UNIVERSITY OF SOUTHAMPTON

Faculty of Engineering and the Environment

Predicting Groundborne Noise and Vibration in Buildings from Railways

Daniel E. J. Lurcock

B.Eng(Hons), MIOA

THESIS FOR THE DEGREE OF
DOCTOR OF ENGINEERING

2018

UNIVERSITY OF SOUTHAMPTON

ABSTRACT

FACULTY OF ENGINEERING AND THE ENVIRONMENT:
Acoustical Engineering

Doctor of Engineering

PREDICTING GROUNDBORNE NOISE AND VIBRATION IN BUILDINGS FROM RAILWAYS

by Daniel Elliot James Lurcock

Groundborne noise and vibration from railways is transmitted to occupants in buildings through the dynamic interaction of several components, including the trackform, tunnel structure, intervening ground, building foundations, building structure, room construction and room acoustics. Due to the number and interdependency of these components it is difficult to accurately predict resulting noise and vibration levels within the building. Consultants often do not have the information, time and skills necessary to employ detailed computer simulations, and must refer instead to simplified empirical prediction methods. However, these methods do not afford the ability to explore the effect of changes to various parameters such as building design.

In this research, vibration measurements from eleven different buildings have been reviewed in order to identify general trends and to validate a finite element (FE) model approach to the prediction of vibration transmission. A generic building FE model has been developed and used as the basis for a parametric study of the effect of a number of parameters on vibration levels at different locations in the building.

Several rooms subject to groundborne noise and vibration have also been used for measurements and to validate a new FE model prediction approach. A generic room FE model has been developed and used as the basis for a parametric study of the effect of a number of parameters on room noise levels. Results of the measurements and FE predictions have been compared with traditional empirical approaches.

The original contributions to knowledge include trends found from the measurement and parametric studies, which have been more extensive than others in the literature. The research also details new approaches to the FE modelling of buildings and point-supported plates as well as methods to couple building vibration with room acoustics. The FE building model has been used to develop a new empirical prediction method for building vibration. The new prediction method will reduce prediction uncertainty and give important insight to building designers into which kinds of design changes might be detrimental or beneficial to groundborne noise and vibration levels.

CONTENTS

AUTHOR'S DECLARATION

I, Daniel Lurcock, declare that the thesis entitled 'Predicting Groundborne Noise and Vibration in Buildings from Railways' and the work presented in the thesis are both my own, and have been generated by me as the result of my own original research. I confirm that:

- this work was done wholly or mainly while in candidature for a research degree at this University;
- where any part of this thesis has previously been submitted for a degree or any other qualification at this University or any other institution, this has been clearly stated;
- where I have consulted the published work of others, this is always clearly attributed;
- where I have quoted from the work of others, the source is always given. With the exception of such quotations, this thesis is entirely my own work;
- I have acknowledged all main sources of help;
- where the thesis is based on work done by myself jointly with others, I have made clear exactly what was done by others and what I have contributed myself;
- output from this research has been published as:

  Lurcock, D.E.J., Thompson, D.J., 2014. Predicting groundborne railway noise and vibration in buildings: A comparison of measurements and methods, in: Proceedings of the Institute of Acoustics. Birmingham, UK, pp. 139–146.

  Lurcock, D.E.J., Thompson, D.J., Bewes, O.G., 2015. Attenuation of Railway Noise and Vibration in Two Concrete Frame Multi-storey Buildings, in: Noise & Vibration Mitigation for Rail Transportation Systems. 126, pp. 297–304.

  Lurcock, D.E.J., Thompson, D.J., Bewes, O.G., 2017. Groundborne Railway Noise and Vibration in Buildings: Results of a Structural and Acoustic Parametric Study, in: Noise & Vibration Mitigation for Rail Transportation Systems. 139, pp. 193-204.

  Lurcock, D.E.J., Thompson, D.J., 2017. A New Empirical Prediction Approach for Groundborne Vibration in Buildings, in: Proceedings of the 24th International Congress on Sound and Vibration, London.

Signed: _____

Date: _____

[BLANK PAGE]

ACKNOWLEDGEMENTS

The author would like to thank the Engineering and Physical Sciences Research Council (EPSRC) and Arup Acoustics for the financial support that has facilitated this research.

Thanks also to:

Prof. David Thompson and Dr. Neil Ferguson (Institute of Sound and Vibration Research (ISVR), University of Southampton), and Dr. Mohammed Hussein (College of Engineering, Qatar University) for their supervision;

Dr. Oliver Bewes, Helen Butcher, Andy Officer (Arup Acoustics) for supervision, access to historical data, and assistance with measurements;

Dr. Ben Waterson, Prof. Philippa Reed and Helene Glasspool for their oversight of the Engineering Doctorate programme in 'Transport and the Environment' at the University of Southampton.

This research has been completed with tremendous support from family. Thank you.

[BLANK PAGE]

SYMBOLS

a	Acceleration, in m.s^{-2}.
a_w	Weighted acceleration, in m.s^{-2}. The weighting curves used in the calculation of the weighted acceleration are defined in BS 6841:1987 [1]; the weighting curve W_b is recommended for vertical motion, with W_d for horizontal motion.
A	Area, in m^2.
β	Ratio of plate thickness to width.
c_B	Bending wave speed, in m.s^{-1}. See Equation (A-1).
c_L	Compressional wave speed, in m.s^{-1}.
c_S	Shear wave speed, in m.s^{-1}.
c_0	Speed of sound in air, in m.s^{-1}.
D	Flexural rigidity, in kg.m^{2}s^{-2}. See Equation (2-11).
E	Young's modulus of elasticity, in Pa.
η	Damping loss factor (often approximated by $\eta \approx 2\zeta$).
f	Frequency, in Hz.
f_n	Natural frequency, in Hz.
f_0	Fundamental natural frequency, in Hz.
Δf	Half-power bandwidth (the interval of the upper and lower frequencies at which the sound pressure level is 3 dB less than at the natural frequency), in Hz.
g	Gravitational acceleration constant, 9.81 m.s^{-2}.
k_z	Vertical stiffness, in N.m^{-1}.
H	Height, in m.
h	Thickness, in m.
l	Length, in m.
$\lambda_{m,n}$	Dimensionless frequency factor, $\lambda_{m,n} = \Omega_{m,n}^2$ See Equation (2-17).
L_A	A-weighted sound pressure level, in dB. Sound pressure level with A-weighting applied (as defined in IEC 61672-1:2002 [2]).
L_{Aeq}	A-weighted equivalent continuous sound pressure level, evaluated over a specific time period.
L_{Amax}	Maximum A-weighted sound pressure level measured during a given time period. In the context of groundborne noise, the level is usually in terms of a running one second L_{Aeq}.
L_{ASmax}	Maximum A-weighted sound pressure level measured during a given time period, with 'slow' exponential time weighting (one second time constant, see [2]). Also denoted by $L_{Amax,S}$.
L_{LF}	The low frequency 'combined' sound pressure level in a room. This is calculated from an average of the corner and more central room positions. See Equation (2-23).

L_p	Sound pressure level, in dB. The logarithmic ratio of a sound pressure to a reference pressure. For sound in air, the reference pressure is usually 2 x 10^{-5} Pa.
$L_{p,\mathrm{norm}}$	Sound pressure level, normalised by reverberation time, in dB. See Equation (6-1).
L_{corner}	The sound pressure level averaged logarithmically over multiple 'room corner' positions, in dB re 2x10^{-5} Pa. See Equation (2-23).
L_{room}	The sound pressure level averaged logarithmically over multiple centrally distributed 'room' positions, in dB re 2x10^{-5} Pa. See Equation (2-23).
L_v	Velocity level, in dB. The logarithmic ratio of a vibration velocity to a reference velocity. The reference velocity is usually 10^{-9} m.s^{-1}.
LV2P	A correction factor (in dB re 2x10^{4} Pa.m^{-1}.s) that can be applied to a velocity level (in dB re 10^{-9} m/s) to predict a re-radiated sound pressure level (in dB re 2 x 10^{-5} Pa). See Equation (6-2).
LV2P$_n$	As above, but with the sound pressure level normalised to reverberation time. See Equation (6-3).
m	Mass, in kg. In some contexts m may refer to an integer that represents a specific mode.
ν	Poisson's ratio.
ω	Angular frequency, in rad.s^{-1}.
$\Omega_{m,n}$	Dimensionless frequency factor, $\Omega_{m,n} = \sqrt{\lambda_{m,n}}$ See Equation (2-12).
p	Sound pressure, in Pascals. The dynamic pressure perturbation above/below the atmospheric pressure, caused by a sound wave in air. In this thesis an integer p is also used to refer to the number of 'bays' in an arrangement of point-supported plates.
p_0	Reference sound pressure. For sound in air, this is usually 2 x 10^{-5} Pa.
ρ	Density of a medium, in kg.m^{-3}.
σ	Radiation efficiency. The proportion of acoustic power transmitted by a structure compared to a theoretical baffled piston. This is used to link structural vibration with resultant noise, and is frequency dependent.
S	Surface area, in m^2.
T, T_{60}	Reverberation time. The time it takes (in seconds) for sound in a room to decay by 60 dB.
v	Velocity, in m.s^{-1}.
$\langle v^2 \rangle$	Mean-squared velocity, in m^2.s^{-2}.
V	Room volume, in m^3.
VDV	Abbreviation for Vibration Dose Value, a measure of vibration exposure as defined in BS 6841:1987 [1].
W	Sound power, in W.
ζ	Damping ratio.
Z	Impedance. The resistance of a medium to velocity input. Defined as the input force divided by the response velocity: $Z = F/v$.

1. INTRODUCTION

1.1 Environmental context

Around the world, the human population is growing in number [3] and a general trend for migration from rural to urban areas has been observed [4]. The demand for housing and the limited availability of land has caused urban planners increasingly to consider residential development on sites close to transport infrastructure. There has also been a rise in motorised transport usage, caused by the increase in both urban population and the distance that people are regularly travelling [5]. These factors have led to increased exposure of the population to transportation noise and vibration sources, including railways.

In the majority of cases, noise from railways, as experienced at a nearby building, propagates to occupants primarily through the air, via façade elements. A diagram of this *airborne* type of propagation is shown in Figure 1-1. This type of propagation causes noise effects from railways over the entire audible frequency range (20 – 20,000 Hz), with the most important components between 100 and 5,000 Hz.

Figure 1-1. Sketch representation of airborne noise path

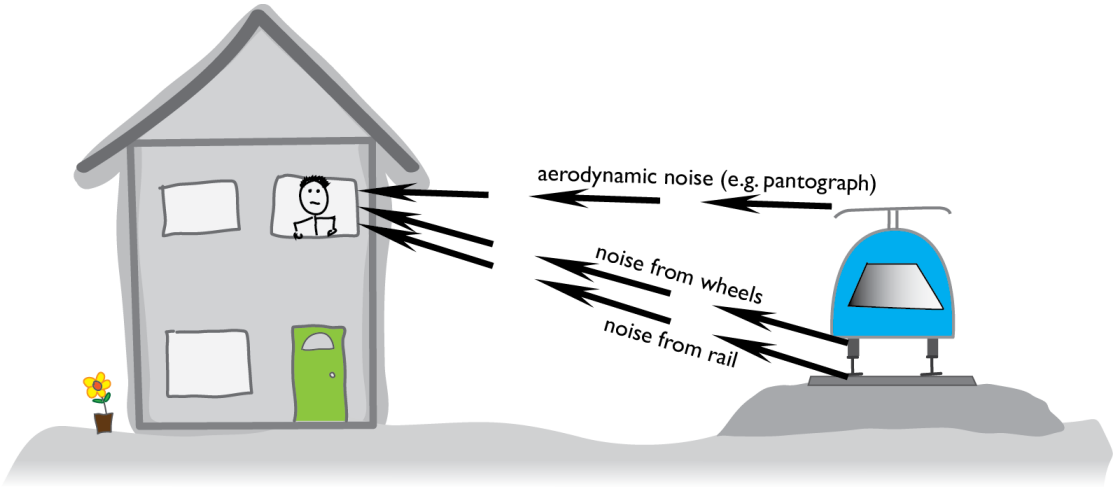

There are many situations in which the airborne noise propagation path has been limited, for example through the installation of acoustically high-performing façades, or trackside noise barriers, or where the trains are running in a tunnel. In such cases, the dominant acoustic transmission path is then *groundborne*, where vibrations propagate via the ground, building foundations, and structure, resulting in (audible) noise and (perceivable) vibration in rooms. A diagram of this type of propagation is shown in Figure 1-2. Where groundborne noise and vibration is concerned, the important frequency ranges are in general around 20 to 250 Hz for the audible noise component, and 4 to 80 Hz for perceivable vibration [6]. These significant

frequency ranges are determined by the frequency dependence of both the railway vibration source, the transmission path, and human perception.

Figure 1-2. Sketch representation of groundborne noise path

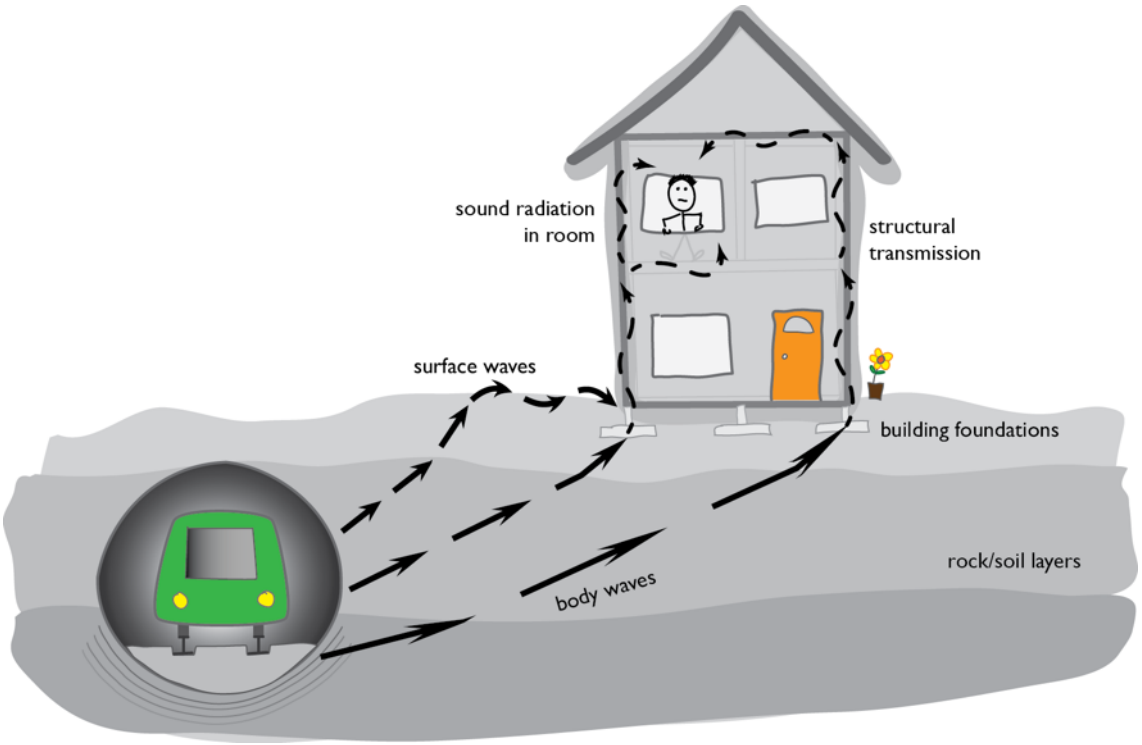

Airborne noise generation and propagation from railways is relatively well understood, with prediction methods able to obtain levels of accuracy within a few decibels [7,8]. This is unfortunately not the case with groundborne noise and vibration, due to the exceedingly complex nature of vibration propagation as well as uncertainties in determining the physical parameters of structures and ground layers. Prediction methods must therefore be improved in order to allow buildings and railway systems to be designed optimally, that is, in order for such designs to incur a minimum cost and resource usage, whilst maintaining appropriate noise and vibration conditions at sensitive receivers.

1.2 Commercial context

Arup is the industrial sponsor of this research. Arup is chiefly a civil engineering consultancy firm, but incorporates a range of multidisciplinary teams, including an acoustics division. Its expertise is called upon for many important development projects globally, including prominent buildings and major transport infrastructure.

Arup often provides consultancy services for new building developments in the vicinity of existing railway systems, as well as new railway systems near existing buildings. A significant proportion

of the acoustics division workload is concerned with the impact assessment of groundborne noise and vibration in such situations.

For new developments close to existing railway infrastructure, the level of vibration at the foundations of the proposed building is usually estimated from vibration measurements on the ground surface or within borehole locations. For new railway infrastructure there are greater uncertainties involved but the level of vibration at the foundations of buildings is usually estimated from a combination of measurements and correction terms for the proposed railway.

The greatest level of uncertainty is associated with predicting the resulting noise and vibration levels within buildings. This is due to a lack of clearly documented and validated methods for predicting: the coupling between ground and foundations; the vibration transmission through the building structure; and the re-radiated sound fields within rooms.

The current Arup prediction approach is typically based on empirical techniques that, whilst considered as constituting 'best practice' and used by acoustical consultants worldwide, are based on limited research from the 1970's. Since this time, building construction methods have changed considerably, with greater use of lightweight materials and complex foundations. In addition, there have since been important changes to railway systems in terms of track and rolling stock design. The current empirical approach does not explicitly account for these factors, and nor does it allow for the exploration of building design modifications such as changes in structure or foundation type, consideration of which is frequently requested by other design team members.

An alternative prediction approach is through the use of numerical methods such as Finite Element (FE) and Boundary Element (BE) analysis, but there is limited experimental validation of such models, and they are expensive for consultants to use in terms of development, calculation and analysis time.

Where uncertainties exist in the prediction methods, it is prudent to adopt a conservative approach. Consequently, consultants are known typically to apply a 10 dB allowance (3.2 times the predicted amplitude) for uncertainty in calculations of groundborne noise. By comparison, conventional airborne noise calculations might attract an allowance of 3 dB (1.4 times the predicted value).

Due to the uncertainties exhibited by the current prediction methodologies and the difficulties in exploring structural design changes, many projects are prescribed with mitigation measures that are potentially overly cautious and therefore more expensive than necessary. However, mitigation against groundborne noise and vibration is inherently expensive in terms of both time

and money, and the use of significant material resources is a growing environmental concern. Furthermore, the inclusion of specialist vibration isolation systems adds complexity to projects.

Further research in this area is therefore important, in order to reduce the potential for over-provision of mitigation, thereby reducing the financial and environmental footprint of many major projects.

1.3 Thesis outline

A review of the relevant literature is given in Chapter 2, which covers background information on the noise and vibration generation and propagation mechanisms as well as prediction methodologies.

In order to identify the kinds of trends to be expected when making predictions, an examination of measured vibration data from a number of buildings is presented in Chapter 3. Furthermore, these measured trends are compared to results from various modelling techniques.

In order for parameter studies to be as accurate as possible, it is important to validate the modelling approach. Chapter 4 presents two such validation studies where measured results from buildings are compared with their counterpart model predictions using a 3D finite element approach. The modelling approach is then used for extensive parameter studies, which are described in Chapter 5. Empirical expressions are derived from the FE model results, with predictions in 1/3 octave bands showing good agreement with trends in the measured and finite element model data.

In order to investigate the conversion of this vibration into re-radiated sound, results from a number of noise measurements are examined in Chapter 6, and compared with existing empirical prediction models. In order to investigate in more detail the influence that the room structure and acoustics might have on re-radiated sound pressure levels, a finite element model of the room is used for a study of various room parameters. Chapter 7 presents validation studies for this approach. The influence of such factors as room size, wall and ceiling configurations, and force input directions on the re-radiated sound pressure levels are presented in Chapter 8. This includes some important observations regarding the relative merits of various room designs.

Conclusions from the research are given in Chapter 9. Further information on historic measurement data, FE model results, data analysis and modelling of structural components is given in the Appendices, which are followed by a list of references.

1.4 Original contributions

The original contributions from this research include the following:

- An extensive review has been conducted of measured vibration data in buildings, with the common trends identified and compared to predictions from several finite element and empirical approaches.
- Using a 3D finite element approach, an extensive parameter study for building vibration has been performed with a larger range of parameters than has previously been available in the literature. The significance of the various building parameters has been assessed qualitatively and quantitatively.
- Findings from the 3D parametric study have been used to derive empirical formulae for predicting building vibration at column and mid-span positions in 1/3 octave band frequencies. The formulae are based on structural natural frequencies and constants relating to building type. Appropriate constants are determined from comparison with the model data and measurement trends.
- A 3D finite element model has been developed and to calculate re-radiated sound pressure levels in rooms. This has been extended with a novel approach that allows the relative sound pressure contributions of individual room surfaces to be approximately determined.
- The 3D finite element room model has been used as a basis for a study for investigating the influence of certain room parameters. The significance of these parameters has been assessed in terms of spatially-averaged sound pressure levels as well as sound pressure contributions from the individual room surfaces.
- Empirical formulae have been derived for predicting the first natural frequency in multi-supported plates. Whereas previous empirical approaches found in the literature only allowed for square bays in a square (p x p) or one-dimensional (1 x p) arrangement, the new formulae can accommodate arbitrary (p x q) arrangements of rectangular bays. For comparable configurations, the new formulae also show improved agreement with finite element model results.

[BLANK PAGE]

2. BACKGROUND & LITERATURE REVIEW

A good recent overview of the mechanisms of groundborne noise and vibration from railways is given by Lombaert et al [9]. For buildings, a useful summary of a number of prediction methods is given as part of the RIVAS project Deliverable D1.6 [10].

2.1 Human response

In order to identify appropriate metrics for predicting and assessing noise and vibration from railways in buildings, it is important first to consider the effects on humans.

It is widely accepted that noise can cause significant negative effects for humans, whether psychologically (for example, through stress or annoyance) or, at extreme sound pressure levels, physiologically (i.e. through damage to hearing) [11]. For the lower values usually associated with groundborne railway noise, the primary concern is the psychological effects; that is, the annoyance caused by interference with sleep and leisure activities (such as music concerts and theatre). Groundborne noise and vibration can also affect work activities, for example those involving sensitive laboratory equipment and/or low-noise test environments.

For vibration from railways it is recognised that in very extreme circumstances damage to buildings *can* occur, although such damage attributed solely to the vibration levels is very rarely observed. It is most unlikely that vibration levels from the passage of trains would ever cause physiological damage to human occupants, but it is recognised that trains do cause vibration in buildings that is in many cases detectable and significant enough to cause annoyance or disturbance [12].

2.1.1 Noise metrics

When humans respond to sound, it is the pressure fluctuation within the air that is the quantity of interest. This pressure fluctuation can be measured using a microphone and recording system and quantified in a number of ways. An example waveform generated from a representative groundborne noise recording is given in Figure 2-1.

Figure 2-1. Example train pass-by waveform

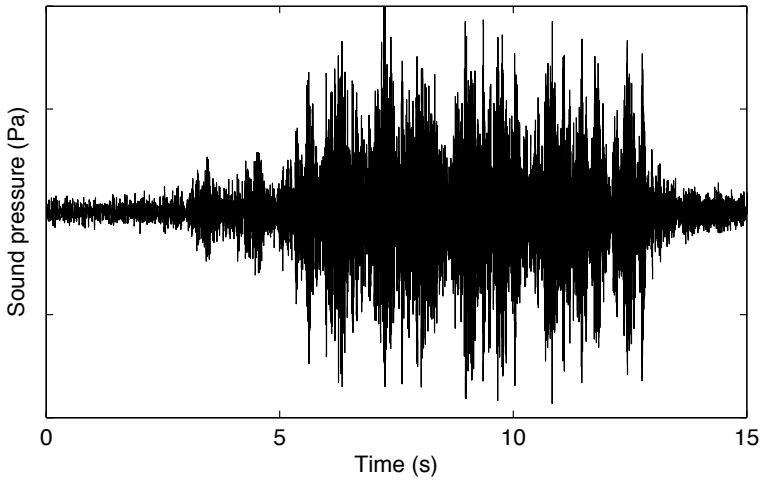

Hearing in humans does not follow a physically linear response, but rather is logarithmic with respect to amplitude. Quantification of sound pressure is therefore usually performed in terms of a logarithmic ratio of the measured pressure to a reference value. This is known as the 'sound pressure level', L_p, as:

$$L_p = 20 \log \frac{p}{p_0} \qquad \text{(dB)} \qquad \textbf{(2-1)}$$

where:

p is the sound pressure, in Pa;

p_0 is the reference sound pressure, in Pa, usually 2 x 10^{-5} Pa.

Due to the periodic nature of acoustic signals, sound pressure signals inherently undulate between positive and negative values (relative to atmospheric pressure); the average is therefore always zero. This is unhelpful for quantification purposes, and so it is usual to apply time averages to the square of the signal. The simplest such method is the root-mean-square (rms) average, which may be performed for a signal over an entire section of interest, or perhaps as a running average with a moving time window. For a given time interval, T, the level of the average rms sound pressure is known as the equivalent continuous sound pressure level, $L_{eq,T}$.

In order to characterise non-steady sounds appropriately, it is necessary to employ additional time-based metrics. A running one-second rms average of the signal is often used, with the maximum level recorded over a period denoted as L_{max}. As an alternative to utilising a running linear average, two types of exponential averaging are frequently used in acoustics: *fast* and *slow*, whose levels are denoted by L_F and L_S respectively. The equations for fast or slow time weighted level $L_\tau(t)$ are given in in IEC 61672-1:2002 [2], reproduced in Equation (2-2).

$$L_\tau(t) = 20\log\left(\frac{\sqrt{(1/\tau)\int_{-\infty}^{t} p^2(\xi)e^{-(t-\xi)/\tau}d\xi}}{p_0}\right) \quad \text{(dB)} \qquad \textbf{(2-2)}$$

where:

τ is the exponential time constant, in s (0.125 s for fast, 1.0 s for slow);

ξ is a dummy variable of time integration from some time in the past, as indicated by $-\infty$ for the lower limit of the integral, to the time of observation, t;

$p(\xi)$ is the instantaneous sound pressure;

p_0 is the reference sound pressure, 2 x 10^{-5} Pa.

For groundborne railway noise (and transportation noise in general) the slow weighting is often preferred to the fast weighting since such sources tend not to include significant short impulses and therefore correspond better with human effects. Where time weightings are used, the signal may be quantified statistically (e.g. the level exceeded for a given percentage of the measurement duration), or in terms of the maximum time-weighted level over a given period, which for a slow time weighted signal is denoted by L_{Smax}.

A summary of some of the quantifiers discussed so far is shown in Figure 2-2 (this is the same pass-by as that represented previously in Figure 2-1).

Figure 2-2. Example groundborne noise metrics for a train pass-by

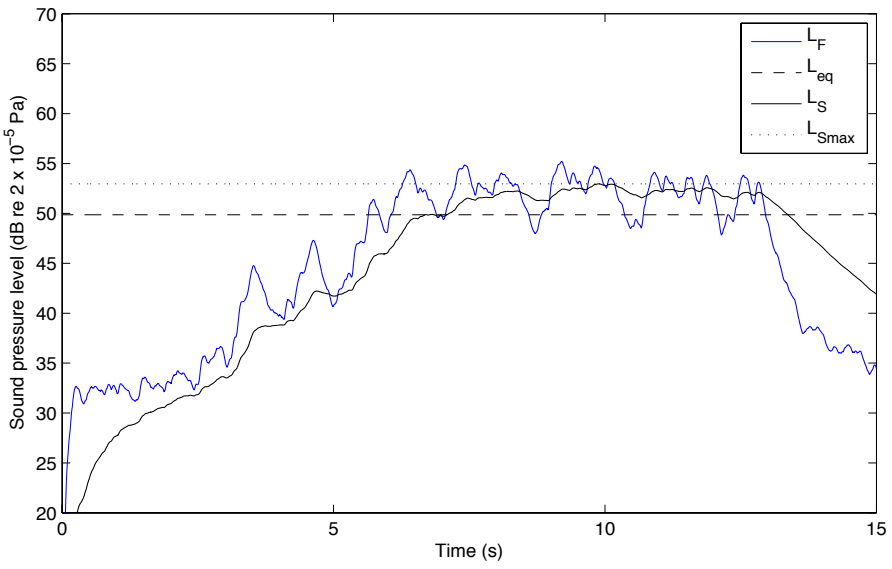

As well as accounting for human perception of noise in the time domain, it is important also to consider perception in the frequency domain. It is helpful therefore to use frequency weighting when quantifying noise. A very popular (but often criticised) frequency weighting is the A-weighting as defined in [2], with the frequency curve reproduced in Figure 2-3. Sound levels

determined from acoustic signals having passed through an A-weighting filter are denoted with an 'A' subscript, e.g. L_A.

Figure 2-3. A-weighting frequency curve

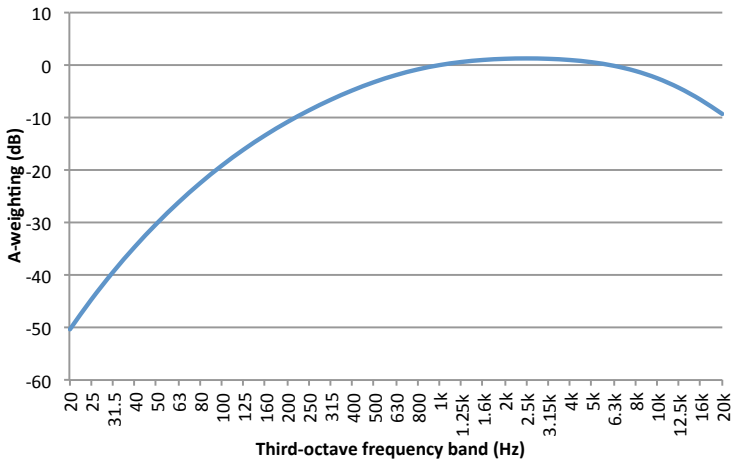

Time weightings and frequency weightings are often used together, for instance L_{ASmax} is defined as the maximum A-weighted sound pressure level over a measurement period with slow time weighting. Here it should be noted that for groundborne noise from trains, there has been shown to be an approximate relationship between L_{ASmax} and L_{AFmax}, such that L_{AFmax} often exceeds L_{ASmax} by around 1-2 dB for continuously welded rail, and 3-4 dB for jointed rail. Furthermore, if evaluated to the 10 dB down points, the L_{Aeq} for a train pass-by is approximately 1-2 dB less than the L_{ASmax} [13]. The dominant frequency range for groundborne noise from trains is typically between 20 and 250 Hz.

2.1.2 Vibration metrics

Vibration can be measured in terms of velocity (with geophones) or acceleration (with accelerometers). When measurements are required for assessment of vibration affecting humans, acceleration is usually the most appropriate physical quantity, with velocity often used as a more appropriate quantity for assessing possible damage to structures, or for predicting re-radiated noise levels.

As with sound quantification, vibration signals must be processed in order to provide meaningful results. The exception is when peak values such as peak particle velocity (PPV) are required, which are obtained directly from the raw velocity signal. It is common practice to convert acceleration signals to velocity signals (if required) by applying time-domain integration. In the frequency domain, for a specific frequency (f in Hz) the magnitudes of acceleration (a in m.s^{-2}) and velocity (v in m.s^{-1}) are related by $a = 2\pi f v$.

The British Standards BS 6472-1:2008 [12] and BS 7385-2:1990 [14] provide guideline information on human response and possible structural damage respectively. For assessing human response, BS 6472 recommends the adoption of the vibration dose value (VDV) parameter, as defined in Equation (2-3).

$$VDV = \left(\int_0^T a_w^4(t)dt \right)^{0.25} \quad \text{(m.s}^{-1.75}\text{)} \qquad \textbf{(2-3)}$$

where:

a_w is the weighted* acceleration, in m.s^{-2};

T is the duration of the assessment period, in s;

t is time, in s.

The W_b weighting (as defined in [1]) is the most commonly used weighting when assessing the effects of railway induced ground vibration on humans. The W_b frequency curve is reproduced in Figure 2-4.

Figure 2-4. W_b-weighting frequency curve

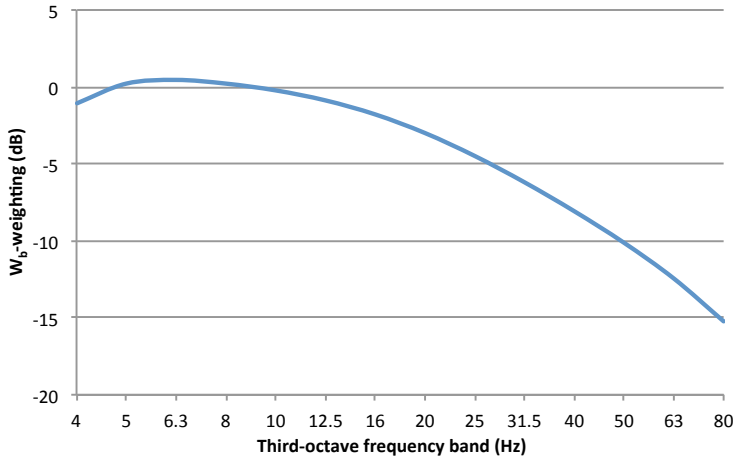

2.1.3 Noise and vibration criteria

Whilst criteria values should not directly influence prediction methodologies, awareness of such criteria assists the researcher in the preparation of prediction models that will be relevant and compatible with the common criteria metrics. Criteria are presented here from published research, national/international standards or guidance, as well as the examination of case histories.

* The weighting curves used in the calculation of the weighted acceleration are defined in BS 6841:1987 [1]; the weighting curve W_b is recommended for vertical motion, with W_d for horizontal motion.

The World Health Organisation (WHO) has suggested that the A-weighted maximum level (fast time weighting, L_{AFmax}) is a suitable indicator for noise effects when the noise consists of a number of discrete events (as occurs with railway noise). It advises that noise events in bedrooms at night should not exceed L_{AFmax} 45 dB to avoid sleep disturbance [11]. Whilst BS 8233:2014 "Guidance on sound insulation and noise reduction for buildings" [15] does give advice for internal ambient noise levels based on the WHO guidance, it adds the caveat that "*projects involving groundborne noise from underground trains, plant or industrial sources usually require expert advice.*"

There are unfortunately no national or international standards that provide specific advice on groundborne railway noise criteria. However, some of the earliest national guidance was provided by the American Public Transport Association (APTA) in 1981 [16], which suggested the L_{Amax} criteria for a range of buildings as presented in Table 2-1.

Table 2-1: APTA Guidelines for Groundborne Noise in Buildings, L_{Amax} (dB)

Environment	Single family dwelling	Multi-family dwelling
Low density residential	30	35
Average density residential	35	40
High density residential	35	40
Commercial	40	45
Industrial/Highway	40	45

More recently, the Federal Transit Administration (FTA) [17], based on the experience of implementing the APTA guidelines, suggested an impact level for buildings which contain habitable rooms (for sleeping) of between 35 and 43 dBA depending on the frequency of the train service. The metric is understood to be a maximum running one-second L_{Aeq}.

London Underground Limited identified a threshold for complaint at L_{Amax} 40 dB [18].

Guidance can also be taken from case studies of important railway infrastructure projects of recent years. The Channel Tunnel Rail Link project, more recently known as High-Speed 1 (HS1) required the construction of 12 miles of tunnels under London, and groundborne noise was a major consideration. The environmental assessment guidance documents classify the impact of groundborne noise as per Table 2-2 [19].

Table 2-2: Groundborne Noise Impact Criteria for Residential dwellings: High-Speed 1 & CrossRail	
Magnitude of Impact / Descriptor*	Groundborne Noise Level (near the centre of the room), L_{ASmax} (dB)
Low	35-39
Medium	40-44
High	45-49
Very High	>49

Similarly, the CrossRail project, involving 13 miles of tunnels underneath London is due to be completed in 2018, with recommended impact criteria for the environmental statement identical to those for the High-Speed 1 project [20]. The Local Authority is to be informed of any residential properties predicted to be exposed to groundborne noise levels at or above L_{ASmax} 35 dB, and mitigation measures should be reasonably adopted in such cases. Additional criteria have also been stipulated for non-residential noise sensitive buildings, with the most stringent criterion of L_{ASmax} 25 dB being assigned to theatres and large auditoria such as concert halls.

BS 6472-1 [12] provides guideline values for human response to vibration in buildings, indicating that for residential buildings at night-time, VDV values around 0.1 $m.s^{-1.75}$ correspond with a "low probability of adverse comment", with values around 0.6 $m.s^{-1.75}$ corresponding with "adverse comment probable". It is also suggested that the threshold for vibration detection for most people is 0.015 $m.s^{-2}$ (this is a weighted vertical peak acceleration).

For structural damage, BS 7385-2 advises that whilst dependent on the dominant frequency and type of building, transient vibration in any direction should not exceed a component peak particle velocity of 15 $mm.s^{-1}$. It is important to note that this value is only an indicator of minor cosmetic damage; significant structural damage would require much greater vibration magnitudes.

Research conducted in the UK [21] suggested that the vibration metric that showed the best correlation with human annoyance was in fact the vibration exposure in the 8 Hz 1/3 octave band for 24 hr rms acceleration. For vertical vibration from railways, weighted rms accelerations of 0.21 $m.s^{-2}$ and VDV values of 0.32 $m.s^{-1.75}$ correspond to around 70% of occupants experiencing a level of annoyance (i.e. slight to high annoyance).

The building vibration criteria for the operational Channel Tunnel Rail Link (CTRL, also referred to as High-Speed 1) and CrossRail projects have been obtained from the environmental

* Magnitudes of impact are often used to inform strategic decision processes, for example in planning considerations for transport infrastructure. In such cases decisions are based on statistical representations of how the proposal might (negatively) affect the population, which may be expressed in terms of the number or proportion of dwellings in each particular impact category.

assessment documents, and are reproduced in Table 2-3. Note that the VDV values are integrated over the whole day or night-time periods. It is seen that these roughly correspond with the recommended values given in BS 6472-1.

Table 2-3: Building Vibration Impact Criteria for Residential dwellings: High-Speed 1 & CrossRail		
Magnitude of Impact / Descriptor	Daytime VDV ($m.s^{-1.75}$)	Night-time VDV ($m.s^{-1.75}$)
Slight	0.22 – 0.31	0.13 – 0.18
Moderate	0.31 – 0.44	0.18 – 0.26
Substantial	0.44 – 0.62	0.26 – 0.37
Severe	>0.62	>0.37

2.2 Vibration propagation in ground

Once vibration has been transmitted to the ground via the railway track system and the tunnel, it propagates as waves through the ground. The ground strata influence the wave propagation since different layers exhibit different physical properties.

For an infinite homogeneous elastic medium, two types of wave can be sustained in relation to compressional or shear body motions. These have differing wave speeds c_L and c_S respectively, given by:

$$c_L = \sqrt{\frac{\lambda + 2\mu}{\rho}}; \quad c_S = \sqrt{\frac{\mu}{\rho}} \qquad (m.s^{-1}) \qquad \textbf{(2-4)}$$

where:

ρ is the density of the medium, in $kg.m^{-3}$;

λ, μ are Lamé constants given by:

$$\lambda = \frac{\nu E}{(1+\nu)(1-2\nu)}; \quad \mu = \frac{E}{2(1+\nu)}$$

where E is the Young's modulus of elasticity, ν is the Poisson's ratio.

Where a boundary exists between ground layers, a component of the incident wave is reflected, and a component is transmitted, with changes in direction observed at non-normal angles of incidence, and where wave speeds differ between the media considered. In addition, at the ground surface there is a coupling between these body waves and 'surface' waves such as Rayleigh waves (vertical displacement) and to a lesser degree, Love waves (transverse displacement). [6]

Compressional waves have the highest wave speeds of these wave types, with surface waves the slowest. Rayleigh waves typically propagate at around 90% of the shear wave speed c_S (dependent on Poisson ratio). Over some ground types, high-speed rail services may approach and even exceed surface wave speeds, which causes significant increases in vibration [22].

Since the shear and compressional waves propagate in all three dimensions, vibration intensity decays with distance from the source. However, for constrained surface waves such as Rayleigh waves, there is very little attenuation with distance for a line source such as that approximated by a railway track.

Propagation through the ground is dependent on the dynamic properties of the ground layer media. Each medium exhibits an impedance, but also an amount of damping; rock has a high impedance but little damping, clay has a smaller impedance, but more significant damping [13,23].

For trains in tunnels, where the majority of excitation is from the tunnel invert, the roof of the tunnel (crown) presents itself as a barrier to the propagation of vibration. This leads to the effect that vibration on the ground surface directly above the tunnel can be less than that at positions offset from the tunnel centreline [24,25].

Due to ground layering and uncertainties surrounding the geological composition, plus the complex nature of the coupling of the various wave types in all three dimensions, it is very difficult to accurately predict the vibrational forces that might act on a built structure in response to even a well-defined input force. This thesis will not set out to quantify such forces, but will assume unit forces at the base of various buildings, and examine differences in propagation through the structures.

2.3 Soil – structure interaction

The dynamic interaction between the ground and a building starts at the foundations. There are a number of different foundation types that are typically considered for buildings; some of these are illustrated in Figure 2-5. These may be grouped into two primary foundation types in relation to their depth: shallow or deep.

Figure 2-5. Some common building foundation types

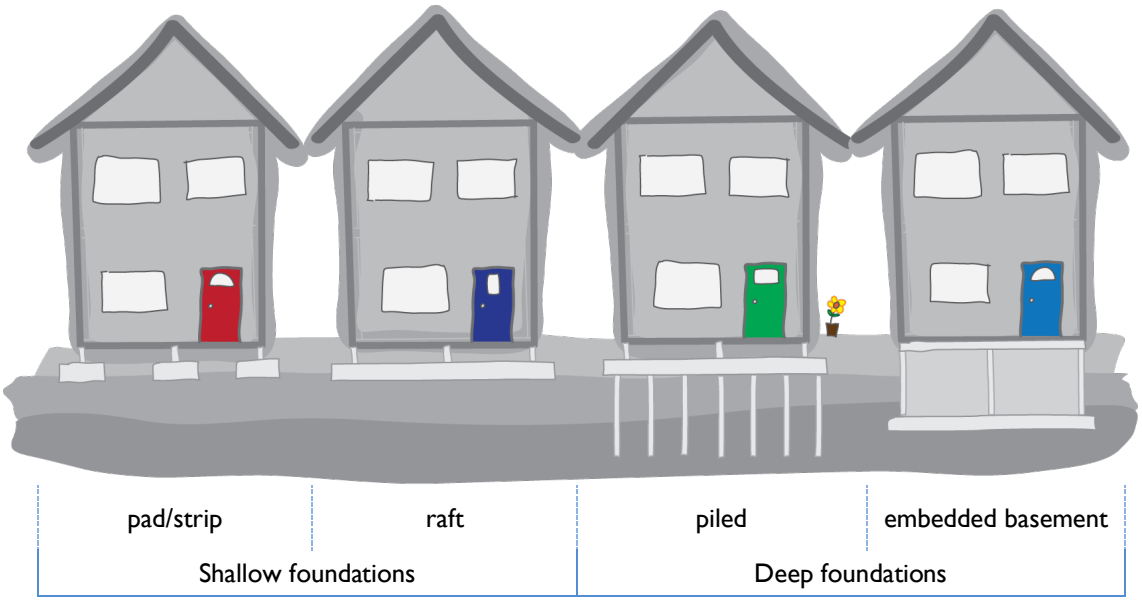

Shallow foundations (or 'spread footings') include pad, strip, and raft foundations, which support a structure by spreading the load over a large area of ground. Deep foundations include piles, sheet piles and diaphragm walls, and provide support to a building by transferring forces to the bottom of the foundation (where stiffer lithologies may be found at greater depths) and also through frictional forces that act upon the entire length of the foundation.

Where it is required to isolate buildings from groundborne vibration, a common solution is to provide resilient elements ('bearings') between the foundations and main building structure. These typically comprise an elastic polymer ('elastomer') layer, or where lower frequency protection is required, metal springs.

Where the building foundations meet the ground, there is dynamic interaction, dependent on the type of foundation (for example shallow spread footings, or deep piles which might traverse soil layers), the soil layer properties, and even the loading. Some helpful representations of the dynamic soil-structure interaction are given in [26] and [27].

For footings resting on an elastic halfspace, the soil acts as a spring. The static vertical stiffness k_z for a stiff circular footing of radius r_0 (in m) has been derived from classical theory as presented by Timoshenko and Goodier [28]:

$$k_z = \frac{2Er_0}{1-\nu^2} \qquad (\text{N.m}^{-1}) \qquad \textbf{(2-5)}$$

where:

E is the Young's modulus of elasticity of the soil in Pa;

ν is the Poisson's ratio of the soil.

When the footing is embedded in the soil, there is an increase in soil resistance, thereby increasing this spring constant. There is also additional stiffness provided through friction at the sides of the footing. Kaldjian [29] prepared a simple finite element model of two configurations: the first with a solid embedded cylinder with a force applied at the surface; the second with the same force applied to a rigid disc at the bottom of the equivalent sized shaft. The effect that the depth to diameter ratio had on the stiffness (relative to the spring constant of a theoretical disc at the surface of an elastic half-space as represented by k_z in Equation (2-5)) is shown in Figure 2-6.

Figure 2-6. Effect of footing embedment on spring constant, from [29]

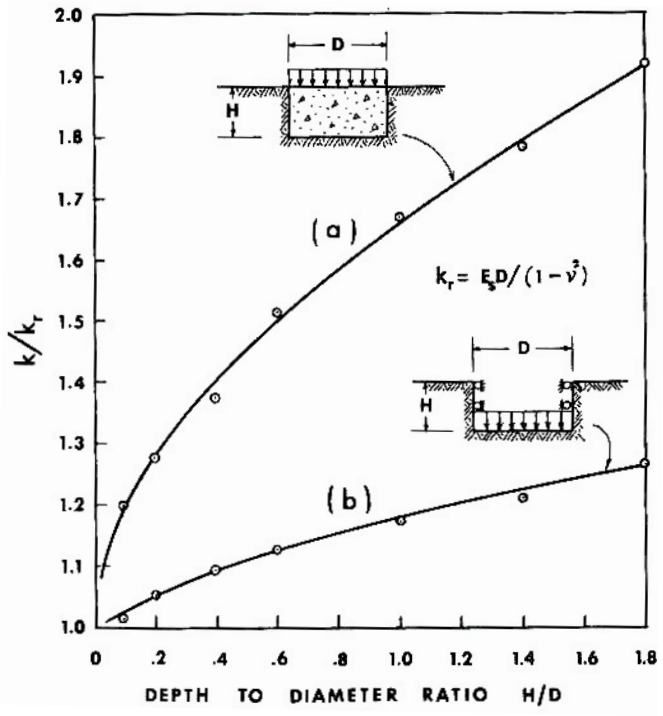

Because shallow foundations are located near the surface, they are influenced primarily by Rayleigh waves. For deep foundations however, the situation is more blurred. The main part of pile foundations presents a very small cross-sectional area compared with the wavelength of any body waves, and therefore there is limited coupling. However, longitudinal vibrations in piles are very efficiently transmitted through the pile, and pile toes* can be situated very close to, and in

* The pile toe is the bottom-most part of the pile.

some cases even in contact with railway tunnel structures. This means that any vibration that *is* transmitted into the foundations at the toe undergoes very little attenuation through the foundation structure [13,30].

Pile foundations represent an interesting case for soil-structure interaction, as their dynamic properties are related to the structure of the pile as well as the soil conditions (which also varies with depth). They can provide load distribution via the pile toe, or via skin friction, or a combination of these two mechanisms. For vertical vibration of an unloaded end-bearing pile of length l (in metres), Young's modulus E (in Pa) and density ρ (in kg.m^{-3}), the system is a classical rod vibration formulation, with the fundamental longitudinal natural frequency f_n given by:

$$f_n = \frac{1}{4l}\sqrt{\frac{E}{\rho}} \quad \text{(Hz)} \tag{2-6}$$

The unloaded longitudinal natural frequency of a 20 m end-bearing concrete pile is therefore around 40 Hz (80 Hz for steel). When a mass m (in kg) is applied to the end, there is a reduction in the natural frequency. The expression linking the applied mass, pile cross-section A (in m^2), and pile length l (in m) is given by:

$$\frac{A\rho l}{m} = \beta \tan \beta \tag{2-7}$$

where:

$\beta = 2\pi f_n l \sqrt{\frac{\rho}{E}}$;

$A\rho l$ is the mass of the pile, in kg.

This relationship is shown graphically in Figure 2-7.

Figure 2-7. Graphical representation of Equation (2-7).

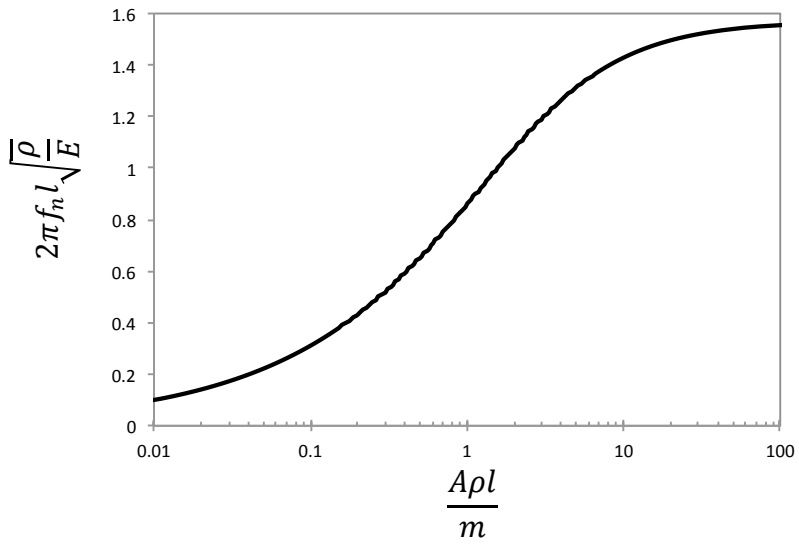

It can be seen that as the applied mass decreases relative to the mass of the pile, the expression tends to $\pi/2$ and the natural frequency tends to that given in Equation (2-6). When the applied mass is much greater than the mass of the pile, then the system behaves like a simple mass on a spring (with stiffness k), for which:

$$f_n = \frac{1}{2\pi}\sqrt{\frac{k}{m}} = \frac{1}{2\pi}\sqrt{\frac{EA}{ml}} \quad \text{(Hz)} \tag{2-8}$$

In reality, the pile is in contact with the soil along its length. The soil modifies the dynamic behaviour through added stiffness and damping. This is difficult to account for, particularly as the soil properties are known to vary significantly with depth.

Examination of pile foundation dynamics has been undertaken by Novak and Sheta [31–33] as well as Kaynia and Kausel [30]. Models of pile foundations developed by Gazetas and Makris [34,35] showed that piles interacting in groups can show resonant behaviour which amplifies incident vibration levels, with the extent of such resonances highly dependent on soil homogeneity.

Acknowledging the lack of research into the dynamics of pile foundations, Kuo and Hunt [36] presented an approach where the response of two different pile groups was modelled due to vibration from an underground tunnel (using the semi-analytical 'Pipe-in-Pipe' model). An important observation was that at frequencies above 15 Hz, piles within a group did not move in phase, and therefore should not be assumed as a rigid collective at such frequencies. It was also found that a pile group containing fewer, but longer piles, exhibited less displacement (that is, reduced ground-foundation coupling) than a group with a greater number of piles at a shallower depth.

2.4 Building transmission

For most buildings, vibration entering the structure at foundation level is very lightly attenuated as it propagates up the building. Jeary [37] summarises that damping occurs due to frictional forces between elements rubbing together and through micro-cracks developing within the material. Damping is therefore amplitude dependent, although it should be noted that for groundborne noise and vibration from transportation sources, amplitudes are small. An earlier empirical expression was given by Ellis [38] for the building's fundamental (swaying) natural frequency f_0 and Jeary equated this to the low amplitude critical damping ratio ζ (in %):

$$\zeta = f_0 = \frac{46}{H} \quad \textbf{(2-9)}$$

where:

H is the height of the building, in metres.

f_0 is the building's fundamental (bending) natural frequency, in Hz.

It should be noted, however, that the measured data suggested that this does not accurately predict the damping in buildings with heights less than around 40 m. Ellis also remarked that for most buildings a damping ratio of between 0.5% and 2.5% (i.e. loss factor between 0.01 and 0.05) is observed for low amplitude motion [38].

Satake et al [39] showed that steel constructions, as used in many modern high-rise buildings, exhibit less damping than otherwise similar reinforced concrete frame buildings. The analysis of 205 buildings for small amplitude excitation showed that steel framed buildings typically exhibited damping loss factors for the translational fundamental natural frequency of less than 0.04; for reinforced concrete buildings this upper value was around 0.1. Damping is said to be less in the lateral direction than the vertical direction, by a factor of 0.83 for steel frame buildings, and 0.75 for concrete. This was thought to be due to greater radiational damping (i.e. energy losses through ground-structure interaction) for vertical vibration.

A number of trends were observed in the data, from which the damping loss factors in the vertical direction could be estimated via the following simplified expressions:

$$\eta_s = \frac{2 \times 74.4}{0.83H \times 100} = \frac{1.79}{H} \quad \textbf{(2-10a)}$$

$$\eta_c = \frac{2 \times 98.9}{0.75H \times 100} = \frac{2.64}{H} \quad \textbf{(2-10b)}$$

where:

η_s is the damping loss factor for steel buildings;

η_c is the damping loss factor for reinforced concrete frame buildings.

It should be noted that the derivation of the above equations was based on buildings with heights in general between 50 and 200 metres. The study included examination of the damping against foundations types. There are difficulties in drawing conclusions from the data because foundation design depends on other factors such as building height and soil conditions, and as such it is not possible to identify the contribution of foundation design in isolation. Nevertheless some broad observations could be made. Buildings with pile foundations in general exhibited slightly greater damping than those with spread footings. It was found that for spread footings, those buildings

with deeper foundations displayed slightly less damping, but it is noted that this is perhaps more likely attributed to the fact that deeper foundations are provided for taller buildings, which inherently exhibit less damping in themselves. For pile foundations, there was found to be no clear correlation between damping and pile length.

Finally, it was noted in the study that the building use had a small effect on damping. Buildings with more non-structural components such as internal partitions (as found in residential, as compared to office accommodation for example) were observed to exhibit slightly greater damping. This effect was seen to be more prominent for steel frame buildings, which tend to have lower damping than reinforced concrete buildings.

It is important to note that most studies on damping focus on the low frequencies associated with the fundamental bending mode. Improving our knowledge of damping at the higher frequencies associated with groundborne noise and vibration will require further research.

Building geometry is an important consideration of vibration propagation through the structure. Where layout is consistent throughout the building, vibrations are more effectively transmitted. Hassan noted that where there are significant changes in layout, or in construction type between floor levels, the changes to impedance result in reflections and dissipation of vibration energy [40].

2.5 Floor dynamics

A background to some of the mechanisms affecting floor vibration is given here, with a focus on out-of-plane modes due to bending wave motion. For a more detailed study and discussion on dynamics of plates, see Appendix A.

2.5.1 Floor response

For human response to noise and vibration in buildings in most of the literature it is assumed that the most important building component is the floor structure. This is because the floor is typically well coupled to the building structure, and because it responds in the vertical axis. This is the axis in which ground vibration from railways tends to be dominant, and in which buildings are stiffest. For perceivable vibration, the floor is of course the common point of entry for human perception. Floor resonances cause elevated noise and vibration at frequencies around their natural frequencies. For many common concrete floor types, this may occur between 10 and 20 Hz for the fundamental modes.

When considering the response of floor slabs in buildings, floors are often assumed to be represented by rectangular plates, with various boundary conditions. In order to understand

better the important parameters in the response, plate theory shall be discussed. Reference will be made to flexural rigidity, D, which is given by:

$$D = \frac{Eh^3}{12(1-\nu^2)} \qquad (\text{kg.m}^2\text{s}^{-2}) \qquad \textbf{(2-11)}$$

where:

E is the Young's modulus of elasticity of the material, in Pa;

h is the thickness of the plate, in m;

ν is Poisson's ratio of the material.

Appendix A contains further discussion and investigation with respect to floor slab natural frequencies. It is important to note from the mode shapes shown in Appendix A that whilst the mid-span position is frequently referred to as a reference location for vibration measurement, this position represents a maxima or minima for most modes.

2.5.2 Thin plate theory

The primary analytical formulation for thin plates was developed by Love [41] in 1888. A good review of the common approaches to determining the natural frequencies of thin rectangular plates is given by Leissa [42]. Where a rectangular plate is simply supported at its edges, its natural frequencies are shown to be given in terms of its dimensionless frequency factor $\Omega_{m,n}$:

$$\Omega_{m,n} = \pi^2 b^2 \left(\frac{m^2}{a^2} + \frac{n^2}{b^2}\right) \qquad \textbf{(2-12)}$$

where:

m, n are the number of half-wavelengths occurring in the x and y directions, respectively;

a, b are the dimensions of the plate in its x and y directions, respectively, in m;

A diagram illustrating the layout of the mode order and plate dimensions is shown in Figure 2-8.

Figure 2-8. Plate mode order and dimensions (m=2; n=3)

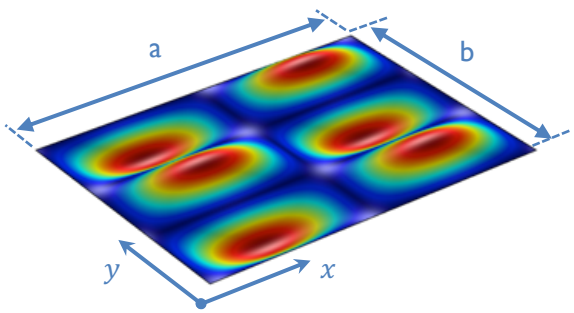

The non-dimensional frequency parameter is related to the frequency through:

$$\Omega = 2\pi f b^2 \sqrt{\frac{\rho h}{D}} \qquad \textbf{(2-13)}$$

where:

f is frequency, in Hz;

ρ is the density of the material, in kg.m^{-3};

h is the thickness of the plate, in m;

D is the flexural rigidity of the plate, as given by Equation (2-11).

(Note that in some of the literature an alternative frequency parameter $\lambda = \Omega^2$ is used) Substituting (2-13) into (2-12) and rearranging leads to:

$$f_{m,n} = \sqrt{\frac{D\pi^2}{4\rho h}}\left(\frac{m^2}{a^2} + \frac{n^2}{b^2}\right) \quad \text{(Hz)} \qquad \textbf{(2-14)}$$

For the case of a thin rectangular plate simply supported at its corner points rather than along its sides, the response is not so straightforward to calculate analytically. Reed [43] outlines two analytical approaches, using Rayleigh-Ritz and trigonometric series solutions. These methods require the use of separate equations for different combinations of odd and even modes. The results are summarised in [42] and [43], with the first seven dimensionless natural frequencies provided for discrete ratios of a/b (1.0, 1.5, 2.0, and 2.5), and for a given Poisson's ratio of 0.3.

Petyt & Mirza [44] used an FE approach to determine the first six modes of rectangular plates supported at points, with close agreement with [43]. They also examined the influence of rigidity at the column/slab joints. It was found that the rigidity of this joint is important for predicting the fundamental natural frequency, but less so for higher frequency modes. As column width increases, the fundamental natural frequency of the slabs also increases, due to this increased rigidity.

For multi-supported plates with square bays, it was observed that modes occur within frequency *bands**, in which the number of modes is equal to the number of bays. The lowest modes occur with motion in the bays that are least constrained, and therefore start at the corner bays, then the side bays, and finally the central bays at the highest mode in the band. The modes of vibration for the first band of frequencies for a 3x3 square grid of 5x5x0.25 m concrete slabs, are

*The 'band' referred to is a nominal grouping of modes, not fractional octave bands.

reproduced in Figure 2-9. The mode shapes have been calculated using FE analysis, assuming pinned points at the slab corners.

Figure 2-9. Modes shapes for the first frequency band of a multi-supported square plate with 3x3 square bays

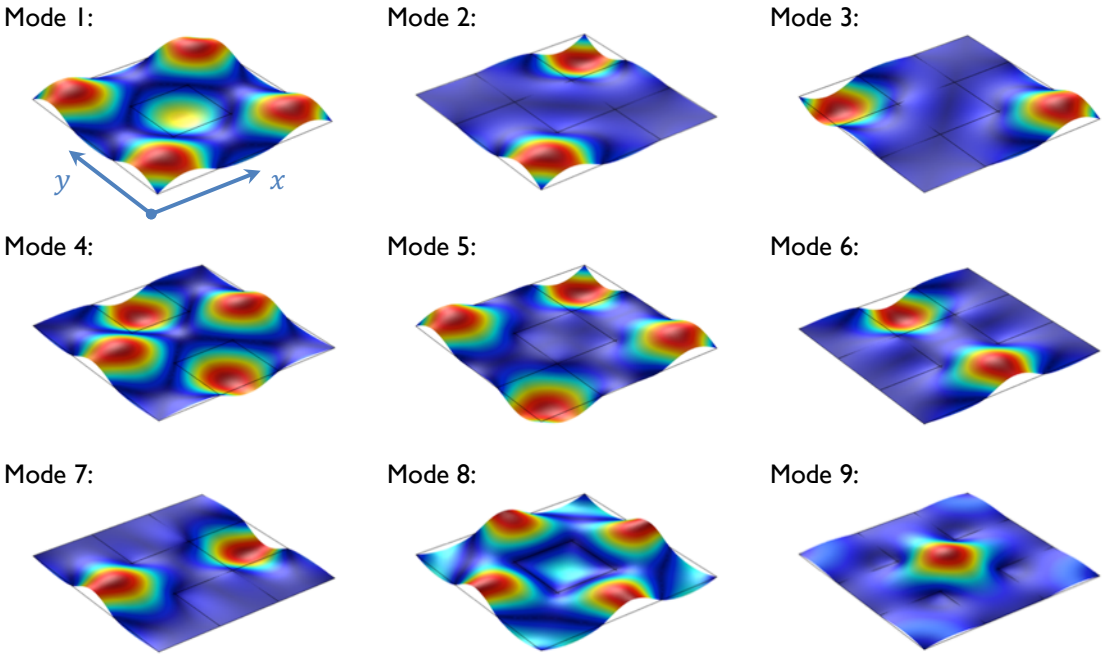

The lowest frequency in the first frequency band for a multi-supported plate in a square (p x p) arrangement was shown by Petyt & Mirza to be approximately predicted from the fundamental frequency parameter of a single bay Ω_{11} using the following relationship:

$$\Omega_{pp1} = p[p(\Omega_{11} + 1) + 1] \ , \qquad \textbf{(2-15)}$$

and for bays in one-dimensional (1 x p) strip arrangements:

$$\Omega_{p1} = p(\Omega_{11} + 1) \qquad \textbf{(2-16)}$$

This approach has been investigated and extended by the author to include for rectangular plates, see Appendix A.

2.5.3 Thick plate theory

Where a plate cannot be considered as 'thin', shear deformations must be taken into account. Mindlin's formulation [45] accounted for this, with approximate expressions for the natural frequency provided by Wang [46]. For a simply supported rectangular plate, the dimensionless frequency factor, $\bar{\lambda}_{m,n}$ is given in terms of the equivalent thin plate frequency factor:

$$\bar{\lambda}_{m,n} = \frac{36\kappa^2(1-\nu)}{\beta^4}\left\{\left[1+\frac{\beta^2\sqrt{\lambda_{m,n}}}{12}\left(1+\frac{2}{(1-\nu)\kappa^2}\right)\right] - \sqrt{\left[1+\frac{\beta^2\sqrt{\lambda_{m,n}}}{12}\left(1+\frac{2}{(1-\nu)\kappa^2}\right)\right]^2 - \frac{\beta^4\lambda_{m,n}}{18(1-\nu)\kappa^2}}\right\} \quad \textbf{(2-17)}$$

where:

κ^2 is the shear correction factor = $\pi^2/12$;

β is the ratio of plate thickness to width, h/b;

$\lambda_{m,n} = \Omega_{m,n}^2$, the thin plate frequency factor.

An expression for the natural frequencies can then be derived by substituting (2-13) into (2-17), but is not presented here for conciseness.

2.5.4 Material properties

When modelling the dynamics of structures, it is important that appropriate values of material parameters are used. An appropriate value for the Young's modulus of elasticity of concrete is deemed to be 20 to 30 GPa, taken from various literature for the static case. However, it is important to note that due to non-linearities in micro-cracking, the *dynamic* stiffness of concrete differs from the static one. In addition, the dominant vibration transmission mechanism in the columns is through longitudinal compression, whereas for the floor slabs it is through bending.

BS 8110-2:1985 [47] provides the following formula for calculating the dynamic elastic modulus of concrete from the static one, and vice versa.

$$E_{\text{dynamic}} = \frac{E_{\text{static}} + 19}{1.25} \quad \textbf{(2-18)}$$

where:

E_{dynamic} , E_{static} are the Young's moduli of elasticity, in GPa.

The relationship between static and dynamic elastic modulus in concrete was shown by Han and Kim [48] to be only slightly dependent on curing temperature and age. For results where the static elastic modulus was around 27 GPa, the dynamic elastic modulus was around 37 GPa, which shows agreement with Equation (2-18).

Where micro-cracks exist in the concrete, there is an effective reduction in stiffness for non-reinforced concrete, although this is minimal for reinforced concrete [49], at least for the case of load testing with samples in compression. Structural elements such as floor slabs that have sections undergoing tension are expected to experience a reduction in flexural rigidity together

with an increase in damping due to micro-cracks. However, this phenomenon is not well understood, and is the subject of continuing research.

2.5.5 Non-structural floor components

Many building designs incorporate additional elements as part of the finished floor, which could include the following:

- Hard finished floorings such as timber laminate, perhaps on a foam underlay;
- Shallow resilient overlay floor surfaces (for impact sound reduction);
- Floating screed, perhaps including underfloor heating;
- Lightweight floating floors, using resilient battens or cradle systems;
- Raised access systems (particularly in commercial developments).

These non-structural components are often neglected in groundborne noise and vibration predictions, and yet it would be expected that they would have an important influence. In measurements by Anderson in [50], raised access flooring was shown to provide substantial floor vibration amplification of up to 25 dB at 125 Hz, which should certainly be taken into account when designing or taking measurements in buildings.

2.6 Re-radiated noise

When a room surface vibrates, it causes a local pressure perturbation in the air. The resulting sound pressure within the room is often called 're-radiated' or 'structural' noise, the mechanisms of which are discussed in this section. For a more comprehensive coverage of these topics, the reader is referred to two books in particular: "Room Acoustics" by Kuttruff [51] and "Sound Insulation" by Hopkins [52].

It should be noted that in furnished accommodation there may be other factors which cannot be reasonably accounted for in predictions. For example, when recumbent on a mattress an occupant may experience higher vibration levels and/or increased noise perceived through bone conduction. In addition, light fittings, windows, furniture and other such items can rattle, thereby significantly accentuating the presence of any structural vibrations. There is little that can be done by building designers to counter these problems, other than being mindful of these factors when specifying or working to noise and vibration criteria. In some cases, for instance with hotel developments, it may be prudent for the building designers to give general recommendations to the building user with regard to these potential issues.

2.6.1 Vibro-acoustic radiation

Radiated sound power from a room surface is dependent on the surface area, the mean-squared velocity over the surface, and a parameter known as the radiation efficiency, σ. This is the ratio of the sound power radiated by the surface to that which would be radiated by a perfect baffled piston with the same mean-square velocity, and is given by:

$$\sigma = \frac{W}{S\rho_0 c_0 \langle v^2 \rangle} \tag{2-19}$$

where:

W is the radiated sound power, in W;

S is the area of the surface, in m^2;

ρ_0 is the density of air, in $kg.m^{-3}$;

c_0 is the speed of sound in air, in $m.s^{-1}$;

$\langle v^2 \rangle$ is the mean-squared velocity of the surface, in $m^2.s^{-2}$ (averaged over both the time and spatial domains).

The radiation efficiency is frequency dependent but values are difficult to obtain, particularly at low frequencies. However, Roozen et al have recently presented a method of using laser doppler vibrometry and a Rayleigh integral calculation to obtain accurate low frequency sound power level measurements from panels, whilst excluding the acoustic effects of the receiver room [53].

In some cases, the radiation efficiency of a wall or floor panel is simply taken as unity (e.g. [54]). This is often an appropriate approximation for concrete constructions, but not for lightweight panels, which exhibit comparatively lower radiation efficiency in the frequency range of interest, and are influenced significantly by the support frame and even the fastening spacing [55,56]. Additional prediction models for homogeneous panels are given in [57].

2.6.2 Low frequency room acoustics

When a sound wave in the room reaches another surface, acoustic energy is partly reflected and partly absorbed, depending on the acoustic absorption characteristic of the surface. As reflected waves interfere with other sound waves in the room, areas of high and low sound pressure develop. These patterns of interference are known as *room modes*, occurring at frequencies dependent on the physical dimensions of the room. As well as causing strong peaks and dips in the sound pressure frequency spectrum, these effects are strongly dependent on location within the room.

Modes in rectangular rooms can be described as three types: axial, tangential and oblique. Axial modes involve reflections between two parallel surfaces; tangential modes involve four surfaces

in the same room plane; oblique modes involve all six surfaces. Diagrams of these mode types are given in Figure 2-10.

Figure 2-10. Room mode types

Axial	Tangential	Oblique
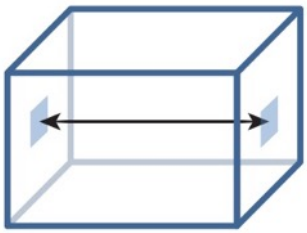	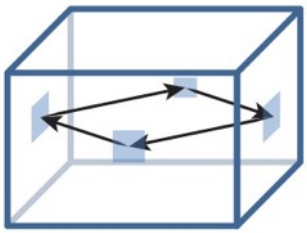	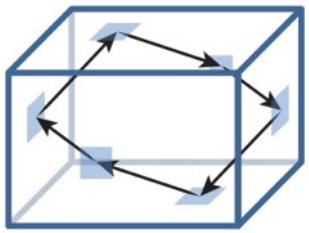

For a cuboid room of dimensions a x b x h with rigid walls, the natural frequencies are given by:

$$f_{p,q,r} = \frac{c_0}{2}\sqrt{\left(\frac{p}{a}\right)^2 + \left(\frac{q}{b}\right)^2 + \left(\frac{r}{h}\right)^2} \quad \text{(Hz)} \qquad \textbf{(2-20)}$$

where:

a, b, h are the room dimensions, in m;

p, q, r are the mode orders in their respective room dimension (e.g. $r = 1$ is the first mode in the h dimension).

Damping is provided through a number of sound absorption mechanisms. The air itself converts some of the sound energy to heat, although this primarily affects high frequencies, and the effect is so small that it would normally only be considered for sound propagating over distances of hundreds of meters or more. At every bounding room surface, a proportion of sound is reflected, and a small amount of sound energy is converted to structural vibration, which propagates away from the room and acts as additional damping. Lightweight panels can also provide absorption through a mechanism whereby at low frequencies the sound pressure is strongly coupled with motion in the panel; damping in the panel materials (and cavity behind) then converts this motion into heat. Absorption is also provided by porous materials within the room, typically in the form of soft furnishings such as curtains, carpets, bedding and cushions etc. As sound propagates through the pores and fibres of such materials, a large proportion of the energy is converted to heat. This is usually the most important mechanism for mid to high frequencies.

Damping influences the frequency response, by reducing and broadening peaks and troughs caused by room modes; it also reduces the time it takes for a sound to decay. *Reverberation time,* T_{60}, is a common measure of room damping, and is defined as the time (in seconds) required for the

sound to decay by 60 dB. Whilst this parameter is frequency dependent, for bedrooms and small living rooms the reverberation time is typically taken as 0.5 s at mid-frequencies.

Since the background noise level will often prevent successful measurement of the full 60 dB decay in the field, 20 dB or 30 dB decay times are usually measured instead, and extrapolated to approximate the true 60 dB reverberation time. Nevertheless, at low frequencies it can be difficult to measure reverberation time accurately due to the decay of analysis filters approaching and even exceeding the acoustic decay rates [58]. Care therefore needs to be taken to utilise appropriate measurement and analysis techniques at these frequencies.

For a given amount of damping in a room, axial modes exhibit longer reverberation times than tangential and oblique modes. There is a greater proportion of axial modes in low frequency bands than at high frequencies, and this tends to correspond to longer reverberation times at the lower frequencies. The frequency-dependent damping provided by porous materials and panel absorption however also plays a part in this effect.

For individual room modes, it can be shown that there is an approximate relationship between the reverberation time and the half-power bandwidth (derived in Appendix D from relationships given in [51]):

$$T = \frac{2.2}{\Delta f} \quad \text{(s)} \tag{2-21}$$

where:

T is the reverberation time, in s;

Δf is the half-power bandwidth of the mode (the interval of the frequencies above and below the natural frequency at which the sound pressure level is 3 dB less than the maximum), in Hz.

The frequency below which the behaviour of a room is generally considered to be dominated by specific modes, is known as the Schroeder cut-off frequency [59] f_S, and is given by:

$$f_S = 2000\sqrt{\frac{T}{V}} \quad \text{(Hz)} \tag{2-22}$$

where:

T is the room reverberation time, in s;

V is the room volume, in m³.

For a cuboid room of dimensions 4 x 3 x 2.6 m, with a reverberation time of 0.5 s, the Schroeder cut-off frequency is around 250 Hz. The natural frequencies as calculated using Equation (2-20) are shown in Figure 2-11 up to 250 Hz. The frequency of the lowest room mode is controlled by the longest room dimension; at 4 metres, the first room mode occurs around 43 Hz.

Figure 2-11. Example room natural frequencies
(cuboid shaped room, 4 x 3 x 2.6 m)

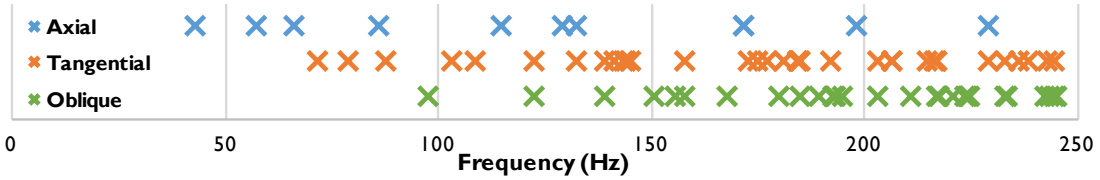

It is evident that in most domestic rooms over the vast majority of the frequency range for groundborne noise the response is strongly influenced by modal behaviour. The lowest room modes are particularly important because around these frequencies there are a small number of modes in a given frequency band (that is, there is a low *modal density*). In these low frequency bands the sound pressure level is therefore dependent on location and room geometry. At high frequencies the modal density is much greater, room modes tend to overlap to a greater extent, and the response is therefore more uniform.

Since at room modes there is a non-uniform distribution of sound pressure, it is difficult to quantify low frequency sound appropriately in small rooms. Indeed it is sometimes recommended that the sound pressure level not be measured at all, but rather should be quantified only through surface vibration measurement based approaches (e.g. [60]). Whilst much of the literature for groundborne noise assessment does not specify the room location(s) for noise evaluation, in some cases it is stated that the evaluation position should be near the centre of the room, but avoiding the very centre of the room due to its prominent modal features. This advice is given in BS ISO 14837-1:2005 [61], which also adds that measurements may be consistent with the ISO 140 series of standards (concerned with the measurement of sound insulation in buildings). BS EN ISO 140-4 for field measurement of airborne sound insulation between rooms has since been superseded by BS EN ISO 16283-1:2014 [62]. In this it is recommended that at low frequencies the sound pressure level may be appropriately described by a weighted logarithmic average of the average sound pressure levels at corner and distributed room positions (based on the findings of Simmons and Hopkins in [63,64]):

$$L_{\mathrm{LF}} = 10\log\frac{2\times 10^{\frac{L_{\mathrm{room}}}{10}} + 10^{\frac{L_{\mathrm{corner}}}{10}}}{3} \quad \text{(dB)} \tag{2-23}$$

where:

L_{room} is the average sound pressure level for the distributed room positions, in dB;

L_{corner} is the average sound pressure level for the corner positions, in dB.

It is important to note that room acoustics should not generally be considered as uncoupled from the structural behaviour of the room surfaces [65]; in the work previously discussed by Roozen et al, it was found that when comparing Rayleigh integral and boundary element models of the receiving room, the radiated sound power of a panel exhibits a dependency on the coupling of structural panel modes to the room modes, resulting in sound power increases of up to 10 dB at some room natural frequencies [53].

At frequencies below the natural frequency of the lowest room mode, propagating waves cannot be sustained. This frequency region is often called the pressure region, where the pressure at all locations in the room is in phase, sound pressure levels are reasonably uniform (dependent on proximity to the first mode) and sound decays rapidly in time [52,66].

2.6.3 Room contents and common structures

Room contents such as furniture can alter the sound field within a room. Large hard objects such as shelves, cabinets and tables can add acoustic diffusion, while soft objects such as beds and sofas also provide absorption. As such, furniture can account for a reduction in sound pressure level of 3-4 dB over the frequency range of interest [67].

Internal walls are often lightweight plasterboard stud partitions or plastered/lined concrete blockwork/masonry. These types differ in the extent of their coupling with the building structure, in their modal response, and their acoustic radiation efficiency.

Ceilings are typically connected to the floor construction through the use of hung framed systems or battens, and may include additional resilient components for improved sound insulation (e.g. between dwellings). The ceiling finish can vary considerably between rooms, for example from plasterboard to lightweight ceiling tiles, and the size of the ceiling cavities can also vary, depending on available floor to soffit heights and the provision of mechanical and electrical services within the ceiling voids. Examples of many ceiling types can be found in [68].

It is intuitive that due to the effect of the mechanisms discussed so far, many of these room surface parameters will have a significant impact on the level of re-radiated noise within a room.

2.7 Prediction methodologies

2.7.1 Introduction to prediction approaches

There are a number of approaches that have historically been taken to understand and predict groundborne noise and vibration in buildings. These approaches can be divided into three types: empirical, analytical or numerical.

Empirical models are developed through experimentation and observation. Vibration and/or noise measurements together with the influential environmental factors may be analysed in order to extract trends that might be used to establish robust prediction methods. Successful empirical models therefore require input data that spans a wide range of influential environmental factors, such as track types, train speeds and lithology conditions for example. Unfortunately, undertaking measurements and acquiring/organising such data requires a great deal of resources. Furthermore, since empirical models are based on observation, they can only be used within the range covered by the observed data, and good model accuracy does not necessarily imply good understanding of the underlying mechanisms, which is important when giving recommendations for design or mitigation.

Analytical models are used to describe a problem in a mathematical form, based on the understandings and assumptions of the underlying physical principles. Whilst good model accuracy implies a good level of understanding of the problem, analytical models can over-simplify the problem in order to keep the mathematics to a manageable complexity, which tends to introduce inaccuracies. In addition, detailed knowledge of material properties is a requirement for accurate models.

Numerical models employ large matrices of model elements to represent complex systems, the equations of which are generally solved through an iteration process. Some popular numerical methods are based on Finite Element, Boundary Element and Finite Difference. These approaches enable three dimensional computer models to be constructed that closely resemble the real situation. However, accurate models require proper and complete knowledge of input data such as component geometry, coupling between elements, material properties as well as boundary conditions. Complex models also require intensive computational resources, with large calculations requiring distributed processing, and calculation times of the order of days or even weeks. Numerical models tend to give very realistic looking results, but the accuracy is always dependent on the quality of the input data. In order to bridge the gap between computationally expensive 3D models and simpler 2D models, an approach of treating the ground as a 2.5D system has been used for predicting vibration from railways (e.g. [69–72]). This is essentially a 3D

representation, but assumes that the geometry is longitudinally invariant, that is, that there are no changes in the track or soil properties with distance along the track.

It should be noted that in recent years there have been some blurring in the distinctions between numerical and analytical methods, where analytical models have become so complex, that numerical methods are required to solve them. These have sometimes been called "semi-analytical" methods (e.g. [73,74]).

2.7.2 Building transmission and re-radiated noise

In acknowledgement of the problem of groundborne noise and vibration in buildings, early investigations of the problem were undertaken by Ungar & Bender [75], who proposed that a 3-4 dB attenuation of vibration might be observed per storey in a building, whilst Lang [76] suggested attenuation of 1 dB per storey. Lang also provided an empirical equation to determine noise level within a basement room from the distance between the tunnel and building walls:

$$L_A = 59 - 20\log r \pm 10 \qquad \text{(dB)} \qquad \textbf{(2-24)}$$

where:

r is the distance between the tunnel and basement walls, in m.

Probably the most widely used groundborne noise prediction model for buildings is that by Kurzweil [77]. Based on empirical analysis of data from North American underground systems, it was proposed that a train pass-by event noise level within a room, for a given octave band, might be predicted from the floor vibration using:

$$L_p = 20\log\frac{a_{rms}}{10^{-6}} - 20\log f + 37 \qquad \text{(dB)} \qquad \textbf{(2-25)}$$

where:

a_{rms} is the rms acceleration, in g;

g is the gravitational acceleration constant 9.81 m.s^{-2};

f is the centre frequency of the frequency band of interest, in Hz.

Equation (2-25) may be written in a simpler form in terms of the velocity:

$$L_p = L_{v,\text{floor}} - 27 \qquad \text{(dB)} \qquad \textbf{(2-26)}$$

where:

$L_{v,\text{floor}}$ is the rms vibration velocity level of the floor, in dB re. 10^{-9} m.s^{-1}.

Within a report from the Transport Cooperative Research Program (TCRP) [78], it has been suggested that indoor sound pressure levels might be over-predicted by around 5 dB by the above approach, and that a more appropriate relationship would therefore be provided by:

$$L_p = L_{v,\text{floor}} - 32 \qquad \text{(dB)} \tag{2-27}$$

It has been further noted [79] that the free-field external vibration level is almost as useful as the floor vibration level in predicting internal sound pressure levels, and corresponds well with Equation (2-26), such that an appropriate approximation may be expressed by:

$$L_p = L_{v,\text{external}} - 27 \qquad \text{(dB)} \tag{2-28}$$

Guidance in the Austrian Standard ONR 199005 [80,81] has included some of the terms which are commonly simplified in the above approaches, to give a more complete expression:

$$L_p = L_{v,\text{floor}} + 10\log(S) - 10\log(V) + 10\log(T) - 20 \qquad \text{(dB)} \tag{2-29}$$

where:

S is the area of the floor surface, in m^2;

V is the volume of the room, in m^3;

T is the reverberation time, in s.

A similar approach has been suggested by Billeter et al [60] which includes a 'radiation transfer function' term to be applied when calculating the sound pressure level in 1/3 octave bands. Whereas other methods tend to assume a radiation efficiency of unity, the radiation transfer function term includes the radiation efficiency and area of the vibrating surface, and the acoustic absorption in the room. The radiation transfer function term can be given for a number of different room scenarios and frequency bands, enabling more accurate predictions to be made. Validation data for the method showed good agreement in general, but the method tended to overestimate the sound pressure levels by on average 2.6 dB.

A summary of a number of methods to predict the noise level from vibration measurements is given by Alten et al [82]. Three empirical approaches are outlined: VIBRA 1-2-3 [83,84], ONR 199005 [80] and Grütz's method [85,86]. Whilst ONR 199005 has been discussed above, it is helpful briefly to present VIBRA 1-2-3 and Grütz's method here.

VIBRA 1-2-3 [83,84] is a proprietary three-part prediction approach developed by Ziegler Consultants: VIBRA-1 provides a simple calculation model for rough predictions; VIBRA-2 provides additional terms to improve the accuracy; VIBRA-3 is a database of measurements that are used as an input for VIBRA-1 and 2. The calculation for structure-borne noise is provided in VIBRA-1 as:

$$L_{Aeq} = L_v - 34 + A + \sigma \qquad \text{(dB)} \tag{2-30}$$

where:

L_v is the rms velocity of the floor vibration during a pass-by over the frequency range 50-125 Hz, in dB re 10^{-9} m.s^{-1};

A is the A-weighting correction at 63 Hz, =-26 dB;

σ is an empirical room factor (not radiation efficiency, but this is included in it). In standard residential rooms this is typically 6-10 dB. The appropriate values are not published in literature, but are selected within the proprietary software.

VIBRA-2 includes transfer functions in 1/3 octave bands:

$$p(f) = \beta(f)v(f) \qquad \text{(Pa)} \tag{2-31}$$

where:

$p(f)$ is the rms sound pressure during a pass-by in any 1/3 octave band, in Pa;

$\beta(f)$ is the transfer spectrum coefficient, in Pa/mm.s^{-1};

$v(f)$ is the rms. vibration velocity at the centre of the floor during a pass-by in any 1/3 octave band, in mm/s.

The empirical transfer spectrum coefficient $\beta(f)$ is obtained through measurements, and is dependent on structure type [87,88].

Grütz [85,86] proposed a simple formula for calculating the L_{Aeq} overall sound pressure level during a train pass-by:

$$L_{Aeq} = c_1 + c_2(L_{v,A} - 34) \qquad \text{(dB)} \tag{2-32}$$

where:

c_1, c_2 are construction dependent constants;

$L_{v,A}$ is the A-weighted rms. velocity level during a pass-by, re 10^{-9} m.s^{-1}.

The constants are dependent on the construction; Table 2-4 gives the values for concrete and timber floor constructions.

Table 2-4. Constants for Grütz's formula

Construction	c_1	c_2
Concrete floor	15.75	0.60
Timber floor	19.88	0.47

The study by Alten et al [82] suggested that ONR 199005 gave good results (i.e. within a couple of dB of measurements in a laboratory) when considering floor vibration, whilst Grütz's method provided good results when considering the vibration of the suspended ceiling. However, it should be noted that due to the many different ceiling configurations, this may not always be the case. There should also be a preference for 1/3 octave band prediction methodologies (such as ONR 199005 and VIBRA-2) when considering detailed scheme designs, due to the frequency dependent characteristics of the source, and possible mitigation measures.

Anderson [50,89], an Arup engineer, examined the measured groundborne noise and vibration levels from two multi-storey buildings located above railways in London. At a development above Fenchurch Street Station, it was found that vibration measured on a loaded pile-cap were around 2-3 dB (3 dB for the unloaded pile-cap) *greater* than those from a nearby bore hole location between 8-100 Hz, but around 15 dB *less* for 200-250 Hz. Measured groundborne noise at the first floor level was said to be predominantly radiated via the plasterboard walls, rather than the concrete floor construction, but for upper levels it was said that radiation from the floor construction was more important. In the same study, examination of an office development at Tottenham Court Road, situated above the Northern Line underground railway, led to the observations of low frequency (4, 8 & 16 Hz octave bands) amplification up the building, with attenuation occurring only at higher frequencies (63 & 125 Hz). However, the addition of exterior cladding appeared to reduce the amount of low frequency amplification up the building, presumably due to increased stiffness. Significant amplification was observed at the mid-span sections of the concrete floor slabs (10 dB at 16 Hz, reducing to around 5 dB in higher frequency bands), although it should also be noted that there was considerable variation in the amplification effects of seemingly identical floor slabs.

Ljunggren [90] developed analytical models of two buildings on rock, based on infinitely long longitudinal rods and impedance elements (the 'Ketten-Leiter model') and an infinite ground impedance. When compared with measured data, it was found that the building response was dominated by the in-plane waves of the structure, such that floor vibrations were well coupled to quasi-longitudinal* waves in the supporting walls, and heavy walls oriented perpendicularly to the structural walls were coupled to transverse waves. Because of the relatively low wave speed of bending waves in structural elements, less power is transmitted to the structure by this wave type. Where the structure is supported by structural columns rather than walls, the quasi-longitudinal waves become even more important, and the well-coupled floor vibrations are then the dominant source of vibration and re-radiated noise. Ljunggren's model did not include any

* Quasi-longitudinal waves are waves within a column or wall, which propagate in-plane, but because of the Poisson's ratio of the material, there is also expansion and contraction in the out-of-plane direction.

reflection effects from the roof of the building, which may be influential, particularly for low-rise buildings.

Hassan [91] developed an analytical model that, unlike Ljunggren's earlier model [90], took into account reflection from the roof of the building, and a finite (but high) ground impedance. The agreement with measurements was good at low frequencies (up to 125 Hz). Additional work [40] showed that offsetting the ground floor columns horizontally compared with the basement columns led to a significant reduction of vibration levels in the rest of the building, particularly at lower frequencies of the range of interest (although the lowest frequency presented was the 31.5 Hz octave band).

Sanayei et al [92] undertook prediction of vibration of a multi-storey building in Massachusetts subject to vibration from a nearby subway. A simple analytical model was developed, with parameters refined through experiments whereby an electrodynamic shaker was used to excite the top of a building column. The resulting analytical predictions were compared with a measurement of vibration due to railway operations, and good agreement was found. It was discovered that floor bending stiffness had the most significant influence on vibration propagation, more so than the floor mass per unit area.

Chua et al [93] describe a modelling approach for a situation where two sets of double box tunnels ran between the ribbed foundation walls of a proposed Singapore office development. An analytical model of the train-track system was used to represent the force input to a 2D FE model. Measurements showed levels of vibration that were within 4 dB of the predicted values.

Statistical Energy Analysis (SEA) was first introduced as a concept for modelling acoustic propagation through structures in the early 1960's as part of spacecraft design. SEA methods acknowledge that there are many uncertainties in structural modelling, and attempts to simplify the problem to give a more general solution to the prediction. It therefore considers general factors such as power input to the system and coupling loss factors between components and subsystems. Its use as a tool for predicting sound and vibration in buildings was pioneered by Craik, whose book on the subject [94] has been important for acousticians interested in its application.

SEA analysis is best used where there are a large number of structural and acoustic modes in a considered frequency band. However, at low frequencies this is generally not the case, and separate account is required of resonant and non-resonant structural response, with modal frequencies calculated through analytical or FE methods [95,96]. In addition, the radiation

efficiency is highly dependent on frequency and difficult to determine at low frequencies, which makes SEA less useful in this frequency range.

Jean [97] describes a 2D coupled FE-BE model to calculate the power input to foundations (both pile and wall foundations are considered). The results were similar to those from more computationally expensive 3D models, and it was suggested that it could be coupled with other methods such as SEA for predicting the vibration transmission through the structure. Later work [69] extended the model to 2.5D, and whilst good agreement was found with 3D models, the predictions showed poor agreement with measured ground surface to building vibration transfer functions. It was suggested that the discrepancy is therefore less dependent on the 3D vs 2.5D model geometry and more influenced by other model aspects, such as the assumption of soil homogeneity.

Talbot and Hunt [98] described an approach whereby a row of piles may be represented using a BE model, with periodic spacing of the pile-soil structure continuing to infinity. The model showed good agreement with Kaynia's model [30]. Further work by Talbot and Hunt [99] when examining base isolation of structures led to some important conclusions, namely that modal vibration of the structure greatly reduces the performance of any base isolation measures employed, and that decoupling a structure from its foundations leads to increased vibration at the foundations, and as such comparing vibration levels above and below isolation measures does not give the complete overall isolation performance. An alternative measure of a power flow insertion loss was therefore proposed.

Vibration of a building due to the passing of a truck on a nearby road was predicted and measured by Pyl et al [100]. The prediction model was based on a 3D FE building model coupled to an unbounded BE model of the (layered) soil. Good agreement was found.

Nagy et al [54] acknowledged the value of FE modelling of buildings when accurate low frequency response was required. A simple approach of quantifying the sound field within a cuboid room was developed, without resorting to BE analysis, that involved the use of the Rayleigh integral and a modified Green's function in order to account for reflections. Detailed simultaneous noise and vibration measurements were undertaken in a room in a Parisian building subject to underground train vibrations. It was noted that the surface with the highest vibration levels was not the floor*. The measurements were compared with predictions made using the Rayleigh integral technique, SEA, Kurzweil's formula, and BE analysis. Best agreement with measurements was found using the BE method. The Rayleigh integral method gave only slightly less agreement but was more

* It is not stated which specific room surface did actually exhibit the greatest vibration levels.

computationally efficient than the BE method. The Rayleigh integral method is however best suited for rooms with relatively high absorption, where the number of reflections can be limited in number.

A fully 3D FE model of a building, soil and elevated track system was developed by Ju [101], which showed very good agreement with measurements for free-field positions (although there were no such validation measurements for the building). It was found that the resonant characteristics of the track system were important, especially when coinciding with natural modes of the building. It was also shown that the addition of piles to the building foundations was predicted to reduce transmitted vibration slightly in the vertical axis compared with the original raft foundation condition, whilst negligible effect was found on the horizontal vibration levels.

Villot et al [102] presented a 2.5D coupled FE-BE model of a building from a surface force excitation. Good agreement was found (overall levels within 3 dB of measurements), and the model was then used to ascertain the influence of various building parameters. It was found that changes in the floor slab thickness had only a small effect on floor vibration levels, by shifting the modal frequencies, but not actually influencing the level significantly. It was also shown that doubling the floor span resulted in reduced modal frequencies and significantly increased vibration levels. It was commented that the model approach would be effective for expanding the database of an empirical approach.

Sanayei et al presented a simplified analytical prediction approach in [103]. A four-storey building was approximated by a single column with impedance values (calculated from thin-plate theory) representing the floors. The impedance values gave good agreement with measured data. Predictions of vibration levels in the building gave reasonable agreement with measurements, although they tended to underestimate the vibration levels, by up to around 10 dB at some frequencies. In addition, it is thought that better agreement was found in the case study (where the vibration source was close to the building) than might be expected for other buildings. An extension to the model investigated the effect of increasing the thickness of one of the floors, in order to act as a "blocking floor". The concept of a blocking floor is based on the understanding that a change in impedance would cause vibrational energy to be reflected downwards, thereby reducing the amount of vibrational energy transmitted upwards through the building. It is predicted that a blocking floor with double the usual thickness could reduce vibration at upper floors by around 3 dB at frequencies above 30 Hz.

Analysis of scaled physical models is sometimes appropriate when investigating vibration problems in some types of structures. As part of an undergraduate project by Teow [104] (partly supervised by the author), vibration transmission results for a portal frame structure constructed

from LEGO™ bricks have been obtained. A reproduced graphic of the test structure is given in Figure 2-12.

Figure 2-12. Scaled physical model graphic

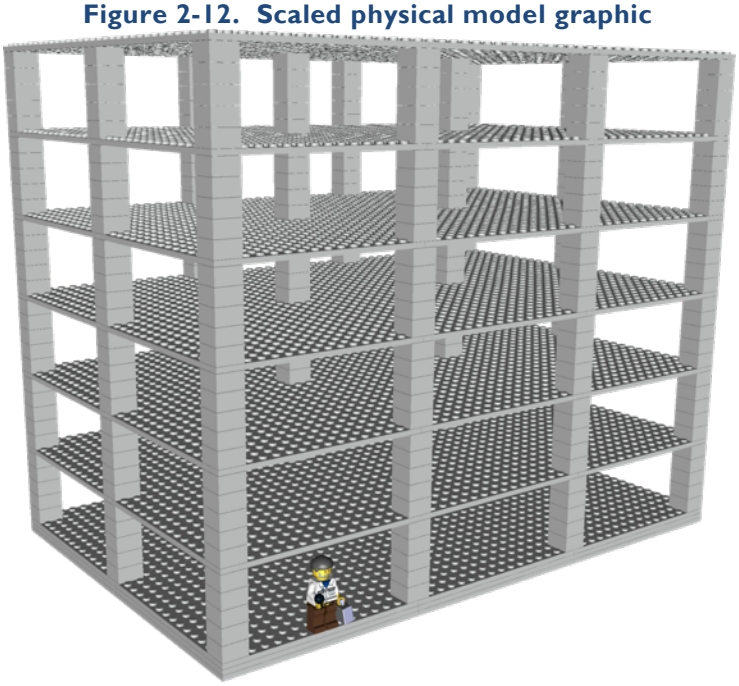

One of the disadvantages with scale modelling is the difficulty in ensuring that all of the vibration mechanisms scale in similar fashions. Due to the particular physical model constraints of the LEGO™ approach (e.g. structural components are only available in discrete sizes) and the components chosen for the study, the floor plates' first natural frequency occurred at a lower frequency than the building model's first extensional mode, which differs from that normally experienced in real buildings. Therefore, it was necessary to consider the transmission through the structure and the response of the floor plate as separate mechanisms, with separate frequency scaling factors. This approach still requires the use of other techniques to obtain the estimated natural frequencies, in order to determine the scaling factors. For building transmission, the model frequency scaling factor was found to be about 35. For the mid-span floor amplification, the factor was about 10. Since the measurements were only performed up to 1600 Hz the upper limit of the building transmission predictions was around 50 Hz, which is insufficient for predicting groundborne noise and vibration in the actual frequency range of interest.

2.7.3 Complete train-to-room models

Nelson and Saurenman introduces a methodology [105] which is also included in the Transportation Noise Reference Book (TNRB) [23] for predicting groundborne noise and vibration in buildings once the free-field vibration level is established through measurement or analytical approaches. A set of empirical values for the coupling loss of various types of building and foundations were provided, as taken from the Handbook of Urban Rail Noise and Vibration

Control [106]. Guidance on inter-storey attenuation is provided as well as the extent of amplification to be expected for suspended floor constructions. The TNRB empirical guidance values for inter-storey and mid-span floor amplification are reproduced in Figure 2-13 and Figure 2-14, respectively.

This is an approach used by many acousticians as the basis for groundborne noise and vibration predictions in buildings, despite concern over the validity and universal application of such guidance, particularly in the context of more modern construction techniques.

Figure 2-13. TNRB storey amplification [23]

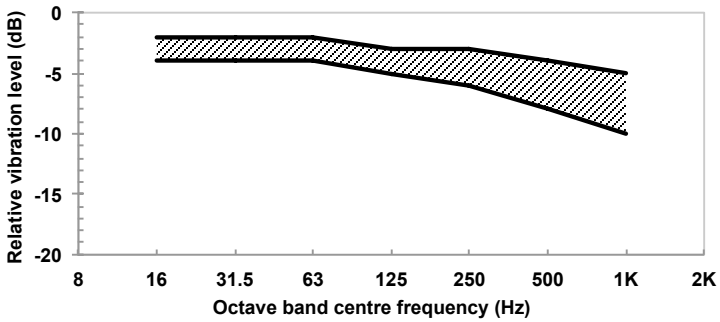

Figure 2-14. TNRB mid-span floor slab amplification [23]

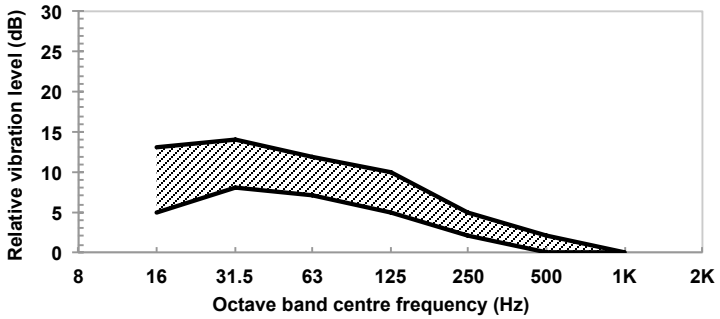

Probably the most comprehensive empirical approach to groundborne noise and vibration prediction is that described as part of the environmental assessment methodology for the Channel Tunnel Rail Link (now known as High Speed 1, or HS1), as developed by Greer et al [24,79,107,108]. As a result of the analysis of a number of noise and vibration measurements, simple expressions were developed for predicting groundborne noise and vibration in buildings. The empirical relationships were based on measurements undertaken in twelve residential buildings as part of a joint collaborative study between British Rail and London Underground Ltd. It was found that groundborne noise decayed by 1 dB per storey in a high rise building, and 2 dB per storey in a typical house. VDV vibration levels on the ground floor are stated to be approximately twice those measured externally (four times for upper storeys). The HS1 methodology gave good agreement with validation measurements, and has been used extensively since. However, it should be noted that the approach was predominantly based on family homes

typical of the historical and geographical context (brick houses on strip foundations, with wooden floors). Piled foundations were deliberately not accounted for in the calculation methodology. Improvements to the model are currently being undertaken by Arup for use in the planning and assessment of the proposed HS2 line.

Gjelstrup et al [109] described an approach where measurements have been undertaken at multiple locations in Denmark and Austria and used to derive an empirical expression, with terms for the vibration source from the train, train speed correction, ground propagation, ground to building coupling, transmission within the building and an error estimate. The terms for speed and ground propagation were provided from theoretical formulae. This is a similar approach to that described for the HS1 prediction study [107], and vibration levels calculated using a single soil layer were slightly over-predicted, while the implementation of two soil layers in the model resulted in slight under-prediction. The model predicted a 3 dB reduction in vibration between ground floor and first floor, whereas the measurements showed a 4 dB increase.

Madshus et al [110] described a database for collecting and analysing vibration data in Scandinavian countries. The focus was on low frequency vibration (i.e. rather than groundborne noise) in areas of soft soil. The database model included the provision of information for five independent parameters: a train type specific vibration level (at a reference distance of 15 m, for a train travelling on standard track at 70 km/h); the measured train speed; distance to receiver; track quality; and building amplification. Bahrekazemi [111] used much of this data in order to prepare a semi-empirical model (EnVib-01) for prediction of vibration levels at any point between the train and building floor, for a known train load distribution. Whilst intended as a tool for scoping, the approach gave good agreement with independent measurements [112].

Melke [113] proposed a prediction procedure based on a chain of transmission losses calculated from analytical expressions for each system component. Whilst this is a convenient representation of the problem, in reality the interdependency of many system factors would be expected to lead to inaccuracies in this approach.

Trochides [114] presented a simplified model of a tunnel in soil affecting a nearby building. The soil was modelled as homogeneous, and the tunnel and building structures were modelled as simple concrete boxes. The model was principally derived analytically, with SEA used to predict vibration levels in the building. Good agreement was found with a 1:10 scale model.

Fiala et al [115] suggested an approach where the problem is tackled as three subsystems. The first is a lumped parameter vehicle model on infinite beams attached to a layered half-space BE ground model. Second, the incident wave field is applied to an FE model of the building structure,

and third. the room response is calculated using a spectral FE model, which is said to be straightforward and a good alternative to a Rayleigh integral based approach [54] when acoustic absorption is low. A case study of a three-storey portal frame office building was used to test the methodology and study the effect of various mitigation options. It was found that whilst floating floors produced little benefit, box-in-box room constructions were successful in reducing groundborne noise by nearly 10 dB, but base isolation was more effective still, reducing noise levels by closer to 15 dB relative to the non-mitigated case. The predictions considered frequencies only up to 150 Hz and were not validated against measurement data.

Romero et al [116] described a coupled FE-BE-FE model of the whole train to building transmission path. The vehicle was modelled as a multibody, with the track structure as finite elements. This was then coupled to a boundary element formulation for the soil, which was in turn coupled to a FE model of a concrete frame building with a continuous slab foundation. Damping of ζ=2% (i.e. loss factor of 0.04) was assumed for the building structure. The model was used in order to tune mitigation options for the track, so as to avoid resonant behaviour of the track system occurring in the same frequency region as those for the building structure. The predictions were not validated against measured data, and the software used was a proprietary Matlab toolbox, which is not freely available.

Coquel's PhD thesis [117] investigated the applicability of a number of modelling techniques, and utilised a coupled FE-BE approach for a parametric study. When predicting vibration within a residential building, the FE approach was found to be no more accurate than a SEA approach, although in general FE provided closer agreement with measurements below 80 Hz. When examining foundation types, it was found that the soil characteristics played a more important role than foundation type. When modelling soil characteristics, results obtained with a 2D layered model were equivalent to a 2.5D homogeneous model.

As part of the RIVAS prediction procedure for mitigation solutions, a number of tools were used to predict the transfer functions for various stages of the transmission, as summarised in [118]. A 2.5D BE model developed by Sheng et al [70] was used to obtain the free-field vibration level near a building, with the Vibra-2 empirical model [83] used to predict ground-to-foundation, and foundation-to-building floor transfer functions. For re-radiated sound, it was acknowledged that the expression given in Equation (2-26) is appropriate, if considering the average sound pressure in the room, with the vibration evaluation point located on the floor surface in the centre of the room.

A common approach to predicting railway noise and vibration is through the direct measurement and application of transfer functions. Steinhauser and Steinhauser [119,120] outlined such an

approach, where a 'VibroScan' mobile vibrator was used to measure the transfer function between a tunnel (prior to track construction) and nearby buildings. These were successfully used to predict the mitigation requirements for the track design. A similar study was presented by Lackner [121], where a vibratory roller was used as the excitation source to measure the tunnel to building basement transfer function, and then (presumably with the vibratory roller situated outside the building) to measure the transfer function between basement and upper storeys. The prediction method allowed for the successful specification of a floating slab track system within the tunnel. Finally, a study by Ralbovsky and Alten [122] in Austria implemented a portable vibration generator in a tunnel. The responses were measured in the time domain, with corrections applied in order to obtain transfer functions for multiple segments of track. The predicted axle forces were then applied to each transfer function and superimposed to obtain the total vibration level at the receptor location. It was predicted that groundborne vibration should be within the limits specified, and whilst validation measurements were not undertaken, the prediction was considered successful by the absence of complaints.

Whilst the measurement of transfer functions has been shown to allow good predictions of train noise and vibration levels, in many cases the direct measurement is not possible, for example when tracks or buildings do not yet exist.

2.8 Uncertainty

The simplified nature of any of the prediction methods discussed compared to the real situation means that there is error inherent in any prediction. Certain methods exhibit higher errors than others, and it is usually the responsibility of the acoustical engineer to evaluate whether the amount of likely error is acceptable for the particular application, and to make allowance by incorporating appropriate safety margins into the building design.

In the introduction it was stated that groundborne noise and vibration predictions are often considered to be acceptable if they are within +/-10 dB of the measurements. However, it should perhaps be expected that the true extent of differences between measurements and predictions is uncertain, due to reluctance of consultants to conduct commissioning measurements and/or publish measured data that is significantly different from the predictions.

The main sources of prediction error are from insufficient resolution and/or accuracy of input data; error vulnerabilities can often be identified through sensitivity studies of the various input parameters. In some studies, more accurate results have been achieved by introducing stochastic variation into some of the input parameters. Error can also originate from incorrect assumptions/simplifications used in calculations, or uncertainties in the measurement of baseline data.

In predicting groundborne noise and vibration in buildings, the uncertainties typically fall into one of three categories: time-based (parameters that could change with time, such as deterioration in rail conditions etc), location-based, or prediction based (assumptions of conditions used in prediction models):

Time based:

- Wheel condition,
- Rail roughness,
- Train type,
- Train speed,
- Ground properties (e.g. seasonal variations).

Location based:

- Ground properties (e.g. variation in ground layers across a site),
- Noise/vibration measurement positions.

Prediction based:

- Ground properties (e.g. interpretation of the ground data when being implemented into the model),
- Building properties,
- Data resolution,
- Prediction method accuracy.

A major deficiency of many of the available prediction methods, is the lack of quantification of uncertainty. This is rarely presented by the authors and yet is a crucial factor for consultants seeking to build appropriate margins of safety into their building designs. Quantification of uncertainty is generally approached on a statistical basis, with allowable error dependent on the sensitivity of the application. For example, it might be determined that a design is acceptable if there is less than a 5% chance that a particular noise or vibration metric (i.e. based on a given prediction method) might be exceeded. In many cases the lack of uncertainty quantification is due to limited validation of prediction methods with measured data, which should therefore be an important aspect of research work in this area.

A useful summary of the uncertainty caused by six common simplifications for ground vibration predictions is given by Jones et al [123], for: twin tunnels; piled foundations and buried structures; discontinuous slab tracks; soil inhomogeneity; non-horizontal soil layers; and tunnel-soil voids.

The scope of this work does not include a detailed study of uncertainty, but by examining a large enough number of measurement sites and prediction model variations, the output of this research will inform an assessment of the variability in measurements and predictions.

2.9 Discussion

Review of the current literature has shown that there remains a lack of validated approaches to providing detailed guidance to designers looking to predict groundborne noise and vibration from trains in buildings, particularly when considering various building designs.

It has been seen in the literature that a large number of models have been developed for predicting surface vibration from at-grade railway lines, but fewer for underground railway lines. It is expected that that there is greater uncertainty in predicting vibration from trains travelling in tunnels due to the greater variation in soil properties at depths than typically exists on the surface.

There are a relatively small number of models available to predict the groundborne noise and vibration within buildings. Building structures tend to be so dissimilar that simplified empirical expressions cannot offer the accuracy required by many building designers. On the other hand, numerical models are difficult to prepare and few have been validated experimentally. There is very little work that has used validated numerical models to extend the simple empirical predictions.

Due to the complexity of the full noise and vibration transmission path, studies have often focussed on distinct aspects of the problem, typically dealing with only a small part of the path. Added to a lack of experimental validation, this further increases the difficulties in determining prediction uncertainty.

Arup are sponsors of this research and are often instructed to assist with building and infrastructure design where groundborne noise and vibration from railways is likely to be an issue. A summary of the current Arup prediction approach with respect to the constituent subsystems is given in Table 2-5. This is representative of the approaches taken by many other acoustic consultancies across the world.

Table 2-5: Summary of current Arup approach		
Subsystem	Approach	Pros (+) and cons (–)
Surface vibration to building vibration	Transfer functions from TNRB [23]	+ convenient – dated – source of info unclear – specific designs or modifications not possible
Transmission in building	Transfer functions from TNRB [23], plus experience of other buildings (e.g. [50])	+ convenient – no understanding of important mechanisms – does not allow prediction of wall or ceiling vibration – uncertainty not defined – specific designs or modifications not possible
Sound radiation into room	Kurzweil-type empirical equation [77–79]	+ convenient – no account for frequency content – no account for surface finishes or room geometry – uncertainty of absorption in rooms at the low frequencies associated with noise from modern railways – no account for room constructions or modifications

In response to the current gaps in the literature, and limitations of prediction methodologies currently used by acoustic consultants, this research will use detailed measurements of groundborne noise and vibration in a number of buildings and rooms in order to validate numerical models that can be used for extensive parametric study, with the results used to inform new and/or extended empirical predictions.

This research will examine results from 3D FE building and room models, with the acknowledgement that such models will require significant computational resources. Whilst this approach may be seen as being less elegant than either analytical or coupled FE-BE approaches, a consistent FE approach will have the advantage of being methodically simple, easy to visualise, and readily reproducible by others working in the field.

[BLANK PAGE]

3. Comparison of Vibration in a Range of Buildings

When making predictions of vibration, it is helpful to have an understanding of the kinds of trends that are observed from measurements in existing buildings. Measurements can also be used to ascertain the variability that might be expected both between and within buildings. Furthermore, these results can be used to determine the prediction method accuracies and suitability for further study into the influence of structural parameters. This chapter presents such comparisons through analysis of site measurements, empirical models and numerical models (1D, 2D and 3D). Some of the results from this chapter were presented by the author in [124].

Whilst full results are frequency dependent, presentation of the frequency spectra can cause figures to be overly complex. Therefore, frequency weighted vibration values are given in two forms:

- A-weighted vertical velocity level. This is used as an indicator for re-radiated noise, placing a greater emphasis on the higher frequency bands (see Figure 2-3). The level is in decibels, relative to 10^{-9} m.s^{-1}.
- W_b-weighted vertical acceleration level. This is used as an indicator for perceivable vibration, with emphasis on the lower frequency bands of consideration (see Figure 2-4). The level is in decibels, relative to 10^{-6} m.s^{-2}.

The frequency range for the above values is generally 4 to 200 Hz (i.e. with maximum one-third octave frequency band results weighted and then summed logarithmically), but is dependent on the measured data available.

3.1 Measurement data

In order to identify trends for vibration propagation through buildings, it is helpful to obtain and analyse vibration data from measurements. As well as being a useful reference in its own right, such data can also be used to validate prediction methodologies.

The accuracy of groundborne vibration measurements is of great importance; further details on suitable approaches to measuring and analysing groundborne noise and vibration data are given in Appendix B. The reader is also referred to the comprehensive guidance in [13].

A number of measurement case studies are presented here, with data obtained from projects on which Arup has provided consultancy advice over a number of years. These are presented as an

overview of the available data, for the purposes of assessing whether model results give the same kind of trends that are seen in measurements taken in different buildings. Only the vertical vibration measurements are discussed here, with no details of project specific assessment or design. Additional information about each case study is given in Appendix C, including 1/3 octave band measurement data.

The results provided in this section are averages over a number of pass-bys. There are variabilities in the pass-bys and therefore there are three statistical parameters that are helpful when interpreting the data:

- Mean: the average of the data;
- 95% confidence interval: the interval either side of the stated mean in which we are 95% certain that the true mean lies;
- Standard deviation: the average amount that the data deviates from the (stated) mean.

Note that the confidence interval is a measure of statistic quality, whereas the standard deviation is measure of the spread of data either side of the mean. Where data for individual train pass-bys has been readily available in the historic data, the 95% confidence interval and standard deviation are shown.

3.1.1 Tottenham Court Road, London (TCR)

The Tottenham Court Road building (TCR) is a reinforced concrete frame building, completed in 1991. Consisting of six storeys plus a basement level, it is supported by a concrete raft foundation and is located close to the Northern Line of the London Underground. Floor slabs are understood to be 0.25 m thick. Measurements of vibration levels from trains were undertaken by Arup engineers at a mid-span and a column position concurrently, repeated at each floor level. Detailed measurement and background information is given in [125–127] and Appendix C.1, , including standard deviations and 95% confidence intervals for the averaged results. The maximum (slow time weighting) one-third octave band vertical velocity levels, averaged over several trains, are shown in Figure 3-1 for the mid-span locations. It should be noted that at the basement, second and third storeys, only three train pass-bys were recorded for each, which may have included different types of train. Whilst the number of pass-bys and confidence intervals were improved at the other storeys (see Appendix C.1), care should be taken when attempting to distinguish trends in this data. For overall vibration levels, the confidence interval of the average W_b-weighted vertical acceleration was 4-6 dB, and 3-4 dB for A-weighted vertical velocity.

Figure 3-1. TCR: Maximum velocity levels at each storey, mid-span

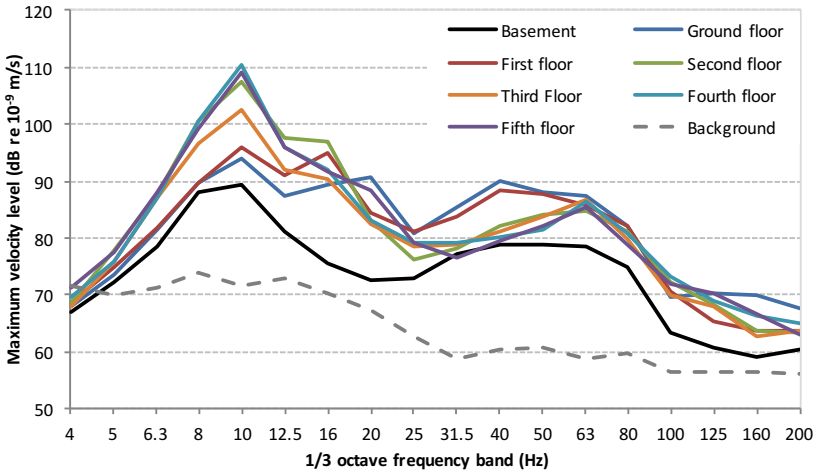

The overall maximum A-weighted vertical velocity levels (i.e. corresponding with groundborne noise level) are plotted against storey in Figure 3-2. The maximum W_b-weighted vertical acceleration levels (i.e. corresponding with perceivable vibration) are shown in Figure 3-3.

Figure 3-2. TCR: Overall A-weighted max. velocity levels with storey

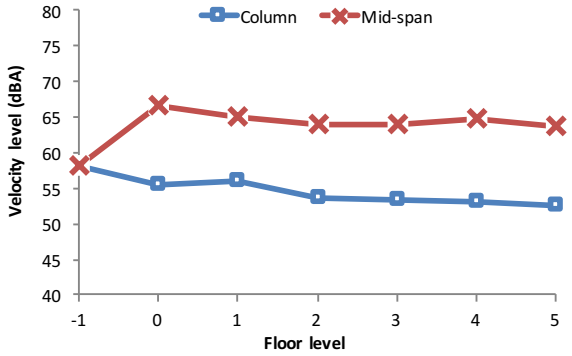

Figure 3-3. TCR: Overall W_b-weighted max. acceleration levels with storey

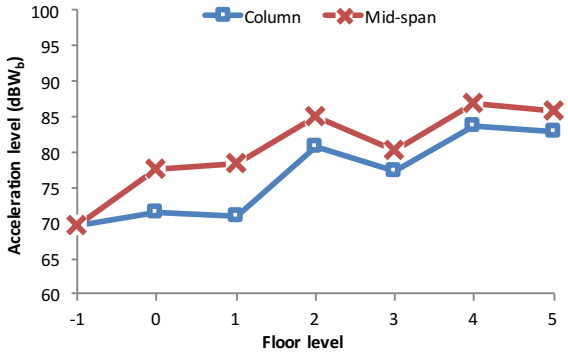

Figure 3-1 shows a peak at 10 Hz, which corresponds to the building's fundamental mode of vibration in the vertical direction. At this mode, vibration increases with height up the building, with a maximum at roof level. The influence of the floor slab modes is seen particularly in the 16 and 20 Hz frequency bands, for which there is a significant increase (up to 15 dB) between basement and ground floor (i.e. the first suspended slab). Note that the floor slab natural frequency occurs at a slightly higher frequency at ground floor level (20 Hz), probably due to the additional stiffening boundaries at this level, provided by the basement walls.

When considering the A-weighted vibration levels, the column positions show a slight reduction of about 2 dB between basement and ground floor level, whereas amplification of around 8 dB is observed between the mid-span points of the basement and ground floor suspended slab, due to floor modes. Above ground floor, both mid-span and column positions showed attenuation with each floor level of about 0.5 dB (for statistical values of gradient, coefficient of determination and

standard error values for each measurement data set see Table 3-1). For the W_b-weighted acceleration levels, mid-span positions show an increase of about 5 dB between basement and ground floor, which is a factor of the building and floor modes; at column positions this increase was around 2 dB. Column and mid-span positions exhibit a steady increase of about 2 dB per storey, due to the fundamental vertical building mode (for statistical values see Table 3-2).

3.1.2 York Way, near King's Cross, London (KX)

The building at York Way (KX) is a large reinforced concrete frame building (with irregularly spaced columns and structural walls), completed in 2014 and consists of eight storeys plus a basement level. Situated close to King's Cross railway station, the building is located directly above the Piccadilly Line of the London Underground. Due to the sensitivity of residential areas of the development, the building has been constructed on isolation springs, designed to achieve a natural frequency of 2.5 Hz. The following measurements were obtained by Arup engineers and the author in December 2012 at individual storeys concurrently with a continuous measurement at basement level. At the time of the measurements, it was understood that the springs were not fully released, and as such should not provide the full attenuation expected.

The overall maximum A-weighted vertical velocity levels are plotted against storey in Figure 3-4. The maximum W_b-weighted vertical acceleration levels are shown in Figure 3-5. Additional measurement data is given in Appendix C.2, including the 95% confidence intervals for the mean results, and the standard deviation of the pass-by results. For overall vibration levels, the confidence interval of the mean for the W_b-weighted vertical acceleration and A-weighted vertical velocity was of the order of 1 dB, with standard deviations around these means of about 2 dB.

Figure 3-4. KX: Overall A-weighted max. velocity levels with storey

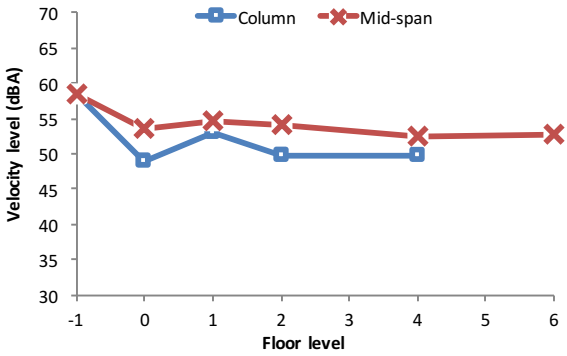

Figure 3-5. KX: Overall W_b-weighted max. acceleration levels with storey

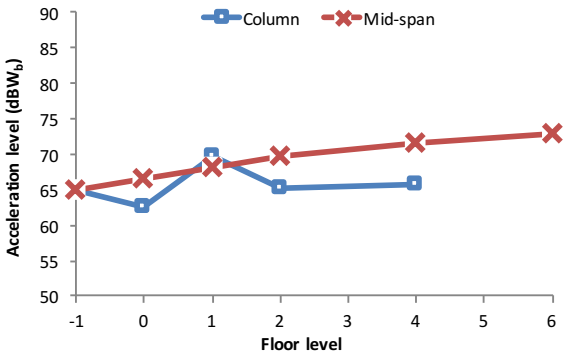

For the overall A-weighted velocity levels, the column positions show about 10 dB of attenuation between basement and ground floor, 5 dB for the mid-span positions. Both the column and mid-span positions exhibited negligible attenuation per storey thereafter. In view of these results, it

is possible that the building isolation was having a significant effect on the building response, despite the springs not having been considered as released.

For the W_b-weighted acceleration levels, there is amplification of around 5 dB between basement and ground floor, above which the vibration at mid-span exhibits amplification of just over 1 dB per storey, whilst the column positions display a more modest amplification of less than 0.5 dB per storey.

3.1.3 York Road, London (YO-B & YO-T)

The building at York Road is a reinforced concrete frame office building (known as Elizabeth House) that has two main parts: a long six storey building (referred here as YO-B) and a sixteen storey tower (referred here as YO-T). Situated on York Road, close to London Waterloo railway station, the buildings are located above or near a number of underground lines: the Northern, Bakerloo, and to a lesser extent the Jubilee, and Waterloo & City lines. There are proposals for the demolition of the existing buildings and construction of a new development on the site. The measurements presented were undertaken in September 2011 and October 2012 by Arup engineers and the author.

For YO-B the overall maximum A-weighted vertical velocity levels are plotted against storey in Figure 3-6. The maximum W_b-weighted vertical acceleration levels are shown in Figure 3-7. Additional measurement data is given in Appendix C.3, including the 95% confidence intervals for the mean results, and the standard deviation of the pass-by results. For overall vibration levels, the confidence interval of the mean for the W_b-weighted vertical acceleration and A-weighted vertical velocity was of the order of 2 dB, with standard deviations around these means of about 2-4 dB.

Figure 3-6. YO-B: Overall A-weighted max. velocity levels with storey

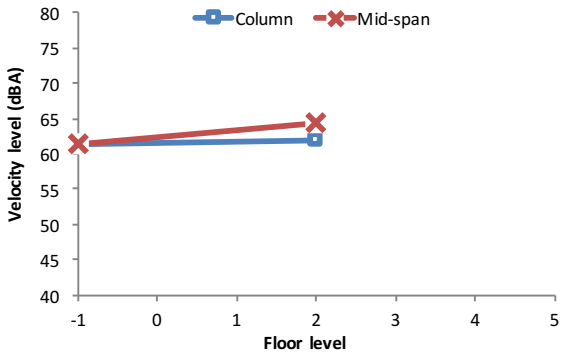

Figure 3-7. YO-B: Overall W_b-weighted max. acceleration levels with storey

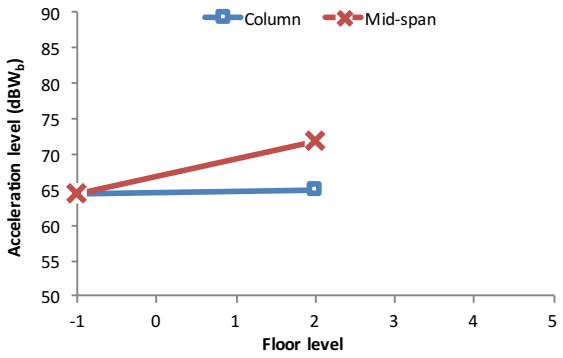

The A-weighted velocity levels show about 3 dB amplification between basement and 2nd floor mid-span, with negligible amplification or attenuation for the column location. The W_b-weighted acceleration levels show about 6 dB and 12 dB amplification between these storeys for the column

and mid-span locations respectively. However, with measurements only available at basement and 2nd floor, there is insufficient data for meaningful trends to be identified.

For YO-T (the tower) the overall maximum A-weighted vertical velocity levels with storey are shown in Figure 3-8. The maximum W_b-weighted vertical acceleration levels are shown in Figure 3-9. These results should be treated with caution (particularly A-weighted levels): the results exhibited a peak around 100 Hz that is uncharacteristic and is likely to be affected by a mounting resonance due to the use of a heavy mounting block on a carpeted surface for the 1st and 4th floor measurements. For overall vibration levels, the confidence interval of the mean for the W_b-weighted vertical acceleration and A-weighted vertical velocity was of the order of 1 dB, with standard deviations around these means of about 2-4 dB..

Figure 3-8. YO-T: Overall A-weighted max. velocity levels with storey

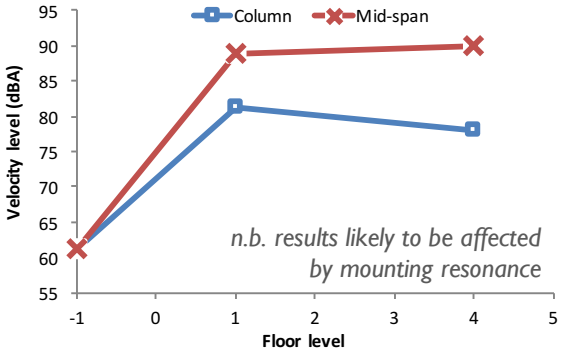

Figure 3-9. YO-T: Overall W_b-weighted max. acceleration levels with storey

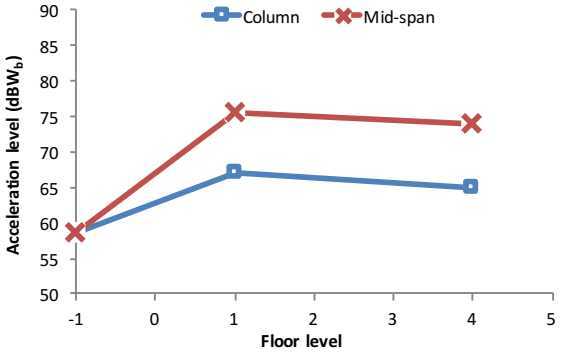

3.1.4 Lexington Ave, New York (LX-S & LX-C)

As part of an investigation for a proposed high-rise hotel on Lexington Avenue, New York, two buildings were considered in 2007. The buildings are located close to the IRT Lexington Avenue Line and IND Sixth Avenue Line in New York. The building (LX–S) that was pre-existing on the proposed site had a steel frame construction of 10 storeys, and has since been demolished. The other building (LX-C) was adjacent to the proposed site; a concrete frame building of 36 storeys.

Measurements were recorded by Arup engineers at only mid-span locations, and only down to 12.5 Hz. For LX-S the overall maximum A-weighted vertical velocity levels are plotted against storey in Figure 3-10. The maximum W_b-weighted vertical acceleration levels are shown in Figure 3-11. For LX-C the overall maximum A-weighted vertical velocity levels are shown in Figure 3-12. The maximum W_b-weighted vertical acceleration levels are shown in Figure 3-13. Additional measurement data is given in Appendix C.4. Note that whilst the American convention is that British ground floor level is known as 'first floor', and so on up the building, the British convention has been maintained in the figures and discussion for consistency with the other data in this thesis.

Figure 3-10. LX-S: Overall A-weighted max. velocity levels with storey

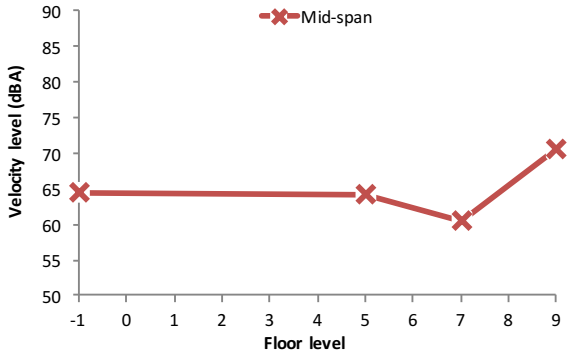

Figure 3-11. LX-S: Overall W_b-weighted max. acceleration levels with storey

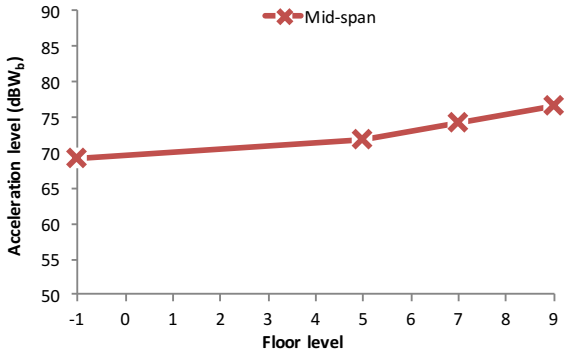

Figure 3-12. LX-C: Overall A-weighted max. velocity levels with storey

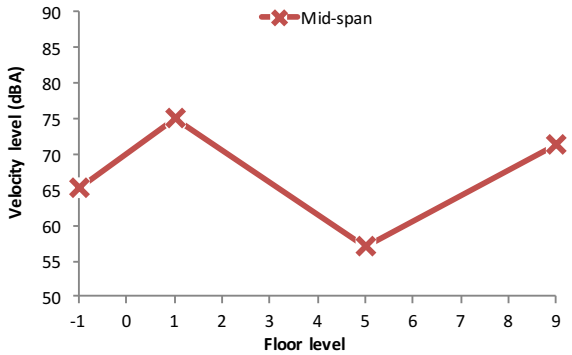

Figure 3-13. LX-C: Overall W_b-weighted max. acceleration levels with storey

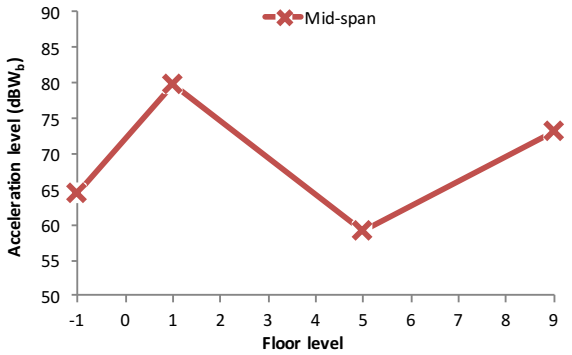

For LX-S, the overall A-weighted velocity level would be expected to be amplified at the ground floor relative to basement, and therefore it is possible that there is approximately 1 dB per storey attenuation between ground and 6th floor, with amplification observed for the uppermost two storeys. For the W_b-weighted acceleration, assuming amplification between basement and ground floor, there is a small amount of further amplification observed up the building of about 0.5 dB per storey.

For LX-C, the frequency spectrum at 4th floor does not follow the same shape as the other measurements (see Appendix C.4), and is likely to have been affected by a local structural feature or perhaps a transducer mounting problem. Ignoring the result at this level would lead to the suggestion that 10 dB amplification occurs between basement and first floor for overall A-weighted velocity level, and only slight attenuation per storey thereafter, less than 0.5 dB per storey. For the W_b-weighted acceleration level, ignoring the result at 4th floor, there is amplification between basement and 1st floor of about 15 dB, and thereafter slight attenuation of less than 0.5 dB per storey.

It is difficult to draw firm conclusions from the LX-S and LX-C data due to the small number of measurement storeys and the scatter in the data.

3.1.5 New Oxford Road, London (NX-1 to NX-4)

The building at New Oxford Road (NX-1 to NX-4) is a steel frame building with concrete floors that previously accommodated the main London postal sorting office. As such it possesses particularly large floor spans (about 12 x 9 m), ceiling heights (about 6 m) and slab thicknesses for the basement and first four storeys. Three, more conventional storeys are situated above these, but were not included in the vibration measurement programme. The building is understood to be constructed on a concrete raft foundation, and is situated close to the Central Line of the London Underground. Vibration measurements were undertaken by the author in 2013 at mid-span locations, at four different distances (ranging from about 5 m at NX-1 to about 60 m at NX-4) from the façade closest to the Central Line.

The overall maximum A–weighted velocity levels are plotted against storey for the measurement points NX-1 to NX-4 in Figure 3-14, with the W_b-weighted acceleration results shown in Figure 3-15. Additional measurement data is given in Appendix C.5, including the 95% confidence intervals for the mean results, and the standard deviation of the pass-by results. For overall vibration levels, the confidence interval of the mean for the W_b-weighted vertical acceleration and A-weighted vertical velocity was generally less than 1 dB at basement level, rising to around 3 dB at 3rd floor, with standard deviations of similar magnitudes.

In order to assess horizontal attenuation across the building structure, these results are shown against distance from the façade in Figure 3-16 and Figure 3-17, with the building facade limits represented as dashed grey lines. Additional measurement data is given in Appendix C.5.

Figure 3-14. NX-1 to 4: Overall A-weighted max. velocity levels with storey (mid-span)

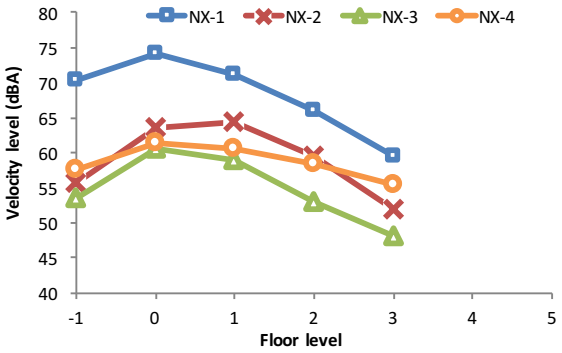

Figure 3-15. NX-1 to 4: Overall W_b-weighted max. acceleration levels with storey (mid-span)

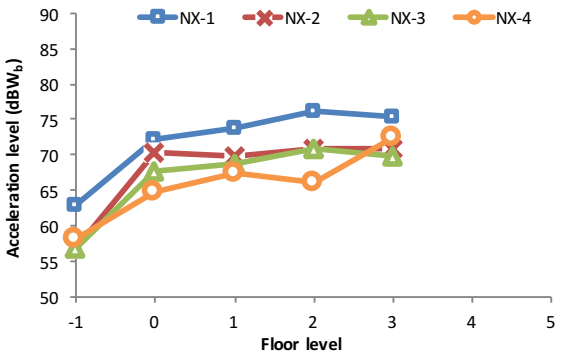

Figure 3-16. NX-1 to 4: Overall A-weighted max. velocity levels with façade distance (mid-span)

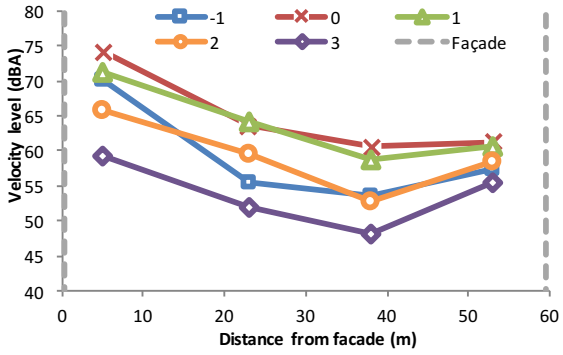

Figure 3-17. NX-1 to 4: Overall W_b-weighted max. acceleration levels with façade distance (mid-span)

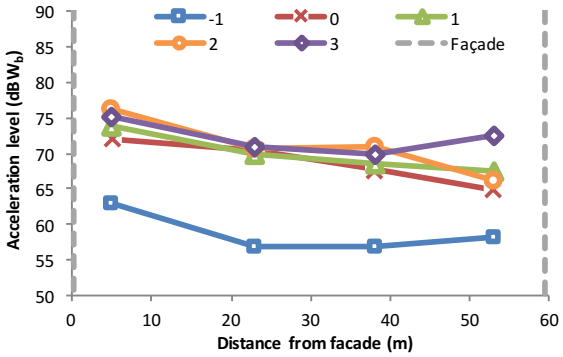

The measurements show an increase of around 5 dB in A-weighted vibration between basement and ground floor (i.e. the first suspended floor slab). Above ground floor, the positions exhibit an attenuation 2 to 5 dB per storey. For the W_b-weighted acceleration, there is a large variation in amplification between basement and ground floor, 2 to 15 dB. Thereafter, amplification of 2 to 5 dB per storey is exhibited, with the positions nearest the façades having the greater amplification rates.

From Figure 3-16 it can be seen that there is a decrease in A-weighted vibration level with horizontal distance from the closest façade to the vibration source. This gave reductions of up to 15 dB at basement level and 10 dB at 3rd floor level, although this reduction is likely also to be related to the building size as well as proximity to the railway. This attenuation can be seen to be more limited near the façade on the opposite side of the building; this is likely to be due to the presence of additional structural elements increasing the structural stiffness in this region. In general, the W_b-weighted acceleration (Figure 3-17) showed a slight reduction in level over the horizontal distance from the façade at all storeys, although the trends are less clear than for the A-weighted vibration.

The results show that there is a significant dependence on horizontal location as well as floor level, which should be considered when measuring or predicting groundborne noise and vibration in buildings.

3.1.6 City Road, London (CR-N & CR-S)

A development at City Road consisted of a number of buildings affected by the nearby Northern Line of the London Underground, and a tunnel section of the (National Rail) Moorgate to Welwyn Garden City line. Measurement of vibration was conducted by the author in two of the buildings in 2014: one to the North of the site (CR-N); and the other to the South of the site (CR-S). The majority of the buildings have since been demolished.

Detailed construction information on the two buildings is not known, but CR-N is understood to have been a steel frame building of five storeys plus a basement level. The floor construction could only be examined in one area (at a service penetration), and was concrete with a double floating floor consisting of a screed layer on ~25 mm dense mineral fibre insulation on floorboards on another layer of ~75 mm dense mineral fibre insulation. It is not known whether the floor construction was representative of the rest of the floors in this building. CR-S was a five-storey (plus basement) building of steel frame construction, and the floor consisted of a weak concrete between metal channels, which were in turn supported on the steel beams*.

For CR-N the A–weighted velocity and W_b-weighted acceleration levels are plotted against storey in Figure 3-18 and Figure 3-19 respectively. For CR-S the A–weighted velocity and W_b-weighted acceleration levels are shown in Figure 3-20 and Figure 3-21 respectively. Additional measurement data is given in Appendix C.6, including the 95% confidence intervals for the mean results, and the standard deviation of the pass-by results. For overall vibration levels at CR-N, the confidence interval of the mean for the W_b-weighted vertical acceleration and A-weighted vertical velocity was generally of the order of 1-3 dB, with standard deviations around these means of about 3-4 dB. At CR-S, the confidence interval of the mean for the W_b-weighted vertical acceleration and A-weighted vertical velocity was generally of the order of 2-3 dB, with standard deviations around these means of about 3-7 dB. The relatively large standard deviation values are due to differences between trains running on different train lines and/or tunnels which have been included together in the analysis.

Figure 3-18. CR-N: Overall A-weighted max. velocity levels with storey

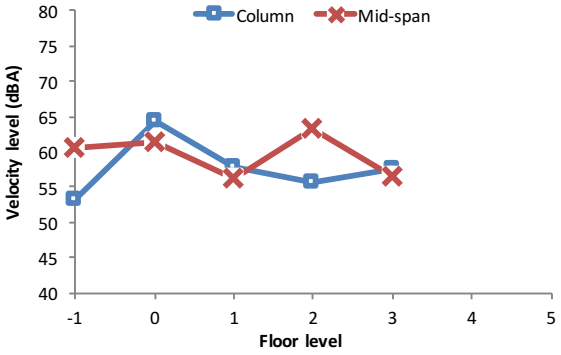

Figure 3-19. CR-N: Overall W_b-weighted max. acceleration levels with storey

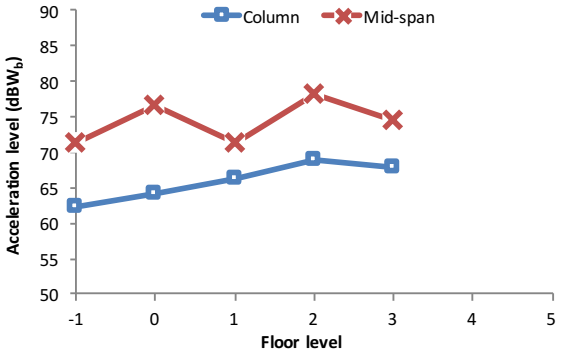

* According to the site contact, this style of floor construction was apparently known as 'pigs', although no other information about such a system has been found through a cursory literature search.

Figure 3-20. CR-S: Overall A-weighted max. velocity levels with storey

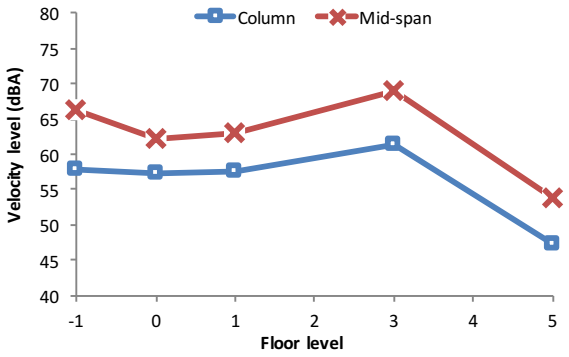

Figure 3-21. CR-S: Overall W_b-weighted max. acceleration levels with storey

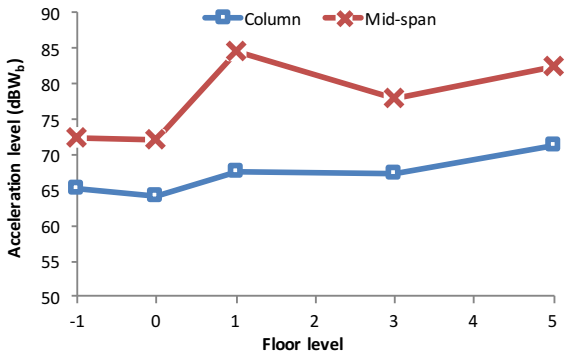

For CR-N, the A-weighted velocity results at column positions showed about 10 dB amplification between basement and ground floor, with an average of about 3 dB attenuation per storey thereafter. Interestingly, the mid-span results did not exhibit amplification between basement and ground floor, and no average attenuation with storey was observed, although there was deviation either side of an average value of about 60 dBA. The W_b-weighted acceleration results showed amplification of about 10 dB between basement and ground floor at the mid-span location, but none for the column location. Above ground floor, both column and mid-span positions exhibited about 1 dB amplification per storey, although the mid-span positions showed greater variance around this general trend. It should be noted that the presence of a floating floor construction is likely to be affecting these measurements, and may result in local anomalies.

For CR-S, the A-weighted levels at column positions showed a constant level between basement, ground and first floor, slight (~1 dB) amplification to 3rd floor and attenuation to 5th floor of around 12 dB. The results for the mid-span showed a similar trend, albeit with about 3 dB attenuation between basement and ground floor. The W_b-weighted results for the column positions showed little change between basement and ground floor, and a general trend of slight amplification of about 1 dB per storey. The mid-span results showed little difference between basement and ground floor but a 20 dB amplification between ground floor and first floor. The result at first floor is significantly higher than usually might be observed when comparing the data to other buildings, and may be influenced by other factors such as local structural anomalies or vibration sources. If this position is ignored, then the general trend above ground floor might be interpreted as around 3 dB amplification per storey.

3.1.7 Portland Place, London (IOP)

As part of a joint investigation (in the MOTIV project*) into groundborne noise and vibration at a location near the Bakerloo Line of the London Underground, vibration measurements have been obtained by the author at multiple storeys of a nearby building in 2014. The building of interest is located on Portland Place and consists of five storeys plus a basement. The basement floor was solid (i.e. stone or concrete); the ground floor level appeared solid, but was assumed to be a concrete screed on a timber floor; the upper floors appeared to be traditional timber joists, supported from the masonry walls. Due to its size and construction, this building is thought to be representative of many traditional residential buildings in the UK.

Only mid-span vibration values were recorded. The A–weighted maximum velocity levels are shown in Figure 3-22, with the W_b-weighted maximum acceleration levels shown in Figure 3-23. Additional measurement data is given in Appendix C.7, including the 95% confidence intervals for the mean results, and the standard deviation of the pass-by results. For overall vibration levels, the confidence interval of the mean for the W_b-weighted vertical acceleration and A-weighted vertical velocity was generally of the order of 1-2 dB, with standard deviations around these means of about 2 dB.

Figure 3-22. IOP: Overall A-weighted max. velocity levels with storey

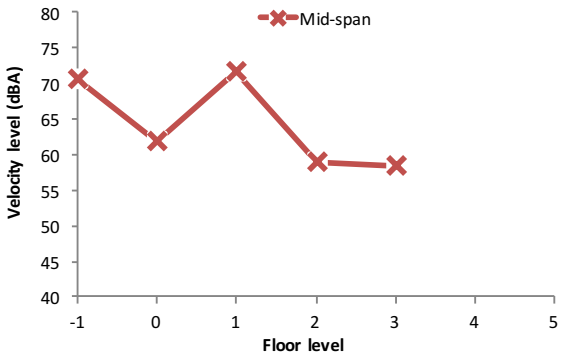

Figure 3-23. IOP: Overall W_b-weighted max. acceleration levels with storey

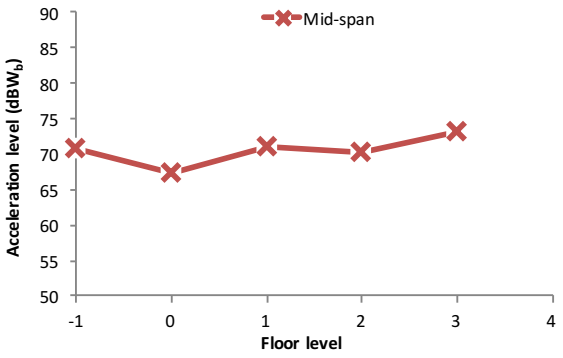

The A-weighted velocity data shows a reduction of around 10 dB between basement and ground floor. Thereafter there is amplification of about 10 dB to the first floor, although there is the possibility that the results of 1st, 2nd and 3rd floors may be affected by non-ideal mounting conditions affecting the A-weighted velocity measurement (the floor was carpeted in these areas; the accelerometer was mounted on a spiked plate placed on the carpet). If the result at first floor is ignored, a slight attenuation above ground floor level is observed, of around 1 dB per storey.

* A joint project between the universities of Southampton and Cambridge, and industry stakeholders, aimed at improving the **M**odelling **O**f **T**rain-**I**nduced **V**ibration. See http://motivproject.co.uk/

For the W_b-weighted acceleration levels, a slight decrease is noted between basement and ground floor, of about 2 dB. Thereafter, amplification is observed of about 5 dB per storey.

3.1.8 Blomfield St, London (BLO)

A traditional six-storey (plus basement) building with masonry and timber floor construction close to the Liverpool St station has been demolished as part of the CrossRail station construction works. The building was subject to particularly high levels of vibration from the Circle Line of the London Underground, which runs in a cutting adjacent to the building. Vibration measurements were undertaken by Arup engineers in 2010 prior to demolition.

Only mid-span measurement positions were recorded, and only down to 12.5 Hz. The A–weighted maximum velocity levels are plotted against storey in Figure 3-24, with the W_b-weighted maximum acceleration levels shown in Figure 3-25. Additional measurement data is given in Appendix C.8.

Figure 3-24. BLO: Overall A-weighted max. velocity levels with storey

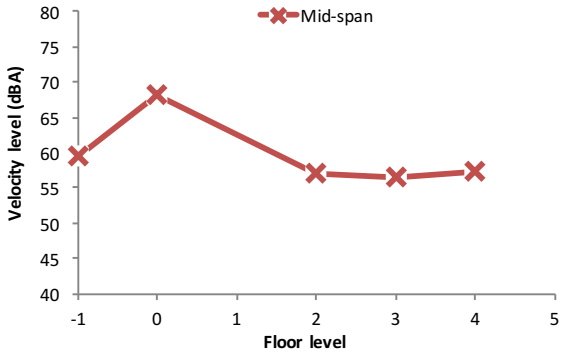

Figure 3-25. BLO: Overall W_b-weighted max. acceleration levels with storey

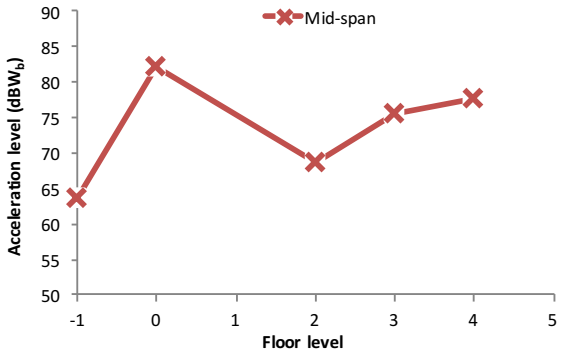

It should be noted that at ground floor the accelerometer was mounted in a heavy spiked block on a carpet; it is possible that this mounting configuration is contributing to the significant amplification recorded. If data from this level is ignored, the overall A-weighted velocity levels show attenuation of less than 1 dB per storey, whilst the W_b-weighted acceleration shows amplification of around 2 dB per storey.

3.1.9 Summary results

It is helpful to collate the measured results from the ten buildings presented here in order to reveal common trends present in the data. The measured basement vertical vibration levels in terms of average maximum one-third octave band levels (at mid-span locations) are shown for all buildings outlined above in Figure 3-26. The average and the range of plus/minus one standard deviation (σ) are also presented. Note that some results have been excluded from the average in bands which were deemed to be contaminated by transducer mounting conditions or localised

anomalies. The result is presented as an indication of the kinds of vibration levels and spectrum shape that are commonly present in the basements of buildings affected by vibration from nearby underground trains. It should be noted that each individual building result is itself an average over several pass-bys; the standard deviation shown here only represents the deviation of the case study buildings from the average, not the deviation between individual train pass-by measurements.

Figure 3-26. Measurement case study summary: Average maximum vibration levels at basement level

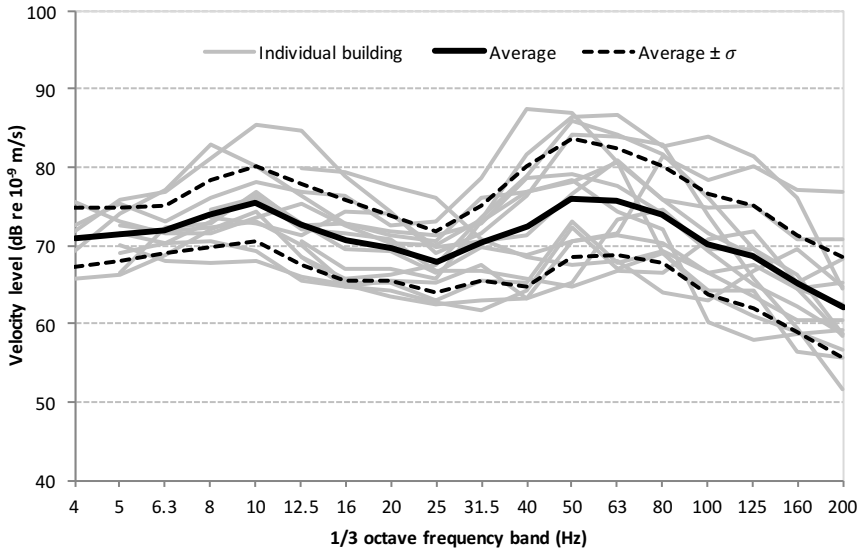

The average vibration level curve contains two broad peaks at around 10 and 50 Hz. The upper peak is believed to be a feature of the coupled wheel/track resonance. The 10 Hz peak is deemed to coincide with dynamic effects of the vehicle primary suspension, although for slowly moving trains (e.g. near stations), effects of the sleeper passing frequency can also be significant in this frequency region [128,129]. Average maximum velocity levels are in the region of 75 dB in one-third octave frequency bands up to about 80 Hz, reducing to about 65 dB at 160 Hz. The standard deviation increases from less than 5 dB at low frequencies to 8 dB at higher frequencies.

Figure 3-27 gives the mid-span A-weighted velocity at each storey relative to the basement for each of the buildings. Note that the values for each building are calculated from the average 1/3 octave band vibration level at each storey relative to the basement, with these relative values then applied to the average basement spectrum given in Figure 3-26. This approach is necessary because in order to compare the vibration transmission characteristics of different buildings, a common input spectrum is required. The W_b-weighted acceleration levels relative to basement are shown in Figure 3-28, calculated in the same way. Average values have only been calculated up to the 5th floor due to the significantly smaller sample size of data above this floor level.

Figure 3-27. Measurement summary: Average basement-relative A-weighted velocity level with storey, mid-span

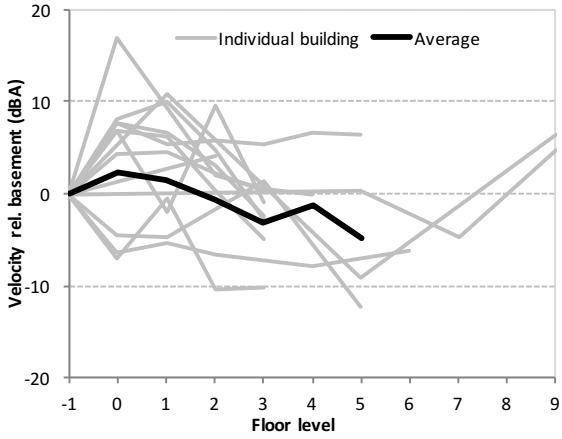

Figure 3-28. Measurement summary: Average basement-relative W_b-weighted acceleration level with storey, mid-span

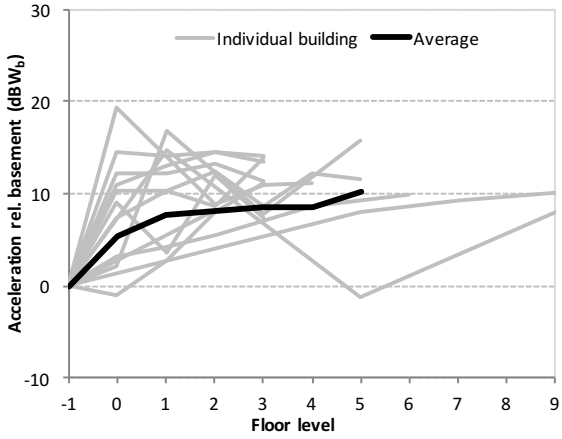

There is a significant spread in the measured data, particularly in the transition between basement and ground floor, probably due to the influence of special floor constructions at basement and ground floor levels, and the range in basement slab conditions (e.g. discrete vs continuously supported foundation types).

The statistical values for inter-storey amplification above ground floor are shown in Table 3-1 for the overall A-weighted velocity levels, and Table 3-2 for the W_b-weighted acceleration levels. In these tables, *m* represents the gradient of the line used for the linear regression (in dB/storey); R^2 the coefficient of determination; σ_e the standard error (in dB). Not all buildings have been included in the regression analysis trends due to incomplete data sets (for example, where no ground floor measurement data was available). The 'average' value shown is for linear regression of the dataset that has been generated from the average values at each storey and one-third octave band relative to basement (e.g. the dark line Figure 3-29).

The average of the results for A-weighted levels is seen to exhibit an attenuation of approximately 1 dB per storey above ground floor. The average W_b-weighted acceleration level shows amplification up the buildings of about 1 dB per storey above ground floor. The correlation for the average data is relatively good for the mid-span positions, but somewhat reduced for the column positions, due to the reduced sample size.

The results show that assuming linear regression of overall mid-span vibration levels from basement measurements is likely to give inaccurate predictions; a ground floor mid-span data point is important. There were also significant differences noted between buildings with respect to the gradient and R^2 values. This suggests that without including prediction terms on a frequency-dependent basis, the accuracy of overall vibration level predictions will be limited.

Table 3-1. Inter-storey amplification trends above ground floor, A-weighted velocity level						
Building	Mid-span			Column		
	m (dB/storey)	R^2	σ_e (dB)	m (dB/storey)	R^2	σ_e (dB)
TCR	-0.5	0.61	0.18	-0.7	0.82	0.15
KX	-0.3	0.45	0.17	-0.1	0.00	0.75
NX-1	-4.9	0.98	0.54	-	-	-
NX-2	-4.0	0.82	1.32	-	-	-
NX-3	-4.3	0.96	0.60	-	-	-
NX-4	-2.0	0.93	0.37	-	-	-
CR-N	-0.7	0.08	1.84	-2.3	0.60	1.31
CR-S	-1.3	0.21	1.78	-1.7	0.39	1.48
IOP	-2.3	0.23	2.97	-	-	-
BLO	-2.9	0.75	1.16	-	-	-
Average	-1.3	0.83	0.30	-1.2	0.34	0.87

Table 3-2. Inter-storey amplification trends above ground floor, W_b-weighted acceleration level						
Building	Mid-span			Column		
	m (dB/storey)	R^2	σ_e (dB)	m (dB/storey)	R^2	σ_e (dB)
TCR	1.8	0.66	0.64	2.6	0.77	0.72
KX	1.0	0.97	0.11	0.9	0.86	0.25
NX-1	1.2	0.74	0.50	-	-	-
NX-2	0.2	0.33	0.18	-	-	-
NX-3	0.8	0.66	0.43	-	-	-
NX-4	2.2	0.69	1.04	-	-	-
CR-N	0.0	0.00	1.62	1.4	0.75	0.57
CR-S	1.1	0.22	1.53	1.2	0.85	0.35
IOP	1.6	0.8	0.58	-	-	-
BLO	-1.1	0.11	2.22	-	-	-
Average	0.6	0.84	0.13	0.6	0.57	0.28

The mid-span vibration levels at 3rd floor are given in Figure 3-29, relative to the basement vibration. The data from this particular storey is presented because it is available for many of the buildings, and is more typical of other storeys than the ground floor. The peaks noted in the measured spectra in the region 6.3 to 16 Hz are due to natural frequencies of the floor slabs. The averaging procedure excludes these effects to a considerable degree, since they occur in

isolated frequency bands, which differ between buildings and even between seemingly similar floors within the same building. Accounting for the natural frequencies correctly would be important when considering the assessment of perceptible vibration. The average result shows amplification relative to basement level at frequencies below around 50 Hz and attenuation at frequencies above this.

Figure 3-29. Measurement case study summary: Average basement-relative velocity level, 3rd floor (mid-span)

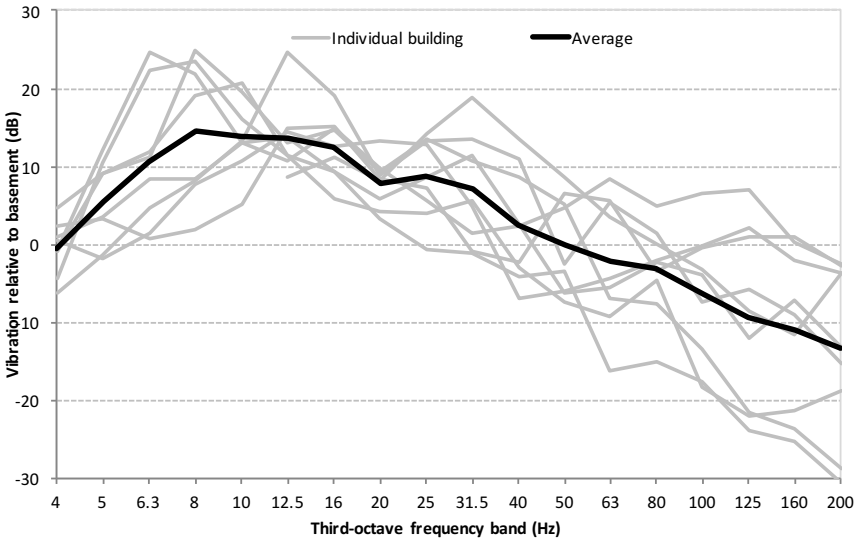

Whilst the data presented for the case studies has covered a wide range of building types, some useful trends have been observed. However, there are difficulties in identifying systematic differences between building types (for example concrete vs steel frame constructions) due to insufficient data and the large number of variables. Therefore the use of models can be useful, for which the influence of building parameters can be determined more clearly.

3.2 Prediction models

It is of interest to compare results from some prediction methods with the data from the measurements, in order to ascertain which types of prediction model might be appropriate for a given circumstance.

For comparison of the approaches, a portal frame is assumed for a generic building with the parameters as given in Table 3-3. Structural damping is accounted for by including the damping loss factor to make the Young's modulus of elasticity complex. For each model, vertical velocity was evaluated for the floor surfaces near all columns and at all mid-span positions; these were converted to 1/3 octave band values, and averaged (where applicable) for each storey. The ground is not included, but the building is excited by a force that is uniform over its base (with a vertical magnitude twice that of the horizontal directions) and the results are expressed as

transmissibility (i.e. the ratio of vibration spectra) from basement to other storeys. Each model was solved in the frequency domain for 1301 frequency points from 3 to 200 Hz, spaced to give finer resolution at the lower frequencies*. Further details are provided in 4.1.3.

Table 3-3. Generic building model portal frame parameters	
Parameter	Value
Number of storeys	Six, plus a basement
Column	Square cross-section, side length 0.5 m
Floor slab dimensions	8 x 6 x 0.27 m
Ceiling height	3 m
Number of floor slabs per storey	4 x 3
Young's modulus of concrete	27 GPa
Density of concrete	2300 $kg.m^{-3}$
Material damping (loss factor)	0.05

The values given in Table 3-3 do not necessarily represent any of the buildings for which measurement data is available; the influence of parameter values will be studied later in Chapter 5.

3.2.1 3D FE models

Prediction of building dynamics using 3D finite element (FE) techniques is the most computationally intensive approach considered, but given appropriate input parameters it should provide the most accurate prediction. Three models with differing levels of complexity are considered as shown in Figure 3-30. For reference, the number of degrees of freedom (DoF) and calculation time are also given, for a reasonably powerful desktop computer**.

Figure 3-30. 3D FE model description		
Full model with structural shafts	Full simplified portal frame	Single 1 x 1 portal frame
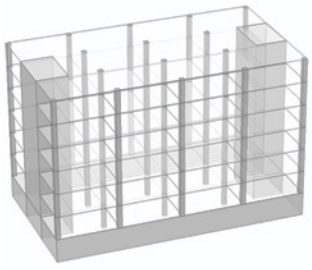	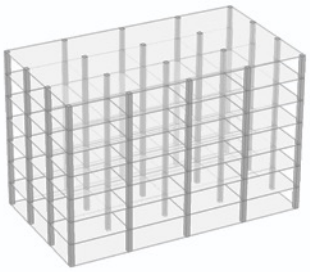	
DoF: 224,250 Calculation time: ~18 hours	DoF: 245,910 Calculation time: ~24 hours	DoF: 21,642 Calculation time: 2 hours

* This was not true logarithmic spacing; the frequency spacing was as follows: 0.02 Hz (3 to 10 Hz), 0.05 (10 to 20 Hz), 0.1 Hz (20 to 50 Hz), 0.2 Hz (50 to 100 Hz), 0.5 Hz (100 to 200 Hz).

** In this thesis, "reasonably powerful desktop computer" refers to the author's desktop computer for this research, consisting of an Apple iMac with 3.1 GHz Intel i7 quad-core processor, 16GB RAM.

A major consideration with finite element analysis is computation time, particularly with such large and complex models as buildings. The computation time of a frequency domain study is strongly dependent on the number of degrees of freedom of the system and the number of frequency points required, as well as the capability of the computer system to be used. It is therefore necessary to optimise the modelling parameters in order to strike the best balance between accuracy and speed of calculation.

FE modelling was performed using COMSOL Multiphysics. In each model, the columns were modelled as solids (tetrahedral mesh) and the walls and floor were modelled as shells (triangular mesh). Quadratic elements were used, with a maximum size of 1.5 m, sufficient to account for bending wavelengths in the frequency range of interest (up to 200 Hz)[130]. Appendix A gives further discussion on element size and FE model convergence.

3.2.2 2D FE models

2D FE analysis is considerably less computationally intensive than its 3D counterpart, due to the reduced number of degrees of freedom required. Figure 3-31 shows the geometries of the 2D models considered. The frames are modelled with beam elements, with appropriate cross-sectional parameters. Each of the models is based on a floor span of 8 m.

Figure 3-31. 2D FE model description

4-bay model	Single bay model
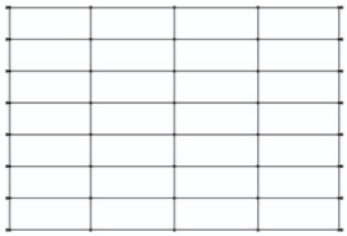	
DoF: 1011 Calculation time: ~ 1 min	DoF: 612 Calculation time: 1 min

3.2.3 1D FE model

A simple 1D FE analysis is also considered in which the building is represented by a sequence of point masses representing the floors, connected by rods representing the columns. This model does not allow for the inclusion of any amplification at mid-span locations. This has been accounted for by assuming 'one-way-coupling' between the 1D model and a plate model, that is, by applying the calculated mid-span amplification calculated from a 3D plate model to the results obtained at each point mass in the 1D model. The 3D plate model was specified with a unit

vertical displacement at the corners, but had no rotational constraints. The geometries used are shown in Figure 3-32. Whilst this approach has been performed using FE methods, it would be straightforward to implement through an analytical approach.

Figure 3-32. 1D FE model description	
1D model	3D plate model
	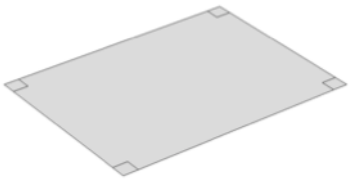
DoF: 87 Calculation time: ~ 15 s	DoF: 2910 Calculation time: ~ 25 min

3.2.4 Empirical model

For comparison, the empirical method given in TNRB [23] is also included, taking the midpoints of the ranges of values suggested therein for floor-to-floor attenuation and floor mid-span amplification.

3.3 Results

The predicted vibration levels from each of the models are expressed for each storey (averaged over multiple bays where appropriate) relative to the basement level, in each 1/3 octave band. A-weighted velocity levels have been calculated by normalising the vibration values at basement level to the average measured frequency spectrum from the measurement case studies (i.e. Figure 3-26). These are then also expressed as basement-relative levels and presented in Figure 3-33, for mid-span locations. The measured average from Figure 3-27 is also shown for comparison. The W_b-weighted acceleration levels have been calculated in the same way, and are presented in Figure 3-34 (with the measured average from Figure 3-28).

1/3 octave band velocity level predictions for the 3rd floor are shown in Figure 3-35. The measured average from Figure 3-29 is shown for comparison.

It is clear that the average building response is best represented by the 2D and 3D FE prediction models although there are differences in the frequency spectra.

Figure 3-33. Model prediction approaches: Predicted basement-relative A-weighted velocity, mid-span

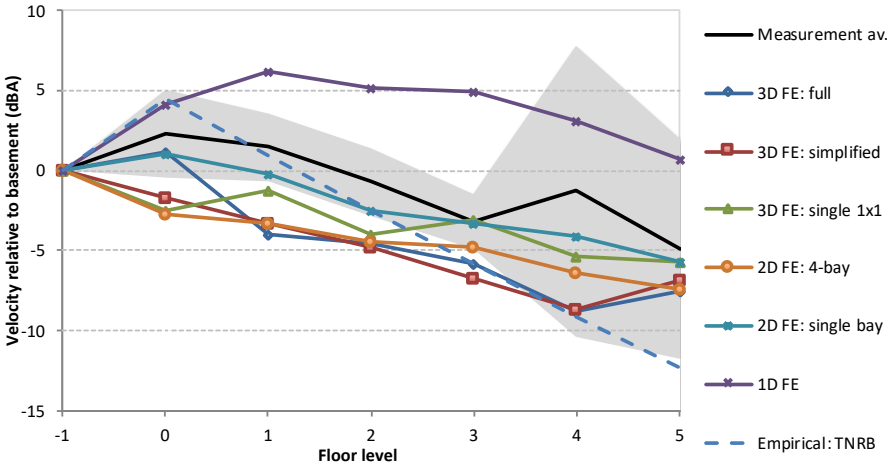

Figure 3-34. Model prediction approaches: Predicted basement-relative W_b-weighted acceleration, mid-span

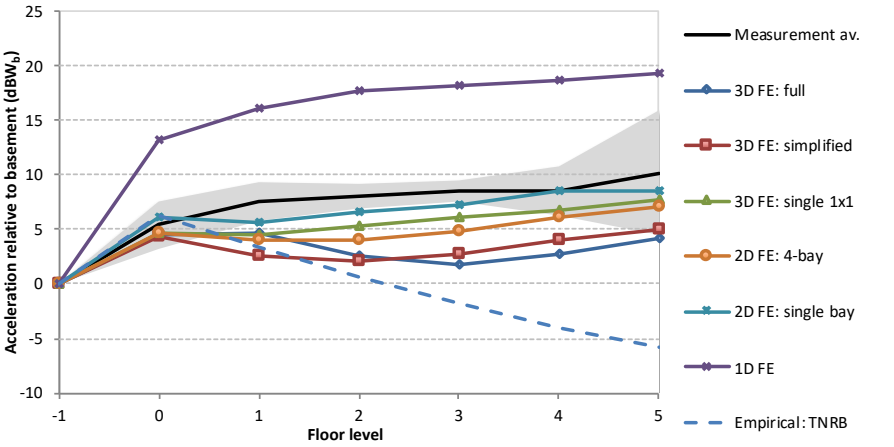

Figure 3-35. Model prediction approaches: Predicted basement-relative 3rd floor vibration, mid-span

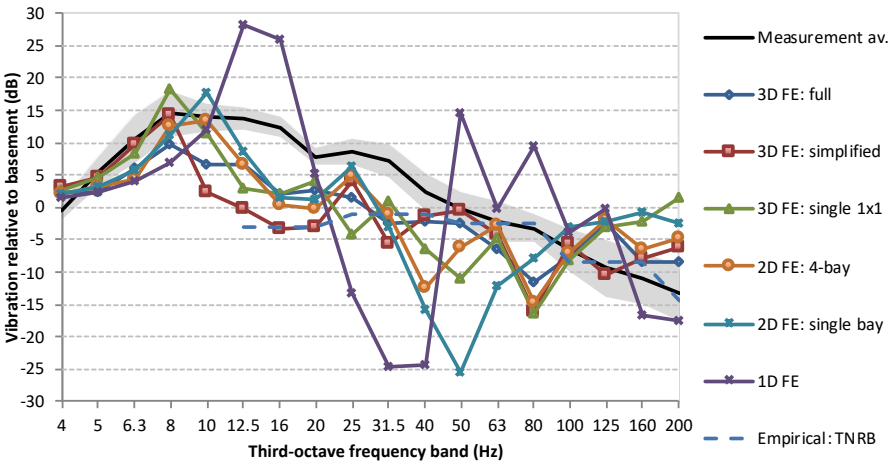

The results shown in Figure 3-33 indicate that, for the A-weighted velocity levels, the 2D and 3D FE models give similar results, and show trends similar to the average measured results, with an approximate attenuation of around 1 dBA per storey above ground level. The 1D FE and

empirical predictions give results that show less good agreement with the trend observed for average measurements.

For W_b-weighted acceleration levels, Figure 3-34 shows that in general the 3D and 2D models showed best agreement with the measured trend, although the inter-storey amplification above ground floor was less than that observed in the measurements; in fact the 1D model seemed to give the best representation of the measured trend for amplification between storeys above ground floor.

When considering the frequency spectra shown for the 3rd floor in Figure 3-35, the 2D and 3D FE models again give similar results, although the peaks in these results around 8 to 10 Hz (due to floor natural frequencies) are much more pronounced than seen in the average measurement results. This is mainly due to the averaging of the measurement results, where floor natural frequencies have occurred in multiple frequency bands. In addition, the peaks for the larger FE models also appear to be less prominent than those with only a single floor span in the horizontal plane. This is also due to the averaging of results from different bays over a given storey for the larger models, where the natural frequencies of individual bays may vary according to their boundary conditions.

The 3D single bay model gave results which showed similar characteristics to the full 3D model, so may be useful when exploring the effect of certain parameters on the structural vibration. The single bay 2D model is less helpful however, for example showing a significant dip in the vibration response at around 50 Hz that is not present for any of the other models. Considering the modest difference in calculation time between the single and multi-bay 2D models, the multi-bay model would normally be the more suitable approach.

It is seen that the simple 1D approach is not reliable, and would be likely to over-predict the A-weighted vibration levels by as much as 8 dB. It is insufficient to use a single point on a simplified model to approximate the whole floor of a complex building in which even individual bays exhibit different vibration responses.

In general, the 2D and 3D FE models show close enough agreement to the average measurement trends that they can be considered suitable for parametric study to investigate the effect of structural parameters on average vibration levels. However, it is important to note that in many cases a single point response is required from a model, for example when assessing the groundborne noise and vibration levels for an individual room. In such instances, care should be taken when using predictions based on storey-averaged results.

3.4 Summary

The purpose of this chapter was to examine the measurements from several buildings of different types in order to identify, if possible, common trends in the vibration data. Such trends could then be compared to predictions from various models.

The measurement results showed significant variation between buildings, but nevertheless a number of trends relating to floor-to-floor attenuation and mid-span amplification were observed. When compared to FE and empirical models it was found that 2D and 3D FE models of multi-bay building structures provided the closest agreement with the measurement trends, and would be suitable for further parameter studies.

The next chapter will explain the development of a more detailed 3D FE building model, with the approach validated against two of the case studies (the TCR and KX buildings). Later, the same approach will be used to develop a 'generic' building model for the purpose of examining the influence of various structural parameters.

[BLANK PAGE]

4. Building Vibration Model: Validation Studies

It is proposed to use 3D finite element models to investigate the effects of various structural parameters on vibration transmission within buildings. To validate the method prior to carrying out the parametric study, it is helpful to compare results from this approach to measurements from physical buildings. Two validation studies are presented in this chapter, for two large multi-storey reinforced concrete frame buildings, that were considered in Section 3.1. Of the buildings considered, it is these buildings for which the most information is available in terms of measurement data and construction details. Both buildings are located in London and affected by vibration from nearby underground railways. Some of the results of these studies were presented by the author as a conference paper in [125], which was also published in [131].

4.1 Case Study A: Tottenham Court Road, London

4.1.1 Background

The first case study is the building at Tottenham Court Road that was presented in Section 3.1.1. The construction of the building was completed in 1991. Arup had been appointed as consulting engineers for the project, and had undertaken vibration measurements within the building, at different stages of construction. The main results of the initial investigation were analysed and presented by Anderson in 1992. His study is published as an Arup internal technical report [50] and was presented at Euronoise in the same year [89]. The development has previously been used by Serra Tur [132], although this was limited to octave band data as presented in [89].

The building consists of six storeys plus a basement level, with a ground level footprint of around 40 m long by 25 m wide, and a height (above ground level) of around 25 m. The building is used as office accommodation for upper storeys, with retail and associated storage at ground and basement level, respectively.

The structural frame of the building is reinforced concrete, with column diameters of 0.67 m. The suspended slab thickness is 0.25 m for most of the building (0.3 m at ground floor and roof level).

The ceiling heights (floor to soffit) of the upper building levels are understood to be 3.4 m, with 3.9 m at ground floor level, and 3.5 m at basement level.

The foundations of the building are understood to consist of a concrete raft with a depth of 0.9 m. A section of the development is given in Figure 4-1.

Figure 4-1. Case study A, schematic section *(from Arup project archive)*

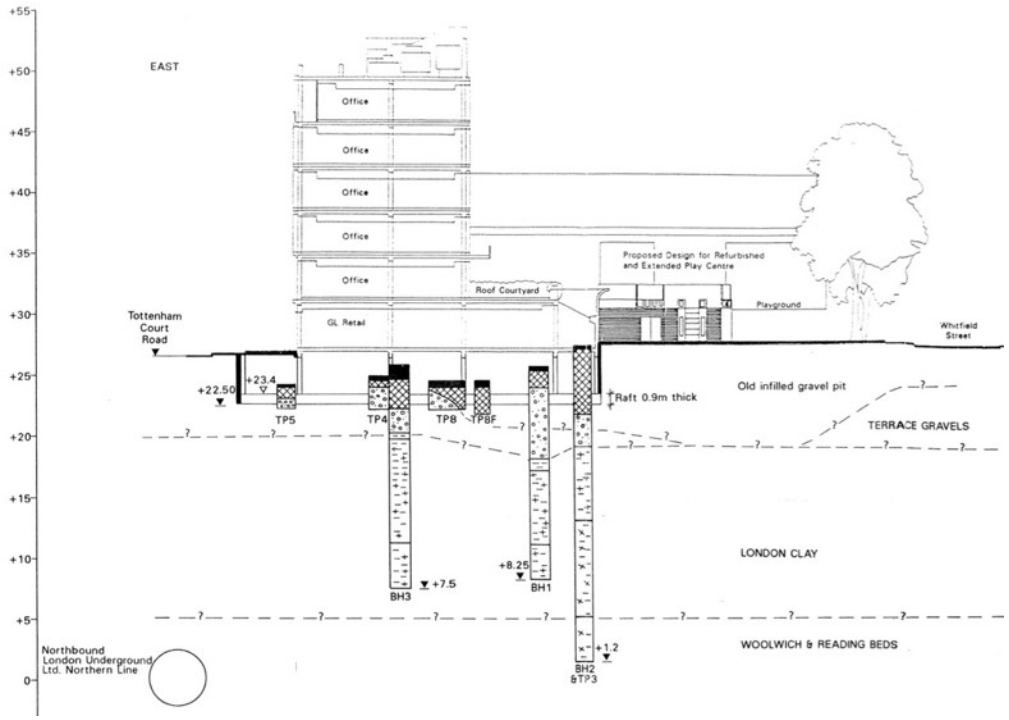

4.1.2 Vibration measurements

Three sets of vibration measurements were undertaken at various stages of construction:

- March 1991: structure complete, no cladding or plant
- April 1991: some cladding and some plant installed
- August 1991: cladding complete, services, suspended ceilings and raised access floors nearing completion.

The focus of this study shall be on the first set of results, as these are anticipated to be easiest to be reproduced through finite element modelling, which requires simplification of the building structure.

Time history data of signals from vertically mounted accelerometers was recorded for each storey, at both mid-span and column locations. For column locations, measurements were made on the floor surface in the vicinity of a structural column. Continuous measurements of 10-15 minutes were made separately at each storey, with mid-span and column position data obtained concurrently. The recordings were later separated into train events by ear, and analysed to extract velocity in 1/3 octave bands. The maximum vertical velocity levels (averaged over several train pass-bys) are presented in Figure 4-2 for column positions, and Figure 4-3 for mid-span positions.

Figure 4-2. Case Study A (TCR) measured maximum vertical velocity level, column positions

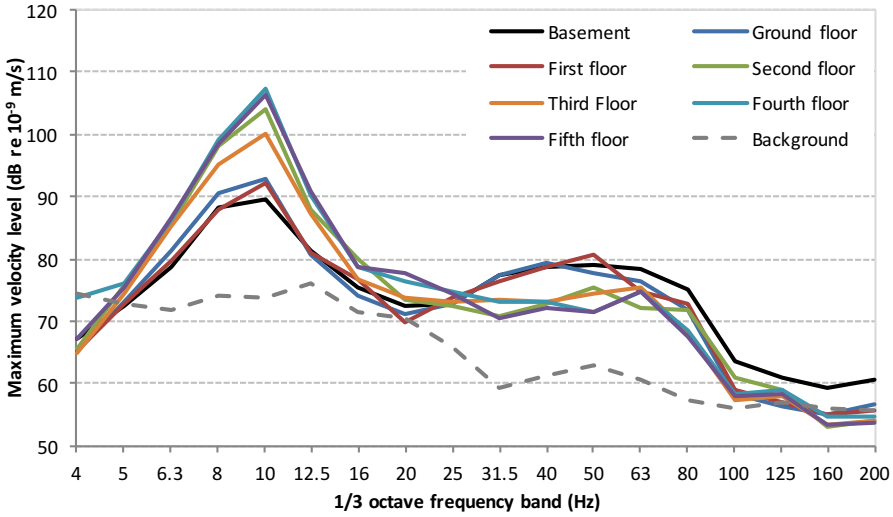

Figure 4-3. Case Study A (TCR) measured maximum vertical velocity level, mid-span positions

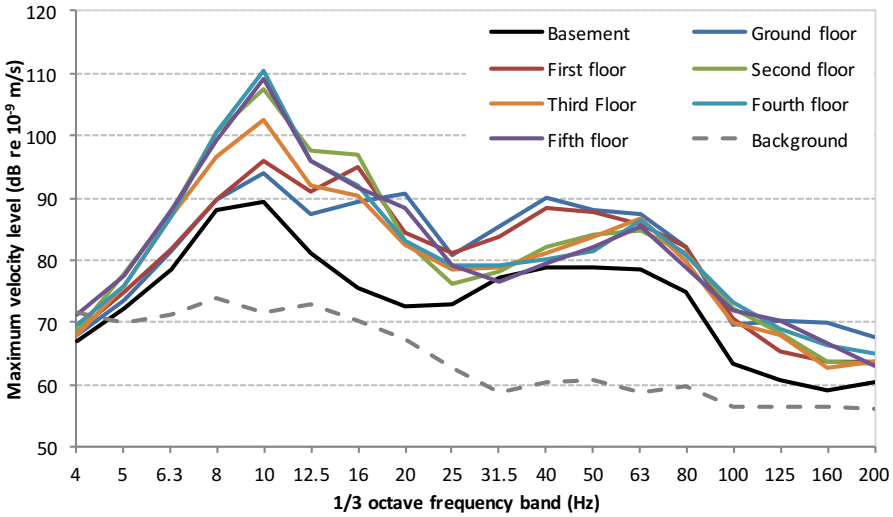

4.1.3 FE model description

A finite element model of the building has been developed using COMSOL Multiphysics™, using the geometry and material information supplied in previous literature and project reports. Note that the stair shafts have not been included in the model, and are stated in the previous literature to be non-structural.

The computation time of a frequency domain study is strongly dependent on the number of degrees of freedom of the system and the number of frequency points required. It is therefore necessary to optimise the modelling parameters in order to strike the best balance between accuracy and speed of calculation. The number of degrees of freedom depends largely on the mesh resolution. Where linear elements are used, the rule of thumb is that a minimum of five to six elements are required per wavelength, at the maximum frequency of interest. Where quadratic elements are used, as have been used in this study, this may decrease to around 2 or 3.

For the bending wavelengths considered in the study, a maximum element size of around 1.5 m is appropriate in order to achieve accurate results for a frequency range up to 200 Hz. Additional considerations are the aspect ratio of the elements (that is, the elements should not be too thin or distorted), and the size growth rate of adjacent elements [130,133,134]. Appendix A gives further discussion on element size and FE model convergence.

The mesh used in the study is shown in Figure 4-4. The columns are modelled as solid elements, with the floors and basement walls modelled as shell elements. The number of degrees of freedom is 439,434.

Figure 4-4. Case study A, model mesh

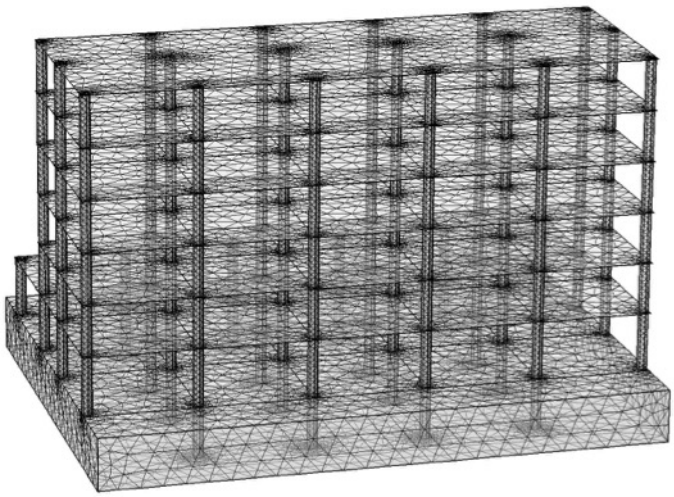

Sufficient frequency resolution is also required so that the calculation results accurately represent the whole frequency range without excluding the full effect of particular system resonances. The number of frequencies required therefore depends on the frequency region considered and the amount of damping in the system. An initial study was carried out that suggested that the frequency range 3 to 200 Hz can be accurately represented by 1301 frequency points, spaced with a finer resolution at the low frequencies*.

Material parameters have been taken from various literature and the COMSOL material library. The material constants used in the model are shown in Table 4-1. The columns have been assigned a slightly higher density than the floors due to a greater proportion of reinforcing steelwork understood to be contained therein. Structural damping has been included in the model by including a constant damping loss factor to make Young's modulus of elasticity complex.

* This was not true logarithmic spacing; the frequency spacing was as follows: 0.02 Hz (3 to 10 Hz), 0.05 (10 to 20 Hz), 0.1 Hz (20 to 50 Hz), 0.2 Hz (50 to 100 Hz), 0.5 Hz (100 to 200 Hz).

Table 4-1: Case study A, material parameters		
	Columns	Floors
Density (kg.m^{-3})	2500	2400
Young's modulus (GPa)	26	26
Damping loss factor	0.05	0.05

The excitation of the building structure is modelled as a distributed force per unit area over the external surfaces of the basement. The direction of the input force has the vector $[F_x,F_y,F_z]$, where x is the axis along the longer length of the building, y is the axis along the shorter width of the building, and z is the axis up the height of the building. The vertical force is set to twice that of the lateral forces, which are set to equal values, such that $F_z=2F_x=2F_y$. This is in accordance with observations at this building from triaxial vibration measurement data at basement levels. Calculations took approximately 36 seconds per frequency with a reasonably powerful desktop computer.

The vertical vibration response of the model is evaluated at a number of column and mid-span locations for each storey as shown in plan in Figure 4-5. It should be noted that some of these points were excluded at first floor and above, as appropriate for the building geometry. 218 response points were evaluated in total. The single point positions, estimated to have been close to the measured positions, are shown circled.

Figure 4-5. Case study A, model evaluation positions, plan view

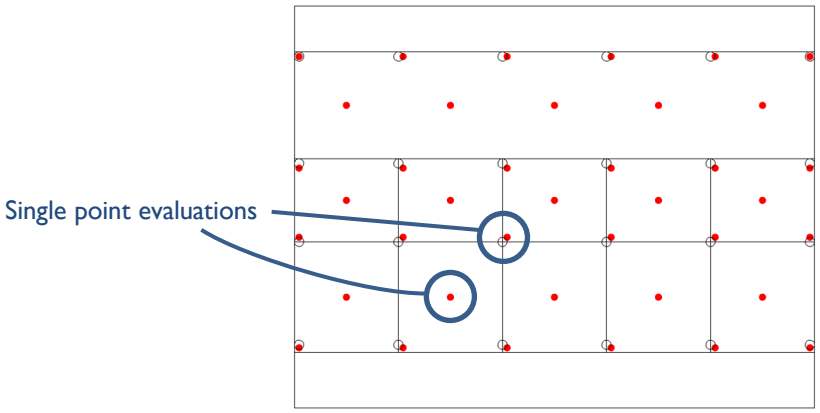

The operational deflection at 10.4 Hz is shown in Figure 4-6, which shows the response of the building around a floor natural frequency. Note that the local floor natural frequencies do not all occur at the same frequency due to differences in boundary conditions.

Figure 4-6. Case study A, operational deflection shape, 10.4 Hz

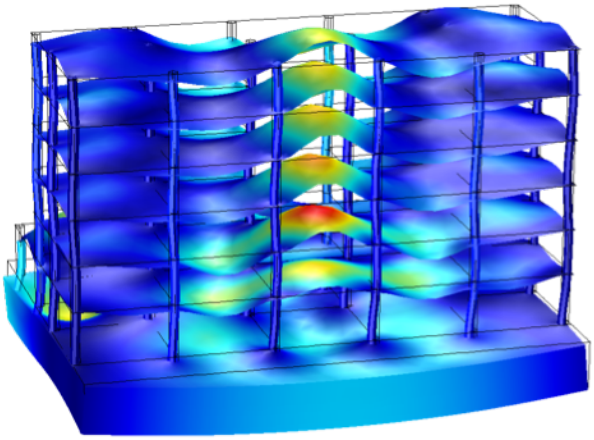

Since the input force profile of the real situation is not available, it is not possible to obtain absolute vibration levels directly from the FE model. Absolute values are therefore obtained by using the model to calculate 1/3 octave band vertical velocity levels at each evaluation point, and expressing these values *relative* to the average 1/3 octave band vibration at basement level, and then applying these relative values to the measured basement vibration level.

4.1.4 FE model results

For the column locations, predicted maximum vertical velocity levels are given in Figure 4-7 in one-third octave bands for each storey. Since multiple locations were evaluated for each storey, the arithmetic mean and plus/minus one standard deviation values are shown, as well as the results from a single evaluation position on each storey that was deemed to be representative of the measurement location. The corresponding overall W_b-weighted acceleration levels and A-weighted velocity are given in Figure 4-8 and Figure 4-9, respectively. For the mid-span positions, the equivalent results are given in Figure 4-10 (one-third octave bands), Figure 4-11 (W_b-weighted acceleration) and Figure 4-12 (A-weighted velocity).

Figure 4-7. Case study A: predicted vibration levels, column positions

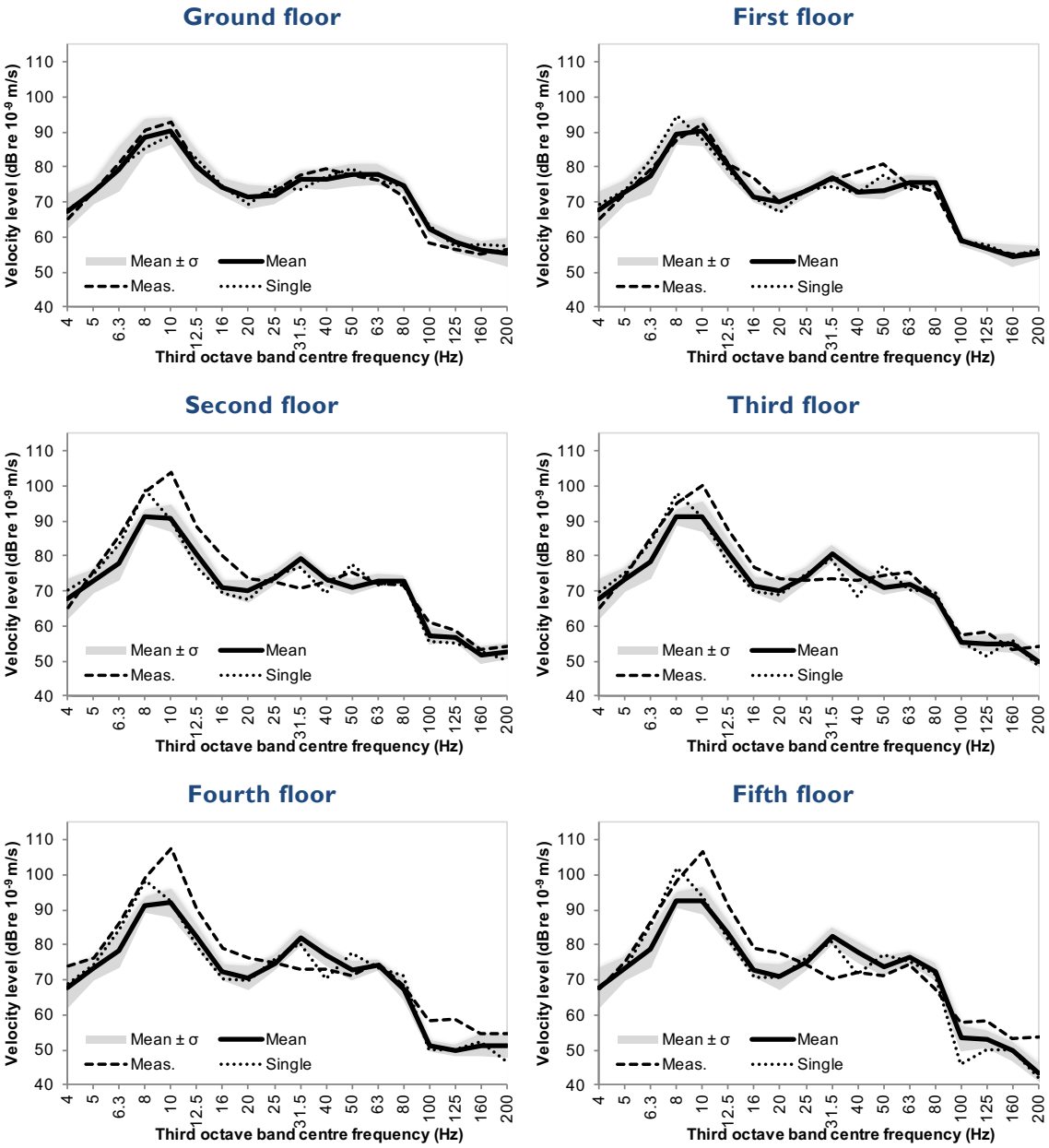

Figure 4-8. Case study A: Column W_b-weighted acceleration levels with storey

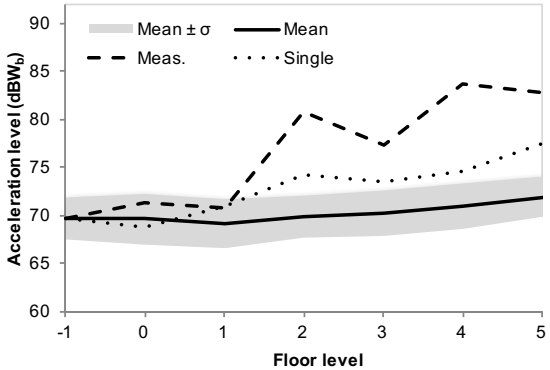

Figure 4-9. Case study A: Column A-weighted velocity levels with storey

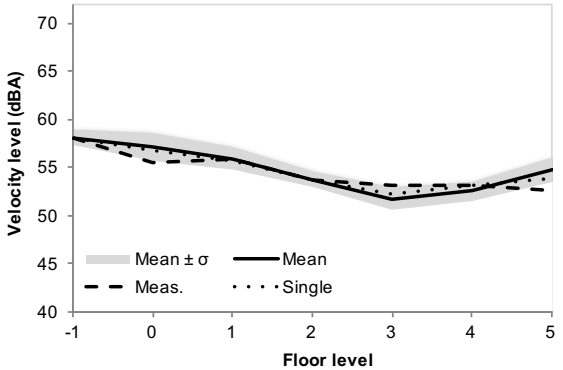

Figure 4-10. Case Study A: predicted vibration levels, mid-span positions

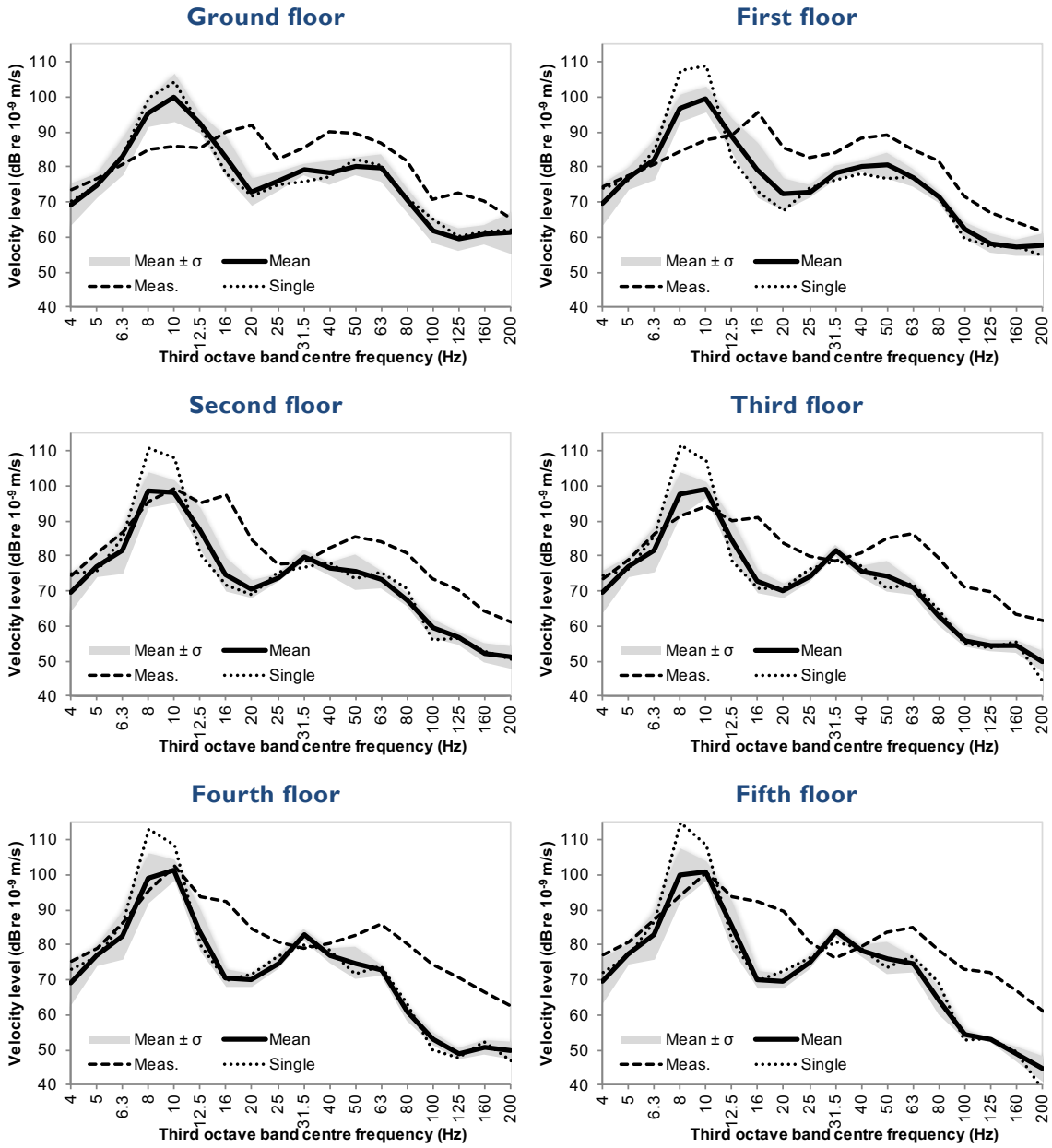

Figure 4-11. Case study A: Mid-span W_b-weighted acceleration levels with storey

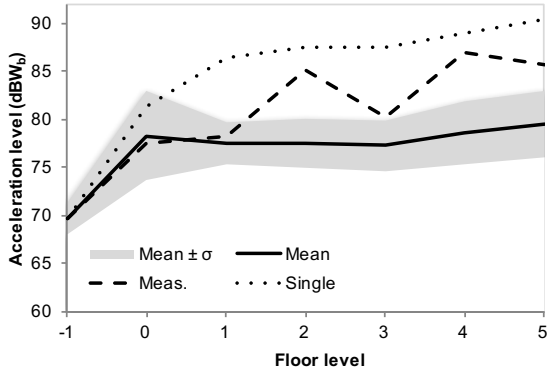

Figure 4-12. Case study A: Mid-span A-weighted velocity levels with storey

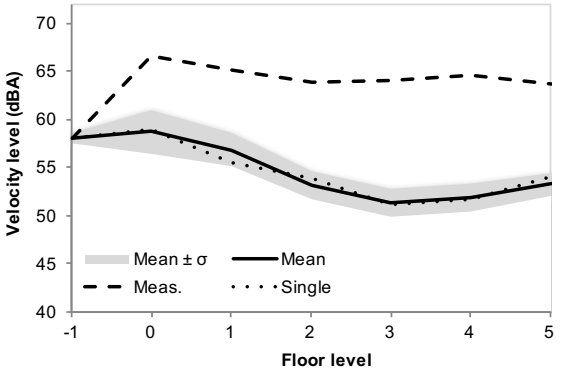

For the column positions, the model data showed reasonable agreement with the measured data, although towards the upper storeys the shape of the measured spectrum appears shifted towards

higher frequencies compared with the predicted data. This is likely due to be stiffening structural elements that existed in the building but are not included in the model. This observation occurs to an even greater extent for the mid-span positions; it is likely that there may have been structural beams as part of the floor construction, but which were not included in the model.

There is a difference between results calculated from averages of multiple positions per storey, and the results calculated from consideration of a single point per storey. Whilst the single-position results are in general within plus/minus one standard deviation of the mean for each storey for the column position, the mid-span results do not tend to lie within the standard deviation at frequencies below about 20 Hz. Consideration of a single point provided better agreement with the measurements than average results for the column positions, but less so for the mid-span positions. This is due to the sensitivity of the single-point approach to the mid-span dynamics both at the basement and the floor level of interest (that is, compared with considering the column positions, there are effectively two additional transfer functions involved, each introducing uncertainty).

In summary, the FE model approach showed similar trends to the measured data, despite difficulties in using historical data and uncertainties about the building structure. The next section describes an additional validation exercise for a recently completed building, for which more detailed measurements and construction details are available.

4.2 Case Study B: York Way, near King's Cross, London

4.2.1 Background

The redevelopment of an area north of the London King's Cross railway station includes a large mixed use development for which Arup were appointed to provide acoustic design advice. This serves as the second case study. Some vibration measurements from this building were briefly presented in Section 3.1.2.

The development is located adjacent to York Way, which runs alongside King's Cross Station. The building lies directly above the Piccadilly Line of the London Underground, the crown of which is around 22 m below ground level (10 m below the pile toes). A section of the development is given in Figure 4-13, showing the location of the tunnels relative to the building.

Figure 4-13. Case study B, building section *(from Arup project drawings)*

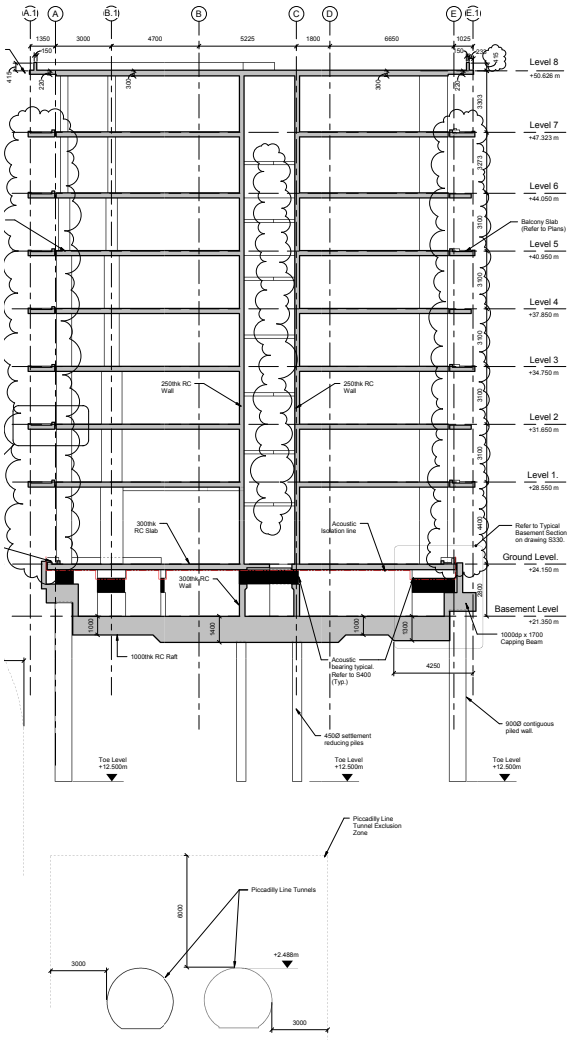

Due to the involvement of Arup in the design of the building, access to detailed structural drawings of the building was possible, which is convenient for modelling purposes.

The building consists of eight storeys plus a basement level, with a ground level footprint of around 115 m long by 25 m wide, and a height (above ground level) of around 27 m. The building use is residential for the upper storeys, retail at ground floor, and car parking in the basement area.

The structural frame of the building is reinforced concrete, with various column sizes and structural walls as well as lift and stair cores. Some of the column cross-sections reduce with floor level up the building. The suspended slab thickness is for the most part 0.27 m (0.3 m at ground and roof level). The ceiling heights (floor to soffit) of the upper building levels are 2.8 m, with 4.1 m at ground floor level, and 2.5 m at basement level.

The foundations of the building consist of a ~1 m deep slab supported on pile foundations. The main building structure has been built upon acoustic bearings (shown as black elements in Figure 4-13), which are installed between basement and ground floor levels.

4.2.2 Vibration measurements

Five sets of vibration measurements were undertaken at various stages of construction:

- Aug 2011: vibration measurements at boreholes and at ground surface, no building structure.
- Aug 2012: structure complete up to 3rd floor, measurements undertaken at basement level only.
- Oct 2012: structure complete up to 4th floor (some areas up to 6th floor), measurements undertaken up to 4th floor.
- Dec 2012: structure complete, measurements undertaken up to 6th floor. Some cladding was installed, and partition metal frameworks installed.
- Jul 2013: structure complete, all cladding, internal partitions, services and façade elements installed. Measurements undertaken up to 7th floor.

The design of the acoustic bearing system is such that the bearings are installed pre-compressed, causing a rigid link for early stages of construction. However, as the loading increases, the bearings compress to or beyond the limit of their retaining bolts. This means that the bearing system is likely to have had a greater effect on the dynamic response of the building for the later measurements.

The focus of the validation study will be on the Dec 2012 measurements, as they represent the bare structural core condition that will be modelled. However, it is of interest to observe whether the recorded vibration levels at basement level might change in response to the progress of the building construction. As such, recorded maximum (slow weighted) vertical velocity levels in the basement are shown in Figure 4-14. It is seen that, below the 12.5 Hz band, vibration levels decreased by as much as 5 dB as the building construction progressed. This may be due to the increased mass of the building, or possibly due to a change in the railway track system. At the higher frequencies there is less of an observable correlation with construction progress, although the most recent measurements seemed to display slightly reduced vibration levels (by about 2 to 3 dB) between 50 and 160 Hz. This decrease is counter-intuitive; if this observation is due to an increased effect of the acoustic bearings, one would expect to see an increase in vibration at the basement level in this frequency range.

It should be noted that there were slight changes in measurement instrumentation between some of the measurements presented. However, each system was verified with a calibrated portable shaker at the time of the measurements and therefore any resultant variation due to instrumentation is expected to be small. For all measurements, at column locations,

measurements were made on the floor surface in the vicinity of a structural column. For any given storey, column and mid-span recordings were made concurrently. Whilst measurements at each storey were performed separately, these were concurrent with measurements in the basement. The basement measurements therefore served as a reference, enabling spurious data measured at other storeys to be identified.

Figure 4-14. Case study B (KX), measured vertical velocity levels at basement

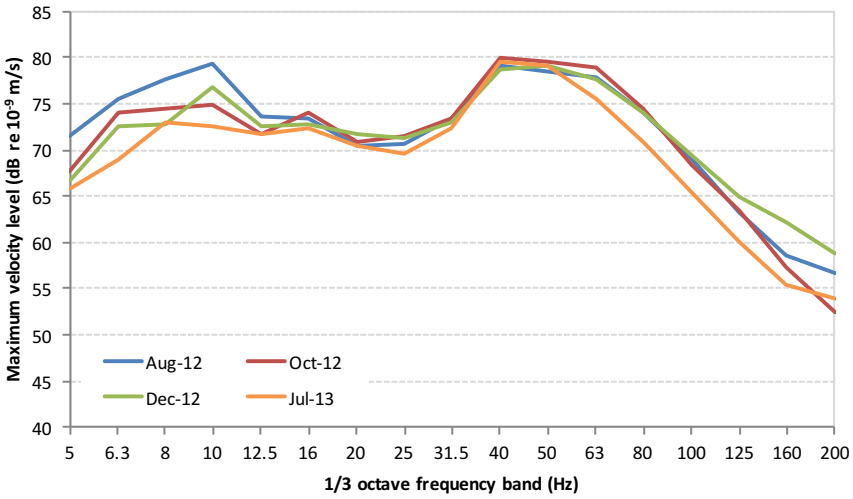

For the Dec 2012 visit, measurements were undertaken at basement, ground, 1st floor, 2nd floor and 4th floor, at mid-span and column positions, plus a 6th floor mid-span location. The data acquisition system utilised PCB 393B12 accelerometers and three Rion DA-20 multichannel digital recorders. The accelerometers were mounted on studded metal plates which were fixed to the floor surfaces with epoxy resin adhesive. Continuous vibration recordings of at least 30 minutes were made at each location. The recordings were later separated into train events by manual waveform analysis, and analysed in order to extract velocity spectra in 1/3 octave bands. The average maximum vertical velocity levels are presented in Figure 4-15 for column positions, and Figure 4-16 for mid-span positions.

Figure 4-15. Case study B (KX) measured maximum vertical velocity level, column positions

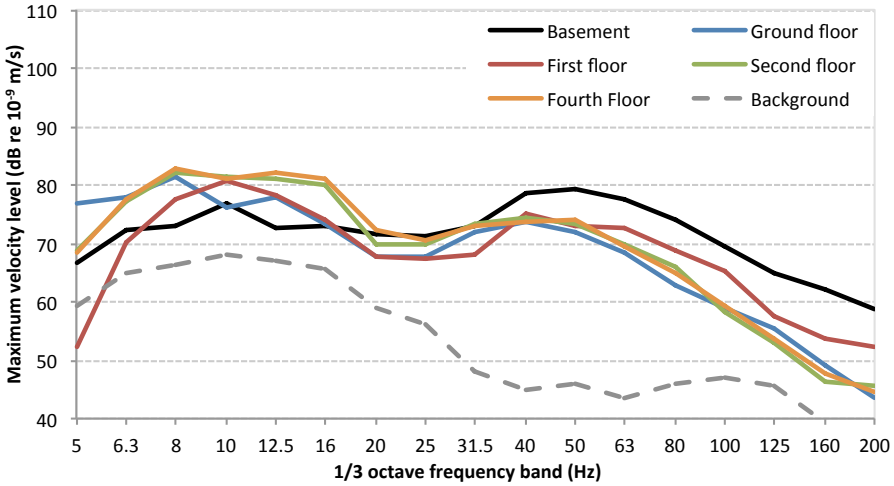

Figure 4-16. Case study B (KX) measured maximum vertical velocity level, mid-span positions

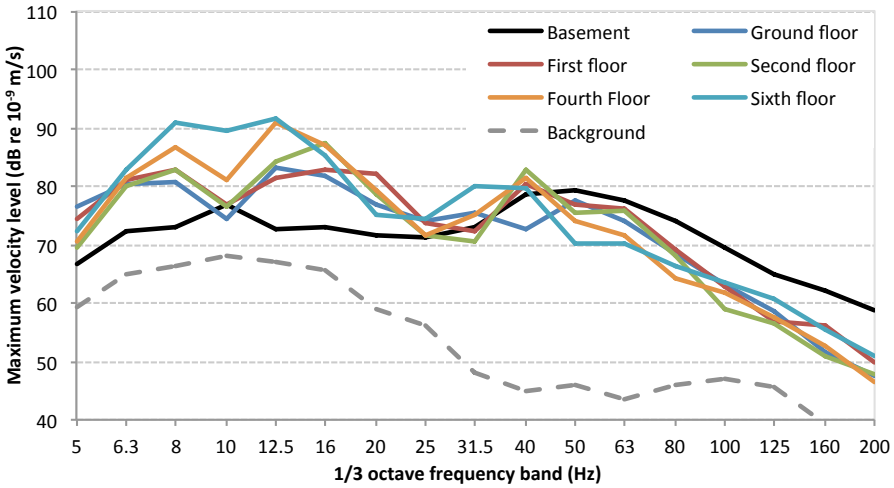

4.2.3 FE model description

A finite element model of the building has been developed using COMSOL Multiphysics™. For the bending wavelengths considered in the study, a maximum element size of around 1.5 m is appropriate in order to achieve accurate results for a frequency range up to 200 Hz. This represents approximately half a wavelength for the floors and shafts, which is at the limit of validity for quadratic elements.

The mesh used in the study is shown in Figure 4-17. The basement and column elements are modelled as solid elements, whilst the floor and shaft walls are modelled as shell elements (Mindlin-Reissner formulation, accounting for transverse shear deformation). The number of

degrees of freedom is 2,625,171. 1301 frequency points were employed in the frequency domain study as before, spaced with a finer resolution at the low frequencies*.

Figure 4-17. Case study B, model mesh

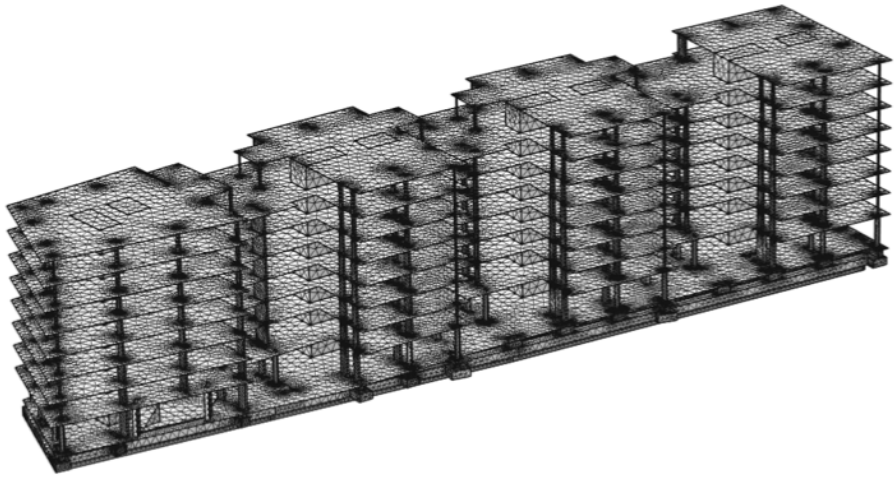

Material parameters have been taken from various literature and the COMSOL material library. The material constants used in the model are shown in Table 4-2. Structural damping has been included in the model by including the damping loss factor to make the Young's modulus of elasticity complex.

Table 4-2: Case study B, material parameters

	Columns	Floors
Density (kg.m^{-3})	2400	2400
Young's modulus (GPa)	27	27
Damping loss factor	0.05	0.05

The excitation of the building structure is modelled as a distributed force per unit area over the external surfaces of the basement. The direction of the input force has the vector (F_x,F_y,F_z), where x is the axis along the longer length of the building, y is the axis along the shorter width of the building, and z is the axis up the height of the building. The vertical force is set to five times that of the lateral forces, which are set to equal values, such that F_z=5F_x=5F_y. This is in accordance with observations from triaxial vibration measurement data at basement levels.

Calculations took approximately 30 minutes per frequency with a reasonably powerful desktop computer. The speed of calculation for this model could be improved with the use of increased

* As before, the frequency spacing was: 0.02 Hz (3 to 10 Hz), 0.05 (10 to 20 Hz), 0.1 Hz (20 to 50 Hz), 0.2 Hz (50 to 100 Hz), 0.5 Hz (100 to 200 Hz).

RAM and/or a solid-state hard drive; see Appendix E for a discussion on optimising computers for modelling.

The vertical vibration response of the model is evaluated at a number of column and mid-span locations for each storey as shown in plan in Figure 4-18. 848 points were evaluated in total. The operational deflection shape at 9.1 Hz is shown in Figure 4-19, which highlights local modes in several of the floor areas. This shows clearly that local modes are an important mechanism for spatial variation of vibration levels within each storey.

Figure 4-18. Case study B, model evaluation positions, plan view

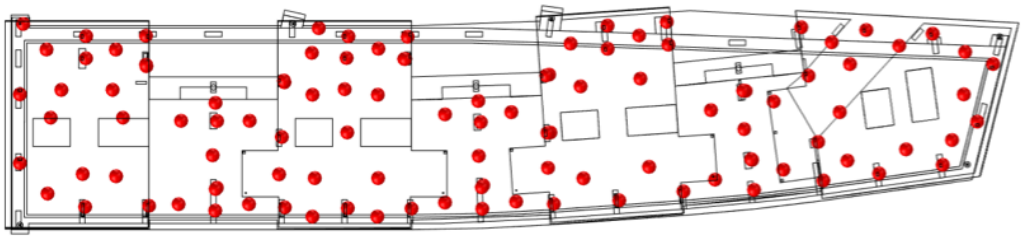

Figure 4-19. Case study B, operational deflection shape, 9.1 Hz

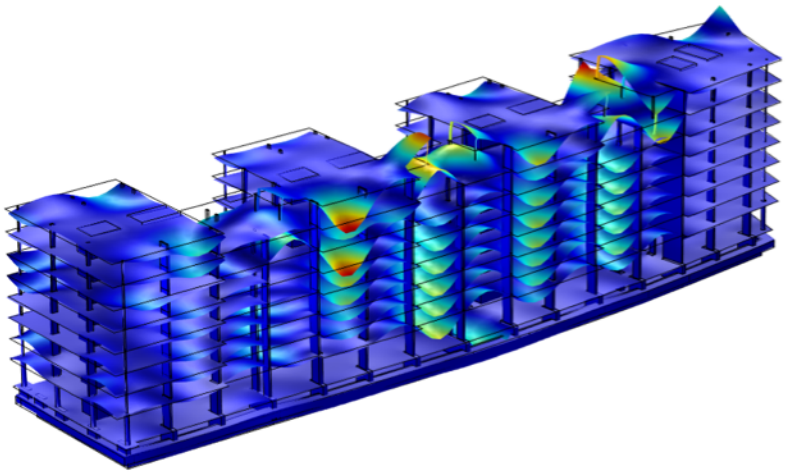

Since the input force profile of the real situation is not available, it is not possible to obtain absolute vibration levels directly from the FE model. Absolute values are therefore obtained by using the model to calculate 1/3 octave band vertical velocity levels at each evaluation point, and expressing these values *relative* to the average 1/3 octave band vibration at basement level, and then combining these relative values with the measured basement vibration level.

4.2.4 FE model results

For the column locations, predicted maximum vertical velocity levels are given in Figure 4-20 in one-third octave bands for each storey. Since multiple locations were evaluated for each storey, the arithmetic mean and plus/minus one standard deviation values are given, as well as the results

from a single evaluation position on each storey that was deemed to be representative of the measurement location. The corresponding overall W_b-weighted acceleration and A-weighted velocity levels are given in Figure 4-21 and Figure 4-22, respectively. One-third octave band results for the third and fifth floors have been excluded due to absence of measurement data and for the sake of brevity.

For the mid-span positions, the equivalent results are given in Figure 4-23 (one-third octave bands), Figure 4-24 (W_b-weighted acceleration) and Figure 4-25 (A-weighted velocity).

Figure 4-20. Case study B: predicted vibration levels, column positions

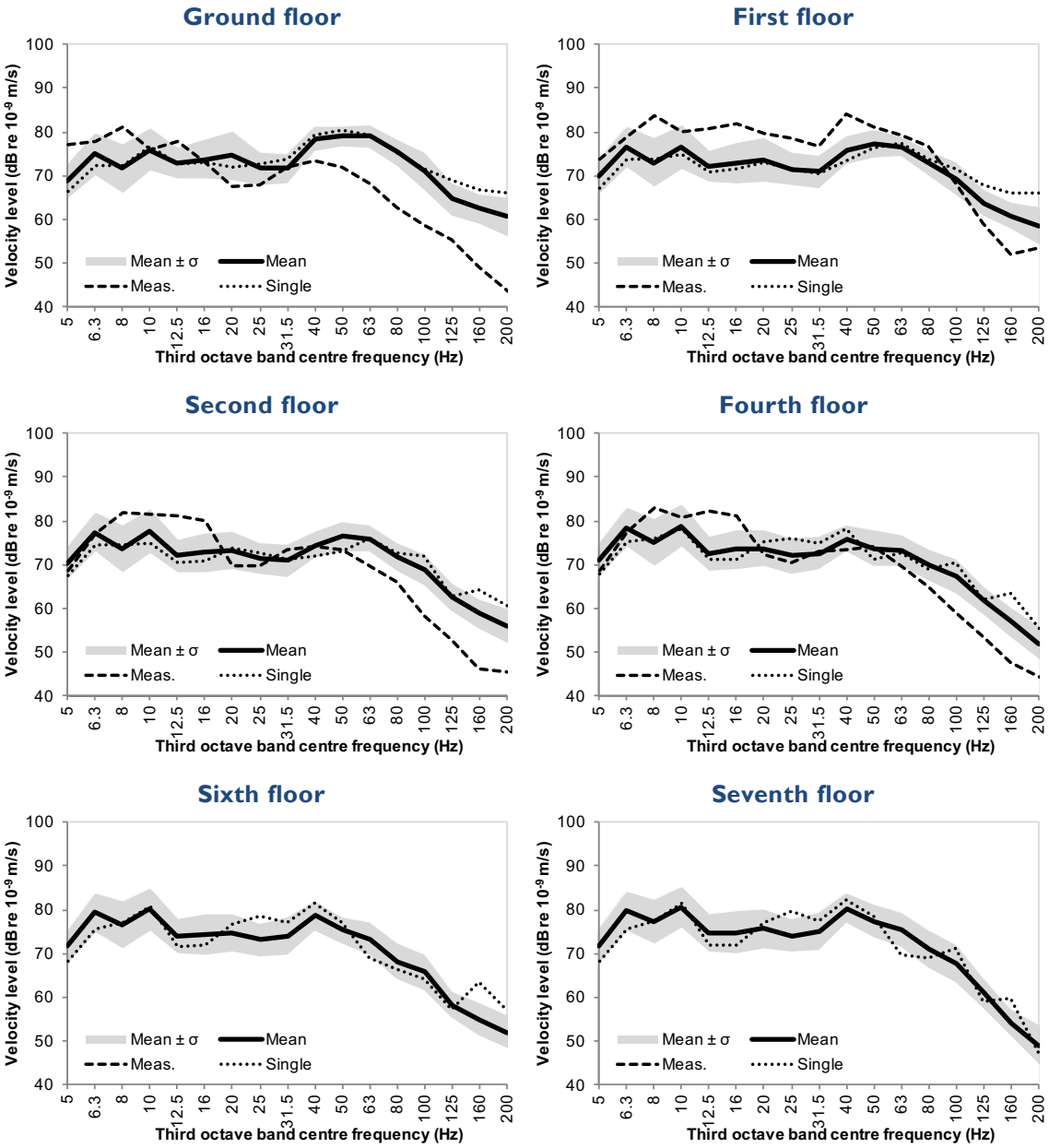

Figure 4-21. Case study B: Column W_b-weighted acceleration levels with storey

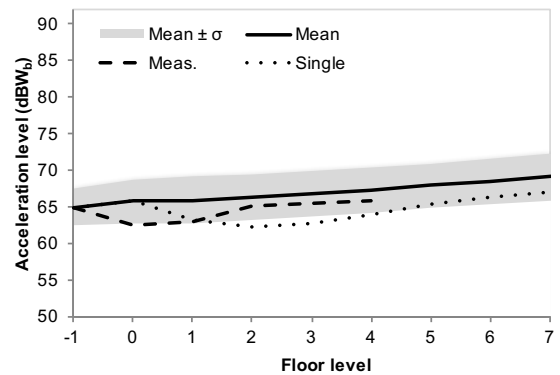

Figure 4-22. Case study B: Column A-weighted velocity levels with storey

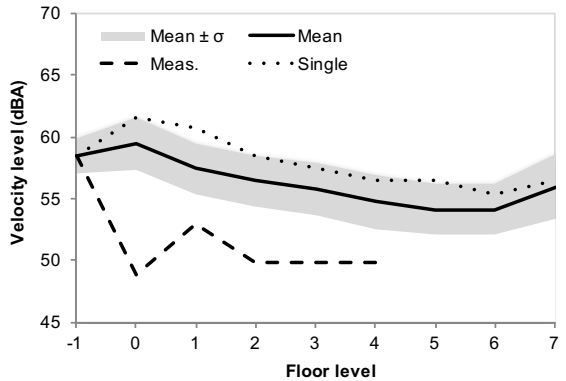

Figure 4-23. Case study B: predicted vibration levels, mid-span positions

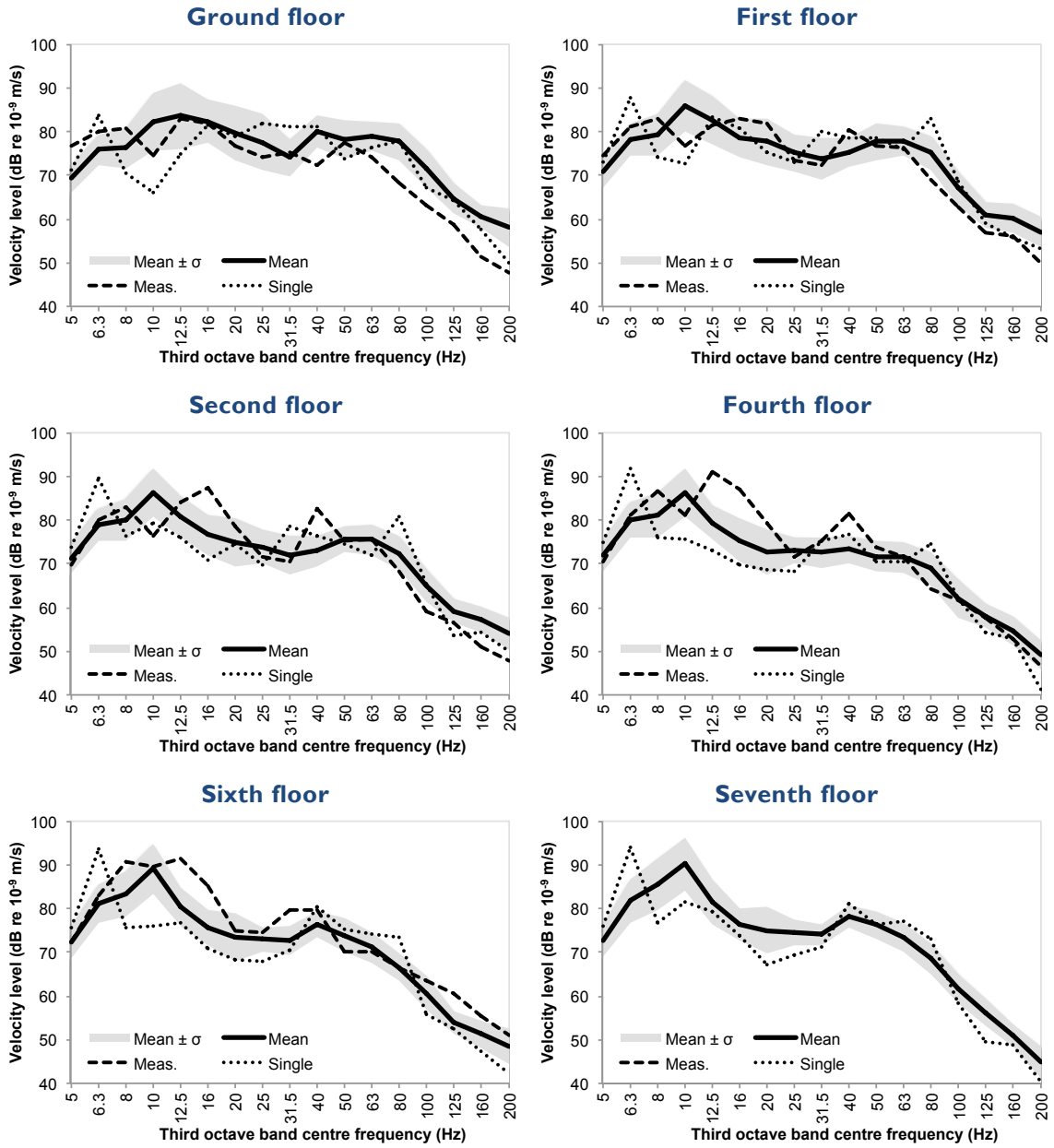

Figure 4-24. Case study B: Mid-span W_b-weighted acceleration levels with storey

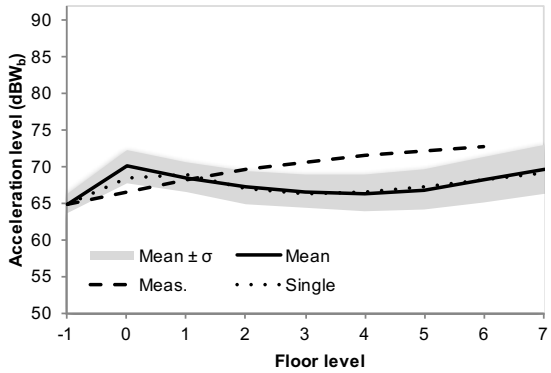

Figure 4-25. Case study B: Mid-span A-weighted velocity levels with storey

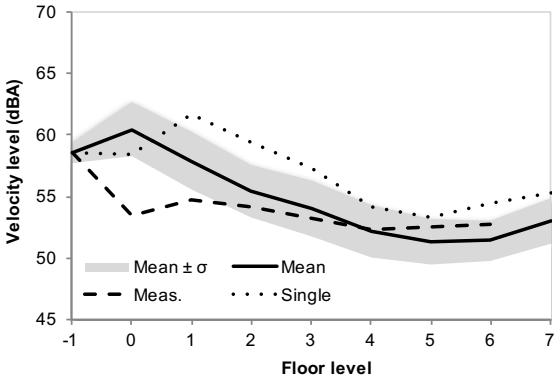

For the column positions, the model data show modest agreement with the measured data, although for all storeys, the results above 40 Hz were typically less than those measured, by about

5-10 dB. This was observed at all storeys, so is likely to be caused by a difference between the modelled and real structure between basement and ground floor, most likely due to the acoustic isolation bearings. Above ground floor, the predicted amplification/attenuation per storey for the A-weighted velocity and W_b-weighted acceleration values shows reasonable agreement with measured data.

The mid-span predictions show slightly better agreement with measured data, although the floor resonances do not always occur in the same frequency bands; as with case study A, it is likely that there are stiffening components which have not been included in the model. The single-position predictions contain a peak in the spectrum in the 6.3 Hz frequency band that was not observed in either the measurements or the averaged predictions. From inspection of the results, this was caused by a dip in the spectrum at the corresponding basement position, and illustrates that care should be taken when making predictions based on values relative to a single reference point, as any anomalies in the reference data will inevitably be present in all the predictions.

There are some differences between the average and single-position results. As found with case study A, the single-position results are in general within plus/minus one standard deviation of the mean for each storey for the column position, but less so for the mid-span position below about 20 Hz.

4.2.5 FE model study extension: reduced building model

The calculation of case study B was carried out in separate calculation runs for a number of frequency regions in order to keep file sizes manageable and reduce the impact of any potential problems that might occur during a calculation run. The calculation therefore took a great deal of time to run*.

It was hypothesised that the whole building might not be required, and that a reduced model of the building might provide acceptable results. The building considered in case study B is made up of four 'cores' with interconnecting sections. The results of a prediction model based on only one of these cores are presented below. A view of the mesh used for the study is given in Figure 4-26. Other than its size, the model had the same material and mesh properties as the full model. The number of degrees of freedom was reduced to 398,280.

* Whilst the computational time was theoretically in the region of 30 days, if the added time for dealing with any problems, for saving files and for restarting the next run (at a convenient moment) is considered, it is more realistic to assume a calculation time of twice this length.

Figure 4-26. Case study B reduced model mesh

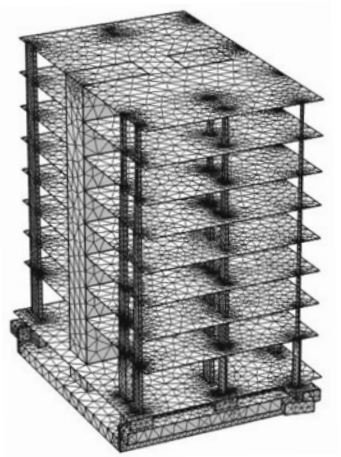

For the column locations, predicted maximum vertical velocity spectra are given in Figure 4-27 in 1/3 octave bands for the ground and fourth floors. This is shown alongside results from the full model and the measurements. Storey-average results are presented in addition to results from a single evaluation position on each storey that was deemed to be representative of the measurement location. The corresponding overall W_b-weighted acceleration and A-weighted velocity levels are given in Figure 4-28 and Figure 4-29, respectively. For the mid-span positions, the equivalent results are given in Figure 4-30 (one-third octave bands), Figure 4-31 (W_b-weighted acceleration) and Figure 4-32 (A-weighted velocity).

Figure 4-27. Case study B reduced model: predicted vibration, column positions

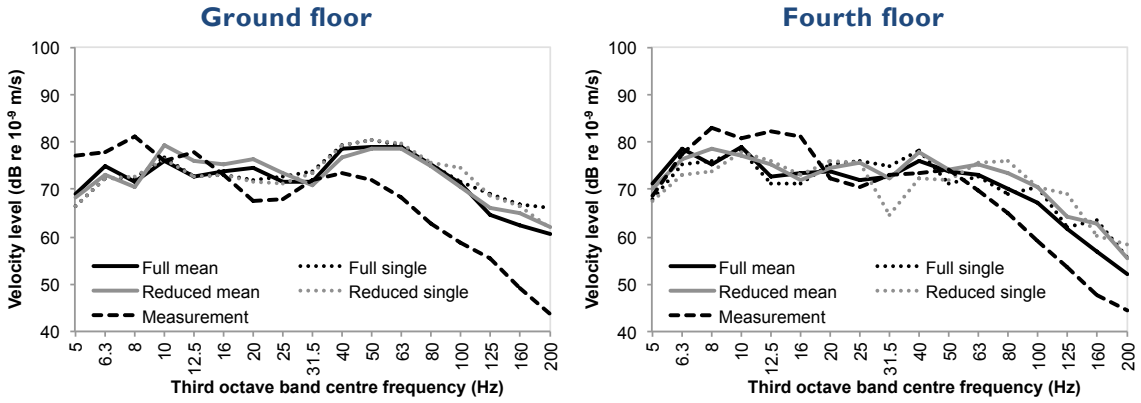

Figure 4-28. Case study B reduced model: Column W_b-weighted acceleration levels with storey

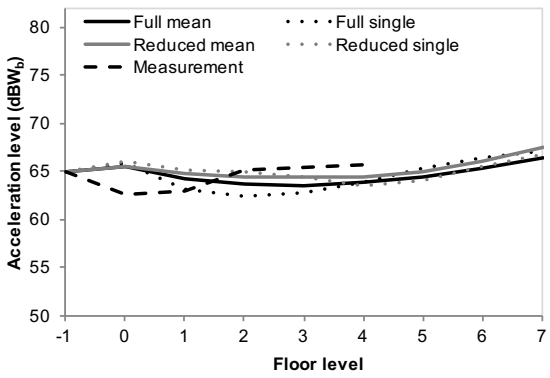

Figure 4-29. Case study B reduced model: Column A-weighted velocity levels with storey

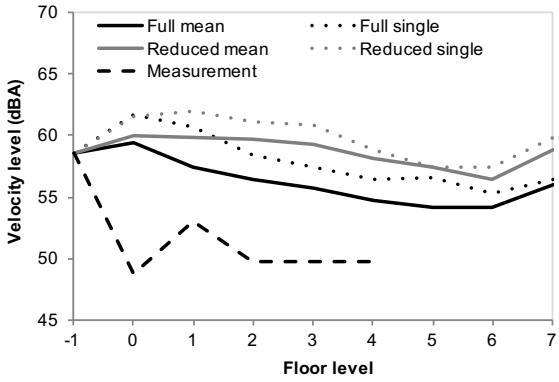

Figure 4-30. Case study B reduced model: predicted vibration, mid-span positions

Ground floor

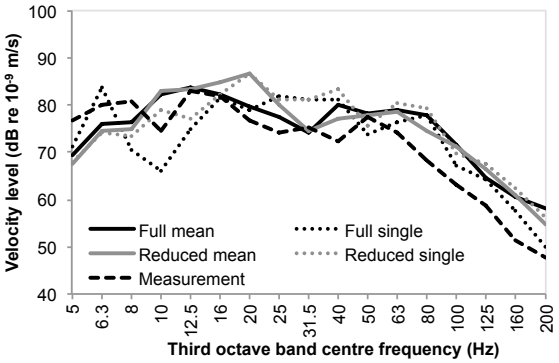

Fourth floor

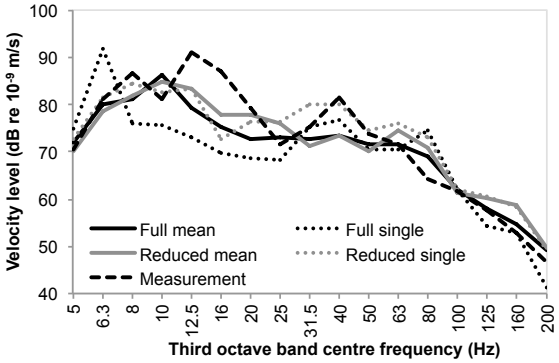

Figure 4-31. Case study B reduced model: Mid-span W_b-weighted acceleration levels with storey

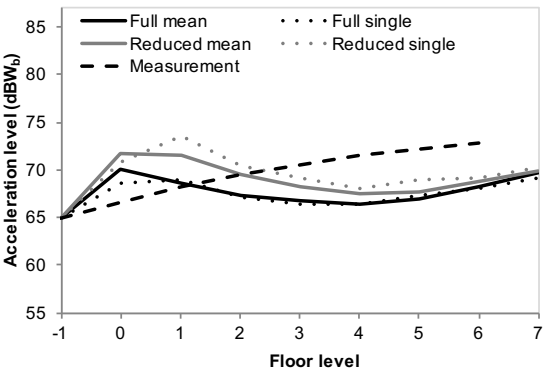

Figure 4-32. Case study B reduced model: Mid-span A-weighted velocity levels with storey

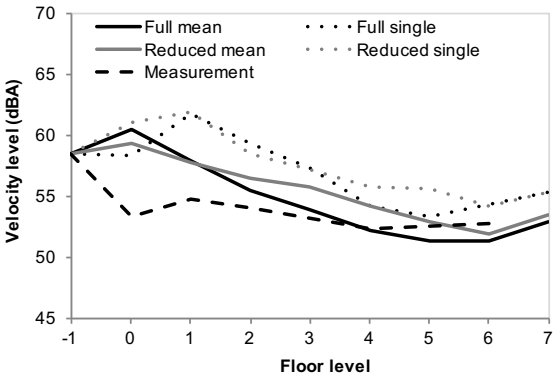

At column positions the results for the reduced model are seen to be close in value to the results from the full model. The storey-average results for the full and reduced models were slightly more similar than the single-point results. The results were particularly close when considering frequencies below 50 Hz. At higher frequencies, at first floor and above, the reduced model gave

results which were about 2 dB higher than the full model. This can be seen most clearly in the overall A-weighted level results; there is marginal difference in the overall W_b-weighted results.

For the mid-span positions, similar observations can be made; slight differences are found between the results for the full and reduced models, particularly for the single-point evaluated results. It should be noted however, that subsequent to the calculation of the full model, one of the supporting columns at the mid-span single-point evaluation position was found not to have been fully connected to the slab. This was deemed to have limited effect on the results when considering average vibration levels over each storey, but may contribute to some of the differences noted between the two models' single-point mid-span results.

Given the small differences between results from the two models, it can be concluded that for the particular building in case study B, a reduced model is capable of providing equivalent results to the full model, at a much reduced time and computational cost. However, the design of this building was such that there were clearly defined parts of the building which were considered a suitable basis for the reduced model; buildings which do not possess such clearly defined parts may be less suitable for model reduction. Further study into the influence of building geometry is therefore required.

4.3 Summary

Two case studies have been presented for multi-storey concrete frame buildings affected by vibration from underground railways in London. For each of the case studies vibration measurements have been compared with FE models. Both case studies have shown agreement between predicted and measured results with some limitations that are attributed mainly to incomplete information or simplification of the building structure. For case study A, the stair shafts have not been included in the model, and are stated in the previous literature to be non-structural. There are some questions over the effect that these would have on the building dynamics. For case study B, the largest uncertainty is over the effect of the acoustic bearings, which were not included in the model, but are expected to influence the building dynamics in their partially-released state. As such, this case study showed best agreement with measurement data when considering relative vibration levels above ground floor.

A direct comparison of model predictions is possible, if the relative vibration values are applied to a constant basement vibration spectrum. The two case study models are compared with the generic 3D model (which is similar to the case study A model, see Section 3.2.1) and average measurement values (see Section 3.1.9). The W_b-weighted and A-weighted results for column and mid-span positions are presented in Figure 4-33 to Figure 4-36, using the basement vibration

values from the average measurement data (see Figure 3-26). The model results shown are based on average vibration values over each storey for each model.

Figure 4-33. 3D FE model comparison Column W_b-weighted acceleration levels with storey

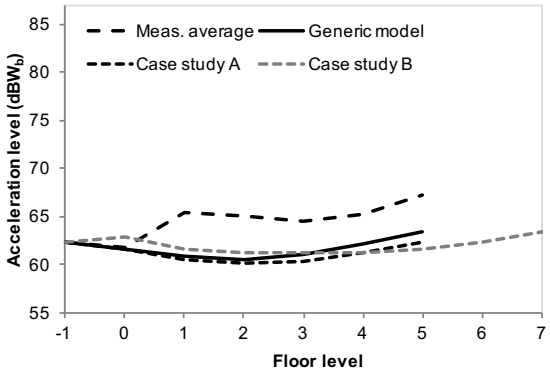

Figure 4-34. 3D FE model comparison: Column A-weighted velocity levels with storey

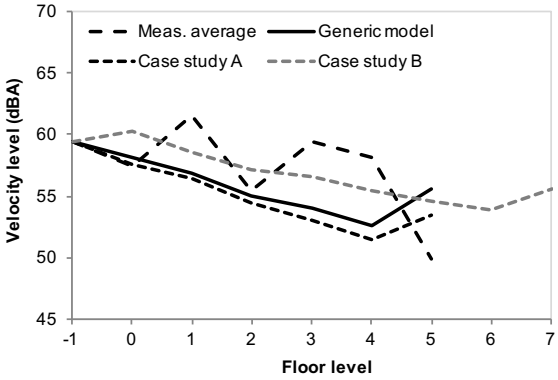

Figure 4-35. 3D FE model comparison: Mid-span W_b-weighted acceleration levels with storey

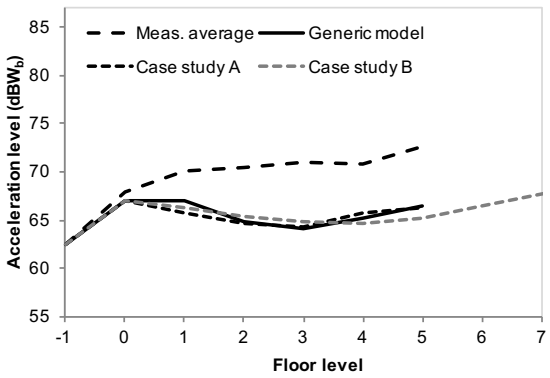

Figure 4-36. 3D FE model comparison: Mid-span A-weighted velocity levels with storey

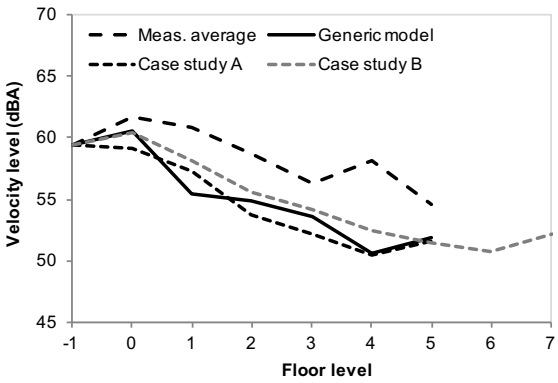

It is seen that the greatest differences between the model results were for the column A-weighted results (Figure 4-34), for which case study B gave values 2-3 dB higher than the other models. For the other results there was typically less than 1 dB difference between model values. In general, the case study B results were closer to the average measurements than the other models. This is likely to be due to the fact that case study B exhibited greater irregularity than the other models, and is perhaps more representative of the measurement dataset that is based on data averaged over a number of different buildings. The influence of irregularity requires further investigation.

There are uncertainties related to the assumed material properties, because it is difficult to estimate these parameters without detailed information about the composition of each building element. Material properties are considered isotropic, whereas in reality, with directional

features such as reinforcement bars and in-situ concrete deck profiles, the properties may perhaps be better described as orthotropic.

The conclusion from the case studies is that the FE analysis approach is suitable for investigating the influence of structural parameters on a building, but it is important that detailed information about the structure is obtained and where possible implemented in the model in order for accurate absolute vibration level predictions to be made.

5. BUILDING VIBRATION MODEL: PARAMETRIC STUDY

Further to the gaps in knowledge highlighted by the literature review and a proposed model approach confirmed by the case studies, a study into the influence of a number of structural parameters on the vibration in a generic building is presented in this chapter.

5.1 FE model description

The starting point for the parametric study is a default model, to which any changes may be compared. Through discussion with experienced engineers from industry partners Arup, a default generic building model has therefore been developed which is deemed to be representative of many modern buildings affected by groundborne noise from railways. The material parameters for the default building model are given in Table 5-1, and the building has the following geometric features:

- Six storeys plus basement
- Two structural shafts
- 1 m thick concrete raft foundation
- Structural basement walls
- 4x3 grid arrangement of slabs, each 8 m x 6 m x 0.27 m
- Cuboid columns, with a cross-section of 0.5 x 0.5 m
- 3.0 m storey height (floor to soffit)

Table 5-1. Material parameters used in generic model

	Columns	Floors
Density ($kg.m^{-3}$)	2500	2400
Young's modulus (GPa)	26	26
Damping loss factor	0.05	0.05

The floors and structural wall surfaces are modelled as shell elements, with the columns modelled as solids. Note that it is also possible to model the columns as beam elements, see Appendix A for further discussion. The mesh of the default configuration is shown in Figure 5-1; the number of degrees of freedom is 224,250, taking 17.5 hours to run a full calculation with a reasonably powerful desktop computer.

Figure 5-1. Generic building default model mesh

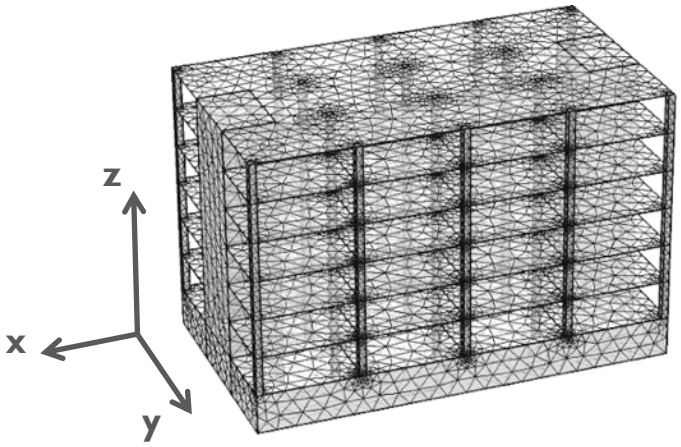

The input force to the building structure is modelled as a distributed force per unit area over the external surfaces of the basement. The direction of the input force has the vector $[F_x,F_y,F_z]$, where *x* is the axis along the longer length of the building, *y* is the axis along the shorter width of the building, and *z* is the axis up the height of the building. Using this nomenclature, the force vector is [0.5,0.5,1]N.

The vertical vibration response of the model is evaluated at a number of column and mid-span locations for each storey as shown in plan in Figure 5-2.

Figure 5-2. Generic building model evaluation positions, plan view (single position locations encircled)

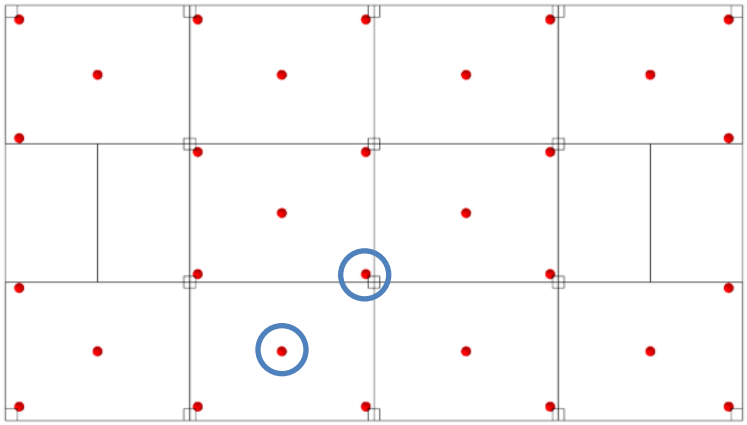

Whilst storey-averaged results are presented primarily, results for single positions are also given for the default model. 210 points are evaluated in total for the default model, but this number varies as appropriate for each individual building model in the parametric study. It should be noted that throughout this study, relative results are calculated from one-third octave band data, not directly from the narrow-band frequency results. The data is converted into one-third octave bands at each evaluation point prior to any per-storey averaging or relative comparisons.

A large number of parametric variations have been considered using this model as a starting point, as listed below:

- Building height in number of storeys (2 to 12) – *Page 109*
- Storey height (3 to 6 m) (all storeys above basement level) – *Page 112*
- Ground floor storey height (3 to 6 m) – *Page 114*
- Slab size (four different width/length combinations) – *Page 115*
- Slab thickness (0.25 to 0.3 m) – *Page 119*
- Building length in number of slabs (3 to 6) – *Page 119*
- Building width in number of slabs (3 to 5) – *Page 120*
- Column cross-section (0.16 to 0.64 m^2 square, and 0.25 m^2 circular) – *Page 121*
- Structural damping (loss factor of 0.01 to 0.1) – *Page 124*
- Material density (default values multiplied by factors of 0.7 to 2) – *Page 127*
- Material stiffness (Young's modulus of elasticity) (20 to 60 GPa) – *Page 129*
- Input force direction (vectors [0,0,1],[0.5,0.5,1] and [1,1,1]) – *Page 132*
- Input force location (various configurations) – *Page 132*
- Internal walls (various stiffness and damping values) – *Page 122*
- Other geometry adjustments – *Page 136*
    - Irregular spacing of columns
    - High mass single storey "blocking floor"
    - Absence of structural shafts
    - Absence of structural shafts and basement walls

The full results for all the parametric variations cannot be given here due to the space required, and are therefore only given for the default model. The parametric study results in subsequent sections are summarised in Appendix F in terms of overall W_b and A-weighted values relative to the basement at column and mid-span locations as well as first floor mid-span locations relative to column locations. In addition, a graph and accompanying table for each study shows the maximum average amplification values (for mid-span and column positions relative to the basement), and the storey at which that maximum occurs. Where appropriate to aid with discussion, some of these results are also reproduced in the main body of the text.

All overall weighted levels have been calculated through the application of the basement spectrum of the average measurement values (see Section 3.1.9).

Throughout the presentation of results, an asterisk (*) denotes the default parameter value, and in the majority of figures this is presented by a solid black line.

5.2 Default model

5.2.1 Transmission through the building

Some of the prominent operational deflection shapes are shown in Figure 5-3. This shows a low frequency translational mode at 3.3 Hz and a vertical building mode at 10.2 Hz, which is also close to a natural frequency of some of the floor slabs.

Figure 5-3. Generic building default model, operational deflection shapes

3.3 Hz

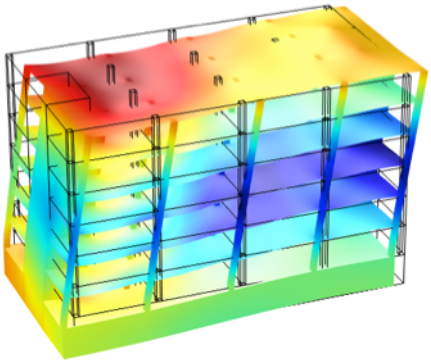

10.2 Hz

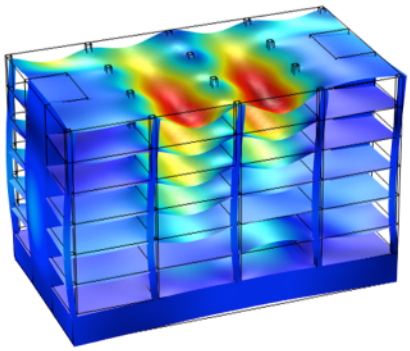

The mean vertical vibration level at each storey relative to the basement is given in Figure 5-4 for the column positions and Figure 5-5 for the mid-span positions. Since the vertical vibration values were evaluated at every column and mid-span position, the mean value is presented for each storey, along with the range of values within ± one standard deviation of the mean. Each figure also includes a 3D surface plot representation of the data, together with a schematic diagram to assist in interpreting the results. The values for the standard deviation and 95% confidence intervals of the storey averages are given in Table 5-2 to Table 5-5.

Figure 5-4. Generic building default model, vertical vibration relative to basement, column positions

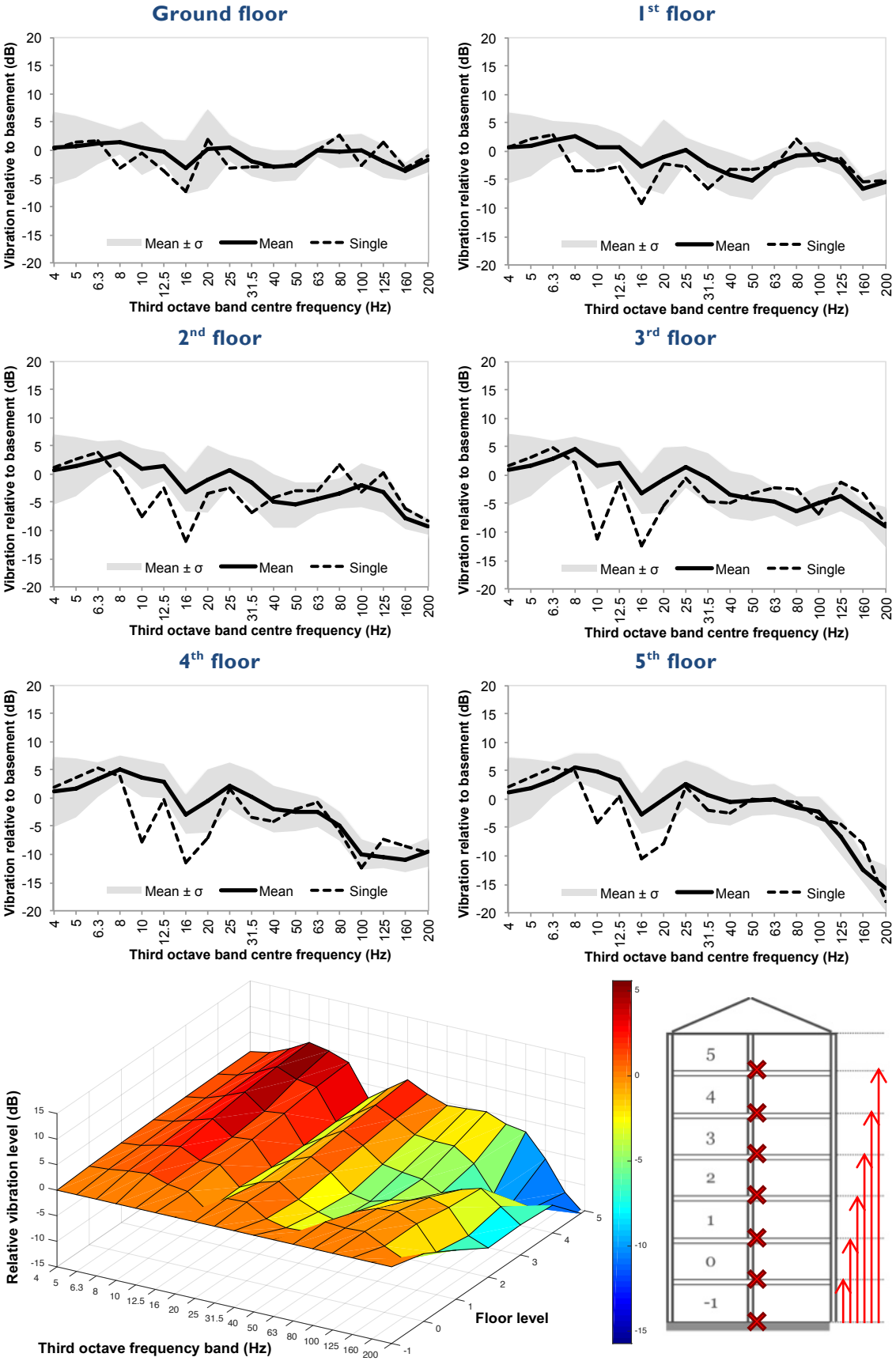

Figure 5-5. Generic building default model, vertical vibration relative to basement, mid-span positions

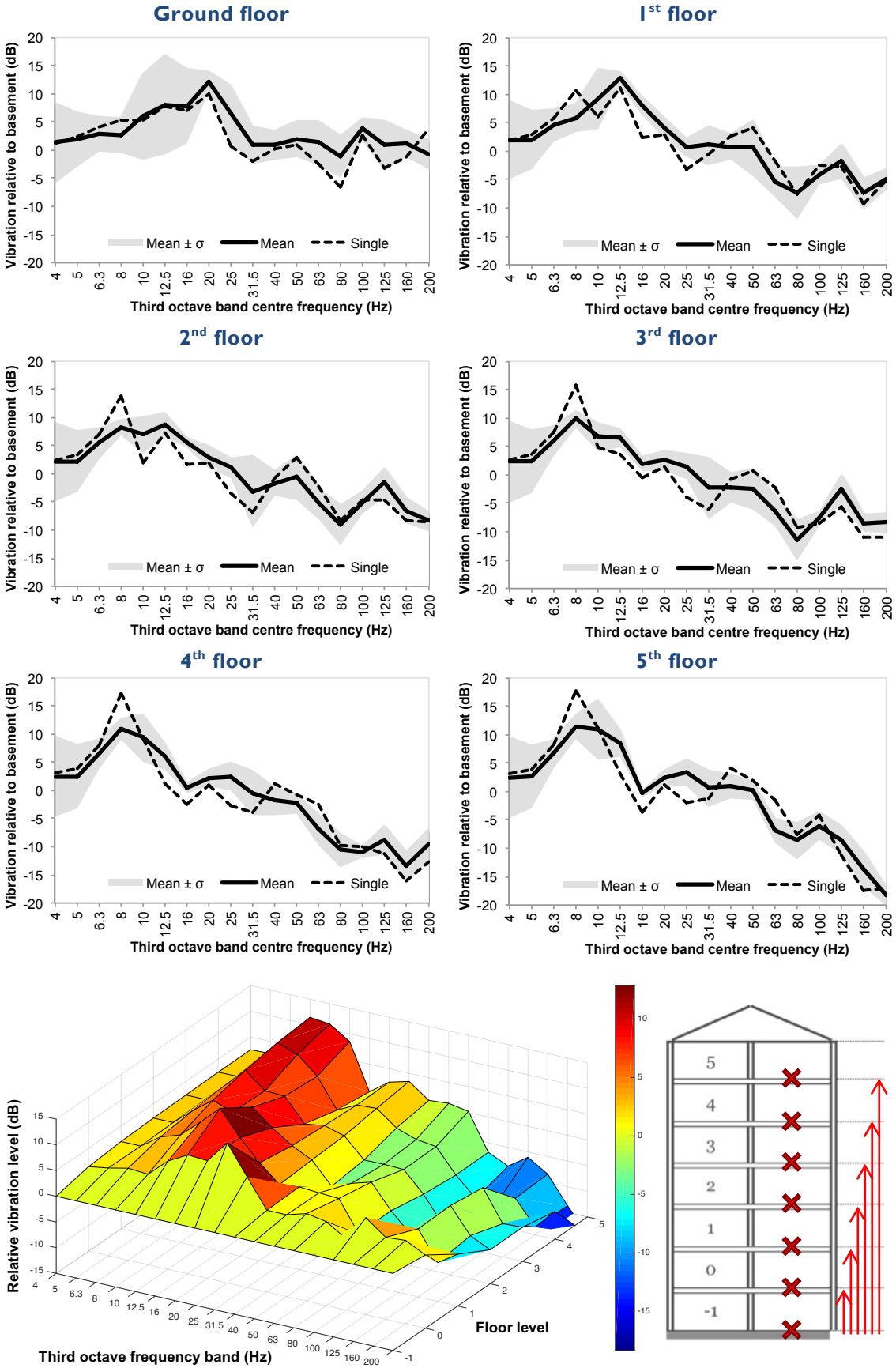

Table 5-2. Generic default building: 95% confidence intervals for mean (column) (dB)																				
Storey	1/3 octave band frequency (Hz)																		Overall	
	4	5	6.3	8	10	12.5	16	20	25	31.5	40	50	63	80	100	125	160	200	L_{Wb}	L_A
-1	2.9	2.5	2.1	1.5	2.3	1.2	2.6	3.9	1.2	1.6	1.7	0.8	1.4	0.8	0.6	0.6	0.6	0.7	0.5	0.3
0	3.0	2.5	1.7	1.0	2.2	1.0	2.2	3.3	1.1	1.2	1.3	1.3	0.6	1.3	1.4	1.4	0.7	1.0	0.5	0.5
1	3.0	2.5	1.6	1.1	1.8	1.2	1.6	3.1	1.1	1.6	1.8	1.6	1.0	1.0	1.0	1.0	1.0	1.0	0.7	0.4
2	2.9	2.5	1.5	1.1	1.7	1.2	1.6	2.8	1.3	1.9	2.2	1.9	1.3	1.2	1.8	1.8	0.9	0.7	0.9	0.7
3	2.9	2.4	1.5	1.0	2.0	1.3	1.6	2.7	1.7	2.1	2.0	1.9	1.1	1.2	1.4	1.2	0.9	1.6	0.9	0.6
4	2.9	2.4	1.4	1.1	1.5	1.4	1.6	2.6	1.9	2.2	1.9	1.6	1.2	1.2	1.2	0.9	1.1	1.2	0.8	0.5
5	2.9	2.4	1.4	1.2	1.5	1.5	1.6	2.5	1.9	2.3	1.9	1.2	1.3	0.9	1.3	1.5	1.0	1.9	0.8	0.6

Table 5-3. Generic default building: 95% confidence intervals for mean (mid-span) (dB)																				
Storey	1/3 octave band frequency (Hz)																		Overall	
	4	5	6.3	8	10	12.5	16	20	25	31.5	40	50	63	80	100	125	160	200	L_{Wb}	L_A
-1	5.2	3.5	2.2	2.1	5.1	3.5	4.5	1.7	1.6	1.2	0.8	1.5	1.7	0.7	0.4	0.7	0.2	0.4	0.7	0.5
0	5.1	3.5	2.2	2.3	5.5	6.4	4.8	1.3	3.6	2.4	1.9	2.4	2.8	2.8	1.5	3.2	1.7	1.9	2.1	1.4
1	5.0	3.8	2.1	1.9	3.9	0.9	1.2	1.4	1.2	2.5	1.7	3.6	2.0	3.3	1.2	2.2	2.0	1.4	1.2	1.9
2	5.0	3.9	1.9	1.1	2.4	1.6	0.7	1.5	1.3	4.6	1.6	2.9	2.0	2.7	1.5	1.9	1.7	1.3	1.0	1.5
3	5.1	4.0	1.9	1.1	1.9	1.2	0.9	1.3	1.6	3.9	1.9	2.6	2.0	2.6	1.0	1.9	1.1	1.3	0.8	1.4
4	5.2	4.0	1.9	1.4	3.1	1.7	0.7	1.2	1.8	2.9	1.8	1.3	2.0	2.2	0.8	1.9	1.9	2.1	1.1	1.1
5	5.2	4.0	1.9	1.6	3.8	1.8	0.4	1.1	1.8	2.3	1.5	1.2	1.5	2.4	1.8	1.8	2.2	1.3	1.2	1.1

Table 5-4. Generic default building: standard deviations (column) (dB)																				
Storey	1/3 octave band frequency (Hz)																		Overall	
	4	5	6.3	8	10	12.5	16	20	25	31.5	40	50	63	80	100	125	160	200	L_{Wb}	L_A
-1	6.3	5.2	4.5	3.3	4.9	2.6	5.5	8.3	2.6	3.5	3.6	1.8	3.0	1.6	1.3	1.3	1.3	1.5	1.1	0.6
0	6.4	5.4	3.6	2.2	4.7	2.2	4.7	7.0	2.4	2.6	2.9	2.7	1.3	2.8	3.0	2.9	1.5	2.2	1.2	1.0
1	6.3	5.3	3.4	2.5	3.9	2.5	3.5	6.6	2.4	3.4	3.8	3.4	2.2	2.1	2.1	2.2	2.0	2.1	1.6	0.9
2	6.3	5.2	3.2	2.3	3.6	2.6	3.5	6.0	2.8	4.1	4.7	4.1	2.8	2.6	3.9	3.8	1.9	1.5	2.0	1.5
3	6.3	5.2	3.1	2.2	4.2	2.8	3.5	5.7	3.6	4.5	4.2	4.0	2.4	2.6	2.9	2.6	1.8	3.5	1.8	1.4
4	6.2	5.2	3.1	2.4	3.3	3.0	3.5	5.6	4.1	4.7	4.0	3.4	2.6	2.5	2.6	2.0	2.2	2.6	1.7	1.1
5	6.2	5.2	3.0	2.5	3.2	3.2	3.5	5.3	4.1	4.9	4.0	2.7	2.8	1.9	2.7	3.2	2.2	4.0	1.7	1.2

Table 5-5. Generic default building: standard deviations (mid-span) (dB)																				
Storey	1/3 octave band frequency (Hz)																		Overall	
	4	5	6.3	8	10	12.5	16	20	25	31.5	40	50	63	80	100	125	160	200	L_{Wb}	L_A
-1	7.3	4.9	3.0	3.0	7.2	4.9	6.3	2.4	2.2	1.7	1.2	2.0	2.4	1.0	0.5	0.9	0.3	0.5	1.0	0.7
0	7.2	4.9	3.1	3.2	7.7	9.0	6.7	1.9	5.1	3.4	2.6	3.4	3.9	3.9	2.1	4.5	2.4	2.6	2.9	1.9
1	6.9	5.3	2.9	2.6	5.4	1.3	1.7	2.0	1.7	3.5	2.4	5.1	2.7	4.6	1.7	3.1	2.8	1.9	1.6	2.6
2	7.0	5.5	2.7	1.5	3.3	2.3	0.9	2.1	1.8	6.4	2.3	4.0	2.8	3.8	2.1	2.7	2.3	1.8	1.4	2.1
3	7.1	5.6	2.7	1.5	2.6	1.6	1.3	1.9	2.3	5.4	2.6	3.7	2.8	3.7	1.3	2.7	1.6	1.9	1.2	2.0
4	7.2	5.7	2.6	2.0	4.3	2.4	0.9	1.7	2.5	4.0	2.5	1.8	2.8	3.0	1.1	2.7	2.7	2.9	1.5	1.5
5	7.3	5.6	2.6	2.2	5.4	2.5	0.6	1.5	2.5	3.3	2.1	1.6	2.1	3.3	2.5	2.5	3.1	1.8	1.7	1.5

The overall W_b and A-weighted results with storey are given in Figure 5-6 and Figure 5-7 respectively for the column positions. The equivalent results for the mid-span locations are given in Figure 5-8 and Figure 5-9.

Figure 5-6. Generic default building, W_b-weighted basement-relative column acceleration levels with storey

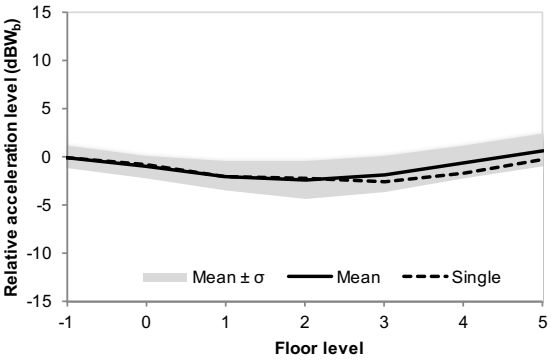

Figure 5-7. Generic default building, A-weighted basement-relative column velocity levels with storey

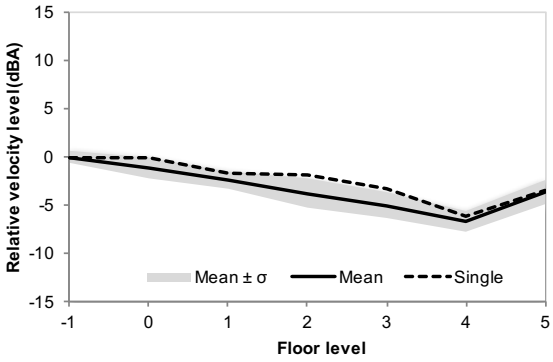

Figure 5-8. Generic default building, W_b-weighted basement-relative mid-span acceleration levels with storey

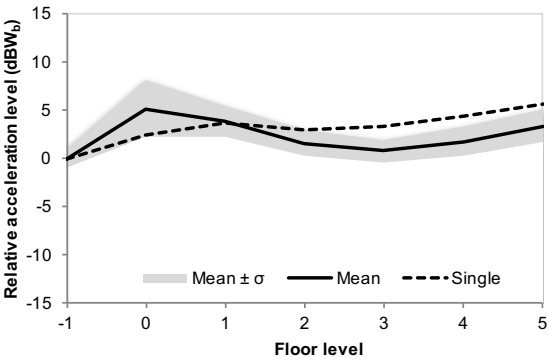

Figure 5-9. Generic default building, A-weighted basement-relative mid-span velocity levels with storey

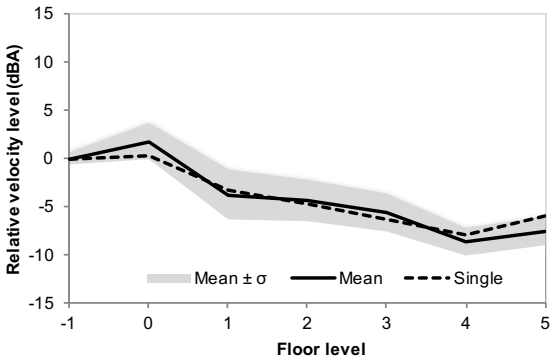

For the column location results (Figure 5-4), the maximum average vibration relative to basement is around 5 dB, occurring at 8 Hz at the uppermost storey. In general, the results show positive inter-storey amplification below around 31.5 Hz, with maximum amplification of around 1 dB per storey at 8 Hz. Above 31.5 Hz there is inter-storey attenuation, the rate of which increases with frequency (around 2 dB per storey at 160 Hz). For the overall W_b-weighted acceleration level (Figure 5-6), there is only very slight amplification up the building (about 2 dB at the uppermost storey relative to the basement). For A-weighted overall velocity level in Figure 5-7, a steady inter-storey attenuation is observed of around 1 dB per storey until the penultimate floor level, with a 2 dB increase between this and the uppermost storey. The overall W_b and A-weighted results for the single evaluation locations are within or close to the standard deviation range. However, the one-third octave data show significant dips in the vibration level at the column location in the 10 and 16 Hz one-third octave bands. This effect may be due to modes in the floor slabs acting as tuned absorbers for the column locations. The additional mechanism is due to building modes causing location dependent minima, which are more pronounced for single column results, than for mid-span or storey-averaged column results.

For mid-span locations the maximum average vibration relative to the basement (Figure 5-5) is around 13 dB at 12.5 Hz on the first floor. As for the column locations, in general inter-storey amplification is observed below around 31.5 Hz, with attenuation above this frequency (around 2 dB per storey at 160 Hz). At the lower frequencies there is a reduction in frequency of the main response peak, which is at 20 Hz at ground floor, and decreases to 8 Hz at the uppermost storey. At the lower floors, it is the floor slab natural frequencies that determine this peak, but at the upper storeys the building modes have a more important role, particularly because the fundamental (extensional) building mode occurs at a lower frequency than the floor mode such that there is amplification at mid-span. In the 8 Hz frequency band (which contains the building's fundamental extensional natural frequency), the inter-storey amplification is steady, at around 2 dB per storey over the height of the building. For the overall W_b-weighted vibration level in Figure 5-8, there is an increase of around 6 dB between basement and ground floor, and little change over the rest of the building height. For A-weighted overall vibration levels in Figure 5-9 there is a 2 dB increase in vibration between basement and ground floor and about 2 dB attenuation per storey above this, with a slight 1 dB increase between the penultimate and uppermost storeys. The single position results provide similar levels to the storey-averaged results, generally within or close to the standard deviation range. However, the peaks for the single position results are more pronounced, with the single position peak value about 5 dB greater than the storey-averaged mean at 2nd floor and above.

5.2.2 Mid-span amplification

The mid-span vibration levels are plotted relative to column positions in one-third octave frequency bands for each storey in Figure 5-10. The overall W_b and A-weighted relative levels are given in Figure 5-11 and Figure 5-12.

Figure 5-10. Generic building default model, vertical vibration at mid-span relative to column positions

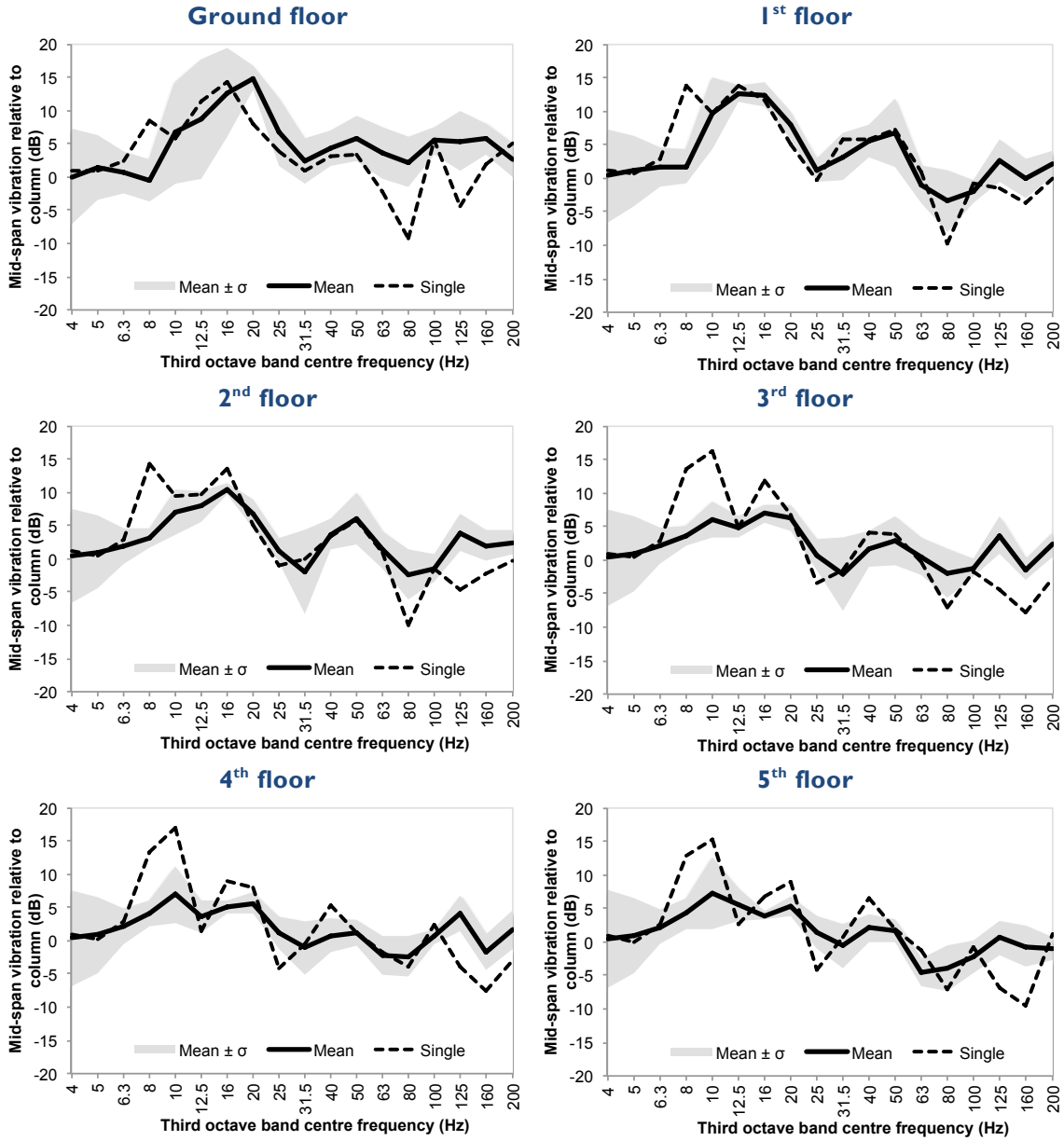

Figure 5-11. Generic default building, W_b-weighted column-relative mid-span acceleration levels with storey

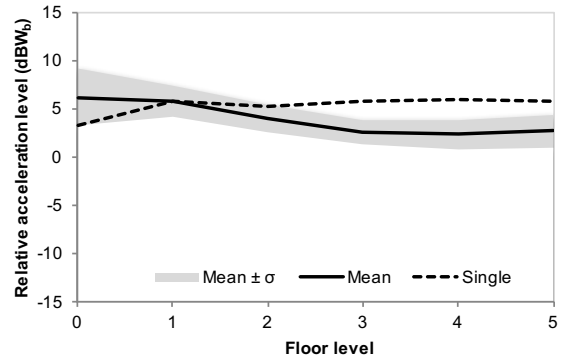

Figure 5-12. Generic default building, A-weighted column-relative mid-span velocity levels with storey

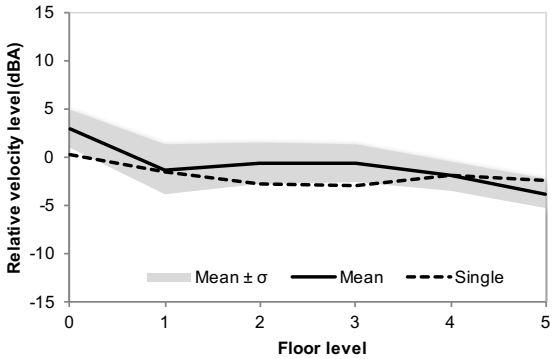

Figure 5-10 demonstrates that the average mid-span amplification is not constant with storey; there is greater amplification noted for the lower storeys. The greater variation observed at ground floor for the W_b-weighted results is due to the different boundary conditions occurring for different floor slabs at this storey, which results in a wider variation in floor slab natural frequency. Figure 5-11 and Figure 5-12 show the effect of the mid-span amplification on the overall W_b and A-weighted vibration levels at the various storeys. For W_b-weighted acceleration, there is a relatively constant ~5 dB amplification at all storeys; for the A-weighted velocity level there is about 3 dB amplification at ground floor, with this value reducing by about 1 dB per storey. It is interesting to note that the reduction in mid-span amplification is not so much due to reduced mid-span vibration levels, but rather due to increased column vibration levels. The single position results are quite different compared to the storey-averaged results when assessing mid-span amplification. From inspection of the figures, it can be seen that this is mainly due to the very location specific response at the column position, with specific dips in the column response spectrum (Figure 5-4) that are not seen in the column averaged results. The vibration of a floor slab is driven by its four supporting columns; the results here indicate that caution should be used when predicting mid-span vibration levels from vibration results at a single column location.

5.2.3 Axis dependency of attenuation

So far, it has been assumed that vertical vibration is the quantity of interest. This is a consequence of the vertical axis usually having the largest vibration magnitudes, as well as being the axis of greatest sensitivity for perceivable vibration and re-radiated noise. However, a short study of the vibration attenuation in each axis is given here; the mid-span and column W_b and A-weighted results are presented in Figure 5-13 to Figure 5-16. The axes are as labelled in Figure 5-1.

Figure 5-13. Generic default building, W_b-weighted basement-relative column acceleration levels with storey, each axis

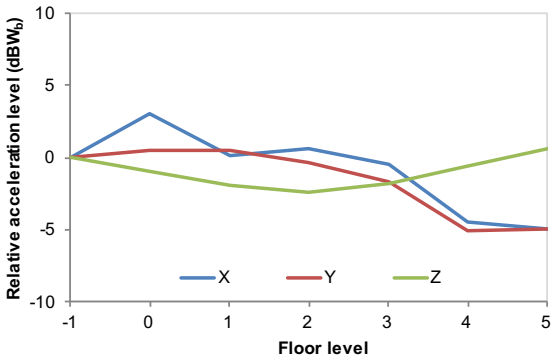

Figure 5-14. Generic default building, A-weighted basement-relative column velocity levels with storey, each axis

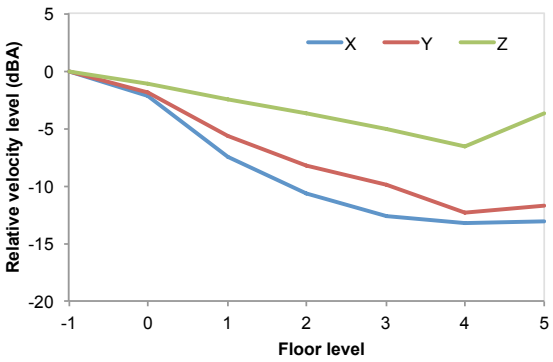

Figure 5-15. Generic default building, W_b-weighted basement-relative mid-span acceleration levels with storey, each axis

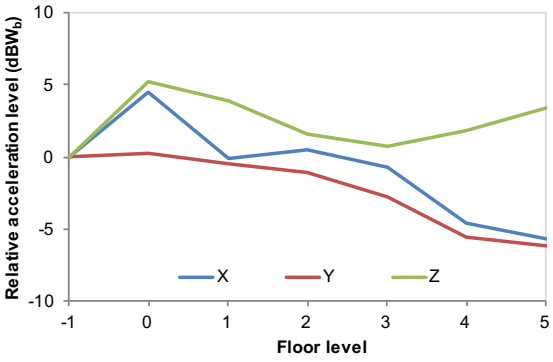

Figure 5-16. Generic default building, A-weighted basement-relative mid-span velocity levels with storey, each axis

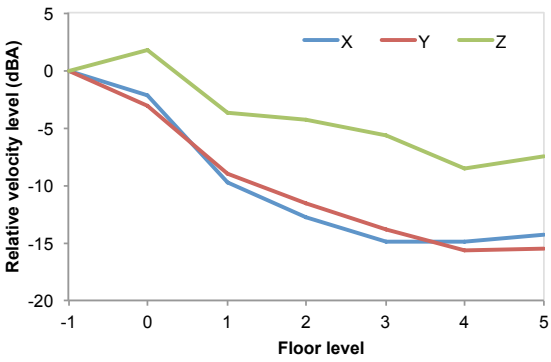

For A-weighted vibration, the vertical component is less attenuated through the building structure than the horizontal components, and it is therefore appropriate that vertical vibration is the primary consideration. However, this was not the case with the W_b-weighted* vibration. The W_b-weighted vibration at column positions is dominated by building modes, with the most significant modes being different for the vertical and horizontal directions. It is therefore important that where there is a sensitivity to low frequency horizontal vibration, for example when designing laboratory facilities, horizontal vibration should be fully accounted for in measurements and predictions.

5.2.4 Variability

The default generic building model displays variability with an average standard deviation of 3 to 4 dB across the frequency range. Variability in the case of the columns (Figure 5-4) was slightly greater at lower frequencies. For the mid-span locations (Figure 5-5), significant variability was displayed on the ground floor between 10 and 16 Hz, with a standard deviation of around 8 dB.

It is not intuitive that an apparently regular structure should exhibit such variability. However, whilst the slab sizes are all identical, there are a number of factors which result in the natural frequencies for the slabs occupying separate one-third octave bands. The first factor is the presence of the shafts, which provide an additional supported boundary to some sections of the floor at each storey. The second is due to the boundary conditions at the perimeter: the slabs at the perimeter of the building's upper floors have at least one free edge; those in the centre of the building have none. At ground floor level the perimeter slabs do not have a free boundary, but are supported by the basement walls, which accounts for the largest variability that is observed

* It should be noted that the W_b weighting curve would normally only be used for the vertical vibration, and when assessing low levels of vibration, see BS 6841:1987 [1]. The W_b weighting is only used here on the horizontal components for consistency in this particular comparison.

at this storey. The third factor is due to the finite size of the columns, which requires the columns at the perimeter of each floor level to be moved inward slightly.

For mid-span amplification (Figure 5-10), the most significant effects are observed at ground floor, with vibration an average of 15 dB greater at mid-span positions than column positions at 20 Hz. The standard deviation at this frequency is relatively small, only about 2 dB. At 16 Hz, whilst the average amplification is slightly less (~13 dB), there is a much greater variation, such that the mean + σ amplification is nearly 20 dB. The mid-span amplification decreases in level and frequency with height up the building; at the uppermost storey the dominant peak in the mid-span amplification is around 7 dB at 10 Hz for average vibration values.

5.3 Height properties

5.3.1 Building height

The effect of building height has been investigated by altering the number of storeys of the FE building model. The range used is between two and twelve; the resulting model geometries are presented in Table 5-6. All other parameters are kept fixed. For the full results, refer to Appendix Section F.1.

Table 5-6. Generic building parametric study: Building height, configurations

No. storeys	Image	No. storeys	Image
2	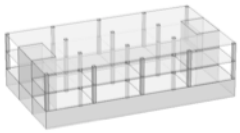	4	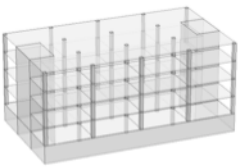
6 *	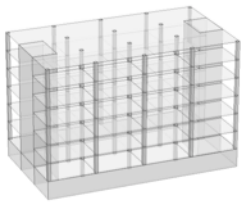	8	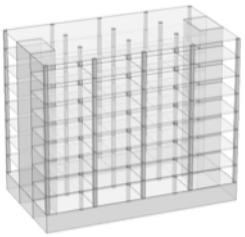
10	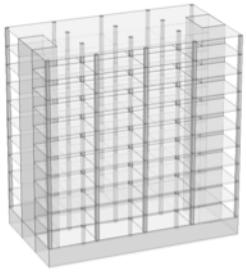	12	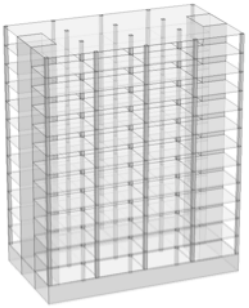

Figure 5-17 to Figure 5-20 show the overall vertical vibration levels evaluated at mid-span and column locations, with the overall vibration level calculated from W_b and A-weighted values. The results are shown by floor level (as for the rest of the models in the parametric study).

Figure 5-17. Parametric study: Building height in number of storeys, W_b-weighted basement-relative column acceleration levels with storey

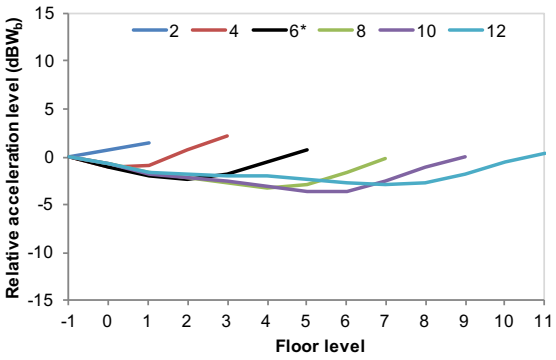

Figure 5-18. Parametric study: Building height in number of storeys, A-weighted basement-relative column velocity levels with storey

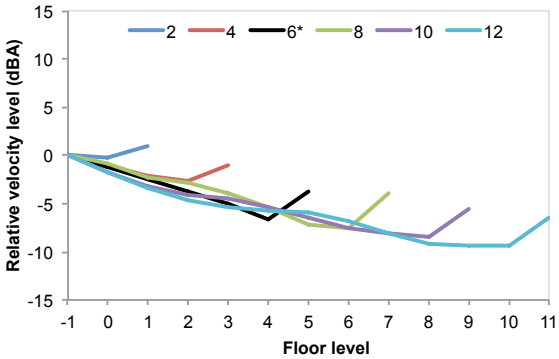

Figure 5-19. Parametric study: Building height in number of storeys, W_b-weighted basement-relative mid-span acceleration levels with storey

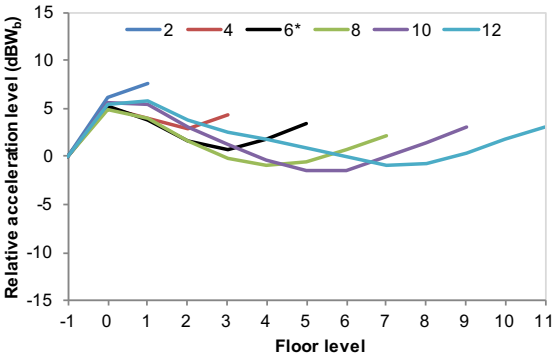

Figure 5-20. Parametric study: Building height in number of storeys, A-weighted basement-relative mid-span velocity levels with storey

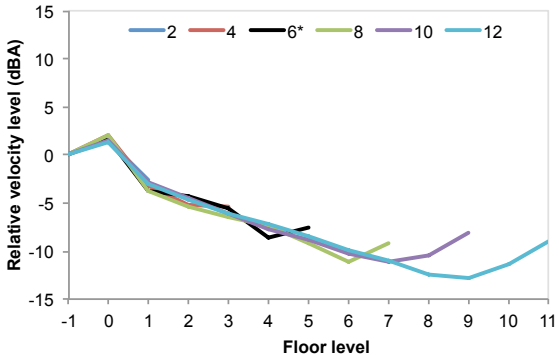

Whilst it is instructive to consider the attenuation or amplification of vibration through the building structure, there are many occasions for which the main parameter of interest is the highest level of vibration within a building. The maximum of the average column one-third octave vibration levels for each storey is therefore shown in Appendix F.1., in which the data is also presented in tabular form, along with the storey at which the highest average vibration value occurs. Data is presented in the same manner (in the Appendix) for the mid-span positions.

The first floor average mid-span vibration relative to column vibration is given in Figure 5-21.

Figure 5-21. Parametric study: Building height in number of storeys, average vertical vibration level at mid-span relative to column positions, first floor

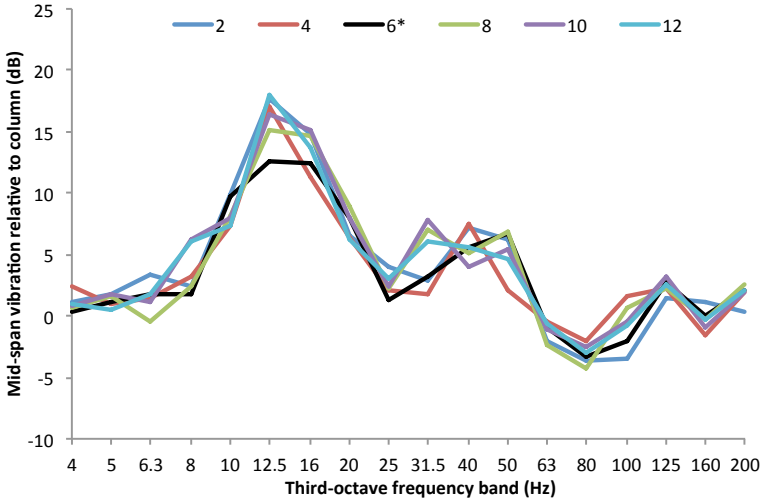

The results show that for each building height configuration, at column positions the maximum overall W_b-weighted value (Figure 5-17) is largely unaffected, occurring in each case at the uppermost storey with a value of 1-2 dB greater than at the basement. The shapes of the lines form a slight curve; a steady inter-storey amplification is not observed. There is an observable difference between buildings of different heights, for example when considering the vibration level at 5th floor, the six storey building model gave results about 4 dB greater than for the 10 storey building. For A-weighted vibration levels (Figure 5-18), all building configurations displayed a fairly steady inter-storey attenuation of 1 dB per storey until the penultimate floor level, where amplification to the uppermost storey is observed (1 dB for the shortest building; 3 dB for the tallest).

For the mid-span overall W_b-weighted results (Figure 5-19), all building configurations show amplification between the basement and ground floor of around 6 dB, with a further 1 dB up to 1st floor (except the two storey building, which displayed a ~3 dB increase between ground and first floor, the top storey). Above first floor, the overall level is more dependent on the building configuration, with lines that curve upward slightly, such that inter-storey amplification is observed at the upper storeys. For the A-weighted results (Figure 5-20), all results show ~1 dB amplification between the basement and ground floor, and around 4 dB attenuation between ground and first floor (1 dB for the two storey building). Above first floor, all buildings display inter-storey attenuation of ~1 dB per storey, but with amplification of 1-2 dB for the uppermost one or two storeys.

For maximum one-third octave band values at column positions (Table F-1), at low frequencies the taller buildings give higher levels (6 dB for the tallest building; 3 dB for the shortest) which always occur at the uppermost storey, but at higher frequencies the shorter buildings give the

higher results. At mid-span locations (Table F-2) the maximum always occurs at first floor and in the 12.5 Hz frequency band. The value is always 13-14 dB relative to the basement, with the exception of the shortest building, where the first floor is its uppermost floor, for which the value is around 17 dB.

5.3.2 Storey height

The effect of storey height (i.e. floor to soffit) has been investigated by altering the height of all storeys of the FE building model, above basement level. The values of storey height that have been used for the study are 3, 4, 5 and 6 m, with the model geometries shown in Table 5-7. Figure 5-22 to Figure 5-25 show the overall W_b and A-weighted vertical vibration levels evaluated at mid-span and column locations. The results are discussed at the end of this section. For the full results, refer to Appendix Section F.2.

Table 5-7. Generic building parametric study: Storey height, configurations

Storey height	Image	Storey height	Image
3.0 m *	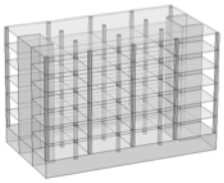	4.0 m	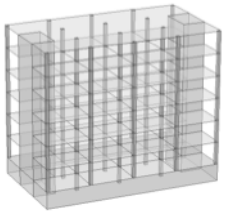
5.0 m	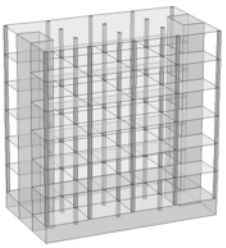	6.0 m	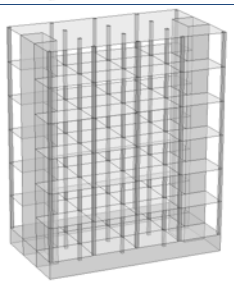

Figure 5-22. Parametric study: Storey height, W_b-weighted basement-relative column acceleration levels with storey

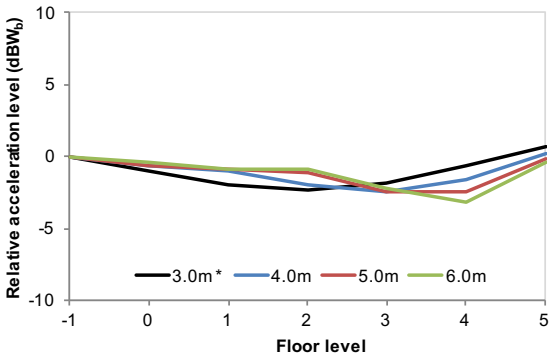

Figure 5-23. Parametric study: Storey height, A-weighted basement-relative column velocity levels with storey

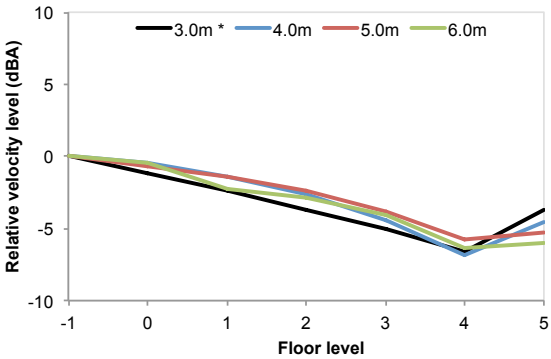

Figure 5-24. Parametric study: Storey height, W_b-weighted basement-relative mid-span acceleration levels with storey

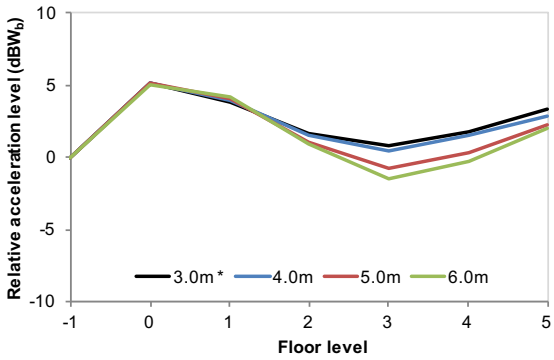

Figure 5-25. Parametric study: Storey height, A-weighted basement-relative mid-span velocity levels with storey

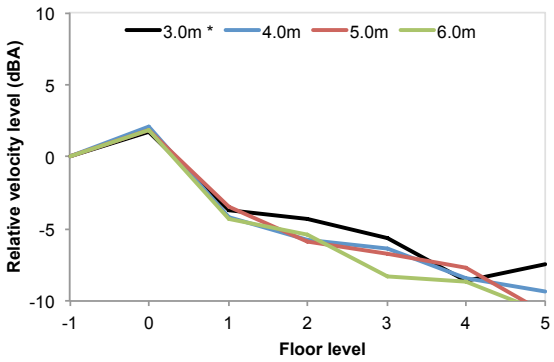

The storey height has a moderate effect on the propagation of vibration through the structure for the values considered. At column locations the W_b-weighted acceleration values (Figure 5-22) are similar at the low storeys and the uppermost storey, but buildings with greater storey heights exhibit slightly reduced vibration levels at the intermediate storeys (by up to about 1 dB). A similar observation can be made for the mid-span locations (Figure 5-24), but a slightly greater influence is noted at the intermediate storeys with storey height accounting for a reduction in vibration of up to 3 dB. For A-weighted velocity levels at column and mid-span locations (Figure 5-23 and Figure 5-25), there are slight differences between the model results (up to 1-2 dB), but the differences are not consistent between models, making it difficult to identify trends.

When comparing these results with the previously presented results for number of storeys (with a constant storey height) interesting results are obtained to demonstrate whether the number of storeys is important when investigating the influence of building height. The mid-span vibration levels relative to the basement are shown in Figure 5-26 for overall W_b- weighted levels, and in Figure 5-27 for the overall A-weighted levels. It should be noted that evaluation of the vibration at roof level is also included in these results, with the marker removed.

Figure 5-26. Parametric study: Storey height and number of storeys, W_b-weighted basement-relative mid-span acceleration levels with storey

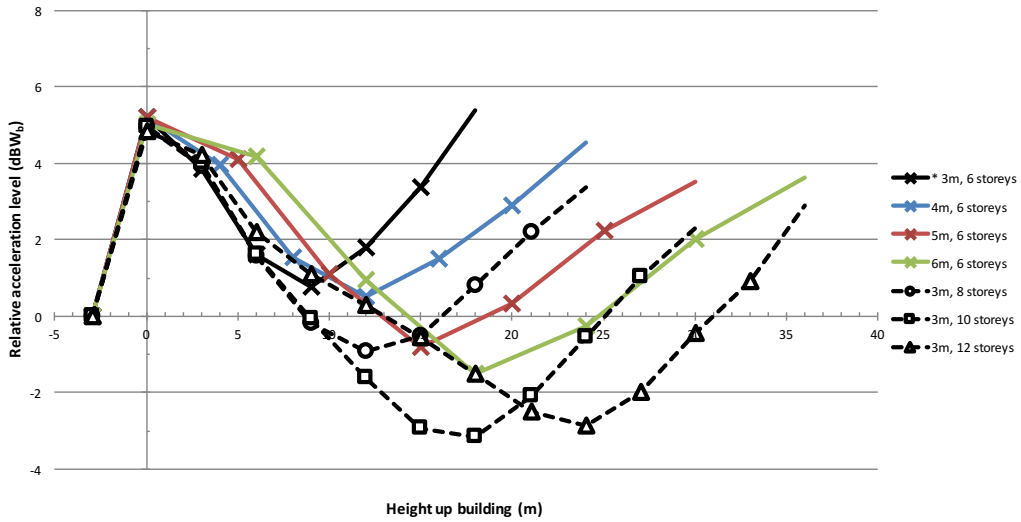

Figure 5-27. Parametric study: Storey height and number of storeys, A-weighted basement-relative mid-span velocity levels with storey

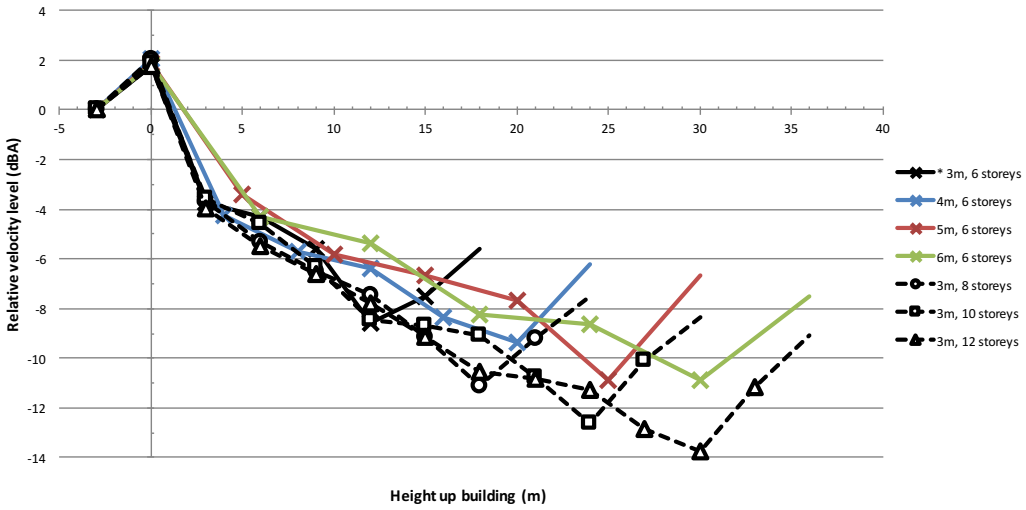

The results show that for buildings of otherwise equal height, those with more storeys typically exhibit greater vibration attenuation, having slightly reduced mid-span vibration levels at their uppermost storeys (by up to about 2 dB and 4 dB for W_b and A-weighted vibration respectively). The height up the building at which the minima occur is shown to be independent of the number of storeys, occurring at around half way up the building for the overall W_b-weighted vibration, and at the uppermost or penultimate storey for A-weighted vibration.

5.3.3 Ground floor storey height

The influence of ground floor storey height is studied as many modern buildings are designed as mixed use, for example with commercial units at ground level and office or residential accommodation at upper levels. In such buildings, the ground floor often is required to have a different height from the rest of the storeys. The values of ground floor storey height that have

been used for the study are 3, 4, 5 and 6 m, with the model geometries shown in Table 5-8. For the full results, refer to Appendix Section F.3.

Table 5-8. Generic building parametric study: Ground floor storey height, configurations

GF storey height	Image	GF storey height	Image
3.0 m *	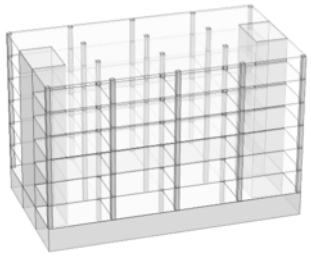	4.0 m	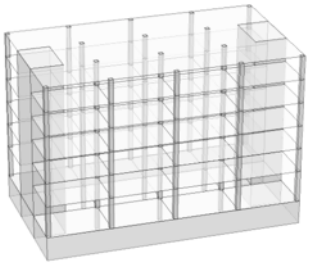
5.0 m	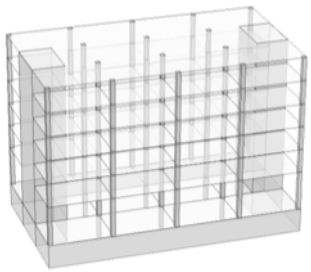	6.0 m	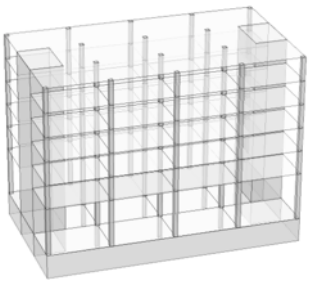

Adjustments to the ground floor storey height are seen to have only a minor influence, which predominantly affects the mid-span low frequency results between ground and first floor levels (Figure F-17); increasing the height from 3.0 to 6.0 m reduces overall W_b-weighted vibration levels at all storeys above ground floor by around 1 dB. There is a ~2 dB reduction in maximum one-third octave band level for the mid-span results (Table F-6) by increasing the ground floor height from 3.0 to 6.0 m.

5.4 Slab dimensions

5.4.1 Floor slab size

The effect of floor slab size has been investigated by altering the dimensions of the floor slabs in the FE building model. Four configurations have been used with the model geometries presented in Table 5-9. Figure 5-28 to Figure 5-31 show the overall W_b and A-weighted vertical vibration levels evaluated at mid-span and column locations. The results are discussed at the end of this section. For the full results, refer to Appendix Section F.4.

Table 5-9. Generic building parametric study: Floor slab size, configurations			
Slab size	Image	Slab size	Image
7 m x 5 m	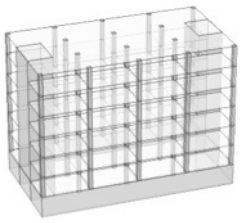	8 m x 6 m *	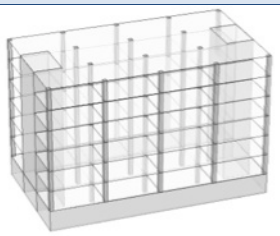
9 m x 7 m	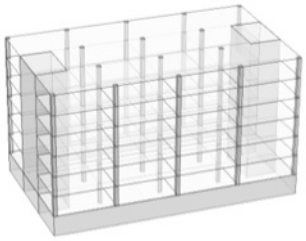	7 m x 7 m	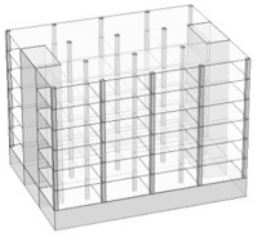

Figure 5-28. Parametric study: Floor slab size, W_b-weighted basement-relative column acceleration levels with storey

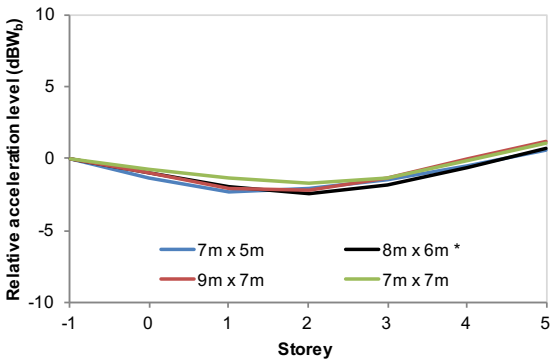

Figure 5-29. Parametric study: Floor slab size, A-weighted basement-relative column velocity levels with storey

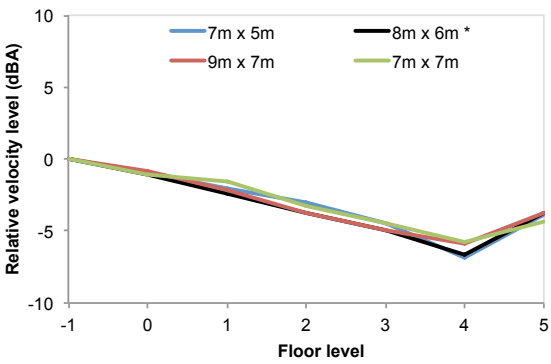

Figure 5-30. Parametric study: Floor slab size, W_b-weighted basement-relative mid-span acceleration levels with storey

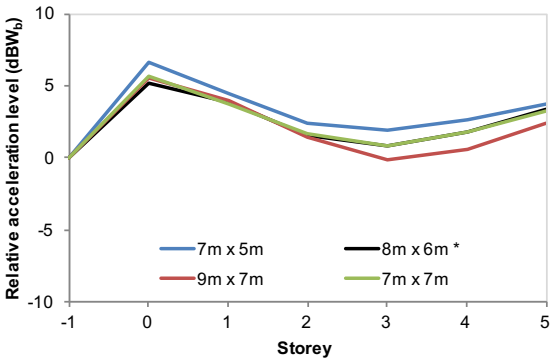

Figure 5-31. Parametric study: Floor slab size, A-weighted basement-relative mid-span velocity levels with storey

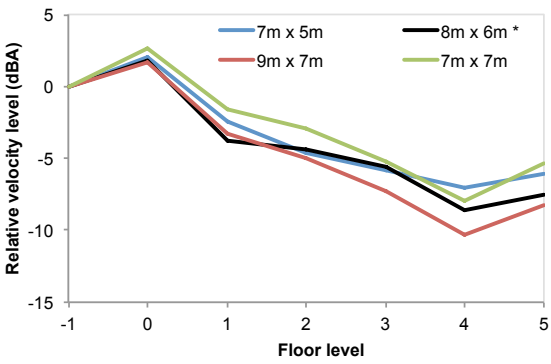

The maximum of the average column one-third octave vibration levels for each storey is shown in Figure 5-32. For mid-span positions, the equivalent results are given in Figure 5-33.

Figure 5-32. Parametric study: Floor slab size, maximum vertical vibration level relative to basement, column positions

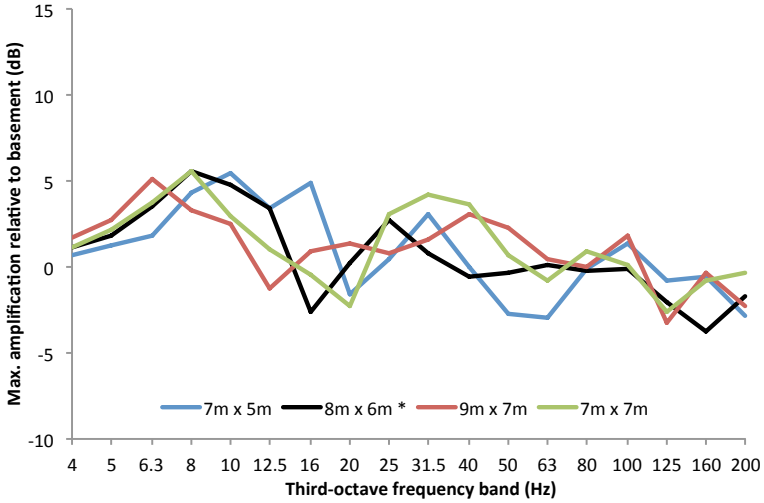

Figure 5-33. Parametric study: Floor slab size, maximum vertical vibration level relative to basement, mid-span positions

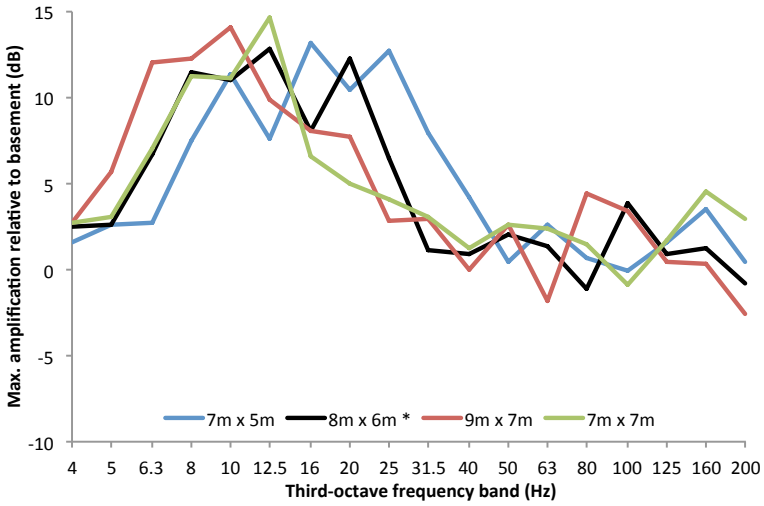

The first floor average mid-span vibration relative to column vibration is given in Figure 5-34.

Figure 5-34. Parametric study: Floor slab size, average vertical vibration level at mid-span relative to column positions, first floor

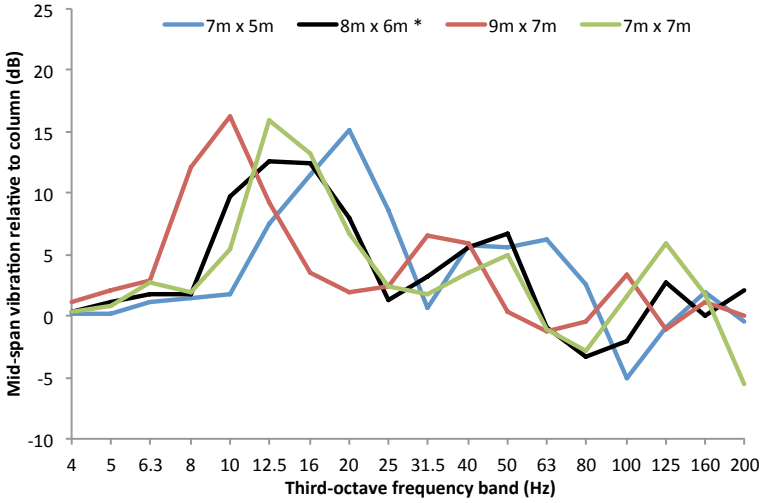

The results for floor slab size show that for column positions there is negligible effect on overall W_b-weighted levels (Figure 5-28), but for A-weighted levels (Figure 5-29) the 7x7 m and 7x5 m slab models exhibit slightly higher vibration levels (~1 dB) than the other configurations at first floor and above.

For mid-span locations, the largest 9x7 m slab displays the highest overall W_b-weighted vibration levels (Figure 5-30), around 2 dB greater than the other configurations at first floor. In the A-weighted results (Figure 5-31), there seems to be a good correlation between slab size and vibration level, which is in general progressive over the height of the building such that at the uppermost storey the 7x5 m slab exhibits vibration levels 3-4 dB higher than the 9x7 m slab. The inference is therefore that when groundborne noise is a consideration, larger slab sizes should be preferred over smaller ones (with all other relevant parameters remaining constant), whereas for perceivable vibration the opposite is the case.

For maximum one-third octave band levels at column positions (Figure 5-32), the slab configurations all give roughly the same maximum level, although the frequency at which this occurs is shifted. This appears not to be due to the natural frequencies of the slabs themselves but due to the increased mass of the larger slabs causing a shift in the column response. For the mid-span values (Figure 5-33), the frequencies of maximum response are also shifted, although the actual values are of the same order (in contrast to the observation by Villot et al in [102]). The 7x7 m slab shows a slightly greater response than the other configurations (by ~1-2 dB), probably because of its square shape.

5.4.2 Floor slab thickness

No images are given for the slab thickness configurations because the thickness is a parameter of the floor shell elements, with no visual change in model geometry. For the full results, refer to Appendix Section F.5.

The results show negligible differences for the overall column vibration levels over the range of floor thicknesses studied (Figure F-29 and Figure F-30). For the overall mid-span W_b and A-weighted vibration levels (Figure F-31 and Figure F-32), the 0.25 m slab gives results which were fairly consistently greater than the 0.30 m slab configuration, by 1-2 dB at first floor and above. The implication is that for controlling groundborne noise and vibration at mid-span locations, thicker slabs should be preferred (all other relevant parameters remaining equal).

For maximum one-third octave band levels, no significant influence is observed for the column positions (Table F-9). It may be relevant to note that the variation in floor mass caused by the range of slab thickness values considered, is about half of the range considered in the preceding section concerned with the floor slab size. For the mid-span positions (Table F-10), the thicker slabs result in a marginally greater maximum response. The 0.25 m slab has its maximum response at the uppermost storey, which is understood to be due to the column resonance becoming closer in frequency to the fundamental natural frequency of the slab.

It should be noted that the changes in modal frequencies associated with the floor thickness observed by Villot et al in [102] were not observed in the results of this study, probably due to the limited practical range of values for this parameter (i.e. it would be unusual to find suspended concrete floors with a thickness much outside of the parameters investigated here).

5.5 Building arrangement

5.5.1 Building length

The effect of building length has been investigated by altering the number of floor bays along the length of the FE building model. Four configurations have been used between three and six bays; the resulting model geometries are presented in Table 5-10. For the full results, refer to Appendix Section F.6.

Table 5-10. Generic building parametric study: Building length, configurations			
No. slabs	Image	No. slabs	Image
3	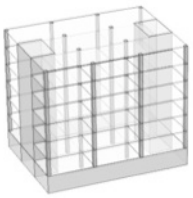	4 *	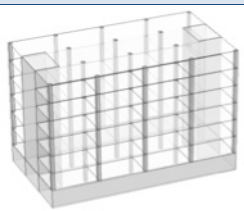
5	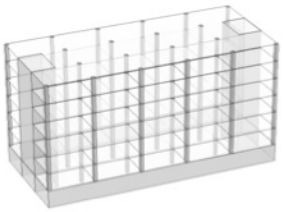	6	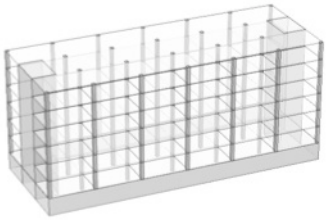

The results show that the building length has a small effect on the vibration levels, at both column and mid-span locations, but a particular trend between building length and vibration is not readily observable. The building with the shortest length (3 slabs) seems to exhibit marginally greater vibration levels (less than 1 dB) compared with the other building models at first floor and above, whereas the longest building seems to give marginally lower vibration levels.

For the maximum one-third octave bands, the length of the building appears to have a slight smoothing effect on the results for the column positions (Figure F-40), and to a lesser extent the mid-span locations (Figure F-41), with the longest building showing a maximum vibration level 1-2 dB less than that for the shortest building.

5.5.2 Building width

In a similar way, the effect of building width has been investigated by altering the number of floor bays across the width of the FE building model. Three configurations have been used between three and five bays; the resulting model geometries are presented in Table 5-11. Note that for the building with four bays in the width, the shaft placement was adjusted from the centreline of the building. For the full results, refer to Appendix Section F.7.

Table 5-11. Generic building parametric study: Building width, configurations			
No. slabs	Image	No. slabs	Image
3*	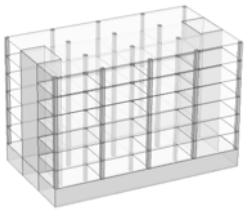	4	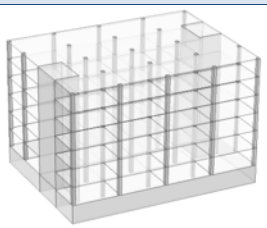
5	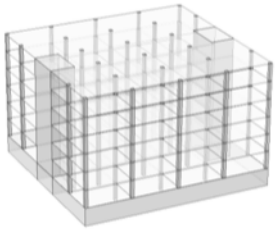	-	-

The results show negligible differences between the four and five slab width models in terms of the overall vibration levels, but a marginal difference between these and the three slab width model: for the A-weighted value at column locations (Figure F-44), the difference is progressive with increasing storey, and amounts to levels around 1 dB higher at the uppermost storey for the three slab width model. In terms of W_b-weighted overall vibration level at mid-span locations (Figure F-45) the three slab width model gives vibration levels about 1 dB less than the others from ground floor up.

For the maximum one-third octave band values at both column and mid-span locations, the three slab width model gives a maximum level which is around 2 dB less than the other models.

5.5.3 Column cross-section

The effect of column cross-section has been investigated by altering the cross-sectional area and shape of the FE building model columns. Six configurations have been used, which are described in Table 5-12. The images for the resulting model geometries are not shown as the visual differences are small. For the full results, refer to Appendix Section F.8.

Table 5-12. Generic building parametric study: Column cross-section		
Label	Description	Cross-sectional area (m^2)
0.16sq.m square	Square cross-section with side length 0.40 m	0.16
0.25sq.m square*	Square cross-section with side length 0.50 m	0.25
0.36sq.m square	Square cross-section with side length 0.60 m	0.36
0.49sq.m square	Square cross-section with side length 0.70 m	0.49
0.64sq.m square	Square cross-section with side length 0.80 m	0.64
0.25sq.m circle	Circular cross-section with diameter 0.56 m	0.25

The first floor average mid-span vibration relative to column vibration is given in Figure 5-35.

Figure 5-35. Parametric study: Column cross-section, average vertical vibration level at mid-span relative to column positions, first floor

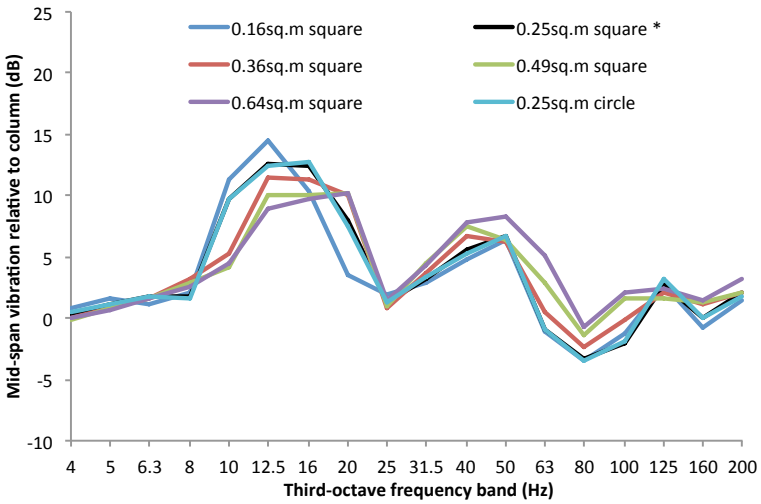

For different cross-sections there is little observable difference at column positions for the parameter values examined. The more significant effect is seen at mid-span, which is not an intuitive observation. The difference is most prominent at 3rd and 4th floors of the building, where it is seen that for both W_b and A-weighted values (Figure F-52 and Figure F-53), there is a spread of 4-5 dB between model results, with the greater predicted vibration levels provided by the columns with the largest cross-sectional area.

It has been shown that a circular or square cross-section shape is of no consequence, so long as the cross-sectional area (or perhaps more accurately, the second moment of area, which differs by only about 5% for a square and circle of equal area) is maintained.

Modelling the columns as beam elements is considered in Appendix A.

5.5.4 Internal walls

The effect of internal walls on the building response has been investigated by the inclusion of vertical plates in the model at ground floor and above. Concrete walls have been assumed with the following properties: thickness 0.1 m; density 2400 kg.m^{-3}; Young's modulus 26 GPa; damping loss factor 0.05. In addition, two cases have been considered with the stiffness increased by a factor of 2 (to 52 GPa), and with the damping increased by a factor of 2 (to a loss factor of 0.1). Views of the model geometry are given in Figure 5-36. Figure 5-37 to Figure 5-40 show the overall W_b and A-weighted vertical vibration levels evaluated at mid-span and column locations. The results are discussed at the end of this section. For the full results, refer to Appendix Section F.9.

Figure 5-36. Generic building parametric study: Internal walls			
	Image		Image
Default *	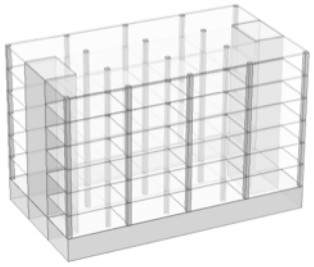	Internal walls	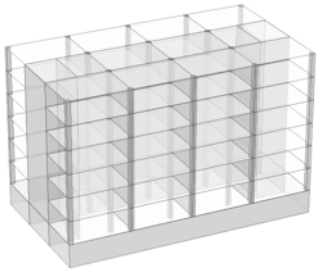

Figure 5-37. Parametric study: Int. walls, W_b-weighted basement-relative mid-span acceleration levels with storey

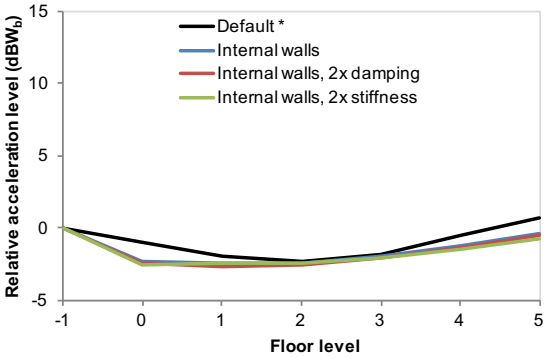

Figure 5-38. Parametric study: Int. walls, A-weighted basement-relative column velocity levels with storey

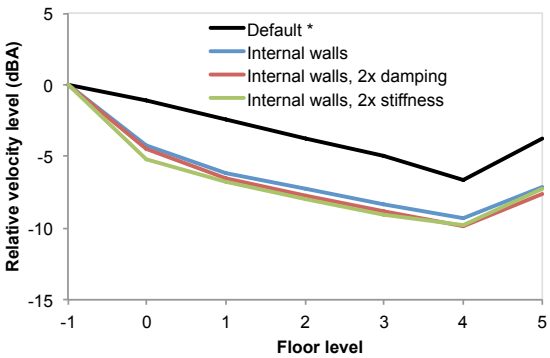

Figure 5-39. Parametric study: Int. walls, W_b-weighted basement-relative mid-span acceleration levels with storey

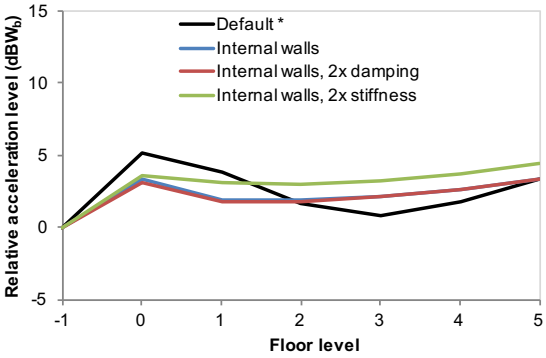

Figure 5-40. Parametric study: Int. walls, A-weighted basement-relative mid-span velocity levels with storey

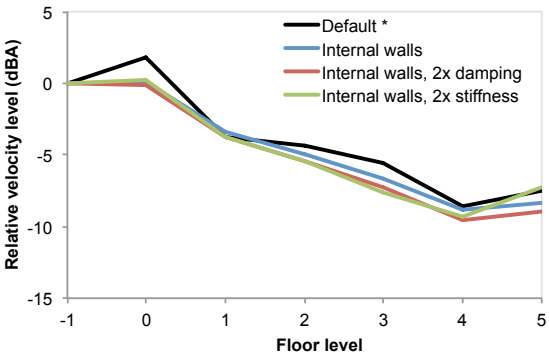

The results show that the presence of internal walls may have an appreciable influence on vibration propagation through the building. With the internal walls in place the whole building is stiffer, which tends to shift the response spectra upward in frequency. In addition, the stiffness of upper floors becomes more significant compared with the stiffness at basement level (which is not modelled as having internal walls). This results in a slight decoupling of the upper building from the basement level, and explains the additional attenuation observed between basement and ground floor levels for column locations at higher frequencies and in terms of the A-weighted level. This effect is less evident for the mid-span locations, due to this 'decoupling' effect being

offset by the upward shift in the response spectrum, which increases the mid-span vibration energy in the audible range.

It is found that once internal walls are included in the model, alterations to the stiffness or damping of the internal walls for the range of values considered do not have a significant effect. In particular, the influence of damping is negligible, whilst doubling the stiffness causes some changes in the response spectrum that result in a slight increase in the mid-span W_b-weighted overall vibration levels above ground floor.

5.6 Material properties

5.6.1 Structural damping

The effect of structural damping has been investigated by altering the loss factor for the materials in the FE model. Four conditions have been used: 0.01, 0.05 and 0.1 throughout the building, and an additional 'mixed' case where a higher value of damping was specified for the basement slab (0.05) compared to the rest of the building model (0.005). Whilst it is convenient to assume a single damping value throughout the building, the mixed case may be more realistic due to the increased damping at basement level through radiation into the ground. Figure 5-41 to Figure 5-44 show the overall W_b and A-weighted vertical vibration levels evaluated at mid-span and column locations. The results are discussed at the end of this section. For the full results, refer to Appendix Section F.10.

Figure 5-41. Parametric study: Structural damping (by loss factor), W_b-weighted basement-relative column acceleration levels with storey

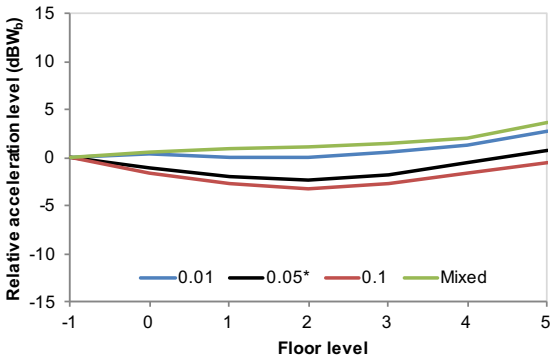

Figure 5-42. Parametric study: Structural damping (by loss factor), A-weighted basement-relative column velocity levels with storey

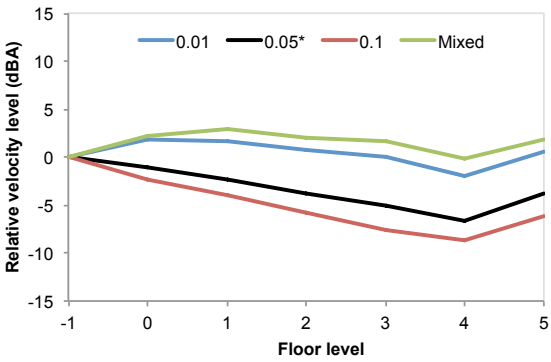

Figure 5-43. Parametric study: Structural damping (by loss factor), W_b-weighted basement-relative mid-span acceleration levels with storey

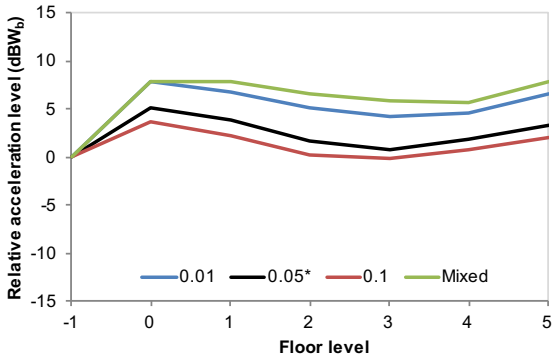

Figure 5-44. Parametric study: Structural damping (by loss factor), A-weighted basement-relative mid-span velocity levels with storey

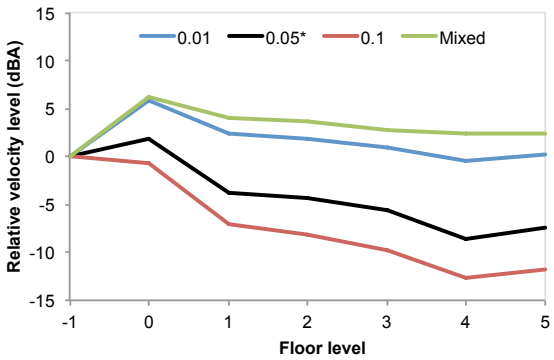

The maximum of the average column one-third octave vibration levels for each storey is shown in Figure 5-45. For mid-span positions, the equivalent results are given in Figure 5-46.

Figure 5-45. Parametric study: Structural damping, maximum vertical vibration level relative to basement, column positions

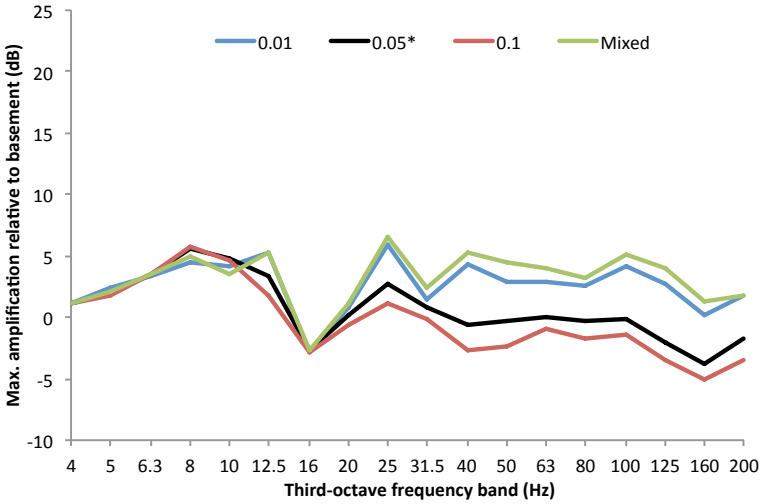

Figure 5-46. Parametric study: Structural damping, maximum vertical vibration level relative to basement, mid-span positions

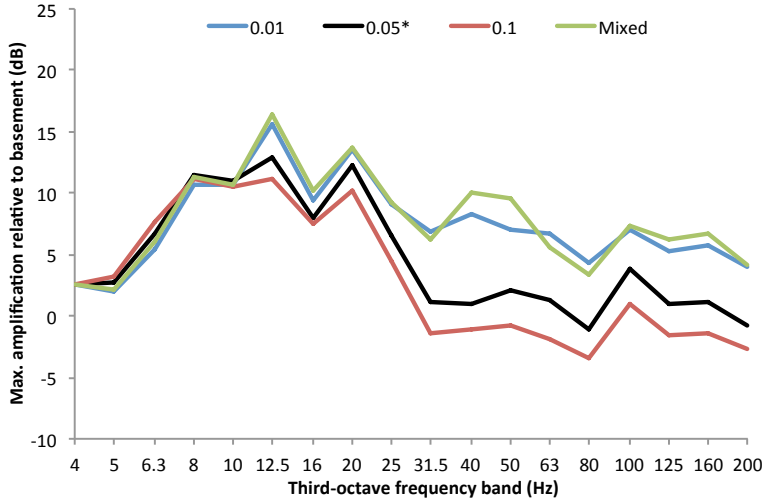

The first floor average mid-span vibration relative to column vibration is given in Figure 5-47.

Figure 5-47. Parametric study: Structural damping, average vertical vibration level at mid-span relative to column positions, first floor

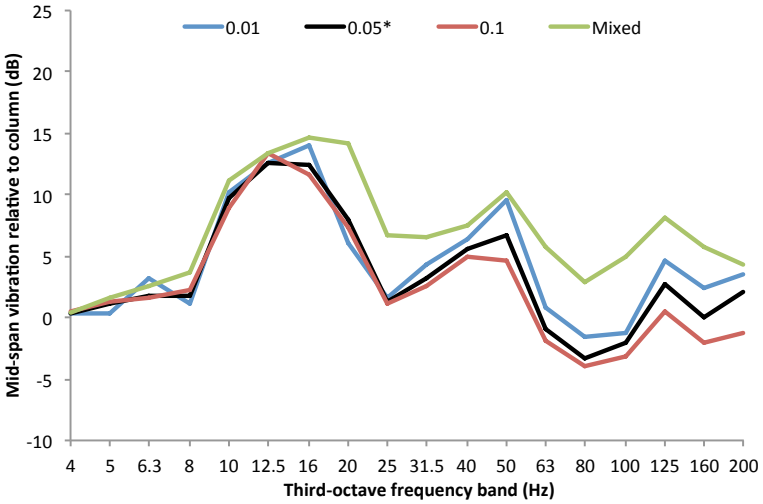

The structural damping of the building is shown to be important. For column positions, it is seen to have greatest effect at high frequencies, such that it accounts for negligible variation in the W_b-weighted velocity level over all storeys (Figure 5-41), but up to 7 dB for the A-weighted levels (Figure 5-42), where increasing the damping resulted in reduced vibration levels.

For the mid-span positions the damping accounts for a slightly greater variation of around 2 dB for the W_b-weighted overall vibration (Figure 5-43), and 10 dB for the A-weighted (Figure 5-44). Most of the variation in amplification occurs between basement and ground floor for all overall values.

For the maximum one-third octave band levels, the damping had the most significant effect at the mid-span positions (Figure 5-46), accounting for a difference of up to around 5 dB at 12.5 Hz.

It should be noted that the frequency resolution of the FE analysis was not adjusted for this study, and therefore for the lowest values of damping the vibration values may be underestimated.

The results show that for the generic building model presented here, the damping loss factor of 0.05 throughout the building corresponds best with trends observed in measured data (comparing Figure 5-44 with Figure 3-27).

Above ground floor, the mixed damping case showed reduced inter-storey attenuation at the upper frequencies compared to the other damping cases and measurement trends. It is therefore likely that this value of damping is too low. Whilst it seems reasonable that the basement levels should exhibit higher damping than the rest of the building, further work is required to ascertain whether other combinations of damping values provide more representative results.

5.6.2 Material density

The effect of material density on the building dynamics is investigated by applying a multiplication factor to the default values given in Table 5-1 by 0.7, 1.3, 1.6 and 2.0. Figure 5-48 to Figure 5-51 show the overall W_b and A-weighted vertical vibration levels evaluated at mid-span and column locations. The results are discussed at the end of this section. For the full results, refer to Appendix Section F.11.

Figure 5-48. Parametric study: Density multiplication factor, W_b-weighted basement-relative mid-span acceleration levels with storey

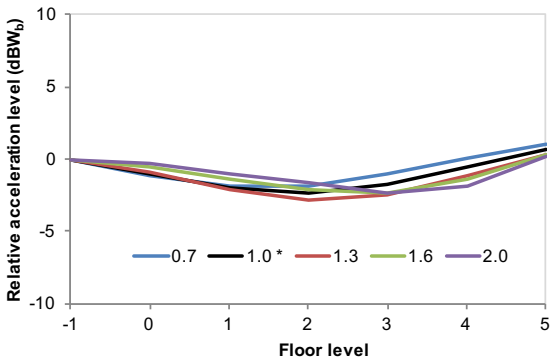

Figure 5-49. Parametric study: Density multiplication factor, A-weighted basement-relative column velocity levels with storey

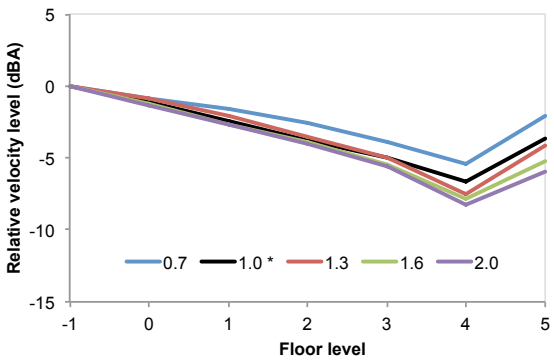

Figure 5-50. Parametric study: Density multiplication factor, W_b-weighted basement-relative mid-span acceleration levels with storey

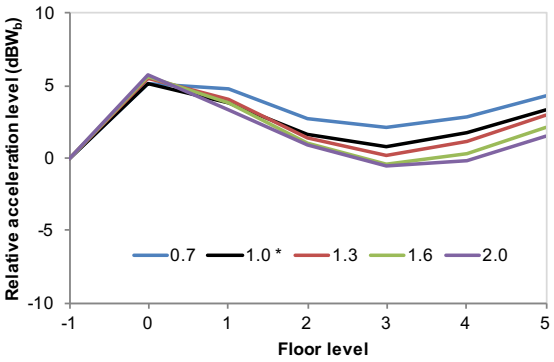

Figure 5-51. Parametric study: Density multiplication factor, A-weighted basement-relative mid-span velocity levels with storey

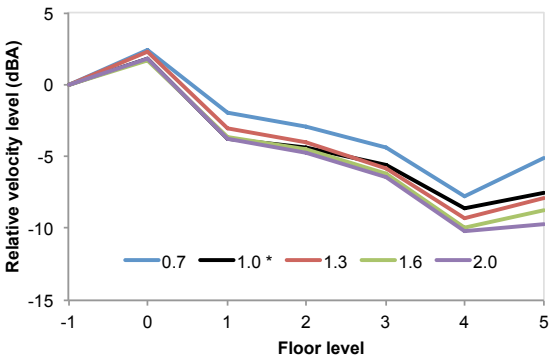

The maximum of the average column one-third octave vibration levels for each storey is shown in Figure 5-52. For mid-span positions, the equivalent results are given in Figure 5-53.

Figure 5-52. Parametric study: Density multiplication factor, maximum vertical vibration level relative to basement, column positions

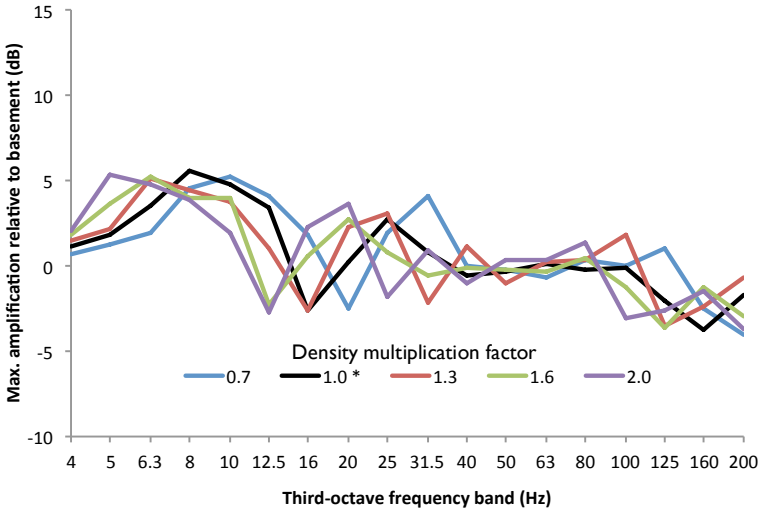

Figure 5-53. Parametric study: Density multiplication factor, maximum vertical vibration level relative to basement, mid-span positions

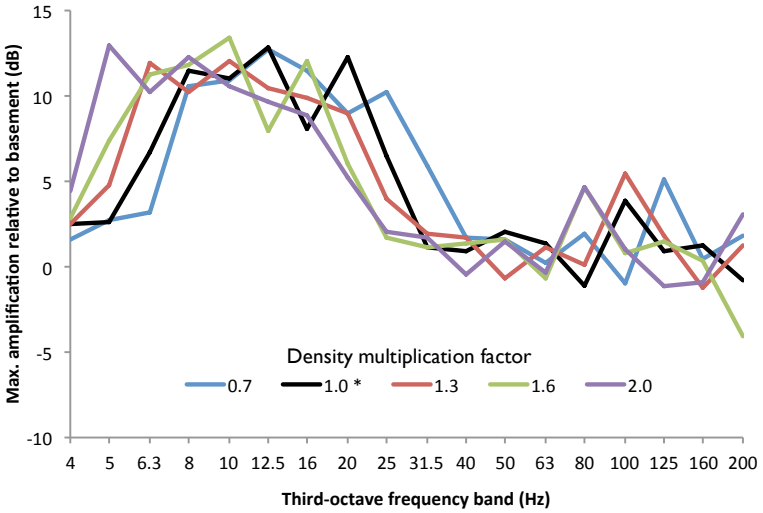

The first floor average mid-span vibration relative to column vibration is given in Figure 5-54.

Figure 5-54. Parametric study: Density multiplication factor, average vertical vibration level at mid-span relative to column positions, first floor

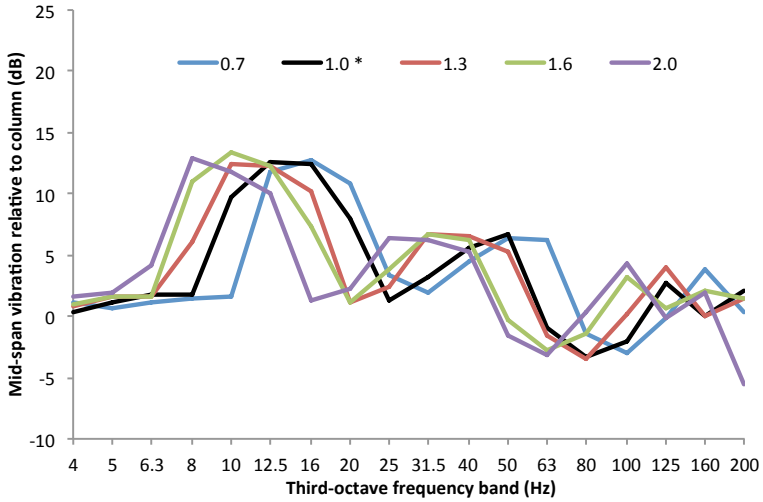

The results in Figure 5-49 and Figure 5-51 show that overall A-weighted levels are slightly more attenuated in buildings where denser materials are used. The effect is progressive with increasing storey such that by the uppermost storey a ~4 dB spread of levels is observed (column and mid-span positions). However, the range of density factors considered in this study is exaggerated compared with the values likely to be encountered in a typical building design situation, for which a spread of around 2 dB at top floor might be more realistic. When considering overall W_b-weighted levels, a spread of about 2 dB is observed at mid-span positions (mainly at ground and first floor), with negligible difference at column positions. The highest levels in this region correspond to the models with the greatest density. However, by inspection of the maximum results, it is found that the amplification levels are not inherently increased with the greater density materials, but a downward shift in frequency spectrum is noted. It is therefore important to note that the observations relating to overall vibration levels may not be the case for all input spectra.

5.6.3 Material stiffness (Young's modulus of elasticity)

The effect of material stiffness on the building dynamics are investigated by calculating the response for the following values of Young's modulus 20, 26, 40 and 60 GPa. Figure 5-55 to Figure 5-58 show the overall W_b and A-weighted vertical vibration levels evaluated at mid-span and column locations. The results are discussed at the end of this section. For the full results, refer to Appendix Section F.12.

Figure 5-55. Parametric study: Material stiffness, W_b-weighted basement-relative column acceleration levels with storey

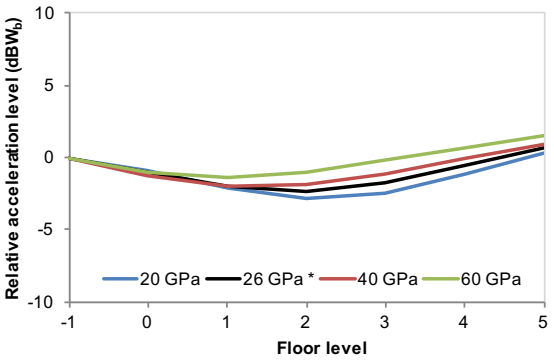

Figure 5-56. Parametric study: Material stiffness, A-weighted basement-relative column velocity levels with storey

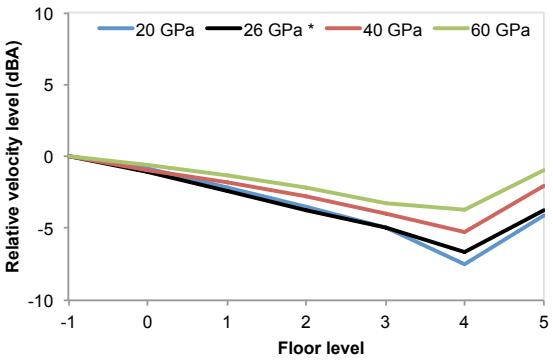

Figure 5-57. Parametric study: Material stiffness, W_b-weighted basement-relative mid-span acceleration levels with storey

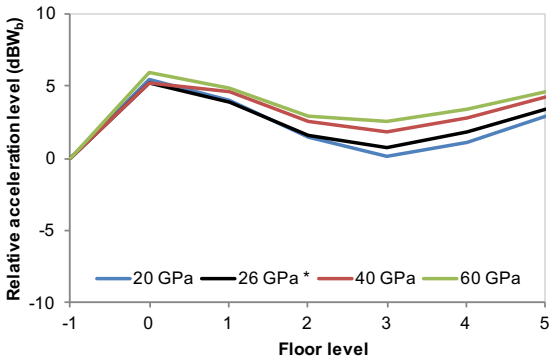

Figure 5-58. Parametric study: Material stiffness, A-weighted basement-relative mid-span velocity levels with storey

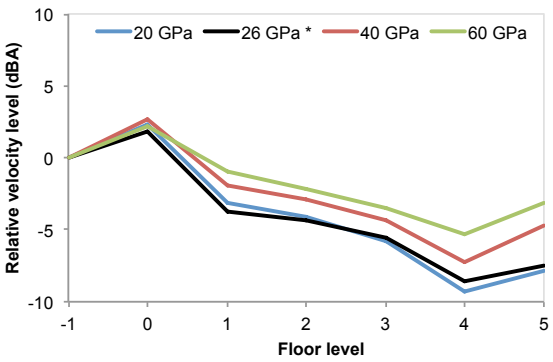

The maximum of the average column one-third octave vibration levels for each storey is shown in Figure 5-59. For mid-span positions, the equivalent results are given in Figure 5-60.

Figure 5-59. Parametric study: Material stiffness, maximum vertical vibration level relative to basement, column positions

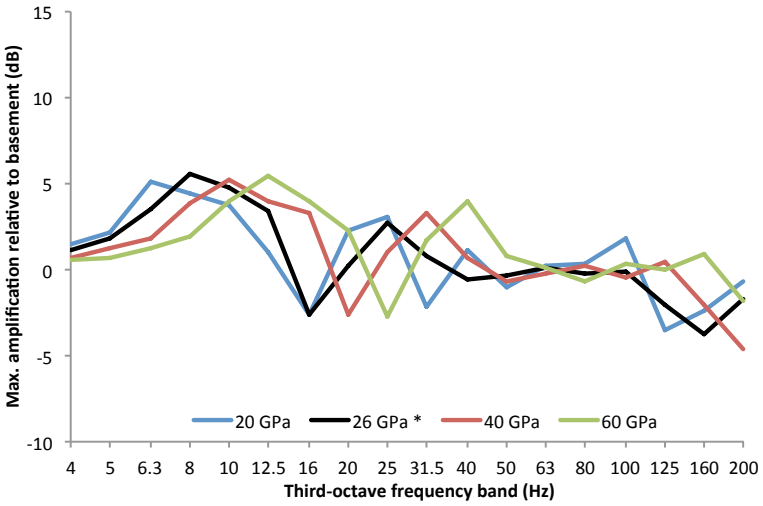

Figure 5-60. Parametric study: Material stiffness, maximum vertical vibration level relative to basement, mid-span positions

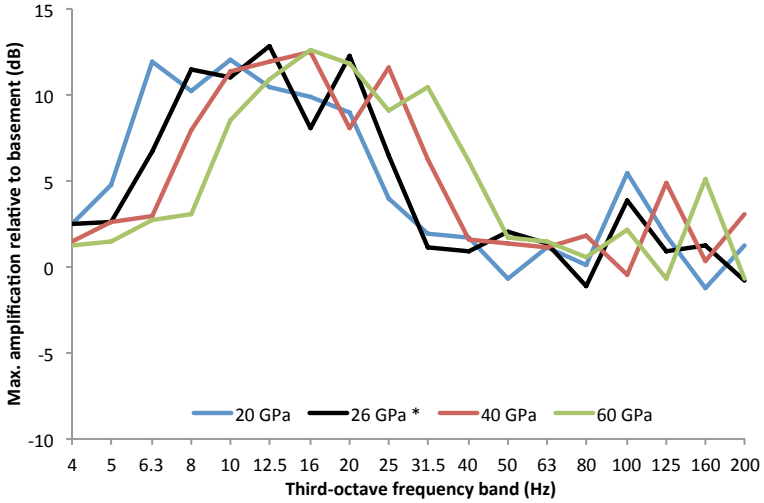

The first floor average mid-span vibration relative to column vibration is given in Figure 5-61.

Figure 5-61. Parametric study: Material stiffness in Young's modulus of elasticity, average vertical vibration level at mid-span relative to column positions, first floor

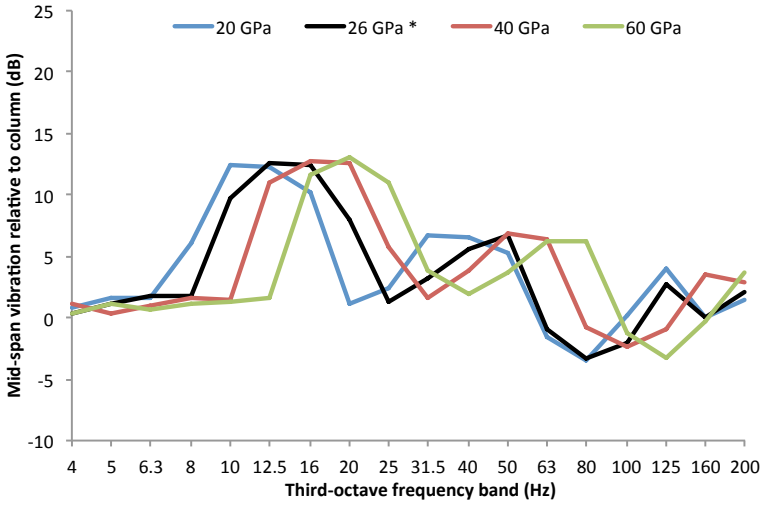

The investigation into the effect of material stiffness on the response of the building shows that, similar to the density, changing the parameter shifts the frequency response (increasing stiffness shifts the curve to higher frequencies), but not the maximum amount of amplification. As the frequency content of the response rises, the major response peaks are pushed further into the audible frequency region, and as such the A-weighted overall levels are seen to increase; doubling the stiffness results in an increase of around 2 dB in the mid-span A-weighted velocity level at first floor. When considering W_b-weighted vibration levels, stiffness is shown not to have an appreciable effect on vibration levels near columns, but for mid-span locations doubling the stiffness results in a reduction in vibration levels mainly at ground and first floor by about 2 dB.

5.7 Building excitation

5.7.1 Input force direction

The effect of the input force direction on the building response is investigated by calculating the response for force input with the following vectors: [0,0,1], [0.5,0.5,1] and [1,1,1], where the format is [*x*,*y*,*z*] and the axes are as described in Section 5.1. For the full results, refer to Appendix Section F.13.

The study on input force direction shows a slight relationship between direction and vibration level within the building. For the overall levels, this is only really seen in the A-weighted mid-span data (Figure F-88), accounting for a spread of around 3 dB at ground floor, but diminishing by the 2nd floor. Within this spread, the case with equal force in each direction gives the highest velocity levels, the case with only vertical force the lowest.

For the maximum one-third octave band values, there is no significant trend observed for column locations, but for the mid-span locations (Figure F-90) up to 16 Hz there is about 1 dB greater vibration levels for the case with only vertical excitation ([0,0,1]), than that with excitation equal in all directions ([1,1,1]). In the 63 and 80 Hz bands the opposite is true; a variation of 6-8 dB is observed where the case with only vertical excitation ([0,0,1]) exhibits the lowest vibration levels.

5.7.2 Input force location

In order to investigate the influence of the force location at the base of the building, the FE model response has been calculated for six cases, each of which has the input force acting over a different region. For brevity, it is helpful to shorten some of the descriptions for the parameters in this study. The shortened descriptions are shown in brackets and italicised together with the full descriptions and diagrams in Table 5-13. For the full results, refer to Appendix Section F.14.

Table 5-13. Generic building parametric study: Input force location, configurations			
	Image		Image
Base slab with structural walls *(Base + walls)* *	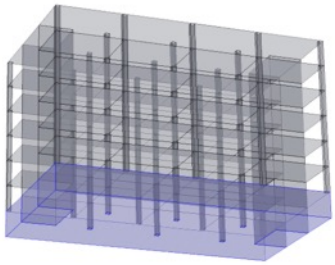	Base slab only *(Base only)*	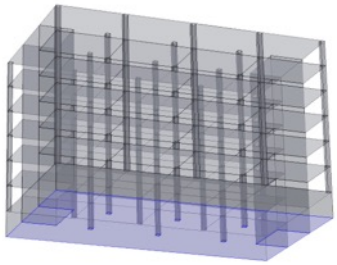
Base strip, central, over building width *(Base-strip, mid width)*	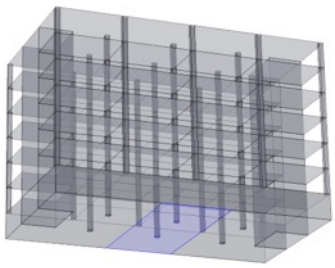	Base strip, at end, over building width *(Base-strip, end width)*	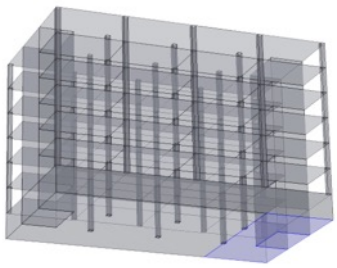
Base strip, central, over building length *(Base-strip, mid length)*	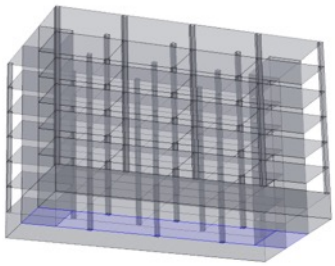	Base strip, at side, over building length *(Base-strip, side length)*	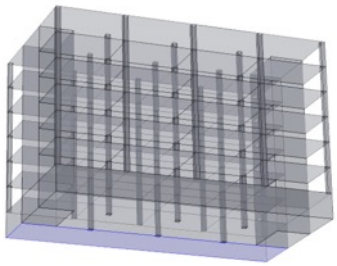

It should be noted that for this parametric study, the vibration at basement level was only evaluated within the region of excitation.

Figure 5-62 to Figure 5-65 show the overall W_b and A-weighted vertical vibration levels evaluated at mid-span and column locations. The results are discussed at the end of this section. Note that in Figure 5-62, the lines for the "Base + walls *" and "Base only" conditions are obscured in the centre of the figure by other lines.

Figure 5-62. Parametric study: Input force location, W_b-weighted basement-relative column acceleration levels with storey

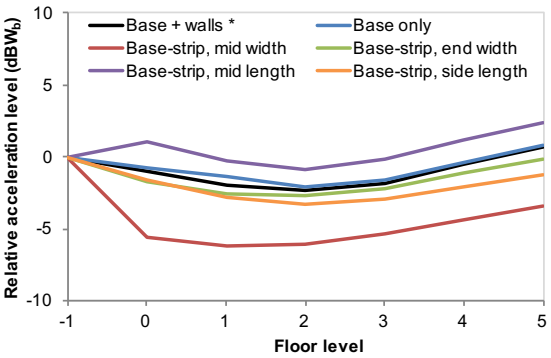

Figure 5-63. Parametric study: Input force location, A-weighted basement-relative column velocity levels with storey

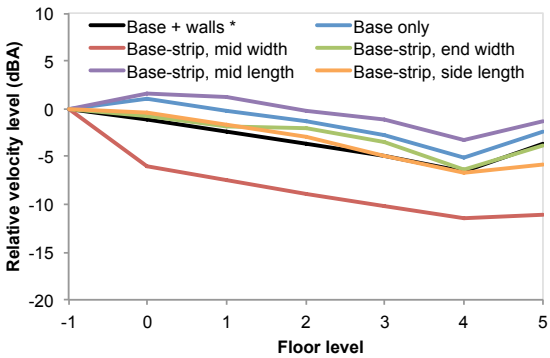

Figure 5-64. Parametric study: Input force location, W_b-weighted basement-relative mid-span acceleration levels with storey

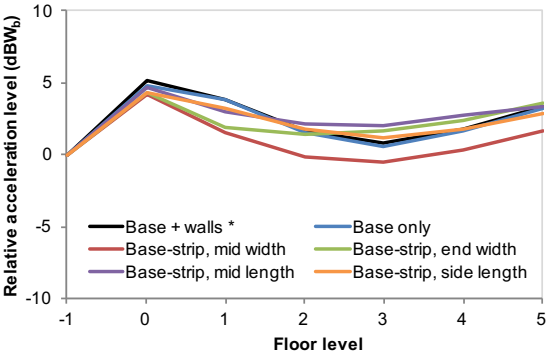

Figure 5-65. Parametric study: Input force location, A-weighted basement-relative mid-span velocity levels with storey

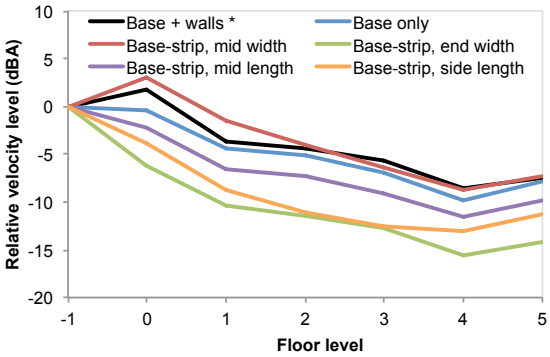

The maximum of the average column one-third octave vibration levels for each storey is shown in Figure 5-66. For mid-span positions, the equivalent results are given in Figure 5-67.

Figure 5-66. Parametric study: Input force location, maximum vertical vibration level relative to basement, column positions

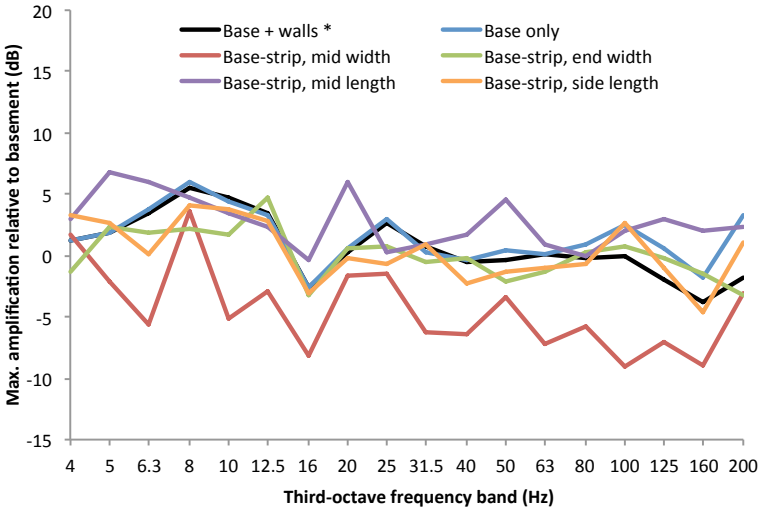

Figure 5-67. Parametric study: Input force location. maximum vertical vibration level relative to basement, mid-span positions

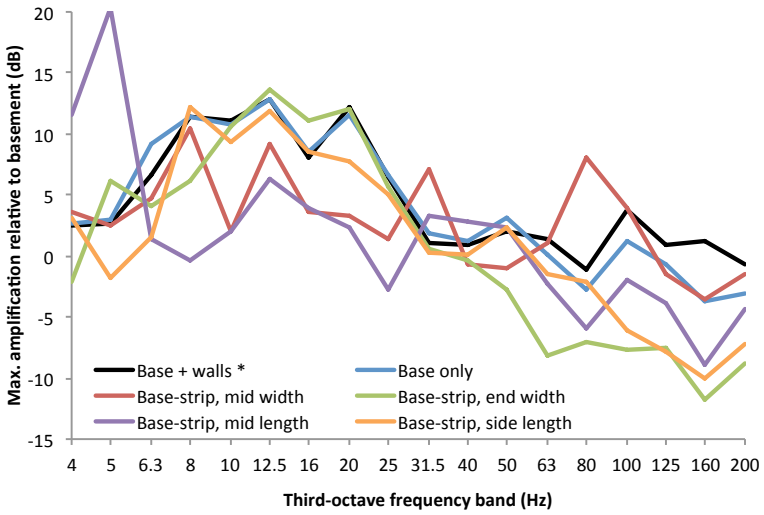

The first floor average mid-span vibration relative to column vibration is given in Figure 5-68.

Figure 5-68. Parametric study: Input force location, average vertical vibration level at mid-span relative to column positions, first floor

The input force location is found to have an important effect on the levels of vibration within the building between basement and ground floor levels, and a minor effect at upper storeys. For the overall W_b-weighted vibration levels, the case with the base strip located along the central length of the building gives the greatest relative vibration levels. The effect is more prominent at the mid-span positions where levels are 5 dB greater than for the default case (see Figure 5-64), than at column positions where levels are about 2 dB greater (see Figure 5-62). The reason for this case exhibiting the greatest relative vibration levels is that the input force location includes both of the structural shafts, and therefore vibration is efficiently transmitted to the upper storeys. By contrast, the case where the input force location is located across the central width of the building gives the lowest relative levels (for overall W_b-weighted vibration), probably because this forcing

region is not connected directly to any structural shafts, and therefore vibration is not so efficiently transmitted to the upper storeys of the building.

The patterns noted above for the overall W_b-weighted vibration also hold for the overall A-weighted vibration, but only for the column positions (Figure 5-63). For the mid-span positions (Figure 5-65), the case with the input force acting over the central width of the building actually causes a slightly greater vibration level increase (about 2 dB) than the other cases between the basement and ground floor levels. The mechanism for this is not fully understood, but it is dominated by the influence of a strong response around the 80 Hz one-third octave band (see Figure 5-67). The case in which the input force acts across the width at one end of the building shows the lowest relative A-weighted vibration levels at the mid-span positions, which is caused by greater reductions between basement and ground floor at frequencies above the 31.5 Hz band, although the mechanism is not fully understood.

Given both the lack of understanding about the physical mechanisms and the significant variation in results shown, it is recommended that further work should be done to investigate the effect of input force location. However, ideally this would be explored with a building model that is coupled to a representative ground model.

5.8 Other factors

The effect of some other model factors of interest are investigated, including the presence of structural shafts and basement walls, irregular column layout, and the inclusion of a double-mass floor construction at first floor to act as a "blocking floor" (following the approach of Sanayei et al [103]). Those factors which require changes to the geometry are shown in Table 5-14. Figure 5-69 to Figure 5-72 show the overall W_b and A-weighted vertical vibration levels evaluated at mid-span and column locations. The results are discussed at the end of this section. For the full results, refer to Appendix Section F.15.

Table 5-14. Generic building parametric study: Other factors, configurations			
	Image		Image
Default*	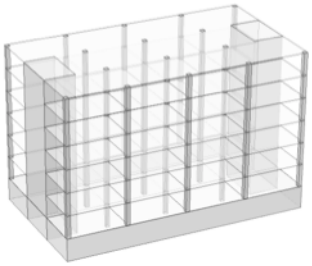	Irregular column layout	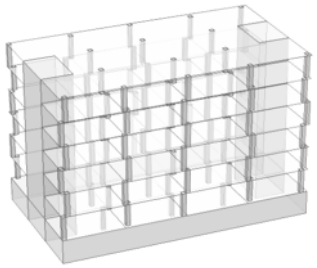
Without shafts	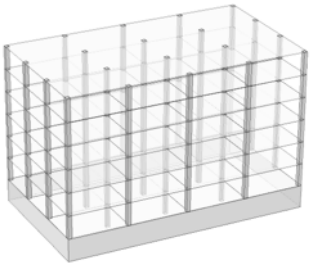	Without shafts & walls	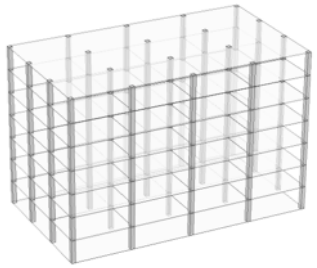

Figure 5-69. Parametric study: Other factors, W_b-weighted basement-relative mid-span acceleration levels with storey

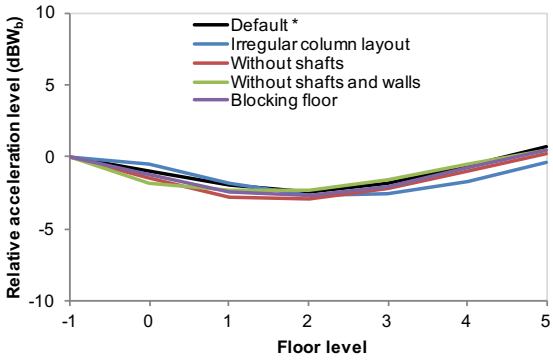

Figure 5-70. Parametric study: Other factors, A-weighted basement-relative column velocity levels with storey

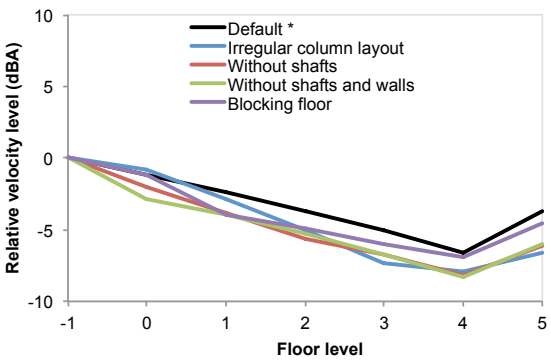

Figure 5-71. Parametric study: Other factors, W_b-weighted basement-relative mid-span acceleration levels with storey

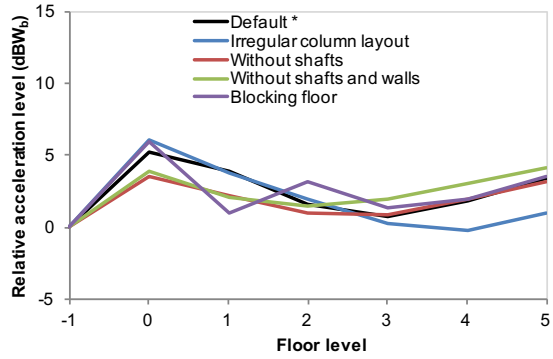

Figure 5-72. Parametric study: Other factors, A-weighted basement-relative mid-span velocity levels with storey

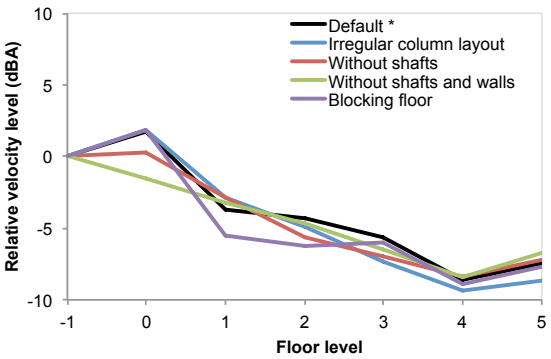

The maximum of the average column one-third octave vibration levels for each storey is shown in Figure 5-73. For mid-span positions, the equivalent results are given in Figure 5-74.

Figure 5-73. Parametric study: Other factors, maximum vertical vibration level relative to basement, column positions

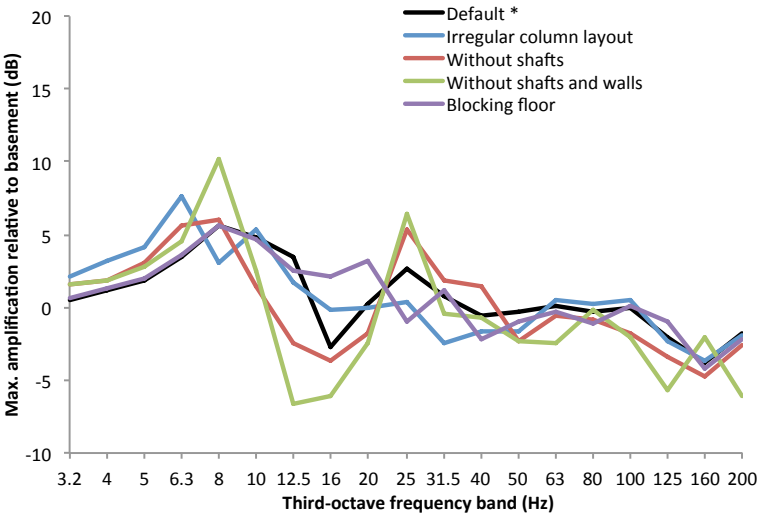

Figure 5-74. Parametric study: Other factors, maximum vertical vibration level relative to basement, mid-span positions

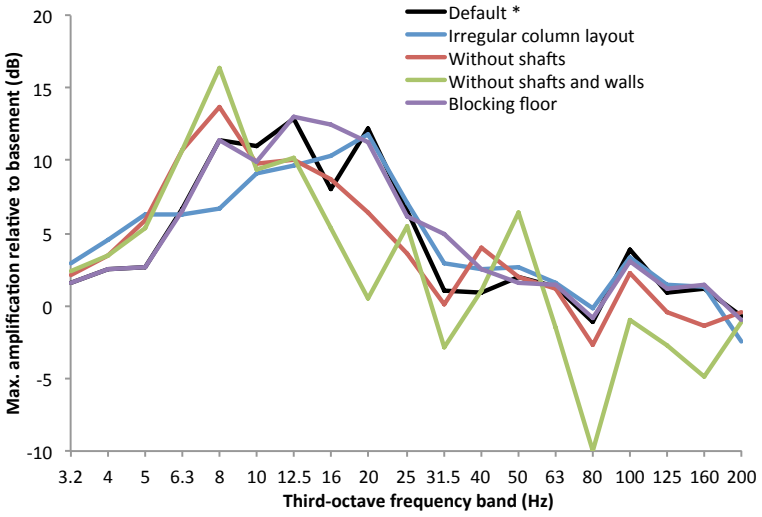

The first floor average mid-span vibration relative to column vibration is given in Figure 5-75.

Figure 5-75. Parametric study: Other factors, average vertical vibration level at mid-span relative to column positions, first floor

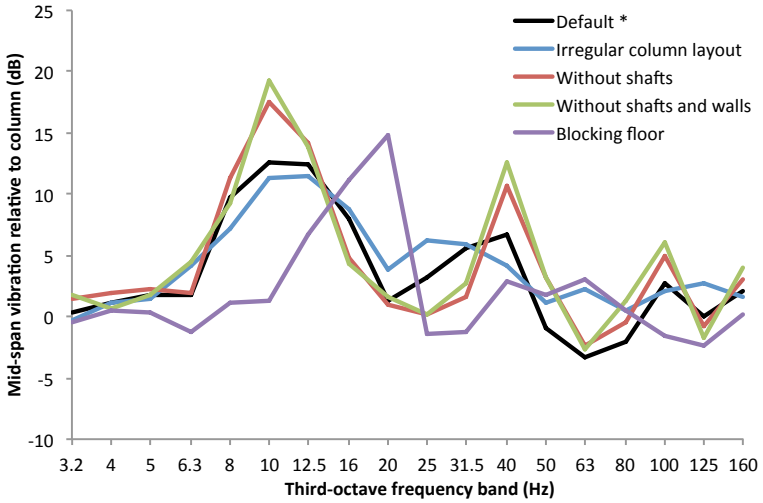

In terms of overall W_b-weighted vibration levels, it is found that at column locations (Figure 5-69), most geometry configurations give similar results, with the model that excludes structural shafts and walls showing levels around 1 dB greater than the others above first floor. At mid-span locations (Figure 5-71), greater variation occurs above first floor, up to around 5 dB at the uppermost storey. It is found that making the column layout more irregular could reduce overall vibration levels at the uppermost storey by 2 dB compared to the default condition. Omitting structural shafts causes an increase in overall vibration level of around 1 dB above first floor; additionally excluding structural walls between basement and ground floor increases these levels by a further 1 dB. Introduction of a double mass 'blocking' floor at first floor gives reduced vibration levels at its own storey by about 4 dB, but the storey directly above exhibits slightly greater vibration levels (1 dB) than for the case with no blocking floor, and at third floor and above there is negligible difference between the vibration levels compared to the default case.

In terms of A-weighted overall vibration levels (Figure 5-70 and Figure 5-72), the geometric adjustments investigated have a less pronounced influence. The main observations are that the configuration with irregular layouts accounts for a reduction in level of around 1 dB at the uppermost storey for mid-span positions, and the blocking floor shows a reduction in mid-span velocity level of about 2 dB itself, but with negligible differences at third floor and above. This is a different finding to Sanayei et al in [103], which predicted reductions of up to 3 dB at floor levels above the blocking floor.

In terms of maximum vibration in one-third octave bands, the irregular column layout is seen in general to reduce the prominence of peaks, whilst the omission of structural walls and shafts tends to coincide with an increase in these peaks. This is true at both mid-span and column positions.

5.9 Summary

A 3D FE model approach has been used as the basis of an extensive investigation into the influence that various parameters have on the transmission of vibration through a building structure. For most of the parameters, the influence is not observed as a straightforward amplification or attenuation, but rather in shifting natural frequencies of the building and floor slabs. This has an indirect influence on overall noise and vibration levels, which is dependent on the spectrum of the input. It is therefore recommended that in the development of more refined empirical approaches, the building and floor slab natural frequencies should be considered.

5.10 Development of empirical expressions

The results from the historical measurements and models have shown that whilst there are many individual factors that affect the level of vibration within a room, the most significant physical mechanisms are the vertical building modes, the level of damping and the modal characteristics of the floor plate. For simplicity of calculations, it is convenient to consider these as separate correction terms to be applied to a given vibration level at the base of the building. In this section, such correction terms are defined and then the results of this empirical model are compared with results from FE calculations and measurements.

5.10.1 Proposed empirical formulae

The approach to develop representative correction terms is based on deriving simple formulae that fit the observed trends in the model and measurement data.

The amplitude of the fundamental vertical building mode is greatest at roof level. The vertical vibration at column positions relative to basement, in this frequency range, has been found to have a spectrum shape $C_1(f)$ that can be expressed by the fundamental natural frequency, a maximum amplitude factor, and a frequency peak width term:

$$C_1(f) = C_{1,1} e^{-\left(\frac{f-f_0}{C_{1,2}}\right)^2} \quad \text{(dB)} \qquad \textbf{(5-1)}$$

where:

f_0 is the fundamental vertical natural frequency, in Hz. This may be known from measurements, or estimated from prediction models of the building;

$C_{1,1}$ is an amplitude factor, which will represent the total amplification in decibels at the roof level (relative to basement), at f_0;

$C_{1,2}$ is a frequency term in Hz, controlling the width of the peak in the correction term at f_0. For the generic concrete frame building model, a value of 5 Hz is suitable.

The spectra for the column vibration at roof level relative to basement are given in Figure 5-76 for the generic building FE model (mean and +/- one standard deviation), the equivalent empirical

expression (with f_0 =8 Hz, $C_{1,1}$ =8 dB, $C_{1,2}$ =5 Hz), and an alternative empirical expression (f_0=10 Hz, $C_{1,1}$=12 dB, $C_{1,2}$=4 Hz). The purpose of the alternative empirical expression is to show the influence of adjustments to the various terms.

Figure 5-76. Proposed empirical predictions, fundamental building mode correction at roof level

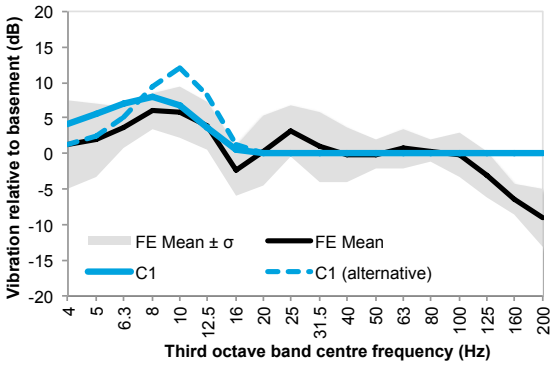

The influence of $C_1(f)$ must be zero at basement and maximum at roof level, as indicated diagrammatically in Figure 5-77, with n representing the storey index (where n=0 is the lowest basement level, and $n = N$ at the roof):. For the intermediate storeys there is an approximate logarithmic relationship with height up the building. This is observed in the measured and model data, such that for a building of N storeys (including basement levels), the influence of $C_1(f)$ at a storey index n can be expressed as $(\log_{10}(\frac{9n}{N} + 1)\, C_1(f)$. This 'influence' relationship with storey is shown for the generic building FE results and empirical expression in Figure 5-78, in which the basement-relative vibration level (in dB) in the frequency band dominated by the fundamental vertical building mode (8 Hz) has been normalised to the maximum basement-relative value (in dB) at roof level.

Figure 5-77. Indicative shape of $C_{1(f)}$ term and influence with storey

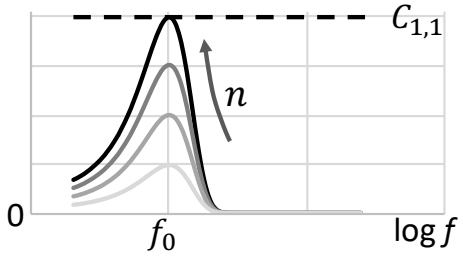

Figure 5-78. Proposed empirical predictions, fundamental building mode influence with storey

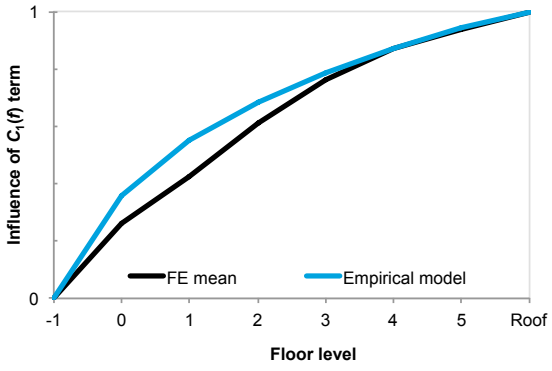

At higher frequencies, the measurements and models show an approximately steady damping loss in decibels on a per-storey basis. The shape of the per-storey attenuation spectrum $C_2(f)$ has

been found to be expressed suitably with a single constant that represents a -0.5 dB cut-off frequency for a function that acts as a low-pass filter:

$$C_2(f) = -\log_{10}\left(1 + \left(\frac{f}{C_{2,1}}\right) + \left(\frac{f}{C_{2,1}}\right)^4\right) \quad \text{(dB)} \qquad \textbf{(5-2)}$$

where:

$C_{2,1}$ is a frequency term in Hz, acting like a cut-off frequency for a low-pass filter. For the generic concrete frame building model, a value of 50 Hz is suitable.

The shape of the $C_2(f)$ term is shown in Figure 5-79. The influence of $C_2(f)$ at a storey index n can be expressed simply as $nC_2(f)$. The spectrum is shown for the generic building FE model, the equivalent empirical expression ($C_{2,1}$ =50 Hz), and an alternative empirical expression ($C_{2,1}$=25 Hz) in Figure 5-80 for 3rd floor. Uppermost storeys exhibit slightly reduced agreement in this frequency range due to roof effects that are not included in this approach.

Figure 5-79. Indicative shape of $C_{2(f)}$ term and influence with storey

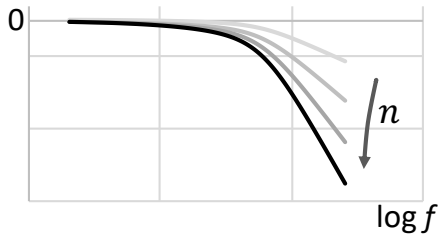

Figure 5-80. Proposed empirical predictions, per-storey attenuation correction at 3rd floor (n=4)

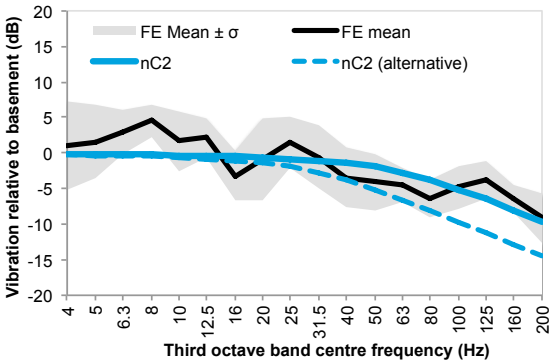

Combining the terms considered thus far, it is proposed that the vibration level at column locations, $L_{v,col}$ for a given 1/3 octave frequency band* f (in Hz) and at a given storey index n might be estimated from:

$$L_{v,col}(f,n) = L_{v,base}(f) + \log_{10}\left(\frac{9n}{N} + 1\right) C_1(f) + nC_2(f) \quad \text{(dB)} \qquad \textbf{(5-3)}$$

The vertical vibration at mid-span locations relative to column locations, has been found to be dependent on the floor slab modal effects. It is useful therefore to consider a number of modal frequencies for modes that have maximum amplitudes at the centre of the floorspan. $f_{(1,2,3)}$ are defined here as the first natural frequencies of a floor slab that provide an antinode at the floor's centre (i.e. the (1,1),(1,3) and (3,3) modes). Focus is given to these particular modes as they

* *Whilst the empirical formulae are derived for use with 1/3 octave frequency band data, the approach may be suitable for alternative frequency spacings, although this use would require further investigation.*

dominate the response at the centre of the floor slabs, which is the location used for many of the re-radiated noise prediction approaches in the literature. For a given floor slab, the mid-span correction spectrum $C_3(f)$, can be expressed as:

$$C_3(f) = 3.3C_{3,1}\log_{10}\left(1 + e^{-\left(\frac{f-f_1}{C_{3,2}}\right)^2} + 0.5e^{-\left(\frac{f-f_2}{C_{3,2}}\right)^2} + 0.5e^{-\left(\frac{f-f_3}{C_{3,2}}\right)^2}\right) \quad \text{(dB)} \quad \textbf{(5-4)}$$

where:

$f_{(1,2,3)}$ are the first three floor natural frequencies (in Hz) of the floor slab of interest that have an antinode at the centre of the floor span. These frequencies may be known from measurements, or estimated from prediction models.

$C_{3,1}$ is an amplitude factor, which will represent the total amplification in decibels at f_1.

$C_{3,2}$ is a frequency term in Hz, controlling the width of the peaks in the correction term at the resonance frequencies.

The shape of the $C_3(f)$ term is shown in Figure 5-81:

Figure 5-81. Indicative shape of $C_{3(f)}$ term

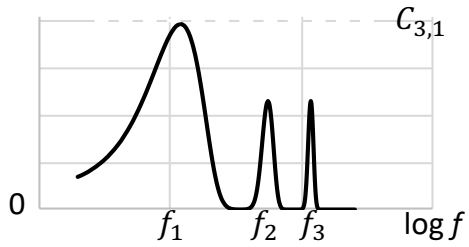

Natural frequencies were calculated for a single plate with the same geometry and material parameters as for a floor slab at 1st floor in the generic building model (i.e. 8 m x 6 m x 0.27 m concrete). This was done using a 3D finite element model, with symmetric boundary conditions specified for the edges. Using this approach, $f_{(1,2,3)}$ were found to be 12, 55 and 117 Hz respectively, with the mode shapes shown in Figure 5-82.

Figure 5-82. Example $f_{(1,2,3)}$ modeshapes and frequencies for a concrete floor slab

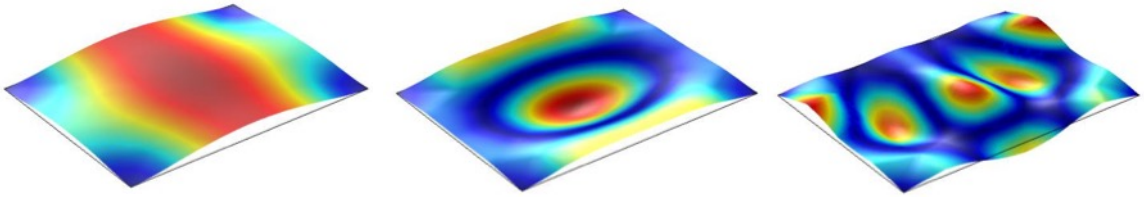

12 Hz (f_1) 55 Hz (f_2) 117 Hz (f_3)

The spectrum of $C_3(f)$ at 2nd floor is shown in Figure 5-88 for the generic building FE model, the equivalent empirical expression ($f_{(1,2,3)}$=12, 55, 116 Hz respectively, $C_{3,1}$=10 dB, $C_{3,2}$=7 Hz), and an alternative expression (with $f_{(1,2,3)}$=22, 113, 238 Hz, $C_{3,1}$=13 dB, $C_{3,2}$=10 Hz).

Figure 5-83. Proposed empirical predictions, mid-span correction at 2nd floor (n=3)

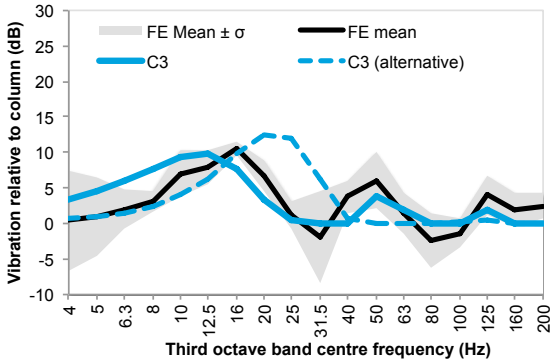

Combining the previous terms, it is proposed that the vibration level at a mid-span location, $L_{v,mid}(f,n)$ might then be estimated from:

$$L_{v,mid}(f,n) = L_{v,col} + C_3(f)$$
$$= L_{v,base} + \log_{10}\left(\frac{9n}{N} + 1\right) C_1(f) + nC_2(f) + C_3(f) \quad \text{(dB)} \qquad \textbf{(5-5)}$$

It should be noted that the empirical formulae suggested above follow the approximate shape of the most significant amplification factors; regions of the frequency spectrum which exhibit limited amplification are not so well represented, and are typically over-predicted. Nevertheless, by ensuring the most significant amplification effects are included appropriately, the overall weighted values are likely to be similar to results from more detailed models and/or measurements.

5.10.2 Results

Results from the proposed empirical formulae may be compared against results from the full finite element model of the generic building previously presented in Chapter 5.2. Results for the one-third octave band vertical vibration level are shown in Figure 5-84, relative to the average basement vibration level. The equivalent results for mid-span positions are shown in Figure 5-85.

It should be noted that to obtain the empirical model results, the modal frequencies for the building and floor plates have been estimated using simplified models, not the full FE model. For example, for each storey the modal frequencies were predicted from a simplified FE model of an individual floor plate, with boundary conditions, thickness and material parameters appropriate for the storey under consideration. This approach is considered representative of how the proposed empirical formulae approach might be used by others. However, the values of some of the empirical constants have been determined by adjusting the empirical model to fit results from full FE building models as well as measurement data.

Table 5-15. Empirical constants used in comparison model	
Constant	Value
N	7
f_0	8 Hz
$C_{1,1}$	8 dB
$C_{1,2}$	5 Hz
$C_{2,1}$	50 Hz
$f_{1,n}$	20 Hz at n =1 (ground floor) 12 Hz at n >1
$f_{2,n}$	77 Hz at n =1 (ground floor) 55 Hz at n >1
$f_{3,n}$	171 Hz at n =1 (ground floor) 117 Hz at n >1
$C_{3,1}$	10 dB
$C_{3,2}$	7 Hz

Figure 5-84 shows that, for the column positions, the proposed empirical formulae give results that are similar in shape to the full FE model results. The exception is at the uppermost storey (5th floor), at which the FE model gave results a few dB higher between 63 and 125 Hz. This is due to roof effects, which are not included in the empirical model. The results from the single point analysis demonstrate prominent dips in the spectrum that are not represented in the average data or empirical data. However, appropriate representation of the peaks is likely to be more important, since models are usually used to determine reasonably 'worst-case' values.

In the mid-span results in Figure 5-85 the FE and proposed empirical predictions again have a similar shape. There are some differences noted in the floor plate modal frequencies (the main peak is at 10 Hz for the empirical model, but 8 Hz for the full FE model), which suggests that the simplified FE model of a single floor plate may tend to overestimate the resulting modal frequencies slightly. The $C_{3,1}$ term was chosen to give a closer peak magnitude to the single point than averaged data, as this is more appropriate when evaluating vibration for individual rooms.

Overall A and W_b-weighted results at the column and mid-span positions are presented in Figure 5-86 to Figure 5-89, using the average measured spectrum (see Figure 3-26) as the basement input. The results from the proposed empirical formulae are shown together with results from the full FE model; the average measured data; measurements from a similar building ('TCR', see Chapter 3.1.1); and data predictions using the middle of the range suggested in the Transportation Noise Reference Book (TNRB) [23].

These comparisons show that the empirical results in general lie between the measured and full FE results. The empirical results are in most cases much closer to these results than the simpler TNRB predictions, particularly for the W_b-weighted acceleration, which is more sensitive to the low frequency floor and building modes.

Figure 5-84. Generic building, FE and proposed empirical predictions, vertical vibration relative to basement, column positions

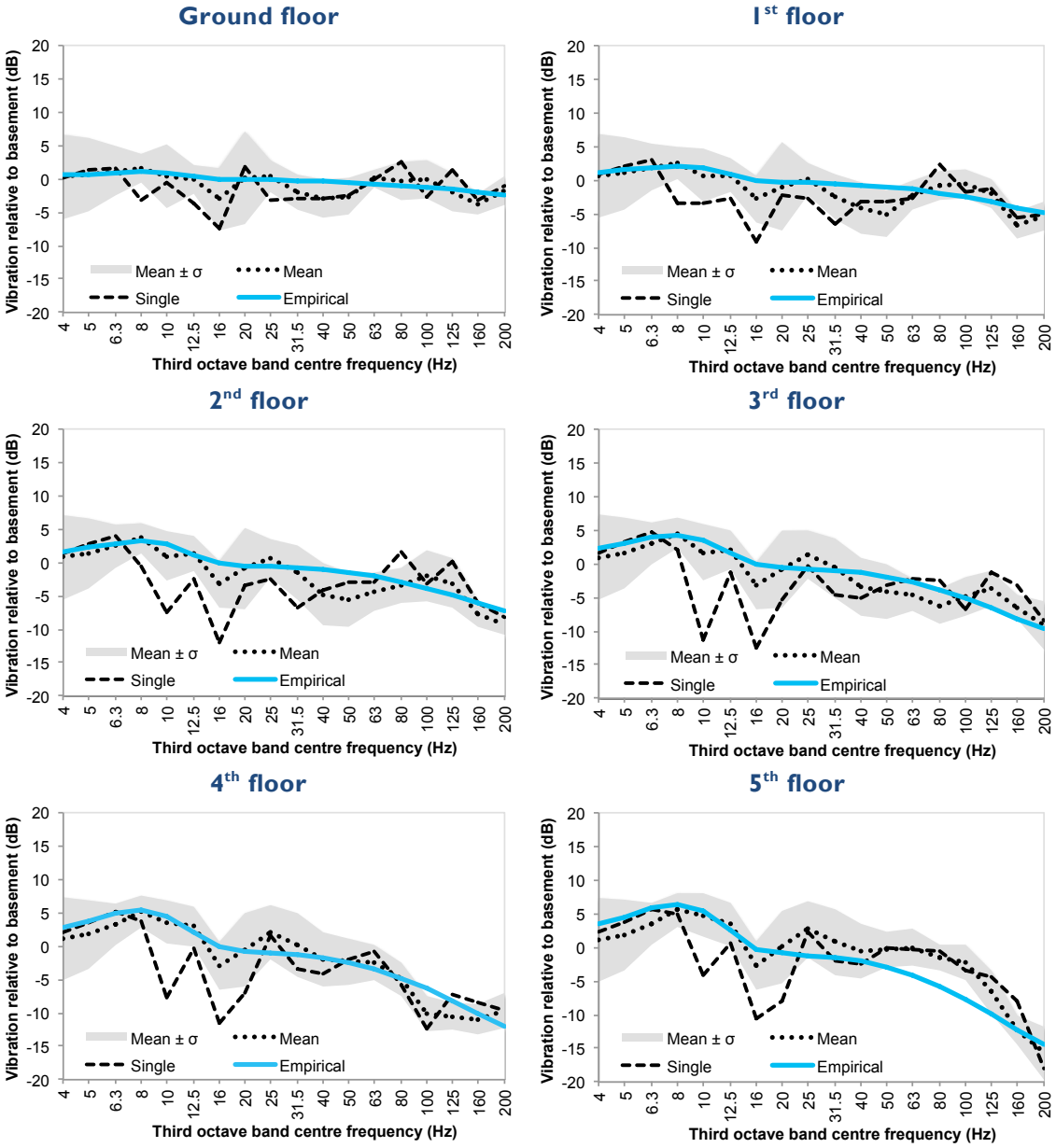

Figure 5-85. Generic building, FE and proposed empirical predictions, vertical vibration relative to basement, mid-span positions

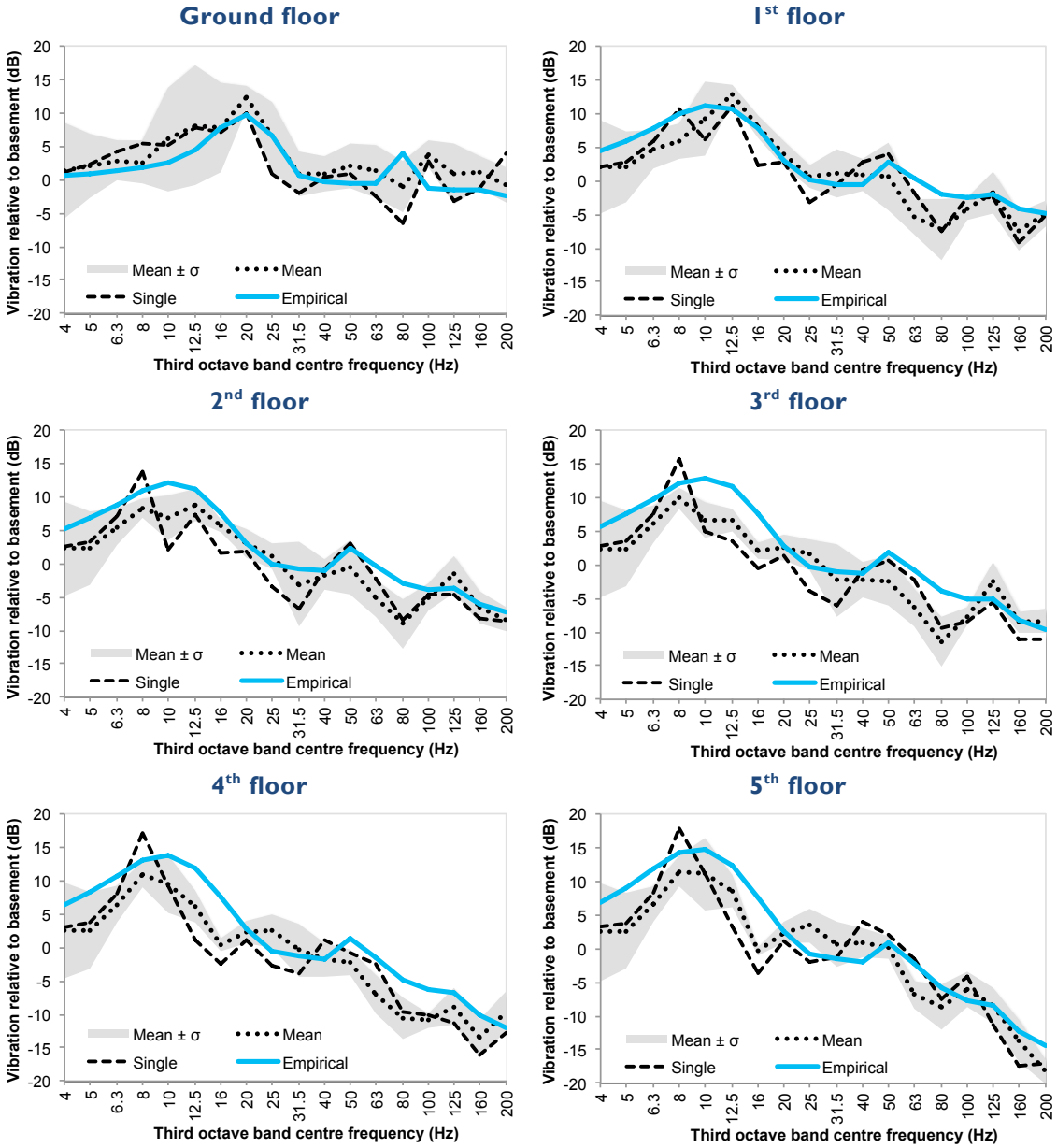

Figure 5-86. Generic building, proposed empirical predictions, W_b-weighted basement-relative column acceleration levels with storey

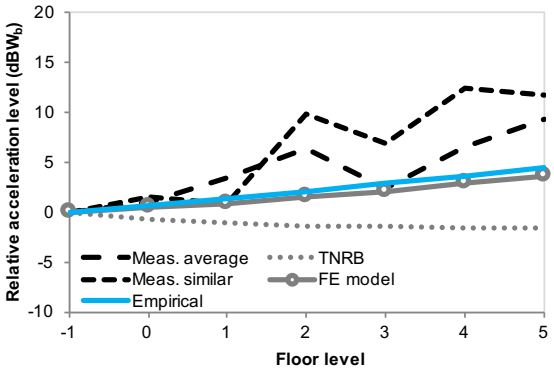

Figure 5-87. Generic building, proposed empirical predictions, A-weighted basement-relative column velocity levels with storey

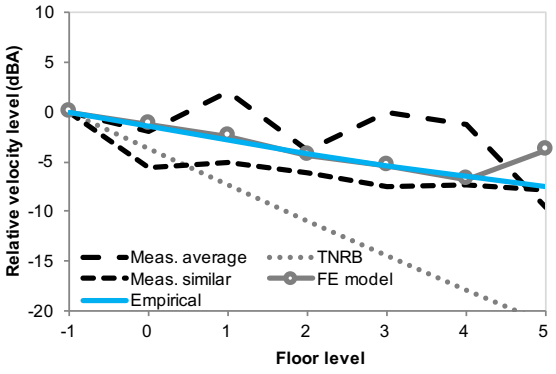

Figure 5-88. Generic building, proposed empirical predictions, W_b-weighted basement-relative mid-span acceleration levels with storey

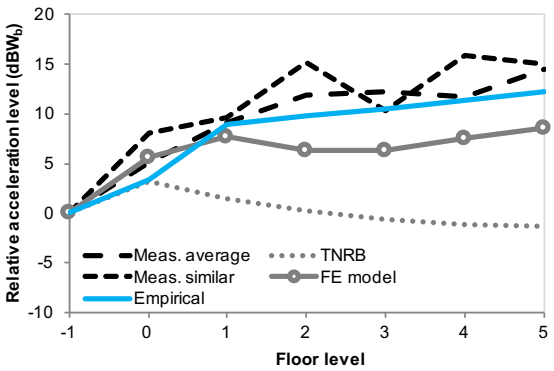

Figure 5-89. Generic building, proposed empirical predictions, A-weighted basement-relative mid-span velocity levels with storey

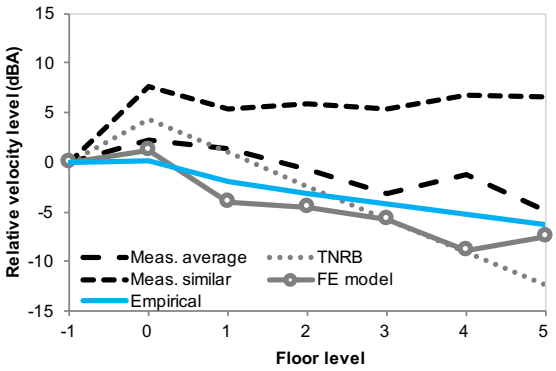

When interpreting overall vibration levels, it is important to consider the dependence on the input spectrum. In order to investigate this dependency further, the proposed empirical results are shown for three different input spectra, $L_{v,base}(f)$: the average measured spectrum (as used above); the measured spectrum from the 'TCR' case study (see Section 3.1.1); and the measured spectrum from the 'IOP' case study (see Section 3.1.7). These spectra were chosen for the investigation, due to their differences in shape, and for convenience they are reproduced in Figure 5-90. The associated results are shown in Figure 5-91 to Figure 5-94. For the TCR spectrum, the peak at 8 Hz is close to the natural frequency of the first extensional building mode used in the empirical model. It should also be noted that in the A-weighted results shown in Figure 5-92 and Figure 5-94, the lines for the average and IOP spectra are similar.

It is shown that the input spectrum can make an appreciable difference to the predicted vibration attenuation within the building, accounting for differences up to 0.5 dB per storey for overall A and W_b-weighted vibration levels for input spectra that could be encountered in the field. Input spectra which have a bias toward lower frequencies (e.g. TCR) lead to slightly greater

amplification of W_b-weighted vibration, and slightly lower attenuation of A-weighted vibration when compared with results employing input spectra that have a greater high frequency bias (e.g. IOP).

Figure 5-90. Basement spectra used for proposed empirical approach spectral sensitivity investigation

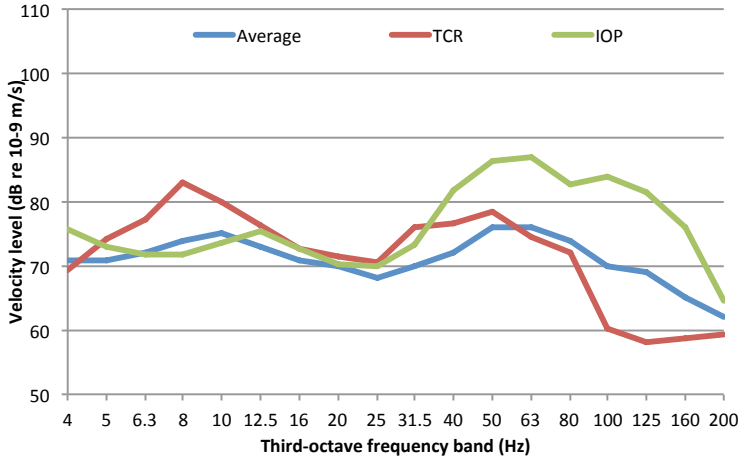

Figure 5-91. Empirical predictions with various input spectra, W_b-weighted basement-relative column acceleration levels with storey

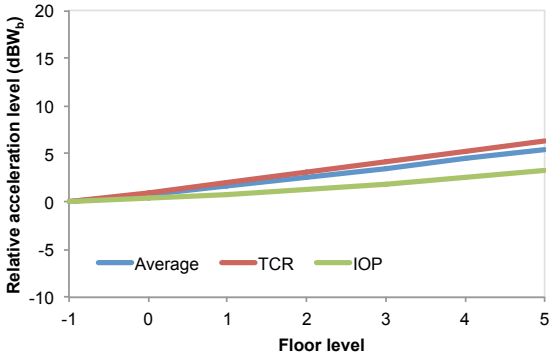

Figure 5-92. Empirical predictions with various input spectra, A-weighted basement-relative column velocity levels with storey

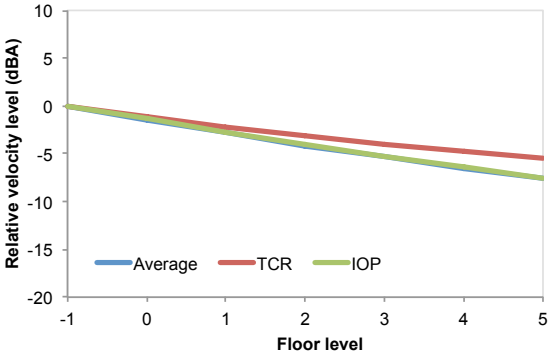

Figure 5-93. Empirical predictions with various input spectra, W_b-weighted basement-relative mid-span acceleration levels with storey

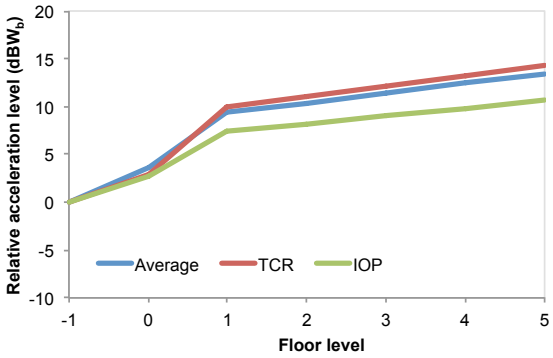

Figure 5-94. Empirical predictions with various input spectra, A-weighted basement-relative mid-span velocity levels with storey

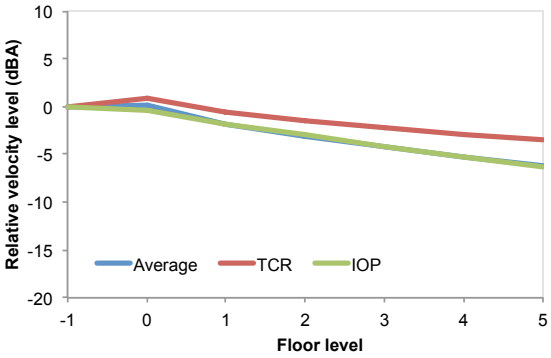

5.10.3 Summary

The results have shown that the proposed empirical formulae provide a useful approach to predicting railway vibration in buildings without resorting to full FE models of the whole building structure. Results predicted with the empirical formulae show an improvement in accuracy over the more simplified TNRB model, and the approach has the additional advantage of allowing for parametric investigations. For example, the attenuation through a building might be compared for two cases in which the floor plates exhibit different modal frequencies.

Whilst the empirical approach shows promise, it is recommended that further work be conducted in order to extend comparisons to other measurements and detailed FE models. Results from such exercises can also be used to derive correction terms and constants for a range of building types. Further development of the empirical formulae might also include accounting for higher order building modes.

6. RE-RADIATED NOISE MEASUREMENTS

In order to investigate the influence of various parameters on the groundborne noise level in a room, it is necessary to undertake simultaneous sound and vibration measurements in affected rooms. This chapter gives the details and results of measurements that have been conducted at four sites in London.

6.1 Site locations and dates

Ten rooms in total were used for the measurements, from four occupied hotels affected by groundborne noise and vibration from the London Underground. The hotels were chosen by using internet based mapping to identify hotels within the vicinity of known underground track alignments. Measurements within the hotels were made with the proprietors' knowledge and permission whilst the author was staying as a guest.

The building construction of the hotels varied, but they were all traditional buildings. Each hotel had rooms at its lowest storey, which was the lower ground floor, and was accessed from the street via steps to the upper ground level. A photograph taken by the author of a hotel building similar to those used for the measurements is shown in Figure 6-1. The actual hotels studied are anonymised and listed as follows:

- Hotel 1 (H1): Pembridge Square, Notting Hill
    - Affected by Circle & District Line
    - Measurements in three rooms (all lower ground level)
- Hotel 2 (H2): Norfolk Square, Paddington
    - Affected mainly by Circle & District Line, but the Bakerloo line is also nearby
    - Measurements in four rooms (three at lower ground level, one at upper ground level)
- Hotel 3 (H3): Norfolk Square, Paddington
    - Affected mainly by Circle & District Line, but the Bakerloo line is also nearby
    - Measurements in two rooms (one at upper ground level, one at lower ground level)
- Hotel 4 (H4): Bolsover Street, Fitzrovia
    - Affected by Victoria Line
    - Measurements in one room (lower ground level)

All rooms were carpeted guest rooms with the exception of a dining area at Hotel 2. A map of the measurement sites is shown in Figure 6-2, along with the track alignments of the London Underground.

Figure 6-1. Indicative building style for hotel measurements

Figure 6-2. Map showing hotel measurement locations and London Underground track alignment

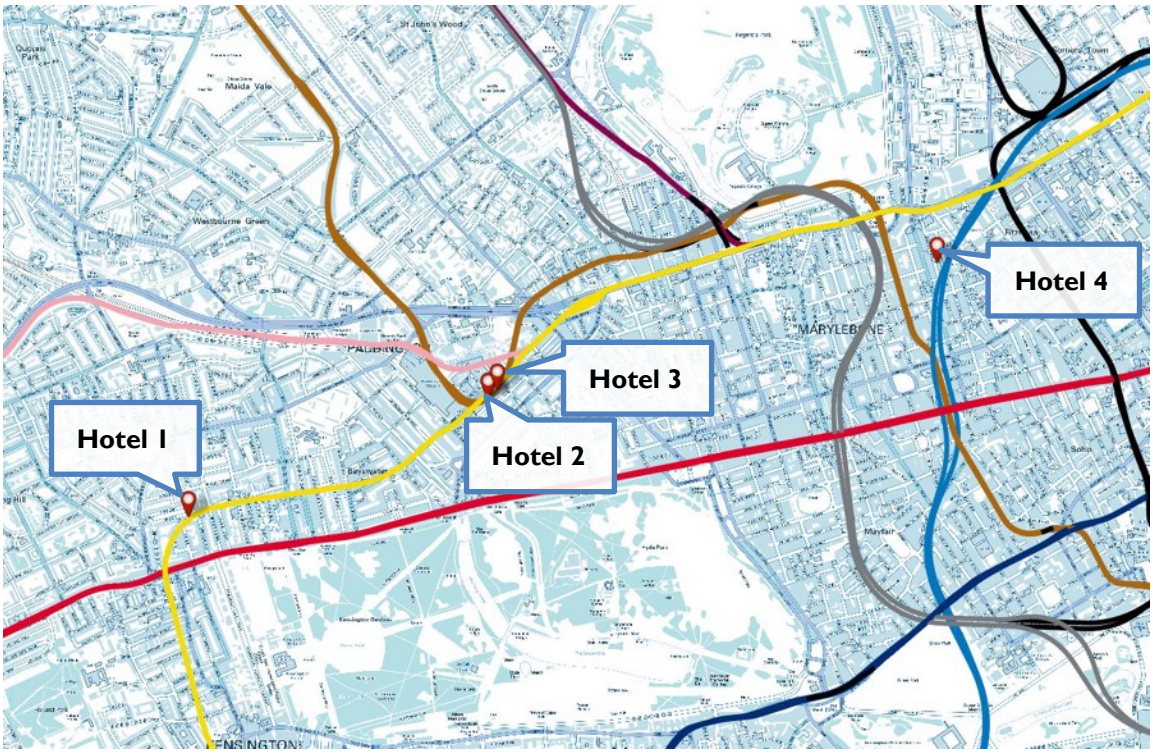

6.2 Methodology

The general approach to the measurements was to use several microphone positions (typically four to six, dependent on room geometry and furniture restrictions) in each room. Microphones

in 'corner' positions were situated approximately 0.5 m from the room surface where possible. Microphones in more central 'room' positions were set at random heights between 1.1 and 1.7 m.

A fixed accelerometer 'control' position was chosen, usually on the floor surface in the corner of the room where carpets could be lifted, but in some cases a windowsill location was used as an alternative. A roving accelerometer was used for vibration measurements, where possible, at multiple positions on each primary room surface (i.e. each wall, the floor, and the ceiling). Data was acquired from the control and roving position concurrently. Accelerometers were fixed using adhesive wax, which is suitable for measurements at and well above the frequency range of interest. Several train pass-bys were recorded for each position, in an attempt to include at least two or three clean pass-by readings for each train direction. The acceleration and sound pressure was recorded as raw waveforms and/or 100ms logged levels in 1/3 octave frequency bands.

The absorption in each room was quantified through reverberation time measurements using a sealed-enclosure low frequency loudspeaker with a sound analyser using the interrupted noise or swept sine techniques. When evaluating reverberation time measurements, it should be noted that at low frequencies, the interrupted noise method can overestimate the reverberation time due to the slow filter response, which provides a lower bound. The lower limit was determined through measurements with the signal generator output connected directly to the input of the analyser, with the results given in Table 6-1.

Table 6-1. Lower limit for reverberation measurements with interrupted noise method (T_{30}, s)

1/3 octave frequency band (Hz)											
20	25	31.5	40	50	63	80	100	125	160	200	250
1.04	0.82	0.63	0.47	0.43	0.33	0.25	0.2	0.17	0.14	0.12	0.09

At Hotels 1 to 3, sound pressure level measurements were undertaken using a Rion NL-52 sound level meter. A Norsonic NOR-121 analyser was used to obtain reverberation time measurements (using the swept-sine method) and to measure the vibration in two channels simultaneously. Channel one was used for the roving PCB 333B42 accelerometer; channel two was used for the PCB 393B12 accelerometer installed at the reference position.

At Hotel 4, a Prosig P8000 multi-channel data acquisition system was used with five PCB 378B02 microphones to measure sound pressure level at multiple positions simultaneously, along with two reference accelerometer positions (each using a PCB 393B12 accelerometer). A PCB 356B18 accelerometer was used as a roving transducer, with only the signal from the axis normal to the surface recorded. A Brüel & Kjaer 2260 analyser was used to measure reverberation times (using the interrupted noise method).

A list of the equipment used for the measurements is given in Table 6-2.

Table 6-2. Re-radiated noise measurements: list of equipment	
Data acquisition	Transducers:
Norsonic NOR-121 two-channel analyser Brüel & Kjaer 2260 analyser Prosig P8000 multi-channel data acquisition system Rion NL-52 sound level meter	Dynaudio Acoustics BM-9S sound source PCB Piezotronics 393B12 10V/g accelerometers PCB Piezotronics 356B18 1V/g triaxial accelerometer PCB Piezotronics 333B42 500mV/g accelerometer PCB Piezotronics 378B02 microphone and preamplifier sets

6.3 Results

The full results and details for each room are given in Appendix G, with the pertinent results provided in this section for discussion.

6.3.1 Hotel 1, Room 1

Measurements were made by the author during the evening of 11th February 2015. Eight microphone positions were used, at room, corner and pillow positions. Six accelerometer positions were used on the wall surfaces, with three ceiling positions and a single floor reference measurement position which was located near the corner of the floor, but on a structural wall element. An additional floor position was used in the centre of the lightweight floor of an en-suite bathroom. The room floor construction was understood to be concrete slab. The room layout and measurement positions are shown diagrammatically in Figure 6-3. The height of the room was 2.5 m. From the width 3.5 m, the first mode is estimated to occur at around 50 Hz.

Figure 6-3. Hotel 1, Room 1:
Groundborne noise and vibration measurement locations

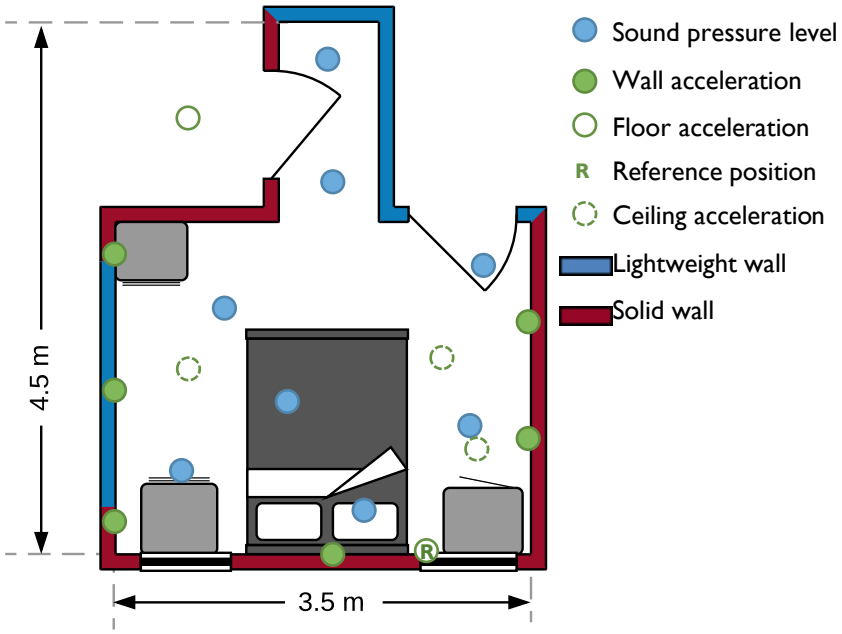

At the reference vibration position, a total of 86 train pass-bys were recorded, with the L_{Smax} vertical velocity results (over each pass-by) shown in Figure 6-4. The results comprise two different frequency signatures that can be deduced to correspond to trains running in two different directions in the two nearby tunnels, and which are seen to differ above 125 Hz by up to about 10 dB. Within each train type, there is good consistency between pass-bys, with a spread of generally up to around 5 dB.

Figure 6-4. Hotel 1, Room 1: maximum velocity level of pass-bys at reference position (86 pass-bys)

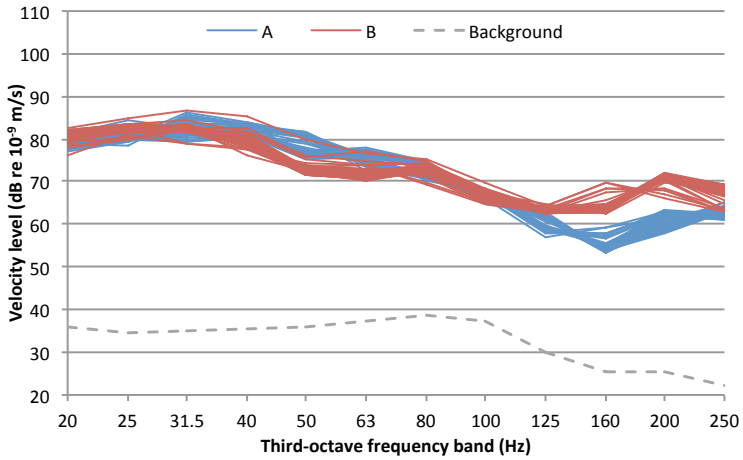

For straightforward comparison of the noise and vibration measurements, train pass-bys have been averaged for results obtained at each vibration or sound pressure measurement position. The averaging was performed by taking a logarithmic mean of the L_{Smax} velocity values in each one-third octave band for each train type, and performing an arithmetic mean over the two train types. For the vibration values, the results for each measurement position are shown in Figure

6-5; the sound pressure results at each microphone position are given in Figure 6-6. The combined A-weighted average maximum sound pressure level, which takes into account the low frequency spatial distribution (see Equation (2-23)), is 44 dBA.

Figure 6-5. Hotel 1, Room 1: average maximum velocity level of pass-bys at various accelerometer measurement positions

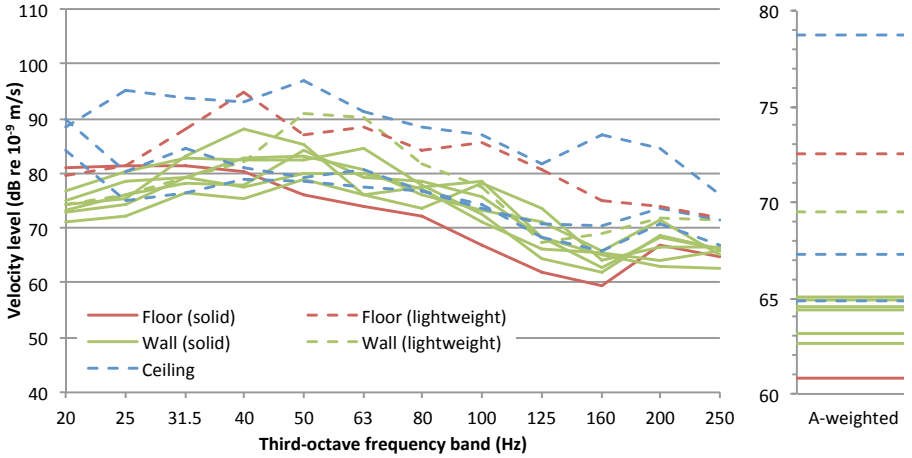

Figure 6-6. Hotel 1, Room 1: average maximum sound pressure level of pass-bys at various microphone measurement positions

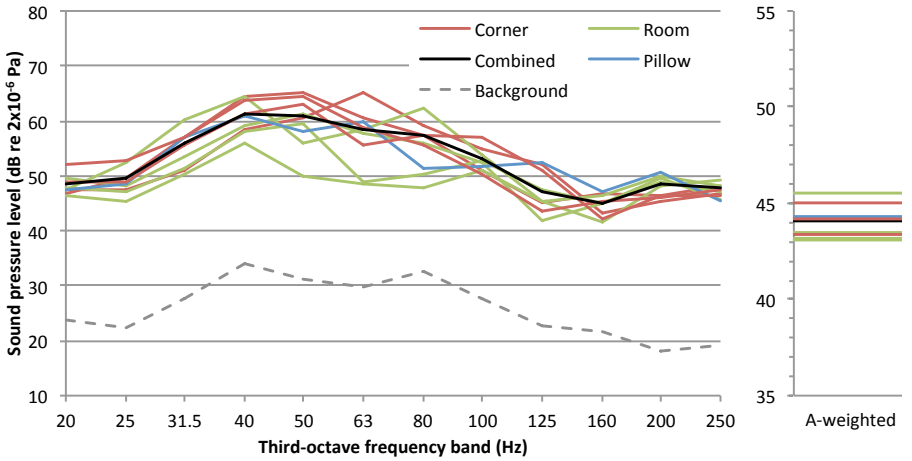

Figure 6-5 shows that the vibration levels could vary by up to 15-20 dB when measured at different points on seemingly similar surfaces. This is probably due to modal patterns within the structures, as well as the presence of supporting elements (for lightweight/framed elements). The solid walls seemed to give the more consistent results, generally lying within 5 dB of each other. It should be noted that whilst solid floors might be assumed to give relatively consistent results over their surface, they are usually overlaid with a timber sheet material such as plywood, which provides additional non-uniform characteristics.

Figure 6-6 shows that one-third octave band sound pressure levels within the room can vary considerably, up to about 15 dB. The frequency range between 40 and 100 Hz will contain a limited number of modes, which supports the suggestion that it is the modal response that causes

the sound pressure levels to be non-uniform in this range. In general, the highest sound pressure levels are at the corner positions, with the lowest at more central room positions. The combined sound pressure level corresponds closely to the pillow position.

The reverberation time results for the room are shown in Table 6-3. Although the results are all greater than the minimum values listed in Table 6-1, this room's first mode is estimated to occur at around 50 Hz, so results below this frequency are likely to be dominated by structural resonances and limitations of the instrumentation. They are therefore represented by grey type in the table.

Table 6-3. Hotel 1, Room1: reverberation time (T_{30}, s)

1/3 octave frequency band (Hz)											
20	25	31.5	40	50	63	80	100	125	160	200	250
1.23	1.03	1.07	0.89	0.75	0.57	0.64	0.32	0.42	0.75	0.36	0.43

In order to compare the data from several rooms and thereby identify trends, it is helpful to normalise the sound pressure levels with respect to the reverberation time:

$$L_{p,\mathrm{norm}} = L_p - 10\log_{10} T \quad \text{(dB)} \qquad \textbf{(6-1)}$$

Note that there are quantities in acoustics that are normalised to a 'standard' reverberation time of 0.5 s (e.g. D_{nT}, the standardised level difference, as defined in [62]). However, due to the frequency dependence of the reverberation time at low frequencies, it is appropriate that full normalisation is considered here. The normalised combined sound pressure level is presented in Figure 6-7, with the A-weighted spectrum shown on a secondary scale (to the right of the graph). This shows that the frequency range that dominates the overall A-weighted sound pressure level (44 dBA) is about 80 to 250 Hz.

Figure 6-7. Hotel 1, Room 1: average maximum sound pressure level of pass-bys (combined value) normalised to reverberation time

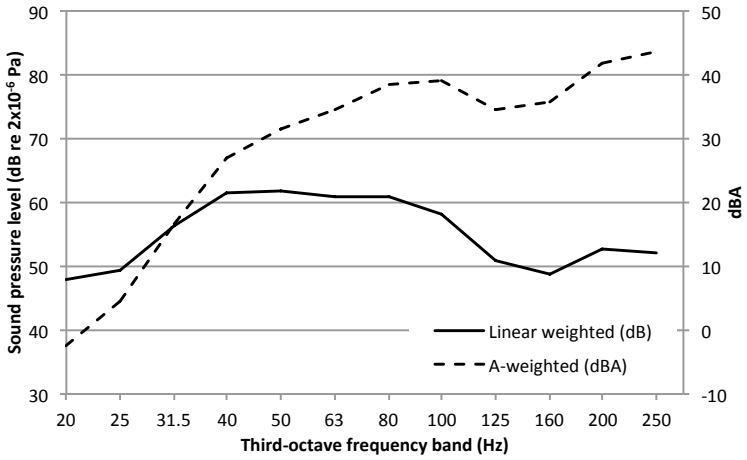

As a step towards predicting sound pressure levels from room vibration levels, for convenience a new general correction term is introduced:

$$LV2P = L_p - L_v \qquad \text{(dB re 2x10}^4\text{ Pa.m}^{-1}\text{.s)} \qquad \textbf{(6-2)}$$

where:

L_p is a sound pressure level during a pass-by, in dB re 2x10^{-5} Pa;

L_v is a vibration velocity level during a pass-by, in dB re 10^{-9} m.s^{-1}.

Note that the terms above are deliberately ambiguous; the appropriate pressure and velocity level metrics will be investigated in this and the following chapters. Where reverberation time normalised sound pressure levels are used, the general term can be defined as:

$$\begin{aligned} LV2P_n &= L_{p,\mathrm{norm}} - L_v \\ &= LV2P - 10\log_{10} T \end{aligned} \qquad \text{(dB re 2x10}^4\text{ Pa.m}^{-1}\text{.s)} \qquad \textbf{(6-3)}$$

As covered in the literature review, the Kurzweil approach [77] suggests a *LV2P* of -27 dB relative to the floor, and the TCRP research -32 dB [78]. For this particular room geometry, ONR 199005 [80] would suggest a $LV2P_n$ of -24 dB, based on the sound pressure level normalised for reverberation time.

The *LV2P* values obtained from the various room measurements are shown in Figure 6-8. Each line represents the average *LV2P* (over multiple train pass-bys) between a single measurement position and the combined room sound pressure level. For sound pressure levels normalised by the reverberation time, the $LV2P_n$ values are shown in Figure 6-9. A-weighted values are also shown in the figures; these are calculated from the single figure $L_{p,\mathrm{A}} - L_{v,A}$ values.

The results show that the *LV2P* and values are not constant with frequency, and this is also the case for the reverberation normalised $LV2P_n$ values. The best agreement with existing guidance is found with the non-normalised lightweight floor location (from the nearby en-suite bathroom) and the Kurzweil approach (i.e. an *LV2P* value of 27 dB). Using the solid floor corner location measurement as a basis for prediction using existing guidance could lead to fairly significant (> 10 dB) under-estimates of the resulting sound pressure level, unless additional corrections are applied to account for mid-floor effects.

Grütz's approach [85,86] for a concrete structure would suggest that to obtain the A-weighted sound pressure level of 44 dBA, the A-weighted vibration velocity level of the surface of interest would be about 81 dBA; this is similar to the velocity level of the ceiling measurement that exhibited the greatest vibration.

Figure 6-8. Hotel 1, Room 1: sound pressure level of pass-bys minus velocity level (dB re $2x10^4$ $Pa.m^{-1}.s$)

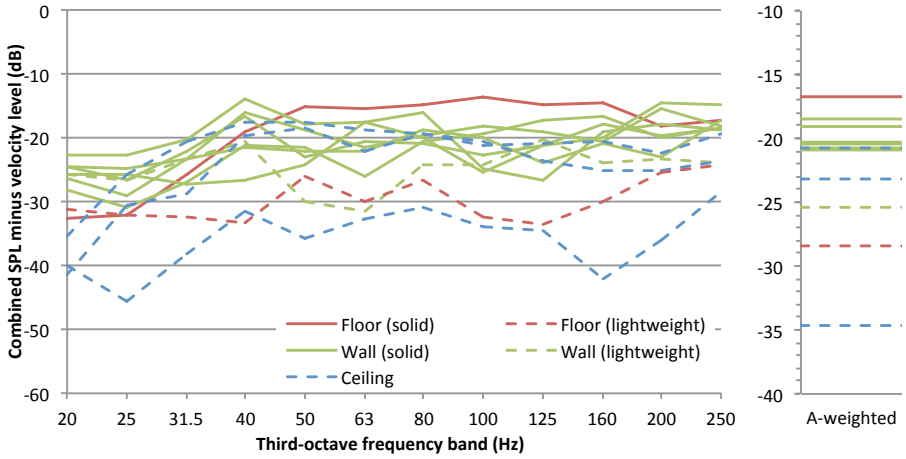

Figure 6-9. Hotel 1, Room 1: sound pressure level of pass-bys minus velocity level (normalised to reverberation time) (dB re $2x10^4$ $Pa.m^{-1}.s$)

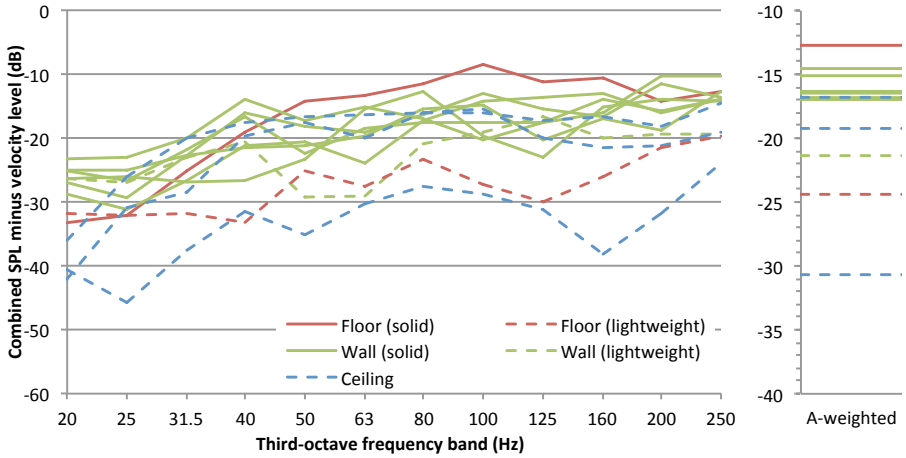

6.3.2 Hotel 1, Room 2

Measurements were made by the author over the evening of 11th March 2015. Nine microphone positions were used, at room, corner and pillow positions. Seven accelerometer positions were used on the wall surfaces, with two ceiling positions and a single floor reference measurement position which was located near the corner of the floor. The room floor construction was understood to be concrete slab. The room layout and measurement positions are shown diagrammatically in Figure 6-10. The height of the room was 2.6 m. From the main dimension 4.8 m, this room's first mode is estimated to occur at around 36 Hz.

Figure 6-10. Hotel 1, Room 2:
Groundborne noise and vibration measurement locations

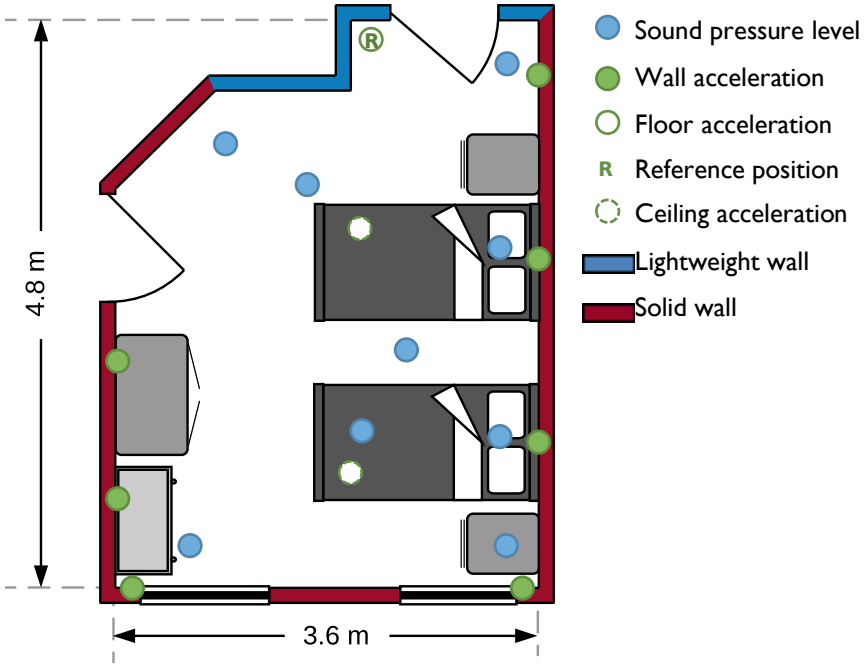

Vibration levels varied by up to 10-15 dB when measured at different points on seemingly similar surfaces. The floor gave the highest vibration levels at the upper frequency range (above 100 Hz), with the ceiling giving the highest levels at the low end of the frequency range (below 50 Hz). Most of the walls gave results that were reasonably consistent with the ceiling above 50 Hz, which is interesting given the fact that the wall vibration measurements were in the horizontal plane whereas the ceiling measurements were in the vertical plane.

Sound pressure levels within this room varied by up to about 15 dB, due to acoustic modes. The highest sound pressure levels are at the corner positions, with the lowest at more central room positions. The combined sound pressure level again corresponded closely to the pillow position.

The combined sound pressure level normalised by reverberation time is presented in Figure 6-11, with the A-weighted spectrum shown on a secondary scale (to the right of the graph). This shows that the frequency range that dominated the overall A-weighted sound pressure level (45 dBA) is about 80 to 250 Hz.

Figure 6-11. Hotel 1, Room 2: average maximum sound pressure level of pass-bys (combined value) normalised to reverberation time

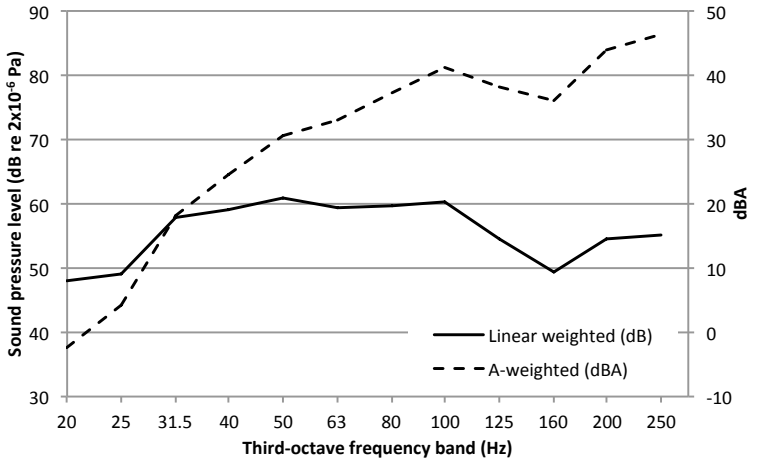

The results show that the *LV2P* and $LV2P_n$ values are not constant with frequency. Nevertheless, use of Kurzweil's prediction approach (-27 dB) with the non-normalised solid floor vibration measurement as a basis (even though this was not in the centre of the room) would have resulted in A-weighted sound pressure levels that were within two or three decibels of those measured.

Grütz's approach for a concrete structure would suggest that to obtain the A-weighted sound pressure level of 45 dBA, the A-weighted vibration velocity level of the surface of interest would be about 84 dBA; this is significantly greater than any of the measurement positions.

6.3.3 Hotel 1, Room 3

Measurements were made by the author over the evening of 11th March 2015. Seven microphone positions were used, at room, corner and pillow positions. Six accelerometer positions were used on the wall surfaces, with two ceiling positions and a single floor reference measurement position which was located near the corner of the floor. The room floor construction was understood to be concrete slab. The room was larger than most typical hotel rooms, with the layout and measurement positions shown diagrammatically in Figure 6-12. The height of the room was 2.8 m. This room's first mode is estimated, from the main dimension 6.2 m, to occur at around 28 Hz.

Figure 6-12. Hotel 1, Room 3:
Groundborne noise and vibration measurement locations

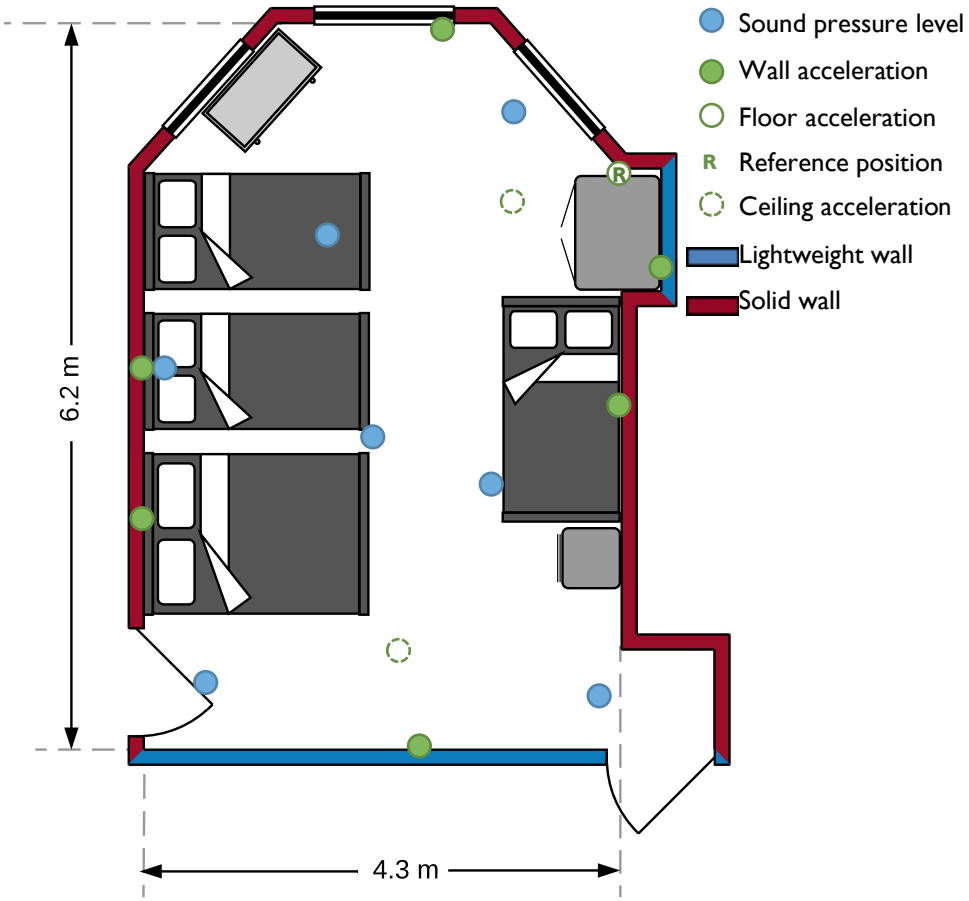

Vibration levels were shown to vary by up to 10-15 dB when measured at different points on seemingly similar surfaces. The floor gave the lowest vibration levels for the majority of the frequency range, whilst above 100 Hz the lightweight walls had the highest vibration levels.

Sound pressure levels within this room vary by up to about 15 dB, due to acoustic modes. The highest sound pressure levels are at the corner positions, with the lowest at more central room positions. The combined sound pressure level parameter again represented the pillow position well. There was a reduced sound pressure level at high frequencies compared with other rooms measured in this building. This room was located on the opposite side of the building to the other rooms, and further away from the railway source, which was in a shallow 'cut-and-cover' track construction. It is therefore likely that there are high frequency losses across the building structure which are causing the reduced sound pressure levels in this frequency range for this room.

The reverberation time normalised combined sound pressure level is presented in Figure 6-13, with the A-weighted spectrum shown on a secondary scale (to the right of the graph). This shows

that the overall A-weighted sound pressure level (37 dBA) has a reasonably uniform frequency contribution above 31.5 Hz.

Figure 6-13. Hotel 1, Room 3: average maximum sound pressure level of pass-bys (combined value) normalised to reverberation time

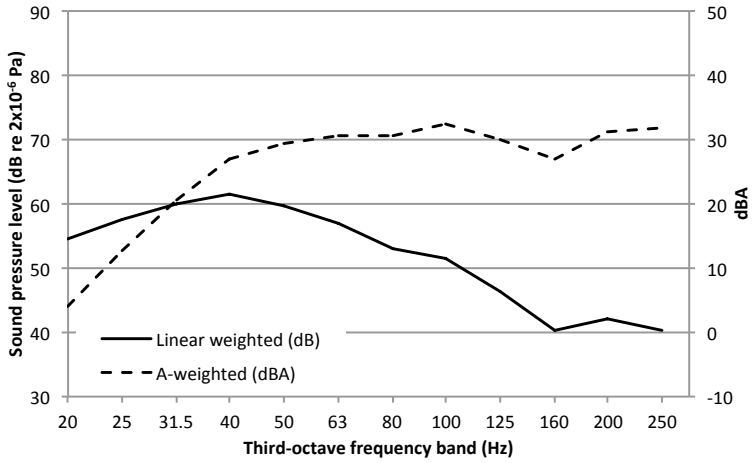

The results show that the most consistent difference between sound pressure level and vibration levels is achieved with the solid wall vibration levels, which were about 20 dB greater than the combined sound pressure level (non-normalised to reverberation time).

Grütz's approach for a concrete structure would suggest that to obtain the A-weighted sound pressure level of 37 dBA, the A-weighted vibration velocity level of the surface of interest would be about 70 dBA; this is somewhat greater than any of the measurement positions.

6.3.4 Hotel 2, Room 1

Measurements were made by the author over the afternoon/evening of 23rd March 2015. Seven microphone positions were used, at room, corner and pillow positions. Eight accelerometer positions were used on the wall surfaces, with one ceiling position. There were difficulties in obtaining reliable vibration measurements on the floor of this room due to the presence of largely non-liftable carpet; therefore a solid windowsill was used for the reference position, which was on a solid façade. However, towards the end of the period, measurements were successfully recorded for a small number of pass-bys at a floor corner location, and the construction was confirmed to be concrete slab. The room layout and measurement positions are shown diagrammatically in Figure 6-14. The height of the room was 2.8 m. From the room's main dimension of 3.0 m, this room's first mode is estimated to occur at around 60 Hz, although the presence of the coupled lobby space may cause this to occur at a slightly lower frequency.

Figure 6-14. Hotel 2, Room 1:
Groundborne noise and vibration measurement locations

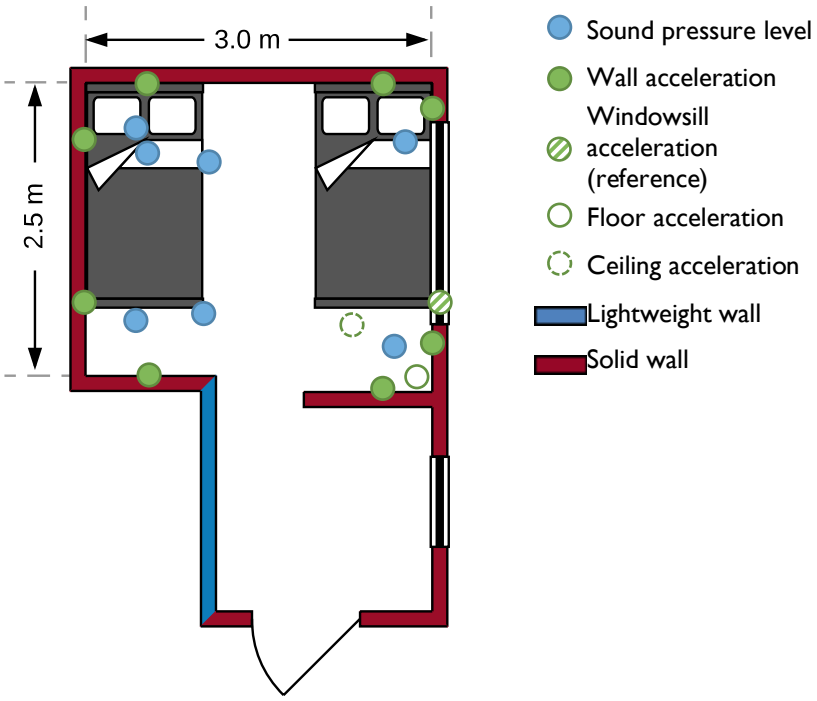

Vibration levels vary by up to 10 dB when measured at different points on seemingly similar surfaces. The ceiling exhibited the greatest vibration levels; about 10 dB greater than the floor measurements for the majority of the frequecy range.

Sound pressure levels within this room varied by up to about 15 dB, due to acoustic modes. The greatest sound pressure levels are at the corner positions, with the least at the more central room positions. Note that for this room, the pillow measurement position was at a corner.

The combined sound pressure level normalised by the reverberation time is presented in Figure 6-15, with the A-weighted spectrum shown on a secondary scale (to the right of the graph). This shows that the overall A-weighted sound pressure level (41 dBA) is dominated by contributions between 50 and 160 Hz.

Figure 6-15. Hotel 2, Room 1: average maximum sound pressure level of pass-bys (combined value) normalised to reverberation time

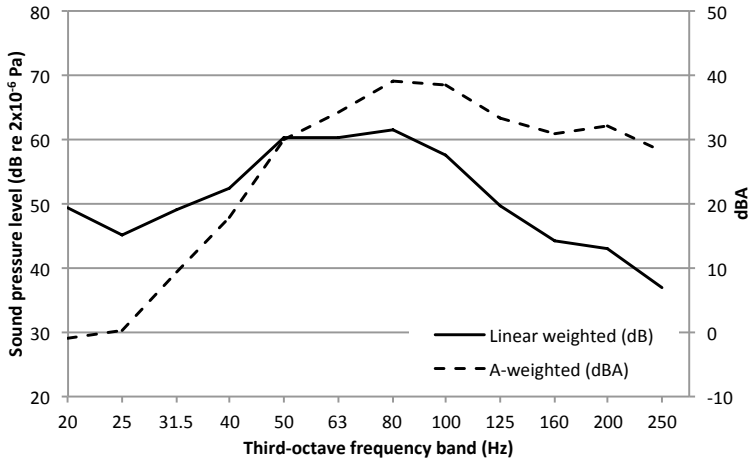

The results show that none of the surface vibration measurements provide a consistent difference with sound pressure level. Nevertheless, reasonable agreement with respect to existing guidance is found by applying the Kurzweil *LV2P* value of -27 dB to the floor corner vibration measurements; this approach would have resulted in an underestimate of the sound pressure level (at a central room position) of about 2 dB. Applying the ONR 199005 prediction would have provided similar agreement.

Grütz's approach for a concrete structure would suggest that to obtain the A-weighted sound pressure level of 41 dBA, the A-weighted vibration velocity level of the surface of interest would be about 76 dBA; this is somewhat greater than any of the measurement positions.

6.3.5 Hotel 2, Room 2

Measurements were made by the author over the morning of 25th March 2015. Nine microphone positions were used, at room, corner and pillow positions. Eight accelerometer positions were used on the wall surfaces, with two ceiling positions and a single floor reference measurement position which was located near the corner of the floor. The construction was understood to be concrete slab, overlaid with plywood. The room layout and measurement positions are shown diagrammatically in Figure 6-16. The height of the room was 2.8 m. This room's first mode is estimated to occur at around 60 Hz.

Figure 6-16. Hotel 2, Room 2:
Groundborne noise and vibration measurement locations

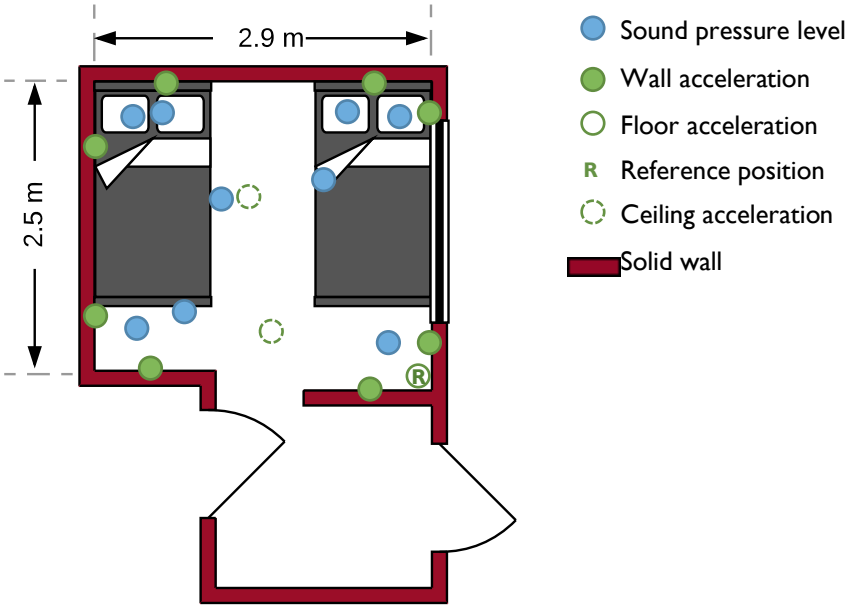

Vibration levels varied by up to about 15 dB when measured at different points on seemingly similar surfaces. The ceiling exhibited the greatest vibration levels below 100 Hz; about 5-10 dB greater than the floor measurements. Above 100 Hz, the floor exhibited the greatest vibration levels, up to 10-15 dB more than the other surfaces at 250 Hz.

Sound pressure levels within this room varied by up to about 10 dB, due to acoustic modes. The greatest sound pressure levels are at the corner positions, with the least at more central room positions. Note that for this room, the pillow measurement positions were also at corners of the room.

The combined sound pressure level normalised to the reverberation time is presented in Figure 6-17, with the A-weighted spectrum shown on a secondary scale (to the right of the graph). This shows that the overall A-weighted sound pressure level (42 dBA) is dominated by contributions between 50 and 160 Hz.

Figure 6-17. Hotel 2, Room 2: average maximum sound pressure level of pass-bys (combined value) normalised to reverberation time

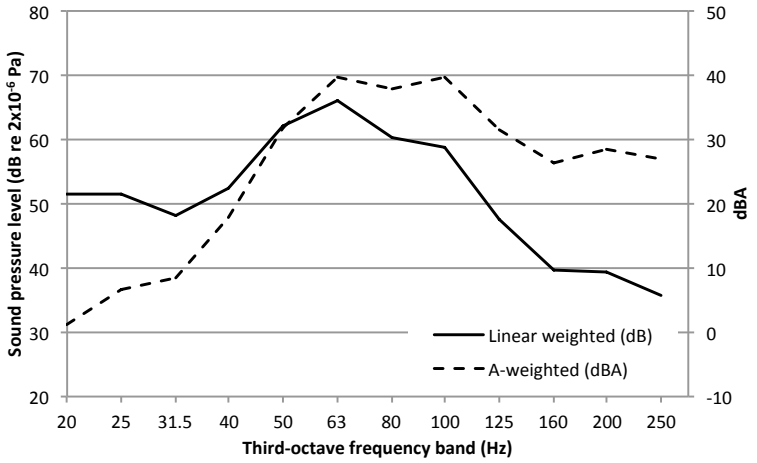

The results show that none of the surface vibration measurements provide a consistent difference with sound pressure level. The best agreement with respect to existing guidance is found with the floor results and the TCRP *LV2P* value of -32 dB, which would likely to overpredict the A-weighted sound pressure level near the centre of the room by around 2 dB.

Grütz's approach for a concrete structure would suggest that to obtain the A-weighted sound pressure level of 42 dBA, the A-weighted vibration velocity level of the surface of interest would be about 77 dBA; this is within a few decibels of the ceiling position with the greatest vibration levels.

6.3.6 Hotel 2, Room 3

Measurements were made by the author over the afternoon/evening of 24th March 2015. Seven microphone positions were used, at room and corner positions. Eight accelerometer positions were used on the wall surfaces, with two ceiling positions and two floor positions; the reference measurement position was located near the corner of the floor. The room floor construction was understood to be concrete slab, with a laminate flooring finish. Being a dining room, the room was larger than a typical bedroom, with the layout and measurement positions shown diagrammatically in Figure 6-18. The height of the room was 2.65 m, and from the main dimension 5.4 m its first mode is estimated to occur at around 30 Hz.

Figure 6-18. Hotel 2, Room 3:
Groundborne noise and vibration measurement locations

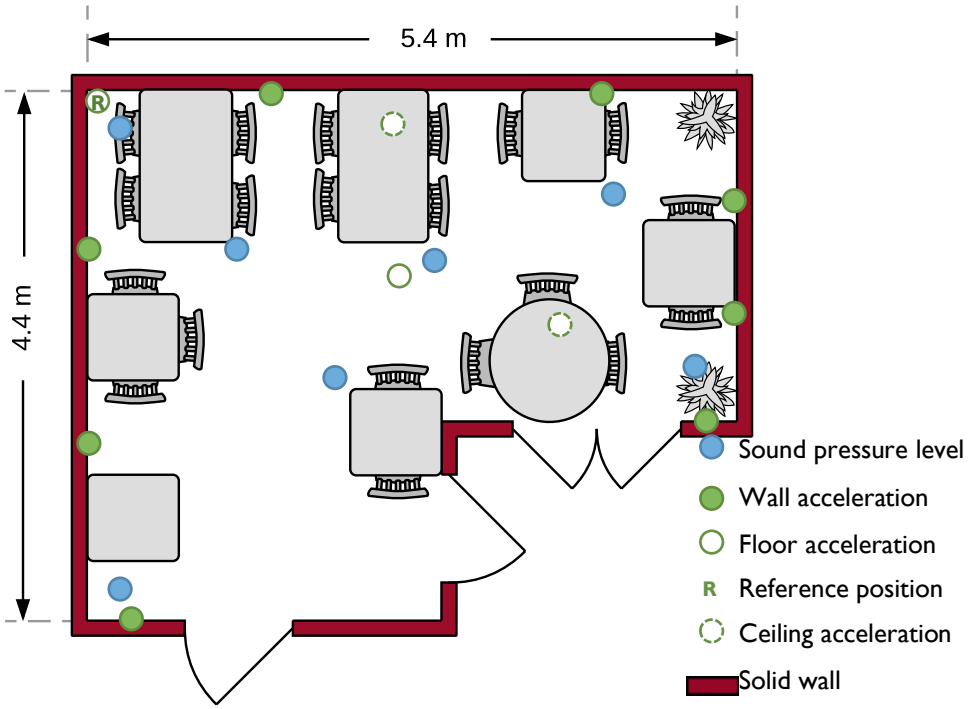

Vibration levels were shown to vary by up to 10-15 dB when measured at different points on seemingly similar surfaces, although the various solid wall positions gave reasonably similar vibration levels. The ceiling gave the greatest vibration levels for the majority of the frequency range, although above 50 Hz the ceiling vibration levels were similar to the mid-span floor position. The mid-span floor position exhibited vibration levels that were about 10-15 dB greater than at the corner floor position over most of the frequency range.

Sound pressure levels within this room varied by up to about 20 dB, due to acoustic modes. The highest sound pressure levels are at the corner positions, with the lowest at more central room positions.

The combined sound pressure level normalised to reverberation time is presented in Figure 6-19, with the A-weighted spectrum shown on a secondary scale (to the right of the graph). This shows that the overall A-weighted sound pressure level (47 dBA) is dominated by contributions between about 63 and 160 Hz.

Figure 6-19. Hotel 2, Room 3: average maximum sound pressure level of pass-bys (combined value) normalised to reverberation time

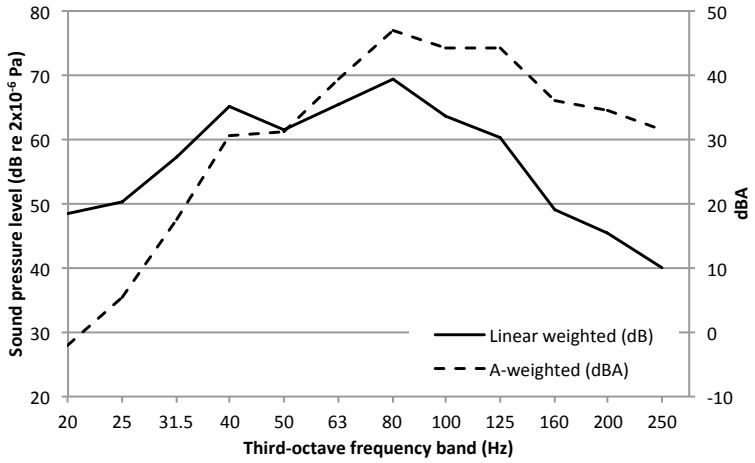

The results show that the most consistent *LV2P* value is achieved with the mid-span floor vibration measurements, with a value of around -24 dB. When considering a central room position, the sound pressure levels would be slightly lower, and would be predicted within a couple of decibels by the Kurzweil and ONR 199005 approaches.

Grütz's approach for a concrete structure would suggest that to obtain the A-weighted sound pressure level of 47 dBA, the A-weighted vibration velocity level of the surface of interest would be about 87 dBA; this is somewhat greater than any of the measurement positions.

6.3.7 Hotel 2, Room 4

Measurements were made by the author over the morning of 24th March 2015. Eight microphone positions were used, at room, corner and pillow positions. Eight accelerometer positions were used on the wall surfaces, with a single ceiling position and two floor positions; the reference measurement position was located near the corner of the floor. The room floor construction was understood to be a timber joist type. The room layout and measurement positions are shown diagrammatically in Figure 6-20. The height of the room was 2.65 m. From the main dimension of 4.4 m, this room's first mode is estimated to occur at around 40 Hz.

Figure 6-20. Hotel 2, Room 4:
Groundborne noise and vibration measurement locations

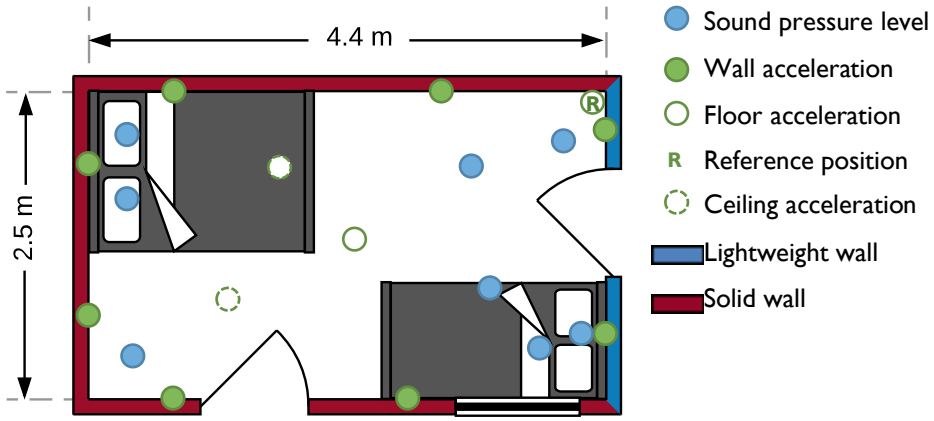

Vibration levels were shown to vary by up to 10-15 dB when measured at different points on seemingly similar surfaces. The ceiling exhibited the greatest vibration levels over the majority of the frequency range. The mid-span floor vibration was about 10 dB greater than at the corner floor position below 63 Hz.

Sound pressure levels within this room varied by up to about 15-20 dB due to acoustic modes, with one of the pillow positions (near a corner) exhibiting particularly high sound pressure levels.

The combined sound pressure level normalised by reverberation time is presented in Figure 6-21, with the A-weighted spectrum shown on a secondary scale (to the right of the graph). This shows that the overall A-weighted sound pressure level (39 dBA) is dominated by contributions between 40 and 125 Hz.

Figure 6-21. Hotel 2, Room 4: average maximum sound pressure level of pass-bys (combined value) normalised to reverberation time

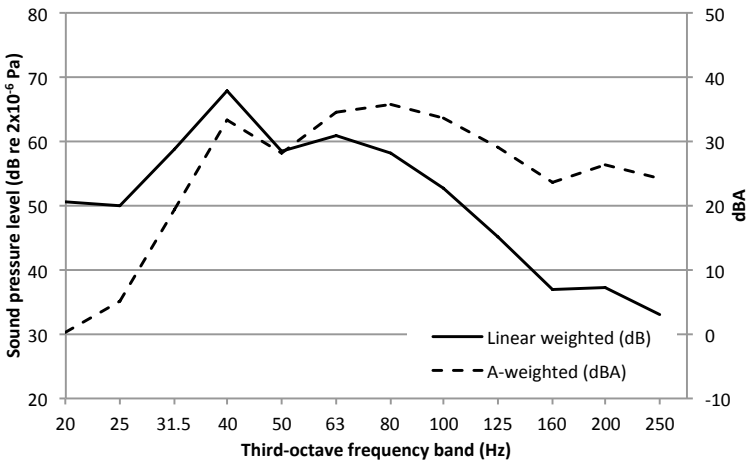

The results show that none of the surface vibration measurements provide a consistent difference with sound pressure level, although when considering the A-weighted values, the *LV2P* value for the mid-span floor location was about -23 dB. When accounting for the difference between the

combined and a central room sound pressure level, the Kurzweil and ONR 199005 predictions would have given overall values similar to those measured.

Grütz's approach for a concrete structure would suggest that to obtain the A-weighted sound pressure level of 39 dBA, the A-weighted vibration velocity level of the surface of interest would be about 74 dBA; this is a similar level to that measured at the ceiling positions.

6.3.8 Hotel 3, Room 1

Measurements were made by the author over the evening of 19th March 2015. Five microphone positions were used, at room, corner and pillow positions. Seven accelerometer positions were used on the wall surfaces, with two ceiling positions and two floor positions. The room floor construction was understood to be a concrete slab, but was finished with a poorly fitted laminate flooring, which was springy underfoot. The reference vibration measurement position was therefore chosen to be on a windowsill. The room layout and measurement positions are shown diagrammatically in Figure 6-22. The height of the room was 3.0 m. From the main dimension of 3.0 m, this room's first mode is estimated to occur at around 60 Hz.

Figure 6-22. Hotel 3, Room 1:
Groundborne noise and vibration measurement locations

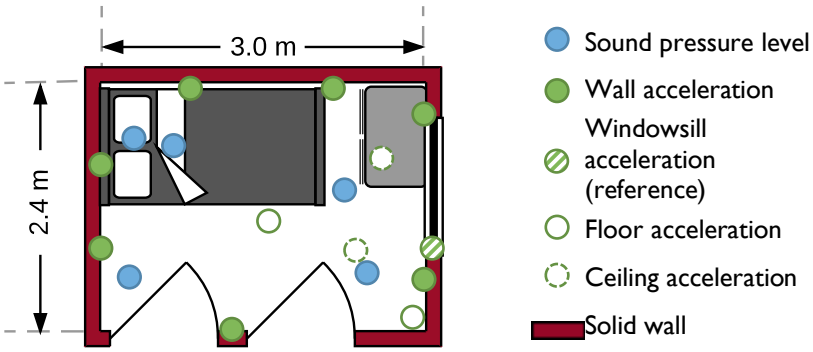

Vibration levels varied by up to 10 dB when measured at different points on seemingly similar surfaces, but for the floor the mid-span vibration exceeded the vibration at the corner by up to 20 dB. Whilst for many cases this might be expected to be the case due to structural modes of the floor, in this case it is anticipated to be due to resonant behaviour of the laminate flooring surface.

Sound pressure levels within this room varied by up to about 10 dB due to acoustic modes, with the pillow position (near a corner) exhibiting the greatest sound pressure levels.

The combined sound pressure level normalised to reverberation time is presented in Figure 6-23, with the A-weighted spectrum shown on a secondary scale (to the right of the graph). This shows

that the overall A-weighted sound pressure level (40 dBA) is dominated by contributions between 50 and 125 Hz.

Figure 6-23. Hotel 3, Room 1: average maximum sound pressure level of pass-bys (combined value) normalised to reverberation time

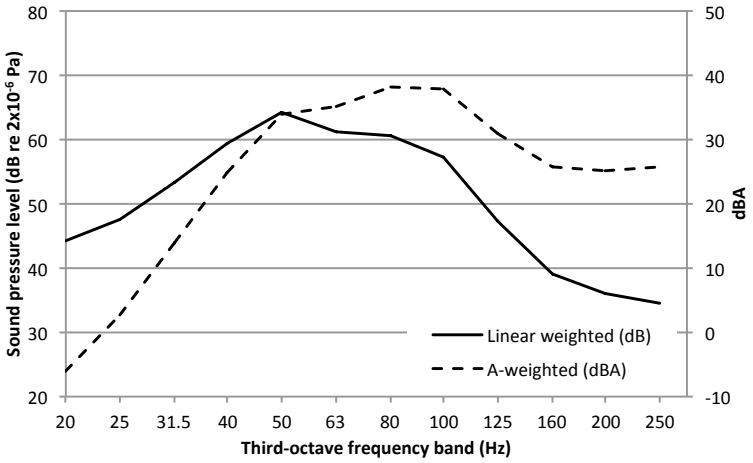

The results show that none of the surface vibration measurements provide a consistent difference with sound pressure level. Use of the mid-span floor vibration results would lead to overestimates of sound pressure at a central room position by around 11 dB for Kurzweil; the 6 dB for TCRP; and 11 dB for the ONR 199005 approach.

Grütz's approach for a concrete structure would suggest that to obtain the A-weighted sound pressure level of 40 dBA, the A-weighted vibration velocity level of the surface of interest would be about 74 dBA; this is within a few decibels of the mid-span floor vibration measurement.

6.3.9 Hotel 3, Room 2

Measurements were made by the author over the afternoon of 19th March 2015. Six microphone positions were used, at room, corner and pillow positions. Six accelerometer positions were used on the wall surfaces, with two ceiling positions and a single floor position. The room floor construction was understood to be of timber joist type, and was finished with laminate flooring. The reference vibration measurement position was therefore chosen to be on a windowsill. The room layout and measurement positions are shown diagrammatically in Figure 6-24. The height of the room was 2.3 m. From the main dimension of 3.0 m, this room's first mode is estimated to occur at around 60 Hz.

Figure 6-24. Hotel 3, Room 2: Groundborne noise and vibration measurement locations

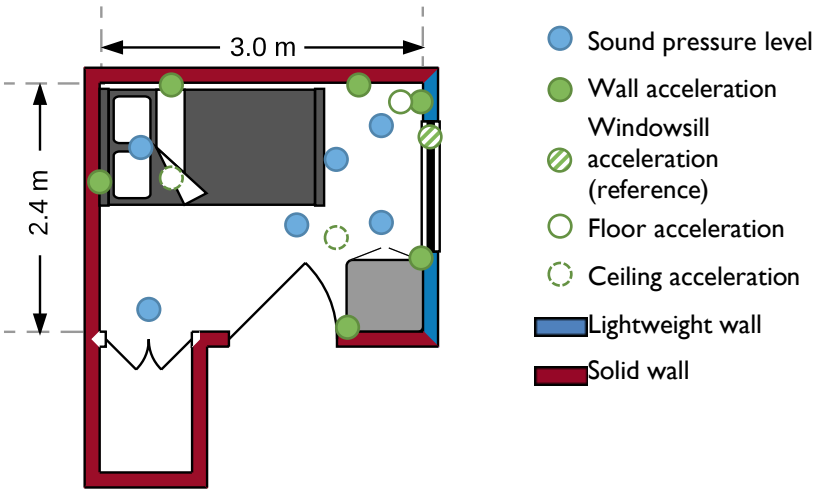

Vibration levels were shown to vary by up to 10-15 dB when measured at different points on seemingly similar surfaces, and up to 20 dB for different points on the floor. Whilst for many cases this might be expected to be the case due to structural modes of the floor, in this case it is anticipated to be due to non-uniform behaviour of the laminate flooring surface.

Sound pressure levels within this room varied by up to about 15 dB due to acoustic modes.

The combined sound pressure level normalised by reverberation time is presented in Figure 6-25, with the A-weighted spectrum shown on a secondary scale (to the right of the graph). This shows that the overall A-weighted sound pressure level (37 dBA) is dominated by contributions between 40 and 125 Hz.

Figure 6-25. Hotel 3, Room 2: average maximum sound pressure level of pass-bys (combined value) normalised to reverberation time

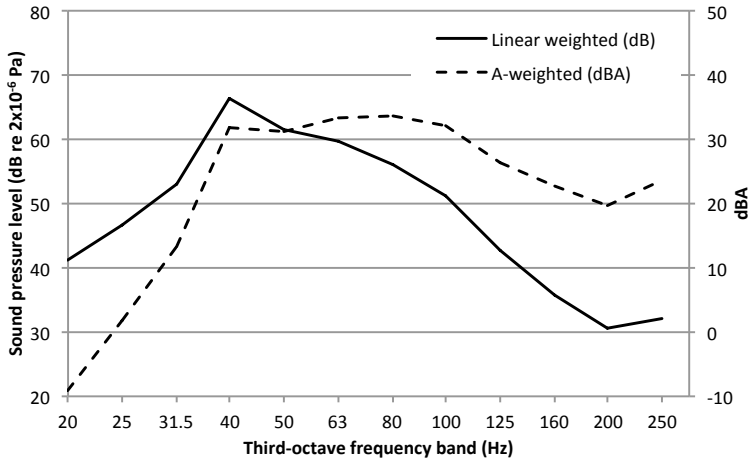

The results show that the most consistent *LV2P* values were provided by the solid wall locations with values of around -23 dB. Use of the TCRP approach to predict sound pressure levels near

the centre of the room from the mid-span floor vibration results would lead to an overestimate of groundborne sound pressure by around 2 dB.

Grütz's approach for a concrete structure would suggest that to obtain the A-weighted sound pressure level of 37 dBA, the A-weighted vibration velocity level of the surface of interest would be about 71 dBA; this is within a few decibels of the mid-span floor vibration measurement.

6.3.10 Hotel 4, Room 1

Measurements were made by the author and Oliver Bewes in a basement room of the hotel during the evening of 11th March 2014. Four microphone positions were used, at room and pillow positions. Thirteen accelerometer positions were used on the wall surfaces, with four ceiling positions and two floor positions (one in the corner of the room where the carpet could be lifted, and one on the tiled floor surface of the adjacent en-suite bathroom, both of these served as reference positions). The room floor construction was understood to be concrete slab. The room layout and measurement positions are shown diagrammatically in Figure 6-26. The height of the room was 2.7 m. From the main dimension of 5.7 m, this room's first mode is estimated to occur at around 30 Hz.

Figure 6-26. Hotel 4, Room 1:
Groundborne noise and vibration measurement locations

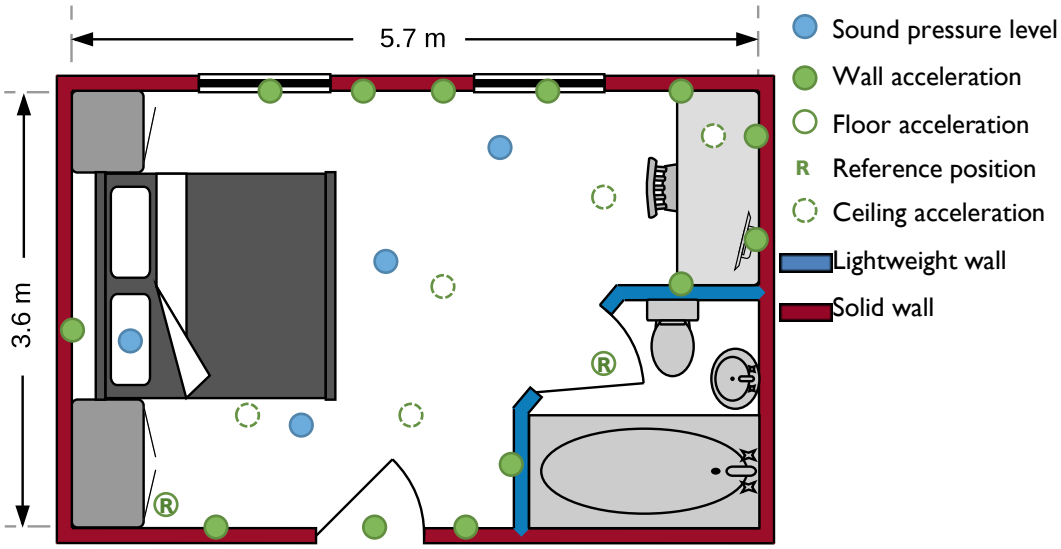

Vibration levels were shown to vary by up to 10-15 dB when measured at different points on seemingly similar surfaces. The ceiling provided the greatest vibration levels, which were about 20 dB greater than the floor measurements.

Sound pressure levels within this room varied by up to about 10 dB due to acoustic modes.

The combined sound pressure level normalised by reverberation time is presented in Figure 6-27, with the A-weighted spectrum shown on a secondary scale (to the right of the graph). This shows that the overall A-weighted sound pressure level (35 dBA) is dominated by contributions between 80 and 250 Hz.

Figure 6-27. Hotel 4, Room 1: average maximum sound pressure level of pass-bys (combined value) normalised to reverberation time

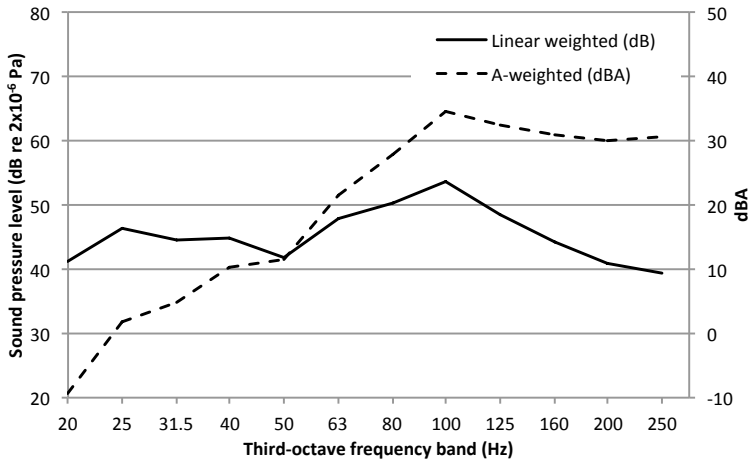

The results show that the most consistent *LV2P* values were provided by the floor locations, with values of around -23 dB. Use of Kurzweil's approach with the mid-span floor vibration results would lead to a reasonably close estimate of groundborne sound pressure at a room centre location, with the ONR 199005 approach also predicting the sound pressure within a couple of decibels.

Grütz's approach for a concrete structure would suggest that to obtain the A-weighted sound pressure level of 35 dBA, the A-weighted vibration velocity level of the surface of interest would be about 66 dBA; this is around the value of the ceiling measurement with the least vibration or the wall measurements with the higher levels of vibration.

6.4 Observations

6.4.1 Vibration

The measurements at the various locations around London showed that the train pass-by vibration levels fell into well-defined 'types', within which the 1/3 octave band vibration levels typically exhibited a spread of about 5 dB. The most obvious type designation is due to trains running in opposite directions on different tracks and in different tunnels.

For the room surfaces, there was significant variation between different measurement locations on lightweight surfaces due to modal patterns and the presence of discrete supporting elements. The solid wall structures seem to give slightly more consistent vibration levels, but this is likely

to be simply due to the greater number of solid wall measurement locations that have been included; a spread of around 10 dB is still observed. The reason for the differences is not clear, but is likely to be due to distinctions in construction (e.g. external vs internal solid walls) as well as the particular horizontal axis represented by each measurement.

As expected, the lightweight surfaces exhibited the greatest vibration levels, which for most of the rooms meant that the highest vibration levels were from a suspended ceiling. Vertical vibration levels at the corners of floors tended to be similar in magnitude to vertical measurements on the windowsills and even normal vibration on solid wall surfaces.

The measurement regime highlighted a number of difficulties in taking representative vibration measurements on floor surfaces. The first challenge is that most rooms encountered were carpeted. There are no reliable methods for mounting accelerometers over the top of a carpet for the frequency range of interest in groundborne railway vibration. Whilst mounting blocks with spiked feet exist on the market, the spikes are rarely sharp enough to pass through the carpet pile, and even if they can, the mounting system tends to consist of a relatively heavy block on slender supports which brings additional mounting resonances into the frequency range of interest. For timber floors it may be possible to obtain a reliable mechanical fixing by screwing a mounting to the floorboards through the carpet. However, in the rooms used in this project most of the floors were concrete, therefore a simple screw fixing was not possible. The result of this is that mid-span floor vibration measurements were not always possible. Nevertheless, it was usually possible to pull the carpet up at a room corner to obtain a good accelerometer fixing to the structural floor surface at a corner position.

Rooms that were not carpeted were usually finished with a laminate flooring. This is typically laid on a thin underlay, which is likely to introduce additional dynamic effects that affect the vibration readings. Furthermore, depending on how well the flooring has been fitted and how level the floor is, the flooring surface can be unsupported in places (especially at the edges), which would cause strong localised effects in the frequency range of interest. Since such flooring is usually laid underneath a skirting or finishing trim at the edges, it is not normally practical to lift the flooring to obtain a measurement on the structural floor surface.

These difficulties in obtaining reliable floor vibration measurements are particularly important to note due to the popularity of using floor vibration values to predict likely re-radiated noise levels.

6.4.2 Sound pressure

The results of the sound pressure measurements show that groundborne noise is nearly always loudest at the corners of the room. In addition, at least in the case of hotel accommodation,

pillow locations were quite often located near the room corners, and as such, recumbent occupants are likely to be exposed to the highest sound pressure levels. It is therefore recommended that the low frequency combined sound pressure level parameter be used (as defined in BS EN ISO 16283-1:2014 [62], see Equation (2-23)) to characterise groundborne noise in rooms. The average maximum combined sound pressure levels for all the rooms are presented in Figure 6-28. Overall averaged maximum levels were between 35 and 47 dBA. The highest overall A-weighted sound pressure level recorded for any single pass-by was L_{ASmax} 67 dB (in Hotel 2, Room 3). The A-weighted spectra are shown in Figure 6-29, which shows that the frequency region of 50 to 160 Hz tends to dominate the A-weighted results.

Figure 6-28. Re-radiated noise measurement summary: Average maximum combined sound pressure levels

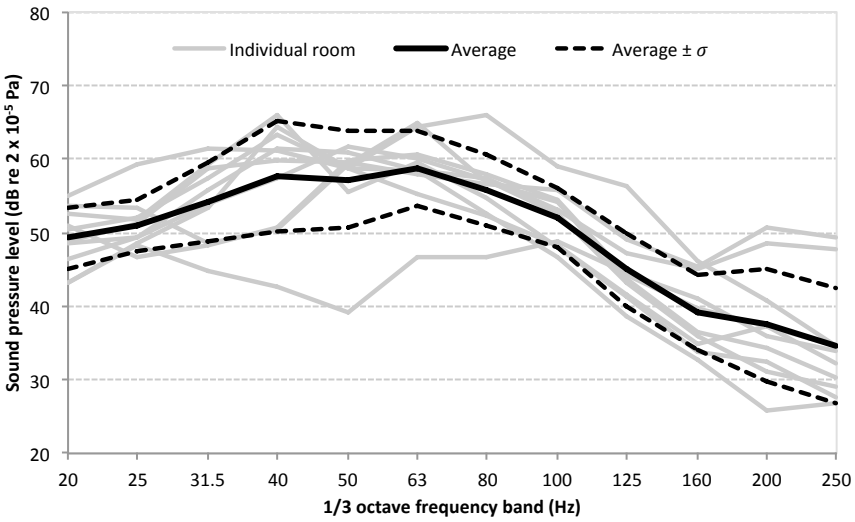

Figure 6-29. Re-radiated noise measurement summary: Average A-weighted maximum combined sound pressure levels

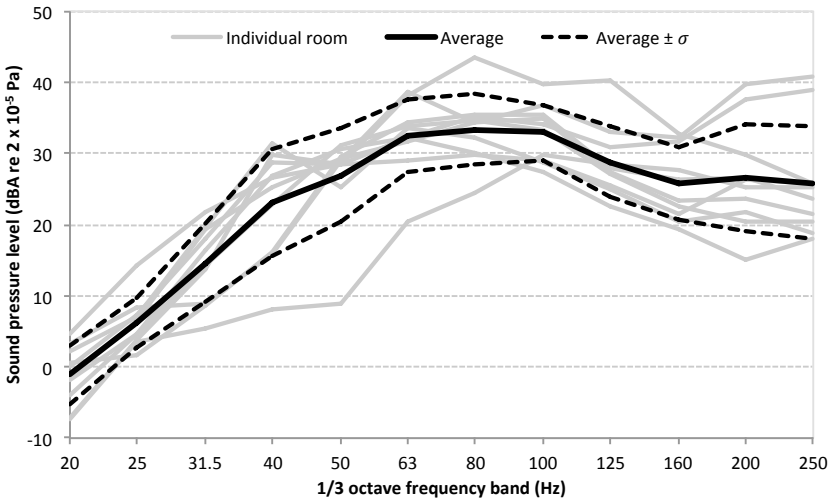

In general the influence of the room modes was seen in the sound pressure results, with spectrum peaks at corner positions and dips at more central room positions around the expected first natural frequencies. Interestingly, many of the rooms exhibited differences in their sound

pressure spectra at frequencies below the first expected acoustic mode. The reason for this is not known, as it is anticipated that at such frequencies the room would be in the pressure-response frequency region where the sound pressure would be reasonably uniform.

Reverberation times in the rooms were generally similar, ranging from around 1 s at the 1/3 octave band of the first room mode, down to around 0.3 s at the upper end of the frequency range (i.e. 200 to 250 Hz). This is to be expected, as most of the rooms were of a similar size and furnishment. The larger rooms of course exhibited longer reverberation times, with the dining room (Hotel 2, Room 3) result extending to 0.8 s in the 250 Hz band on account of its size and hard floor surface. This room exhibited the highest sound pressure levels, which are probably mainly due to the reverberant sound pressure component.

6.4.3 Accuracy of empirical predictions

It is appropriate to compare the measurement results to predictions from some of the empirical approaches that utilise vibration as a means to predict the re-radiated sound pressure levels. The empirical approaches considered here are Kurzweil [77], TCRP [78], Grütz [85,86] and ONR 199005 [80,81].

The first challenge when considering empirical prediction accuracy is the point outlined previously: that it is often difficult to obtain reliable measurements at mid-span floor locations in furnished rooms, and yet this is the location specified for most of the prediction methodologies. For the few rooms where a reasonably reliable mid-span floor vibration measurement was available, the measured *LV2P* (or $LV2P_n$) values were similar to those suggested by the Kurzweil and ONR 199005 approaches (when considering sound pressure levels at a central room location).

Where mid-span vibration measurements were not available, the floor corner positions (or even a solid windowsill position) usually provided a close alternative for the Kurzweil and ONR 199005 predictions. It is therefore considered that it is a valid approach to, if necessary, include an appropriate mid-span correction to data measured at a corner position as part of a re-radiated noise prediction.

It is noted that for the rooms measured, the Kurzweil and ONR 199005 approaches tended to give better predictions than the TCRP approach. However, the measurements were all based in London, in similar buildings; the TCRP method may provide better agreement with alternative railway stock, geology and architecture that exists in other cities worldwide.

The Grütz approach gave inconsistent agreement with the measurements; in some rooms the noise level would have been predicted well with the ceiling vibration measurements, whereas in

other rooms there were no surfaces that would have given a reasonable estimation of the noise level.

The Kurzweil and TCRP approaches assume a constant *LV2P* value with frequency: -27 dB for Kurzweil and -32 dB for TCRP. However, the results show that the *LV2P* value is rarely constant with frequency, and as such the accuracy of these predictions will be dependent on the source spectrum. The ONR approach does include some frequency dependence in the reverberation time correction, but even when considering the reverberation time normalised sound pressure levels, *LV2P* values still varied significantly with frequency. The implication of these findings is that there is little benefit in normalising the results to reverberation time, if a constant *LV2P* value is assumed.

Whilst a constant *LV2P* value was not observed in the results, several of the rooms exhibited a similar *LV2P* spectrum shape. It was often seen that around the room's first mode, reverberation time normalised $LV2P_n$ values were about -20 dB, and increased with frequency at about 3 dB per octave. This was particularly consistent for the wall measurements. Hotel 4 Room 1 exhibited the same increase with frequency, but the trend was shifted downwards by about 6 dB. Part of this is due to the absence of corner microphone measurement positions at this location. However, this hotel was affected by a different underground line than the other hotels, and therefore it is possible that the pattern observed is dependent somehow on the incident groundborne vibration.

6.5 Summary

In this chapter, the results from an extensive measurement campaign have been presented, in which ten rooms affected by groundborne noise have been examined. Results have been compared against four empirical prediction models, with most rooms showing poor agreement with all models. One of the main problems identified was the difficulty in obtaining reliable mid-span floor vibration measurements in furnished rooms.

A trend in $LV2P_n$ has been identified where the $LV2P_n$ is -20 dB at the room's first mode, and increases with frequency at a rate of 3 dB per octave. It is recommended that this should be investigated in future work.

In light of the difficulties in successfully applying the existing empirical methods to the measurement data, an improved understanding of re-radiated noise mechanisms is required in order to work towards a more refined empirical prediction approach. The mechanisms might be understood better by using a more detailed model to investigate the relative contributions of the room surfaces, and the influence that various parameters could have on the re-radiated sound pressure level. Due to the 3D dependencies of the re-radiated noise mechanisms, a 3D FE

technique is appropriate. The next chapter describes a 3D FE model approach which is validated against measurements from a room believed to be of similar construction and geometry, and is then subsequently used to investigate the influence of various parameters.

7. RE-RADIATED NOISE MODEL: VALIDATION STUDY

In the previous chapter, the case studies revealed a requirement for an improved understanding of re-radiated noise mechanisms, and it was proposed that this could be achieved through a 3D FE model approach. This chapter describes such an approach, with validation against measurements from a room believed to be of similar construction and geometry.

7.1 FE modelling approach

When modelling the re-radiated noise within a room using 3D FE analysis, it would be convenient to assume that the building/room structure, and the room acoustics are *one-way-coupled*, that is, that whilst the room acoustics do not affect the building/room structure, the building/room structure vibration is used as an input to the room acoustics model. With this approach, FE model sizes can be kept to a minimum, with solutions calculated more quickly than in the fully-coupled case. Another important benefit is that it can more readily allow for the comparison of noise contributions from individual surfaces.

In an empty room, since there is negligible air attenuation at the frequencies and distances considered for re-radiated noise, all the damping is provided at the room boundaries. For the room acoustics model, this might be modelled as an acoustic impedance at the surfaces. However, in a one-way-coupled approach the input to the acoustic model is given by specifying the boundary surface velocities as calculated from the structural model. It is not possible to specify both the velocity and impedance at the same point, and therefore there are difficulties in accommodating this approach.

One possible solution is to introduce an equivalent room damping in the air volume rather than at the boundaries. This has been investigated and documented in Appendix D, which describes a short study where the room frequency response around an axial mode was examined for a range of air damping values (the damping was specified in terms of attenuation per unit length (dB/m), which is a specific parameter provided by COMSOL Multiphysics). The appropriate air volume attenuation for a given reverberation time was found to be constant with frequency, and largely independent of room geometry for the range of rooms considered.

7.1.1 FE model description

In order for the modelled room surfaces to exhibit realistic vibration fields, an assembly representative of a small building structure was prepared, which could subsequently be coupled

to the room model. The structure consisted of a two-storey 2x2 portal frame arrangement, with each portal frame having dimensions of 8 m x 6 m. The height of each storey was 3.0 m. A diagram of the model is given in Figure 7-1. Note that the compass graphic shown in the figure is to assist with identification of individual walls. The dimensions and construction materials of the room model were chosen to be similar to one of the measured rooms, Hotel 3, Room 1, described in Chapter 6.3.8, which will be used for validation of the model approach.

Floors were represented as 270 mm thick concrete plates (represented by shell elements), supported by concrete columns with a 0.5 m x 0.5 m square cross-section (represented by beam elements). The mesh was specified with a maximum element size of 1.2 m, which is sufficient for frequencies up to around 300 Hz. The force input to the building structure was specified as a force per unit area with a vertical value twice that in the horizontal axes, applied over the entire basement floor surface (the blue shaded area in Figure 7-1).

A room structure of dimensions 2.35 m x 3.02 m was coupled to the building structure as seen Figure 7-1. The walls were defined as plate elements of 200 mm concrete, connected to the floor and the soffit. The ceiling was defined as 15 mm plasterboard, at a height of 2.96 m.

The ceiling displacement was coupled to the soffit over a rigid grid framework with supports spaced at a maximum of every 1.2 m in the y-direction, and 0.45 m in the x-direction, which is a typical recommendation for plasterboard ceiling systems (e.g. in [68]). The ceiling was connected to the walls via a 100 mm perimeter strip, which was assigned a lower stiffness than the rest of the ceiling (halved Young's modulus). The mesh used for the wall and ceiling surfaces had a maximum element size of 0.3 m (suitable for up to around 500 Hz for the ceiling, 3000 Hz for the walls). The internal volume of the room was specified as air, with a mesh of maximum element size 0.4 m (suitable for up to around 400 Hz). No air was included within the ceiling cavity, or in the rest of the building.

Figure 7-1. Re-radiated noise model: Validation model geometry

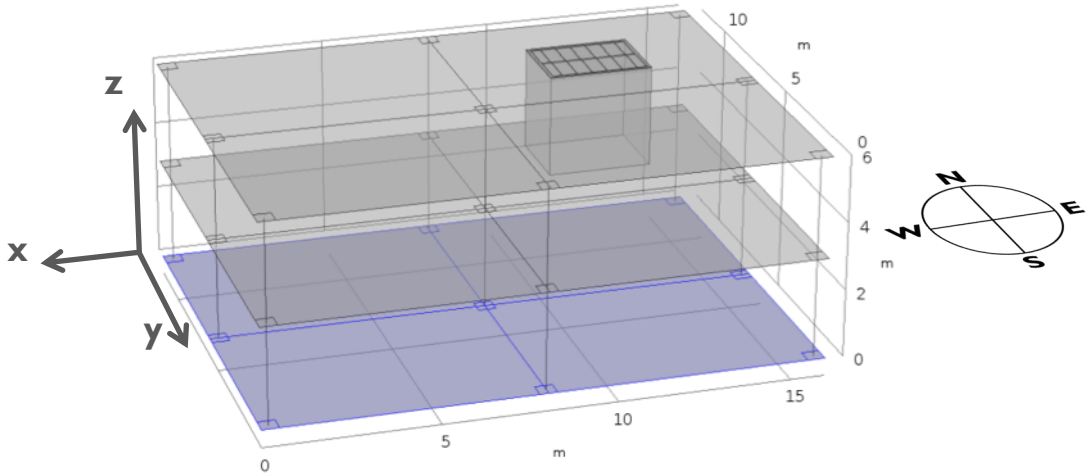

The material parameters used in the model are given in Table 7-1. The damping loss factors were included by making the Young's modulus values complex. Whilst material parameters for concrete have been discussed previously, the values for the plasterboard have been taken from the material library for the INSUL acoustic prediction software [135] as well through reference to literature (e.g. [52,136]).

Table 7-1. Material parameters used in re-radiated noise FE model			
	Concrete (floors & walls)	Concrete (columns)	Plasterboard (ceiling)
Density ($kg.m^{-3}$)	2400	2500	650
Young's modulus (GPa)	26.0	26.0	2.0
Poisson's ratio	0.33	0.33	0.20
Damping loss factor	0.05	0.05	0.02

7.1.2 Room damping

Initially, for the fully-coupled model, no additional damping was applied to the internal air volume, relying only on the damping in the structure. For a source in one corner and a receiver in the opposite corner, the pressure responses around a number of room modes were obtained with frequency resolutions as fine as 0.005 Hz; such fine resolutions were required because of the light damping in the system. The reverberation time was calculated from the width of the peaks at the natural frequencies, using the relationships described in Appendix D, with the results shown in Table 7-2.

Table 7-2. FE acoustics modelling: Calculated reverberation times for fully-coupled model without additional air attenuation	
f_m (Hz)	T_{60} (s)
57	44
58	110
73	20
113	20
116	17
163	13

Table 7-2 shows values for reverberation time that are clearly much greater than would be experienced in reality, even in a room considered to be completely unfurnished. The main reason for the discrepancies is likely to be due to insufficient coupling between the air volume and the wall surfaces, i.e. that the surface impedances are too high, which equates to an acoustic absorption that is too low. In addition, there may also be insufficient damping assumed for the materials; Utley & Pope suggest that damping in large panels can be significantly higher than the

internal damping of the material due to the mounting conditions [136]. The other reason for the discrepancy is the exclusion of room features that are nearly always present, for example windows and doors. These provide a mechanism for radiation damping, as well as scattering to some extent (at the upper end of the frequency range considered). As it is not feasible to account for all these features in this study, it is proposed that a constant air attenuation value of 0.35 dB/m be used for the modelling, corresponding to a reverberation time of 0.5 seconds (calculated in Appendix D). This will provide results that can be readily compared between situations, and extrapolated to other acoustic conditions by normalising the results to the reverberation time (e.g. Equation (6-1)).

7.2 Results

With the proposed air attenuation value, sufficient frequency resolution (i.e. at least 5 points per half-power bandwidth) was provided with a frequency spacing of 0.2 Hz over the range of 16 to 281 Hz (1325 frequency points).

The fully-coupled model had just over 80,000 degrees of freedom, taking approximately 5 hours to calculate on a reasonably powerful desktop computer. When considering the structure only (with no air volume) the number of degrees of freedom reduced to 65,000, with calculations taking around an hour to compute. The air volume had 15,000 degrees of freedom when considered by itself, with calculations completed in under 10 minutes.

7.2.1 Comparison of point evaluations and surface/volume averages

Due to modal patterns within structures and acoustic volumes in the frequency range of interest, there will be some variability between values evaluated at different discrete points. Note that in most cases, it is likely that relatively few acoustic or vibration evaluation points will be used by consultants undertaking measurements in the field for the purposes of survey-grade predictions. This is due to constraints on time and equipment resources.

For each of the primary room surfaces in the model, eight points have been used to evaluate the normal vibration, as shown in Figure 7-2. In order to accommodate alternative room geometries, the evaluation positions have been specified as functions of the surface dimensions, with the algebraic expressions shown in the adjacent table.

Figure 7-2. Re-radiated noise model: Surface vibration evaluation points

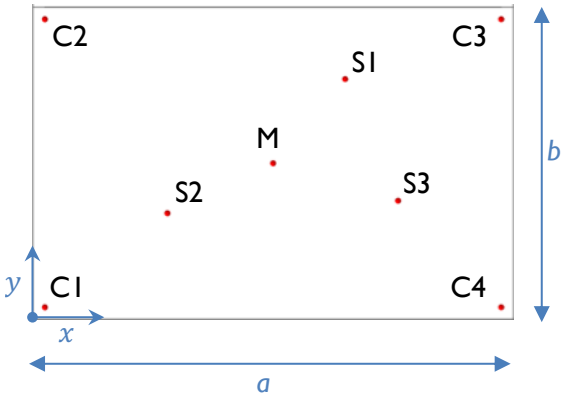

Position	x (m)	y (m)
C1	0.1	0.1
C2	0.1	b – 0.1
C3	a – 0.1	b – 0.1
C4	a – 0.1	0.1
M	a/2	b/2
S1	0.65a	0.77b
S2	0.28a	0.34b
S3	0.76a	0.38b

An alternative method for evaluating the vibration over a surface is the root mean square (rms) over all the FE model nodes. This averaging has a bias towards the higher values of surface vibration, such that resonant peaks are not unduly attenuated in the averaging process. The vibration spectra in 1/3 octave bands for three surfaces are provided in Figure 7-3 (North wall), Figure 7-4 (floor) and Figure 7-5 (ceiling). The results show that the corner positions give the lowest values, whilst the midpoint give inconsistent values with respect to the others, due it being located either at a node or antinode of any of the main surface modes. The centrally distributed points would give similar values to the surface rms if arithmetically averaged. Note the peak at 125 Hz for the ceiling vibration level, which is due to the point S1 being positioned close to an antinode of the ceiling with respect to its local support grid. This demonstrates the importance of using an average of multiple measurement points when evaluating the vibration of room surfaces.

Figure 7-3. Normal vibration variation over surface: North wall

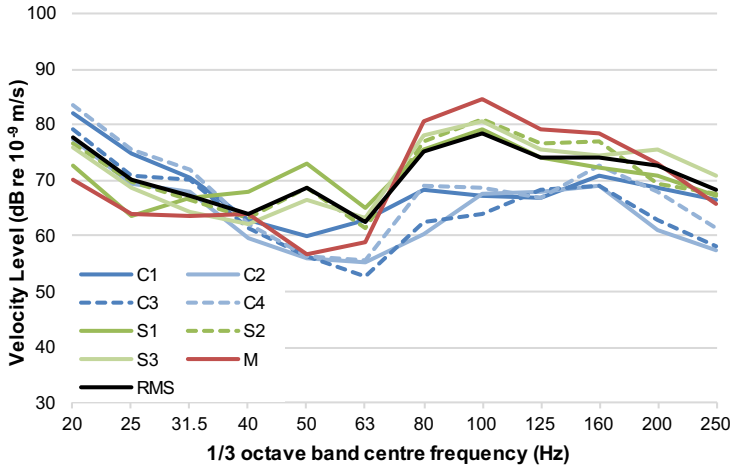

Figure 7-4. Normal vibration variation over surface: Floor

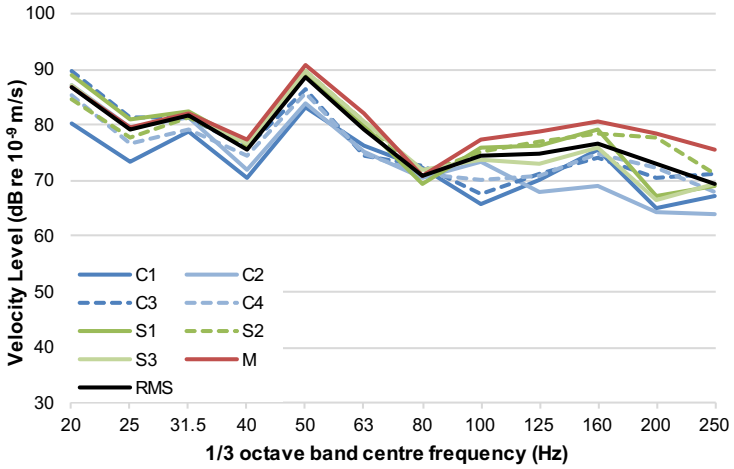

Figure 7-5. Normal vibration variation over surface: Ceiling

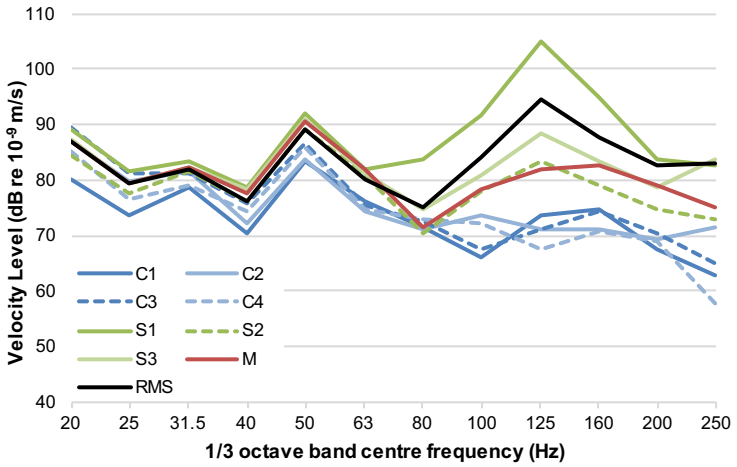

To evaluate the sound pressure, a total of twelve points have been used, as shown in Figure 7-6. In order to accommodate alternative room geometries, the evaluation positions have been specified as functions of the room dimensions, with the algebraic expressions shown in the adjacent table. Positions C1-C8 are at the room corners (0.5 m from each surface); R1-R3 are distributed around the central portion of the room; M is at the geometric centre of the room. The results are shown in Figure 7-7. For reference, the combined sound pressure level value (see Equation (2-23)) is also determined. Note that the corner positions give similar values, and therefore for clarity only C1, C2, C7 and C8 are shown in the Figure.

The results show that, as with the measurements, the corner positions give the highest sound pressure levels, with the lowest occurring at the room centre. Room position R3 gives similar results to the centre of the room, because for the present case the height of this position coincides with the room's vertical centre. The significant differences observed between positions R1 to R3 (up to 60 dB in the 50 Hz band) highlight the importance of using a number of positions to evaluate the sound pressure level in the room. The combined sound pressure level appears

to represent appropriately the sound pressure in the room that is most likely to be experienced by the occupants.

Figure 7-6. Re-radiated noise model: Sound pressure evaluation points

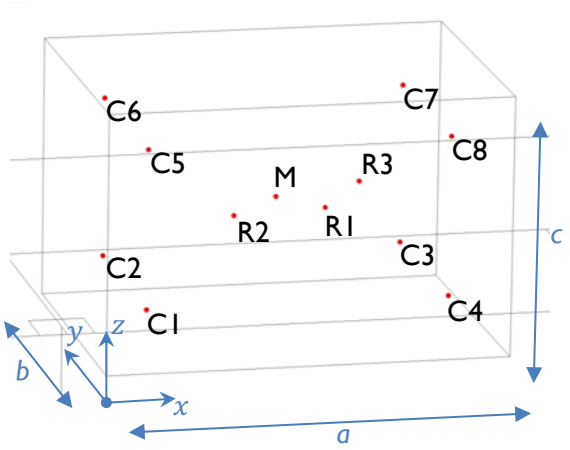

Position	x (m)	y (m)	z (m)
C1-C8	0.50 and a – 0.50	0.50 and b – 0.50	0.50 and c – 0.50
M	0.50a	0.50b	0.50c
R1	0.66a	0.70b	1.00
R2	0.37a	0.35b	1.25
R3	0.69a	0.40b	1.50

Figure 7-7. Sound pressure variation within room

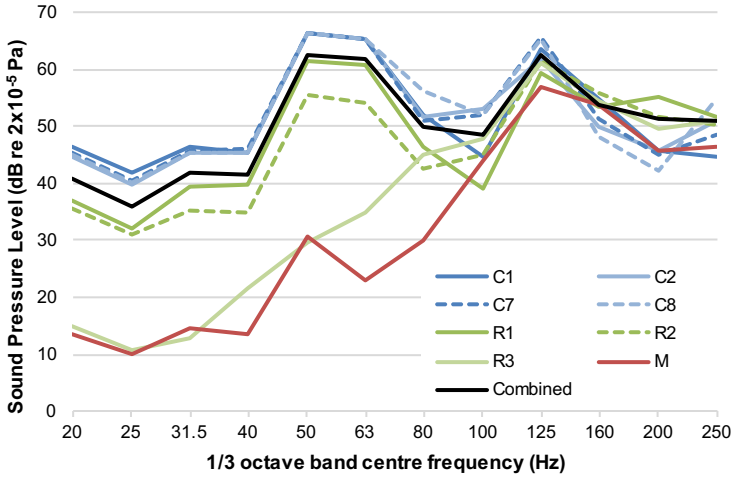

7.2.2 Comparison of fully-coupled and one-way-coupled models

The validity of a one-way-coupled approach can be determined by comparing vibration values with and without a fully-coupled room air volume. For excitation distributed over the base of the structure, the surface-averaged (rms) velocity levels for the floor, a wall, and the ceiling are shown in Figure 7-8. The lines for fully-coupled and uncoupled vibration are almost indistinguishable from each other for the wall and floor, but for the lighter plasterboard ceiling, the presence of the air in the room has an important effect between 110 and 160 Hz. This occurs through increased damping and the interaction of modes of the room and ceiling structure. It should therefore be concluded that when modelling the vibration of the system, it is appropriate to include a coupled air volume if dealing with lightweight surfaces, but this can be neglected if only heavy surfaces are included such as concrete or masonry. In reality, however, nearly all

modern domestic rooms will include at least one such lightweight surface (e.g. a plasterboard ceiling).

Figure 7-8. Vibration of room surfaces, with and without air in the room

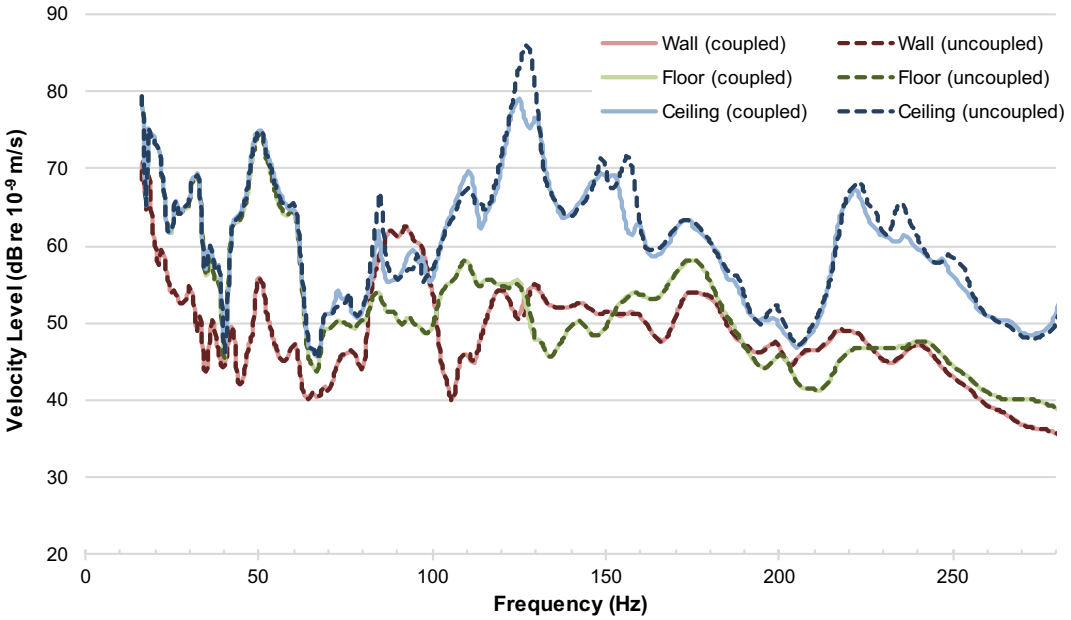

Whilst a constant attenuation of 0.35 dB/m has been specified for the air volume, the additional effect of the structural coupling on the room acoustics is shown in Figure 7-9, which shows the sound pressure level at one corner of the room in response to a point source with one Watt* of sound power (at each frequency) at the far-most corner. Here it is seen that the structure provides additional damping to the air volume between 100 and 170 Hz. In this frequency range there is interaction between the room and ceiling modes, and coupling with the floor/walls due to coincidence with bending waves. The inference from the data is that by omitting these specific effects of the room surfaces, the sound pressure level in the room might be slightly overestimated. However, it is envisaged that these effects could still be accounted for in calculations that are normalised to the reverberation time, where the reverberation time has been measured or modelled in detail.

* *Note that one Watt of sound power is a very high value. These results are not intended to be representative of an actual source, but rather the focus should be on any differences noted between the spectra.*

Figure 7-9. Sound pressure level in the room due to an acoustic source, with and without structural coupling

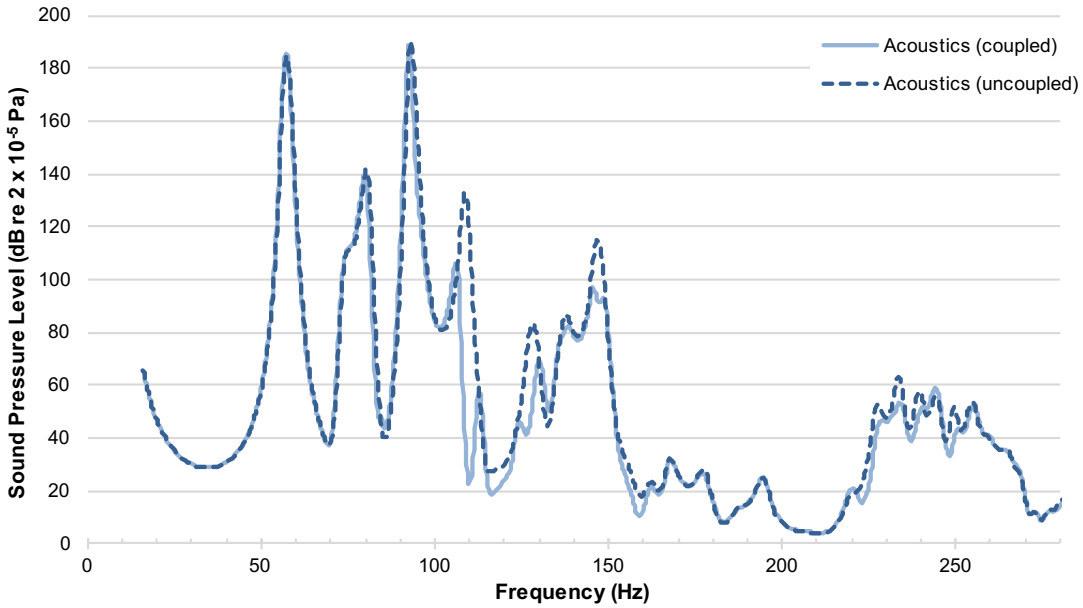

Should the one-way-coupled approach not provide the required accuracy (i.e. where there are lightweight room surfaces), a hybrid approach may be considered in which the surface acceleration values from a fully-coupled model are used as the input to a room-only model. Of course, the benefits of improved calculation time are lost with this approach, but there remains the potential to assess the noise level contributions from each surface separately. Results from the two approaches are compared with the fully-coupled model in Figure 7-10, which shows the combined sound pressure level in the room in response to the structural input at the base of the building structure. The results show that whilst the one-way-coupled model that used the structural-only solution as its input gives values very similar to the fully-coupled model in nearly all frequency bands (except 125 Hz), the model that used the fully-coupled solution as its input gives values that are almost identical to the fully-coupled solution result in all frequency bands.

Figure 7-10. Sound pressure level in the room due to a structural source, fully-coupled and one-way-coupled model results

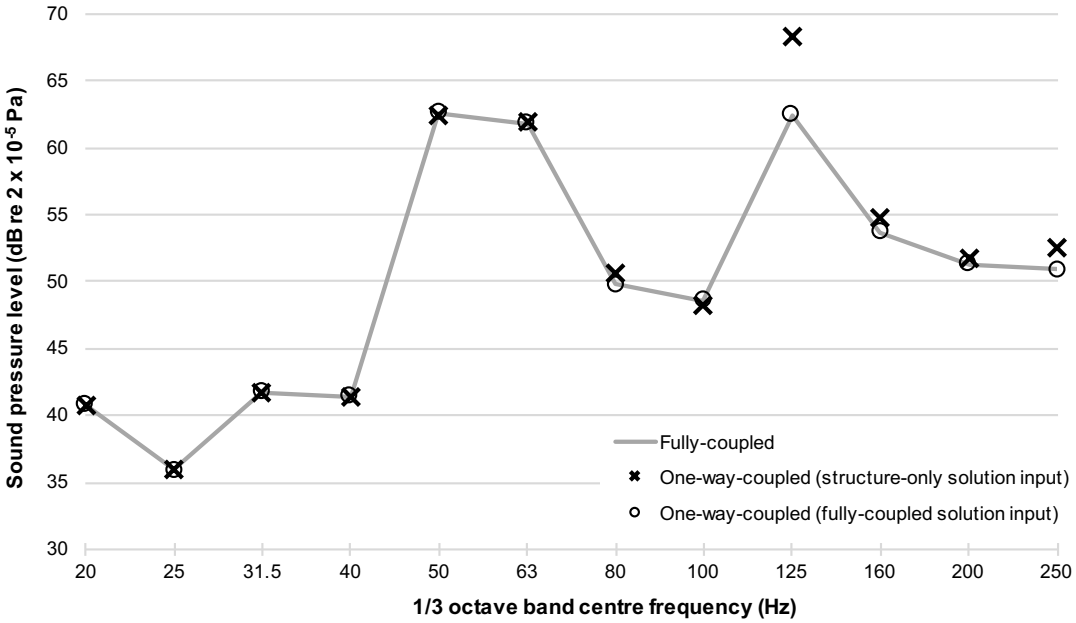

Using the one-way-coupled model with the input from the fully-coupled solution, the sound pressure level contributions from each surface can be identified, and are shown in Figure 7-11. These results suggest that the floor and ceiling are roughly equal in their contributions to the overall noise level at most frequencies, but a peak exists in the 125 Hz band for the ceiling, which is due to a mode of the plasterboard on its regular grid. In this frequency band there is also a mode of the local floor (and soffit) between the room walls. The peak at around 50-63 Hz is due to the first mode of the floors between the supporting columns. When the four walls are combined, it would be reasonable to expect that at most frequencies it is these that contribute most to the A-weighted sound pressure level, with the exception for the 125 Hz peak caused by the ceiling. However, since the contributions of each surface are frequency dependent, this depends on the input spectrum.

Note that below 40 Hz there are no local structural or acoustic modes and the room behaves as a single entity. In this frequency range, surface vibrations will be of similar magnitude and phase for all room surfaces, and the resulting sound pressures will be reduced. However, when using the one-way-coupled model to calculate the sound pressure level contributions from each surface separately, all surfaces other than the surface of interest are set to zero displacement. This causes the discrepancy seen below 40 Hz where calculated contributions from the floor and ceiling are greater than the total sound pressure level calculated with the fully-coupled model. When using the one-way-coupled technique for individual surfaces in isolation, results below the natural frequency of the lowest local structural mode should be discarded.

Figure 7-11. Sound pressure level in the room due to a structural source, fully-coupled and one-way-coupled model results

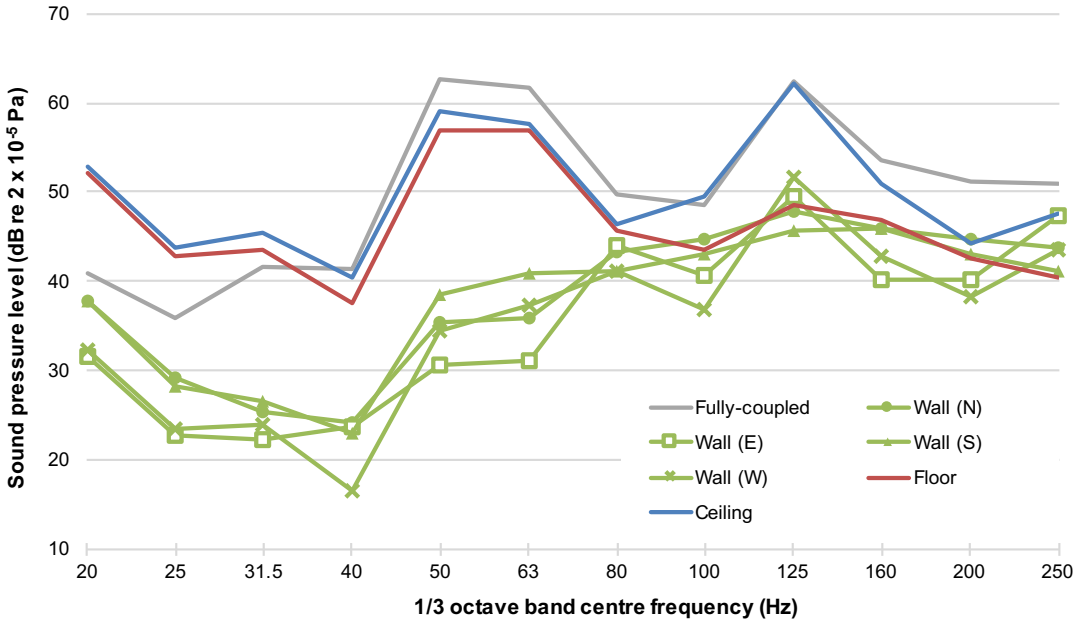

7.2.3 Comparison with measurements

The dimensions and construction materials used in the room model described above were chosen to be similar to one of the measured rooms, Hotel 3, Room 1, described in Chapter 6.3.8. It is possible to compare the $LV2P_n$ values directly by normalising the measured results to the measured reverberation time, and the results from the (fully-coupled) model to the assumed reverberation time of 0.5 s in each frequency band,. Note that the results from the model are based on a root mean squared surface average velocity (in the normal direction) whereas the measurement results are based on an average of the measurement points, typically two or three points per surface. In both cases the combined sound pressure level has been used, derived from the corner and central room positions. Measured results are shown in Figure 7-12; results from the model are shown in Figure 7-13.

It should be noted that $LV2P_n$ values for surfaces that are not contributing to the combined sound pressure level are meaningless. Attention should therefore be focussed on the wall/ceiling surfaces between 40-80 Hz, and all surfaces at frequencies above this. At around 125 Hz, attention should be focussed on the ceiling surface results.

Figure 7-12. Hotel 3, Room 1: measured *LV2P*$_n$ (dB re 2x10^4 Pa.m^{-1}.s)

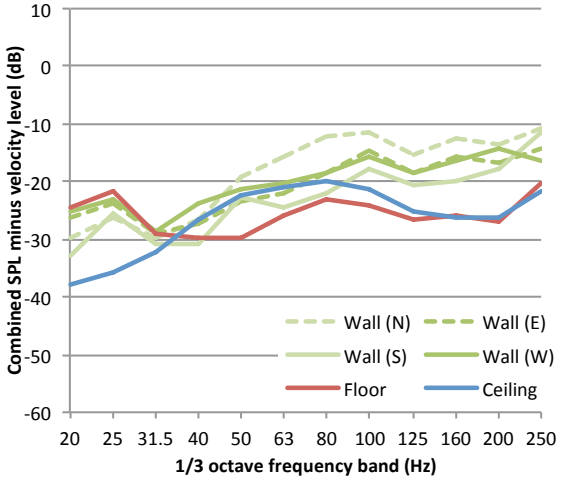

Figure 7-13. Hotel 3, Room 1: FE model *LV2P*$_n$ (dB re 2x10^4 Pa.m^{-1}.s)

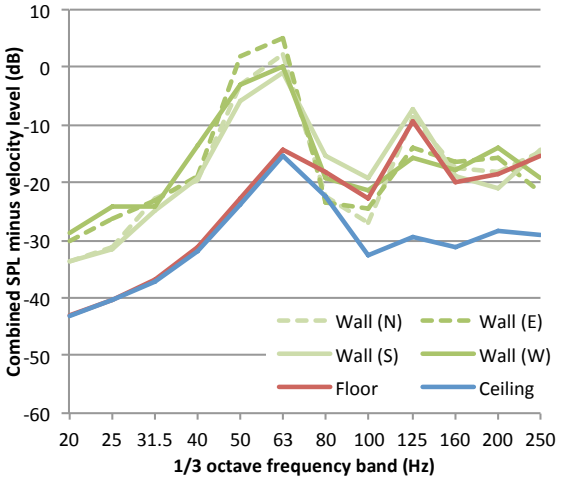

The results show differences between the measured and predicted values, and this is likely to be mainly due to inadequate specification of materials and boundary conditions (which were not fully known for the measured room). This mainly affects the values in the region below 80 Hz, which is the frequency region where the walls and floor structure exhibit strong modes in the model. The influence of doors and windows, as well as furniture such as beds and cupboards, is not explicitly included in the model; these features would be expected to break up the well-defined modal pattern that exists in the modelled surfaces, such that measured results appear comparatively less resonant.

Despite these factors, when taking into account the significance of the surfaces in their appropriate frequency regions the predictions give results that are of a comparable magnitude to the measured values,

7.3 Summary

This chapter has described an approach for modelling re-radiated noise in a room using a finite element model of a 3D air volume coupled with a 3D building structure. The initial results from the fully-coupled model predicted reverberation times in excess of those that would normally be expected in reality. This was considered to be due to insufficient acoustic absorption and damping specified in the materials, as well as the exclusion of room features such as doors and windows. In order to increase the amount of damping in the model, a value for attenuation in the air volume has been introduced that corresponds to a reverberation time of approximately 0.5 s. *LV2P* Results are then normalised to the reverberation time as part of the analysis.

Different extents of coupling between the air volume and structure have been investigated, and it is found that the coupling is important in the presence of lightweight room surfaces such as plasterboard ceilings. A technique where the surface vibration levels from a fully-coupled model

are applied to an air-volume-only room model is demonstrated to give results that are equivalent to the fully-coupled model at and above the first natural frequencies of the room structure. Whilst there are no savings in computational resources with this method, the benefits are that the re-radiated noise level contributions of each room surface may be determined separately.

When the model results are compared with measurements in a similar room, some differences are found. These have been attributed to inadequacies in the geometry and material specification, as well as the exclusion of furniture, doors and windows in the model. Nevertheless, when the sound pressure level contribution of each surface is considered in the appropriate frequency ranges, the model gives $LV2P_n$ values that are of comparable magnitude to those measured.

It is important to consider the differences between model and measurements if undertaking predictions of absolute sound pressure values. However, the current modelling approach is considered to be suitable as a basis for a parametric study on the influence of room and structural parameters on re-radiated noise.

Having established the validity of this approach, it is used in the next chapter in a parametric study.

[BLANK PAGE]

8. RE-RADIATED NOISE MODEL: PARAMETRIC STUDY

Further to the validation of the FE approach for calculating the re-radiated sound pressure levels in a room, as described in the previous chapter, a study into the influence of a number of room parameters on the re-radiated noise level in a generic room is presented in this chapter.

8.1 FE model description

The parametric study utilises a 'default' room model, which is intended to be representative of a generic residential room. The default model is specified with a force input at the base with a force per unit area of [0.5,0.5,1] N/m² in the [*x,y,z*] directions (see Figure 7-1 for the model axes orientations). The general form of the model is as described in Chapter 7.1, but with the room dimensions of 4 m x 3 m, and an internal ceiling height of 2.6 m. A view of the model geometry is presented in Figure 8-1.

Figure 8-1. Generic room: default geometry

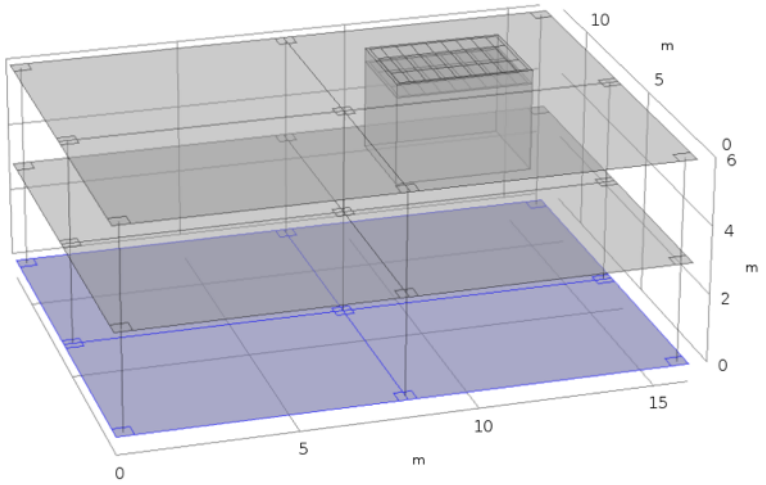

A number of parameter variations have been considered using this model as a starting point, as listed below:

- Room size (three configurations) – Section 8.2.2.
- Ceiling (with/without ceiling; with/without air in ceiling cavity) – Section 8.2.3.
- Walls (load-bearing concrete, non-load-bearing concrete, plasterboard) – Section 8.2.4.
- Force input direction (mainly vertical, vertical only, mainly horizontal) – Section 8.2.5.

8.2 Results

In order to make representative comparisons of overall noise and vibration levels, one-third octave band results are normalised to a basement vibration level with the average measured spectrum shown in Figure 3-26. For the various parametric studies, the full results are provided in Appendix H, with a summary of the results discussed in this chapter. Note that results labelled with an asterisk represent the default model condition.

8.2.1 Default model

The fully-coupled default model has just over 80,000 degrees of freedom, taking approximately 5 hours to calculate on a reasonably powerful desktop computer (with 1325 frequency points). The resulting rms normal velocity levels of each room surface are presented in Figure 8-2. The combined sound pressure level contributions of each surface type (normalised to the reverberation time) have been calculated using the one-way-coupled approach and are shown in Figure 8-3, together with the result from the fully-coupled model. The total contribution from all wall surfaces has been calculated by performing an energy summation of the contributions of each wall surface in each third octave band. Overall A-weighted sound pressure levels are shown in the legend. Note that results in frequency bands outside the range of validity for the one-way-coupled approach have been excluded from the figure.

Figure 8-2. Generic room: rms normal velocity level by surface, default model

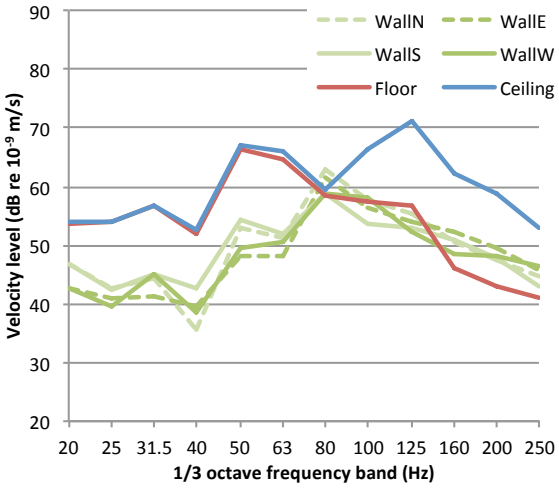

Figure 8-3. Generic room: sound pressure level contributions by surface, default model

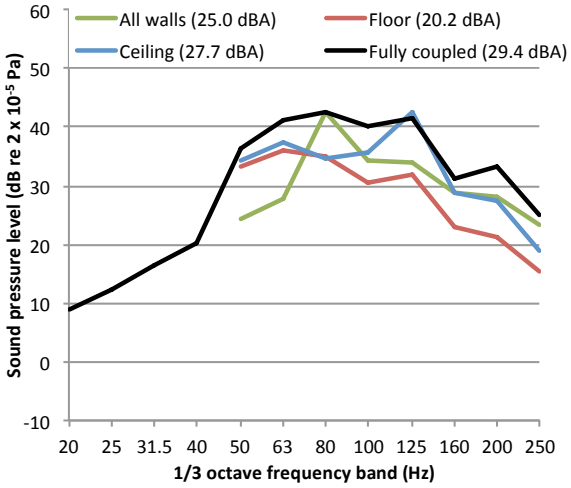

Figure 8-2 shows that the wall surfaces each have similar vibration levels over the frequency range. The floor and ceiling have similar vibration levels below 100 Hz, above which the modal behaviour of the plasterboard ceiling plays a significant role. Note that in the model it is assumed that the ceiling is rigidly connected to the soffit; however, in practice the stiffness of the ceiling support system would be expected to influence the results from a lower frequency.

Figure 8-3 shows that the relative contributions of the surface types is dependent on frequency, for example below 80 Hz the floor and ceiling are dominant; at 80 Hz the walls; and at 125 Hz the ceiling.

The $LV2P_n$ values for each surface expressed relative to the total re-radiated noise level (fully-coupled model) are shown in Figure 8-4. The $LV2P_n$ values for each surface expressed relative to its contribution (one-way-coupled model) are shown in Figure 8-5. Overall A-weighted sound pressure levels are shown in the legends, although it is important to note that these values are provided for indicative purposes only, as they are dependent on the input spectrum. Note that results in frequency bands outside the range of validity for the one-way-coupled approach have been excluded from the figure.

Figure 8-4. Generic room: $LV2P_n$ values by surface, relative to total sound pressure level, default model (dB re $2x10^4$ $Pa.m^{-1}.s$)

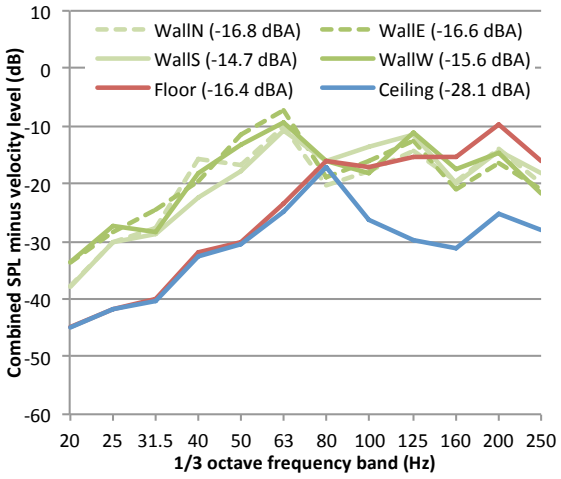

Figure 8-5. Generic room: $LV2P_n$ values by surface, relative to sound pressure level surface contributions, default model (dB re $2x10^4$ $Pa.m^{-1}.s$)

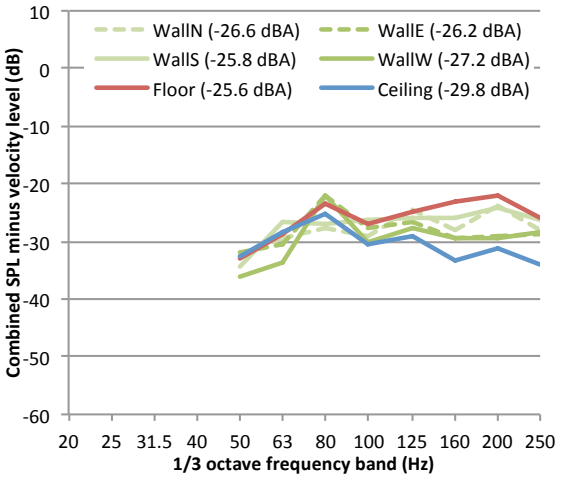

Figure 8-4 shows that, when expressed relative to the total noise level in the room, the $LV2P_n$ values for each surface are highly dependent on the surface and frequency. However, relative to the noise level contributions calculated from the one-way-coupled model, the $LV2P_n$ values in Figure 8-5 show a much reduced dependence on both surface and frequency, lying typically between about -24 and -31 dB. The differences between values are likely to be mainly due to differences in radiation efficiency for each surface. Note that for the floor, the $LV2P_n$ values are about -26 dB. At a reverberation time of 0.5 s, this is equivalent to *LV2P* values of around -29 dB, which is in the region of the Kurzweil (-27 dB) and TCRP (-32 dB) recommendations [77,78].

In addition to the observations made with respect to the comparison between measured and calculated *LV2P* values in Chapter 7.2.3, comparison of the two figures above supports a clear conclusion that is also intuitive; that a constant *LV2P* value for a *single* surface relative to the *total* re-radiated noise level can only be assumed in situations where the noise contributions from that

surface are dominant across the whole frequency range. For most re-radiated noise models in the literature, it is assumed that this is the case for the floor surface, but this may not always be the case, particularly where other surfaces exhibit strong modes in individual frequency bands. This is likely to be most significant source of error for the majority of empirical re-radiated noise predictions.

8.2.2 Room size

In addition to the default model room geometry, the model was run for two alternative room sizes; the dimensions and images of the room models are shown in Table 8-1. The room sizes given are for the interior air volume dimensions.

Table 8-1. Generic room: Room size, configurations

Size (m)	Image	Size (m)	Image
l=2.7 w=2.3 h=2.6*	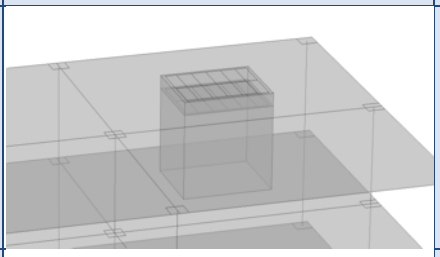	l=4.0* w=3.0* h=2.6*	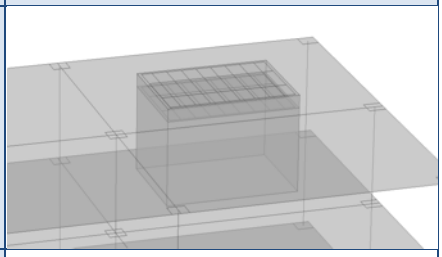
l=6.0 w=5.0 h=2.6*	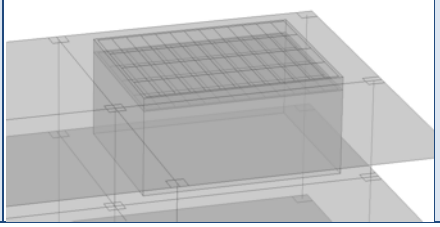	-	-

The full results for surface vibration levels and noise contributions are provided in Appendix H. A summary of the influence of the room size on the combined sound pressure level is given in Figure 8-6, with overall A-weighted values shown in the legend.

Figure 8-6. Generic room: predicted sound pressure level (normalised to reverberation time), by room size

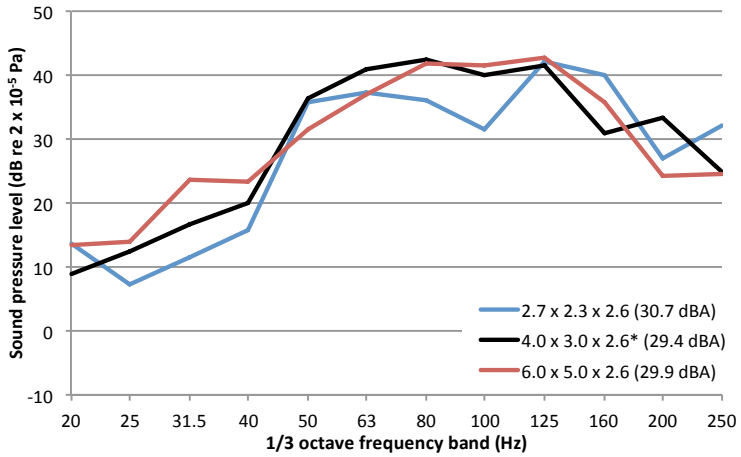

The results show that altering the room size influences a number of the mechanisms that contribute to re-radiated noise (see Figure H-5 to Figure H-8). The floor (and soffit) natural frequencies have been shifted, although since the spacing of the ceiling grid was maintained for each model, the frequency and magnitude of the main ceiling modes is unchanged. For the walls a shift can be noted in the natural frequencies, and walls in the larger room exhibit a flatter spectrum compared with the other room models. This is likely to be because the aspect ratio of the walls for the larger room is greater than for the smaller rooms, which reduces the likelihood of lower order modes from each of the local axes occurring in the same frequency bands.

For a given ceiling height, smaller rooms have a greater proportion of wall area to floor/ceiling area, and therefore the walls have a greater relative contribution to the total sound pressure level. The room modes in smaller rooms also occur at higher frequencies which is important when A-weighting is used for assessment, due to the increased emphasis on the upper frequencies (see Figure 2-3).

In summary, whilst it might be expected that larger rooms would inherently exhibit greater re-radiated sound pressure levels than smaller rooms simply due to an increase in the area of radiating surfaces, the natural frequencies of the surfaces remain important to consider, especially their relation to acoustic room modes and the input spectrum.

It should be noted, however, that larger room volumes typically exhibit greater reverberation times, which will also contribute to the sound pressure levels in practice (although not when the results are normalised as here).

8.2.3 Ceiling

In addition to the default ceiling specification, two alternative ceiling conditions are explored. In the first condition the air within the ceiling cavity is included; in the second condition the ceiling is completely omitted, such that the room volume is bounded by the exposed soffit. For the condition where the ceiling is omitted, the column height is reduced to 2.6 m (from 3.0 m) in order to maintain equivalent room volumes.

The full results of surface vibration levels and noise contributions are provided in Appendix H; as before a summary of the influence of the ceiling conditions on the combined sound pressure level is given in Figure 8-7, with overall A-weighted values shown in the legend.

Figure 8-7. Generic room: predicted sound pressure level (normalised to reverberation time), by ceiling condition

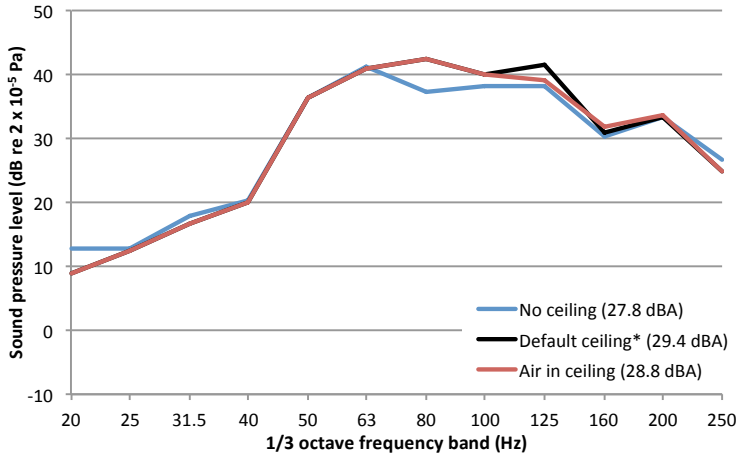

The results show that inclusion of air in the ceiling void has a minor effect in the 125 Hz frequency band. This is the band at which the ceiling vibration exhibits its primary mode of the plasterboard between the support framework, and it has already been discussed that air coupling can be important for lightweight surfaces (see discussion around Figure 7-8). At this frequency the air in the cavity is providing additional damping to the ceiling. Note that the ceiling framework has been specified as rigidly connected to the soffit; for ceiling support systems that incorporate resilient elements or are independent from the soffit (i.e. only supported from perimeter walls), the air and presence of any additional acoustic absorption within the cavity would be expected to have a more significant influence.

When comparing the conditions with and without the ceiling, it should be observed that the velocity levels of the floor and ceiling in each of the models are very similar below 100 Hz. Therefore, any differences between the two models below 100 Hz are likely to be due to the differences in storey height between the models rather than the inclusion of the ceiling. Nevertheless the inclusion of the ceiling is seen to increase the total sound pressure level in the 80, 100 and 125 Hz frequency bands by 2-3 dB. The increase would be more significant than this if the contributions from the walls and floor were neglected (these exhibit modes in this frequency region). This is demonstrated by comparing the sound pressure level contributions from the ceiling in Figure 8-8. These results suggest that the inclusion of a plasterboard ceiling on a rigidly connected frame might increase the contribution from the top of the room by up to 7 dB. For ceiling systems with independent or resilient supports, there will be a mass-spring-mass resonance; sufficiently above this frequency the ceiling would provide attenuation of re-radiated noise from the soffit. The influence of such non-rigid ceiling supports requires further investigation.

Figure 8-8. Generic room: sound pressure level ceiling contributions, by ceiling condition

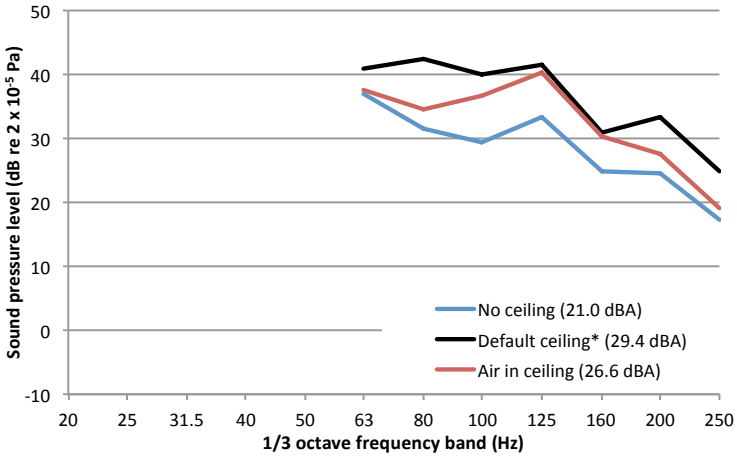

8.2.4 Walls

The default room model was specified with 200 mm concrete walls that were structurally connected to the soffit of the floor slab above. An alternative wall configuration is specified here whereby the walls are stopped slightly short of the soffit (10 mm) such that there is no structural connection. The intention of this configuration is to represent modern buildings that may include such gaps at the wallhead. The reason for this is to allow for deflections in the floor slabs caused by thermal expansion or changes in loading conditions. A further alternative wall construction has also been specified consisting of 25 mm plasterboard supported by a 80 mm square section timber framework. Frames were spaced at 600 mm centres in accordance with current practice and recommendations (e.g. [68]). This lightweight wall system also stops 10 mm short of the soffit. Images of the conditions are shown in Table 8-2. Note that these gaps do not coincide with the acoustic model, since they are above ceiling level and no air is included in the ceiling void in these models.

Table 8-2. Generic room: Wall configurations			
	Image		Image
200mm concrete, load-bearing*	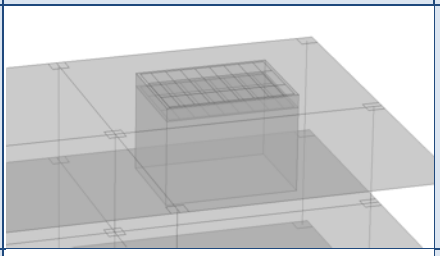	200 mm concrete, non-load-bearing	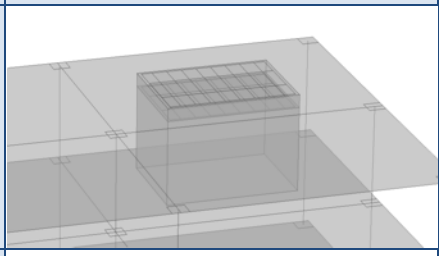
25 mm plasterboard on frame	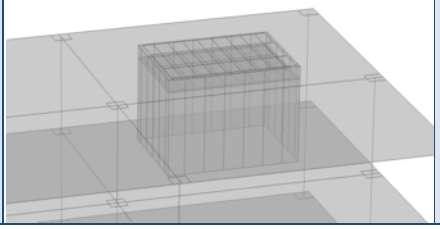	-	-

A summary of the influence of the ceiling conditions on the combined sound pressure level is given in Figure 8-9, with the full results provided in Appendix H.

Figure 8-9. Generic room: predicted sound pressure level (normalised to reverberation time), by wall condition

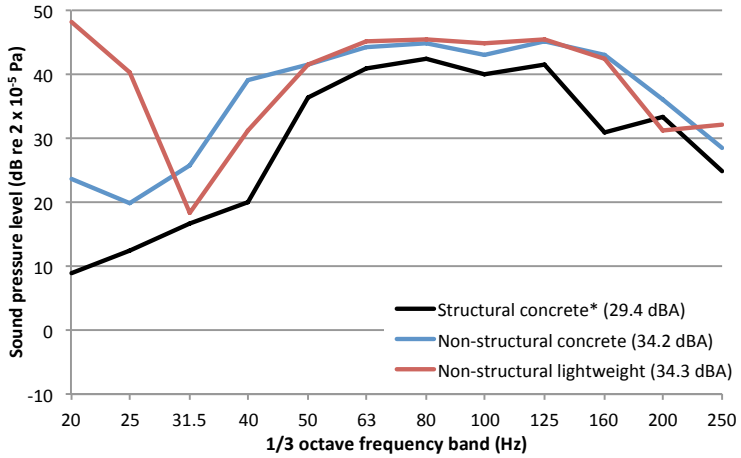

The results suggest that the wall connection to the soffit is relatively important, with the rooms with non-load-bearing walls exhibiting sound pressure levels around 5 dBA greater than the room with load-bearing concrete walls. Inspection of the results in the appendix leads to the conclusion that for the conditions where the walls are non-load-bearing, there is an increased contribution from the ceiling. This is due to the floor slab above only being supported on the columns leading to an increase in its vibration. With the modelled non-load-bearing walls, the ceiling is still connected to the walls via a small perimeter strip of reduced stiffness; the increased ceiling vibration as well as the free condition at the wall heads causes an increase in the concrete wall vibration by around 3 dB across most of the frequency range, although the band at which the concrete walls exhibit their first mode (80 Hz) does not change with the decoupling from the

soffit, probably because the walls are still constrained at the ceiling interface. For non-load-bearing walls, the perimeter ceiling interface is therefore likely to be important.

Due to their low stiffness, the first modes of the lightweight walls occur at a low frequency, around 20 Hz, which is the primary cause for the large increases in sound pressure level in the 20 and 25 Hz bands. The primary mode of the plasterboard on the wall frame occurs around the 160 Hz band, which causes contributions from the wall to increase by about 10 dB in this band, relative to the concrete walls (see Figure H-24).

8.2.5 Force input direction

The default model was specified with a force input at the base with a force per unit area of [0.5,0.5,1] N/m^2 in the [*x,y,z*] directions (see Figure 7-1 for the axis orientations). Two alternative conditions have been specified; a mainly horizontal condition (nominally [1,1,0.5] N/m^2) and an entirely vertical condition (nominally [0,0,1] N/m^2). The results have been adjusted in each case to maintain an equivalent total input force for each of the models. The full results are provided in Appendix H; a summary of the influence of the force direction on the combined sound pressure level is given in Figure 8-10.

Figure 8-10. Generic room: predicted sound pressure level (normalised to reverberation time), by force input direction

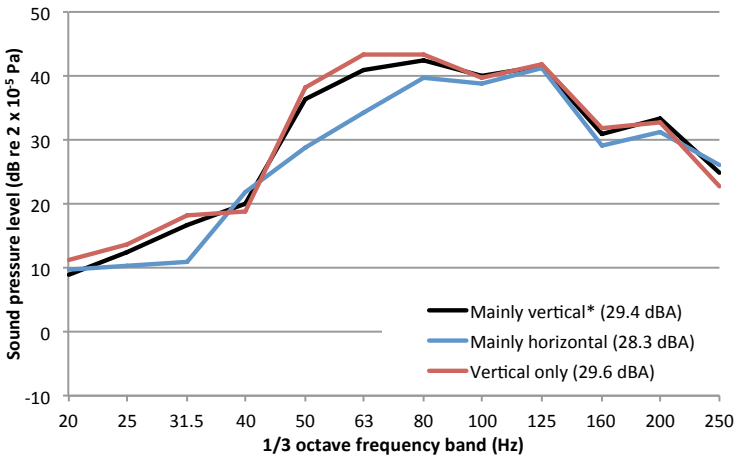

It can be observed from Figure 8-10 that the force input direction does not have a significant influence on the total re-radiated sound pressure level above 80 Hz. For the vertical-only condition, the vibration levels (and sound pressure contributions) of the floor and ceiling are increased by about 2 dB below 80 Hz. This is due to the increased proportion of force in the direction normal to these surfaces. Similarly, for the mainly-horizontal condition the contributions from the floor and ceiling are reduced, which accounts for the reductions in total sound pressure level by up to about 7 dB below 80 Hz. It would be expected that for the mainly-horizontal condition the walls might exhibit a relative increase in vibration and sound pressure contributions, but this is not the case, with the exception of a very minor increase (1-2 dB) at the

lowest contributing frequencies. In addition, the peak in the vibration spectrum for the walls is shifted from the 80 to the 100 Hz band by increasing the horizontal force components. The mechanism for this is unclear, but is possibly due to interactions between the upper and lower floor slabs.

8.3 Summary

In this chapter, an FE model of a generic room has been presented, which has been used as the basis of an investigation into the influence of certain room and building parameters on the re-radiated sound pressure level.

With respect to the size of the room, it was found that (when normalised by reverberation time), larger rooms might not necessarily exhibit higher re-radiated sound pressure levels than smaller rooms due to the influence of modes in the room volume and bounding surfaces. When designing rooms for low noise, the coincidence of these modes with peaks in the input spectrum is therefore important.

When examining the influence of the ceiling, it was found that, compared with an exposed soffit condition, provision of a ceiling (on a rigidly connected frame) could increase the re-radiated noise contributions from the top of the room by up to 7 dB due to additional structural modes being introduced. The inclusion of air within the ceiling cavity resulted in a slightly reduced ceiling contribution due to increased damping.

The structural connection of walls to the soffit was found to have an important influence on the re-radiated sound pressure levels. The main source of difference was found to be the ceiling, since the inclusion of load-bearing walls reduces the mobility of the floor slab above. As a result, the models with non-load-bearing walls exhibited overall sound pressure levels about 5 dBA greater than the model with load-bearing walls. The lightweight walls had a significantly lower fundamental natural frequency (around 20 Hz) than the concrete walls, but also introduced additional modes at higher frequencies (around 160 Hz), which contributed to the total sound pressure level.

The input force direction was found to have only a minor influence on sound pressure levels above 80 Hz, but below this frequency the force in the vertical direction is most important. Whilst the low frequency floor and ceiling contributions could be attributed to the amount of force that was in the vertical direction, the influence of the horizontal components is more difficult to understand due to the complex interactions between the floor slabs and columns.

Further to the observations made from the parametric study described in this chapter, it is suggested that future investigations could include:

- Additional wall types e.g. different concrete block densities, and the influence of plasterboard wall linings;
- Additional ceiling types e.g. resilient ceiling frames, independent ceilings, suspended ceiling tile systems;
- Floor treatments e.g. floating floor systems such as resilient screeds, cradle and batten systems;
- Detailed room geometry e.g. window and door reveals, room furniture.

[BLANK PAGE]

9. Conclusions and Further Work

9.1 Conclusions

As part of this research, several aspects of buildings and rooms have been explored in order to improve understanding of the most important groundborne noise and vibration mechanisms. Specific conclusions from the research are summarised in this section.

9.1.1 Review of building vibration measurements and modelling

Measurement data from eleven buildings has been reviewed. Whilst these buildings had different sizes, age and construction types, a number of trends have been identified that are common to many of the buildings. These include the fact that typically up to about 15 dB amplification occurs with height up the building at low frequencies (below about 25 Hz), but attenuation occurs at higher frequencies. However, there is significant variability between different buildings, particularly in the transmission between basement and ground floor. Measurement spectra at the basement of all buildings have been compared and show similar shapes, with broad peaks around 10 and 50 Hz. Despite the measurements representing different buildings and underground railways, the standard deviation is about 5-7 dB.

Results from the measurements have also been compared with predictions from a range of finite element model approaches of varying complexity, and with an existing empirical approach. It has been found that multi-bay finite element model approaches correspond well with the measurement trends, and give results which are an improvement over the existing empirical method.

9.1.2 3D finite element modelling of buildings

A 3D finite element modelling approach has been developed for predicting the levels of vibration in a building, relative to the levels in the basement. The approach has been validated against measurements in two large concrete frame buildings in London with reasonable agreement, although there are many uncertainties in the geometry, excitation, material parameters, and boundary conditions of physical buildings.

The 3D finite element approach has been used to develop a 'generic' building model for parametric study. This has been used to examine the influence of many structural parameters on the transmission of vibration through the building. Damping has been shown to be important, and a loss factor of around 0.05 gives best agreement with the measurement trends. The presence of internal (structural) walls has been shown to lead to slightly reduced vibration levels for the

upper floors of a building. The inclusion of a 'blocking' floor, with a mass twice that of the other floors, has been shown to have limited effect for floors above. As well as providing useful observations for the dependence on each of the parameters, it has been found that building vibration is strongly dependent on the modes of the global building structure and the local floor slabs. It is therefore recommended that improved empirical models should include these effects.

9.1.3 Empirical formulae for building vibration

Using the information from the 3D finite element modelling and measurement data review, a new empirical approach has been developed for predicting groundborne vibration in buildings in 1/3 octave bands. The approach uses terms allowing for the influence of the resonance frequencies of the building and floor slabs, which may be obtained through measurements or other models. In addition a number of constants are required, which are related to the building type.

The approach includes three main terms, which are applied to the basement vibration level to predict the vibration elsewhere in the building. The first term is a function of the building's vertical natural frequency and the storey of interest, and affects a low frequency peak. The second term is also storey dependent, but is used to account for reductions in high frequency vibration on a per-storey basis. The third term is used to predict the additional vibration amplification at a mid-span location, and therefore includes terms for floor slab natural frequencies, amplitude, and peak width.

Results from this empirical approach have shown good agreement with results from the full finite element model, but its accuracy and usefulness for physical buildings will depend on the availability of terms for various building types.

9.1.4 Measurements of re-radiated sound

Measurements in ten rooms affected by re-radiated noise from underground railways have been undertaken, in which the sound pressure level has been measured at multiple positions throughout the room, and vibration levels of each surface have also been obtained. Maximum A-weighted combined sound pressure levels are generally between 35 and 47 dBA, and the frequency range that dominates the A-weighted results is 50 to 160 Hz. The highest maximum sound pressure level measured during any single pass-by at a single measurement location was 67 dBA. The measurement data shows that groundborne noise levels at the centre of the room are generally lower than in other parts of the room due to the influence of room modes. Whilst the room corner positions represent the highest sound pressure levels, it has been found that positions close to the pillow in bedrooms can exhibit sound pressure levels just as high, particularly as in many cases the pillow position is actually located close to a room corner. It is therefore important to include the corner positions of the room as part of the assessment of re-

radiated sound pressure level. The low frequency combined sound pressure level parameter (as defined in BS EN ISO 16283-1:2014 [62]) is recommended to characterise groundborne noise in rooms.

Despite the large number of measurements, the data does not agree well with the existing empirical prediction methods in the literature and large variability is found. One of the reasons for this is the difficulty in obtaining reliable measurements of vibration on the floor surface of a furnished room. In order to understand further the re-radiated noise transmission mechanisms, it is recommended that finite element modelling is used.

9.1.5 3D finite element modelling of re-radiated sound

A 3D finite element model approach has been developed to calculate re-radiated sound pressure levels in rooms. The finite element model consists of a small building structure coupled to a room structure. 'One-way' coupling is used to excite the bounding surfaces of an air volume within the room.

The finite element model has been extended with an approach that allows the relative sound pressure contributions of individual room surfaces to be approximately determined at frequencies above the fundamental local structural and acoustic natural frequencies. It is found that different surfaces can dominate the sound pressure level in different frequency ranges, according to their modal frequencies. This helps to explain most of the discrepancies found with the empirical guidance when considering the difference between surface velocity and sound pressure levels.

9.1.6 Parameter study for re-radiated sound

The 3D finite element model approach has been used as a basis to investigate the influence of a number of room parameters on the re-radiated noise level. It has been found that, compared with an exposed soffit condition, a ceiling on a rigidly connected frame might cause re-radiated sound pressure levels in the room to be increased slightly (1-2 dBA).

The connection of the wall to the soffit has been found to be important; a load-bearing concrete wall is predicted to provide room sound pressure levels 5 dBA less than for a non-load-bearing concrete wall. The main reason is that load-bearing walls reduce vibration in the upper floor slab (and ceiling).

Room size is shown to have a negligible influence on re-radiated sound pressure level for a given reverberation time, although due to shifting of natural frequencies, the influence is dependent on the input spectrum.

9.1.7 Empirical formulae for predicting modes in multi-supported plates

As part of an investigation into predicting natural frequencies in plates, refined empirical formulae have been derived for predicting the first natural frequency of a multi-supported plate. The new formulae provide more accurate results, and allow for a greater range of plate size configurations compared with the approach previously available in the literature.

9.2 Recommendations for further work

9.2.1 Building vibration modelling

It is recommended that further work should include using the 3D finite element modelling approach to predict vibration transmission in other building types, such as steel frame, masonry and lightweight timber frame buildings. In addition, the influence of the ground coupling requires further understanding. Therefore the inclusion of different foundation types and ground types in future parameter studies is recommended.

9.2.2 Empirical building vibration terms

The empirical prediction approach developed in this research for building vibration should be extended to include additional terms. It is recommended that further work should include modelling (e.g. in conjunction with the suggestions in Section 9.2.1 above) and/or measurements of additional building types and situations, to obtain updated constants for different building types.

In addition to obtaining these constants for different building types, it is also recommended that suitable methods to determine the building and floor slab natural frequencies be identified and validated against measurements. This will further assist in the adoption and development of the empirical expressions.

9.2.3 Re-radiated noise model

Only a relatively small number of parameters have been investigated using the finite element approach described for the re-radiated noise study. It is therefore recommended that the approach be extended to include the following:

- Additional wall types e.g. different concrete block densities, and the influence of plasterboard wall linings;
- Additional ceiling types e.g. resilient ceiling frames, independent ceilings, suspended ceiling tile systems;
- Floor treatments e.g. floating floor systems such as resilient screeds, cradle and batten systems;

- Detailed room geometry e.g. window and door reveals, room furniture.

It is also recommended that studies be conducted with the room located in a different type of building structure, such as a timber frame house.

[BLANK PAGE]

APPENDIX A: VIBRATION OF STRUCTURAL COMPONENTS

Modelling approach

In order to understand how changes in individual parameters might affect vibration propagation through a building structure, it is not possible to rely on measurements in actual buildings. The use of models is therefore appropriate. Finite element analysis is a modelling technique whereby a structure may be represented digitally through a mesh of interconnected nodes. When the material properties, force input and boundary conditions of the structure are known, an equation of motion for the system may be derived in matrix form, which can be solved for discrete input frequencies in order to obtain the structural response at any point on the structure to an input force.

A number of finite element analysis software packages are available. This research has used the Structural Mechanics module of COMSOL Multiphysics due to its (relative) ease-of-use and computing platform interoperability.

Model mesh

A major consideration with a finite element analysis approach is computation time, particularly with such physically large and complex models as buildings. The computation time of a full simulation is determined by the number of degrees of freedom of the system and the number of frequency points required, as well as the capability of the computer system to be used. It is therefore necessary to optimise the modelling parameters in order to strike the best balance between accuracy and speed of calculation.

The number of degrees of freedom depends largely on the mesh resolution. Where linear elements are used, the rule of thumb is that a minimum of five to six elements are required per wavelength, at the maximum frequency of interest. Where quadratic elements are used, as have been used in this study, this may decrease to around 2. Additional considerations are the aspect ratio of the elements (that is, the elements should not be too thin or distorted), and the size growth rate of adjacent elements [130,133,134].

Modelling plates

Single plates

When predicting the dynamic response of plates, it is important to consider whether thin plate theory is sufficient, or whether shear deformations within the plate must be accounted for, using thick plate theory. This may be tested by comparing predicted natural frequencies using each theory. The predicted uppermost modes for an 8 x 6 x 0.25 m concrete slab with pinned edges are given in Table A-1 for frequencies up to 200 Hz, and Table A-2 for frequencies up to 281 Hz. The predictions are from the analytical expressions for thin and thick plates given in Equation (2-14) and (2-17) respectively. The images of the mode shapes are from the FE convergence study described in the next few pages.

The fundamental (1,1) natural frequency is predicted by thin theory to be at 17.0 Hz, and by thick theory at 16.9 Hz. Whilst the predicted natural frequencies are close, differences of up to 8% are noted in the predicted vibration modes around 280 Hz. It is thus shown that for the slab considered, assumption of a thin plate may be adequate for predicting the first modes, but for the upper frequencies, a thick plate approach would normally be required in order to achieve appropriate accuracy.

Table A-1. Analytical plate mode predictions, up to 200 Hz			
Mode (m,n)	Predicted frequency (Hz)		Image of mode shape
	Thin theory	Thick theory	
4,3	195.6	185.4	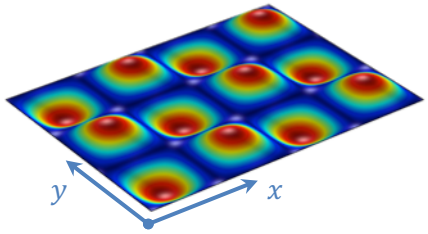
1,4	180.0	171.3	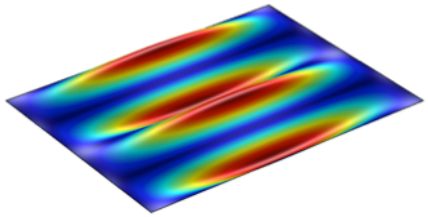
5,1	163.7	156.4	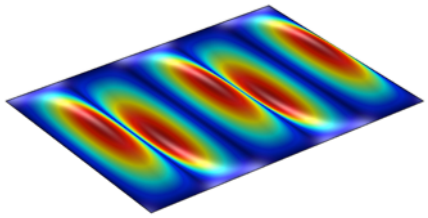
3,3	152.8	146.4	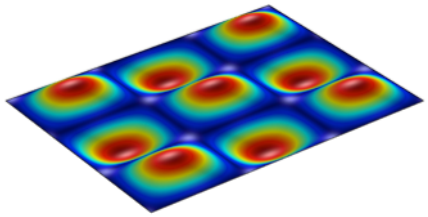
4,2	141.2	135.8	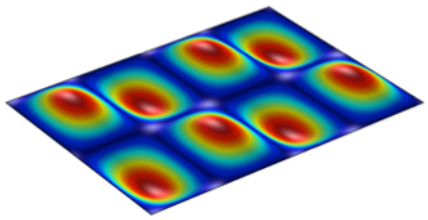
2,3	122.2	118.1	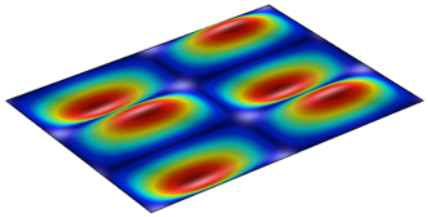

Table A-2. Analytical plate mode predictions, up to 281 Hz			
Mode (m,n)	Predicted frequency (Hz)		Image of mode shape
	Thin theory	Thick theory	
2,5	296.1	273.8	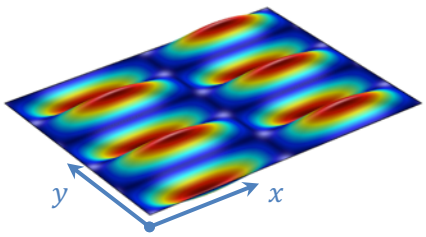
1,5	277.7	257.9	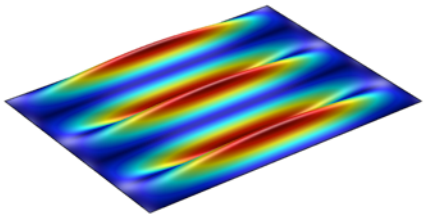
4,4	271.6	252.6	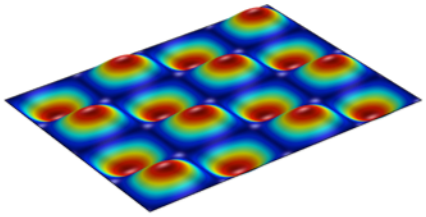
6,2	263.5	245.6	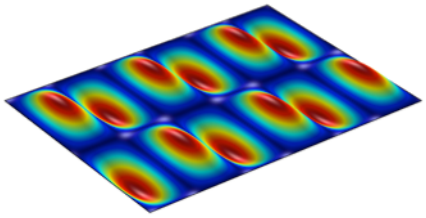
5,3	250.6	234.3	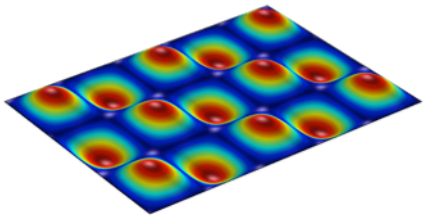
6,1	230.9	216.9	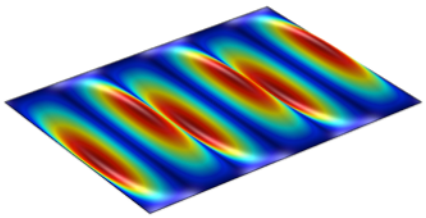

The bending wave speed c_B (in m/s) in a plate is given by:

$$c_B = \left(\frac{D\omega^2}{\rho h}\right)^{\frac{1}{4}} \qquad \textbf{(A-1)}$$

where:

$D = \frac{Eh^3}{12(1-\nu^2)}$;

ω is the angular frequency ($= 2\pi f$) in rad.s^{-1};

h is the thickness of the plate, in m.

Since $c_B = f\lambda$ (where λ is the wavelength, in m), the corresponding minimum wavelength* considered at 200 Hz is 2.80 m. As such, the maximum quadratic element size should normally be 1.40 m. Previous work in this research has considered frequencies up to 200 Hz. In order to provide for the full one-third octave band at 250 Hz in future, the maximum frequency considered must be 281 Hz for which the wavelength is 2.37 m and the maximum quadratic element size should be 1.19 m.

One of the tests for mesh accuracy is the convergence of predicted natural frequencies with reducing element size – particularly towards the analytically predicted natural frequencies. The effect of element size was investigated through an exercise studying the uppermost six modes of a floor slab (simply supported at the edges), with the results shown in Table A-3 for frequencies up to 200 Hz, and Table A-4 for up to 281 Hz. When considering up to 200 Hz, results with maximum element sizes of less than around 1.75 m are of the same order as that with extremely fine element sizes. In order to provide for the full one-third octave band at 250 Hz in future, the maximum frequency considered must be 281 Hz, for which a maximum element size of less than around 1.50m is suitable.

* assuming a 0.25 m thick plate of density 2400 kg.m^{-3}, Poisson's ratio 0.33 and Young's modulus 26 GPa.

Table A-3. FE model convergence, natural frequency prediction (Hz), up to 200 Hz							
		Mode of vibration (m,n)					
		4,3	1,4	5,1	3,3	4,2	2,3
Thin plate theory		195.6	180.0	163.7	152.8	141.2	122.2
Thick plate theory		185.4	171.3	156.4	146.4	135.8	118.1
Max. element size (m)	0.02	182.7	171.0	155.9	144.5	134.1	117.0
	0.05	182.7	171.0	155.9	144.4	134.1	117.0
	0.10	182.6	170.9	155.8	144.4	134.0	116.9
	0.25	181.9	170.2	155.3	143.9	133.6	116.6
	0.50	180.5	168.6	153.9	143.0	132.8	116.0
	0.75	178.9	167.0	152.5	141.9	131.8	115.1
	1.00	177.6	165.5	150.8	140.6	130.6	114.1
	1.25	177.8	166.1	150.5	140.4	130.2	113.4
	1.50	180.5	165.8	153.6	141.5	130.2	114.0
	1.75	184.8	177.2	153.4	144.4	133.6	113.3
	2.00	197.1	182.1	164.1	145.7	134.6	114.1

Table A-4. FE model convergence, natural frequency prediction (Hz), up to 281 Hz							
		Mode of vibration (m,n)					
		2,5	1,5	4,4	6,2	5,3	6,1
Thin plate theory		296.1	277.7	271.6	263.5	250.6	230.9
Thick plate theory		273.8	257.9	252.6	245.6	234.3	216.9
Max. element size (m)	0.02	272.8	257.8	249.5	243.7	231.2	216.5
	0.05	272.7	257.7	249.4	243.7	231.1	216.4
	0.10	272.4	257.5	249.2	243.5	230.9	216.3
	0.25	271.0	256.2	248.0	242.3	229.9	215.3
	0.50	267.5	252.8	245.4	239.6	227.6	212.8
	0.75	264.5	250.3	243.1	237.0	225.4	210.6
	1.00	265.0	251.0	242.6	236.5	225.0	209.9
	1.25	268.9	254.5	244.7	237.2	226.3	210.6
	1.50	277.0	259.8	249.8	242.3	229.5	219.2
	1.75	293.5	n/a	267.0	251.5	241.4	224.7
	2.00	325.7	312.3	301.1	282.8	276.6	256.4

An exercise has been performed using the FE model described for Case Study A (see Section 4.2.3) with the maximum element size reduced from 1.5 to 0.6 m. This had the effect of nearly doubling the number of degrees of freedom of the model from 440k to 870k. The vibration

response to an arbitrary input force at a single point (mid-span on the 5th floor) is shown in Figure A-1. It supports the above conclusion that sufficient model convergence is reached for typical building models (for the frequency range up to 200 Hz) where the maximum element size is less than around 1.75 m.

Figure A-1. FE model convergence:
Predicted vibration of TCR case study building, mid-span

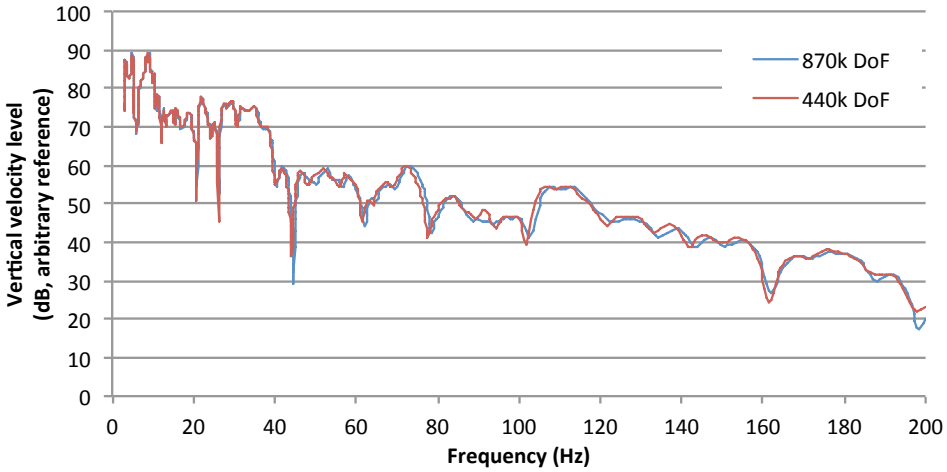

Multiple plates

The approach used by Petyt & Mirza [44] (as discussed in 2.5.1) provided an interesting simple formula for predicting the lowest natural frequency of a multi-supported plate from analysis of a single bay. However, it only considered the case for one-dimensional and square arrangements of square bays. It seems reasonable that it may be possible to approximate the first natural frequency of a multi-supported rectangular plate from consideration of a single rectangular bay. An FE approach has therefore been taken in order to examine this theory, and is outlined below. In the following FE models, the plate is assumed to be concrete with the following material parameters: density 2400 $kg.m^{-3}$; Young's modulus 26 GPa; Poisson ratio 0.3; and thickness 0.25 m. Triangular quadratic elements are used with a maximum length of 1.5 m. The plate is formulated as a thick (Mindlin) plate.

The first exercise examines the case for a p x q arrangement of square bays (up to 5 x 5), each bay having a side length of 7 m. The corresponding first natural frequencies and mode shapes are shown in Table A-5, for arrangements up to 4 x 4.

From inspection of the results, an empirical expression similar to those given in [44] (as reproduced in Equations (2-15) and (2-16)) has been found for predicting the non-dimensional frequency parameter of the first mode of the multi-supported structure from that of the single bay:

$$\Omega_{pq1} = \begin{cases} pq(\Omega_{11} + 2) - 2 & p, q > 1 \\ pq(\Omega_{11} + 1) - 0.5 & p \; or \; q = 1 \end{cases} \quad \textbf{(A-2)}$$

where:

p, q is the number of bays in the arrangement in the x and y directions, respectively.

The case for where there is only a single bay in the width or length should be considered separately. It is important to note that when dealing with the non-dimensional frequency parameter for non-square plates, it is appropriate to replace the b^2 term in Equation (2-13) with ab, such that:

$$\Omega = 2\pi f ab \sqrt{\frac{\rho h}{D}} \quad \textbf{(A-3)}$$

Table A-5. First natural frequency mode shapes, multi-supported p x q arrangement of square bays

p x q	Freq. (Hz)	Image of mode shape	p x q	Freq. (Hz)	Image of mode shape
1x1	5.69	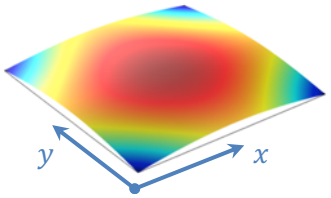	3x3	7.04	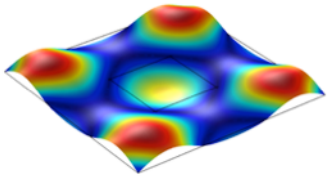
2x1	6.35	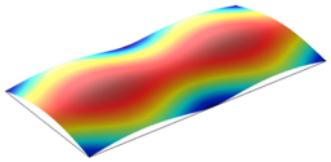	4x1	6.40	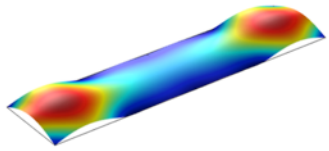
2x2	6.98	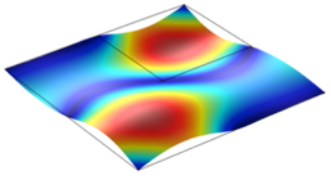	4x2	7.06	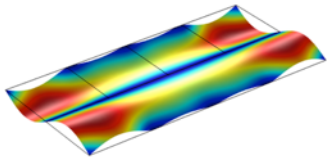
3x1	6.35	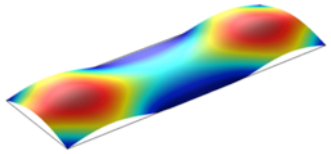	4x3	7.18	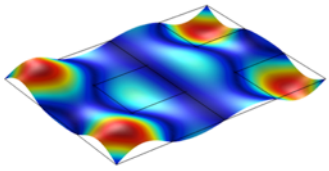
3x2	7.02	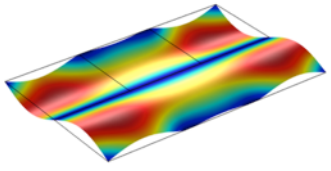	4x4	7.27	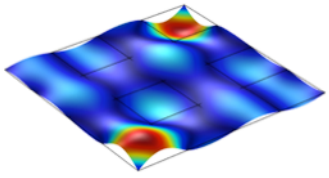

The FE results and empirical predictions of the natural frequencies for all combinations of arrangements up to 5x5 are shown in Table A-6. The proposed empirical expression shows an improvement over those given in [44].

Table A-6. Empirical prediction of first natural frequencies for a multi-supported p x q arrangement of square bays (Hz)							
p x q	FE result	Empirical from [44]	Proposed empirical	p x q	FE result	Empirical from [44]	Proposed empirical
2x1	6.35	6.50	6.30	4x3	7.18	-	7.17
2x2	6.98	6.90	6.90	4x4	7.27	6.70	7.21
3x1	6.35	6.50	6.36	5x1	6.41	6.50	6.42
3x2	7.02	-	7.04	5x2	7.08	-	7.15
3x3	7.04	6.77	7.13	5x3	7.15	-	7.20
4x1	6.40	6.50	6.40	5x4	7.27	-	7.23
4x2	7.06	-	7.11	5x5	7.18	6.66	7.24

The next step toward a more complete approximation for the first natural frequency of a multi-supported plate is the consideration of rectangular bays. A similar FE approach as above has been taken, for bays with lateral dimensions 8 x 6 m, 9 x 5 m, 9 x 3 m, and 9 x 9 m. From inspection of the results, the following empirical formula has been found:

$$\Omega_{pq1} = \begin{cases} \dfrac{pq(\Omega_{11}+2)(\chi+1)}{2} - 2 & p,q > 1 \\ \dfrac{pq(\Omega_{11}+1)(\chi+3)}{4} - 0.5 & p \text{ or } q = 1 \end{cases} \quad \textbf{(A-4)}$$

where:

χ is the small aspect ratio of a bay, i.e. a/b when $a < b$, or b/a when $b < a$;

a, b are the dimensions of an individual bay

The results of the FE study are shown in Table A-7, with the empirically predicted values and % deviation between the methods.

Table A-7. Empirical prediction of first natural frequencies for a multi-supported p x q arrangement of rectangular bays (Hz)												
p x q	8 x 6 m bays $\chi = 0.75$			9 x 5 m bays $\chi = 0.56$			9 x 3 m bays $\chi = 0.33$			9 x 9 m bays $\chi = 1$		
	FE result	Empirical	% Difference	FE result	Empirical	% Difference	FE result	Empirical	% Difference	FE result	Empirical	% Difference
1x1	5.28	-	-	4.47	-	-	4.58	-	-	3.45	-	-
1x2	5.50	5.52	*0.3*	4.56	4.54	*-0.5*	4.63	4.68	*0.9*	3.86	3.82	*-0.9*
1x3	5.54	5.59	*0.8*	4.59	4.61	*0.4*	4.67	4.80	*2.8*	3.85	3.86	*0.2*
1x4	5.57	5.62	*0.9*	4.61	4.65	*0.9*	4.69	4.86	*3.6*	3.89	3.88	*-0.2*
1x5	5.59	5.64	*1.0*	4.62	4.67	*1.1*	4.71	4.90	*4.1*	3.89	3.89	*0.0*
2x1	5.58	5.52	*-1.0*	4.56	4.54	*-0.4*	4.60	4.68	*1.7*	3.86	3.82	*-0.9*
2x2	5.72	5.65	*-1.2*	4.63	4.41	*-4.8*	4.65	4.07	*-12.4*	4.23	4.19	*-1.1*
2x3	5.76	5.79	*0.5*	4.66	4.56	*-2.2*	4.68	4.22	*-9.9*	4.26	4.27	*0.2*
2x4	5.78	5.86	*1.4*	4.68	4.63	*-1.0*	4.70	4.29	*-8.8*	4.29	4.31	*0.5*
2x5	5.79	5.90	*1.8*	4.69	4.67	*-0.3*	4.72	4.34	*-8.1*	4.30	4.33	*0.8*
3x1	5.66	5.59	*-1.3*	4.58	4.61	*0.6*	4.60	4.80	*4.2*	3.85	3.86	*0.2*
3x2	5.80	5.79	*-0.2*	4.65	4.56	*-2.1*	4.65	4.22	*-9.3*	4.26	4.27	*0.2*
3x3	5.83	5.88	*0.8*	4.68	4.65	*-0.6*	4.68	4.32	*-7.9*	4.27	4.32	*1.1*
3x4	5.85	5.93	*1.3*	4.70	4.70	*0.1*	4.71	4.37	*-7.3*	4.36	4.35	*-0.2*
3x5	5.87	5.96	*1.5*	4.71	4.73	*0.5*	4.72	4.39	*-6.9*	4.34	4.37	*0.6*
4x1	5.71	5.62	*-1.5*	4.60	4.65	*1.1*	4.61	4.86	*5.5*	3.89	3.88	*-0.2*
4x2	5.84	5.86	*0.4*	4.67	4.63	*-0.8*	4.65	4.29	*-7.7*	4.29	4.31	*0.5*
4x3	5.87	5.93	*1.0*	4.70	4.70	*0.2*	4.69	4.37	*-6.9*	4.36	4.35	*-0.2*
4x4	5.89	5.96	*1.2*	4.71	4.74	*0.6*	4.71	4.40	*-6.5*	4.41	4.37	*-1.0*
4x5	5.90	5.98	*1.4*	4.72	4.76	*0.8*	4.73	4.42	*-6.4*	4.41	4.38	*-0.7*
5x1	5.73	5.64	*-1.6*	4.61	4.67	*1.4*	4.61	4.90	*6.2*	3.89	3.89	*0.0*
5x2	5.86	5.90	*0.7*	4.67	4.67	*0.0*	4.65	4.34	*-6.8*	4.30	4.33	*0.8*
5x3	5.89	5.96	*1.1*	4.70	4.73	*0.6*	4.69	4.39	*-6.2*	4.34	4.37	*0.6*
5x4	5.91	5.98	*1.2*	4.72	4.76	*0.9*	4.71	4.42	*-6.1*	4.41	4.38	*-0.7*
5x5	5.92	6.00	*1.3*	4.73	4.78	*1.1*	4.73	4.44	*-6.0*	4.41	4.39	*-0.3*

It is shown that the proposed empirical prediction gives values within a couple of percent of the FE results for bay aspect ratios of down to around 0.5, but exhibits reduced accuracy as aspect ratios reduce (affecting the 2x2 arrangement the most). At aspect ratios of 0.33 most results are under-predicted by several percent.

One additional observation from the results is that there is only a small difference in the FE results of inverted arrangement patterns i.e. a 2 x 4 arrangement has a similar first natural frequency to a 4 x 2 arrangement.

Composite structures

When modelling complex structures such as buildings for FE analysis, joints exist between various components, which must be accounted for appropriately. In addition, coupling between different element types such as beams, shells/plates, solids and even fluids may be required. Of particular interest when modelling buildings is the coupling of beam elements (used to represent structural columns and beams) to shell elements representing wall and floor surfaces.

Floors

It is not currently feasible to model floors of a large multi-storey building purely from solid elements due to the number of nodes that would be required to represent the structure accurately for dynamic analysis in the frequency range of interest. This is because of the thin nature of the floor surface; good practice guidance for FE modelling [130] advises against the use of elements which are too distorted in one dimension; therefore small elements would be required.

Floor surfaces are therefore usually required to be modelled with shell/plate elements. Furthermore, due to the thickness of a floor not being insignificant, the Mindlin thick plate theory should be used (see Chapter 2.5 for discussion of thick plate vs thin plate formulations).

The natural frequencies of a floor slab depend on its material and geometric properties, but also on the boundary conditions. A range of different boundary conditions might be found for various slabs over one storey of a building. Where a slab is connected to an adjacent slab, at some natural frequencies the boundary condition might be approximately symmetrical; at the perimeter of the storey the boundary condition might be approximately free (although in reality additional stiffening structures such as beams or façade constructions may reduce the validity of this assumption). For the 6 x 8 m slab that has been considered elsewhere in this chapter, the pinned-boundary fundamental natural frequency might be calculated analytically using Equation (2-14) as 18.5 Hz. The fundamental natural frequencies for more complicated boundary conditions can be obtained using FE analysis. The plate with pinned boundary conditions is calculated as 18.1 Hz through finite element analysis. The predicted fundamental natural frequencies and mode shapes for the concrete plate with a number of boundary conditions are given in Table A-8. In order to reproduce the effect of columns that may be present for a typical floor slab, the corners are

pinned. The frequencies of higher modes for the symmetric boundary condition case are shown in Table A-9.

Table A-8. Fundamental natural frequency for a concrete plate with various boundary conditions

Boundary condition	f_0 (Hz)	Deformation
All boundaries free, corners pinned	5.7	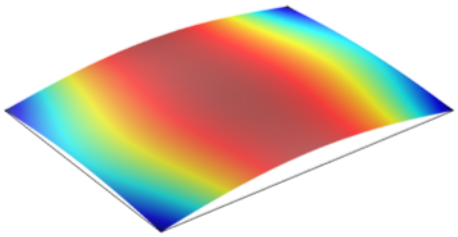
All boundaries pinned	18.1	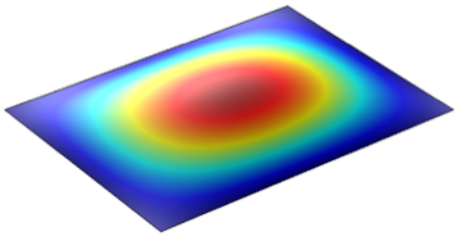
All boundaries symmetric, corners pinned	12.2	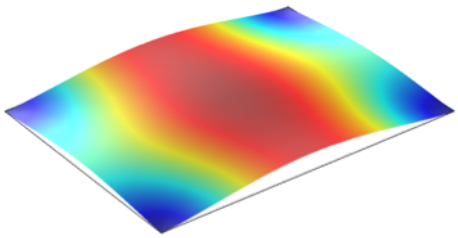
Three boundaries symmetric, short boundary free, corners pinned	9.1	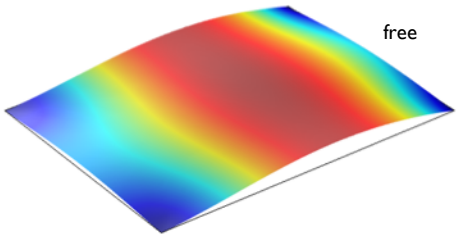
Three boundaries symmetric, long boundary free, corners pinned	10.5	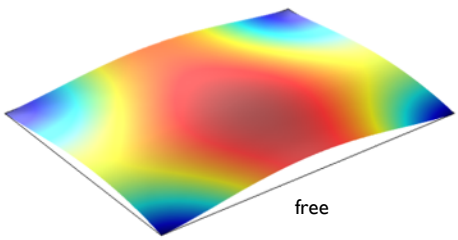
Symmetric along two adjacent sides, other boundaries free, corners pinned	8.3	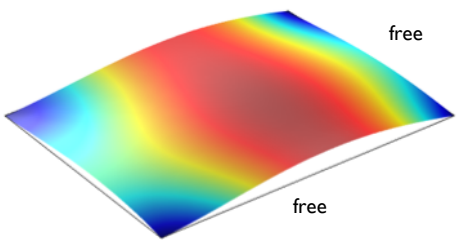

Table A-9. Natural frequencies for a concrete plate with symmetric boundary conditions, corners pinned			
f (Hz)	Mode shape	*f* (Hz)	Mode shape
12.2	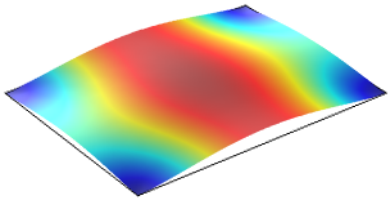	22.0	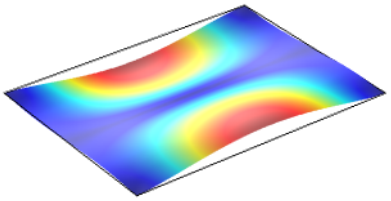
23.8	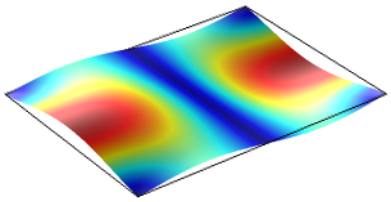	35.2	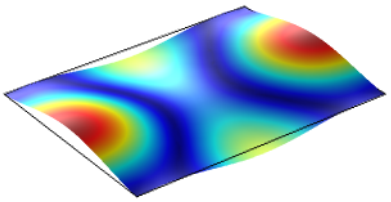
42.5	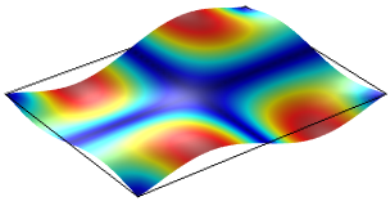	55.5	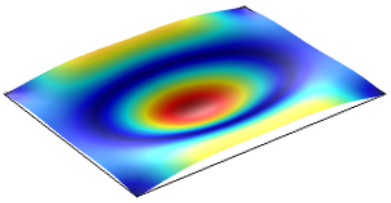
56.3	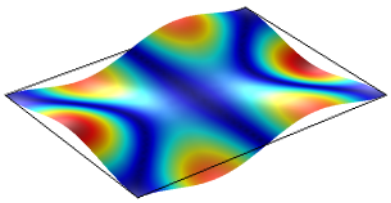	64.9	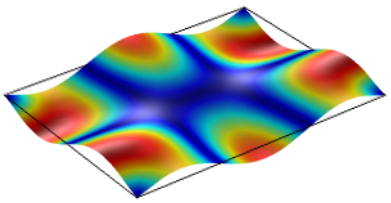
80.4	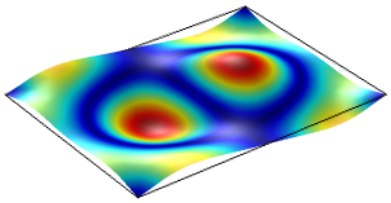	86.3	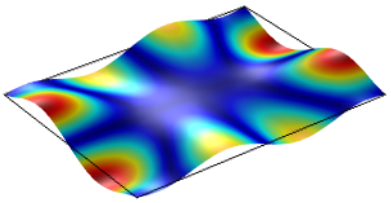
89.7	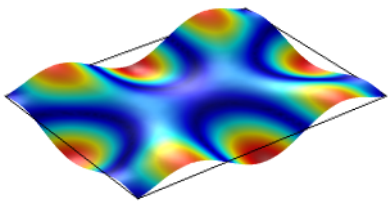	104.3	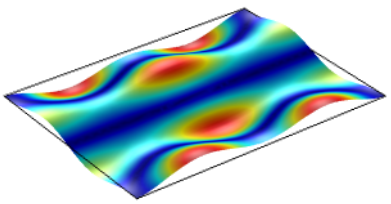

Table A-8 includes several boundary conditions which might be present in a typical building structure, and implies that a variation in natural frequencies is to be expected depending on the location of a floor slab at any given storey. For example, a centrally located floor slab might

exhibit fully symmetric boundary conditions; a slab at the perimeter of the storey may exhibit one or two free boundaries.

It should be noted that as the number of bays increases, the first natural frequency in the first band of natural frequencies is similar to that given by a single slab for the boundary conditions which are symmetric along to adjacent sides, and free along the other adjacent sides, with pinned corners. The last natural frequency in the band is similar to that given by a single slab with symmetric boundary conditions on all edges, and pinned corners.

Where the boundary conditions are not symmetrically distributed, it is shown that the location of maximum amplitude is no longer in the centre of the plate. In addition, only two of the modes shown in Table A-9 exhibit maximum response at the centre of the slab (i.e. at 12.2 and 55.5 Hz). These effects should be considered when evaluating amplification effects at the centre of a floor slab.

Columns

Due to their limited size, it is often feasible to model structural columns with solid elements, despite the requirement for small element size due to the typically small cross-section dimensions. When coupling solid element columns with shell element floors, it is only necessary to link the node displacements.

Due to the slender aspect ratio of most columns, it is often appropriate to model the column with beam elements. In this situation, the cross-sectional area of the beam elements must be specified properly (and in the correct orientation). There are some challenges in coupling the beam element to the shell element of the floor surface in that it is not sufficient to link only the displacements, as the rotation of the column must also be accounted for. The junction also occurs at a single point, whereas in the real situation the junction is an area that corresponds to the cross-section of the column. It is therefore necessary to specify an intersection area on the shell, and to specify that the rotation of this area is equal to the rotation of the beam element at the junction. Furthermore, the stiffness of this intersection area should be accounted for. Figure A-2a and Figure A-2b show the configurations for the different element types.

Figure A-2a. Columns as solid elements

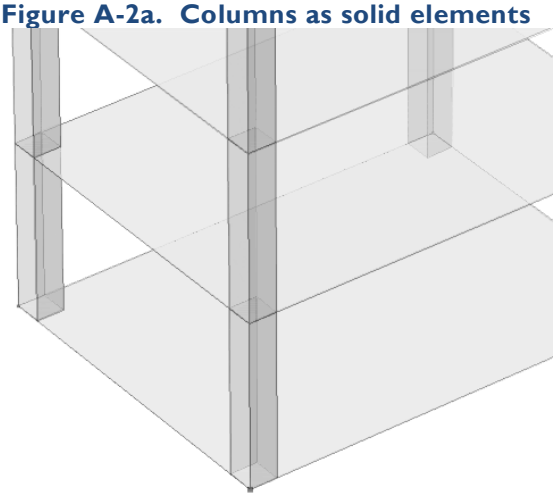

Figure A-2b. Columns as beam elements

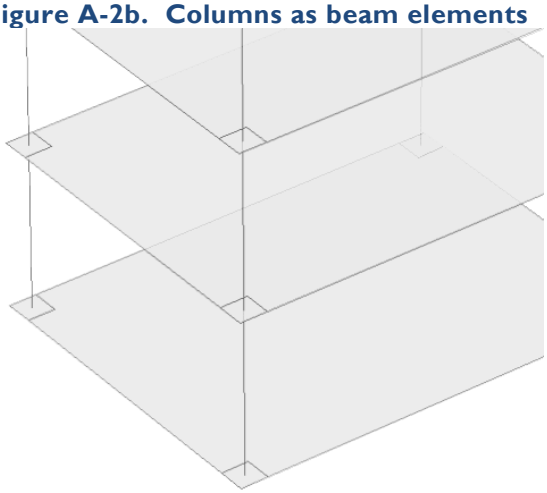

In order to determine the kind of differences that might be expected when using the different element types for structural columns, a study has been conducted on a form of the generic building detailed in Section 5.1. The version of the generic building used is that with no structural walls or cores. The vertical vibration transfer function between a mid-span point on the 5th floor and the same point at basement level is shown in Figure A-3 and Figure A-4 for narrow-band and one-third octave frequency data respectively. Different values of the stiffness of the beam intersection area have been investigated by multiplying the Young's modulus of the material in these areas by the shown factor.

Figure A-3. Vertical vibration transfer function between a mid-span point at fifth floor and basement level with beam and solid elements for columns; narrow-band

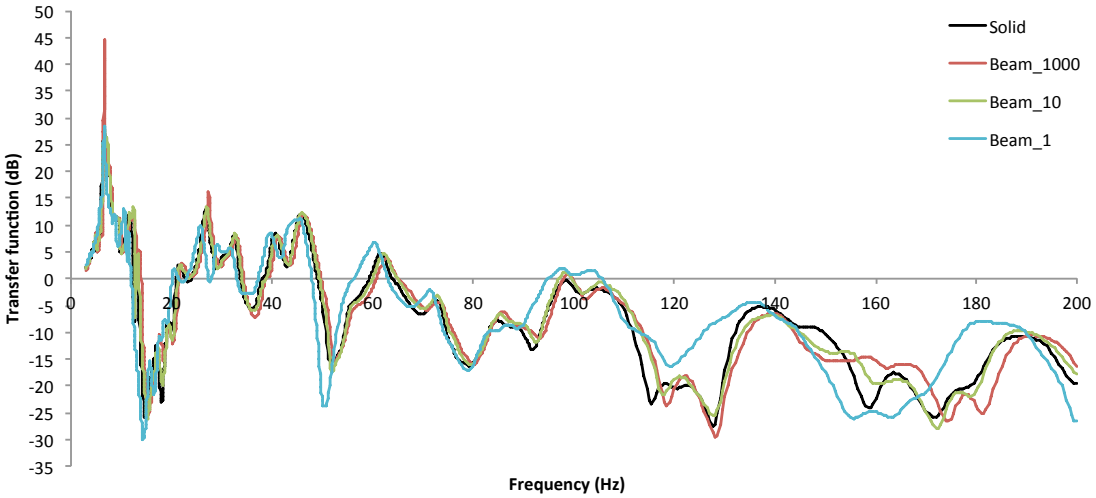

Figure A-4. Vertical vibration transfer function between a mid-span point at fifth floor and basement level with beam and solid elements for columns; third octave bands

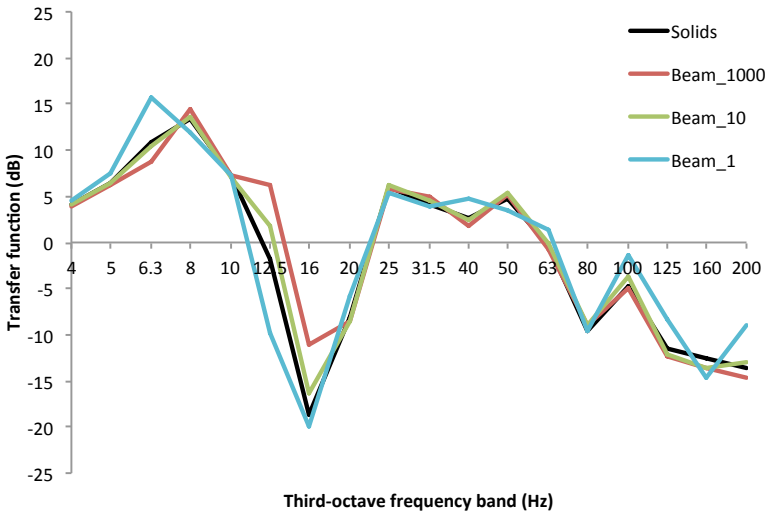

It is seen in the above figure that using beam elements for columns can provide similar results to using solid elements, provided that the intersection area is defined with an increased stiffness (in this case a factor of 10 is suitable). Use of beam elements leads to a significant computational resource saving; for example, for the generic building model the number of degrees of freedom reduced from 245,910 to 165,960 (i.e. 67%) and the calculation time reduced from nearly 24 hours to just over 8 hours.

APPENDIX B: GROUNDBORNE NOISE AND VIBRATION ANALYSIS APPROACH

There are a number of procedures involved in analysing measured noise and vibration data. The general process is outlined in the following flowchart:

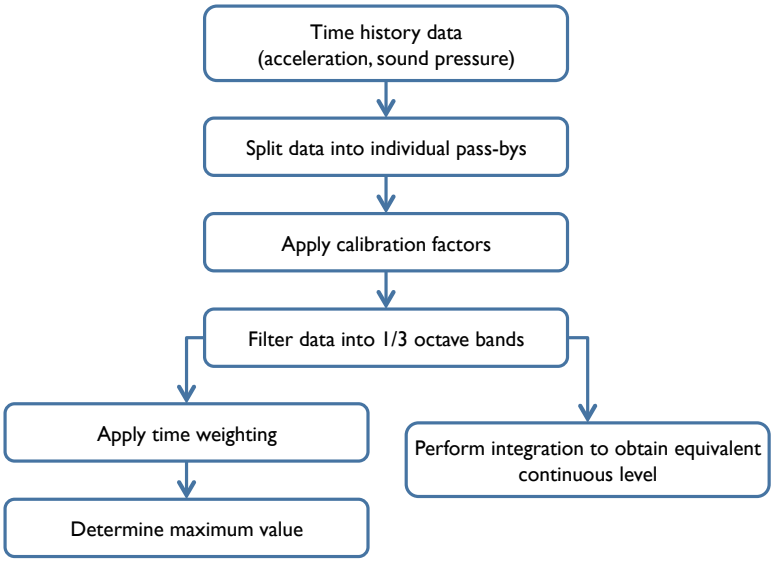

Pre-processing

In the measurement of groundborne noise and vibration, it is usually appropriate to make continuous recordings to be post-processed rather than individual pass-by recordings, due to difficulties in perceiving pass-by events and delays in the start of recordings. The first stage of the analysis is therefore usually to split the continuous recordings into files for individual pass-bys.

The file format used for recorded data will normally be WAV files*. These can often be split using proprietary software from the measurement equipment manufacturer, or a third party audio editor such as Audacity (open source) or Adobe Audition (commercial). Accurate splitting of pass-bys may require examination of the waveform, spectrogram and even listening to the signal directly. It should be noted that in order to listen to the audio signal, it may be necessary to process a 'normalised' (i.e. amplified) version of the waveform, and use headphones with a wide frequency range (small speakers are unlikely to reproduce the low frequencies associated with groundborne noise).

* For the frequency range considered in assessment of groundborne noise, a minimum sampling frequency of 750 Hz is recommended. 24-bit depth is also recommended to preserve dynamic range.

After successfully splitting the files into individual pass-by recordings, it is necessary to apply calibration values to the WAV file data in order to extract the raw recorded quantity in terms of acceleration, velocity, or sound pressure. The usual technique is to load the WAV files into a programming environment (such as Matlab or Python) for this step*.

Frequency analysis

Most meaningful analysis must allow for frequency dependence. For groundborne noise and vibration it is helpful to consider the noise and vibration quantities in terms of 1/3 octave bands. The signal may be split into the 1/3 octave bands by one of two methods:

- FFT Analysis: the signal is analysed at discrete frequency points, with the results for any given band obtained by summing the frequency points therein;
- FIR/IIR Digital Filtering: the signal is processed with a digital filter for each frequency band; usually a Butterworth filter designed to comply with standard limits [137].

Whilst the FFT method is in general quicker to compute, the FIR method is implemented in this research (using the '`butter`' and '`lfilter`' functions of the SciPy Python library).

It should be noted that at low frequencies (less than 1/20th of the sampling frequency) digital filters tend to become unstable. For these frequency bands it is therefore necessary to perform decimation on the data, to reduce the sample rate prior to applying the filter.

Time weighting

In this research, the quantity of interest that is most related to the perceived noise and vibration from railway sources is the maximum level of the signal with a 'slow' time weighting. The 'slow' time weighting provides an exponential time weighting to the input signal with a time constant of one second. This is realised through the following formula:

$$x_n = \sqrt{\alpha x_{n-1}^2 + (1-\alpha) x_{n-1}^2} \qquad \textbf{(B-1)}$$

where:

x_n is the value of the nth sample in the signal;

α is the time weighting term, given by:

* Some difficulties were experienced with the use of 24-bit audio files. Matlab was able to load these, only if the WAV files had been stripped of header information when saved (an option in Adobe Audition). Python (SciPy) is understood to require an additional audio library such as 'audiolab' for such files.

$$\alpha = \frac{1}{f_s T_c + 1} \qquad \textbf{(B-2)}$$

where:

f_s is the sampling frequency of the signal, in Hz;

T_c is the exponential time constant, in seconds*.

There is a slight difficulty in obtaining the very first term of the time-weighted sequence without discarding the first sample. In the measurements analysed in this research, the first sample has been obtained from the rms of the first 0.5 s of the signal.

The maximum value is found for the slow time-weighted signal, for each frequency band. Note that care should be taken when using slow time weightings to quantify maximum levels in low frequency bands, due to limitations of the filter response [58].

* The value of the time constant is taken as 1.0 s for 'slow' and 0.125 s for 'fast' time weighting.

[BLANK PAGE]

APPENDIX C: VIBRATION MEASUREMENT CASE STUDIES

A number of case studies are presented here, with data from projects on which Arup has provided consultancy advice over a number of years. This is presented as an overview of the available data, for the purposes of assessing whether model results give the same kind of trends that are seen in vibration measurements of different buildings. Only the vertical vibration measurements are provided here, with no discussion provided on project specific assessment or design.

C.1: Tottenham Court Road, London (TCR)

Average measured maximum one-third octave band vertical vibration levels are given in Figure C-1 for column positions, and Figure C-2 for mid-span positions. This has been calculated by determining the maximum slow time-weighted vibration level for each one-third octave band during a train pass-by, and averaging the results for each band over several pass-bys. The standard deviations and 95% confidence intervals for these averages are shown in Table C-1 to Table C-4. The overall A-weighted maximum vertical velocity levels (i.e. corresponding with groundborne noise level) are plotted against storey in Figure C-3. The overall W_b-weighted maximum vertical acceleration levels (i.e. corresponding with perceivable vibration) are shown in Figure C-4.

Figure C-1. TCR: Max. vibration levels at each measured storey (column)

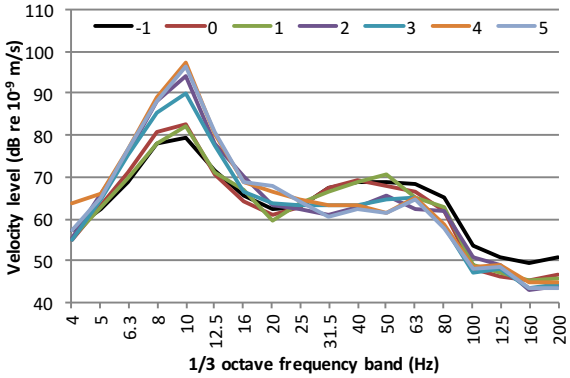

Figure C-2. TCR: Max. vibration levels at each measured storey (mid-span)

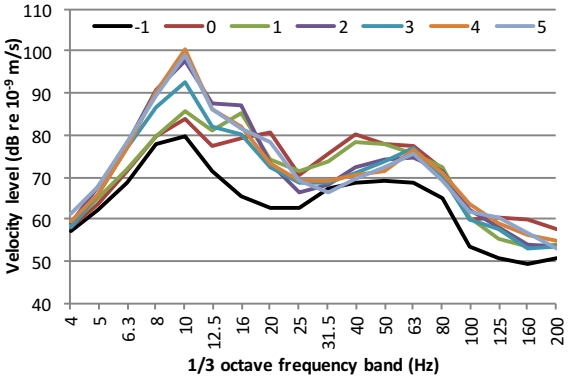

Figure C-3. TCR: Overall A-weighted max. velocity levels with storey

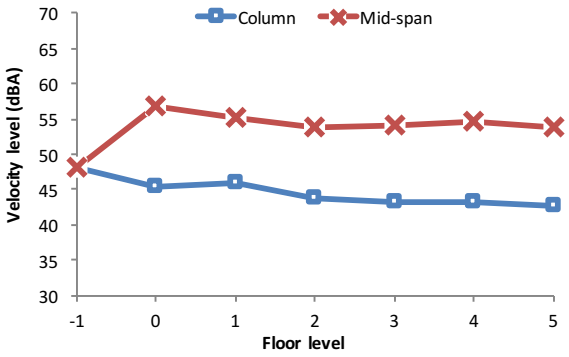

Figure C-4. TCR: Overall W_b-weighted max. acceleration levels with storey

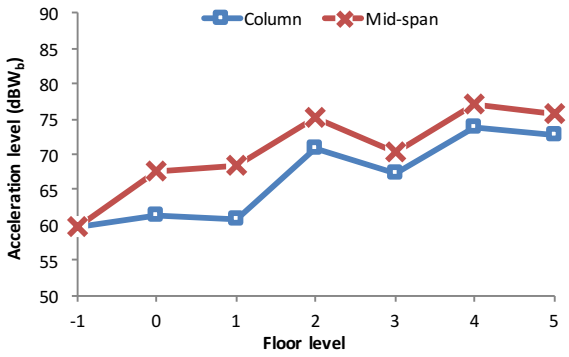

Table C-1. TCR: Measurement 95% confidence intervals for mean (column) (dB)

Storey	No. pass-bys	1/3 octave band frequency (Hz)																		Overall	
		4	5	6.3	8	10	12.5	16	20	25	31.5	40	50	63	80	100	125	160	200	L_{Wb}	L_A
-1	3	3.2	8.1	13.8	18.8	14.5	5.8	9.9	7.3	2.7	4.0	9.4	12.2	11.1	10.0	2.1	14.2	11.0	6.6	7.7	3.0
0	7	2.1	3.6	5.2	6.6	6.2	2.4	2.3	1.3	1.9	3.8	5.1	5.8	5.3	5.2	2.0	1.5	2.0	2.0	2.0	2.8
1	4	3.8	2.7	6.0	7.7	6.5	4.3	4.8	2.6	8.9	9.7	11.9	11.6	6.4	9.9	4.5	4.6	4.9	4.2	3.7	6.6
2	3	2.5	7.8	16.9	22.1	19.4	10.3	4.3	4.4	5.8	10.1	17.1	15.9	3.0	5.8	6.1	3.9	1.9	0.6	11.4	3.9
3	3	4.5	10.0	17.8	18.5	17.5	15.2	6.6	4.3	8.1	12.8	11.3	7.7	6.1	3.0	3.0	2.5	4.0	3.0	10.3	2.7
4	5	7.1	2.8	2.8	3.1	5.0	2.0	1.6	0.5	3.1	6.4	6.5	4.2	3.4	4.0	3.2	2.1	1.7	0.9	3.3	2.0
5	5	1.8	1.6	2.7	0.8	3.9	1.3	0.9	2.1	1.4	4.8	6.0	5.0	3.2	4.2	2.2	3.8	1.8	0.6	2.4	2.1

Table C-2. TCR: Measurement 95% confidence intervals for mean (mid-span) (dB)

Storey	No. pass-bys	1/3 octave band frequency (Hz)																		Overall	
		4	5	6.3	8	10	12.5	16	20	25	31.5	40	50	63	80	100	125	160	200	L_{Wb}	L_A
-1	3	3.5	9.5	12.2	19.2	15.4	3.8	6.2	6.0	1.9	2.4	8.5	13.7	13.0	10.7	2.3	4.3	6.2	10.0	7.3	3.9
0	7	2.7	3.3	5.2	5.9	5.4	2.4	2.0	2.2	0.9	1.7	1.3	2.1	3.6	4.4	2.1	3.1	3.3	3.4	1.1	2.0
1	4	3.5	3.3	7.0	7.2	6.6	3.0	5.1	4.2	7.1	7.4	8.5	7.4	6.7	8.3	3.5	5.3	6.5	5.1	4.1	6.7
2	3	3.5	7.1	17.7	23.6	20.3	4.2	3.0	5.5	3.7	11.9	11.6	10.3	5.7	5.4	5.6	2.2	6.6	1.6	5.6	3.4
3	3	4.6	9.3	18.2	18.8	17.0	8.4	6.3	5.2	7.3	12.3	4.9	5.3	6.6	6.5	5.8	4.0	6.1	4.8	7.0	4.3
4	5	1.8	1.5	2.6	3.1	4.9	1.2	1.2	0.7	3.2	6.0	3.3	2.6	2.8	3.1	4.4	2.4	2.6	1.4	2.2	2.1
5	5	1.5	0.8	2.7	1.1	4.4	1.8	0.8	1.6	1.6	4.1	3.2	2.2	2.1	3.6	3.5	5.3	4.5	2.0	1.9	2.5

Table C-3. TCR: Measurement standard deviations (column) (dB)

Storey	No. pass-bys	1/3 octave band frequency (Hz)																		Overall	
		4	5	6.3	8	10	12.5	16	20	25	31.5	40	50	63	80	100	125	160	200	L_{Wb}	L_A
-1	3	1.3	3.2	5.5	7.6	5.9	2.4	4.0	2.9	1.1	1.6	3.8	4.9	4.5	4.0	0.9	5.7	4.4	2.6	1.2	3.1
0	7	2.3	3.9	5.7	7.2	6.7	2.6	2.5	1.4	2.0	4.1	5.5	6.2	5.7	5.6	2.2	1.6	2.2	2.2	0.9	2.1
1	4	2.4	1.7	3.8	4.8	4.1	2.7	3.0	1.6	5.6	6.1	7.5	7.3	4.0	6.2	2.9	2.9	3.1	2.6	1.7	2.3
2	3	1.0	3.1	6.8	8.9	7.8	4.2	1.7	1.8	2.3	4.1	6.9	6.4	1.2	2.3	2.5	1.6	0.8	0.3	0.7	4.6
3	3	1.8	4.0	7.2	7.5	7.1	6.1	2.7	1.7	3.3	5.1	4.6	3.1	2.5	1.2	1.2	1.0	1.6	1.2	0.9	4.1
4	5	5.7	2.2	2.3	2.5	4.0	1.6	1.3	0.4	2.5	5.2	5.2	3.3	2.7	3.2	2.6	1.7	1.4	0.8	0.7	2.7
5	5	1.5	1.3	2.2	0.6	3.2	1.0	0.7	1.7	1.2	3.9	4.8	4.0	2.6	3.4	1.8	3.1	1.5	0.5	0.2	2.0

Table C-4. TCR: Measurement standard deviations (mid-span) (dB)

Storey	No. pass-bys	1/3 octave band frequency (Hz)																		Overall	
		4	5	6.3	8	10	12.5	16	20	25	31.5	40	50	63	80	100	125	160	200	L_{Wb}	L_A
-1	3	1.4	3.8	4.9	7.7	6.2	1.5	2.5	2.4	0.8	1.0	3.4	5.5	5.2	4.3	0.9	1.7	2.5	4.0	2.4	3.0
0	7	2.9	3.6	5.6	6.4	5.9	2.6	2.2	2.3	0.9	1.9	1.4	2.2	3.9	4.8	2.3	3.3	3.5	3.7	2.4	1.1
1	4	2.2	2.1	4.4	4.5	4.2	1.9	3.2	2.6	4.5	4.6	5.3	4.6	4.2	5.2	2.2	3.3	4.1	3.2	2.4	2.6
2	3	1.4	2.9	7.1	9.5	8.2	1.7	1.2	2.2	1.5	4.8	4.7	4.2	2.3	2.2	2.2	0.9	2.7	0.6	1.4	2.3
3	3	1.9	3.7	7.3	7.6	6.8	3.4	2.5	2.1	3.0	4.9	2.0	2.1	2.7	2.6	2.3	1.6	2.5	1.9	1.8	2.8
4	5	1.4	1.2	2.1	2.5	3.9	1.0	1.0	0.6	2.6	4.8	2.6	2.1	2.3	2.5	3.5	1.9	2.1	1.1	2.2	1.8
5	5	1.2	0.6	2.2	0.9	3.5	1.4	0.7	1.3	1.3	3.3	2.6	1.7	1.7	2.9	2.8	4.3	3.6	1.6	1.0	1.5

C.2: York Way, nr King's Cross, London (KX)

The following measurements were obtained by the author in December 2012. Average maximum one-third octave band vertical vibration levels are given in Figure C-5 for column positions, and Figure C-6 for mid-span positions. The standard deviations and 95% confidence intervals for these averages are shown in Table C-5 to Table C-8. The overall A-weighted maximum vibration levels are plotted against frequency band in Figure C-7. The overall W_b-weighted maximum vertical acceleration levels are shown in Figure C-8.

Figure C-5. KX: Max. vibration levels at each measured storey (column)

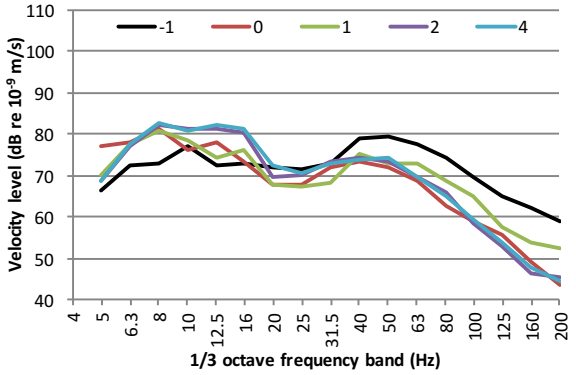

Figure C-6. KX: Max. vibration levels at each measured storey (mid-span)

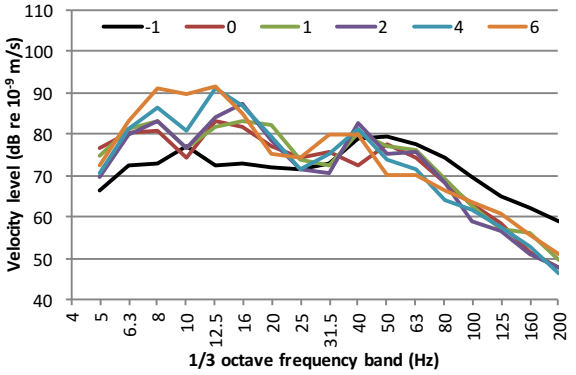

Table C-5. KX: Measurement 95% confidence intervals for mean (column) (dB)

Storey	No. pass-bys	1/3 octave band frequency (Hz)																		Overall	
		4	5	6.3	8	10	12.5	16	20	25	31.5	40	50	63	80	100	125	160	200	L_{Wb}	L_A
-1	41	1.5	0.9	0.8	1.0	1.3	0.7	0.4	0.6	0.5	0.6	0.6	0.6	0.5	0.8	1.0	1.3	1.8	1.4	0.4	0.8
0	8	6.3	5.5	3.7	4.6	3.0	2.5	1.9	2.3	2.1	2.5	3.9	4.4	4.1	2.9	3.3	4.4	4.1	2.3	2.7	2.9
1	27	2.0	1.9	1.5	1.5	1.7	0.9	1.0	1.2	0.8	0.7	0.9	0.8	1.0	0.9	1.1	1.2	1.6	1.9	0.6	0.9
2	20	2.1	1.4	1.1	1.5	2.1	1.4	1.6	0.6	0.8	1.0	0.7	0.7	0.6	1.0	0.9	1.2	1.4	1.8	1.0	0.5
4	28	1.4	1.1	0.8	1.0	1.6	1.1	1.3	0.6	0.7	0.6	0.9	0.8	0.6	0.9	0.9	1.2	1.3	1.3	0.8	0.6

Table C-6. KX: Measurement 95% confidence intervals for mean (mid-span) (dB)

Storey	No. pass-bys	1/3 octave band frequency (Hz)																		Overall	
		4	5	6.3	8	10	12.5	16	20	25	31.5	40	50	63	80	100	125	160	200	L_{Wb}	L_A
-1	41	1.5	0.9	0.8	1.0	1.3	0.7	0.4	0.6	0.5	0.6	0.6	0.6	0.5	0.8	1.0	1.3	1.8	1.4	0.4	0.8
0	8	4.8	5.4	4.4	4.2	2.5	2.6	2.4	2.5	2.6	1.9	2.1	3.6	3.5	5.1	3.7	3.0	2.3	3.7	2.4	3.1
1	27	2.1	1.8	1.6	1.4	1.7	1.1	0.9	1.6	0.8	0.7	0.9	0.9	0.9	0.9	0.9	1.5	1.7	1.7	0.7	0.8
2	20	2.4	1.3	1.3	1.4	1.8	1.4	1.5	1.0	0.8	1.0	1.0	0.6	0.6	1.4	0.9	1.8	1.4	2.2	0.8	0.6
4	28	1.9	1.0	0.9	1.1	1.6	1.2	0.9	1.1	0.9	0.9	1.0	0.8	0.6	0.6	1.5	1.6	1.5	0.8	0.7	0.7
6	16	2.5	1.6	1.4	1.6	2.4	1.3	1.4	1.2	1.4	1.4	1.6	0.8	0.8	1.0	2.3	3.0	2.3	2.2	1.2	1.4

Table C-7. KX: Measurement standard deviations (column) (dB)

Storey	No. pass-bys	1/3 octave band frequency (Hz)																		Overall	
		4	5	6.3	8	10	12.5	16	20	25	31.5	40	50	63	80	100	125	160	200	L_{Wb}	L_A
-1	41	4.9	2.9	2.4	3.2	4.0	2.1	1.3	1.8	1.7	1.8	2.0	1.8	1.6	2.4	3.1	4.0	5.7	4.5	1.3	2.5
0	8	7.5	6.6	4.5	5.5	3.6	3.0	2.3	2.7	2.5	3.0	4.6	5.2	4.9	3.4	3.9	5.3	4.9	2.7	3.3	3.5
1	27	4.9	4.9	3.7	3.9	4.4	2.3	2.5	2.9	2.0	1.8	2.2	2.0	2.5	2.4	2.7	3.1	4.1	4.9	1.5	2.2
2	20	4.5	3.0	2.4	3.1	4.4	3.1	3.3	1.3	1.7	2.2	1.4	1.5	1.3	2.1	1.9	2.5	3.0	3.9	2.2	1.2
4	28	3.6	2.8	2.0	2.7	4.2	2.8	3.4	1.5	1.9	1.5	2.3	2.0	1.4	2.3	2.3	3.0	3.2	3.4	2.1	1.5

Table C-8. KX: Measurement standard deviations (mid-span) (dB)																					
Storey	No. pass-bys	1/3 octave band frequency (Hz)																		Overall	
		4	5	6.3	8	10	12.5	16	20	25	31.5	40	50	63	80	100	125	160	200	L_{Wb}	L_A
-1	41	4.9	2.9	2.4	3.2	4.0	2.1	1.3	1.8	1.7	1.8	2.0	1.8	1.6	2.4	3.1	4.0	5.7	4.5	1.3	2.5
0	8	5.7	6.4	5.3	5.0	3.0	3.2	2.9	3.0	3.2	2.3	2.5	4.3	4.2	6.0	4.5	3.6	2.7	4.5	2.9	3.7
1	27	5.4	4.6	4.0	3.6	4.3	2.7	2.3	4.2	1.9	1.7	2.2	2.2	2.3	2.3	2.3	3.7	4.2	4.3	1.9	2.1
2	20	5.2	2.8	2.7	3.0	3.8	3.0	3.1	2.1	1.6	2.1	2.1	1.3	1.4	3.0	1.9	3.8	3.1	4.7	1.7	1.3
4	28	5.0	2.5	2.3	2.9	4.0	3.2	2.2	3.0	2.2	2.4	2.6	2.1	1.5	1.5	3.8	4.1	3.9	2.0	1.9	1.9
6	16	4.6	3.0	2.5	3.0	4.5	2.5	2.6	2.3	2.6	2.5	3.0	1.5	1.6	2.0	4.3	5.6	4.4	4.1	2.3	2.5

Figure C-7. KX: Overall A-weighted max. velocity levels with storey

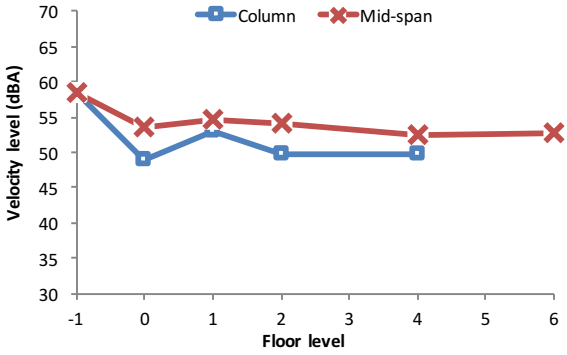

Figure C-8. KX: Overall W_b-weighted max. acceleration levels with storey

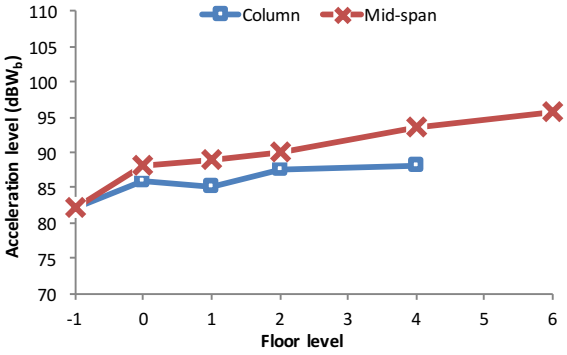

The data at the first floor column location, shows slightly higher vibration levels than expected at the higher frequencies, which may be due to a local structural or transducer mounting anomaly. The one-third octave band results show that in general amplification is observed with storey at frequencies below 20 Hz. The mid-span results indicate that floor span natural frequencies occur in the 8 and 12.5 Hz bands.

C.3: York Road, London (YO-B & YO-T)

Average maximum one-third octave band vertical vibration levels for YO-B are given in Figure C-9 for column positions, and Figure C-10 for mid-span positions. The standard deviations and 95% confidence intervals for these averages are shown in Table C-9 to Table C-12. The overall A-weighted maximum velocity levels with storey are shown in Figure C-11. The overall W_b-weighted maximum vertical acceleration levels are shown in Figure C-12.

Figure C-9. YO-B: Max. vibration levels at each measured storey (column)

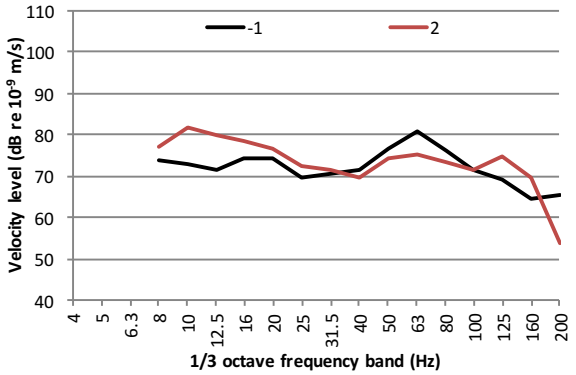

Figure C-10. YO-B: Max. vibration levels at each measured storey (mid-span)

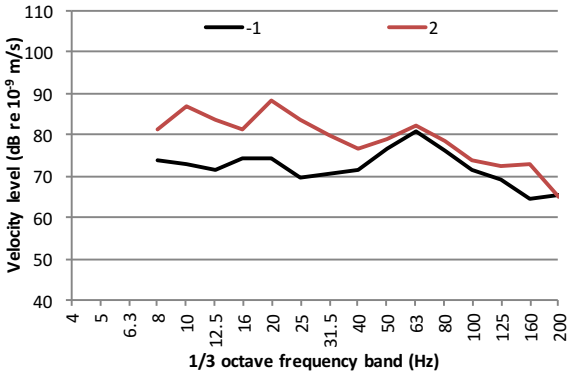

Table C-9. YO-B: Measurement 95% confidence intervals for mean (column) (dB)

Storey	No. pass-bys	1/3 octave band frequency (Hz)															Overall	
		8	10	12.5	16	20	25	31.5	40	50	63	80	100	125	160	200	L_{Wb}	L_A
-1	11	1.8	1.5	2.3	3.8	4.1	2.4	2.0	2.5	3.5	3.6	2.2	2.3	1.8	1.3	2.1	2.3	1.5
2	11	1.6	1.5	2.0	1.9	3.3	1.5	1.4	1.2	2.6	3.5	2.4	1.6	2.4	1.9	1.8	1.2	1.9

Table C-10. YO-B: Measurement 95% confidence intervals for mean (mid-span) (dB)

Storey	No. pass-bys	1/3 octave band frequency (Hz)															Overall	
		8	10	12.5	16	20	25	31.5	40	50	63	80	100	125	160	200	L_{Wb}	L_A
-1	11	1.8	1.5	2.3	3.8	4.1	2.4	2.0	2.5	3.5	3.6	2.2	2.3	1.8	1.3	2.1	2.3	1.5
2	11	1.3	2.0	1.9	3.0	3.4	2.4	2.4	2.1	2.6	4.1	2.7	1.5	2.1	1.9	1.6	1.8	1.9

Table C-11. YO-B: Measurement standard deviations (column) (dB)

Storey	No. pass-bys	1/3 octave band frequency (Hz)															Overall	
		8	10	12.5	16	20	25	31.5	40	50	63	80	100	125	160	200	L_{Wb}	L_A
-1	11	2.7	2.2	3.4	5.7	6.1	3.5	3.0	3.7	5.2	5.3	3.2	3.5	2.6	1.9	3.1	3.5	2.2
2	11	2.4	2.3	2.9	2.8	4.9	2.2	2.1	1.8	3.9	5.3	3.5	2.3	3.6	2.8	2.7	1.8	2.8

Table C-12. YO-B: Measurement standard deviations (mid-span) (dB)

Storey	No. pass-bys	1/3 octave band frequency (Hz)															Overall	
		8	10	12.5	16	20	25	31.5	40	50	63	80	100	125	160	200	L_{Wb}	L_A
-1	11	2.7	2.2	3.4	5.7	6.1	3.5	3.0	3.7	5.2	5.3	3.2	3.5	2.6	1.9	3.1	3.5	2.2
2	11	2.0	2.9	2.8	4.5	5.0	3.5	3.6	3.1	3.8	6.1	4.1	2.2	3.1	2.8	2.4	2.7	2.9

Figure C-11. YO-B: Overall A-weighted max. velocity levels with storey

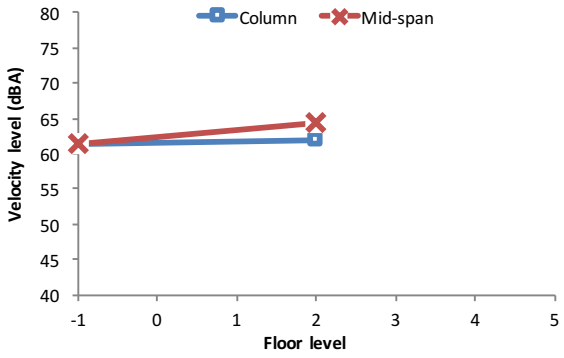

Figure C-12. YO-B: Overall W_b-weighted max. acceleration levels with storey

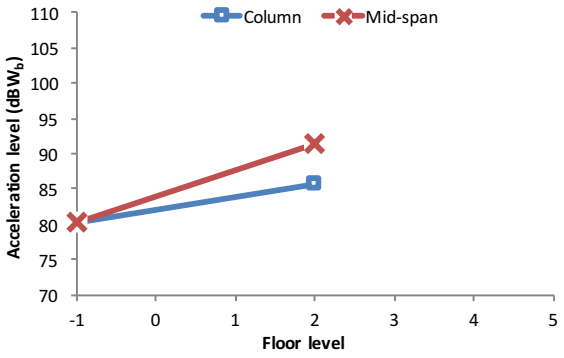

The results broadly show that vibration at 2nd floor has undergone amplification at frequencies below 31.5 Hz, and that the mid-span natural frequency is likely to have occurred within the 20 Hz band. However, with measurements at only basement and 2nd floor, there is insufficient data for meaningful trends to be identified.

Average maximum one-third octave band vertical vibration levels for YO-T (the tower) are given in Figure C-13 for column positions, and Figure C-14 for mid-span positions. The standard deviations and 95% confidence intervals for these averages are shown in Table C-13 to Table C-16. The overall A-weighted maximum velocity levels with storey are shown in Figure C-15. Care should be taken when interpreting these results, as the peak around 100 Hz is uncharacteristic and is likely to be affected by a mounting resonance due to the use of a heavy mounting block on a carpeted surface for the first and fourth floor measurements. The overall W_b-weighted maximum vertical acceleration levels are shown in Figure C-16.

Figure C-13. YO-T: Max. vibration levels at each measured storey (column)

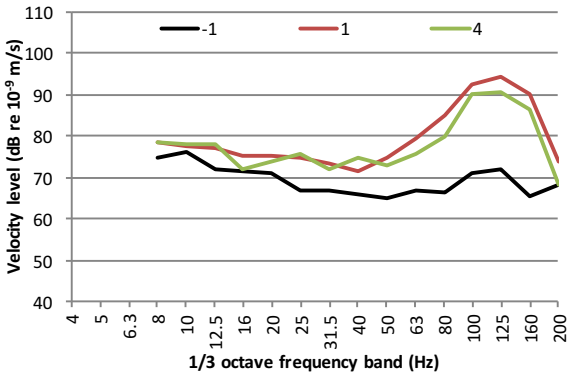

Figure C-14. YO-T: Max. vibration levels at each measured storey (mid-span)

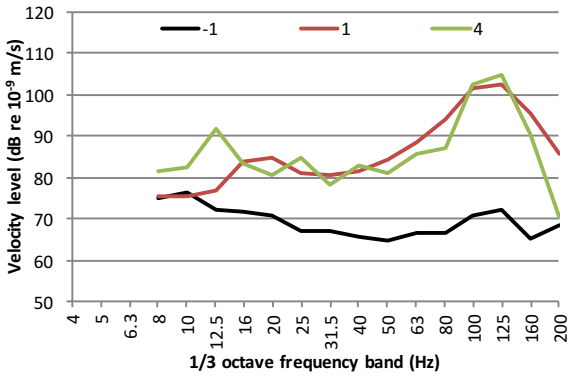

Table C-13. YO-T: Measurement 95% confidence intervals for mean (column) (dB)

Storey	No. pass-bys	1/3 octave band frequency (Hz)															Overall	
		8	10	12.5	16	20	25	31.5	40	50	63	80	100	125	160	200	L_{Wb}	L_A
-1	26	0.9	1.7	1.1	1.5	1.5	1.3	1.6	2.0	2.3	2.7	2.4	1.6	1.7	2.1	1.9	1.1	1.4
1	26	1.9	1.9	2.1	2.2	1.9	1.7	1.6	1.7	1.5	2.0	1.1	1.8	2.4	2.2	1.9	1.5	1.7
4	26	0.7	0.7	1.3	1.1	2.1	2.0	0.8	1.2	0.9	2.5	1.1	1.7	1.5	2.7	1.5	0.8	1.6

Table C-14. YO-T: Measurement standard deviations (column) (dB)

Storey	No. pass-bys	1/3 octave band frequency (Hz)															Overall	
		8	10	12.5	16	20	25	31.5	40	50	63	80	100	125	160	200	L_{Wb}	L_A
-1	26	2.3	4.1	2.7	3.8	3.8	3.2	3.9	4.9	5.6	6.7	5.8	3.9	4.3	5.3	4.7	2.8	3.4
1	26	4.7	4.7	5.1	5.3	4.7	4.2	4.1	4.2	3.6	4.9	2.8	4.5	5.8	5.4	4.6	3.7	4.3
4	26	1.7	1.6	3.3	2.6	5.2	4.9	2.1	3.0	2.1	6.3	2.8	4.2	3.7	6.6	3.8	2.0	4.0

Table C-15. YO-T: Measurement 95% confidence intervals for mean (mid-span) (dB)																		
Storey	No. pass-bys	1/3 octave band frequency (Hz)															Overall	
		8	10	12.5	16	20	25	31.5	40	50	63	80	100	125	160	200	L_{Wb}	L_A
-1	26	0.9	1.7	1.1	1.5	1.5	1.3	1.6	2.0	2.3	2.7	2.4	1.6	1.7	2.1	1.9	1.1	1.4
1	26	1.0	1.3	1.7	1.9	1.4	0.8	1.6	1.8	1.1	2.0	1.0	1.8	2.6	1.5	1.7	1.0	1.5
4	26	1.6	1.6	1.5	1.6	2.8	1.3	1.1	1.1	1.2	3.0	1.2	1.8	1.6	2.2	1.7	1.0	1.4

Table C-16. YO-T: Measurement standard deviations (mid-span) (dB)																		
Storey	No. pass-bys	1/3 octave band frequency (Hz)															Overall	
		8	10	12.5	16	20	25	31.5	40	50	63	80	100	125	160	200	L_{Wb}	L_A
-1	26	2.3	4.1	2.7	3.8	3.8	3.2	3.9	4.9	5.6	6.7	5.8	3.9	4.3	5.3	4.7	2.8	3.4
1	26	2.5	3.3	4.2	4.8	3.5	1.9	4.0	4.5	2.8	4.9	2.4	4.4	6.4	3.7	4.1	2.4	3.8
4	26	3.9	4.0	3.6	3.9	6.8	3.3	2.8	2.7	3.1	7.5	2.9	4.5	4.0	5.5	4.2	2.4	3.4

Figure C-15. YO-T: Overall A-weighted max. velocity levels with storey

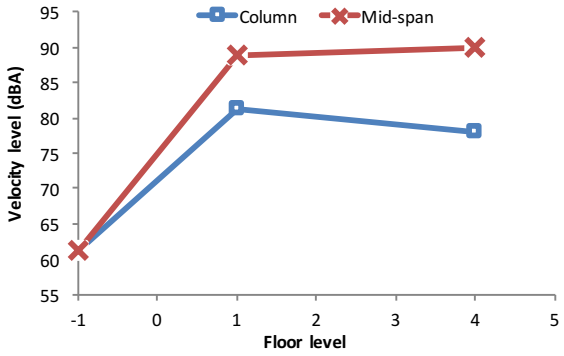

Figure C-16. YO-T: Overall W_b-weighted max. acceleration levels with storey

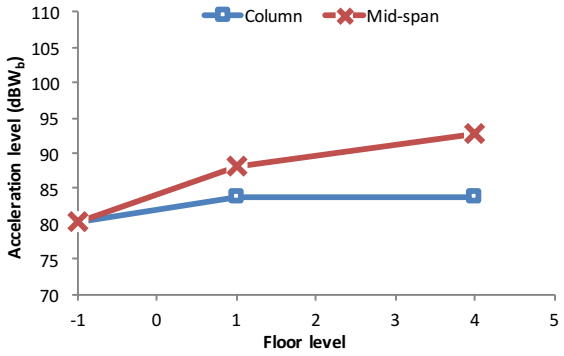

C.4: Lexington Ave, New York (LX-S & LX-C)

Only mid-span measurement positions were recorded, and only down to 12.5 Hz. Average maximum one-third octave band vertical vibration levels are given in Figure C-17 for LX–C, and Figure C-18 for LX-S. The overall A–weighted maximum velocity levels with storey are shown in Figure C-19 and Figure C-20, respectively. The overall W_b-weighted maximum acceleration levels are shown in Figure C-21 and Figure C-22, respectively.

Figure C-17. LX-C: Max. vibration levels at each measured storey (mid-span)

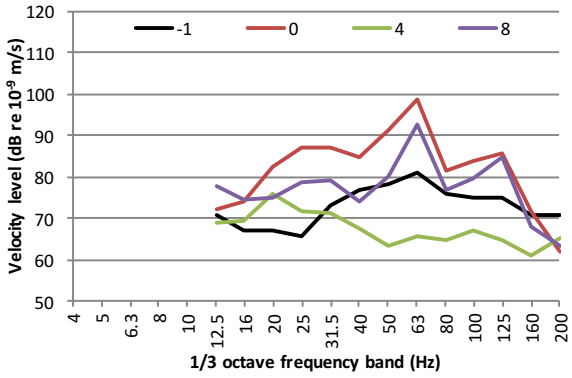

Figure C-18. LX-S: Max. vibration levels at each measured storey (mid-span)

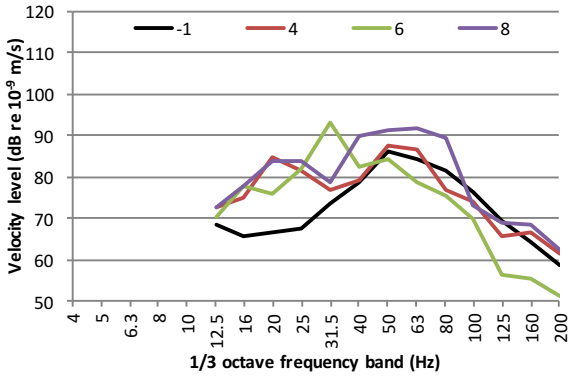

Figure C-19. LX-C: Overall A-weighted max. velocity levels with storey

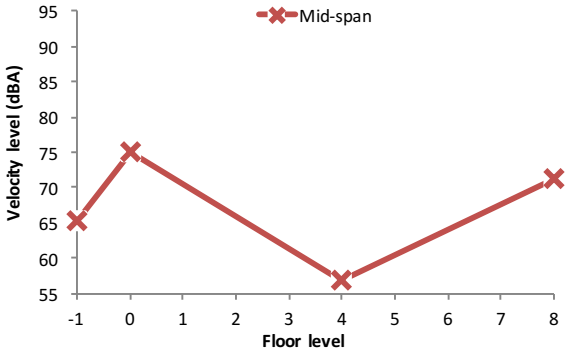

Figure C-20. LX-S: Overall A-weighted max. velocity levels with storey

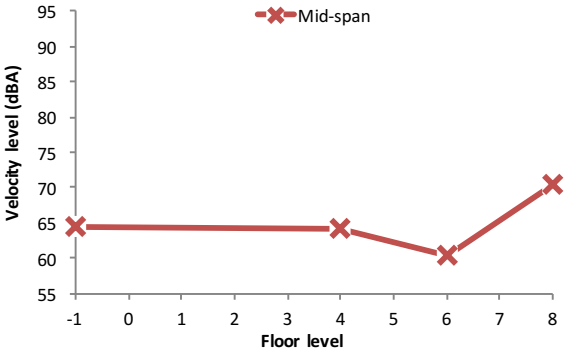

Figure C-21. LX-C: Overall W_b-weighted max. acceleration levels with storey

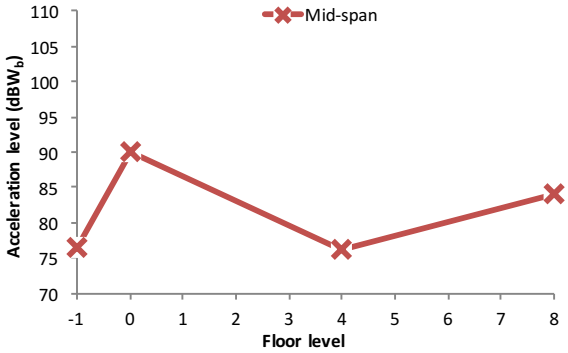

Figure C-22. LX-S: Overall W_b-weighted max. acceleration levels with storey

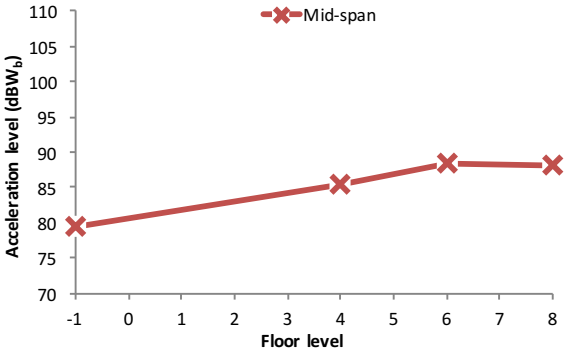

The one-third octave band results are difficult to draw conclusions from without data from column measurement positions. For LX-C, there is a peak in the vibration response in the 63 Hz band, which also coincides with the peak in the input spectrum. The result at 4th floor does not follow the same shape as the other measurements, and is likely to have been affected by a local structural feature. The measurements for LX-S suggest that the floor natural frequency occurs in the 20 Hz band.

C.5: New Oxford Road, London (NX-1 to NX-4)

Average maximum one-third octave band vertical vibration levels for the measurement points NX-1 to NX-4 are given in Figure C-23 to Figure C-26 respectively. The overall A–weighted maximum velocity levels are plotted against storey for the measurement points NX-1 to NX-4 in Figure C-27, with the W_b-weighted maximum acceleration results shown in Figure C-28. In order to assess horizontal attenuation across the building structure, these results are shown against distance from the façade in Figure C-29 and Figure C-30, with the building facade limits represented as dashed grey lines.

Figure C-23. NX-1: Max. vibration levels at each measured storey (mid-span)

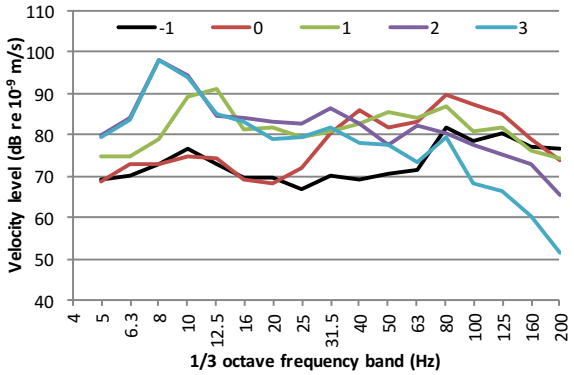

Figure C-24. NX-2: Max. vibration levels at each measured storey (mid-span)

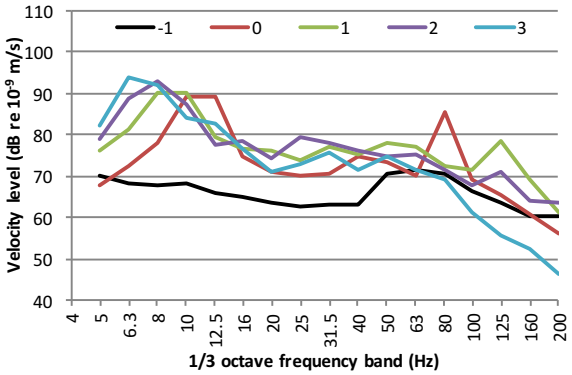

Figure C-25. NX-3: Max. vibration levels at each measured storey (mid-span)

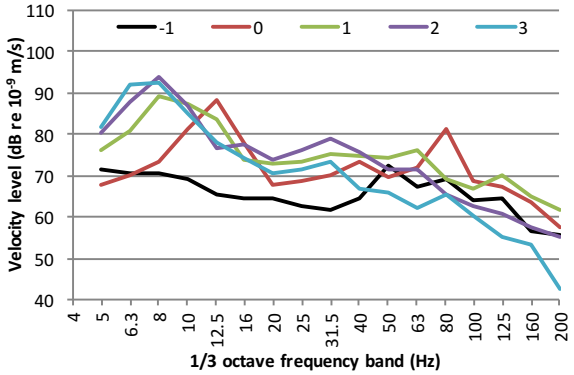

Figure C-26. NX-4: Max. vibration levels at each measured storey (mid-span)

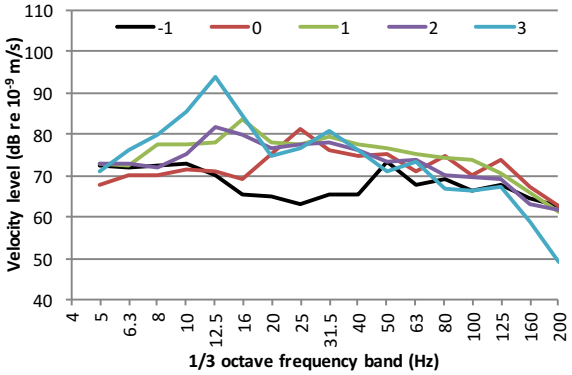

The 95% confidence intervals and standard deviation data over all pass-bys are shown for each storey in Table C-17 to Table C-24. The results show that the average results presented for each storey are a good representation of the actual mean.

Table C-17. NX1: Measurement 95% confidence intervals for mean (mid-span) (dB)

Storey	No. pass-bys	1/3 octave band frequency (Hz)																	Overall	
		5	6.3	8	10	12.5	16	20	25	31.5	40	50	63	80	100	125	160	200	L_{Wb}	L_A
-1	37	0.8	0.9	1.4	1.6	1.7	1.9	0.8	0.6	0.3	0.2	0.2	0.2	0.1	0.2	0.1	0.2	0.2	0.2	0.1
0	43	0.8	0.9	1.1	0.8	1.2	1.3	0.8	0.6	0.8	0.2	0.2	0.2	0.1	0.1	0.1	0.1	0.2	0.2	0.1
1	14	1.5	1.3	1.9	1.8	1.6	0.8	1.6	0.9	1.3	0.5	0.3	0.6	0.2	0.3	0.2	0.2	0.3	0.7	0.1
2	5	4.6	4.5	3.5	4.8	5.0	6.1	5.8	5.5	3.3	5.2	4.5	3.6	5.1	5.1	5.8	5.3	5.0	3.5	4.3
3	8	2.1	3.2	4.3	2.8	3.7	4.1	3.0	1.3	4.3	1.7	0.4	2.7	0.3	0.4	0.4	0.5	0.5	3.0	0.2

Table C-18. NX1: Measurement standard deviations (mid-span) (dB)

Storey	No. pass-bys	1/3 octave band frequency (Hz)																	Overall	
		5	6.3	8	10	12.5	16	20	25	31.5	40	50	63	80	100	125	160	200	L_{Wb}	L_A
-1	37	2.4	2.6	4.3	4.7	5.0	5.8	2.5	1.7	0.9	0.6	0.7	0.5	0.4	0.5	0.3	0.5	0.7	0.7	0.3
0	43	2.5	3.0	3.6	2.7	3.9	4.3	2.6	2.0	2.6	0.5	0.6	0.8	0.3	0.4	0.3	0.4	0.5	0.5	0.2
1	14	2.6	2.3	3.3	3.1	2.7	1.3	2.8	1.5	2.3	0.8	0.6	1.0	0.4	0.4	0.4	0.4	0.5	1.2	0.3
2	5	3.7	3.6	2.8	3.9	4.0	4.9	4.7	4.5	2.7	4.2	3.6	2.9	4.1	4.1	4.7	4.3	4.1	2.8	3.5
3	8	2.6	3.8	5.2	3.4	4.4	4.9	3.6	1.6	5.1	2.0	0.5	3.2	0.4	0.5	0.5	0.6	0.6	3.5	0.3

Table C-19. NX2: Measurement 95% confidence intervals for mean (mid-span) (dB)																				
Storey	No. pass-bys	1/3 octave band frequency (Hz)																	Overall	
		5	6.3	8	10	12.5	16	20	25	31.5	40	50	63	80	100	125	160	200	L_{Wb}	L_A
-1	23	0.7	0.8	1.5	1.4	1.2	1.3	0.8	0.6	0.4	0.3	0.4	0.4	0.3	0.3	0.2	0.2	0.1	0.2	0.1
0	43	1.1	0.8	1.0	1.0	0.8	1.0	0.7	0.7	0.6	0.2	0.2	0.1	0.1	0.1	0.1	0.1	0.1	0.5	0.1
1	14	1.9	2.7	3.2	1.8	1.4	1.6	1.4	1.4	0.8	1.1	0.3	0.6	0.8	0.9	0.5	0.8	0.8	1.8	0.6
2	5	2.0	1.8	3.7	1.8	5.4	4.3	4.8	5.1	4.0	5.4	3.2	1.7	3.9	2.9	3.1	2.1	2.1	2.1	1.6
3	8	3.5	2.0	4.0	2.9	2.9	3.3	2.8	2.0	2.8	2.0	1.3	2.0	0.5	0.5	0.7	0.3	0.5	2.5	0.8

Table C-20. NX2: Measurement standard deviations (mid-span) (dB)																				
Storey	No. pass-bys	1/3 octave band frequency (Hz)																	Overall	
		5	6.3	8	10	12.5	16	20	25	31.5	40	50	63	80	100	125	160	200	L_{Wb}	L_A
-1	23	1.5	1.8	3.5	3.2	2.9	3.0	1.8	1.3	1.0	0.8	0.8	0.8	0.6	0.7	0.5	0.4	0.3	0.6	0.3
0	43	3.5	2.5	3.3	3.3	2.7	3.1	2.3	2.4	1.9	0.7	0.5	0.5	0.3	0.4	0.3	0.5	0.3	1.7	0.3
1	14	3.2	4.6	5.5	3.1	2.4	2.8	2.4	2.4	1.3	1.9	0.6	1.0	1.3	1.6	0.9	1.4	1.4	3.1	1.0
2	5	1.6	1.4	3.0	1.4	4.3	3.4	3.9	4.1	3.2	4.3	2.5	1.4	3.1	2.3	2.5	1.7	1.7	1.7	1.3
3	8	4.2	2.4	4.8	3.5	3.5	3.9	3.3	2.4	3.4	2.4	1.5	2.4	0.7	0.6	0.9	0.3	0.6	3.0	0.9

Table C-21. NX3: Measurement 95% confidence intervals for mean (mid-span) (dB)																				
Storey	No. pass-bys	1/3 octave band frequency (Hz)																	Overall	
		5	6.3	8	10	12.5	16	20	25	31.5	40	50	63	80	100	125	160	200	L_{Wb}	L_A
-1	20	0.7	0.6	0.8	1.6	0.9	1.1	0.6	0.3	0.3	0.3	0.4	0.3	0.2	0.3	0.3	0.2	0.1	0.3	0.1
0	43	0.8	0.7	1.0	1.1	0.8	1.0	0.7	0.6	0.6	0.3	0.7	0.2	0.1	0.2	0.1	0.2	0.1	0.6	0.1
1	14	1.4	1.7	3.3	2.4	1.4	1.0	1.0	1.1	0.8	1.5	0.9	0.4	0.5	1.4	0.2	1.7	1.6	2.0	1.0
2	5	2.2	3.0	3.5	2.2	4.8	6.7	4.9	5.4	5.1	3.5	2.3	3.6	3.1	2.2	3.9	3.0	2.6	2.5	2.0
3	8	3.4	1.9	2.3	3.2	2.5	1.7	2.6	2.5	2.9	1.8	0.9	1.7	0.4	0.6	1.1	1.3	1.9	2.0	0.5

Table C-22. NX3: Measurement standard deviations (mid-span) (dB)																				
Storey	No. pass-bys	1/3 octave band frequency (Hz)																	Overall	
		5	6.3	8	10	12.5	16	20	25	31.5	40	50	63	80	100	125	160	200	L_{Wb}	L_A
-1	20	1.5	1.2	1.7	3.5	1.9	2.3	1.4	0.7	0.7	0.6	0.8	0.6	0.3	0.5	0.6	0.5	0.3	0.6	0.3
0	43	2.6	2.4	3.1	3.7	2.5	3.3	2.2	2.0	2.0	0.9	2.1	0.8	0.4	0.5	0.4	0.5	0.4	1.9	0.3
1	14	2.5	2.9	5.8	4.1	2.5	1.7	1.7	1.9	1.4	2.6	1.6	0.8	0.9	2.4	0.4	2.9	2.8	3.4	1.7
2	5	1.8	2.4	2.8	1.8	3.9	5.4	4.0	4.4	4.1	2.8	1.9	2.9	2.5	1.7	3.1	2.4	2.1	2.0	1.6
3	8	4.1	2.2	2.8	3.8	2.9	2.1	3.1	3.0	3.5	2.2	1.1	2.1	0.4	0.8	1.3	1.6	2.2	2.4	0.6

Table C-23. NX4: Measurement 95% confidence intervals for mean (mid-span) (dB)																				
Storey	No. pass-bys	1/3 octave band frequency (Hz)																	Overall	
		5	6.3	8	10	12.5	16	20	25	31.5	40	50	63	80	100	125	160	200	L_{Wb}	L_A
-1	9	1.2	2.0	1.3	1.9	1.9	1.3	1.6	1.1	0.5	0.8	0.9	0.7	0.6	0.6	0.3	0.4	0.5	0.8	0.2
0	43	0.6	0.7	0.9	1.0	1.2	1.0	0.5	0.5	1.0	0.4	0.5	0.4	0.1	0.1	0.2	0.2	0.3	0.5	0.2
1	14	0.8	1.0	1.8	0.9	1.2	0.7	1.8	0.9	1.7	2.3	2.0	0.9	0.3	1.1	1.0	1.6	1.8	1.0	1.0
2	5	1.3	1.5	3.3	0.8	2.7	3.8	6.2	2.9	3.1	4.8	5.3	5.1	3.3	3.9	2.4	3.2	4.3	3.1	2.4
3	8	2.7	1.5	2.8	4.1	4.2	2.1	2.3	3.5	4.0	2.6	1.3	2.4	1.2	1.3	0.9	1.4	2.1	3.6	0.9

Table C-24. NX4: Measurement standard deviations (mid-span) (dB)																				
Storey	No. pass-bys	1/3 octave band frequency (Hz)																	Overall	
		5	6.3	8	10	12.5	16	20	25	31.5	40	50	63	80	100	125	160	200	L_{Wb}	L_A
-1	9	1.6	2.6	1.6	2.5	2.5	1.7	2.1	1.4	0.7	1.1	1.1	0.9	0.8	0.7	0.4	0.5	0.6	1.0	0.2
0	43	2.1	2.4	2.8	3.4	3.8	3.2	1.8	1.7	3.3	1.4	1.6	1.3	0.4	0.4	0.8	0.7	1.0	1.5	0.5
1	14	1.4	1.7	3.1	1.5	2.0	1.2	3.2	1.6	3.0	4.0	3.4	1.6	0.5	1.9	1.8	2.8	3.1	1.7	1.7
2	5	1.1	1.2	2.7	0.6	2.2	3.1	5.0	2.4	2.5	3.8	4.3	4.1	2.7	3.1	2.0	2.6	3.5	2.5	1.9
3	8	3.2	1.8	3.3	4.9	5.1	2.5	2.8	4.1	4.8	3.1	1.6	2.8	1.4	1.6	1.1	1.7	2.5	4.3	1.0

The measured spectra suggest that most of the floor slabs exhibited natural frequencies between 6.3 and 12.5 Hz. A peak at 80 Hz is present is some of the spectra measured, but this is anticipated to be due an extraneous vibration source rather than being a characteristic of the structural response.

Figure C-27. NX-1 to 4: Overall A-weighted max. velocity levels with storey (mid-span)

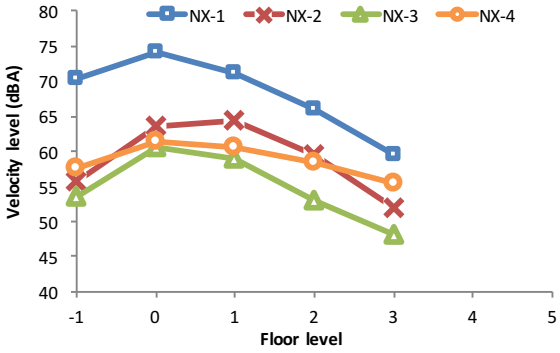

Figure C-28. NX-1 to 4: Overall W_b-weighted max. acceleration levels with storey (mid-span)

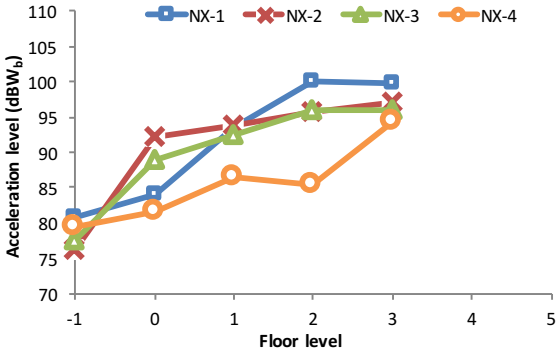

Figure C-29. NX-1 to 4: Overall A-weighted max. velocity levels with façade distance (mid-span)

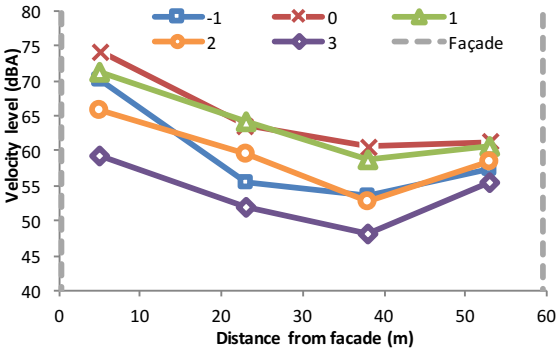

Figure C-30. NX-1 to 4: Overall W_b-weighted max. acceleration levels with façade distance (mid-span)

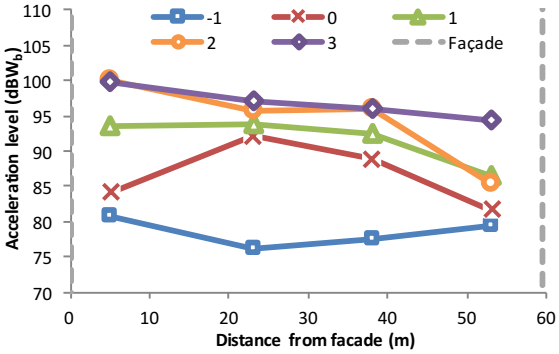

C.6: City Road, London (CR-N & CR-S)

Average maximum one-third octave band vertical vibration levels for CR-N are given in Figure C-31 and Figure C-32 for column and mid-span positions respectively. The standard deviations and 95% confidence intervals for these averages are shown in Table C-25 to Table C-28. The overall A–weighted maximum velocity levels with storey are shown in Figure C-33. The overall W_b-weighted maximum acceleration levels are shown in Figure C-34.

Figure C-31. CR-N: Max. vibration levels at each measured storey (column)

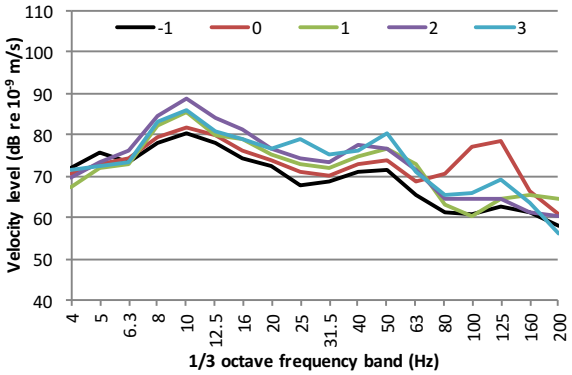

Figure C-32. CR-N: Max. vibration levels at each measured storey (mid-span)

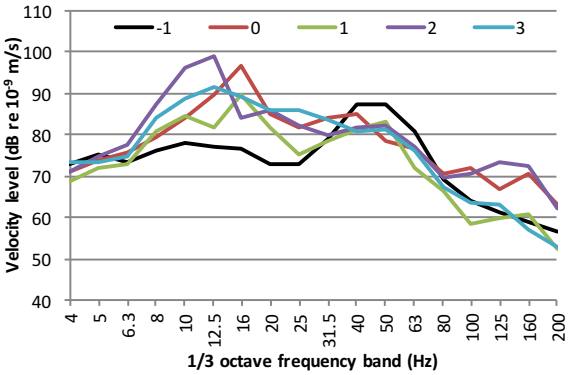

Table C-25. CR-N: Measurement 95% confidence intervals for mean (column) (dB)

Storey	No. pass-bys	1/3 octave band frequency (Hz)																		Overall	
		4	5	6.3	8	10	12.5	16	20	25	31.5	40	50	63	80	100	125	160	200	L_{Wb}	L_A
-1	21	2.3	2.0	1.2	1.1	1.4	1.7	1.1	1.5	2.1	2.5	3.0	3.0	2.5	1.0	1.4	2.1	2.8	3.4	1.3	2.1
0	19	2.0	1.7	1.3	1.2	1.6	1.7	1.8	1.9	3.0	2.7	3.3	3.4	3.0	1.4	1.2	1.4	2.3	3.1	1.5	1.2
1	7	1.1	1.4	1.6	4.0	3.7	2.1	2.5	2.2	2.2	3.2	3.3	4.9	5.7	1.3	1.9	3.7	4.1	6.5	1.8	4.3
2	6	1.6	3.9	3.2	4.2	3.6	4.1	5.5	6.1	5.7	4.5	6.0	6.8	4.3	3.5	1.7	0.5	2.5	2.4	3.9	2.2
3	8	4.3	2.3	1.1	2.8	3.9	1.7	2.6	4.3	5.9	6.0	4.9	6.3	4.3	2.9	2.3	3.6	3.7	4.1	3.1	3.2

Table C-26. CR-N: Measurement 95% confidence intervals for mean (mid-span) (dB)

Storey	No. pass-bys	1/3 octave band frequency (Hz)																		Overall	
		4	5	6.3	8	10	12.5	16	20	25	31.5	40	50	63	80	100	125	160	200	L_{Wb}	L_A
-1	21	2.2	2.1	1.2	1.1	1.5	1.8	1.4	1.4	1.9	2.4	2.2	2.2	1.7	1.1	1.7	2.0	2.5	3.5	1.8	1.8
0	19	2.0	1.8	1.1	1.0	1.7	2.0	2.4	2.0	1.9	3.0	2.9	2.4	2.5	1.8	1.6	1.3	2.8	3.2	2.1	1.9
1	7	1.5	1.0	1.1	3.9	3.2	2.8	1.2	2.6	2.2	2.3	3.4	4.6	4.3	2.5	1.6	4.1	4.2	6.1	1.5	3.8
2	6	1.3	3.4	2.9	4.6	3.5	5.2	5.0	5.1	4.8	3.4	4.7	4.7	3.2	2.4	3.3	4.4	4.9	2.5	4.2	3.6
3	8	3.9	2.2	1.2	2.7	3.7	2.4	3.8	3.5	5.5	4.7	2.6	4.6	3.8	2.4	3.1	3.4	2.4	4.0	2.8	3.2

Table C-27. CR-N: Measurement standard deviations (column) (dB)

Storey	No. pass-bys	1/3 octave band frequency (Hz)																		Overall	
		4	5	6.3	8	10	12.5	16	20	25	31.5	40	50	63	80	100	125	160	200	L_{Wb}	L_A
-1	21	5.0	4.5	2.6	2.4	3.1	3.7	2.5	3.4	4.7	5.6	6.6	6.7	5.4	2.2	3.1	4.5	6.1	7.5	3.0	4.7
0	19	4.2	3.5	2.6	2.5	3.2	3.5	3.7	3.9	6.1	5.6	6.9	7.0	6.2	3.0	2.4	2.9	4.7	6.4	3.2	2.5
1	7	1.2	1.5	1.7	4.3	4.0	2.3	2.7	2.4	2.3	3.4	3.6	5.3	6.2	1.4	2.0	4.0	4.4	7.0	1.9	4.7
2	6	1.5	3.7	3.1	4.0	3.4	3.9	5.2	5.8	5.5	4.2	5.7	6.5	4.1	3.3	1.6	0.5	2.4	2.3	3.7	2.1
3	8	5.2	2.7	1.4	3.3	4.7	2.0	3.1	5.2	7.1	7.1	5.9	7.5	5.1	3.4	2.7	4.3	4.4	4.9	3.8	3.9

Table C-28. CR-N: Measurement standard deviations (mid-span) (dB)

Storey	No. pass-bys	1/3 octave band frequency (Hz)																		Overall	
		4	5	6.3	8	10	12.5	16	20	25	31.5	40	50	63	80	100	125	160	200	L_{Wb}	L_A
-1	21	4.9	4.5	2.7	2.3	3.2	3.9	3.0	3.1	4.2	5.2	4.8	4.9	3.7	2.5	3.7	4.3	5.6	7.7	3.9	4.0
0	19	4.2	3.7	2.2	2.1	3.5	4.2	4.9	4.1	4.0	6.1	6.1	5.0	5.1	3.8	3.4	2.7	5.9	6.6	4.3	4.0
1	7	1.7	1.1	1.2	4.2	3.4	3.0	1.3	2.8	2.4	2.5	3.7	4.9	4.7	2.7	1.7	4.4	4.6	6.6	1.7	4.2
2	6	1.2	3.3	2.8	4.4	3.3	4.9	4.8	4.9	4.6	3.3	4.5	4.5	3.0	2.3	3.2	4.2	4.6	2.3	4.0	3.4
3	8	4.6	2.6	1.5	3.3	4.4	2.9	4.5	4.2	6.5	5.6	3.1	5.4	4.5	2.9	3.8	4.1	2.9	4.8	3.4	3.8

Figure C-33. CR-N: Overall A-weighted max. velocity levels with storey

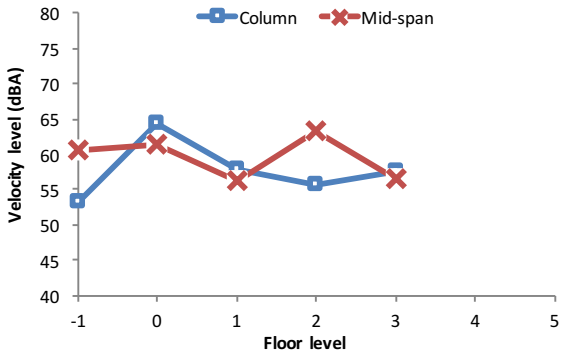

Figure C-34. CR-N: Overall W_b-weighted max. acceleration levels with storey

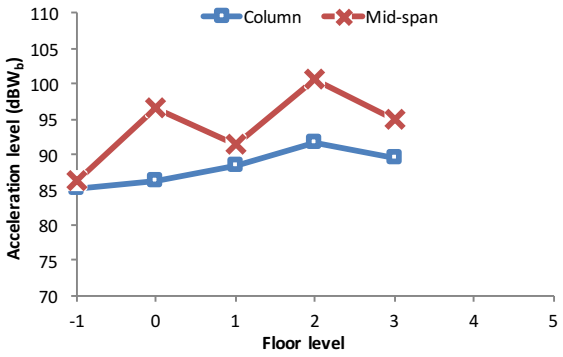

For CR-N, the one-third octave band column results show similar vibration levels at each storey, and even slight amplification with storey across most of the frequency range, which is unusual. The floor natural frequencies occurred in the 12.5 and 16 Hz bands.

Average maximum one-third octave band vertical vibration levels for CR-S are given in Figure C-35 and Figure C-36 for column and mid-span positions respectively. The standard deviations and 95% confidence intervals for these averages are shown in Table C-29 to Table C-32. The overall A–weighted maximum velocity levels with storey are shown in Figure C-37. The overall W_b-weighted maximum acceleration levels are shown in Figure C-38.

Figure C-35. CR-S: Max. vibration levels at each measured storey (column)

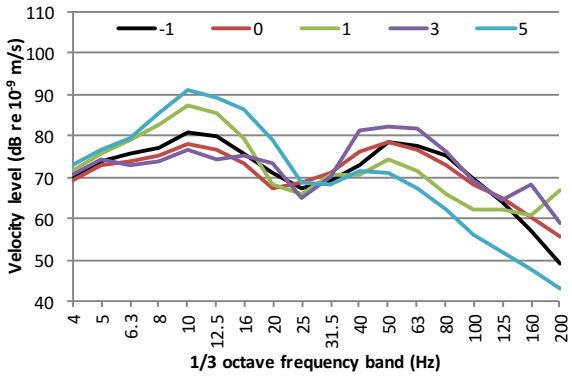

Figure C-36. CR-S: Max. vibration levels at each measured storey (mid-span)

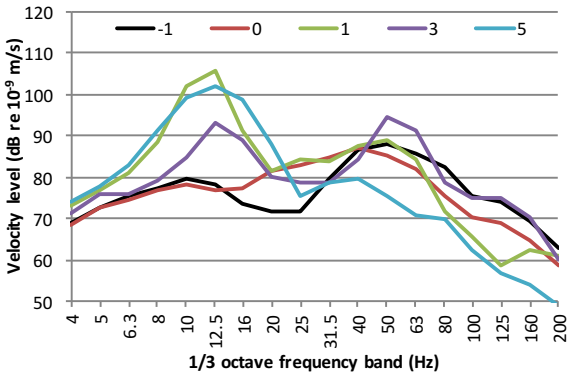

Table C-29. CR-S: Measurement 95% confidence intervals for mean (column) (dB)

Storey	No. pass-bys	1/3 octave band frequency (Hz)																		Overall	
		4	5	6.3	8	10	12.5	16	20	25	31.5	40	50	63	80	100	125	160	200	L_{Wb}	L_A
-1	19	2.0	2.0	1.8	2.6	3.2	3.2	2.9	2.6	1.9	2.3	2.7	3.9	4.4	4.8	3.1	1.9	2.2	2.3	3.3	3.5
0	15	1.6	1.6	1.6	2.4	3.2	2.8	1.7	1.1	2.4	3.3	3.6	4.4	4.7	4.5	2.5	1.6	2.1	2.6	2.7	2.8
1	19	2.0	2.2	2.4	3.1	3.7	3.7	3.2	2.0	2.4	3.0	4.7	4.0	4.8	4.5	3.8	2.4	3.1	3.1	2.7	2.8
2	5	3.5	3.2	1.0	2.0	4.6	5.0	3.3	1.7	0.8	1.6	4.1	2.4	2.9	1.8	3.3	3.1	3.0	2.9	2.5	2.3
3	17	2.0	2.1	2.4	2.8	3.2	3.2	2.9	2.1	1.8	3.0	4.3	4.5	5.7	5.3	2.9	2.2	1.4	1.8	1.8	3.6

Table C-30. CR-S: Measurement 95% confidence intervals for mean (mid-span) (dB)																					
Storey	No. pass-bys	1/3 octave band frequency (Hz)																		Overall	
		4	5	6.3	8	10	12.5	16	20	25	31.5	40	50	63	80	100	125	160	200	L_{Wb}	L_A
-1	19	1.5	1.7	1.7	2.5	2.9	3.0	2.2	2.2	2.4	2.8	3.1	3.4	4.1	4.7	3.1	1.9	2.5	2.3	3.4	3.1
0	15	1.6	1.7	1.5	2.3	3.2	2.7	1.8	1.7	2.2	2.2	3.0	2.8	4.5	3.8	2.2	2.1	2.0	2.5	2.3	2.4
1	18	1.4	1.5	1.9	2.7	3.1	3.1	2.4	1.5	1.3	2.2	3.8	4.4	5.0	4.5	3.7	2.4	2.1	1.9	2.0	3.4
2	5	4.3	3.3	1.3	2.4	4.1	5.7	3.0	4.3	2.0	1.3	2.5	3.8	2.6	3.6	3.5	3.3	3.0	2.2	3.2	2.9
3	17	1.9	2.1	2.2	2.7	3.2	2.8	2.4	1.9	1.6	3.1	3.5	3.7	4.7	4.2	2.7	2.1	1.4	1.9	2.2	2.5

Table C-31. CR-S: Measurement standard deviations (column) (dB)																					
Storey	No. pass-bys	1/3 octave band frequency (Hz)																		Overall	
		4	5	6.3	8	10	12.5	16	20	25	31.5	40	50	63	80	100	125	160	200	L_{Wb}	L_A
-1	19	4.1	4.2	3.7	5.3	6.7	6.7	6.0	5.4	4.0	4.7	5.6	8.1	9.2	10.0	6.4	4.0	4.6	4.8	6.8	7.2
0	15	2.8	2.9	2.9	4.3	5.8	5.0	3.1	2.0	4.4	5.9	6.4	7.9	8.4	8.2	4.4	3.0	3.8	4.7	4.8	5.0
1	19	4.1	4.6	5.1	6.5	7.6	7.7	6.7	4.3	4.9	6.2	9.8	8.4	9.9	9.3	7.9	5.0	6.5	6.4	5.5	5.7
2	5	2.8	2.6	0.8	1.6	3.7	4.0	2.6	1.3	0.7	1.3	3.3	2.0	2.3	1.4	2.7	2.5	2.4	2.3	2.0	1.8
3	17	3.8	4.1	4.7	5.5	6.2	6.2	5.6	4.1	3.6	5.8	8.4	8.8	11.0	10.3	5.6	4.4	2.6	3.5	3.6	7.0

Table C-32. CR-S: Measurement standard deviations (mid-span) (dB)																					
Storey	No. pass-bys	1/3 octave band frequency (Hz)																		Overall	
		4	5	6.3	8	10	12.5	16	20	25	31.5	40	50	63	80	100	125	160	200	L_{Wb}	L_A
-1	19	3.1	3.5	3.4	5.2	6.0	6.2	4.6	4.6	5.0	5.7	6.5	7.0	8.5	9.8	6.5	3.9	5.2	4.9	7.1	6.5
0	15	2.8	3.0	2.8	4.2	5.8	4.9	3.2	3.1	4.0	4.0	5.4	5.0	8.1	6.9	4.0	3.9	3.6	4.4	4.2	4.3
1	18	2.8	3.0	3.8	5.5	6.2	6.2	4.8	3.0	2.6	4.5	7.7	8.8	10.1	9.1	7.4	4.8	4.3	3.8	4.0	6.9
2	5	3.5	2.7	1.0	2.0	3.3	4.6	2.4	3.4	1.6	1.1	2.0	3.1	2.1	2.9	2.8	2.7	2.4	1.8	2.6	2.4
3	17	3.7	4.1	4.3	5.3	6.2	5.5	4.6	3.6	3.0	6.0	6.9	7.3	9.1	8.2	5.3	4.0	2.7	3.8	4.3	4.8

Figure C-37. CR-S: Overall A-weighted max. velocity levels with storey

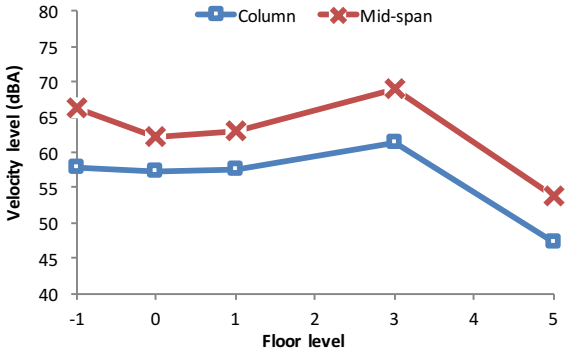

Figure C-38. CR-S: Overall W_b-weighted max. acceleration levels with storey

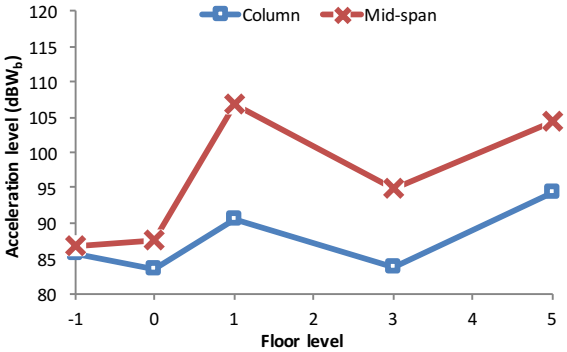

For CR-S, the one-third octave band column results show amplification with storey at frequency bands below 20 Hz, and amplification with storey above around 31.5 Hz. The mid-span results show natural frequencies occurring mainly in the 12.5 Hz frequency band. The exception is the measurement at ground floor, which does not display a clear natural frequency, although there is a broad peak in the vibration level around 40 Hz; the increase in frequency may have been due to additional floor stiffness in the construction at ground floor.

C.7: Portland Place, London (IOP)

Only mid-span vibration values were recorded. Average maximum one-third octave band vertical velocity levels are given in Figure C-39. The standard deviations and 95% confidence intervals for these averages are shown in Table C-33 and Table C-34. The overall A–weighted maximum velocity levels with storey are shown in Figure C-40. The overall W_b-weighted maximum acceleration levels are shown in Figure C-41.

Figure C-39. IOP: Max. vibration levels at each measured storey (mid-span)

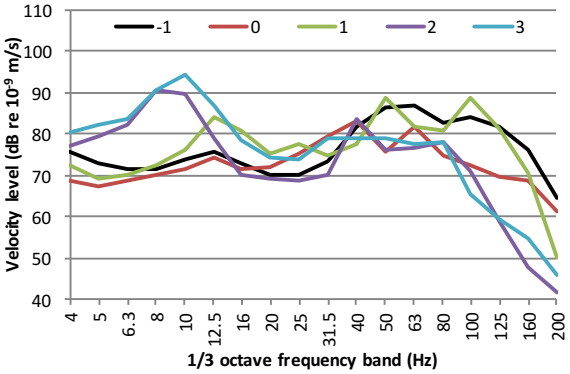

Table C-33. IOP: Measurement 95% confidence intervals for mean (mid-span) (dB)

Storey	No. pass-bys	1/3 octave band frequency (Hz)																		Overall	
		4	5	6.3	8	10	12.5	16	20	25	31.5	40	50	63	80	100	125	160	200	L_{Wb}	L_A
-1	48	0.7	0.8	0.9	0.8	1.3	0.8	0.8	0.7	0.8	0.9	0.7	0.6	0.6	0.5	0.6	0.7	0.8	0.7	0.5	0.6
0	27	1.0	1.2	1.7	1.3	1.7	1.4	0.9	0.9	1.2	1.3	1.4	0.8	0.8	1.5	2.1	2.1	1.4	1.0	0.8	1.1
1	10	3.2	2.1	2.4	1.4	1.8	2.2	2.7	2.3	1.5	2.6	1.8	2.7	1.2	0.8	0.8	1.0	2.0	1.6	1.8	0.7
2	13	2.1	2.3	2.8	2.3	2.3	2.2	1.6	2.0	2.1	2.1	2.1	1.2	1.2	2.0	1.9	3.1	2.6	1.5	1.7	1.3
3	5	8.4	7.3	8.7	7.6	9.0	7.1	8.6	7.1	5.9	4.1	4.4	2.6	2.8	1.3	4.5	3.1	2.4	5.7	6.4	1.4

Table C-34. IOP: Measurement standard deviations (mid-span) (dB)

Storey	No. pass-bys	1/3 octave band frequency (Hz)																		Overall	
		4	5	6.3	8	10	12.5	16	20	25	31.5	40	50	63	80	100	125	160	200	L_{Wb}	L_A
-1	48	2.4	2.7	2.9	2.8	4.3	2.7	2.6	2.4	2.6	3.2	2.3	2.2	2.2	1.8	2.1	2.5	2.7	2.4	1.7	2.0
0	27	2.6	3.1	4.2	3.3	4.3	3.5	2.4	2.2	3.0	3.3	3.4	2.1	1.9	3.8	5.3	5.2	3.5	2.6	1.9	2.7
1	10	4.5	2.9	3.4	2.0	2.5	3.1	3.8	3.3	2.1	3.6	2.5	3.8	1.7	1.1	1.1	1.4	2.9	2.3	2.5	1.0
2	13	3.5	3.8	4.7	3.8	3.8	3.6	2.6	3.2	3.5	3.5	3.5	2.0	2.0	3.2	3.1	5.1	4.3	2.5	2.8	2.1
3	5	6.8	5.8	7.0	6.1	7.2	5.7	6.9	5.7	4.7	3.3	3.5	2.1	2.3	1.0	3.6	2.5	1.9	4.6	5.1	1.1

Figure C-40. IOP: Overall A-weighted max. velocity levels with storey

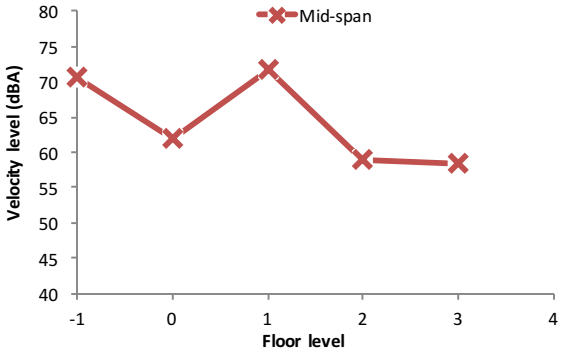

Figure C-41. IOP: Overall W_b-weighted max. acceleration levels with storey

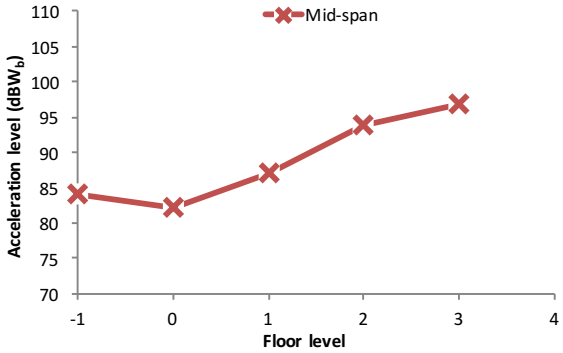

The one-third octave band results show amplification with storey at frequencies below around 20 Hz, with attenuation at higher frequencies. The ground floor did not show a clear natural frequency in the results. The suspended timber floor constructions showed natural frequencies of between 8 and 12.5 Hz, lower than is normally seen for concrete floors. This is probably due to the comparatively low stiffness of the joists. If the ground floor were of a similar construction, it is likely that the overall A-weighted results would have showed amplification of around 5 dB to the ground floor, and attenuation of perhaps as much as 5 dB per storey thereafter. The significant attenuation is expected to be due to high levels of damping in the floor construction and at the interface between timber joist and masonry wall.

C.8: Blomfield St, London (BLO)

Only mid-span measurement positions were recorded, and only down to 12.5 Hz. Average maximum one-third octave band vertical velocity levels for BLO are given in Figure C-42. The overall A–weighted maximum velocity levels with storey are shown in Figure C-43. The overall W_b-weighted maximum acceleration levels are shown in Figure C-44.

Figure C-42. BLO: Max. vibration levels at each measured storey (mid-span)

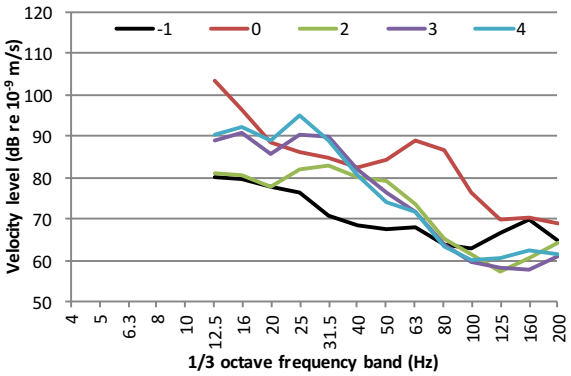

Figure C-43. BLO: Overall A-weighted max. velocity levels with storey

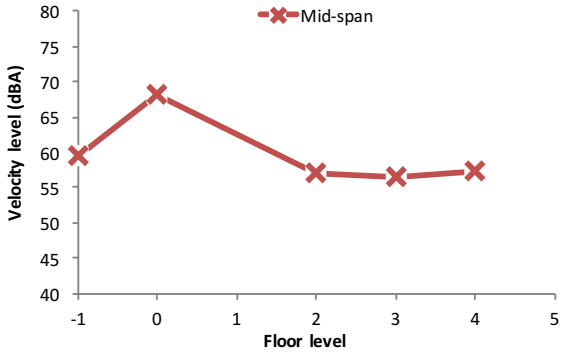

Figure C-44. BLO: Overall W_b-weighted max. acceleration levels with storey

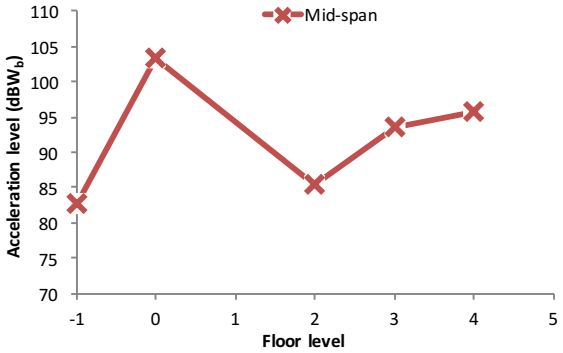

Whilst low frequency data is not available, the one-third octave band data suggests a possible natural frequency for the ground floor of around 12.5 Hz. The natural frequency for the 3rd and 4th floor levels appears to be of the order of 25 Hz.

C.9: Summary results

It is helpful to collate the measured results in order to discover trends present in the data. The measured data for basement vertical vibration levels in terms of average maximum one-third octave band levels (at mid-span locations) are shown for all buildings outlined above in Figure C-45. The average and the range of plus/minus one standard deviation are also presented. Note that some results have been excluded from the average for the 4 Hz frequency band due to the presence of a high-pass filter that was applied to these results. The result presented is only an indication of the kinds of vibration levels that might be present in the basement of a building affected by vibration from nearby underground trains.

Figure C-45. Measurement case study summary: Average maximum vibration levels at basement level

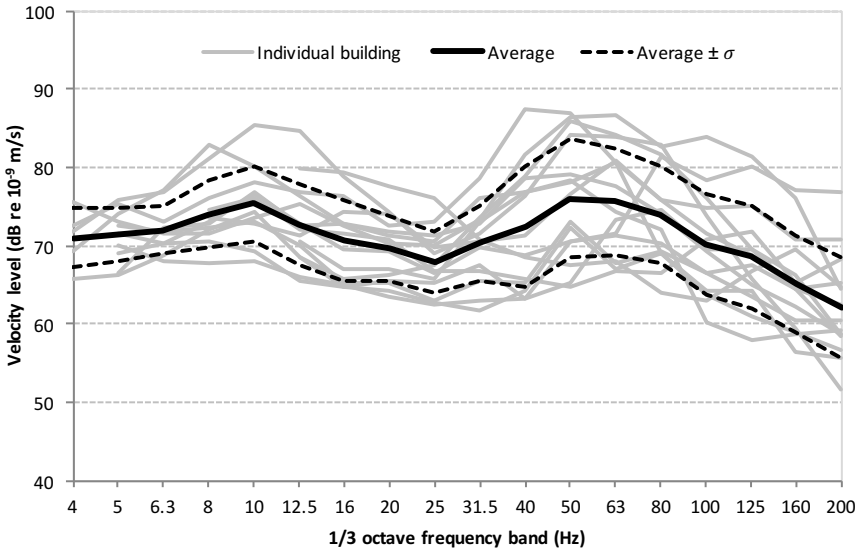

The interesting features of the shape of the average vibration level curve are the peaks around 10 and 50 Hz. The upper peak is a feature of the coupled wheel/track resonance. The 10 Hz peak is deemed to coincide with an anti-resonance of the vehicle primary suspension [128].

Figure C-46 gives the mid-span A-weighted vibration data relative to the basement at each storey for each of the buildings. An average of the relative values over the first six storeys is also given. Note that the average is calculated from the average 1/3 octave band frequency data, and assumes that the vibration at basement level is given by the average spectrum given in Figure C-45. There is a significant spread in the measured data, particularly in the transition between basement and ground floor, probably due to the influence of special floor constructions at basement and ground floor levels, and the range in basement slab conditions (e.g. discrete vs continuously supported foundation type). The average of the results for A-weighted levels is seen to exhibit an attenuation of approximately 1 dB per storey above ground floor.

Figure C-46. Measurement case study summary: Average basement-relative A-weighted velocity level with storey, mid-span

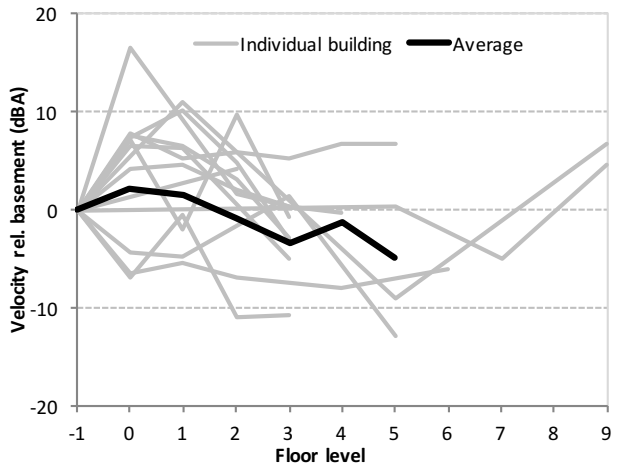

The mid-span vibration levels at 3rd floor are given in Figure C-47, relative to basement vibration. The peaks noted in the measured spectra in the 6.3 to 16 Hz region are due to natural frequencies of the floor slabs. It should be noted that the averaging procedure excludes these effects to a considerable degree, since these effects occur in isolated frequency bands, which differ between buildings and even between seemingly similar floors within the same building. Accounting for the natural frequencies correctly would be an important factor when considering the assessment of perceptible vibration. The average result shows amplification relative to basement level at frequencies below around 50 Hz and attenuation at frequencies above this.

Figure C-47. Measurement case study summary: Average velocity level relative to basement, 3rd floor (mid-span)

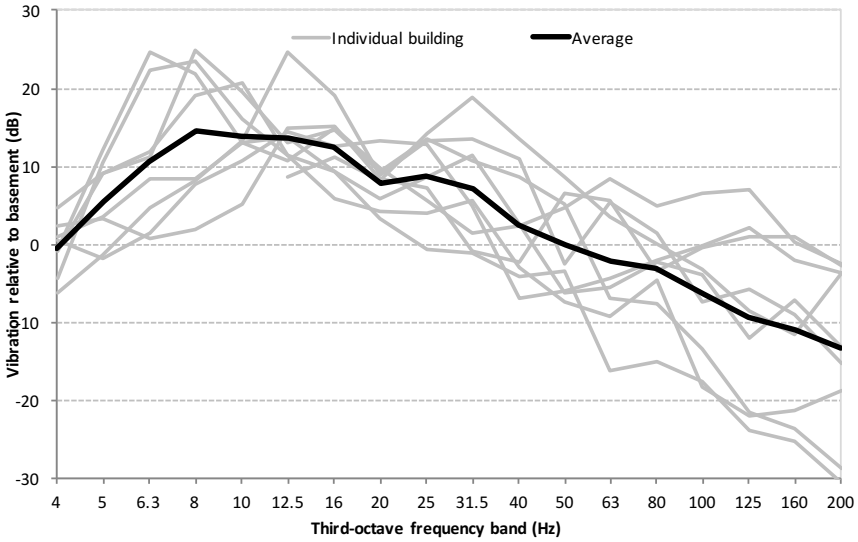

[BLANK PAGE]

APPENDIX D: DAMPING IN FE ROOM MODELS

In order to avoid the necessity of specifying damping at the room boundaries (which conflicts with the requirement to specify velocity at the boundaries), it is possible to specify an equivalent damping in the room volume. With COMSOL Multiphysics, the room volume can be assigned an "attenuation per unit length" parameter (dB/m).

Kuttruff [51] states that the reverberation time in a room, *T* in seconds, may be estimated from the room decay (or *damping*) constant through:

$$T = \frac{3\ln(10)}{\langle\delta\rangle} \approx \frac{6.91}{\langle\delta\rangle} \qquad \textbf{(D-1)}$$

where:

$\langle\delta\rangle$ is the spatially averaged decay constant, in rad.s^{-1}.

For each room mode, the decay constant is related to the loss factor and can therefore be obtained through half-power bandwidth analysis of resonant responses:

$$\delta_i = \pi f_i \eta_i = \pi f_i \frac{\Delta f_i}{f_i} = \pi \Delta f_i \qquad \textbf{(D-2)}$$

where:

η_i is the loss factor at mode i, $(= \frac{\Delta f}{f})$;

f_i is the frequency at mode i, in Hz;

Δf_i is the half-power bandwidth of mode i (the interval of the frequencies above and below the natural frequency at which the sound pressure level is 3 dB less than the mode maximum), in Hz.

For a value of *T* of 0.5 s, the value of the room decay constant would be expected to be around 14 rad.s^{-1}. The reverberation time can be related directly to the half-power bandwidth through:

$$T = \frac{6.91}{\pi \Delta f} = \frac{2.2}{\Delta f} \quad \text{(s)} \qquad \textbf{(D-3)}$$

An initial FE model of a room with dimensions 6 x 4 x 2.5 m has been used in order to determine appropriate values for the volumetric attenuation for given reverberation time conditions. All room boundaries are considered rigid (i.e. perfectly reflective). A pressure source is located at the centre of the room (with an arbitrary sound power), and an evaluation point is located at the

corner of the room. For different values of attenuation per unit length, the half-power bandwidth has been calculated at mode [2,0,0] to obtain the reverberation time, using Equation (D-3). A frequency resolution of 0.02 to 0.005 Hz is used in the analysis (dependent on the damping in each model). Graphs of the pressure responses are shown in Figure D-1, with the interpolated results provided in Table D-1, which include the half-power bandwidths Δf and corresponding values of attenuation per unit length. Note that the headings

Note that the attenuation value corresponding to T_{60}=0.1 s is not available due to the limited frequency range of the study (i.e. the -3 dB points were outside the study range).

Figure D-1. FE acoustics modelling: Sound pressure level response at room node, different values for attenuation per unit distance (in dB/m)

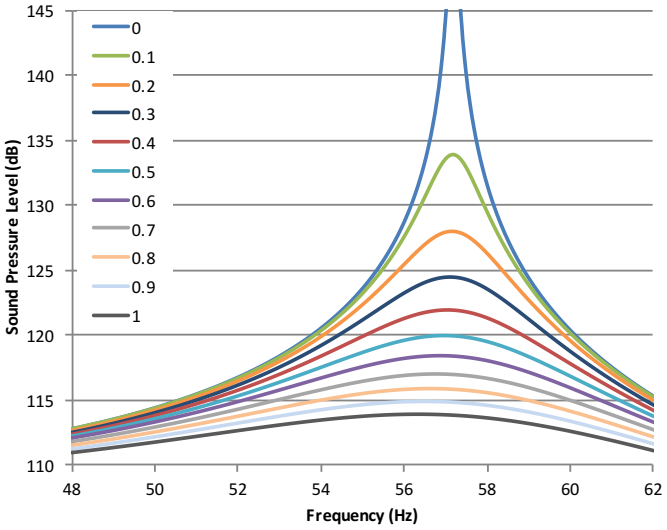

Table D-1. FE acoustics modelling: Appropriate values for attenuation for various reverberation time values

Attenuation (dB/m)	Δf (Hz)	δ (rad.s^{-1})	T_{60} (s)
-	22.0	69.1	0.1
0.82	11.0	34.6	0.2
0.57	7.3	23.0	0.3
0.43	5.5	17.3	0.4
0.35	4.4	13.8	0.5
0.29	3.7	11.5	0.6
0.25	3.1	9.9	0.7
0.21	2.7	8.6	0.8
0.19	2.4	7.7	0.9
0.17	2.2	6.9	1.0

The validity of the above values was tested for a range of room geometries; the approach was repeated for rooms with dimensions 5 x 3 x 2.5 m and 12 x 4 x 2.5 m with very similar results. Therefore, a very simple empirical expression was derived to obtain appropriate air attenuation values for a given reverberation time:

$$Air\ attenuation = \frac{1}{5.75T} \quad \text{(dB/m)} \qquad \textbf{(D-4)}$$

The empirical formula is plotted with the finite element results in Figure D-2, which shows very close agreement in the range of reverberation times for typical domestic rooms.

Figure D-2. FE acoustics modelling: Relationship between reverberation time and attenuation per unit distance

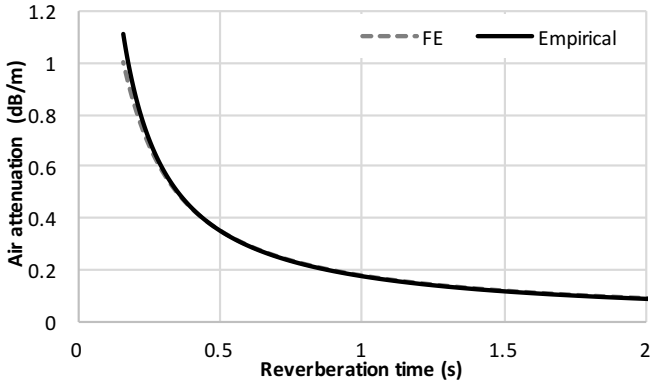

[BLANK PAGE]

APPENDIX E: OPTIMISING COMPUTERS FOR FE MODELLING

Due to the efforts that have been required to reduce the computation time of FE model solutions, it seems appropriate to present a number of observations.

When a solution is required, the computer system must first establish equations of motion in matrix form. During this process, the CPU stores the values in RAM. The CPU then must derive the solution required from the matrices, during which it must access these from the RAM. Solution results are then stored in the RAM. In this scenario, the speed of the calculation depends mainly on the speed of the CPU.

Where there is not sufficient available RAM to store the matrices and solutions, the computer must revert to the use of 'virtual memory' whereby the computer's hard disk drive (HDD) is used. RAM is very fast compared to HDD's, and in this scenario the solution time can increase considerably. Figure E-1shows a diagram of the process.

Figure E-1. FE solution computer resource usage diagram

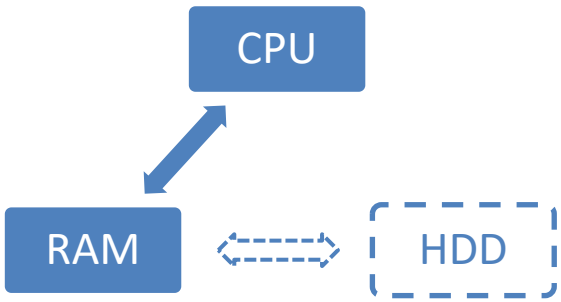

Where virtual memory must be used, the speed of the CPU becomes less important, because the hard disk data transfer speed dominates the time required for the solution. In such cases, the greatest improvement in calculation time comes through increasing the amount of RAM installed. If the maximum amount of RAM has already been installed, then the only remaining option is to increase the hard disk speed. There are three primary routes to achieve this:

Firstly, is the replacement of the main system hard drive with one with a faster speed, perhaps a HDD with a platter speed of up to 10,000 rpm.

Secondly is the use of a RAID 0 array. In this system, data is written to and read from multiple hard drives simultaneously for improved speed.

Thirdly is the use of solid state hard drives (SSD's), which use faster flash based memory. These have a much-reduced storage capacity compared to conventional HDD's, and as such should normally be used in conjunction with another storage system for archiving solutions once calculated. Most computer systems allow the location of the virtual memory to be specified manually, so it is possible to have the virtual memory on a separate (SSD) disk to the main computer operating system. The SSD solution has been trialled in this project, but not found to be successful. A high rate of drive failure was observed, and attributed to excessive use of a small sector of the drive, due to frequent reads and writes to the same location. However, it is understood that this can be resolved through the use of drive firmware updates and enabling 'TRIM' support, which ensures that drive usage is more evenly spread across the drive. Whilst this was therefore not successful for this project, it is expected that the reliability and implementation of SSD technology will be improved in the future.

It should be noted that the speed of the hard drive interface is important when considering high performance hard drive options. For internal hard drives, the SATA III interface provides suitable bandwidth for SSD and HDD systems. For external systems, the current best choices are the Thunderbolt and USB 3.0 interfaces.

APPENDIX F: BUILDING VIBRATION STUDY RESULTS

Results from the generic building FE model parameter study are given here, with discussion provided in Chapter 5. Each set of results includes: figures for W_b and A-weighted vibration levels with storey at column and mid-span locations; tables and figures for maximum (in each frequency band, and over the whole building) vertical vibration level relative to basement (at mid-span and column positions); and a figure for the average mid-span vibration level relative to column locations at first floor.

F.1: Building height

For discussion of these results, please refer to Section 5.3.1.

Figure F-1. Parametric study: Building height in number of storeys, W_b-weighted basement-relative column acceleration levels with storey

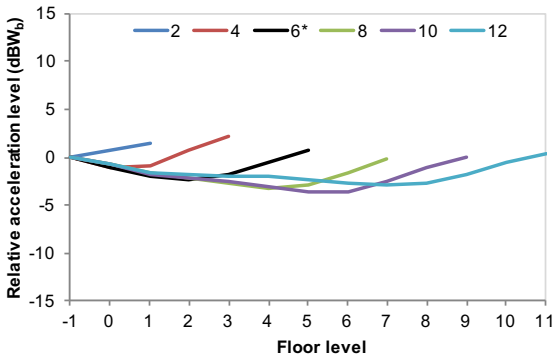

Figure F-2. Parametric study: Building height in number of storeys, A-weighted basement-relative column velocity levels with storey

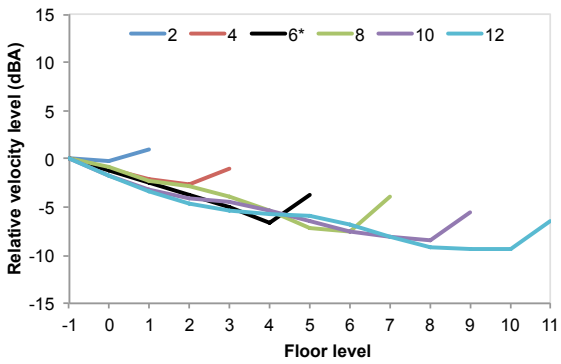

Figure F-3. Parametric study: Building height in number of storeys, W_b-weighted basement-relative mid-span acceleration levels with storey

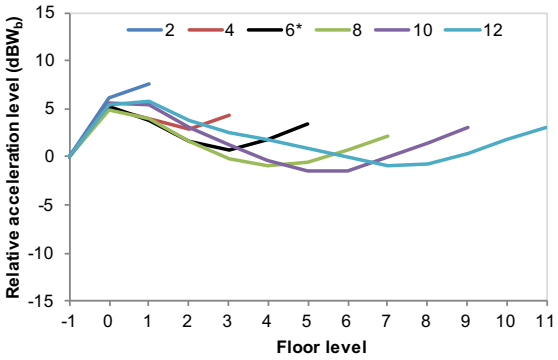

Figure F-4. Parametric study: Building height in number of storeys, A-weighted basement-relative mid-span velocity levels with storey

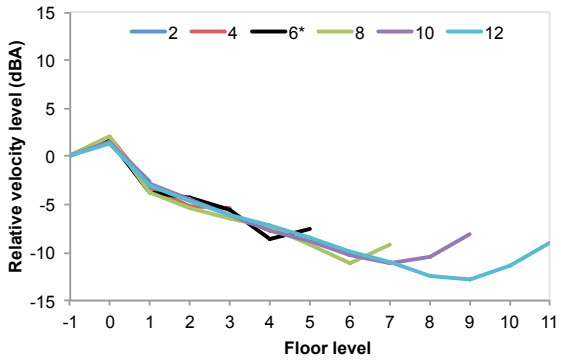

Figure F-5. Parametric study: Building height in number of storeys, maximum vertical vibration level relative to basement, column positions

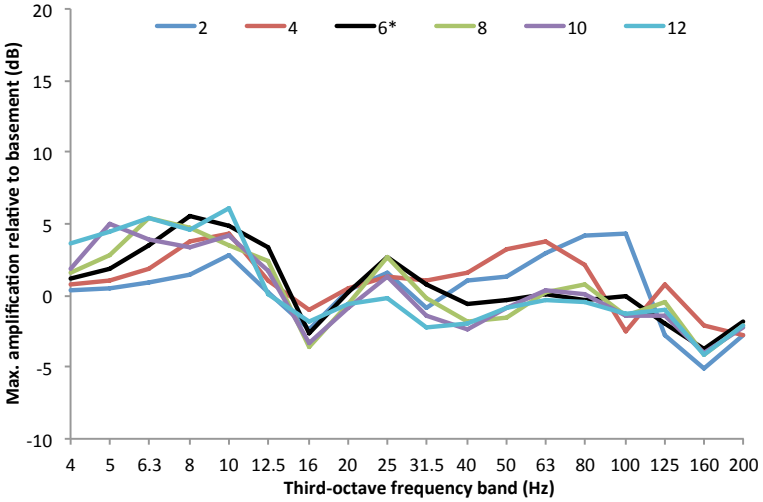

Table F-1. Generic building parametric study: Building height, maximum vertical vibration relative to basement, column positions

No. storeys	Maximum amplification relative to basement level; *Floor level at which maximum occurs*																		
	1/3 octave band frequency (Hz)																	Overall	
	4	5	6.3	8	10	12.5	16	20	25	31.5	40	50	63	80	100	125	160	200	L_{Wb}	L_A
2	0.3 *1*	0.5 *1*	1.0 *1*	1.5 *1*	2.8 *1*	0.2 *1*	-2.3 *1*	0.4 *0*	1.6 *1*	-0.9 *1*	1.1 *1*	1.3 *1*	2.9 *1*	4.2 *1*	**4.4** ***1***	-2.7 *1*	-5.1 *0*	-2.8 *0*	1.5 *1*	1.0 *1*
4	0.8 *3*	1.1 *3*	1.9 *3*	**3.7** ***3***	4.3 *3*	1.0 *3*	-1.0 *3*	0.5 *3*	1.3 *3*	1.0 *3*	1.6 *3*	3.3 *3*	**3.7** ***3***	2.2 *3*	-2.5 *0*	0.7 *0*	-2.1 *1*	-2.8 *0*	2.2 *3*	-1.0 *0*
6*	1.2 *5*	1.9 *5*	3.5 *5*	**5.6** ***5***	4.8 *5*	3.4 *5*	-2.7 *5*	0.2 *0*	2.7 *5*	0.8 *5*	-0.6 *5*	-0.3 *5*	0.1 *0*	-0.3 *0*	-0.1 *0*	-2.0 *1*	-3.8 *0*	-1.8 *0*	0.7 *5*	-1.1 *0*
8	1.2 *7*	1.5 *7*	2.8 *7*	**5.4** ***7***	4.7 *7*	3.5 *7*	2.4 *7*	-3.6 *0*	-0.6 *0*	2.6 *7*	-0.2 *7*	-1.9 *7*	-1.6 *0*	0.3 *0*	0.8 *2*	-1.4 *0*	-0.4 *0*	-4.2 *0*	-0.2 *7*	-0.9 *0*
10	1.9 *9*	**5.0** ***9***	4.0 *9*	3.4 *9*	4.1 *9*	1.7 *9*	-3.3 *0*	-0.9 *0*	1.3 *9*	-1.4 *9*	-2.4 *0*	-0.9 *0*	0.3 *9*	0.0 *3*	-1.5 *0*	-1.4 *0*	-4.0 *0*	-2.2 *0*	0.0 *9*	-1.7 *0*
12	3.6 *11*	4.4 *11*	5.4 *11*	4.6 *11*	**6.0** ***11***	0.1 *11*	-1.8 *0*	-0.7 *0*	-0.2 *11*	-2.2 *0*	-2.0 *0*	-0.9 *0*	-0.3 *11*	-0.5 *1*	-1.3 *0*	-1.0 *0*	-4.1 *0*	-2.0 *0*	0.4 *11*	-1.7 *0*

Figure F-6. Parametric study: Building height in number of storeys, maximum vertical vibration level relative to basement, mid-span positions

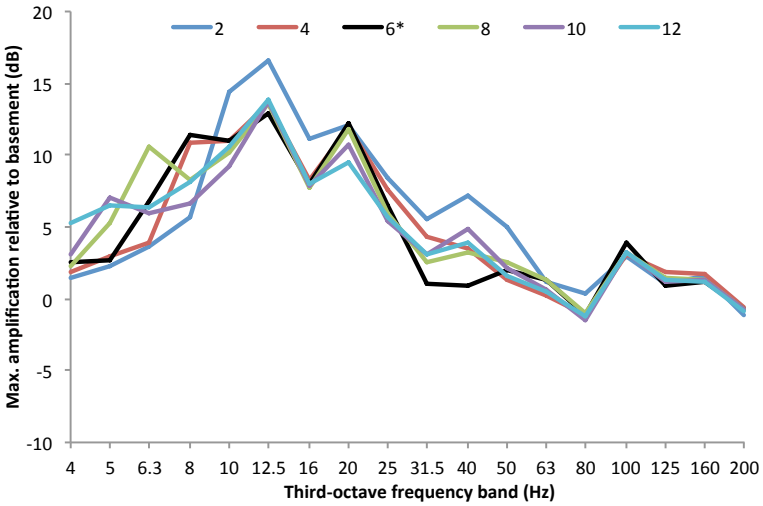

Table F-2. Generic building parametric study: Building height, maximum vertical vibration relative to basement, mid-span positions																				
No. storeys	Maximum amplification relative to basement level; *Floor level at which maximum occurs*																		Overall	
	1/3 octave band frequency (Hz)																			
	4	5	6.3	8	10	12.5	16	20	25	31.5	40	50	63	80	100	125	160	200	L_{Wb}	L_A
2	1.4 *1*	2.3 *1*	3.7 *1*	5.6 *1*	14.4 *1*	**16.6** *1*	11.1 *1*	12.1 *0*	8.4 *0*	5.6 *0*	7.2 *1*	5.0 *1*	1.1 *0*	0.4 *0*	3.0 *0*	1.0 *0*	1.6 *0*	-1.1 *0*	7.5 *1*	1.5 *0*
4	1.8 *3*	3.0 *3*	3.9 *3*	10.9 *3*	11.0 *3*	**13.6** *1*	8.3 *0*	11.9 *0*	7.6 *0*	4.3 *0*	3.5 *3*	1.3 *3*	0.2 *0*	-1.1 *0*	3.1 *0*	1.9 *0*	1.7 *0*	-0.6 *0*	5.1 *0*	2.0 *0*
6*	2.5 *5*	2.7 *5*	6.7 *5*	11.5 *5*	11.0 *5*	**12.9** *1*	8.0 *1*	12.2 *0*	6.5 *0*	1.1 *1*	0.9 *5*	2.0 *0*	1.3 *0*	-1.1 *0*	3.8 *0*	0.9 *0*	1.2 *0*	-0.7 *0*	5.2 *0*	1.8 *0*
8	2.3 *7*	5.2 *7*	10.5 *7*	8.3 *7*	10.2 *7*	**13.6** *1*	7.8 *0*	11.8 *0*	5.9 *0*	2.6 *1*	3.2 *0*	2.5 *0*	1.3 *0*	-1.0 *0*	3.2 *0*	1.4 *0*	1.3 *0*	-0.7 *0*	4.9 *0*	2.0 *0*
10	3.1 *9*	7.1 *9*	5.9 *9*	6.7 *9*	9.3 *9*	**13.7** *1*	7.8 *0*	10.8 *0*	5.3 *0*	3.1 *1*	4.8 *0*	2.1 *0*	0.7 *0*	-1.5 *0*	3.3 *0*	1.1 *0*	1.4 *0*	-0.8 *0*	5.6 *0*	1.5 *0*
12	5.3 *11*	6.5 *11*	6.3 *11*	8.2 *11*	10.6 *11*	**13.8** *1*	8.0 *0*	9.6 *0*	5.6 *0*	3.1 *0*	3.9 *0*	1.6 *0*	0.5 *0*	-1.2 *0*	3.3 *0*	1.3 *0*	1.2 *0*	-0.8 *0*	5.8 *1*	1.3 *0*

Figure F-7. Parametric study: Building height in number of storeys, average vertical vibration level at mid-span relative to column positions, first floor

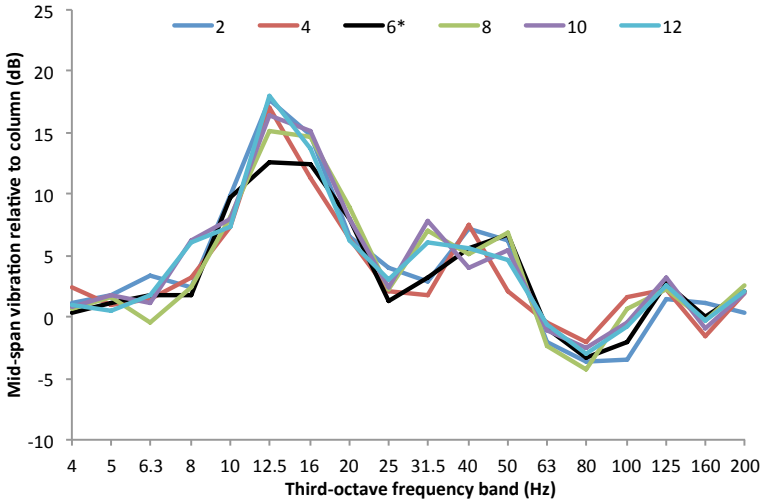

F.2: Storey height

For discussion of these results, please refer to Section 5.3.2.

Figure F-8. Parametric study: Storey height, W_b-weighted basement-relative column acceleration levels with storey

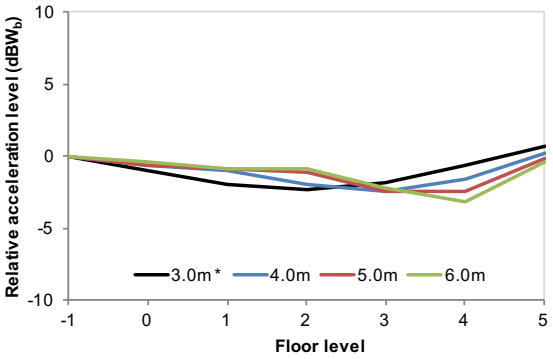

Figure F-9. Parametric study: Storey height, A-weighted basement-relative column velocity levels with storey

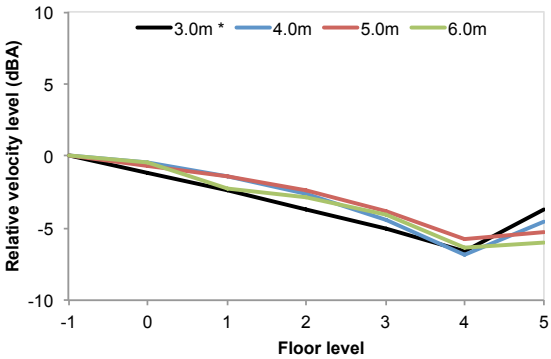

Figure F-10. Parametric study: Storey height, W_b-weighted basement-relative mid-span acceleration levels with storey

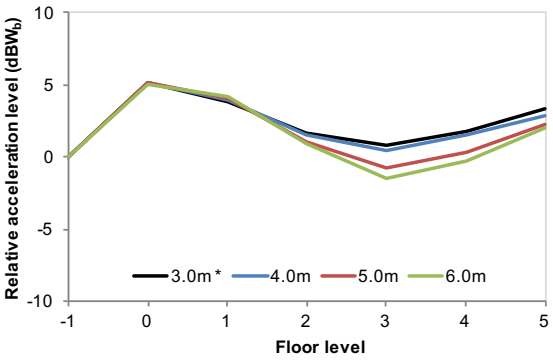

Figure F-11. Parametric study: Storey height, A-weighted basement-relative mid-span velocity levels with storey

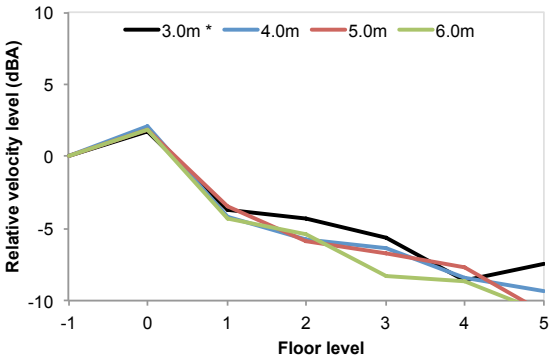

Figure F-12. Parametric study: Storey height, maximum vertical vibration level relative to basement, column positions

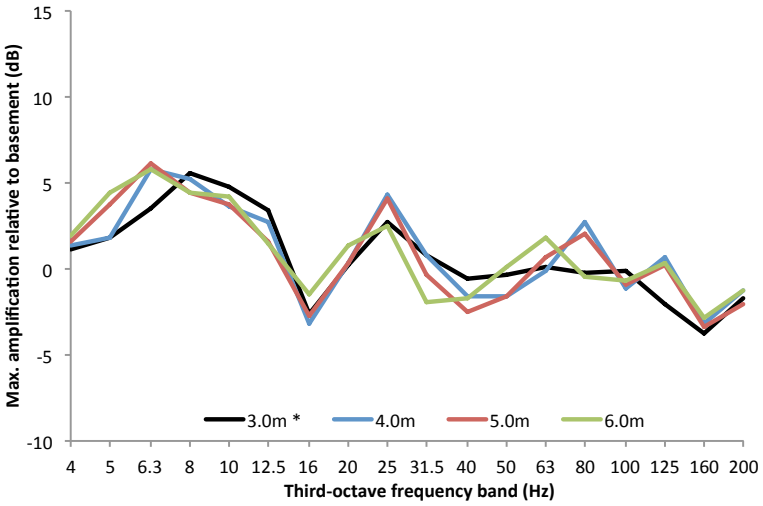

Table F-3. Generic building parametric study: Storey height, maximum vertical vibration relative to basement, column positions																				
Storey height (m)	Maximum amplification relative to basement level; *Floor level at which maximum occurs*																		Overall	
	1/3 octave band frequency (Hz)																			
	4	5	6.3	8	10	12.5	16	20	25	31.5	40	50	63	80	100	125	160	200	L_{Wb}	L_A
3.0 *	1.2 *5*	1.9 *5*	3.5 *5*	**5.6** ***5***	4.8 *5*	3.4 *5*	-2.7 *5*	0.2 *0*	2.7 *5*	0.8 *5*	-0.6 *5*	-0.3 *5*	0.1 *0*	-0.3 *0*	-0.1 *0*	-2.0 *1*	-3.8 *0*	-1.8 *0*	0.7 *5*	-1.1 *0*
4.0	1.0 *5*	1.3 *5*	1.8 *5*	**5.8** ***5***	5.2 *5*	3.6 *5*	2.8 *5*	-3.2 *1*	0.3 *0*	4.3 *5*	0.8 *5*	-1.6 *5*	-1.6 *0*	-0.1 *0*	2.7 *1*	-1.1 *2*	0.7 *0*	-3.2 *0*	0.2 *5*	-0.5 *0*
5.0	1.4 *5*	1.6 *5*	3.7 *5*	**6.1** ***5***	4.4 *5*	3.7 *5*	1.6 *5*	-2.8 *5*	0.3 *5*	4.1 *5*	-0.3 *5*	-2.6 *0*	-1.6 *0*	0.6 *1*	2.0 *2*	-1.0 *0*	0.3 *0*	-3.4 *0*	-0.2 *5*	-0.6 *0*
6.0	1.7 *5*	2.0 *5*	4.4 *5*	**5.8** ***5***	4.4 *5*	4.1 *5*	1.4 *5*	-1.5 *5*	1.4 *5*	2.5 *5*	-2.0 *5*	-1.7 *0*	0.1 *1*	1.8 *2*	-0.5 *2*	-0.7 *0*	0.4 *0*	-2.9 *0*	-0.3 *5*	-0.4 *0*

Figure F-13. Parametric study: Storey height, maximum vertical vibration level relative to basement, mid-span positions

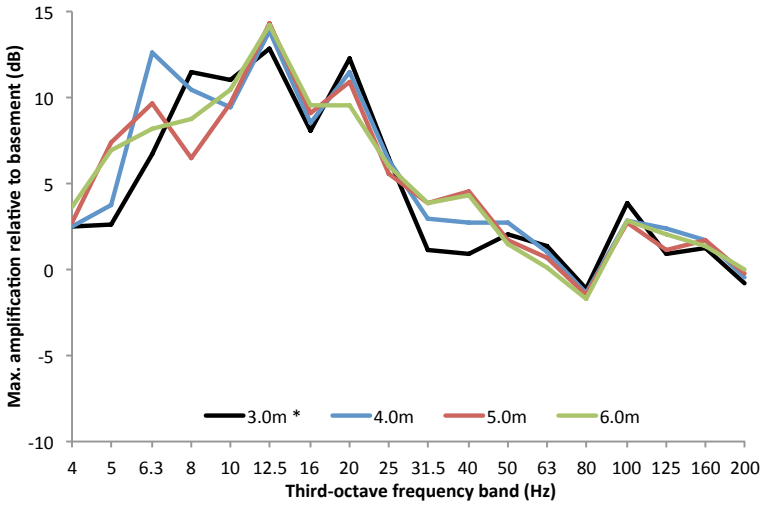

Table F-4. Generic building parametric study: Storey height, maximum vertical vibration relative to basement, mid-span positions																				
Storey height (m)	Maximum amplification relative to basement level; *Floor level at which maximum occurs*																		Overall	
	1/3 octave band frequency (Hz)																			
	4	5	6.3	8	10	12.5	16	20	25	31.5	40	50	63	80	100	125	160	200	L_{Wb}	L_A
3.0 *	2.5 *5*	2.7 *5*	6.7 *5*	11.5 *5*	11.0 *5*	**12.9** ***1***	8.0 *1*	12.2 *0*	6.5 *0*	1.1 *1*	0.9 *5*	2.0 *0*	1.3 *0*	-1.1 *0*	3.8 *0*	0.9 *0*	1.2 *0*	-0.7 *0*	5.2 *0*	1.8 *0*
4.0	2.5 *5*	3.8 *5*	12.6 *5*	10.4 *5*	9.4 *5*	**13.8** ***1***	8.5 *0*	11.5 *0*	6.3 *0*	2.9 *1*	2.7 *0*	2.7 *0*	1.0 *0*	-1.4 *0*	2.9 *0*	2.3 *0*	1.7 *0*	-0.4 *0*	5.2 *0*	2.1 *0*
5.0	2.7 *5*	7.3 *5*	9.7 *5*	6.5 *5*	9.6 *5*	**14.3** ***1***	9.1 *0*	10.9 *0*	5.5 *0*	3.8 *1*	4.6 *0*	1.7 *0*	0.7 *0*	-1.5 *0*	2.8 *0*	1.1 *0*	1.7 *0*	-0.2 *0*	5.2 *0*	1.9 *0*
6.0	3.7 *5*	6.9 *5*	8.1 *5*	8.7 *5*	10.5 *5*	**14.2** ***1***	9.5 *0*	9.5 *0*	6.0 *0*	3.9 *0*	4.3 *0*	1.4 *1*	0.1 *0*	-1.7 *0*	2.8 *0*	2.1 *0*	1.4 *0*	0.0 *0*	5.0 *0*	1.8 *0*

Figure F-14. Parametric study: Storey height, average vertical vibration level at mid-span relative to column positions, first floor

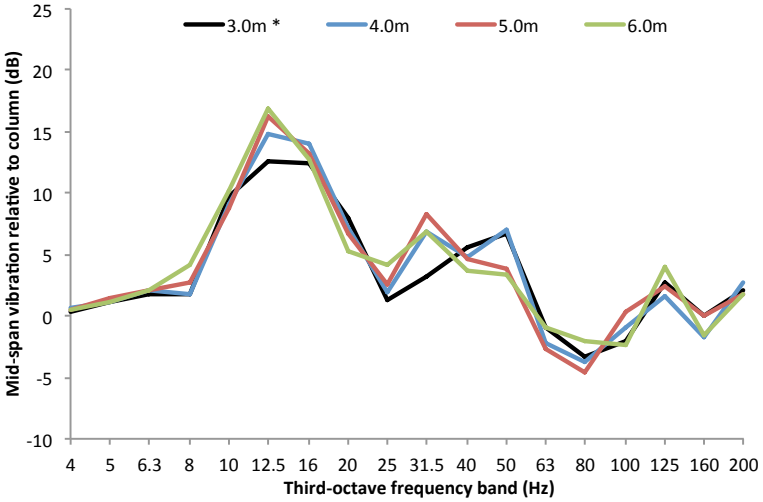

F.3: Ground floor storey height

For discussion of these results, please refer to Section 5.3.3.

Figure F-15. Parametric study: Ground floor storey height, W_b-weighted basement-relative column acceleration levels with storey

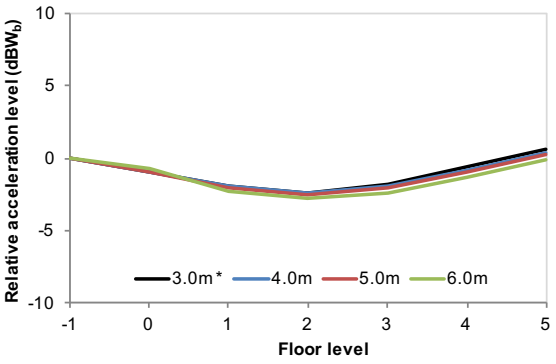

Figure F-16. Parametric study: Ground floor storey height, A-weighted basement-relative column velocity levels with storey

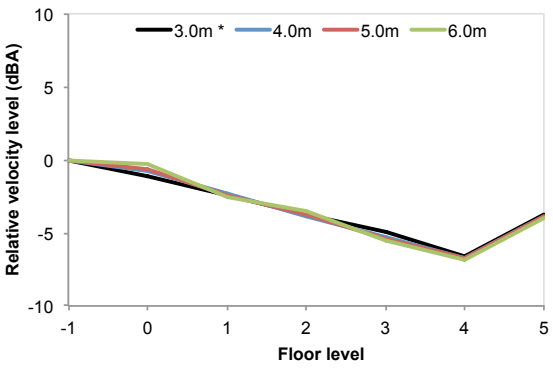

Figure F-17. Parametric study: Ground floor storey height, W_b-weighted basement-relative mid-span acceleration levels with storey

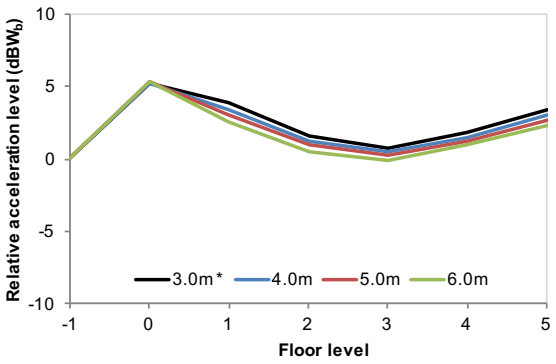

Figure F-18. Parametric study: Ground floor storey height, A-weighted basement-relative mid-span velocity levels with storey

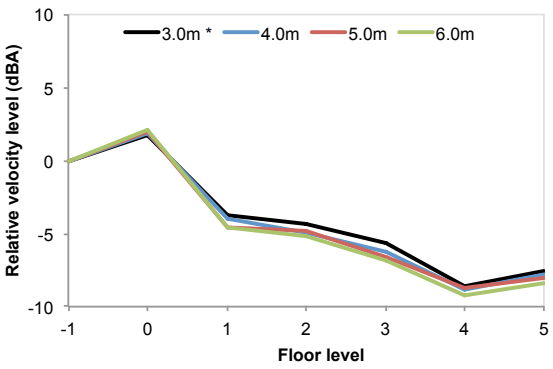

Figure F-19. Parametric study: Ground floor storey height, maximum vertical vibration level relative to basement, column positions

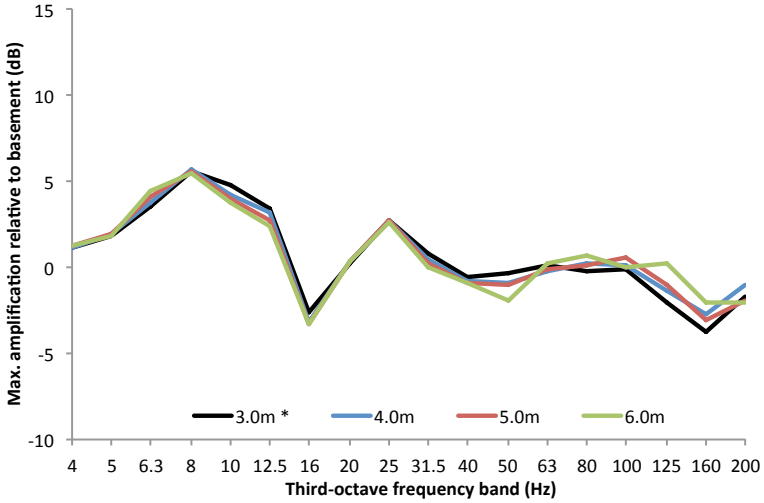

Table F-5. Generic building parametric study: Ground floor storey height, maximum vertical vibration relative to basement, column positions

GF storey height (m)	Maximum amplification relative to basement level; *Floor level at which maximum occurs*																			
	1/3 octave band frequency (Hz)																		Overall	
	4	5	6.3	8	10	12.5	16	20	25	31.5	40	50	63	80	100	125	160	200	L_{Wb}	L_A
3.0 *	1.2 *5*	1.9 *5*	3.5 *5*	**5.6** ***5***	4.8 *5*	3.4 *5*	-2.7 *5*	0.2 *0*	2.7 *5*	0.8 *5*	-0.6 *5*	-0.3 *5*	0.1 *0*	-0.3 *0*	-0.1 *0*	-2.0 *1*	-3.8 *0*	-1.8 *0*	0.7 *5*	-1.1 *0*
4.0	1.2 *5*	1.9 *5*	3.8 *5*	**5.6** ***5***	4.3 *5*	3.1 *5*	-3.2 *1*	0.4 *0*	2.8 *5*	0.5 *5*	-0.7 *5*	-0.9 *5*	-0.2 *0*	0.2 *0*	0.1 *1*	-1.3 *0*	-2.8 *0*	-1.0 *0*	0.4 *5*	-0.8 *0*
5.0	1.2 *5*	1.9 *5*	4.1 *5*	**5.6** ***5***	4.0 *5*	2.7 *5*	-3.3 *0*	0.4 *0*	2.8 *5*	0.3 *5*	-0.9 *5*	-1.0 *5*	-0.1 *0*	0.2 *0*	0.5 *1*	-1.0 *0*	-3.0 *0*	-1.9 *0*	0.3 *5*	-0.7 *0*
6.0	1.3 *5*	1.9 *5*	4.4 *5*	**5.5** ***5***	3.7 *5*	2.4 *5*	-3.3 *0*	0.3 *0*	2.6 *5*	0.0 *5*	-0.9 *5*	-2.0 *0*	0.3 *0*	0.7 *0*	-0.1 *1*	0.2 *0*	-2.0 *0*	-2.1 *0*	0.0 *5*	-0.3 *0*

Figure F-20. Parametric study: Storey height, maximum vertical vibration level relative to basement, mid-span positions

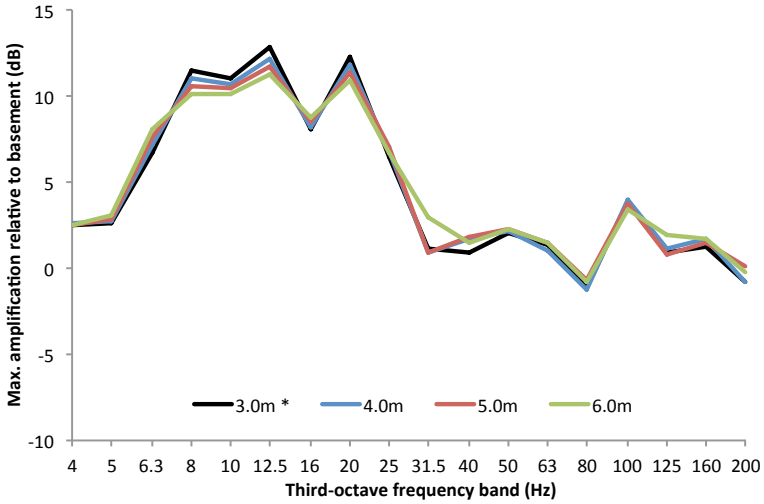

Table F-6. Generic building parametric study: Ground floor storey height, maximum vertical vibration relative to basement, mid-span positions																				
GF storey height (m)	Maximum amplification relative to basement level; *Floor level at which maximum occurs*																		Overall	
	1/3 octave band frequency (Hz)																			
	4	5	6.3	8	10	12.5	16	20	25	31.5	40	50	63	80	100	125	160	200	L_{Wb}	L_A
3.0 *	2.5 *5*	2.7 *5*	6.7 *5*	11.5 *5*	11.0 *5*	**12.9** ***1***	8.0 *1*	12.2 *0*	6.5 *0*	1.1 *1*	0.9 *5*	2.0 *0*	1.3 *0*	-1.1 *0*	3.8 *0*	0.9 *0*	1.2 *0*	-0.7 *0*	5.2 *0*	1.8 *0*
4.0	2.6 *5*	2.8 *5*	7.2 *5*	11.0 *5*	10.7 *5*	**12.2** ***1***	8.2 *0*	11.8 *0*	6.8 *0*	0.9 *0*	1.7 *5*	2.1 *0*	1.0 *0*	-1.2 *0*	4.0 *0*	1.1 *0*	1.7 *0*	-0.8 *0*	5.2 *0*	1.8 *0*
5.0	2.5 *5*	2.9 *5*	7.6 *5*	10.6 *5*	10.5 *5*	**11.8** ***1***	8.5 *0*	11.4 *0*	7.1 *0*	0.9 *0*	1.8 *5*	2.3 *0*	1.5 *0*	-0.7 *0*	3.8 *0*	0.8 *0*	1.4 *0*	0.1 *0*	5.3 *0*	2.0 *0*
6.0	2.5 *5*	3.1 *5*	8.1 *5*	10.2 *5*	10.1 *5*	**11.3** ***1***	8.8 *0*	10.9 *0*	6.7 *0*	3.0 *0*	1.5 *5*	2.3 *0*	1.4 *0*	-0.8 *0*	3.4 *0*	2.0 *0*	1.7 *0*	-0.3 *0*	5.3 *0*	2.1 *0*

Figure F-21. Parametric study: Ground floor storey height, average vertical vibration level at mid-span relative to column positions, first floor

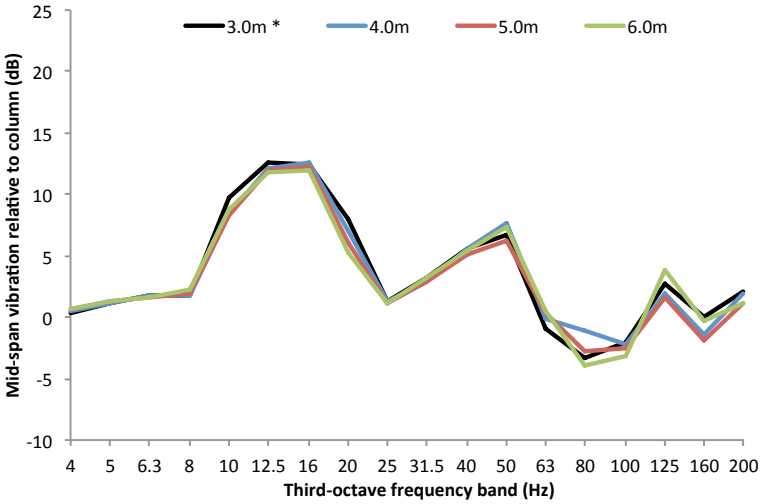

F.4: Floor slab size

For discussion of these results, please refer to Section 5.4.1.

Figure F-22. Parametric study: Floor slab size, W_b-weighted basement-relative column acceleration levels with storey

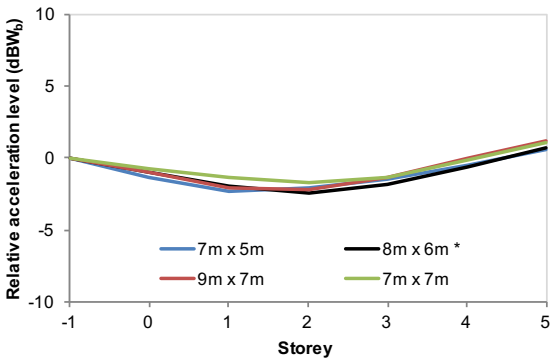

Figure F-23. Parametric study: Floor slab size, A-weighted basement-relative column velocity levels with storey

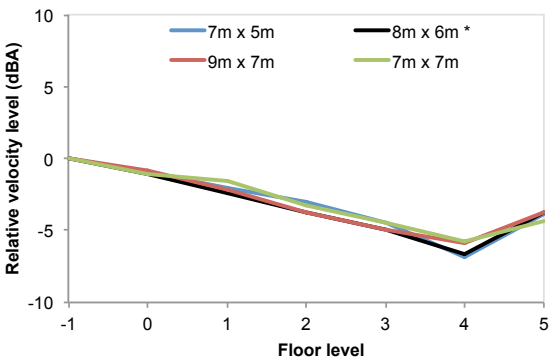

Figure F-24. Parametric study: Floor slab size, W_b-weighted basement-relative mid-span acceleration levels with storey

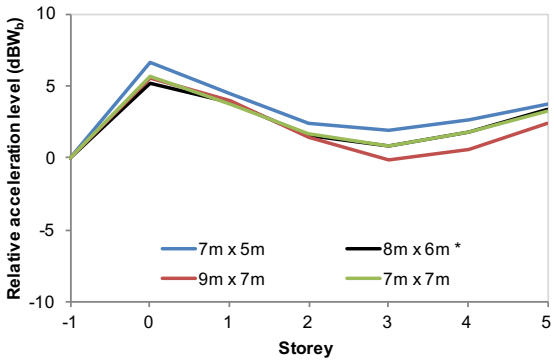

Figure F-25. Parametric study: Floor slab size, A-weighted basement-relative mid-span velocity levels with storey

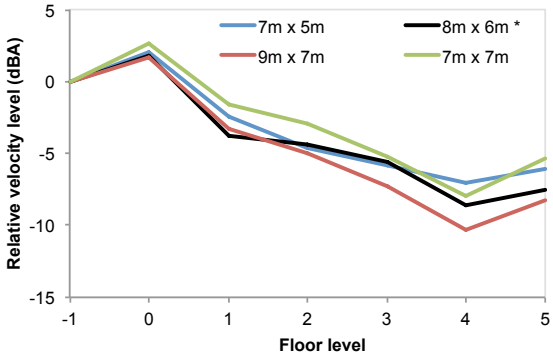

Figure F-26. Parametric study: Floor slab size, maximum vertical vibration level relative to basement, column positions

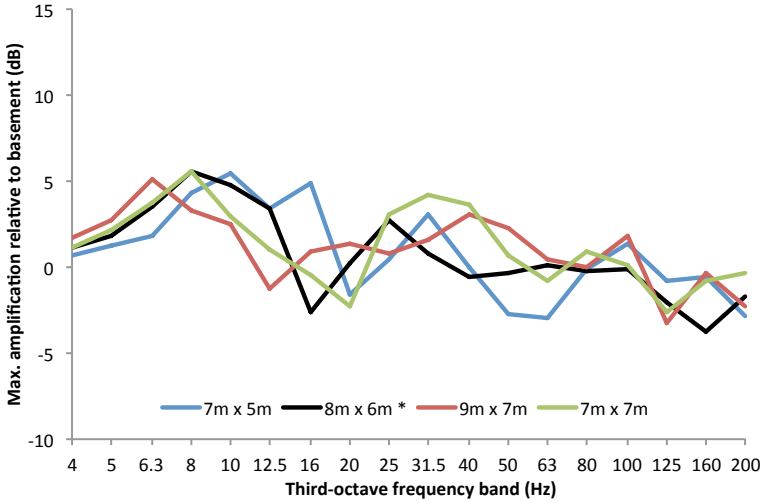

Table F-7. Generic building parametric study: Floor slab size, maximum vertical vibration relative to basement, column positions

Slab size (m x m)	Maximum amplification relative to basement level; *Floor level at which maximum occurs*																		
	1/3 octave band frequency (Hz)																	Overall	
	4	5	6.3	8	10	12.5	16	20	25	31.5	40	50	63	80	100	125	160	200	L_{Wb}	L_A
7x5	0.7 *5*	1.3 *5*	1.8 *5*	4.3 *5*	**5.5** ***5***	3.4 *5*	4.9 *5*	-1.6 *5*	0.4 *5*	3.0 *5*	0.0 *5*	-2.8 *5*	-3.0 *0*	-0.2 *0*	1.4 *1*	-0.8 *2*	-0.5 *0*	-2.9 *0*	0.6 *5*	-1.0 *0*
8x6*	1.2 *5*	1.9 *5*	3.5 *5*	**5.6** ***5***	4.8 *5*	3.4 *5*	-2.7 *5*	0.2 *0*	2.7 *5*	0.8 *5*	-0.6 *5*	-0.3 *5*	0.1 *0*	-0.3 *0*	-0.1 *0*	-2.0 *1*	-3.8 *0*	-1.8 *0*	0.7 *5*	-1.1 *0*
9x7	1.8 *5*	2.7 *5*	**5.2** ***5***	3.2 *5*	2.5 *5*	-1.3 *5*	0.9 *5*	1.3 *5*	0.8 *5*	1.6 *5*	3.0 *5*	2.3 *5*	0.4 *5*	0.0 *0*	1.8 *0*	-3.2 *2*	-0.3 *0*	-2.3 *0*	1.2 *5*	-0.8 *0*
7x7	1.2 *5*	2.2 *5*	3.7 *5*	**5.6** ***5***	3.0 *5*	1.0 *5*	-0.4 *5*	-2.2 *5*	3.0 *5*	4.2 *5*	3.7 *5*	0.7 *5*	-0.8 *0*	0.9 *1*	0.1 *0*	-2.6 *1*	-0.8 *0*	-0.3 *1*	1.1 *5*	-1.0 *0*

Figure F-27. Parametric study: Floor slab size, maximum vertical vibration level relative to basement, mid-span positions

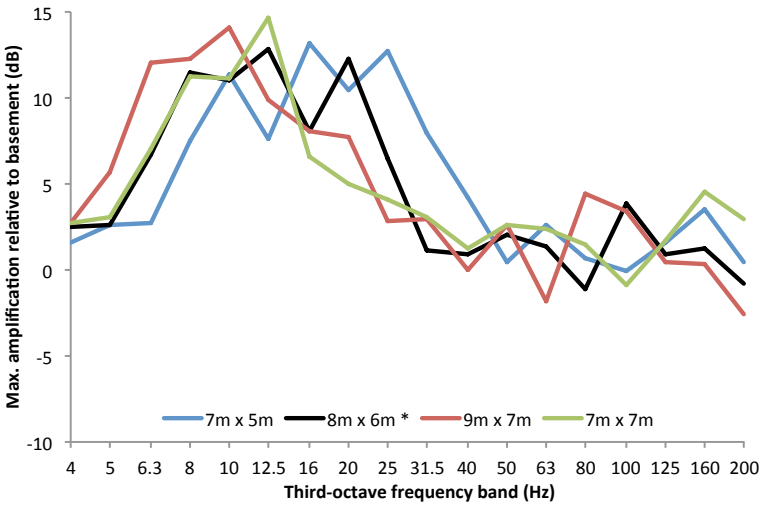

Table F-8. Generic building parametric study: Floor slab size, maximum vertical vibration relative to basement, mid-span positions

Slab size (m x m)	Maximum amplification relative to basement level; *Floor level at which maximum occurs*																		
	1/3 octave band frequency (Hz)																	Overall	
	4	5	6.3	8	10	12.5	16	20	25	31.5	40	50	63	80	100	125	160	200	L_{Wb}	L_A
7x5	1.6	2.7	2.7	7.5	11.4	7.6	**13.2**	10.5	12.7	7.9	4.3	0.5	2.6	0.7	-0.1	1.6	3.5	0.5	6.6	2.0
	5	*5*	*5*	*5*	*5*	*5*	*1*	*1*	*0*	*0*	*0*	*0*	*0*	*0*	*0*	*0*	*0*	*0*	*0*	*0*
8x6*	2.5	2.7	6.7	11.5	11.0	**12.9**	8.0	12.2	6.5	1.1	0.9	2.0	1.3	-1.1	3.8	0.9	1.2	-0.7	5.2	1.8
	5	*5*	*5*	*5*	*5*	*1*	*1*	*0*	*0*	*1*	*5*	*0*	*0*	*0*	*0*	*0*	*0*	*0*	*0*	*0*
9x7	2.7	5.7	12.1	12.3	**14.1**	9.9	8.1	7.8	2.8	3.0	0.0	2.6	-1.8	4.5	3.4	0.4	0.4	-2.6	5.6	1.7
	5	*5*	*5*	*5*	*1*	*0*	*0*	*0*	*0*	*5*	*0*	*0*	*0*	*0*	*0*	*0*	*0*	*0*	*0*	*0*
7x7	2.7	3.0	7.0	11.2	11.2	**14.7**	6.6	5.0	4.1	3.0	1.2	2.6	2.3	1.5	-0.9	1.7	4.6	2.9	5.6	2.7
	5	*5*	*5*	*5*	*5*	*1*	*1*	*0*	*0*	*5*	*5*	*0*	*0*	*0*	*0*	*1*	*0*	*0*	*0*	*0*

Figure F-28. Parametric study: Floor slab size, average vertical vibration level at mid-span relative to column positions, first floor

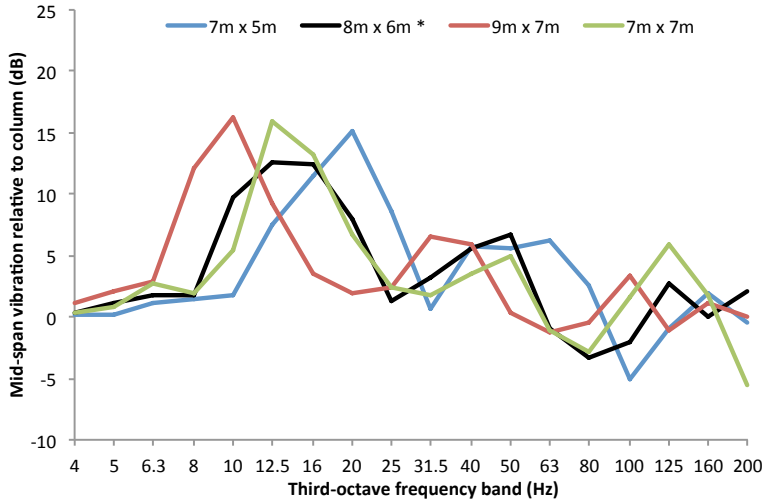

F.5: Floor slab thickness

For discussion of these results, please refer to Section 5.4.2.

Figure F-29. Parametric study: Floor slab thickness, W_b-weighted basement-relative column acceleration levels with storey

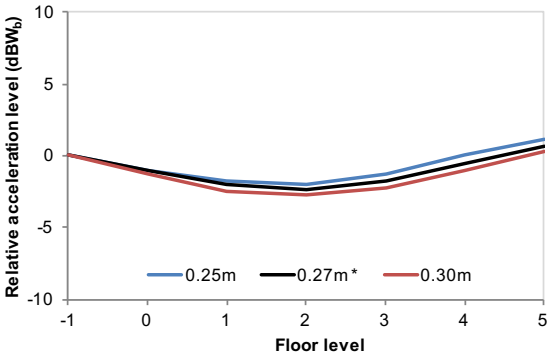

Figure F-30. Parametric study: Floor slab thickness, A-weighted basement-relative column velocity levels with storey

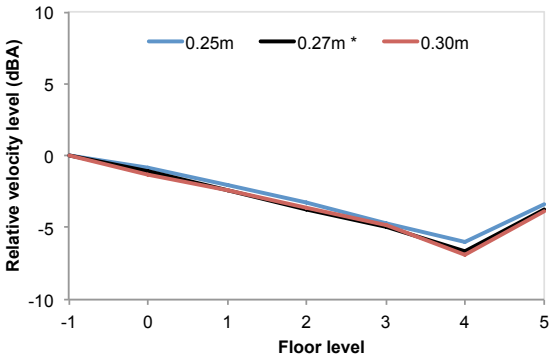

Figure F-31. Parametric study: Floor slab thickness, W_b-weighted basement-relative mid-span acceleration levels with storey

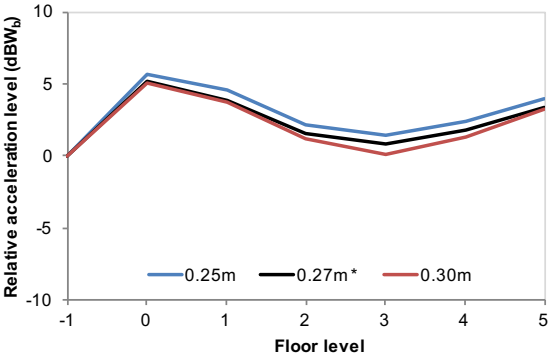

Figure F-32. Parametric study: Floor slab thickness, A-weighted basement-relative mid-span velocity levels with storey

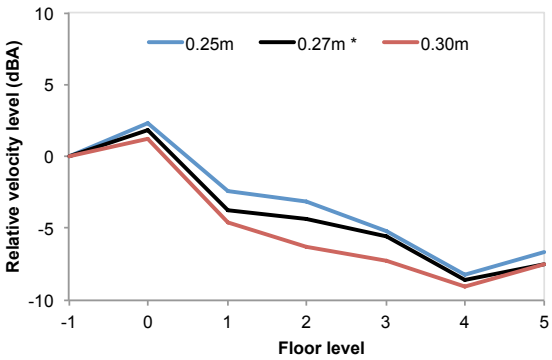

Figure F-33. Parametric study: Floor slab thickness, maximum vertical vibration level relative to basement, column positions

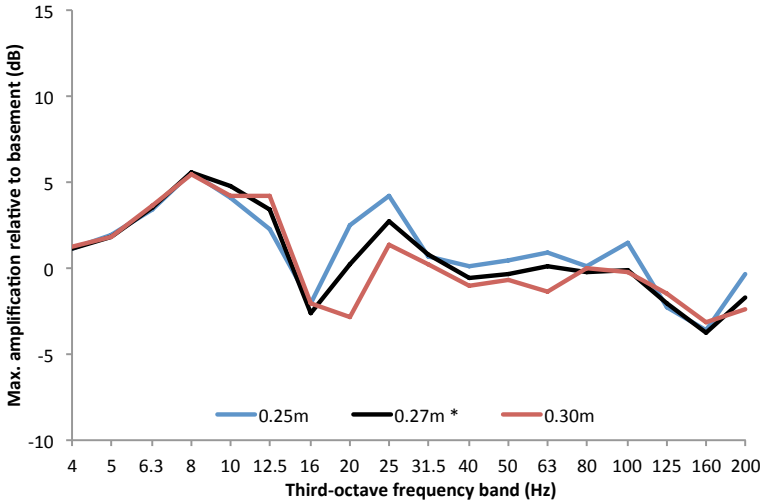

Table F-9. Generic building parametric study: Floor slab thickness, maximum vertical vibration relative to basement, column positions																				
Slab thickness (m)	Maximum amplification relative to basement level; *Floor level at which maximum occurs*																		Overall	
	1/3 octave band frequency (Hz)																			
	4	5	6.3	8	10	12.5	16	20	25	31.5	40	50	63	80	100	125	160	200	L_{Wb}	L_A
0.25	1.1 *5*	1.9 *5*	3.4 *5*	**5.6** ***5***	4.1 *5*	2.2 *5*	-2.0 *0*	2.5 *5*	4.2 *5*	0.7 *5*	0.1 *5*	0.5 *5*	0.9 *5*	0.1 *0*	1.4 *1*	-2.3 *0*	-3.6 *0*	-0.4 *0*	1.2 *5*	-0.8 *0*
0.27*	1.2 *5*	1.9 *5*	3.5 *5*	**5.6** ***5***	4.8 *5*	3.4 *5*	-2.7 *5*	0.2 *0*	2.7 *5*	0.8 *5*	-0.6 *5*	-0.3 *5*	0.1 *0*	-0.3 *0*	-0.1 *0*	-2.0 *1*	-3.8 *0*	-1.8 *0*	0.7 *5*	-1.1 *0*
0.30	1.3 *5*	1.8 *5*	3.7 *5*	**5.5** ***5***	4.2 *5*	4.2 *5*	-2.1 *5*	-2.8 *0*	1.3 *5*	0.3 *5*	-1.0 *5*	-0.7 *5*	-1.3 *0*	-0.1 *0*	-0.2 *0*	-1.4 *1*	-3.1 *0*	-2.4 *0*	0.3 *5*	-1.3 *0*

Figure F-34. Parametric study: Floor slab thickness, maximum vertical vibration level relative to basement, mid-span positions

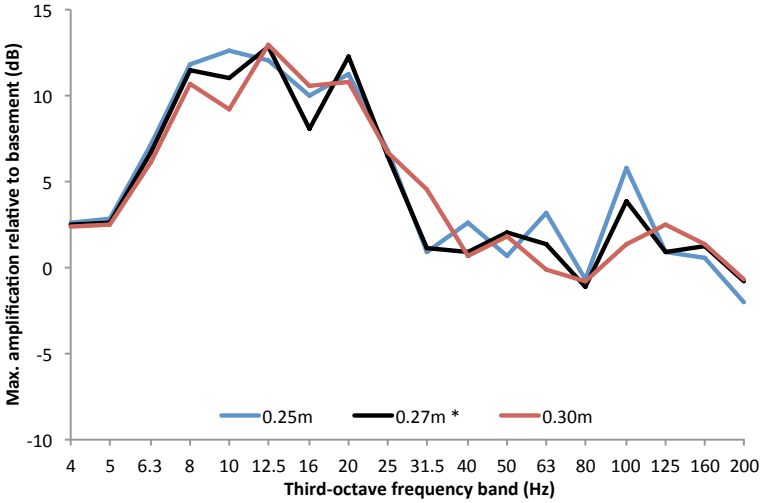

Table F-10. Generic building parametric study: Floor slab thickness, maximum vertical vibration relative to basement, mid-span positions																				
Slab thickness	Maximum amplification relative to basement level; *Floor level at which maximum occurs*																		Overall	
	1/3 octave band frequency (Hz)																			
	4	5	6.3	8	10	12.5	16	20	25	31.5	40	50	63	80	100	125	160	200	L_{Wb}	L_A
0.25	2.6 *5*	2.9 *5*	7.2 *5*	11.9 *5*	**12.6** ***5***	12.0 *1*	10.0 *0*	11.2 *0*	6.9 *0*	0.9 *1*	2.6 *5*	0.7 *0*	3.2 *0*	-0.7 *0*	5.8 *0*	0.9 *0*	0.6 *0*	-2.0 *0*	5.7 *0*	2.3 *0*
0.27*	2.5 *5*	2.7 *5*	6.7 *5*	11.5 *5*	11.0 *5*	**12.9** ***1***	8.0 *1*	12.2 *0*	6.5 *0*	1.1 *1*	0.9 *5*	2.0 *0*	1.3 *0*	-1.1 *0*	3.8 *0*	0.9 *0*	1.2 *0*	-0.7 *0*	5.2 *0*	1.8 *0*
0.30	2.4 *5*	2.5 *5*	6.1 *5*	10.7 *5*	9.2 *5*	**12.9** ***1***	10.6 *1*	10.8 *0*	6.7 *0*	4.6 *0*	0.7 *1*	1.8 *5*	-0.1 *0*	-0.8 *0*	1.4 *0*	2.5 *0*	1.4 *0*	-0.7 *0*	5.0 *0*	1.3 *0*

Figure F-35. Parametric study: Floor slab thickness, average vertical vibration level at mid-span relative to column positions, first floor

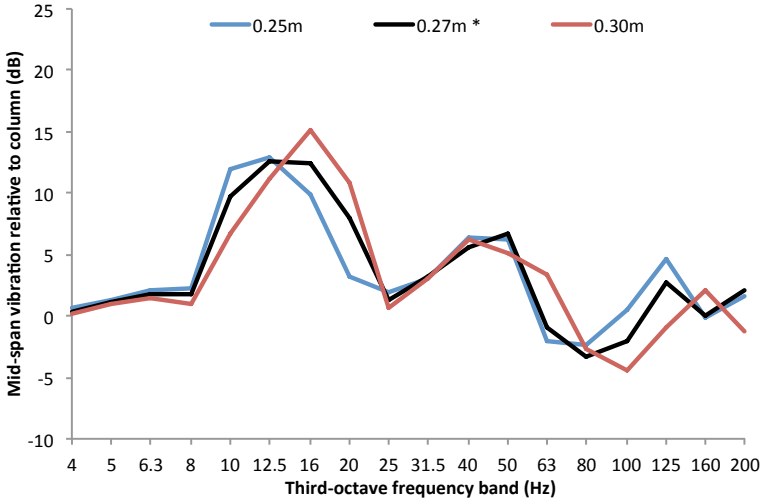

F.6: Building length

For discussion of these results, please refer to Section 5.5.1.

Figure F-36. Parametric study: Building length in slabs, W_b-weighted basement-relative column acceleration levels with storey

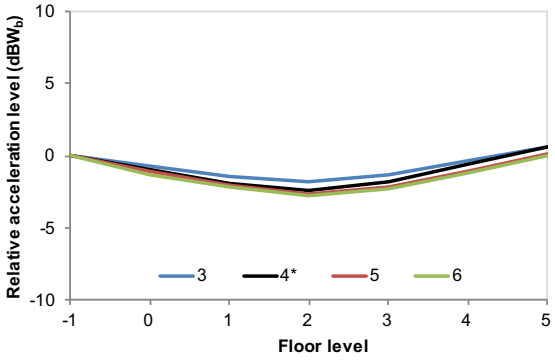

Figure F-37. Parametric study: Building length in slabs, A-weighted basement-relative column velocity levels with storey

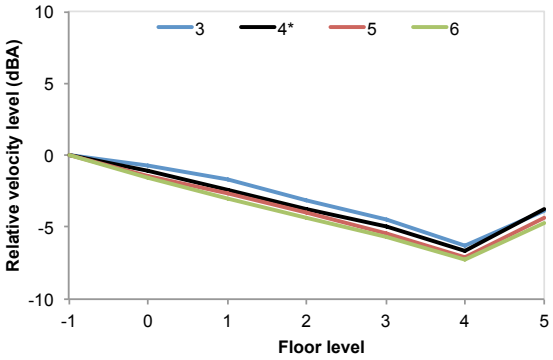

Figure F-38. Parametric study: Building length in slabs, W_b-weighted basement-relative mid-span acceleration levels with storey

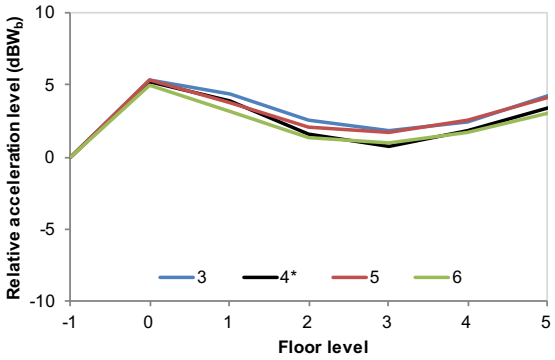

Figure F-39. Parametric study: Building length in slabs, A-weighted basement-relative mid-span velocity levels with storey

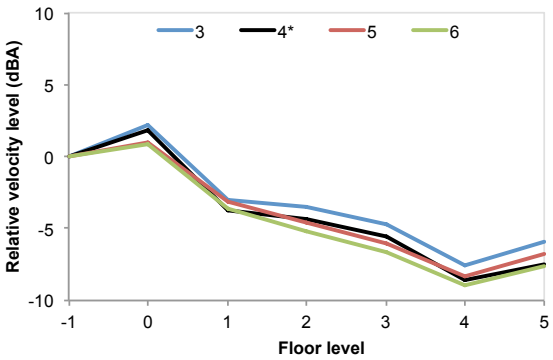

Figure F-40. Parametric study: Building length in slabs, maximum vertical vibration level relative to basement, column positions

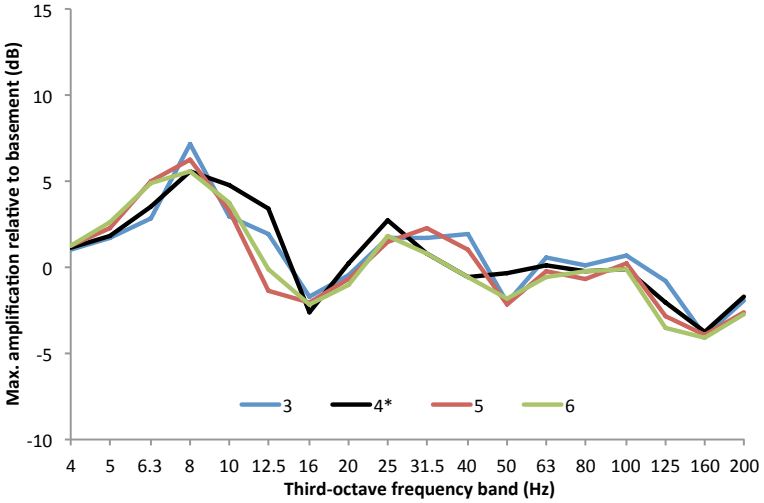

Table F-11. Generic building parametric study: Building length in slabs, maximum vertical vibration relative to basement, column positions

No. slabs	Maximum amplification relative to basement level; *Floor level at which maximum occurs*																			
	1/3 octave band frequency (Hz)																	Overall		
	4	5	6.3	8	10	12.5	16	20	25	31.5	40	50	63	80	100	125	160	200	L_{Wb}	L_A
3	1.1 *5*	1.7 *5*	2.8 *5*	**7.1** ***5***	3.0 *5*	1.9 *5*	-1.7 *1*	-0.5 *5*	1.7 *5*	1.7 *5*	2.0 *5*	-2.1 *0*	0.6 *5*	0.1 *0*	0.7 *0*	-0.8 *0*	-4.0 *0*	-1.9 *0*	0.7 *5*	-0.7 *0*
4*	1.2 *5*	1.9 *5*	3.5 *5*	**5.6** ***5***	4.8 *5*	3.4 *5*	-2.7 *5*	0.2 *0*	2.7 *5*	0.8 *5*	-0.6 *5*	-0.3 *5*	0.1 *0*	-0.3 *0*	-0.1 *0*	-2.0 *1*	-3.8 *0*	-1.8 *0*	0.7 *5*	-1.1 *0*
5	1.3 *5*	2.2 *5*	5.0 *5*	**6.3** ***5***	3.3 *5*	-1.4 *0*	-2.1 *0*	-0.6 *0*	1.5 *5*	2.3 *5*	1.1 *5*	-2.2 *5*	-0.2 *0*	-0.7 *0*	0.2 *0*	-2.9 *0*	-3.9 *0*	-2.6 *0*	0.2 *5*	-1.5 *0*
6	1.2 *5*	2.6 *5*	4.9 *5*	**5.6** ***5***	3.7 *5*	-0.1 *5*	-2.1 *0*	-1.0 *5*	1.8 *5*	0.8 *5*	-0.6 *5*	-1.8 *5*	-0.6 *0*	-0.3 *0*	-0.1 *0*	-3.5 *2*	-4.1 *0*	-2.7 *0*	0.0 *5*	-1.6 *0*

Figure F-41. Parametric study: Building length in slabs, maximum vertical vibration level relative to basement, mid-span positions

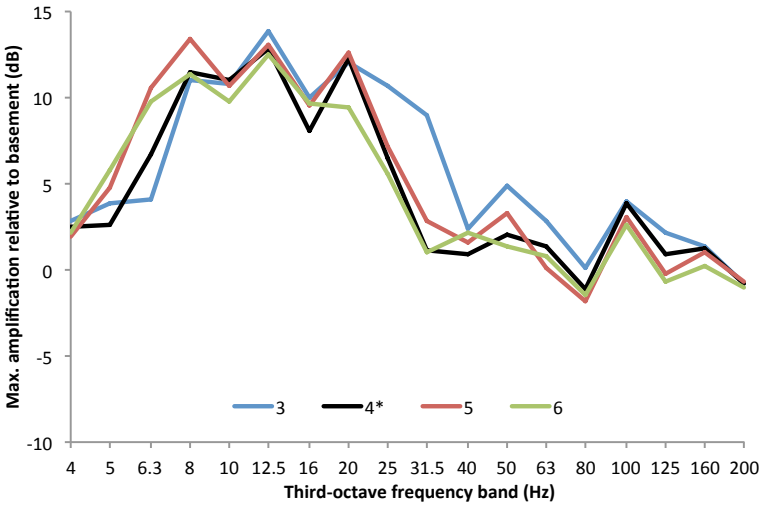

Table F-12. Generic building parametric study: Building length in slabs, maximum vertical vibration relative to basement, mid-span positions																				
No. slabs	Maximum amplification relative to basement level; *Floor level at which maximum occurs*																		Overall	
	1/3 octave band frequency (Hz)																			
	4	5	6.3	8	10	12.5	16	20	25	31.5	40	50	63	80	100	125	160	200	L_{Wb}	L_A
3	2.8	3.9	4.1	11.0	10.8	**13.8**	10.0	12.0	10.6	9.0	2.4	4.9	2.8	0.1	4.0	2.1	1.4	-0.8	5.3	2.2
	5	*5*	*5*	*4*	*5*	***5***	*1*	*0*	*0*	*0*	*0*	*1*	*0*	*0*	*0*	*0*	*0*	*0*	*0*	*0*
4*	2.5	2.7	6.7	11.5	11.0	**12.9**	8.0	12.2	6.5	1.1	0.9	2.0	1.3	-1.1	3.8	0.9	1.2	-0.7	5.2	1.8
	5	*5*	*5*	*5*	*5*	***1***	*1*	*0*	*0*	*1*	*5*	*0*	*0*	*0*	*0*	*0*	*0*	*0*	*0*	*0*
5	2.0	4.7	10.6	**13.4**	10.7	13.1	9.5	12.6	7.1	2.8	1.6	3.3	0.1	-1.9	3.1	-0.2	1.0	-0.7	5.3	1.0
	5	*5*	*5*	***5***	*5*	*1*	*0*	*0*	*0*	*0*	*0*	*1*	*0*	*0*	*0*	*0*	*0*	*0*	*0*	*0*
6	2.2	5.8	9.8	11.3	9.7	**12.5**	9.7	9.5	5.5	1.0	2.2	1.3	0.8	-1.5	2.6	-0.7	0.3	-1.0	4.9	0.8
	5	*5*	*5*	*5*	*5*	***1***	*0*	*0*	*0*	*0*	*0*	*1*	*0*	*0*	*0*	*0*	*0*	*0*	*0*	*0*

Figure F-42. Parametric study: Building length in slabs, average vertical vibration level at mid-span relative to column positions, first floor

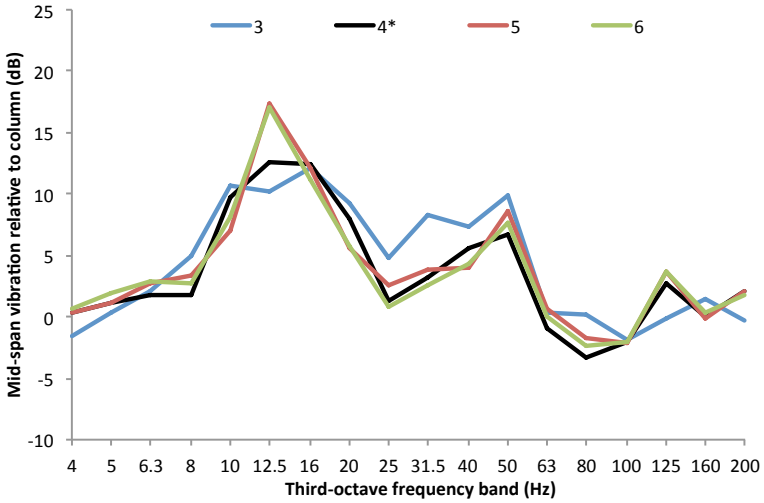

F.7: Building width

For discussion of these results, please refer to Section 5.5.2.

Figure F-43. Parametric study: Building width in slabs, W_b-weighted basement-relative column acceleration levels with storey

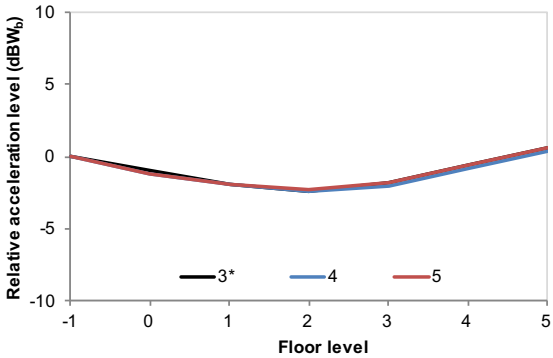

Figure F-44. Parametric study: Building width in slabs, A-weighted basement-relative column velocity levels with storey

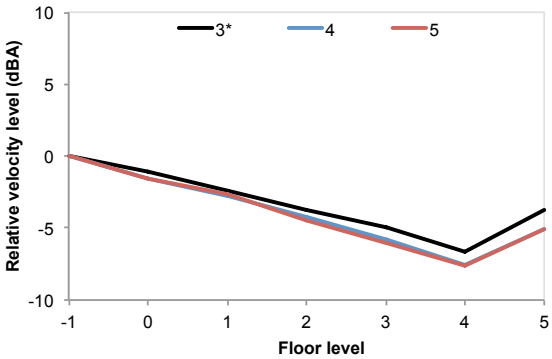

Figure F-45. Parametric study: Building width in slabs, W_b-weighted basement-relative mid-span acceleration levels with storey

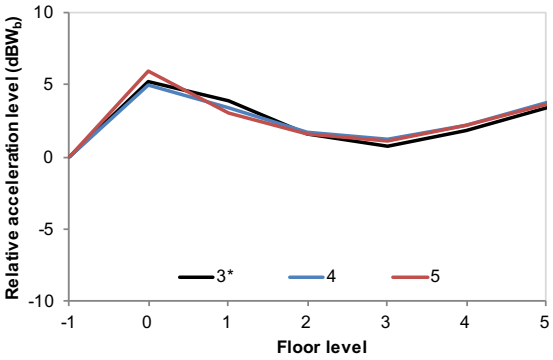

Figure F-46. Parametric study: Building width in slabs, A-weighted basement-relative mid-span velocity levels with storey

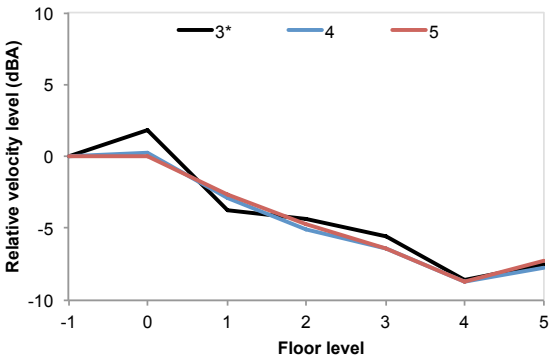

Figure F-47. Parametric study: Building width in slabs, maximum vertical vibration level relative to basement, column positions

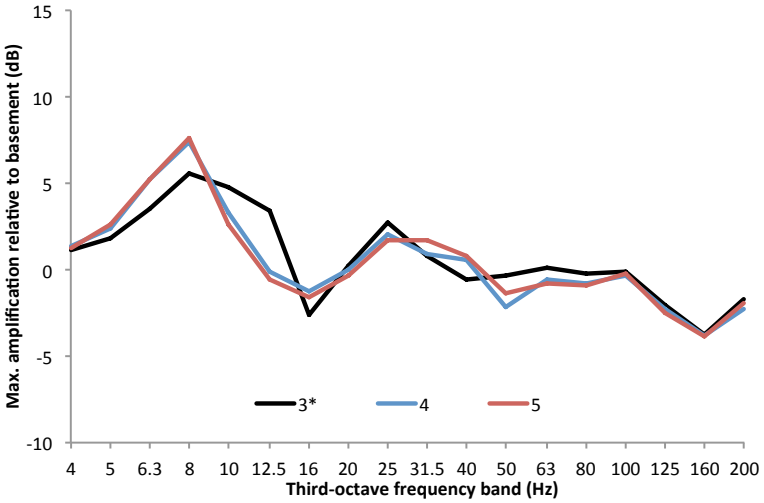

Table F-13. Generic building parametric study: Building width in slabs, maximum vertical vibration relative to basement, column positions

No. slabs	Maximum amplification relative to basement level; *Floor level at which maximum occurs*																		
	1/3 octave band frequency (Hz)																	Overall	
	4	5	6.3	8	10	12.5	16	20	25	31.5	40	50	63	80	100	125	160	200	L_{Wb}	L_A
3*	1.2 *5*	1.9 *5*	3.5 *5*	**5.6** ***5***	4.8 *5*	3.4 *5*	-2.7 *5*	0.2 *0*	2.7 *5*	0.8 *5*	-0.6 *5*	-0.3 *5*	0.1 *0*	-0.3 *0*	-0.1 *0*	-2.0 *1*	-3.8 *0*	-1.8 *0*	0.7 *5*	-1.1 *0*
4	1.3 *5*	2.4 *5*	5.2 *5*	**7.4** ***5***	3.3 *5*	-0.1 *5*	-1.3 *5*	0.0 *5*	2.0 *5*	1.0 *5*	0.6 *5*	-2.2 *5*	-0.6 *0*	-0.8 *0*	-0.3 *0*	-2.3 *0*	-3.8 *0*	-2.2 *0*	0.3 *5*	-1.5 *0*
5	1.2 *5*	2.6 *5*	5.2 *5*	**7.6** ***5***	2.6 *5*	-0.6 *0*	-1.6 *0*	-0.4 *5*	1.7 *5*	1.7 *5*	0.7 *5*	-1.4 *5*	-0.8 *0*	-0.9 *0*	-0.2 *0*	-2.5 *0*	-3.9 *0*	-1.9 *0*	0.6 *5*	-1.5 *0*

Figure F-48. Parametric study: Building width in slabs, maximum vertical vibration level relative to basement, mid-span positions

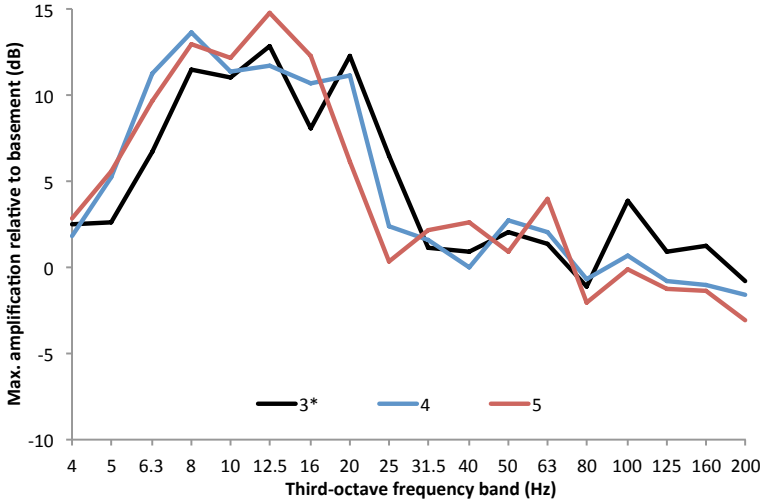

Table F-14. Generic building parametric study: Building width in slabs, maximum vertical vibration relative to basement, mid-span positions

No. slabs	Maximum amplification relative to basement level; *Floor level at which maximum occurs*																		
	1/3 octave band frequency (Hz)																	Overall	
	4	5	6.3	8	10	12.5	16	20	25	31.5	40	50	63	80	100	125	160	200	L_{Wb}	L_A
3*	2.5	2.7	6.7	11.5	11.0	**12.9**	8.0	12.2	6.5	1.1	0.9	2.0	1.3	-1.1	3.8	0.9	1.2	-0.7	5.2	1.8
	5	*5*	*5*	*5*	*5*	***1***	*1*	*0*	*0*	*1*	*5*	*0*	*0*	*0*	*0*	*0*	*0*	*0*	*0*	*0*
4	1.9	5.2	11.3	**13.6**	11.3	11.7	10.6	11.1	2.4	1.5	0.0	2.7	2.0	-0.6	0.6	-0.8	-1.0	-1.6	5.0	0.3
	5	*5*	*5*	***5***	*5*	*1*	*0*	*0*	*0*	*0*	*0*	*1*	*0*	*0*	*0*	*0*	*0*	*0*	*0*	*0*
5	2.8	5.6	9.6	13.0	12.1	**14.8**	12.2	6.1	0.4	2.1	2.6	0.9	4.0	-2.0	-0.1	-1.3	-1.4	-3.1	5.9	0.0
	5	*5*	*5*	*5*	*5*	***0***	*0*	*0*	*5*	*0*	*0*	*1*	*0*	*0*	*0*	*1*	*0*	*0*	*0*	*0*

Figure F-49. Parametric study: Building width in slabs, average vertical vibration level at mid-span relative to column positions, first floor

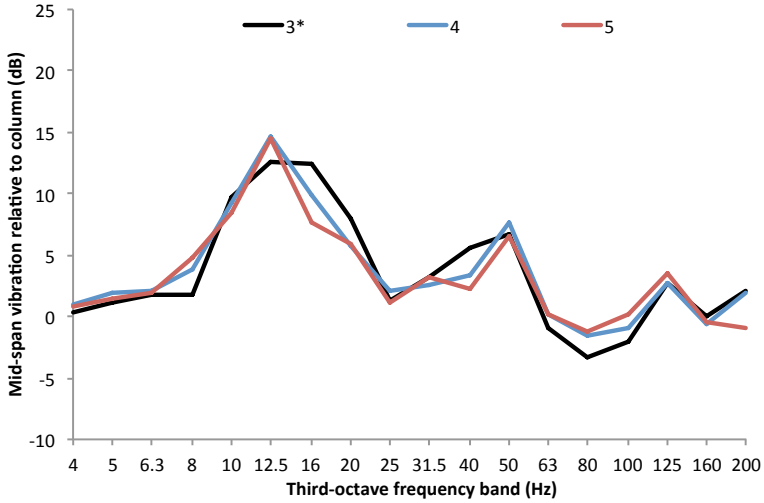

F.8: Column cross-section

For discussion of these results, please refer to Section 5.5.3.

Figure F-50. Parametric study: Column cross-section, W_b-weighted basement-relative column acceleration levels with storey

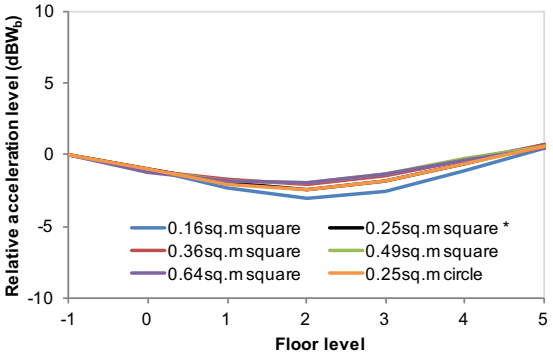

Figure F-51. Parametric study: Column cross-section, A-weighted basement-relative column velocity levels with storey

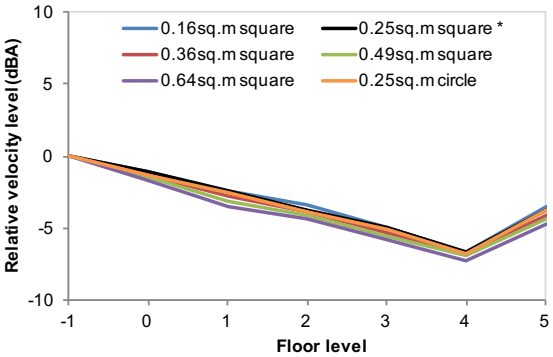

Figure F-52. Parametric study: Column cross-section, W_b-weighted basement-relative mid-span acceleration levels with storey

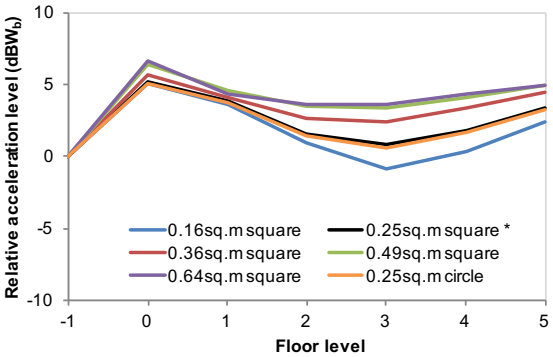

Figure F-53. Parametric study: Column cross-section, A-weighted basement-relative mid-span velocity levels with storey

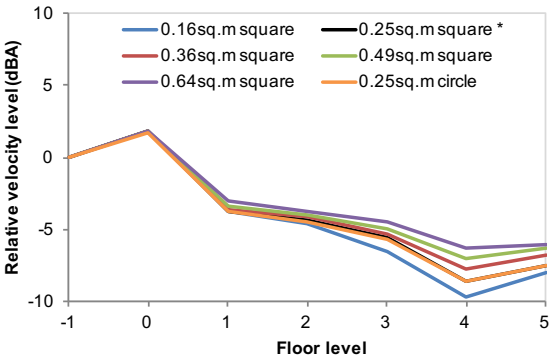

Figure F-54. Parametric study: Column cross-section, maximum vertical vibration level relative to basement, column positions

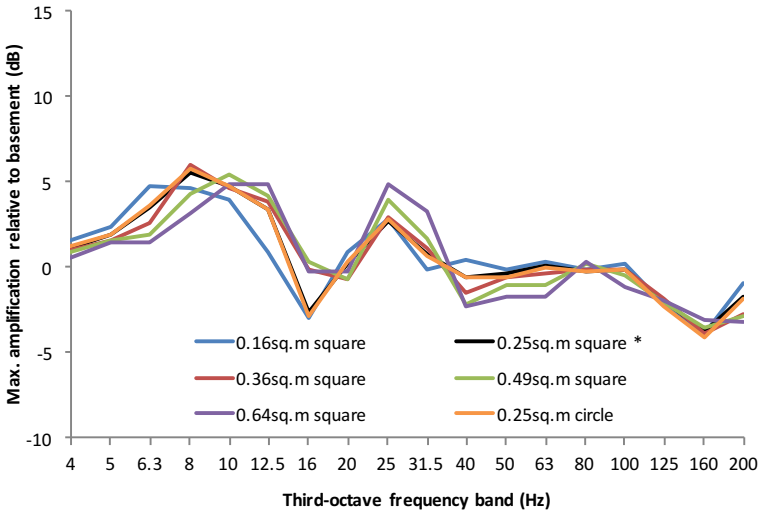

Table F-15. Generic building parametric study: Column cross-section, maximum vertical vibration relative to basement, column positions																				
Cross-section	Maximum amplification relative to basement level; *Floor level at which maximum occurs*																		Overall	
	1/3 octave band frequency (Hz)																			
	4	5	6.3	8	10	12.5	16	20	25	31.5	40	50	63	80	100	125	160	200	L_{Wb}	L_A
0.16 m² square	1.6	2.4	**4.8**	4.6	4.0	0.9	-2.9	0.9	2.8	-0.1	0.5	-0.1	0.4	-0.2	0.2	-2.2	-3.9	-1.0	0.5	-1.1
	5	*5*	***5***	*5*	*5*	*5*	*0*	*5*	*5*	*5*	*5*	*5*	*5*	*0*	*1*	*0*	*0*	*0*	*5*	*0*
0.25 m² square*	1.2	1.9	3.5	**5.6**	4.8	3.4	-2.7	0.2	2.7	0.8	-0.6	-0.3	0.1	-0.3	-0.1	-2.0	-3.8	-1.8	0.7	-1.1
	5	*5*	*5*	***5***	*5*	*5*	*5*	*0*	*5*	*5*	*5*	*5*	*0*	*0*	*0*	*1*	*0*	*0*	*5*	*0*
0.36 m² square	1.0	1.6	2.6	**6.0**	4.7	3.9	-0.1	-0.7	2.9	1.1	-1.5	-0.6	-0.3	-0.1	-0.1	-1.9	-3.9	-2.7	0.7	-1.3
	5	*5*	*5*	***5***	*5*	*5*	*5*	*5*	*5*	*5*	*5*	*5*	*0*	*0*	*0*	*0*	*0*	*0*	*5*	*0*
0.49 m² square	0.8	1.5	1.9	4.3	**5.4**	4.2	0.4	-0.7	3.9	1.7	-2.2	-1.0	-1.0	0.2	-0.5	-2.0	-3.5	-2.9	0.6	-1.5
	5	*5*	*5*	*5*	***5***	*5*	*5*	*5*	*5*	*5*	*5*	*5*	*0*	*0*	*0*	*0*	*0*	*0*	*5*	*0*
0.64 m² square	0.5	1.5	1.5	3.1	**4.9**	**4.9**	-0.3	-0.3	**4.9**	3.2	-2.3	-1.7	-1.7	0.3	-1.2	-2.0	-3.1	-3.2	0.5	-1.6
	5	*5*	*5*	*5*	***5***	***5***	*5*	*5*	***5***	*5*	*5*	*5*	*5*	*0*	*0*	*0*	*0*	*0*	*5*	*0*
0.25 m² circle	1.2	1.9	3.6	**5.8**	4.7	3.4	-2.9	0.4	2.9	0.6	-0.5	-0.6	0.0	-0.3	-0.1	-2.3	-4.1	-1.9	0.6	-1.3
	5	*5*	*5*	***5***	*5*	*5*	*1*	*0*	*5*	*5*	*5*	*5*	*0*	*0*	*0*	*1*	*0*	*0*	*5*	*0*

Figure F-55. Parametric study: Column cross-section, maximum vertical vibration level relative to basement, mid-span positions

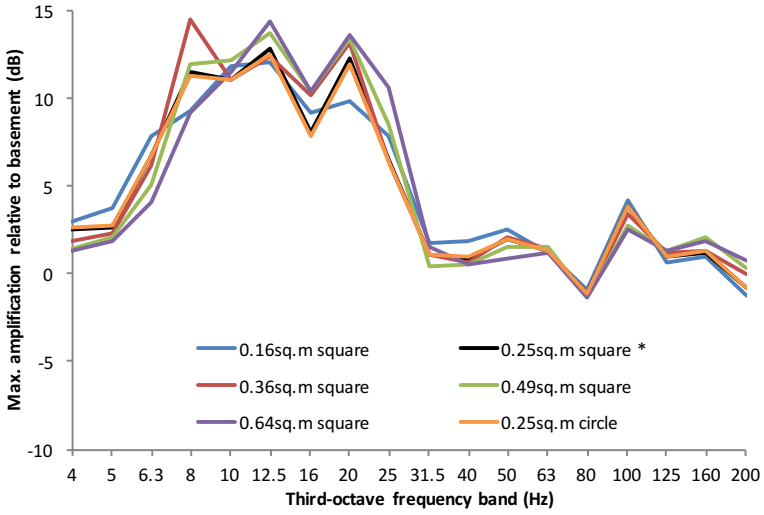

Table F-16. Generic building parametric study: Column cross-section, maximum vertical vibration relative to basement, mid-span positions																				
Cross-section	Maximum amplification relative to basement level; *Floor level at which maximum occurs*																		Overall	
	1/3 octave band frequency (Hz)																			
	4	5	6.3	8	10	12.5	16	20	25	31.5	40	50	63	80	100	125	160	200	L_{Wb}	L_A
0.16 m² square	3.0	3.7	7.9	9.3	11.8	**12.0**	9.2	9.8	7.8	1.7	1.9	2.5	1.2	-0.9	4.2	0.7	1.0	-1.2	5.1	1.8
	5	*5*	*5*	*5*	*5*	***1***	*0*	*0*	*0*	*0*	*0*	*0*	*0*	*0*	*0*	*0*	*0*	*0*	*0*	*0*
0.25 m² square*	2.5	2.7	6.7	11.5	11.0	**12.9**	8.0	12.2	6.5	1.1	0.9	2.0	1.3	-1.1	3.8	0.9	1.2	-0.7	5.2	1.8
	5	*5*	*5*	*5*	*5*	***1***	*1*	*0*	*0*	*1*	*5*	*0*	*0*	*0*	*0*	*0*	*0*	*0*	*0*	*0*
0.36 m² square	1.9	2.3	6.1	**14.5**	11.1	12.3	10.1	13.1	6.4	1.1	0.7	2.1	1.5	-1.2	3.4	1.1	1.4	0.0	5.6	1.8
	5	*5*	*5*	***5***	*5*	*1*	*1*	*0*	*0*	*1*	*5*	*0*	*0*	*0*	*0*	*0*	*0*	*0*	*0*	*0*
0.49 m² square	1.4	2.0	5.1	11.9	12.2	**13.7**	10.4	13.3	8.5	0.5	0.5	1.5	1.6	-1.4	2.8	1.3	2.0	0.3	6.4	1.9
	5	*5*	*5*	*5*	*5*	***5***	*1*	*0*	*0*	*1*	*5*	*0*	*0*	*0*	*0*	*0*	*0*	*0*	*0*	*0*
0.64 m² square	1.3	1.9	4.1	9.2	11.4	**14.3**	10.4	13.6	10.7	1.5	0.6	0.8	1.2	-1.4	2.5	1.3	1.9	0.7	6.7	1.8
	5	*5*	*5*	*5*	*5*	***5***	*1*	*0*	*0*	*5*	*5*	*5*	*0*	*0*	*0*	*0*	*0*	*0*	*0*	*0*
0.25 m² circle	2.6	2.7	6.8	11.3	11.1	**12.5**	7.9	11.9	6.4	1.1	1.0	2.0	1.3	-1.1	3.9	1.0	1.3	-0.8	5.0	1.8
	5	*5*	*5*	*5*	*5*	***1***	*1*	*0*	*0*	*1*	*0*	*0*	*0*	*0*	*0*	*0*	*0*	*0*	*0*	*0*

Figure F-56. Parametric study: Column cross-section, average vertical vibration level at mid-span relative to column positions, first floor

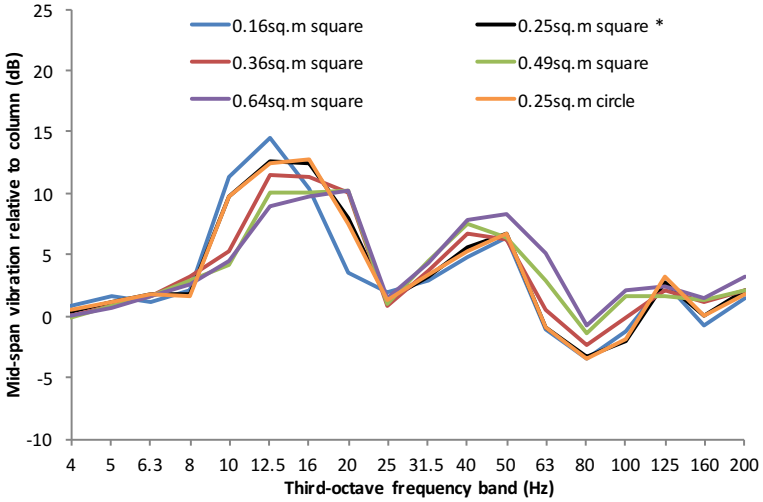

F.9: Internal walls

For discussion of these results, please refer to Section 5.5.4.

Figure F-57. Parametric study: Int. walls, W_b-weighted basement-relative mid-span acceleration levels with storey

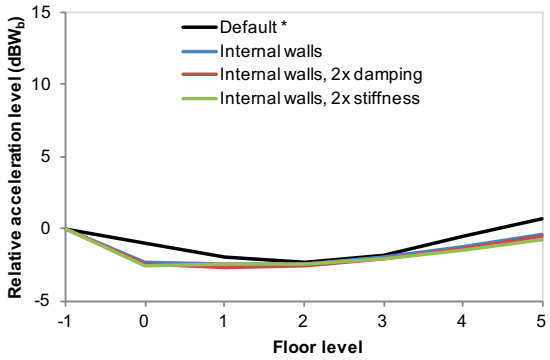

Figure F-58. Parametric study: Int. walls, A-weighted basement-relative column velocity levels with storey

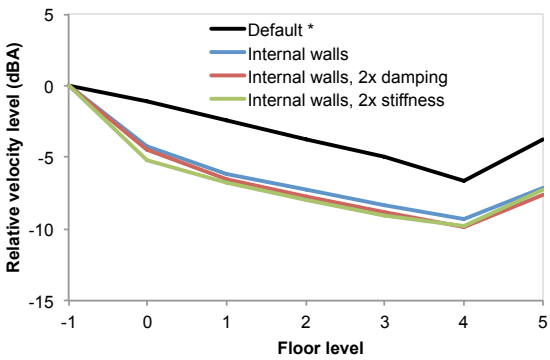

Figure F-59. Parametric study: Int. walls, W_b-weighted basement-relative mid-span acceleration levels with storey

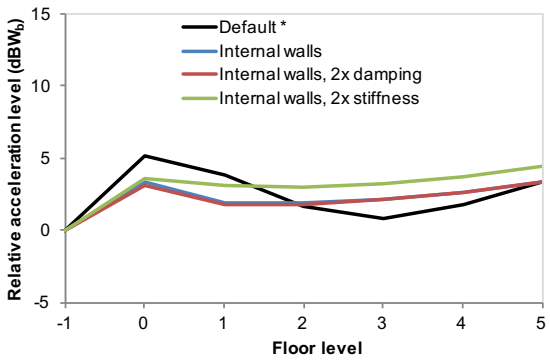

Figure F-60. Parametric study: Int. walls, A-weighted basement-relative mid-span velocity levels with storey

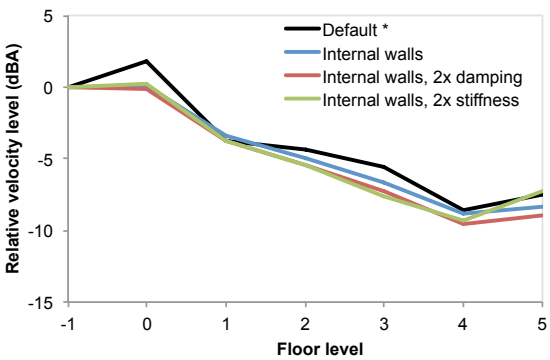

Figure F-61. Parametric study: Int. walls, maximum vertical vibration level relative to basement, column positions

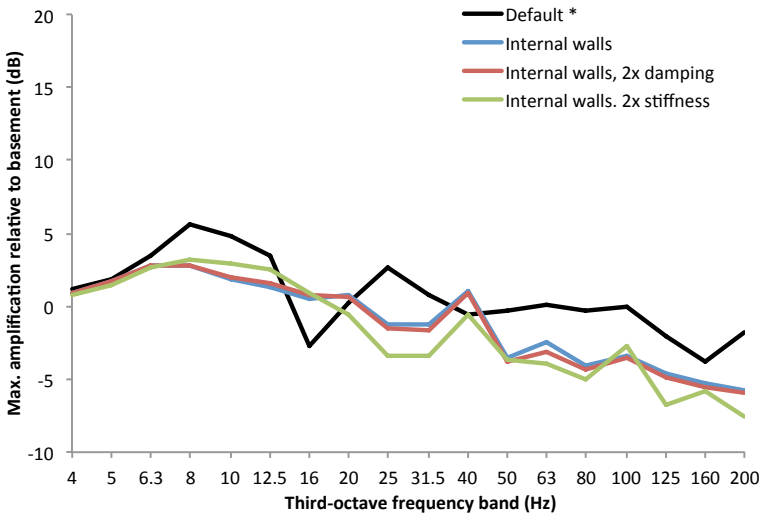

Table F-17. Generic building parametric study: Int. walls, maximum vertical vibration relative to basement, column positions

	Maximum amplification relative to basement level; *Floor level at which maximum occurs*																			
	1/3 octave band frequency (Hz)																		Overall	
	4	5	6.3	8	10	12.5	16	20	25	31.5	40	50	63	80	100	125	160	200	L_{Wb}	L_A
Default*	1.2	1.9	3.5	**5.6**	4.8	3.4	-2.7	0.2	2.7	0.8	-0.6	-0.3	0.1	-0.3	-0.1	-2.0	-3.8	-1.8	0.7	-1.1
	5	*5*	*5*	***5***	*5*	*5*	*5*	*0*	*5*	*5*	*5*	*5*	*0*	*0*	*0*	*1*	*0*	*0*	*5*	*0*
Int. walls	1.0	1.7	2.8	**2.9**	1.8	1.4	0.6	0.7	-1.2	-1.2	1.0	-3.5	-2.5	-4.1	-3.4	-4.6	-5.3	-5.8	-0.4	-4.2
	5	*5*	*5*	***5***	*5*	*5*	*5*	*5*	*5*	*5*	*5*	*5*	*5*	*0*	*0*	*0*	*0*	*0*	*5*	*0*
Int. walls 2x damp.	1.0	1.7	2.8	**2.9**	2.0	1.6	0.8	0.7	-1.5	-1.7	1.0	-3.7	-3.1	-4.3	-3.5	-4.9	-5.5	-5.9	-0.6	-4.4
	5	*5*	*5*	***5***	*5*	*5*	*5*	*5*	*5*	*5*	*5*	*5*	*5*	*0*	*0*	*0*	*0*	*0*	*5*	*0*
Int. walls 2x stiff.	0.8	1.4	2.7	**3.3**	2.9	2.5	0.9	-0.5	-3.4	-3.3	-0.6	-3.6	-4.0	-5.0	-2.8	-6.8	-5.9	-7.6	-0.8	-5.2
	5	*5*	*5*	***5***	*5*	*5*	*5*	*5*	*5*	*5*	*5*	*5*	*5*	*0*	*0*	*0*	*0*	*0*	*5*	*0*

Figure F-62. Parametric study: Int. walls, maximum vertical vibration level relative to basement, mid-span positions

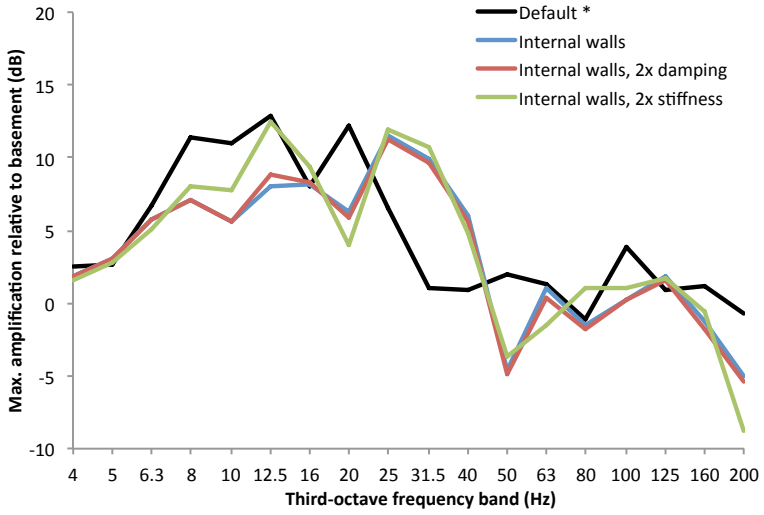

Table F-18. Generic building parametric study: Int. walls, maximum vertical vibration relative to basement, mid-span positions																				
	Maximum amplification relative to basement level; *Floor level at which maximum occurs*																		Overall	
	1/3 octave band frequency (Hz)																			
	4	5	6.3	8	10	12.5	16	20	25	31.5	40	50	63	80	100	125	160	200	L_{Wb}	L_A
Default*	2.5 *5*	2.7 *5*	6.7 *5*	11.5 *5*	11.0 *5*	**12.9** ***1***	8.0 *1*	12.2 *0*	6.5 *0*	1.1 *1*	0.9 *5*	2.0 *0*	1.3 *0*	-1.1 *0*	3.8 *0*	0.9 *0*	1.2 *0*	-0.7 *0*	5.2 *0*	1.8 *0*
Int. walls	1.8 *5*	3.1 *5*	5.8 *5*	7.0 *5*	5.6 *5*	8.0 *5*	8.1 *5*	6.2 *0*	**11.5** ***0***	9.9 *0*	6.1 *5*	-4.6 *0*	1.1 *0*	-1.6 *0*	0.2 *0*	1.8 *0*	-1.2 *0*	-5.1 *0*	3.4 *0*	0.2 *0*
Int. walls 2x damp.	1.8 *5*	3.1 *5*	5.7 *5*	7.0 *5*	5.7 *5*	8.9 *5*	8.3 *5*	5.9 *0*	**11.3** ***0***	9.7 *0*	5.6 *5*	-4.9 *0*	0.3 *0*	-1.8 *0*	0.2 *0*	1.5 *0*	-1.7 *0*	-5.4 *0*	3.3 *5*	-0.1 *0*
Int. walls 2x stiff.	1.6 *5*	2.7 *5*	5.0 *5*	8.0 *5*	7.8 *5*	**12.5** ***5***	9.4 *1*	4.0 *0*	12.0 *0*	10.8 *0*	4.9 *5*	-3.6 *0*	-1.5 *0*	1.0 *0*	1.0 *0*	1.7 *0*	-0.6 *0*	-8.8 *0*	4.4 *5*	0.3 *0*

Figure F-63. Parametric study: Internal walls, average vertical vibration level at mid-span relative to column positions, first floor

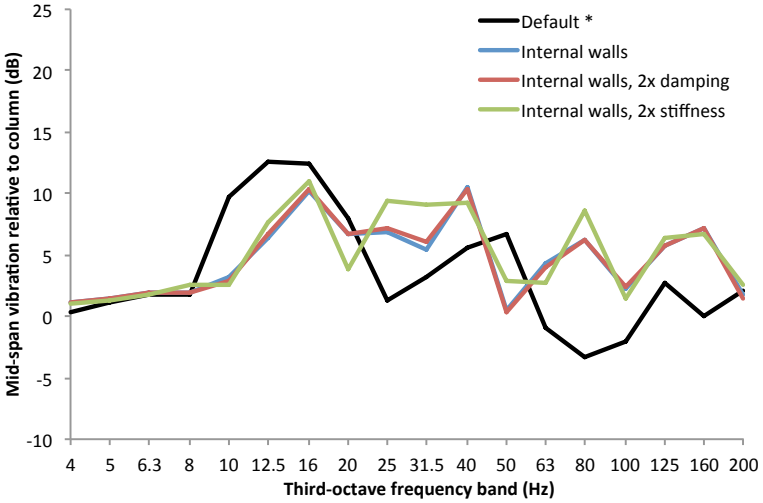

F.10: Structural damping

For discussion of these results, please refer to Section 5.6.1.

Figure F-64. Parametric study: Structural damping (by loss factor), W_b-weighted basement-relative column acceleration levels with storey

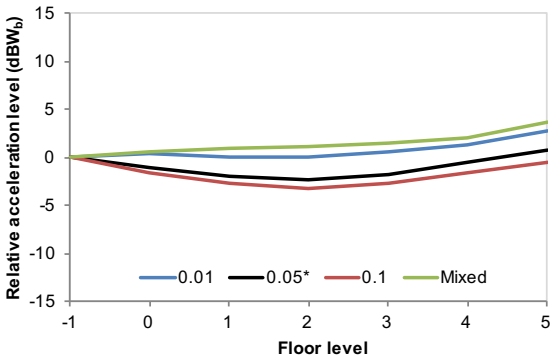

Figure F-65. Parametric study: Structural damping (by loss factor), A-weighted basement-relative column velocity levels with storey

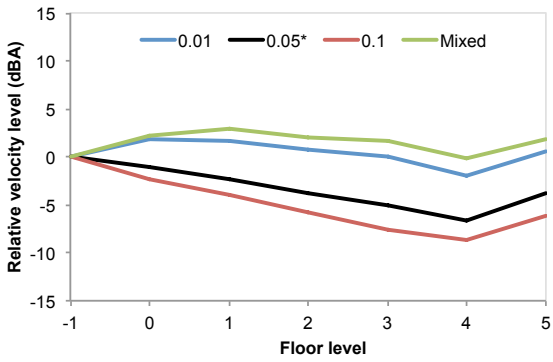

Figure F-66. Parametric study: Structural damping (by loss factor), W_b-weighted basement-relative mid-span acceleration levels with storey

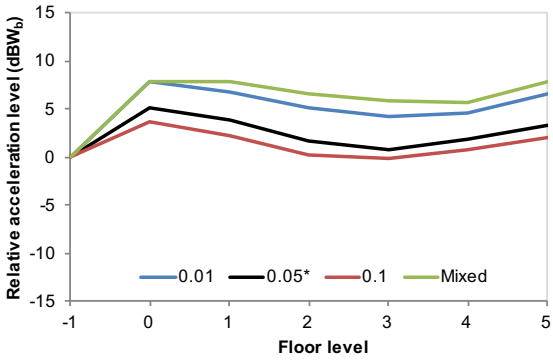

Figure F-67. Parametric study: Structural damping (by loss factor), A-weighted basement-relative mid-span velocity levels with storey

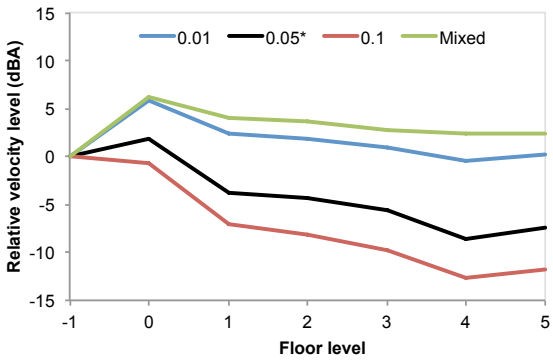

Figure F-68. Parametric study: Structural damping, maximum vertical vibration level relative to basement, column positions

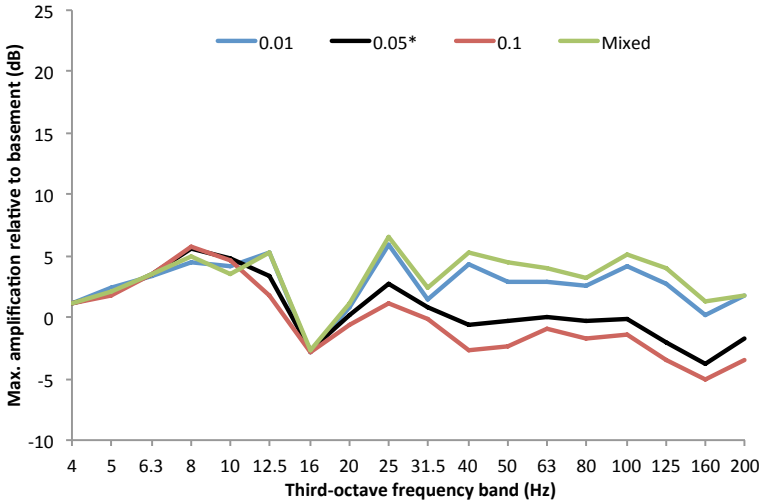

Table F-19. Generic building parametric study: Structural damping, maximum vertical vibration relative to basement, column positions

Loss factor	Maximum amplification relative to basement level; *Floor level at which maximum occurs*																			
	1/3 octave band frequency (Hz)																		Overall	
	4	5	6.3	8	10	12.5	16	20	25	31.5	40	50	63	80	100	125	160	200	L_{Wb}	L_A
0.01	1.2 *5*	2.5 *5*	3.4 *5*	4.4 *5*	4.2 *5*	5.3 *5*	-2.9 *5*	0.9 *5*	**5.9** ***5***	1.4 *5*	4.4 *5*	2.9 *5*	2.9 *5*	2.6 *0*	4.2 *1*	2.8 *1*	0.3 *0*	1.8 *0*	2.8 *5*	1.8 *0*
0.05*	1.2 *5*	1.9 *5*	3.5 *5*	**5.6** ***5***	4.8 *5*	3.4 *5*	-2.7 *5*	0.2 *0*	2.7 *5*	0.8 *5*	-0.6 *5*	-0.3 *5*	0.1 *0*	-0.3 *0*	-0.1 *0*	-2.0 *1*	-3.8 *0*	-1.8 *0*	0.7 *5*	-1.1 *0*
0.1	1.1 *5*	1.7 *5*	3.5 *5*	**5.8** ***5***	4.6 *5*	1.7 *5*	-2.8 *1*	-0.6 *0*	1.1 *5*	-0.2 *5*	-2.7 *5*	-2.4 *5*	-0.9 *0*	-1.7 *0*	-1.5 *0*	-3.4 *0*	-5.1 *0*	-3.6 *0*	-0.5 *5*	-2.3 *0*
Mixed	1.2 *5*	2.2 *5*	3.5 *5*	5.0 *5*	3.5 *5*	5.3 *5*	-2.7 *5*	1.2 *5*	**6.6** ***5***	2.4 *5*	5.3 *5*	4.5 *5*	4.1 *5*	3.2 *5*	5.0 *1*	4.0 *1*	1.2 *0*	1.7 *0*	3.7 *5*	2.9 *1*

Figure F-69. Parametric study: Structural damping, maximum vertical vibration level relative to basement, mid-span positions

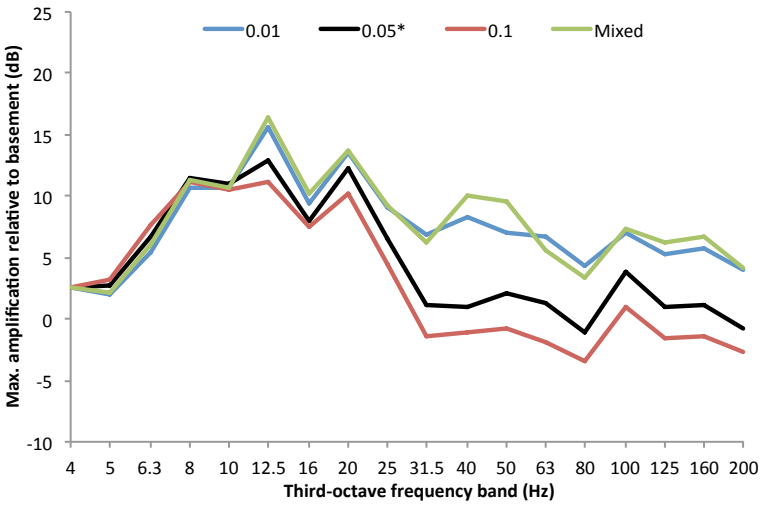

Table F-20. Generic building parametric study: Structural damping, maximum vertical vibration relative to basement, mid-span positions

Loss factor	Maximum amplification relative to basement level; *Floor level at which maximum occurs*																			
	1/3 octave band frequency (Hz)																		Overall	
	4	5	6.3	8	10	12.5	16	20	25	31.5	40	50	63	80	100	125	160	200	L_{Wb}	L_A
0.01	2.6 *5*	2.0 *0*	5.4 *5*	10.7 *5*	10.7 *5*	**15.6** ***1***	9.4 *1*	13.6 *0*	9.1 *0*	6.8 *0*	8.3 *5*	6.9 *0*	6.6 *0*	4.3 *0*	7.1 *0*	5.2 *0*	5.8 *0*	4.0 *0*	7.8 *0*	5.8 *0*
0.05*	2.5 *5*	2.7 *5*	6.7 *5*	11.5 *5*	11.0 *5*	**12.9** ***1***	8.0 *1*	12.2 *0*	6.5 *0*	1.1 *1*	0.9 *5*	2.0 *0*	1.3 *0*	-1.1 *0*	3.8 *0*	0.9 *0*	1.2 *0*	-0.7 *0*	5.2 *0*	1.8 *0*
0.1	2.5 *5*	3.2 *5*	7.6 *5*	**11.2** ***5***	10.5 *5*	11.1 *1*	7.5 *0*	10.3 *0*	4.5 *0*	-1.3 *1*	-1.1 *0*	-0.7 *0*	-1.9 *0*	-3.4 *0*	1.0 *0*	-1.5 *0*	-1.4 *0*	-2.7 *0*	3.7 *0*	-0.7 *0*
Mixed	2.6 *5*	2.1 *5*	6.0 *5*	11.4 *5*	10.6 *5*	**16.4** ***1***	10.2 *1*	13.6 *0*	9.2 *0*	6.3 *0*	10.1 *5*	9.6 *2*	5.6 *0*	3.3 *0*	7.4 *0*	6.2 *0*	6.8 *0*	4.1 *0*	7.9 *5*	6.1 *0*

Figure F-70. Parametric study: Structural damping, average vertical vibration level at mid-span relative to column positions, first floor

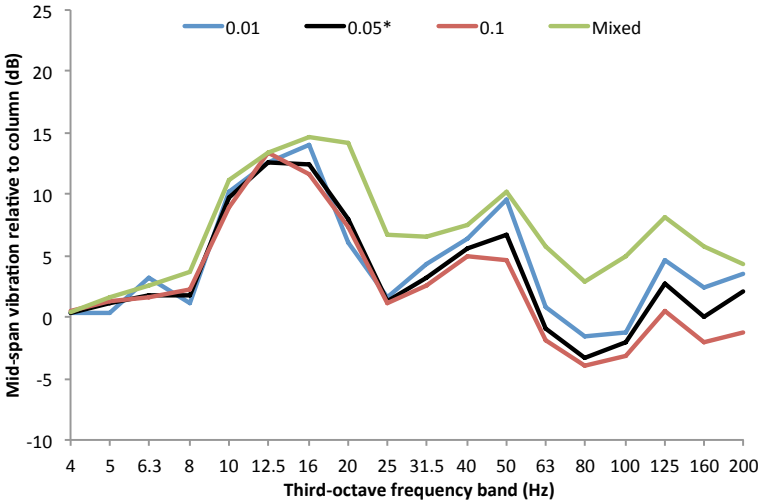

F.11: Material density

For discussion of these results, please refer to Section 5.6.2.

Figure F-71. Parametric study: Density multiplication factor, W_b-weighted basement-relative mid-span acceleration levels with storey

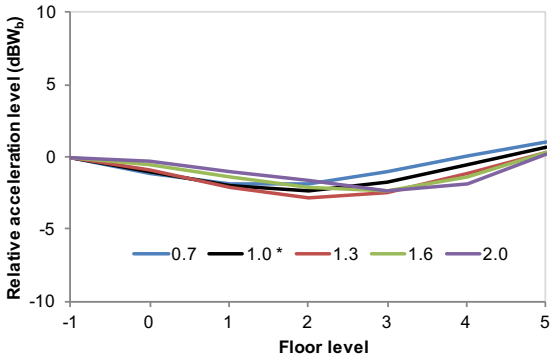

Figure F-72. Parametric study: Density multiplication factor, A-weighted basement-relative column velocity levels with storey

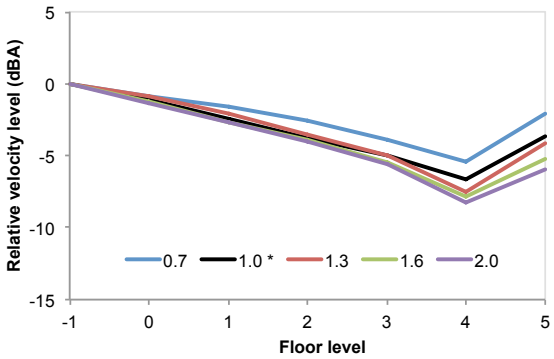

Figure F-73. Parametric study: Density multiplication factor, W_b-weighted basement-relative mid-span acceleration levels with storey

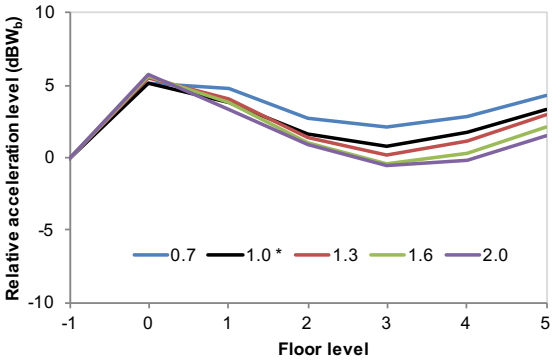

Figure F-74. Parametric study: Density multiplication factor, A-weighted basement-relative mid-span velocity levels with storey

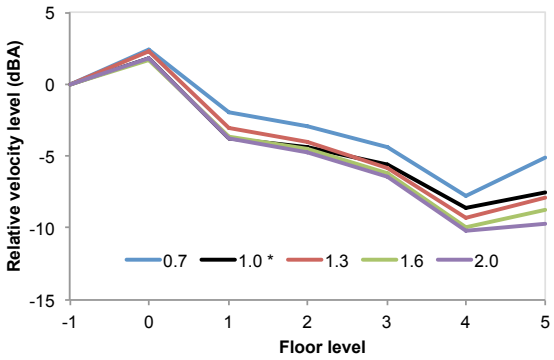

Figure F-75. Parametric study: Density multiplication factor, maximum vertical vibration level relative to basement, column positions

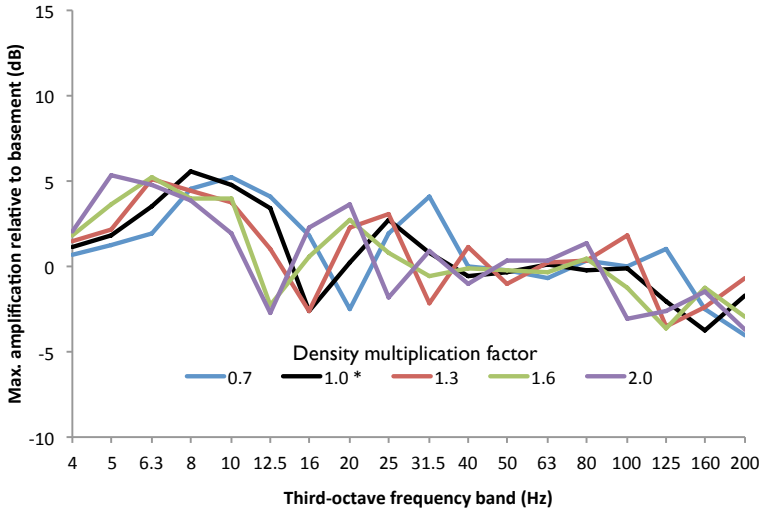

Table F-21. Generic building parametric study: Density multiplication factor, maximum vertical vibration relative to basement, column positions																				
Density factor	Maximum amplification relative to basement level; *Floor level at which maximum occurs*																		Overall	
	1/3 octave band frequency (Hz)																			
	4	5	6.3	8	10	12.5	16	20	25	31.5	40	50	63	80	100	125	160	200	L_{Wb}	L_A
0.7	0.7 *5*	1.2 *5*	1.9 *5*	4.6 *5*	5.2 *5*	4.0 *5*	1.9 *5*	-2.5 *0*	1.9 *5*	4.1 *5*	0.0 *5*	-0.2 *5*	-0.7 *5*	0.4 *5*	0.0 *0*	1.0 *1*	-2.5 *0*	-4.0 *0*	1.1 *5*	-0.8 *0*
1.0 *	1.2 *5*	1.9 *5*	3.5 *5*	**5.6** ***5***	4.8 *5*	3.4 *5*	-2.7 *5*	0.2 *0*	2.7 *5*	0.8 *5*	-0.6 *5*	-0.3 *5*	0.1 *0*	-0.3 *0*	-0.1 *0*	-2.0 *1*	-3.8 *0*	-1.8 *0*	0.7 *5*	-1.1 *0*
1.3	1.5 *5*	2.2 *5*	**5.2** ***5***	4.4 *5*	3.7 *5*	1.0 *5*	-2.6 *1*	2.2 *5*	3.1 *5*	-2.1 *5*	1.1 *5*	-1.0 *5*	0.2 *0*	0.4 *0*	1.8 *1*	-3.5 *0*	-2.4 *0*	-0.7 *0*	0.3 *5*	-0.9 *0*
1.6	1.8 *5*	3.6 *5*	**5.3** ***5***	4.0 *5*	4.0 *5*	-2.2 *5*	0.6 *0*	2.7 *5*	0.8 *5*	-0.5 *5*	-0.1 *5*	-0.2 *5*	-0.3 *0*	0.4 *0*	-1.3 *1*	-3.6 *0*	-1.3 *0*	-2.9 *0*	0.3 *5*	-1.3 *0*
2.0	2.0 *5*	**5.3** ***5***	4.7 *5*	3.9 *5*	1.9 *5*	-2.7 *0*	2.2 *5*	3.6 *5*	-1.8 *5*	1.0 *5*	-1.1 *5*	0.4 *0*	0.3 *0*	1.4 *1*	-3.0 *0*	-2.7 *0*	-1.4 *0*	-3.7 *0*	0.2 *5*	-1.3 *0*

Figure F-76. Parametric study: Density multiplication factor, maximum vertical vibration level relative to basement, mid-span positions

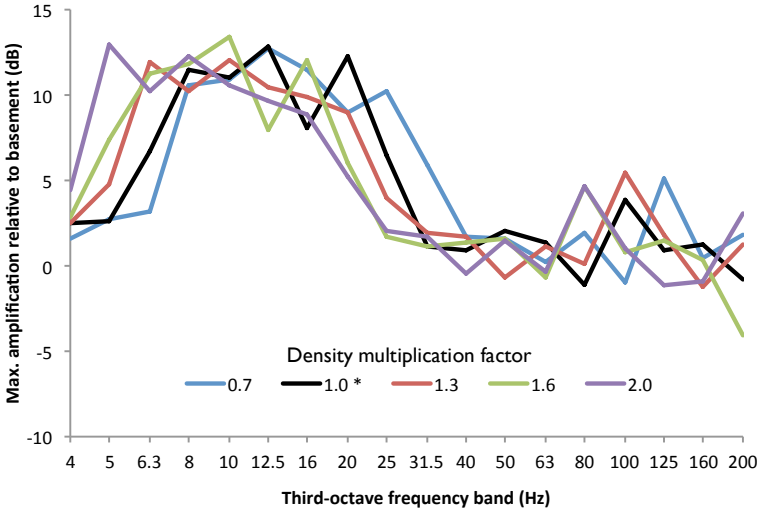

Table F-22. Generic building parametric study: Density multiplication factor, maximum vertical vibration relative to basement, mid-span positions																				
Density factor	Maximum amplification relative to basement level; *Floor level at which maximum occurs*																		Overall	
	1/3 octave band frequency (Hz)																			
	4	5	6.3	8	10	12.5	16	20	25	31.5	40	50	63	80	100	125	160	200	L_{Wb}	L_A
0.7	1.5 *5*	2.8 *5*	3.2 *5*	10.6 *5*	10.9 *5*	**12.7** ***5***	11.5 *1*	9.0 *0*	10.2 *0*	5.9 *0*	1.7 *1*	1.6 *1*	0.3 *0*	1.9 *0*	-1.0 *0*	5.1 *0*	0.4 *0*	1.8 *0*	5.1 *0*	2.4 *0*
1.0 *	2.5 *5*	2.7 *5*	6.7 *5*	11.5 *5*	11.0 *5*	**12.9** ***1***	8.0 *1*	12.2 *0*	6.5 *0*	1.1 *1*	0.9 *5*	2.0 *0*	1.3 *0*	-1.1 *0*	3.8 *0*	0.9 *0*	1.2 *0*	-0.7 *0*	5.2 *0*	1.8 *0*
1.3	2.4 *5*	4.7 *5*	11.9 *5*	10.3 *5*	**12.0** ***1***	10.5 *1*	9.9 *0*	8.9 *0*	4.0 *0*	1.9 *1*	1.7 *0*	-0.6 *0*	1.2 *0*	0.1 *0*	5.4 *0*	1.9 *0*	-1.2 *0*	1.2 *0*	5.5 *0*	2.3 *0*
1.6	2.9 *5*	7.4 *5*	11.2 *5*	11.8 *5*	**13.5** ***1***	8.0 *1*	12.1 *0*	6.0 *0*	1.7 *1*	1.1 *1*	1.3 *0*	1.6 *0*	-0.6 *0*	4.6 *0*	0.8 *0*	1.5 *0*	0.4 *0*	-4.1 *0*	5.7 *0*	1.6 *0*
2.0	4.5 *5*	**13.0** ***5***	10.2 *5*	12.2 *1*	10.6 *1*	9.7 *0*	8.9 *0*	5.2 *0*	2.0 *1*	1.7 *0*	-0.5 *0*	1.5 *0*	-0.3 *0*	4.6 *0*	1.0 *0*	-1.2 *0*	-0.9 *0*	3.0 *0*	5.8 *0*	1.8 *0*

Figure F-77. Parametric study: Density multiplication factor, average vertical vibration level at mid-span relative to column positions, first floor

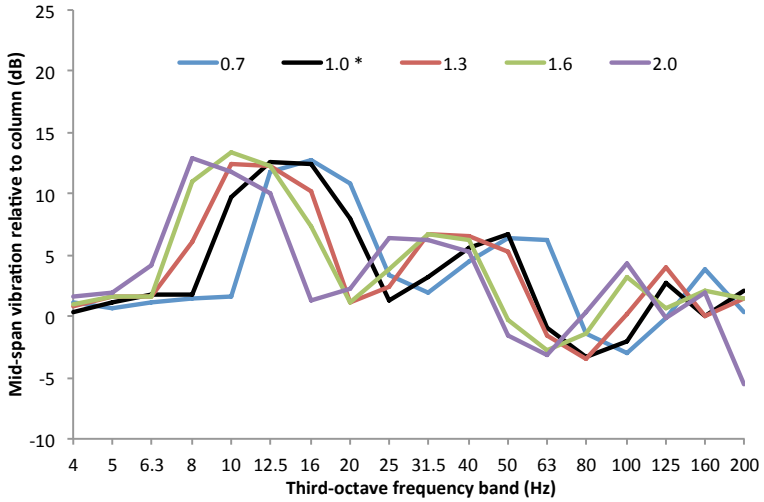

F.12: Material stiffness

For discussion of these results, please refer to Section 5.6.3.

Figure F-78. Parametric study: Material stiffness, W_b-weighted basement-relative column acceleration levels with storey

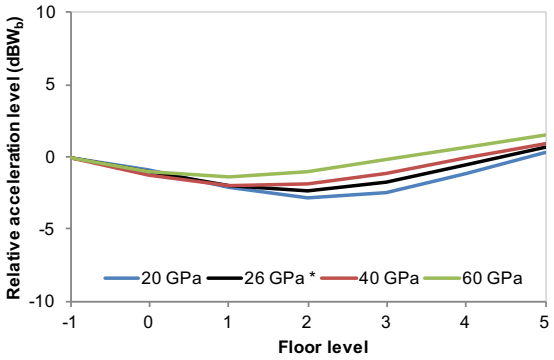

Figure F-79. Parametric study: Material stiffness, A-weighted basement-relative column velocity levels with storey

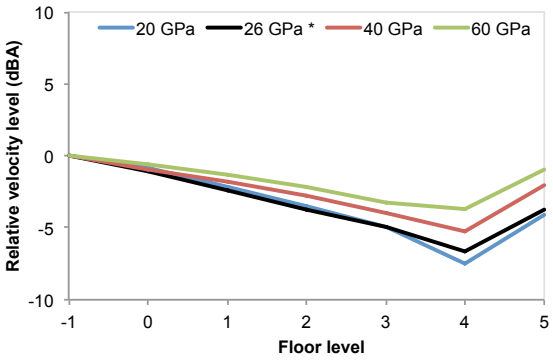

Figure F-80. Parametric study: Material stiffness, W_b-weighted basement-relative mid-span acceleration levels with storey

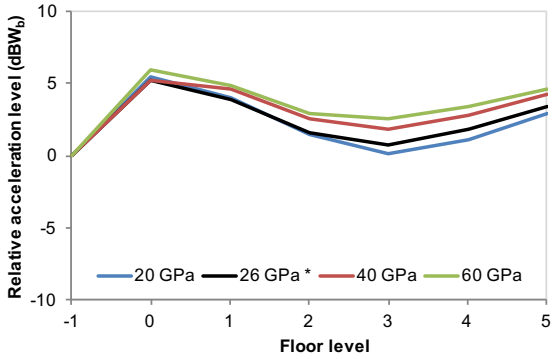

Figure F-81. Parametric study: Material stiffness, A-weighted basement-relative mid-span velocity levels with storey

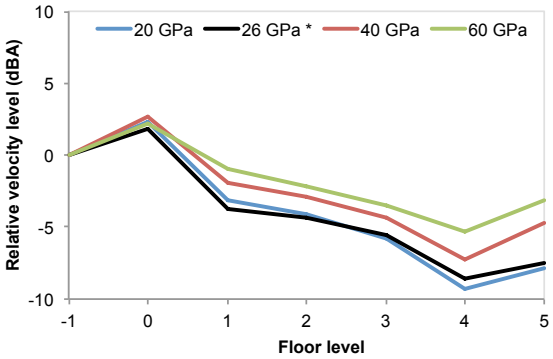

Figure F-82. Parametric study: Material stiffness, maximum vertical vibration level relative to basement, column positions

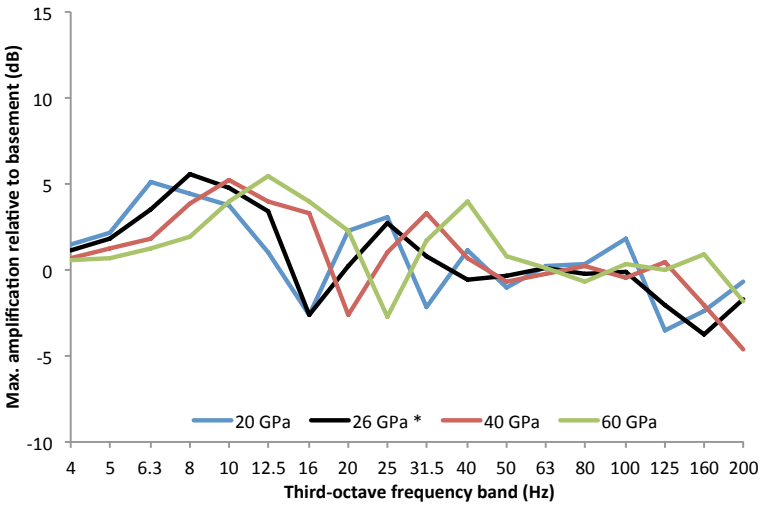

Table F-23. Generic building parametric study: Material stiffness, maximum vertical vibration relative to basement, column positions

Young's mod.	Maximum amplification relative to basement level; *Floor level at which maximum occurs*																		
	1/3 octave band frequency (Hz)																	Overall	
	4	5	6.3	8	10	12.5	16	20	25	31.5	40	50	63	80	100	125	160	200	L_{Wb}	L_A
20	1.5 *5*	2.2 *5*	**5.2** ***5***	4.4 *5*	3.7 *5*	1.0 *5*	-2.6 *1*	2.2 *5*	3.1 *5*	-2.1 *5*	1.1 *5*	-1.0 *5*	0.2 *0*	0.4 *0*	1.8 *1*	-3.5 *0*	-2.4 *0*	-0.7 *0*	0.3 *5*	-0.9 *0*
26 *	1.2 *5*	1.9 *5*	3.5 *5*	**5.6** ***5***	4.8 *5*	3.4 *5*	-2.7 *5*	0.2 *0*	2.7 *5*	0.8 *5*	-0.6 *5*	-0.3 *5*	0.1 *0*	-0.3 *0*	-0.1 *0*	-2.0 *1*	-3.8 *0*	-1.8 *0*	0.7 *5*	-1.1 *0*
40	0.7 *5*	1.2 *5*	1.8 *5*	3.9 *5*	**5.2** ***5***	4.0 *5*	3.3 *5*	-2.6 *5*	1.0 *5*	3.3 *5*	0.7 *5*	-0.7 *5*	-0.3 *5*	0.2 *5*	-0.5 *0*	0.4 *1*	-2.0 *1*	-4.6 *0*	1.0 *5*	-0.9 *0*
60	0.6 *5*	0.7 *5*	1.2 *5*	1.9 *5*	4.0 *5*	**5.4** ***5***	4.0 *5*	2.3 *5*	-2.7 *0*	1.7 *5*	4.0 *5*	0.8 *5*	0.1 *5*	-0.7 *5*	0.4 *0*	0.0 *0*	0.9 *1*	-1.8 *1*	1.5 *5*	-0.6 *0*

Figure F-83. Parametric study: Material stiffness, maximum vertical vibration level relative to basement, mid-span positions

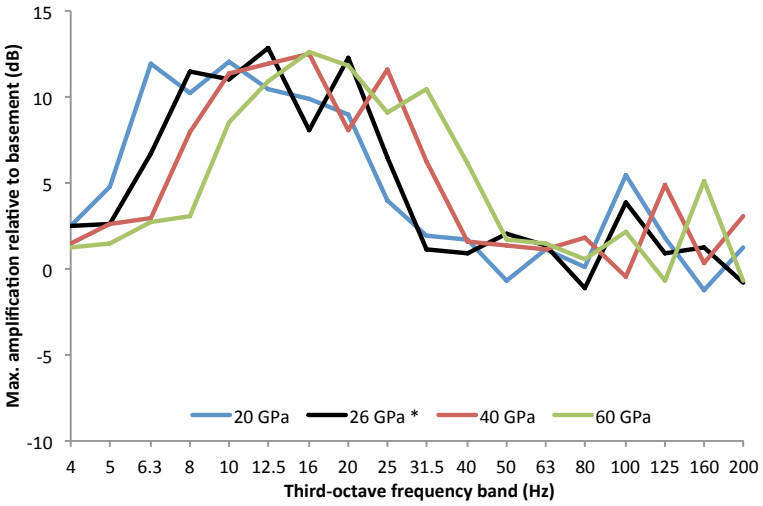

Table F-24. Generic building parametric study: Material stiffness, maximum vertical vibration relative to basement, mid-span positions																				
Young's mod.	Maximum amplification relative to basement level; *Floor level at which maximum occurs*																		Overall	
	1/3 octave band frequency (Hz)																			
	4	5	6.3	8	10	12.5	16	20	25	31.5	40	50	63	80	100	125	160	200	L_{Wb}	L_A
20	2.4 *5*	4.7 *5*	11.9 *5*	10.3 *5*	**12.0** ***1***	10.5 *1*	9.9 *0*	8.9 *0*	4.0 *0*	1.9 *1*	1.7 *0*	-0.6 *0*	1.2 *0*	0.1 *0*	5.4 *0*	1.9 *0*	-1.2 *0*	1.2 *0*	5.5 *0*	2.3 *0*
26 *	2.5 *5*	2.7 *5*	6.7 *5*	11.5 *5*	11.0 *5*	**12.9** ***1***	8.0 *1*	12.2 *0*	6.5 *0*	1.1 *1*	0.9 *5*	2.0 *0*	1.3 *0*	-1.1 *0*	3.8 *0*	0.9 *0*	1.2 *0*	-0.7 *0*	5.2 *0*	1.8 *0*
40	1.5 *5*	2.6 *5*	2.9 *5*	8.0 *5*	11.3 *5*	11.9 *5*	**12.5** ***1***	8.1 *0*	11.6 *0*	6.2 *0*	1.6 *1*	1.3 *1*	1.2 *0*	1.8 *0*	-0.5 *0*	4.8 *0*	0.3 *0*	3.0 *0*	5.2 *0*	2.6 *0*
60	1.3 *5*	1.5 *5*	2.7 *5*	3.1 *5*	8.6 *5*	10.9 *5*	**12.6** ***5***	11.8 *1*	9.1 *0*	10.5 *0*	6.1 *0*	1.7 *1*	1.5 *1*	0.5 *0*	2.1 *0*	-0.7 *0*	5.1 *0*	-0.7 *0*	5.9 *0*	2.2 *0*

Figure F-84. Parametric study: Material stiffness in Young's modulus of elasticity, average vertical vibration level at mid-span relative to column positions, first floor

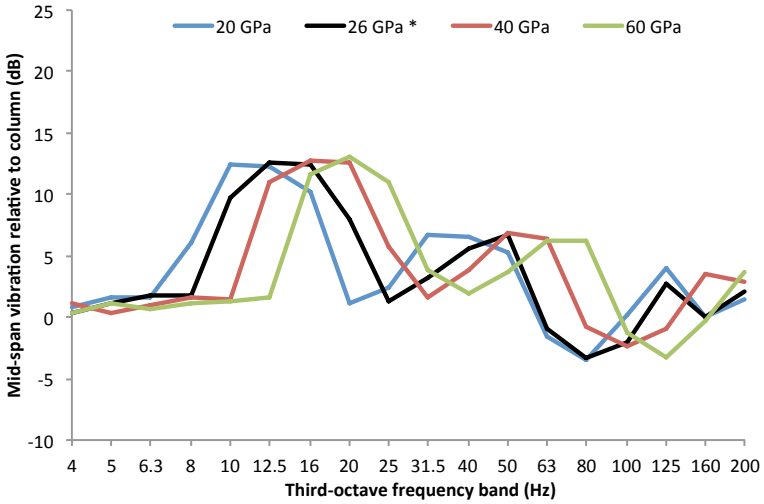

F.13: Input force direction

For discussion of these results, please refer to Section 5.7.1.

Figure F-85. Parametric study: Input force direction (by vector), W_b-weighted basement-relative mid-span acceleration levels with storey

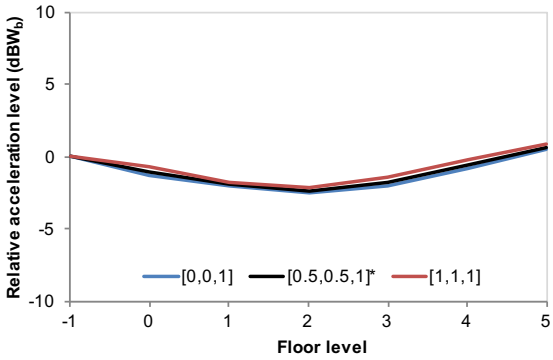

Figure F-86. Parametric study: Input force direction (by vector), A-weighted basement-relative column velocity levels with storey

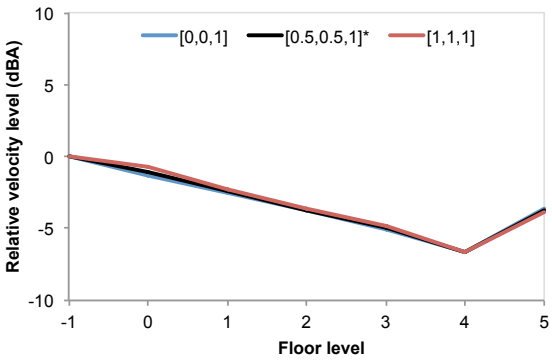

Figure F-87. Parametric study: Input force direction (by vector), W_b-weighted basement-relative mid-span acceleration levels with storey

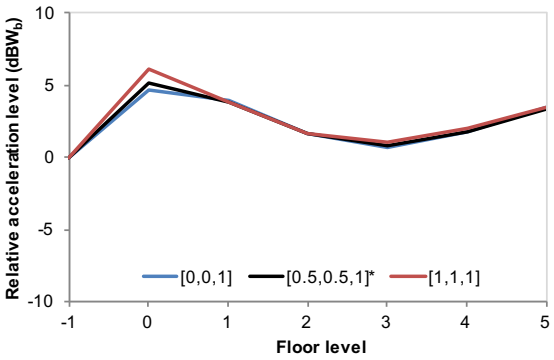

Figure F-88. Parametric study: Input force direction (by vector), A-weighted basement-relative mid-span velocity levels with storey

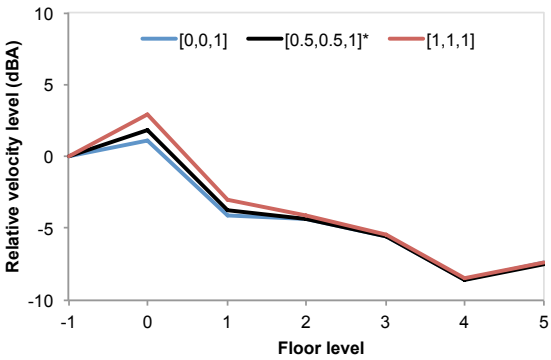

Figure F-89. Parametric study: Input force direction (by vector), maximum vertical vibration level relative to basement, column positions

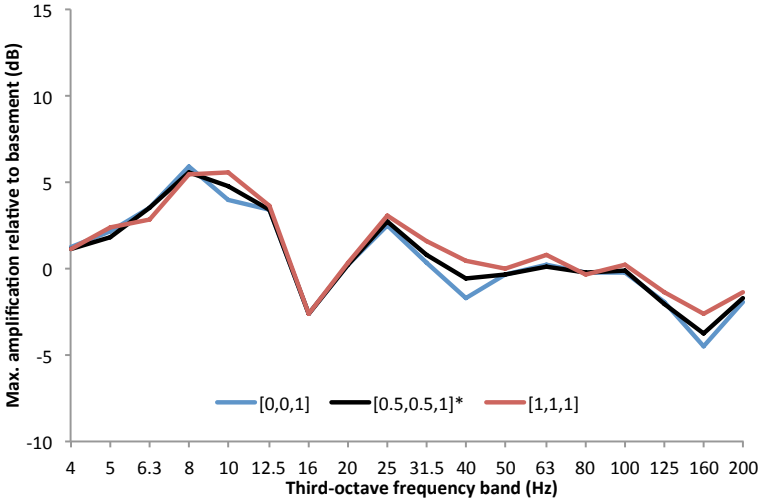

Table F-25. Generic building parametric study: Input force direction, maximum vertical vibration relative to basement, column positions

Force vector [x,y,z]	Maximum amplification relative to basement level; *Floor level at which maximum occurs*																			
	1/3 octave band frequency (Hz)																		Overall	
	4	5	6.3	8	10	12.5	16	20	25	31.5	40	50	63	80	100	125	160	200	L_{Wb}	L_A
[0,0,1]	1.3 *5*	2.2 *5*	3.5 *5*	**5.9** ***5***	3.9 *5*	3.4 *5*	-2.7 *5*	0.2 *0*	2.5 *5*	0.4 *5*	-1.7 *5*	-0.4 *5*	0.2 *5*	-0.2 *0*	-0.2 *0*	-2.0 *0*	-4.5 *0*	-1.9 *0*	0.6 *5*	-1.3 *0*
[0.5,0.5,1]*	1.2 *5*	1.9 *5*	3.5 *5*	**5.6** ***5***	4.8 *5*	3.4 *5*	-2.7 *5*	0.2 *0*	2.7 *5*	0.8 *5*	-0.6 *5*	-0.3 *5*	0.1 *0*	-0.3 *0*	-0.1 *0*	-2.0 *1*	-3.8 *0*	-1.8 *0*	0.7 *5*	-1.1 *0*
[1,1,1]	1.2 *5*	2.4 *5*	2.9 *5*	5.5 *5*	**5.6** ***5***	3.6 *5*	-2.6 *5*	0.3 *5*	3.1 *5*	1.6 *5*	0.5 *5*	0.0 *5*	0.8 *0*	-0.4 *0*	0.2 *0*	-1.3 *1*	-2.6 *0*	-1.4 *0*	0.9 *5*	-0.7 *0*

Figure F-90. Parametric study: Input force direction (by vector), maximum vertical vibration level relative to basement, mid-span positions

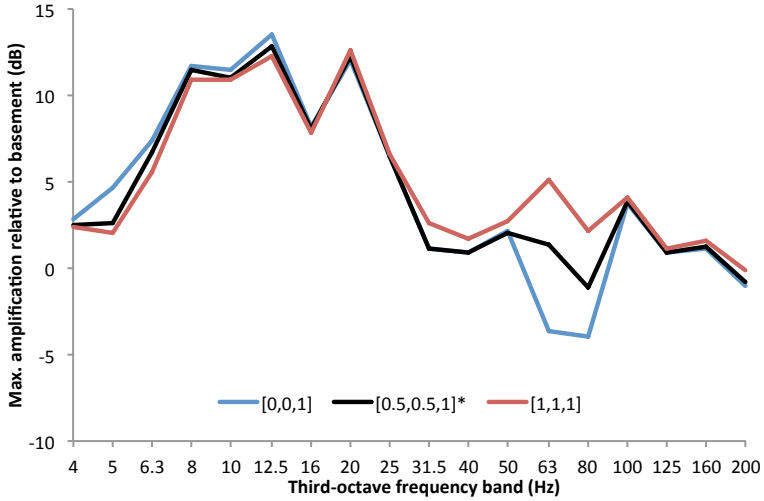

Table F-26. Generic building parametric study: Input force direction, maximum vertical vibration relative to basement, mid-span positions

Force vector [x,y,z]	Maximum amplification relative to basement level; *Floor level at which maximum occurs*																			
	1/3 octave band frequency (Hz)																		Overall	
	4	5	6.3	8	10	12.5	16	20	25	31.5	40	50	63	80	100	125	160	200	L_{Wb}	L_A
[0,0,1]	2.8 *5*	4.7 *5*	7.3 *5*	11.7 *5*	11.5 *5*	**13.5** ***1***	8.1 *1*	12.1 *0*	6.5 *0*	1.2 *1*	0.9 *1*	2.1 *0*	-3.7 *0*	-4.0 *0*	3.8 *0*	0.9 *0*	1.1 *0*	-1.0 *0*	4.7 *0*	1.1 *0*
[0.5,0.5,1]*	2.5 *5*	2.7 *5*	6.7 *5*	11.5 *5*	11.0 *5*	**12.9** ***1***	8.0 *1*	12.2 *0*	6.5 *0*	1.1 *1*	0.9 *5*	2.0 *0*	1.3 *0*	-1.1 *0*	3.8 *0*	0.9 *0*	1.2 *0*	-0.7 *0*	5.2 *0*	1.8 *0*
[1,1,1]	2.4 *5*	2.1 *5*	5.6 *5*	10.9 *5*	10.9 *5*	12.3 *1*	7.8 *0*	**12.6** ***0***	6.6 *0*	2.6 *0*	1.7 *0*	2.8 *0*	5.1 *0*	2.2 *0*	4.0 *0*	1.1 *0*	1.6 *0*	-0.1 *0*	6.1 *0*	2.9 *0*

Figure F-91. Parametric study: Input force direction, average vertical vibration level at mid-span relative to column positions, first floor

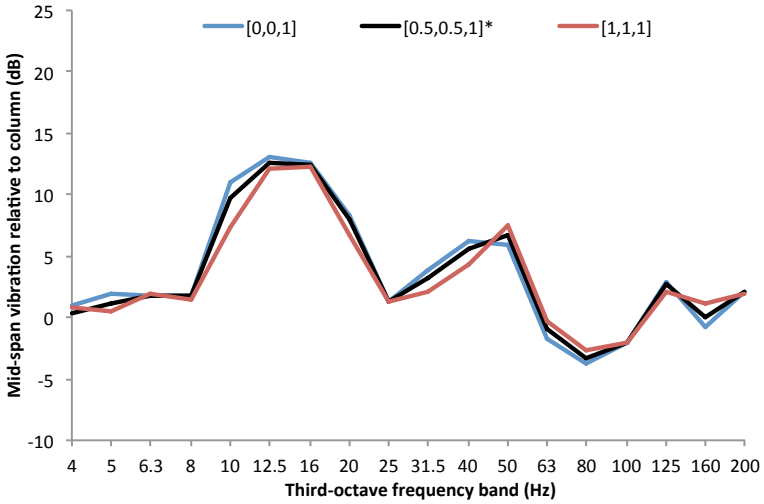

F.14: Input force location

For discussion of these results, please refer to Section 5.7.2.

Figure F-92. Parametric study: Input force location, W_b-weighted basement-relative column acceleration levels with storey

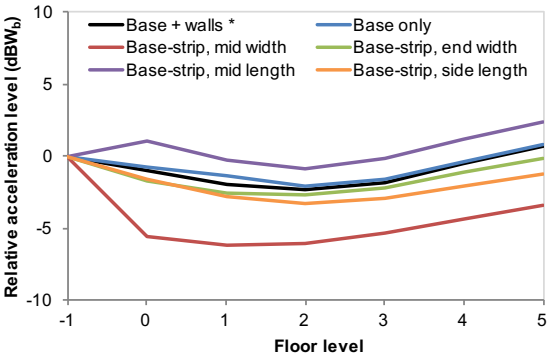

Figure F-93. Parametric study: Input force location, A-weighted basement-relative column velocity levels with storey

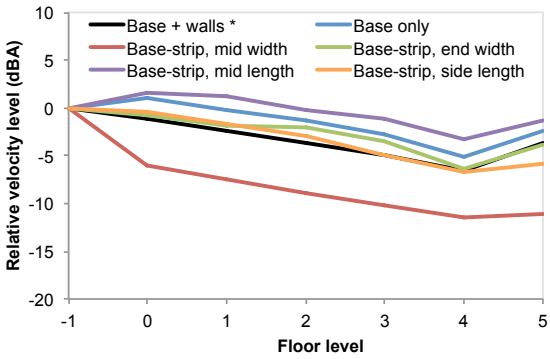

Figure F-94. Parametric study: Input force location, W_b-weighted basement-relative mid-span acceleration levels with storey

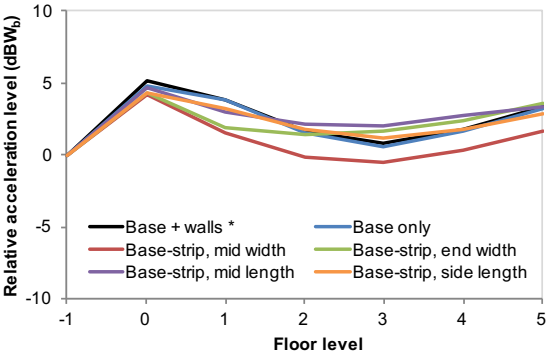

Figure F-95. Parametric study: Input force location, A-weighted basement-relative mid-span velocity levels with storey

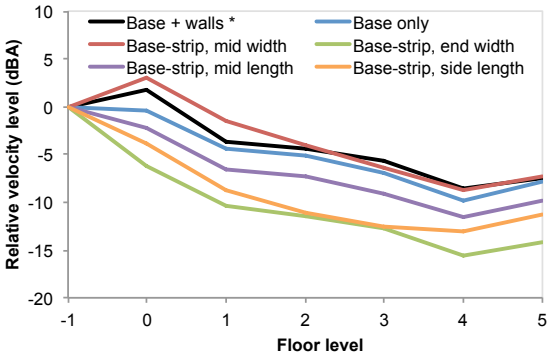

Figure F-96. Parametric study: Input force location, maximum vertical vibration level relative to basement, column positions

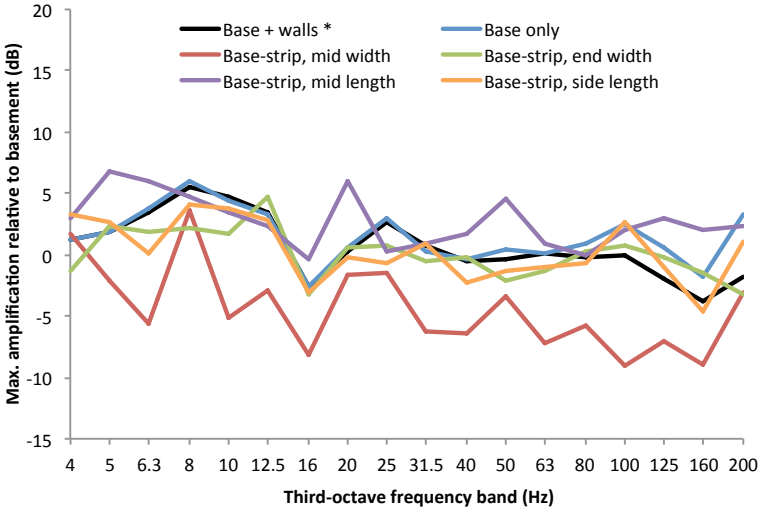

Table F-27. Generic building parametric study: Input force location, maximum vertical vibration relative to basement, column positions																				
Input force	Maximum amplification relative to basement level; *Floor level at which maximum occurs*																		Overall	
	1/3 octave band frequency (Hz)																			
	4	5	6.3	8	10	12.5	16	20	25	31.5	40	50	63	80	100	125	160	200	L_{Wb}	L_A
Base + walls *	1.2 *5*	1.9 *5*	3.5 *5*	**5.6** ***5***	4.8 *5*	3.4 *5*	-2.7 *5*	0.2 *0*	2.7 *5*	0.8 *5*	-0.6 *5*	-0.3 *5*	0.1 *0*	-0.3 *0*	-0.1 *0*	-2.0 *1*	-3.8 *0*	-1.8 *0*	0.7 *5*	-1.1 *0*
Base only	1.2 *5*	1.8 *5*	3.8 *5*	**6.0** ***5***	4.4 *5*	3.3 *5*	-2.6 *5*	0.6 *5*	3.0 *5*	0.3 *5*	-0.3 *5*	0.4 *5*	0.2 *5*	1.0 *0*	2.5 *1*	0.5 *1*	-1.9 *0*	3.2 *0*	0.8 *5*	1.1 *0*
Base-strip, mid width	1.7 *5*	-2.1 *5*	-5.5 *5*	**3.7** ***5***	-5.2 *5*	-2.9 *5*	-8.1 *0*	-1.7 *5*	-1.5 *5*	-6.2 *5*	-6.4 *5*	-3.5 *5*	-7.2 *5*	-5.7 *0*	-9.0 *2*	-7.1 *0*	-8.9 *0*	-3.1 *0*	-3.4 *5*	-6.0 *0*
Base-strip, end width	-1.3 *5*	2.3 *5*	1.9 *5*	2.2 *5*	1.7 *5*	**4.7** ***5***	-3.3 *0*	0.7 *5*	0.8 *5*	-0.5 *5*	-0.2 *5*	-2.2 *5*	-1.3 *5*	0.2 *0*	0.7 *2*	-0.2 *2*	-1.5 *0*	-3.3 *0*	-0.1 *5*	-0.8 *0*
Base-strip, mid length	3.0 *5*	**6.7** ***5***	6.0 *5*	4.8 *5*	3.4 *5*	2.3 *5*	-0.4 *0*	6.0 *5*	0.3 *5*	0.9 *5*	1.6 *5*	4.6 *5*	0.9 *0*	0.0 *0*	2.0 *1*	3.0 *1*	2.1 *0*	2.4 *0*	2.4 *5*	1.7 *0*
Base-strip, side length	3.2 *5*	2.7 *5*	0.1 *5*	4.1 *5*	**3.8** ***5***	2.8 *5*	-3.1 *5*	-0.2 *5*	-0.7 *5*	0.9 *5*	-2.3 *5*	-1.3 *0*	-1.0 *0*	-0.6 *0*	2.6 *0*	-1.1 *0*	-4.6 *0*	1.1 *0*	-1.2 *5*	-0.4 *0*

Figure F-97. Parametric study: Input force location. maximum vertical vibration level relative to basement, mid-span positions

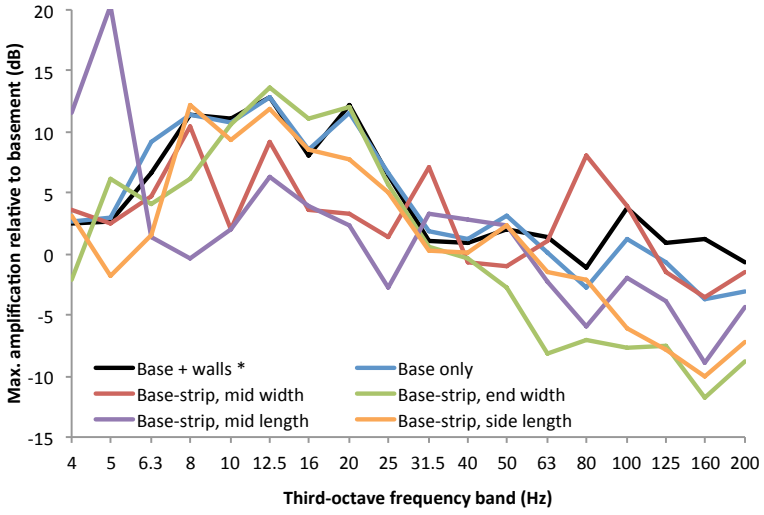

Table F-28. Generic building parametric study: Input force location, maximum vertical vibration relative to basement, mid-span positions																				
Input force	Maximum amplification relative to basement level; *Floor level at which maximum occurs*																		Overall	
	1/3 octave band frequency (Hz)																			
	4	5	6.3	8	10	12.5	16	20	25	31.5	40	50	63	80	100	125	160	200	L_{Wb}	L_A
Base + walls *	2.5 *5*	2.7 *5*	6.7 *5*	11.5 *5*	11.0 *5*	**12.9** ***1***	8.0 *1*	12.2 *0*	6.5 *0*	1.1 *1*	0.9 *5*	2.0 *0*	1.3 *0*	-1.1 *0*	3.8 *0*	0.9 *0*	1.2 *0*	-0.7 *0*	5.2 *0*	1.8 *0*
Base only	2.6 *5*	3.0 *5*	9.2 *5*	11.3 *5*	10.7 *5*	**12.9** ***1***	8.6 *1*	11.6 *0*	6.6 *0*	1.9 *0*	1.2 *5*	3.1 *0*	0.1 *0*	-2.8 *0*	1.2 *0*	-0.7 *0*	-3.7 *0*	-3.1 *0*	4.8 *0*	-0.5 *0*
Base-strip, mid width	3.7 *4*	2.5 *5*	4.7 *5*	**10.5** ***5***	2.1 *1*	9.1 *1*	3.7 *0*	3.2 *0*	1.4 *0*	7.0 *0*	-0.6 *0*	-0.9 *5*	1.1 *0*	8.0 *0*	3.9 *0*	-1.5 *0*	-3.6 *0*	-1.4 *0*	4.2 *0*	3.0 *0*
Base-strip, end width	-2.1 *5*	6.1 *5*	4.1 *5*	6.2 *4*	10.6 *5*	**13.6** ***5***	11.1 *0*	12.1 *0*	5.7 *0*	0.6 *0*	-0.3 *0*	-2.7 *0*	-8.2 *0*	-7.0 *0*	-7.6 *0*	-7.6 *0*	-11.8 *0*	-8.7 *0*	4.4 *0*	-6.3 *0*
Base-strip, mid length	11.5 *5*	**20.3** ***5***	1.4 *5*	-0.4 *5*	2.0 *5*	6.3 *1*	3.9 *0*	2.3 *0*	-2.8 *0*	3.2 *0*	2.8 *0*	2.4 *0*	-2.3 *0*	-5.9 *0*	-1.9 *0*	-3.8 *1*	-8.9 *0*	-4.3 *0*	4.6 *0*	-2.2 *0*
Base-strip, side length	3.1 *5*	-1.8 *0*	1.5 *5*	**12.3** ***5***	9.4 *5*	11.9 *1*	8.5 *0*	7.7 *0*	5.1 *0*	0.3 *5*	0.1 *1*	2.3 *0*	-1.6 *0*	-2.2 *0*	-6.0 *0*	-7.9 *0*	-10.0 *0*	-7.2 *0*	4.3 *0*	-3.9 *0*

Figure F-98. Parametric study: Input force location, average vertical vibration level at mid-span relative to column positions, first floor

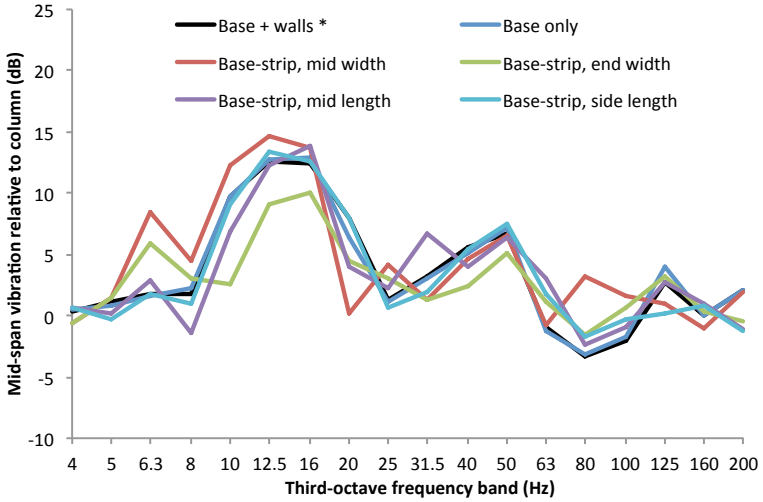

F.15: Other factors

For discussion of these results, please refer to Section 5.8.

Figure F-99. Parametric study: Other factors, W_b-weighted basement-relative mid-span acceleration levels with storey

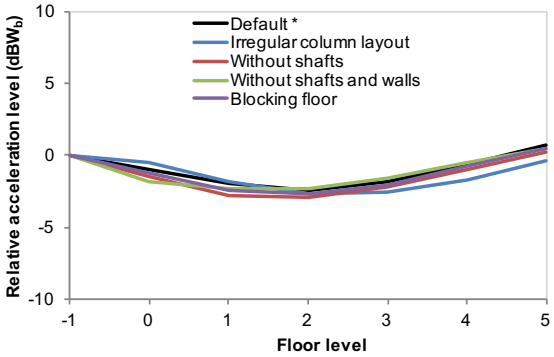

Figure F-100. Parametric study: Other factors, A-weighted basement-relative column velocity levels with storey

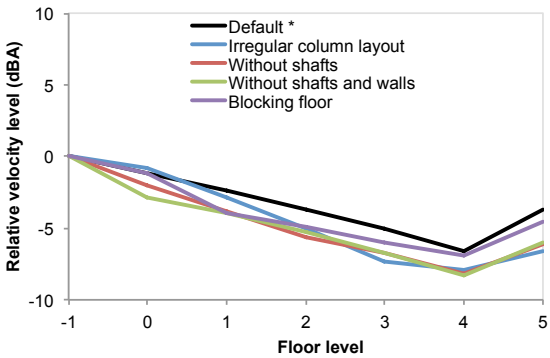

Figure F-101. Parametric study: Other factors, W_b-weighted basement-relative mid-span acceleration levels with storey

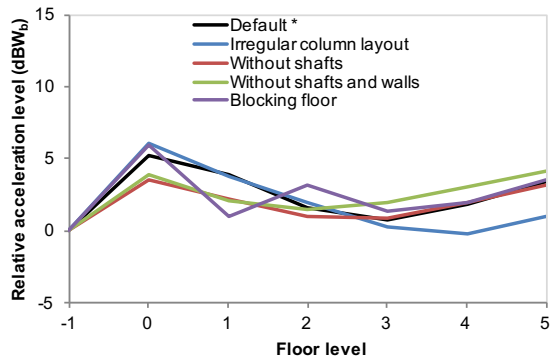

Figure F-102. Parametric study: Other factors, A-weighted basement-relative mid-span velocity levels with storey

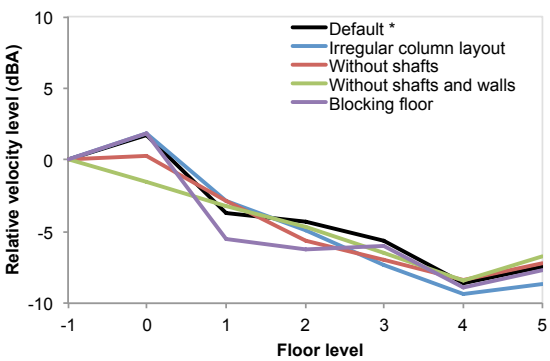

Figure F-103. Parametric study: Other factors, maximum vertical vibration level relative to basement, column positions

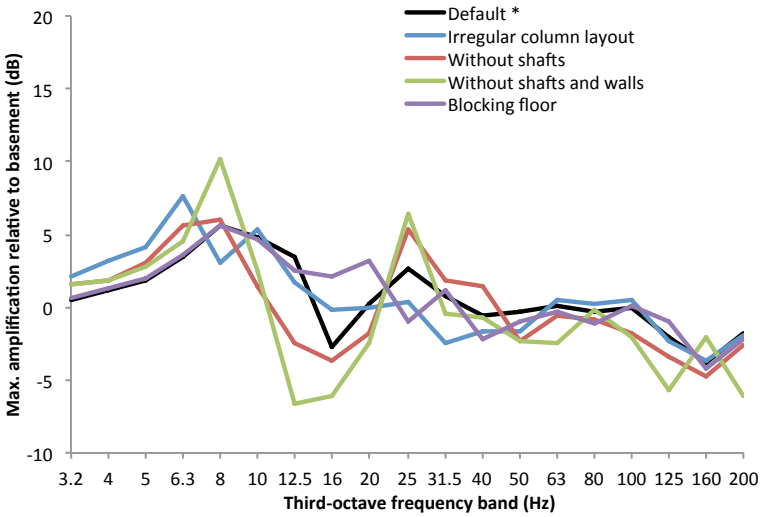

Table F-29. Generic building parametric study: Other factors, maximum vertical vibration relative to basement, column positions

	Maximum amplification relative to basement level; *Floor level at which maximum occurs*																		
	1/3 octave band frequency (Hz)																	Overall	
	4	5	6.3	8	10	12.5	16	20	25	31.5	40	50	63	80	100	125	160	200	L_{Wb}	L_A
Default*	1.2 *5*	1.9 *5*	3.5 *5*	**5.6** ***5***	4.8 *5*	3.4 *5*	-2.7 *5*	0.2 *0*	2.7 *5*	0.8 *5*	-0.6 *5*	-0.3 *5*	0.1 *0*	-0.3 *0*	-0.1 *0*	-2.0 *1*	-3.8 *0*	-1.8 *0*	0.7 *5*	-1.1 *0*
Irregular columns	3.2 *5*	4.2 *5*	**7.7** ***5***	3.1 *5*	5.3 *5*	1.8 *5*	-0.1 *5*	0.0 *5*	0.3 *1*	-2.5 *5*	-1.7 *0*	-1.6 *0*	0.5 *0*	0.3 *0*	0.6 *0*	-2.3 *0*	-3.7 *0*	-2.0 *0*	-0.4 *5*	-0.8 *0*
No shafts	1.8 *5*	3.0 *5*	5.7 *5*	**6.1** ***5***	1.4 *5*	-2.4 *0*	-3.6 *0*	-1.7 *5*	5.3 *5*	1.9 *5*	1.5 *5*	-2.2 *5*	-0.6 *0*	-0.9 *0*	-1.8 *0*	-3.3 *0*	-4.8 *0*	-2.6 *0*	0.3 *5*	-2.1 *0*
No walls	1.8 *5*	2.7 *5*	4.5 *5*	**10.2** ***5***	2.5 *5*	-6.6 *0*	-6.1 *0*	-2.5 *0*	6.4 *5*	-0.5 *5*	-0.6 *5*	-2.3 *5*	-2.4 *5*	-0.2 *0*	-2.1 *1*	-5.6 *0*	-2.0 *0*	-6.0 *0*	0.5 *5*	-2.9 *0*
Blocking floor	1.3 *5*	2.0 *5*	3.6 *5*	**5.6** ***5***	4.7 *5*	2.5 *5*	2.2 *1*	3.3 *5*	-1.0 *5*	1.1 *5*	-2.2 *5*	-1.0 *5*	-0.3 *5*	-1.1 *0*	0.1 *0*	-0.9 *0*	-4.2 *0*	-2.2 *0*	0.4 *5*	-1.1 *0*

Figure F-104. Parametric study: Other factors, maximum vertical vibration level relative to basement, mid-span positions

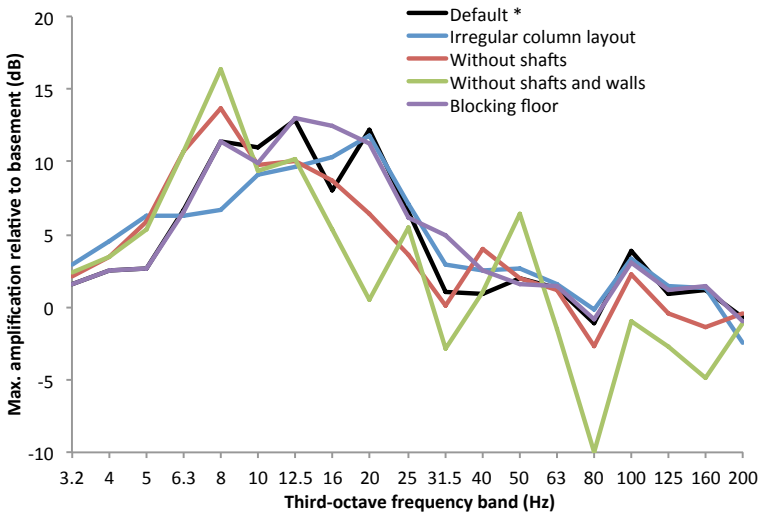

Table F-30. Generic building parametric study: Other factors, maximum vertical vibration relative to basement, mid-span positions																				
	Maximum amplification relative to basement level; *Floor level at which maximum occurs*																		Overall	
	1/3 octave band frequency (Hz)																			
	4	5	6.3	8	10	12.5	16	20	25	31.5	40	50	63	80	100	125	160	200	L_{Wb}	L_A
Default*	2.5	2.7	6.7	11.5	11.0	**12.9**	8.0	12.2	6.5	1.1	0.9	2.0	1.3	-1.1	3.8	0.9	1.2	-0.7	5.2	1.8
	5	*5*	*5*	*5*	*5*	***1***	*1*	*0*	*0*	*1*	*5*	*0*	*0*	*0*	*0*	*0*	*0*	*0*	*0*	*0*
Irregular columns	4.5	6.3	6.3	6.8	9.1	9.7	10.3	**11.8**	7.0	3.0	2.5	2.7	1.6	-0.2	3.3	1.4	1.3	-2.5	6.1	1.9
	5	*5*	*5*	*5*	*5*	*1*	*0*	***0***	*0*	*0*	*0*	*0*	*0*	*0*	*0*	*0*	*0*	*0*	*0*	*0*
No shafts	3.4	5.9	10.7	**13.7**	9.8	10.1	8.7	6.5	3.6	0.1	3.9	2.0	1.2	-2.7	2.3	-0.4	-1.4	-0.5	3.5	0.3
	5	*5*	*5*	***5***	*5*	*1*	*0*	*0*	*5*	*0*	*0*	*1*	*0*	*0*	*0*	*0*	*0*	*0*	*0*	*0*
No walls	3.5	5.4	10.7	**16.4**	9.4	10.2	5.4	0.5	5.4	-2.9	1.1	6.5	-1.5	-10.0	-1.0	-2.8	-4.9	-1.1	4.2	-1.5
	5	*5*	*5*	***5***	*5*	*0*	*0*	*0*	*5*	*5*	*5*	*0*	*5*	*1*	*0*	*0*	*0*	*0*	*5*	*0*
Blocking floor	2.5	2.7	6.6	11.4	10.0	**13.0**	12.4	11.3	6.1	5.0	2.5	1.5	1.4	-0.9	3.1	1.2	1.4	-1.0	6.0	1.8
	5	*5*	*5*	*5*	*5*	***2***	*0*	*1*	*1*	*0*	*0*	*0*	*0*	*0*	*0*	*0*	*0*	*0*	*0*	*0*

Figure F-105. Parametric study: Other factors, average vertical vibration level at mid-span relative to column positions, first floor

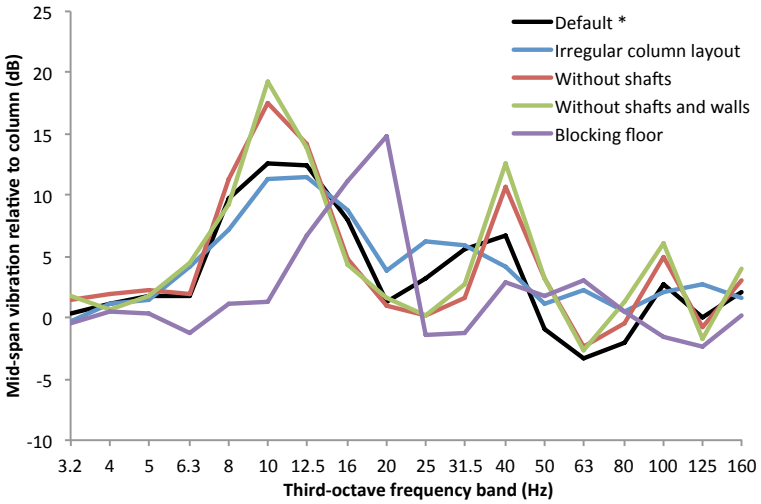

APPENDIX G: RE-RADIATED NOISE MEASUREMENT CASE STUDIES

G.1: Hotel 1, Room 1

At the reference vibration position, a total of 86 train pass-bys were recorded, with the L_{Smax} vertical velocity results (over each pass-by) shown in Figure G-1. The results comprise two different frequency signatures that can be deduced to correspond to trains running in two different directions in the two nearby tunnels, and which are seen to differ above 125 Hz by up to about 10 dB. Within each train type, there is good consistency between pass-bys, with a spread of generally up to around 5 dB.

Figure G-1. Hotel 1, Room 1: maximum velocity level of pass-bys at reference position (86 pass-bys)

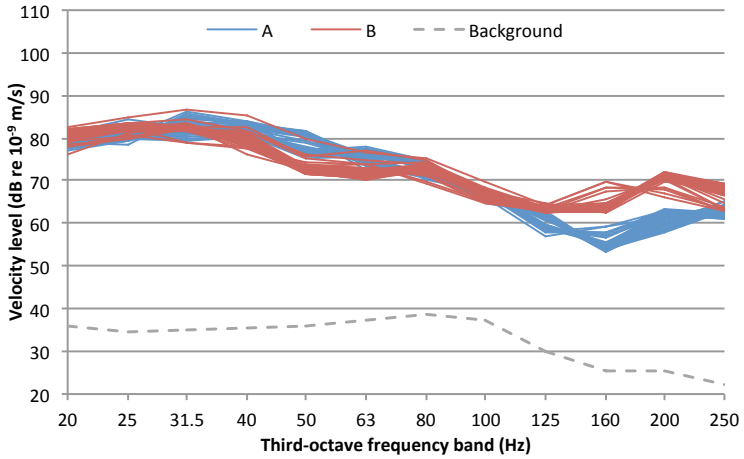

For straightforward comparison of the noise and vibration measurements, train pass-bys have been averaged for results obtained at each vibration or sound pressure measurement position. The averaging was performed by taking a logarithmic mean of the L_{Smax} velocity values in each one-third octave band for each train type, and performing an arithmetic mean over the two train types. For the vibration values, the results for each measurement position are shown in Figure G-2; the sound pressure results at each microphone position are given in Figure G-3. The combined A-weighted average maximum sound pressure level, which takes into account the low frequency spatial distribution (see Equation (2-23)), is 44 dBA.

Figure G-2. Hotel 1, Room 1: average maximum velocity level of pass-bys at various accelerometer measurement positions

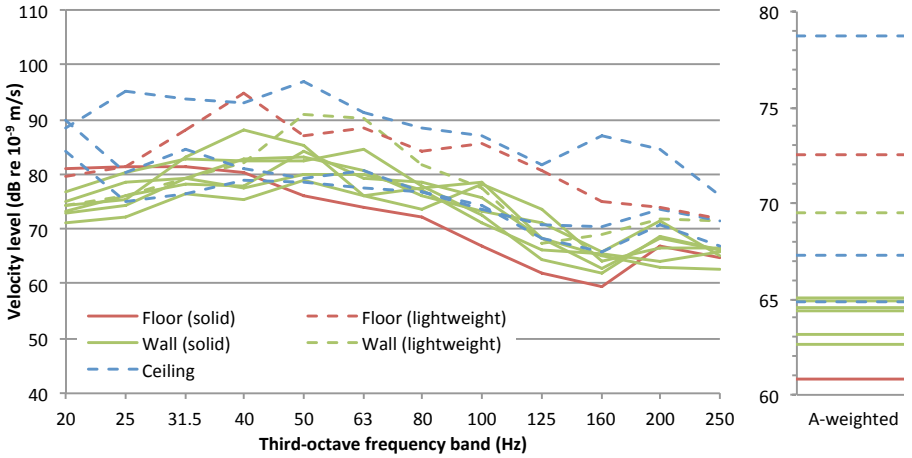

Figure G-3. Hotel 1, Room 1: average maximum sound pressure level of pass-bys at various microphone measurement positions

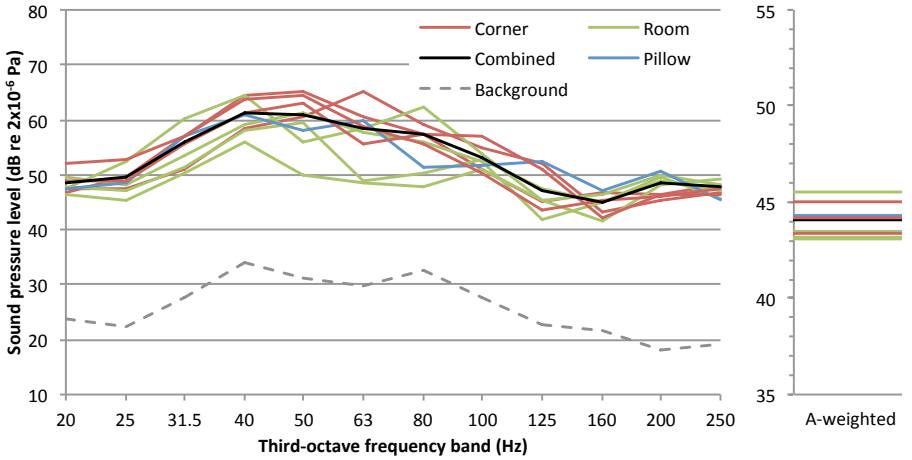

Figure G-2 shows that the vibration levels could vary by up to 15-20 dB when measured at different points on seemingly similar surfaces. This is probably due to modal patterns within the structures, as well as the presence of supporting elements (for lightweight/framed elements). The solid walls seemed to give the more consistent results, generally lying within 5 dB of each other. It should be noted that whilst solid floors might be assumed to give relatively consistent results over their surface, they are usually overlaid with a timber sheet material such as plywood, which provides additional non-uniform characteristics.

Figure G-3 shows that sound pressure levels within the room can vary considerably, up to about 15 dB. The frequency range between 40 and 100 Hz will contain a limited number of modes, which supports the suggestion that it is the modal response that causes the sound pressure levels to be non-uniform in this range. In general, the highest sound pressure levels are at the corner positions, with the lowest at more central room positions. The combined sound pressure level corresponds closely to the pillow position.

The reverberation time results for the room are shown in Table G-1. Although the results are all greater than the minimum values listed in Table 6-1, this room's first mode is estimated to occur at around 50 Hz, so results below this frequency are likely to be dominated by structural resonances and limitations of the instrumentation. They are therefore represented by grey type in the table.

Table G-1. Hotel 1, Room1: reverberation time (T_{30}, s)											
1/3 octave frequency band (Hz)											
20	25	31.5	40	50	63	80	100	125	160	200	250
1.23	1.03	1.07	0.89	0.75	0.57	0.64	0.32	0.42	0.75	0.36	0.43

In order to compare the data from several rooms and thereby identify trends, it is helpful to normalise the sound pressure levels with respect to the reverberation time, which is achieved through the application of Equation (6-1).

The normalised combined sound pressure level is presented in Figure G-4, with the A-weighted spectrum shown on a secondary scale (to the right of the graph). This shows that the frequency range that dominates the overall A-weighted sound pressure level is about 80 to 250 Hz.

Figure G-4. Hotel 1, Room 1: average maximum sound pressure level of pass-bys (combined value) normalised to reverberation time

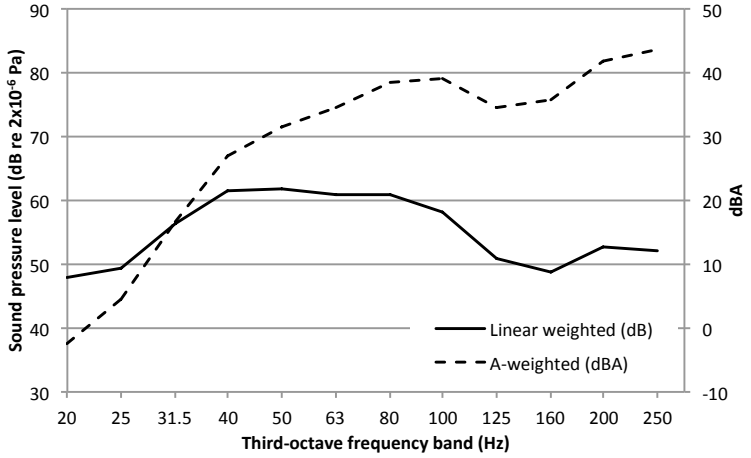

As covered in the literature review, the Kurzweil approach [77] suggests a *LV2P* of -27 dB relative to the floor, and the TCRP research -32 dB [78]. For this particular room geometry, ONR 199005 [80] would suggest a $LV2P_n$ of -24 dB, based on the sound pressure level normalised for reverberation time.

The *LV2P* values obtained from the various vibration measurements and the combined room sound pressure level are shown in Figure G-5. For sound pressure levels normalised by the

reverberation time, the $LV2P_n$ values are shown in Figure G-6. A-weighted values are also shown in the figures; these are calculated from the single figure $L_{p,\mathrm{A}} - L_{v,A}$ values.

Figure G-5. Hotel 1, Room 1: sound pressure level of pass-bys minus velocity level (dB re 2x10⁴ Pa.m⁻¹.s)

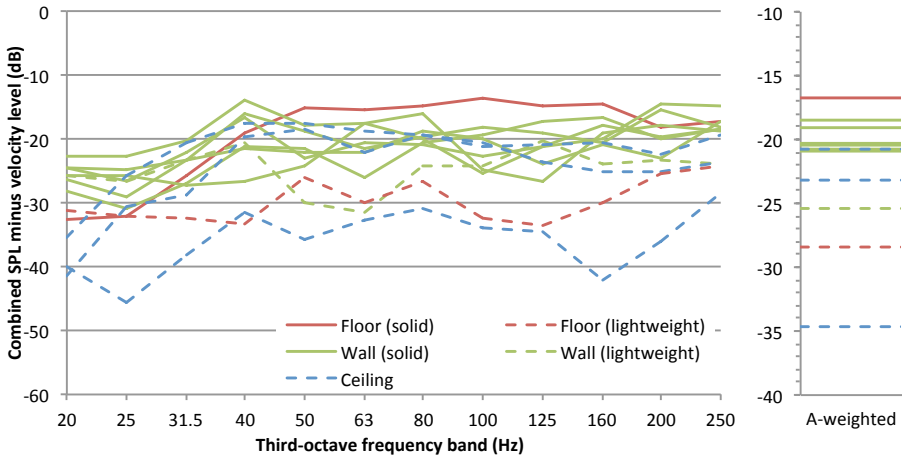

Figure G-6. Hotel 1, Room 1: sound pressure level of pass-bys minus velocity level (normalised to reverberation time) (dB re 2x10⁴ Pa.m⁻¹.s)

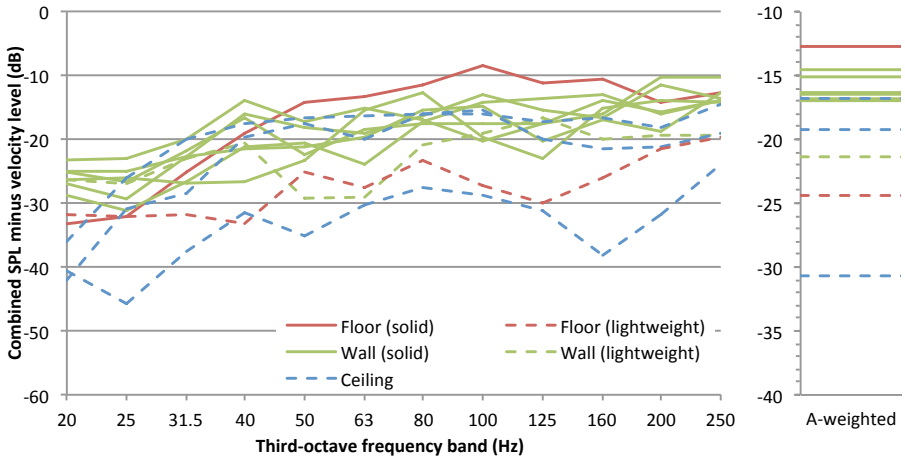

The results show that the *LV2P* and values are not constant with frequency, and this is also the case for the reverberation normalised $LV2P_n$ values. The best agreement with existing guidance is found with the non-normalised lightweight floor location (from the nearby en-suite bathroom) and the Kurzweil approach (i.e. an *LV2P* value of 27 dB). Using the solid floor corner location measurement as a basis for prediction using existing guidance could lead to fairly significant (> 10 dB) under-estimates of the resulting sound pressure level, unless additional corrections are applied to account for mid-floor effects.

Grütz's approach [85,86] for a concrete structure would suggest that to obtain the A-weighted sound pressure level of 44 dBA, the A-weighted vibration velocity level of the surface of interest

would be about 81 dBA; this is similar to the velocity level of the ceiling measurement that exhibited the greatest vibration.

G.2: Hotel 1, Room 2

At the reference vibration position on the floor, a total of 68 train pass-bys were recorded, with the L_{Smax} vertical velocity results shown in Figure G-7. These comprise two different frequency signatures that are assumed to correspond to trains running in two different directions in the two nearby tunnels, and which are seen to differ above 50 Hz by up to about 15 dB. Within each train type, there is good consistency between pass-bys, with a spread of generally less than 5 dB.

Figure G-7. Hotel 1, Room 2: maximum velocity level of pass-bys at reference position (68 pass-bys)

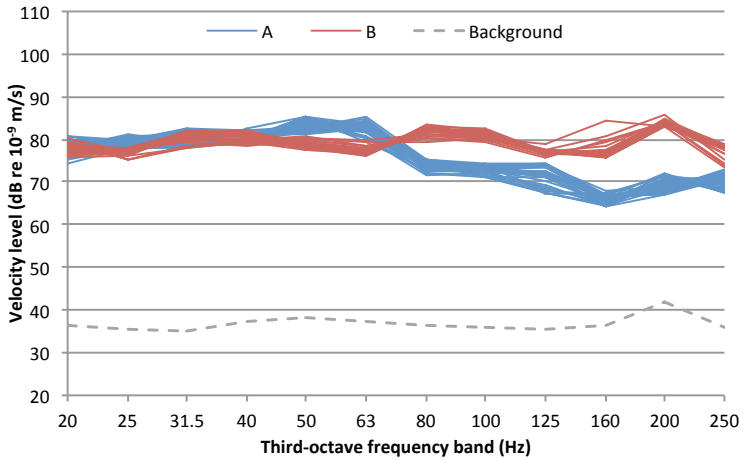

Average L_{Smax} velocity values in each one-third octave band for each measurement position are shown in Figure G-8; the sound pressure results at each microphone position are given in Figure G-9. The combined A-weighted average maximum sound pressure level is 45 dBA.

Figure G-8. Hotel 1, Room 2: average maximum velocity level of pass-bys at various accelerometer measurement positions

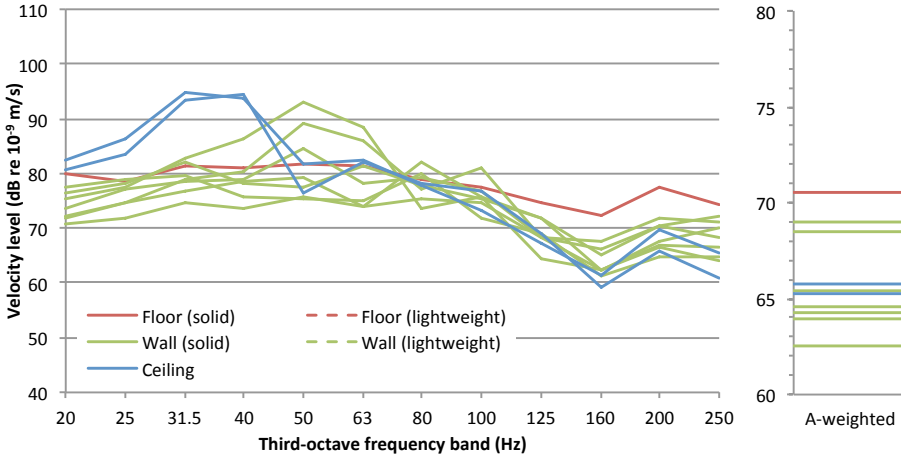

Figure G-9. Hotel 1, Room 2: average maximum sound pressure level of pass-bys at various microphone measurement positions

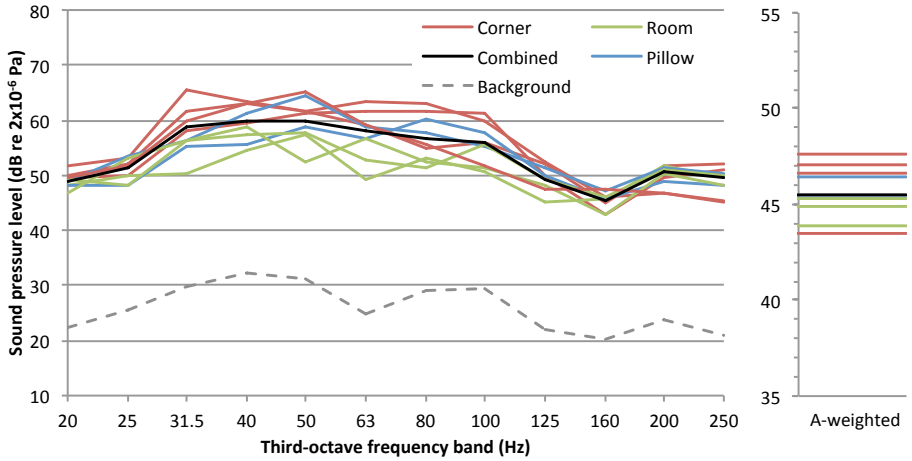

Figure G-8 shows that the vibration levels could vary by up to 10-15 dB when measured at different points on seemingly similar surfaces. The floor gave the highest vibration levels at the upper frequency range (above 100 Hz), with the ceiling giving the highest levels at the low end of the frequency range (below 50 Hz). Most of the walls gave results which were reasonably consistent with the ceilng above 50 Hz, which is interesting given the fact that the wall vibration measurements were in the horizontal plane whereas the ceiling measurements were in the vertical plane.

Figure G-9 shows that sound pressure levels within this room varied by up to about 15 dB, due to acoustic modes. The highest sound pressure levels are at the corner positions, with the lowest at more central room positions. The combined sound pressure level again corresponded closely to the pillow position.

The reverberation time results for the room are shown in Table G-2. The results are all greater than the minimum values listed in Table 6-1; results below the 40 Hz band are likely to be dominated by structural resonances and limitations of the instrumentation.

Table G-2. Hotel 1, Room 2: reverberation time (T_{30}, s)

1/3 octave frequency band (Hz)											
20	25	31.5	40	50	63	80	100	125	160	200	250
1.24	1.74	1.28	1.20	0.77	0.72	0.50	0.35	0.30	0.40	0.39	0.27

The combined sound pressure level normalised by reverberation time is presented in Figure G-10, with the A-weighted spectrum shown on a secondary scale (to the right of the graph). This shows that the frequency range that dominated the overall A-weighted sound pressure level is about 80 to 250 Hz.

Figure G-10. Hotel 1, Room 2: average maximum sound pressure level of pass-bys (combined value) normalised to reverberation time

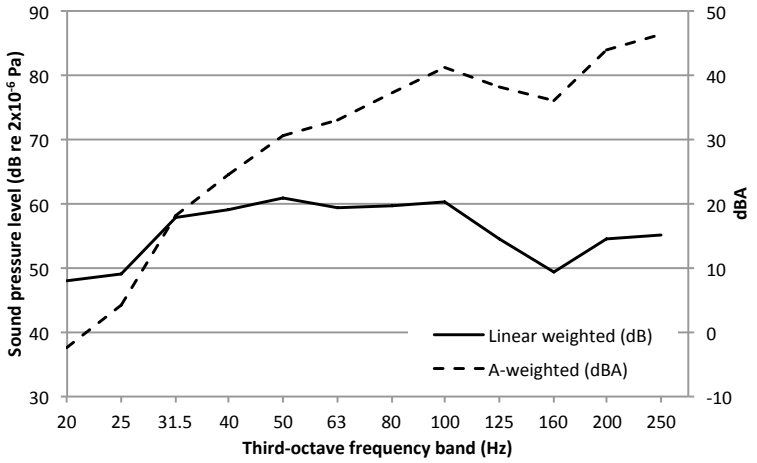

The *LV2P* values obtained from the various vibration measurements and the combined room sound pressure level are shown in Figure G-11. For sound pressure levels normalised by the reverberation time, the $LV2P_n$ values are shown in Figure G-12. For this particular room geometry, ONR 199005 would suggest a $LV2P_n$ of -24 dB.

The results show that the *LV2P* and $LV2P_n$ values are not constant with frequency. Nevertheless, use of Kurzweil's prediction approach (-27 dB) with the non-normalised solid floor vibration measurement as a basis (even though this was not in the centre of the room) would have resulted in A-weighted sound pressure levels that were within two or three decibels of those measured.

Grütz's approach for a concrete structure would suggest that to obtain the A-weighted sound pressure level of 45 dBA, the A-weighted vibration velocity level of the surface of interest would be about 84 dBA; this is significantly greater than any of the measurement positions.

Figure G-11. Hotel 1, Room 2: sound pressure level of pass-bys minus velocity level (dB re 2x10⁴ Pa.m⁻¹.s)

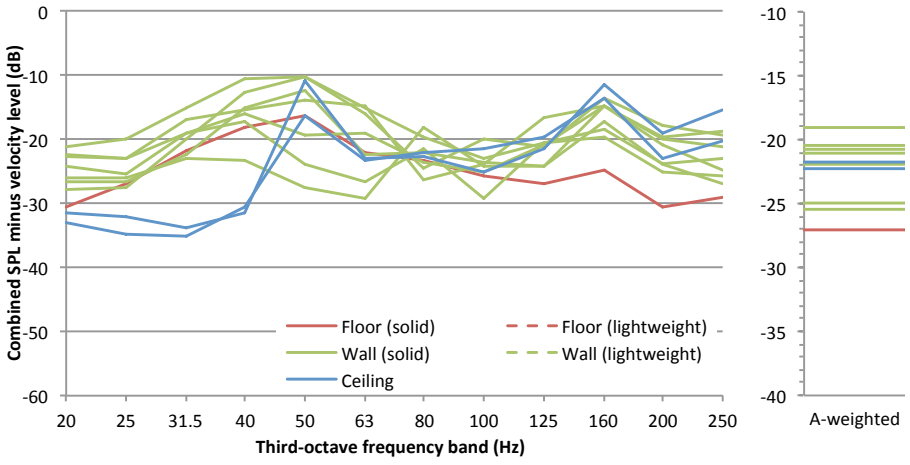

Figure G-12. Hotel 1, Room 2: sound pressure level of pass-bys minus velocity level (normalised to reverberation time) (dB re $2x10^{4}$ $Pa.m^{-1}.s$)

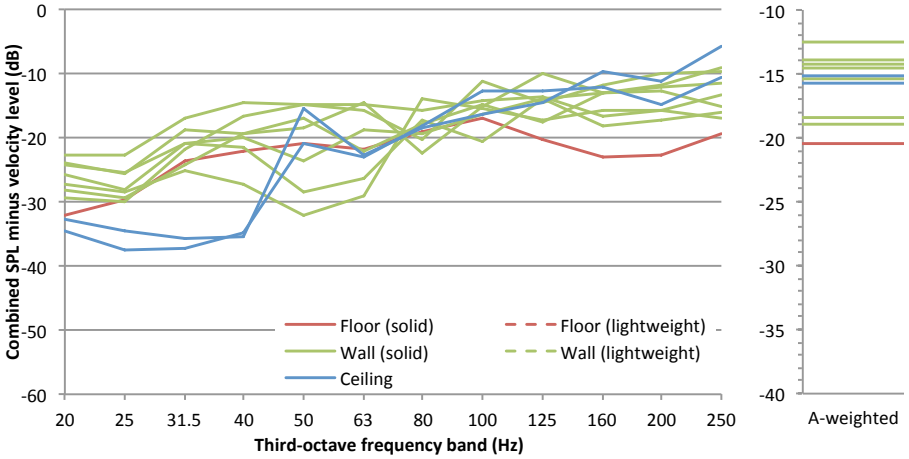

G.3: Hotel 1, Room 3

At the reference vibration position, a total of 56 train pass-bys were recorded, with the L_{Smax} vertical velocity results shown in Figure G-13. These comprise two different frequency signatures that are assumed to correspond to trains running in two different directions in the two nearby tunnels, and which are seen to differ above 63 Hz by up to about 15 dB. Within each train type, there is good consistency between pass-bys, with a spread of generally up to around 5 dB.

Figure G-13. Hotel 1, Room 3: maximum velocity level of pass-bys at reference position (56 pass-bys)

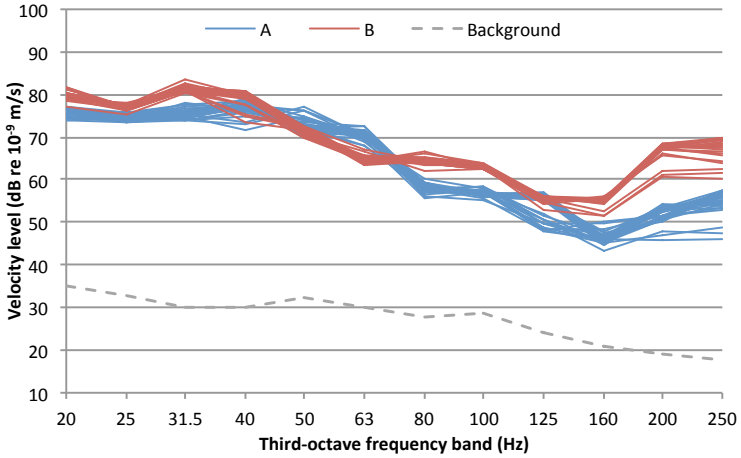

Average L_{Smax} velocity values in each one-third octave band for each measurement position are shown in Figure G-14; the sound pressure results at each microphone position are given in Figure G-15. The combined A-weighted average maximum sound pressure level is 37 dBA.

Figure G-14. Hotel 1, Room 3: average maximum velocity level of pass-bys at various accelerometer measurement positions

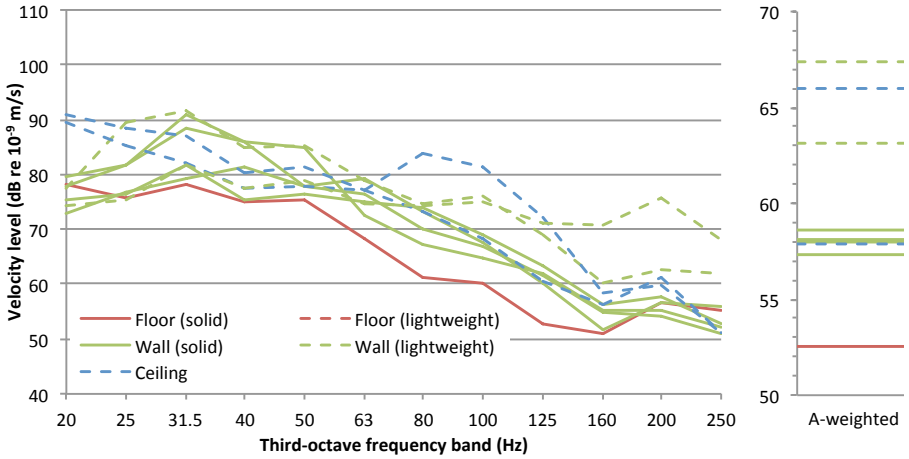

Figure G-15. Hotel 1, Room 3: average maximum sound pressure level of pass-bys at various microphone measurement positions

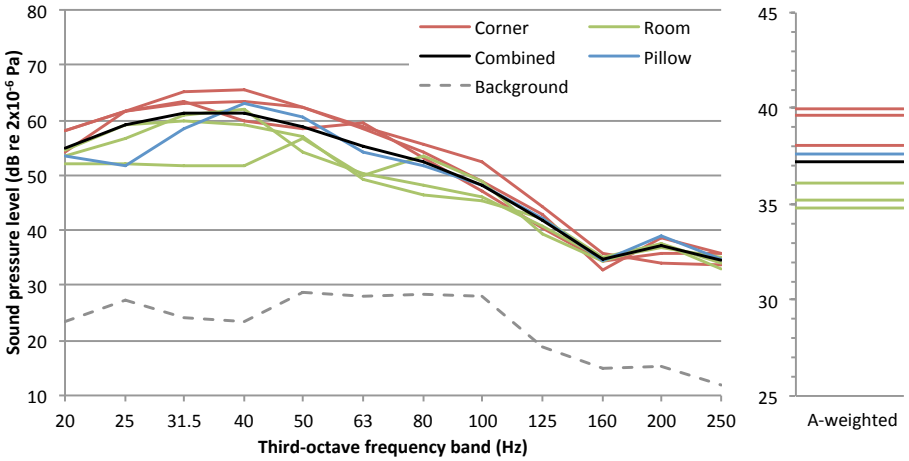

Figure G-14 shows that the vibration levels could vary by up to 10-15 dB when measured at different points on seemingly similar surfaces. The floor gave the lowest vibration levels for the majority of the frequecy range, whilst above 100 Hz the lightweight walls had the highest vibration levels.

Figure G-15 shows that sound pressure levels within this room varied by up to about 15 dB, due to acoustic modes. The highest sound pressure levels are at the corner positions, with the lowest at more central room positions. The combined sound pressure level parameter again represented the pillow position well. There was a reduced sound pressure level at high frequencies compared with other rooms measured in this building. This room was located on the opposite side of the building to the other rooms, and further away from the railway source, which was in a shallow 'cut-and-cover' track construction. It is therefore likely that there are high frequency losses across the building structure which are causing the reduced sound pressure levels in this frequency range for this room.

The reverberation time results for the room are shown in Table G-3. The results are all greater than the minimum values listed in Table 6-1; results below the 31.5 Hz band are likely to be dominated by structural resonances and limitations of the instrumentation.

Table G-3. Hotel 1, Room 3: reverberation time (T_{30}, s)											
1/3 octave frequency band (Hz)											
20	25	31.5	40	50	63	80	100	125	160	200	250
1.16	1.48	1.34	0.89	0.80	0.68	0.83	0.48	0.34	0.28	0.33	0.26

The reverberation time normalised combined sound pressure level is presented in Figure G-16, with the A-weighted spectrum shown on a secondary scale (to the right of the graph). This shows that the overall A-weighted sound pressure level has a reasonably uniform frequency contribution above 31.5 Hz.

Figure G-16. Hotel 1, Room 3: average maximum sound pressure level of pass-bys (combined value) normalised to reverberation time

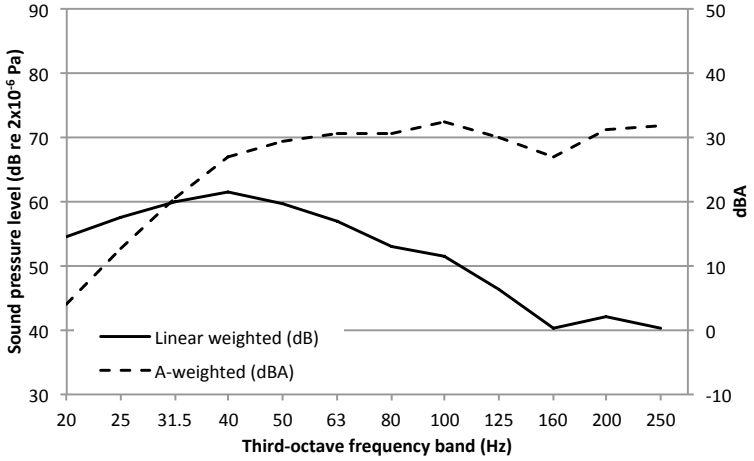

The *LV2P* values obtained using the various vibration measurements and the combined room sound pressure level are shown in Figure G-17. For sound pressure levels normalised by the reverberation time, the *LV2P* values are shown in Figure G-18. For this particular room geometry, ONR 199005 would suggest a $LV2P_n$ of -24 dB.

The results show that the most consistent difference between sound pressure level and vibration levels is achieved with the solid wall vibration levels, which were about 20 dB greater than the combined sound pressure level (non-normalised to reverberation time).

Grütz's approach for a concrete structure would suggest that to obtain the A-weighted sound pressure level of 37 dBA, the A-weighted vibration velocity level of the surface of interest would be about 70 dBA; this is somewhat greater than any of the measurement positions.

Figure G-17. Hotel 1, Room 3: sound pressure level of pass-bys minus velocity level (dB re $2x10^{4}$ $Pa.m^{-1}.s$)

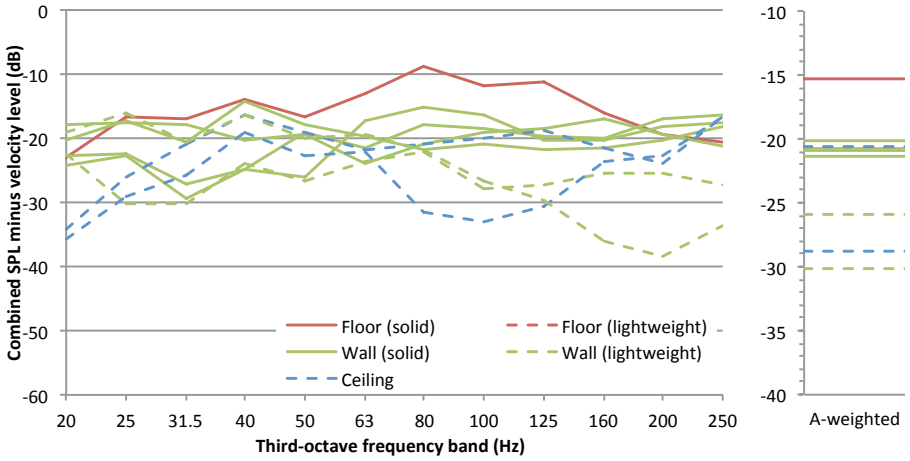

Figure G-18. Hotel 1, Room 3: sound pressure level of pass-bys minus velocity level (normalised to reverberation time) (dB re $2x10^{4}$ $Pa.m^{-1}.s$)

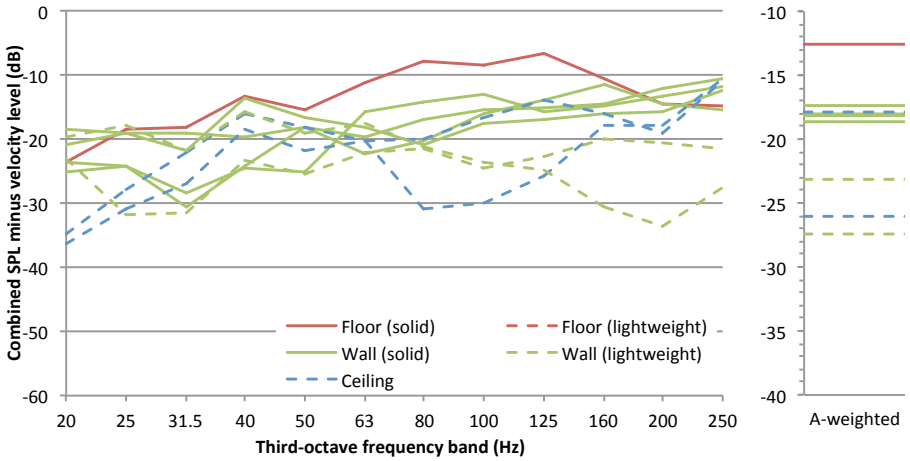

G.4: Hotel 2, Room 1

At the reference vibration position on the floor, a total of 113 train pass-bys were recorded, with the L_{Smax} vertical velocity results shown in Figure G-19. These comprise mainly two different frequency signatures which are seen to differ across the frequency range by up to about 15 dB. The dominant frequency signatures are likely to be due to trains running on two nearby lines; the District/Circle Line, and the Bakerloo line. Within each train type, there is good consistency between pass-bys, with a spread of generally up to around 5 dB, although the results designated as train type B (in Figure G-19) exhibited a spread of up to 15-20 dB in the 63 and 80 Hz bands. This could be due to variability in rolling stock or operational speed.

Figure G-19. Hotel 2, Room 1: maximum velocity level of pass-bys at reference position (113 pass-bys)

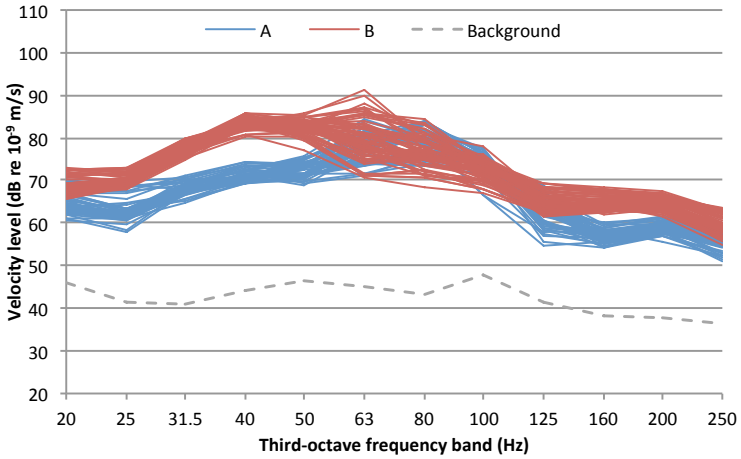

Average L_{Smax} velocity values in each one-third octave band for each measurement position are shown in Figure G-20 (note that the windowsill position has been grouped as a solid floor measurement); the sound pressure results at each microphone position are given in Figure G-21. The combined A-weighted average maximum sound pressure level is 41 dBA.

Figure G-20. Hotel 2, Room 1: average maximum velocity level of pass-bys at various accelerometer measurement positions

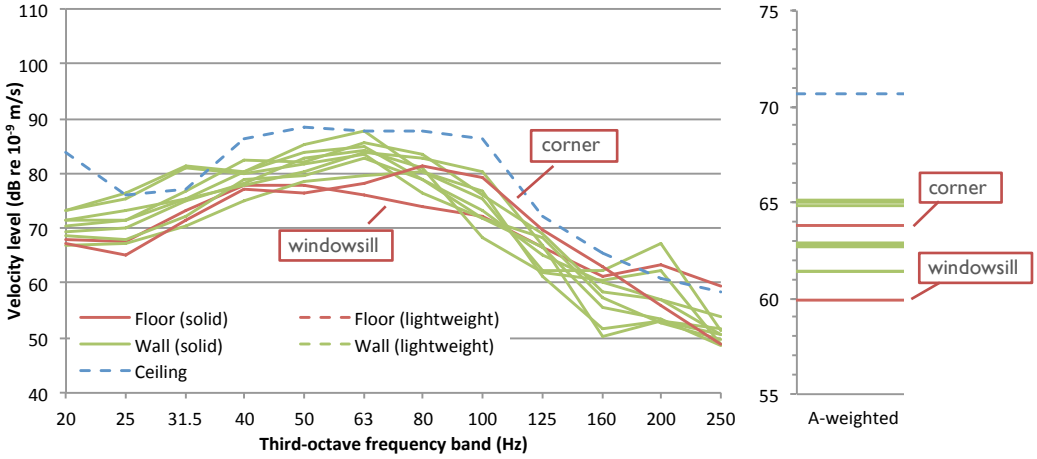

Figure G-21. Hotel 2, Room 1: average maximum sound pressure level of pass-bys at various microphone measurement positions

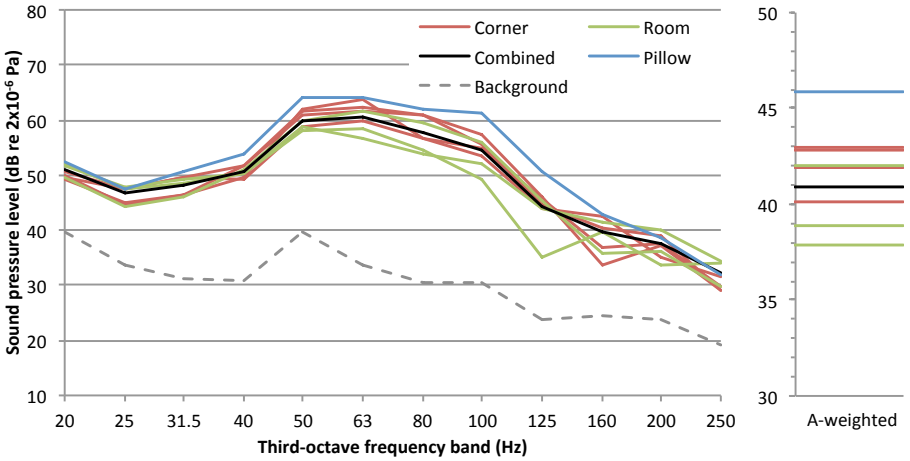

Figure G-20 shows that the vibration levels varied by up to 10 dB when measured at different points on seemingly similar surfaces. The ceiling exhibited the greatest vibration levels; about 10 dB greater than the floor measurements for the majority of the frequecy range.

Figure G-21 shows that sound pressure levels within this room varied by up to about 15 dB, due to acoustic modes. The greatest sound pressure levels are at the corner positions, with the least at the more central room positions. Note that for this room, the pillow measurement position was at a corner.

The reverberation time results for the room are shown in Table G-4. The results are all greater than the minimum values listed in Table 6-1; results below the 63 Hz band are likely to be dominated by structural resonances and limitations of the instrumentation.

Table G-4. Hotel 2, Room 1: reverberation time (T_{30}, s)											
1/3 octave frequency band (Hz)											
20	25	31.5	40	50	63	80	100	125	160	200	250
1.42	1.37	0.86	0.66	0.90	1.02	0.42	0.50	0.28	0.34	0.28	0.34

The combined sound pressure level normalised by the reverberation time is presented in Figure G-22, with the A-weighted spectrum shown on a secondary scale (to the right of the graph). This shows that the overall A-weighted sound pressure level is dominated by contributions between 50 and 160 Hz.

Figure G-22. Hotel 2, Room 1: average maximum sound pressure level of pass-bys (combined value) normalised to reverberation time

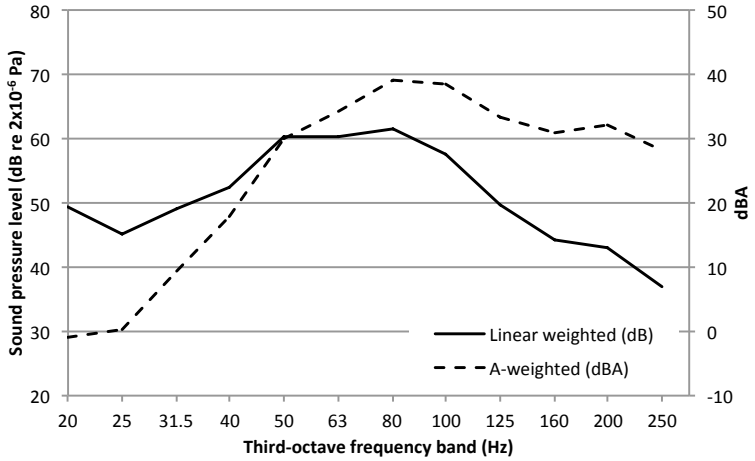

The *LV2P* values for the various vibration measurements and the combined room sound pressure level are shown in Figure G-23. For sound pressure levels normalised to the reverberation time, the $LV2P_n$ values are shown in Figure G-24. For this particular room geometry, ONR 199005 would suggest a $LV2P_n$ of -23 dB.

The results show that none of the surface vibration measurements provide a consistent difference with sound pressure level. Nevertheless, reasonable agreement with respect to existing guidance is found by applying the Kurzweil *LV2P* value of -27 dB to the floor corner vibration measurements; this approach would have resulted in an underestimate of the sound pressure level (at a central room position) of about 2 dB. Applying the ONR 199005 prediction would have provided similar agreement.

Grütz's approach for a concrete structure would suggest that to obtain the A-weighted sound pressure level of 41 dBA, the A-weighted vibration velocity level of the surface of interest would be about 76 dBA; this is somewhat greater than any of the measurement positions.

Figure G-23. Hotel 2, Room 1: sound pressure level of pass-bys minus velocity level (dB re $2x10^4$ Pa.m^{-1}.s)

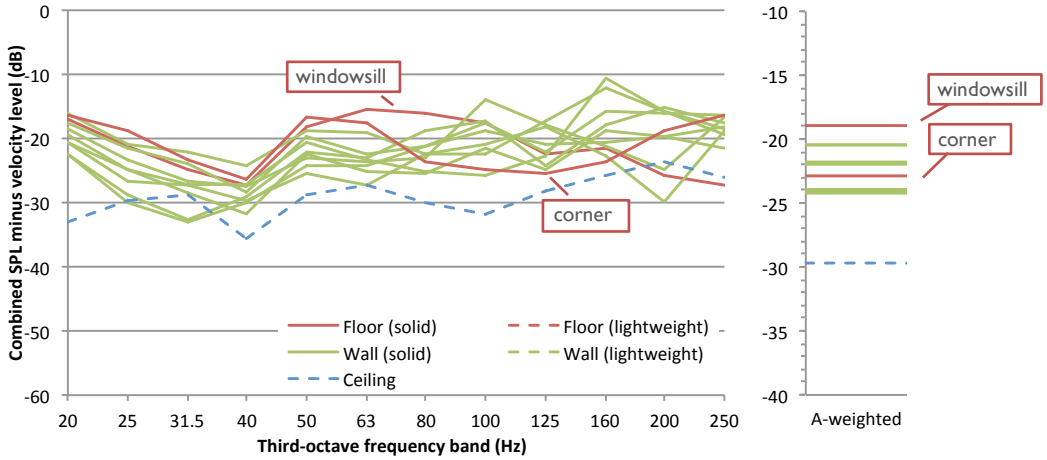

Figure G-24. Hotel 2, Room 1: sound pressure level of pass-bys minus velocity level (normalised to reverberation time) (dB re $2x10^4$ Pa.m^{-1}.s)

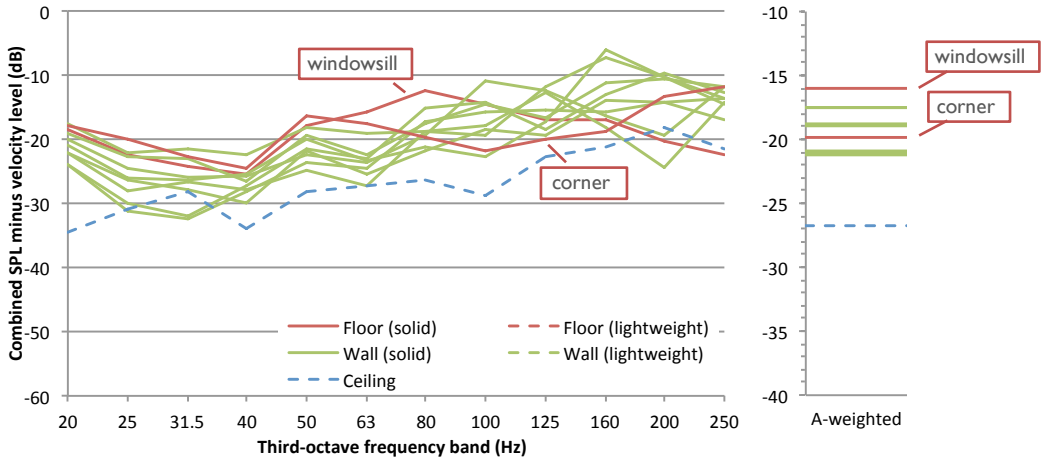

G.5: Hotel 2, Room 2

At the reference vibration position on the floor, a total of 96 train pass-bys were recorded, with the L_{Smax} vertical velocity results shown in Figure G-25. These comprise mainly two different frequency signatures which are seen to differ across the frequency range by up to about 20 dB.

The dominant frequency signatures are likely to be due to trains running on two nearby lines; the District/Circle Line, and the Bakerloo line. Within each train type, there is fairly good consistency between pass-bys, with a spread of generally around 5 dB, although the results designated as train type B exhibited a spread of closer to 10 dB in the 63 and 125 Hz bands.

Figure G-25. Hotel 2, Room 2: maximum velocity level of pass-bys at reference position (96 pass-bys)

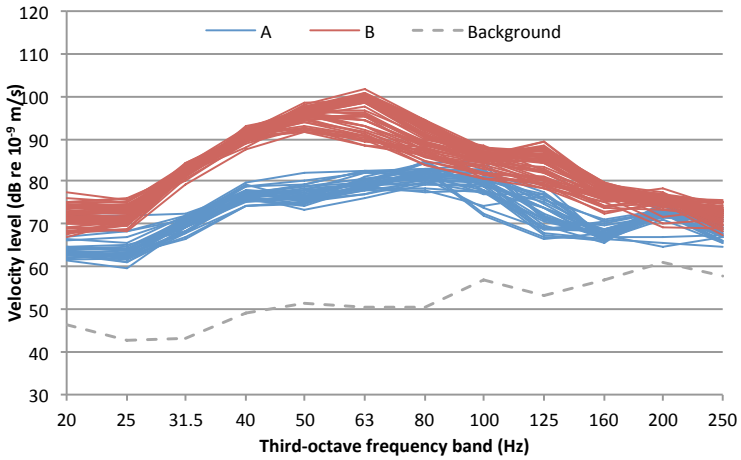

Average L_{Smax} velocity values in each one-third octave band for each measurement position are shown in Figure G-26; the sound pressure results at each microphone position are given in Figure G-27. The combined A-weighted average maximum sound pressure level is 42 dBA.

Figure G-26. Hotel 2, Room 2: average maximum velocity level of pass-bys at various accelerometer measurement positions

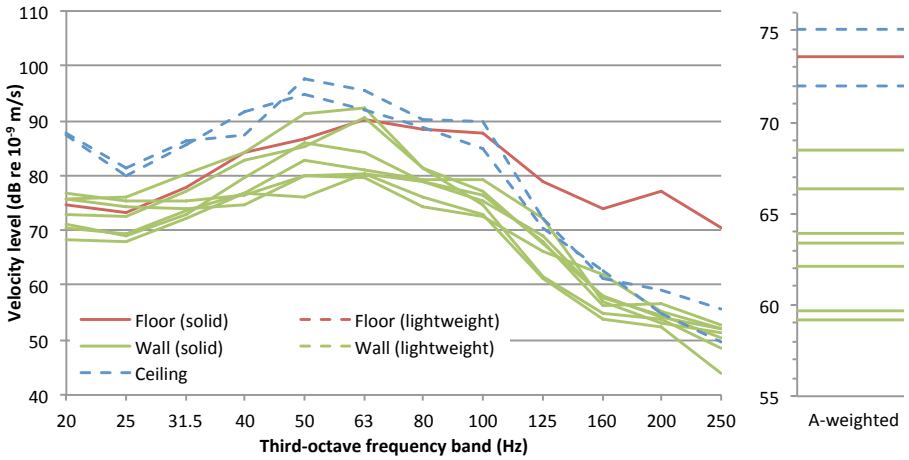

Figure G-27. Hotel 2, Room 2: average maximum sound pressure level of pass-bys at various microphone measurement positions

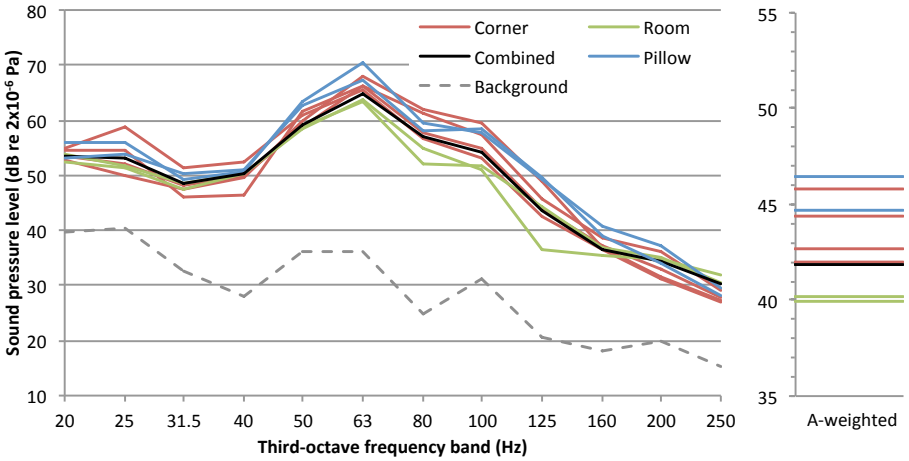

Figure G-26 shows that the vibration levels varied by up to about 15 dB when measured at different points on seemingly similar surfaces. The ceiling exhibited the greatest vibration levels below 100 Hz; about 5-10 dB greater than the floor measurements. Above 100 Hz, the floor exhibited the greatest vibration levels, up to 10-15 dB more than the other surfaces at 250 Hz.

Figure G-27 shows that sound pressure levels within this room varied by up to about 10 dB, due to acoustic modes. The greatest sound pressure levels are at the corner positions, with the least at more central room positions. Note that for this room, the pillow measurement positions were also at corners of the room.

The reverberation time results for the room are shown in Table G-5. The results are all greater than the minimum values listed in Table 6-1; results below the 63 Hz band are likely to be dominated by structural resonances and limitations of the instrumentation.

Table G-5. Hotel 2, Room 2: reverberation time (T_{30}, s)

1/3 octave frequency band (Hz)											
20	25	31.5	40	50	63	80	100	125	160	200	250
1.59	1.55	1.10	0.64	0.53	0.77	0.45	0.34	0.40	0.48	0.33	0.29

The combined sound pressure level normalised to the reverberation time is presented in Figure G-28, with the A-weighted spectrum shown on a secondary scale (to the right of the graph). This shows that the overall A-weighted sound pressure level is dominated by contributions between 50 and 160 Hz.

Figure G-28. Hotel 2, Room 2: average maximum sound pressure level of pass-bys (combined value) normalised to reverberation time

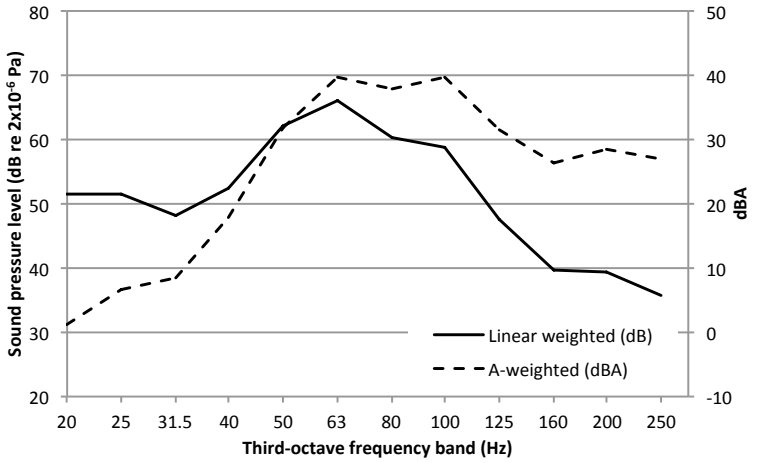

The *LV2P* values for the various vibration measurements and the combined room sound pressure level are shown in Figure G-29. For sound pressure levels normalised to the reverberation time, the $LV2P_n$ values are shown in Figure G-30. For this particular room geometry, ONR 199005 would suggest a $LV2P_n$ of -24 dB.

The results show that none of the surface vibration measurements provide a consistent difference with sound pressure level. The best agreement with respect to existing guidance is found with the floor results and the TCRP *LV2P* value of -32 dB, which would likely to overpredict the A-weighted sound pressure level near the centre of the room by around 2 dB.

Grütz's approach for a concrete structure would suggest that to obtain the A-weighted sound pressure level of 42 dBA, the A-weighted vibration velocity level of the surface of interest would be about 77 dBA; this is within a few decibels of the ceiling position with the greatest vibration levels.

Figure G-29. Hotel 2, Room 2: sound pressure level of pass-bys minus velocity level (dB re 2x10⁴ Pa.m⁻¹.s)

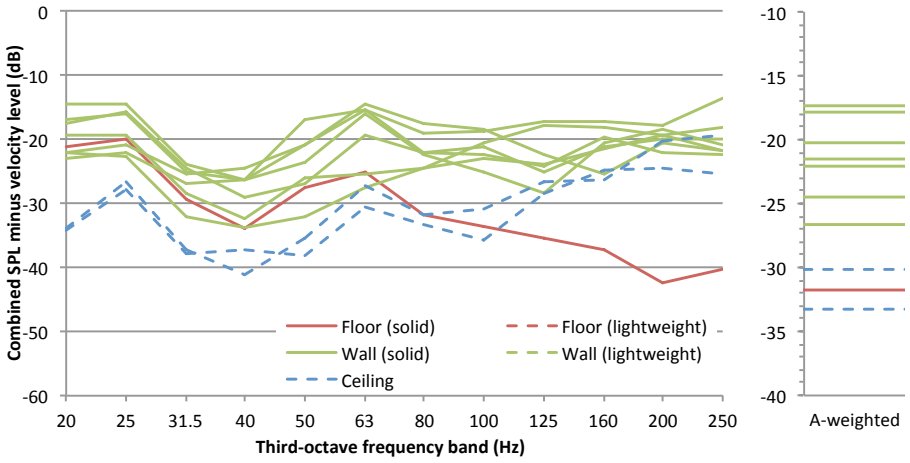

Figure G-30. Hotel 2, Room 2: sound pressure level of pass-bys minus velocity level (normalised to reverberation time) (dB re $2x10^{4}$ $Pa.m^{-1}.s$)

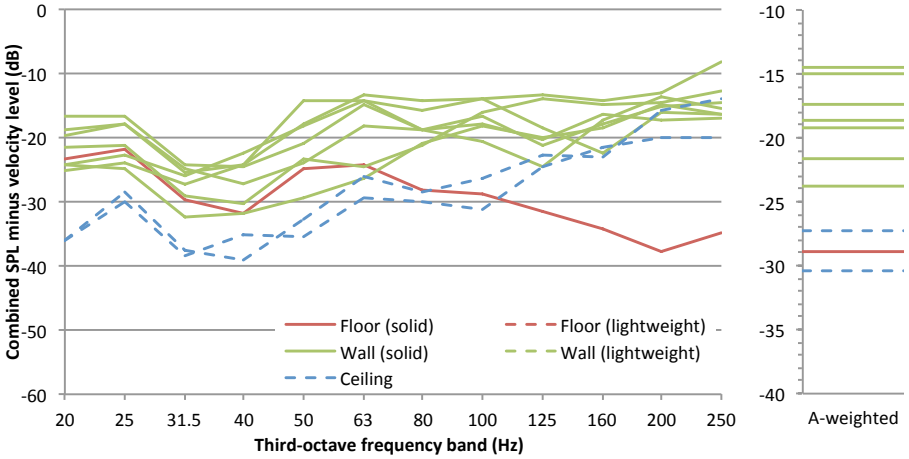

G.6: Hotel 2, Room 3

At the reference vibration position on the floor, a total of 173 train pass-bys were recorded, with the L_{Smax} vertical velocity results shown in Figure G-31. These comprise mainly two different frequency signatures which are seen to differ across the frequency range by up to about 20 dB. Spectra designated as train type A also exhibit two slightly different shapes below 125 Hz. The dominant frequency signatures are likely to be due to trains running on two nearby lines; the District/Circle Line, and the Bakerloo line. Furthermore, each of these lines would be expected to exhibit different frequency signatures for the trains running in two different directions.

Figure G-31. Hotel 2, Room 3: maximum velocity level of pass-bys at reference position (173 pass-bys)

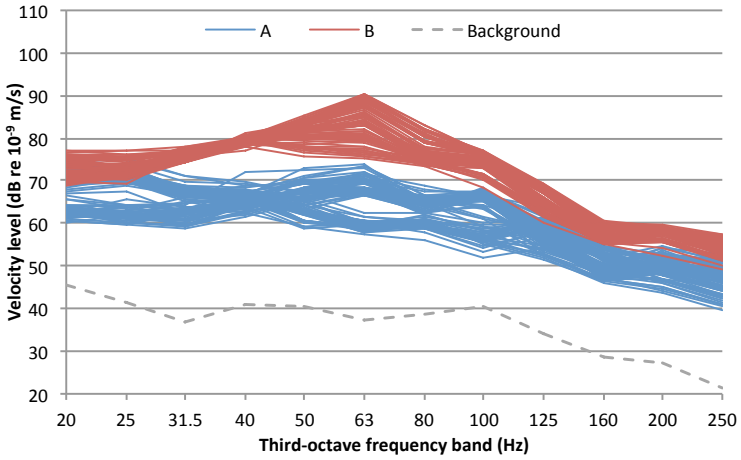

Average L_{Smax} velocity values in each one-third octave band for each measurement position are shown in Figure G-32. It should be noted that for the two floor measurement points, the greater vibration levels were at a mid-span position whereas the lesser vibration levels were at a corner position. The sound pressure results at each microphone position are given in Figure G-33. The combined A-weighted average maximum sound pressure level is 47 dBA.

Figure G-32. Hotel 2, Room 3: average maximum velocity level of pass-bys at various accelerometer measurement positions

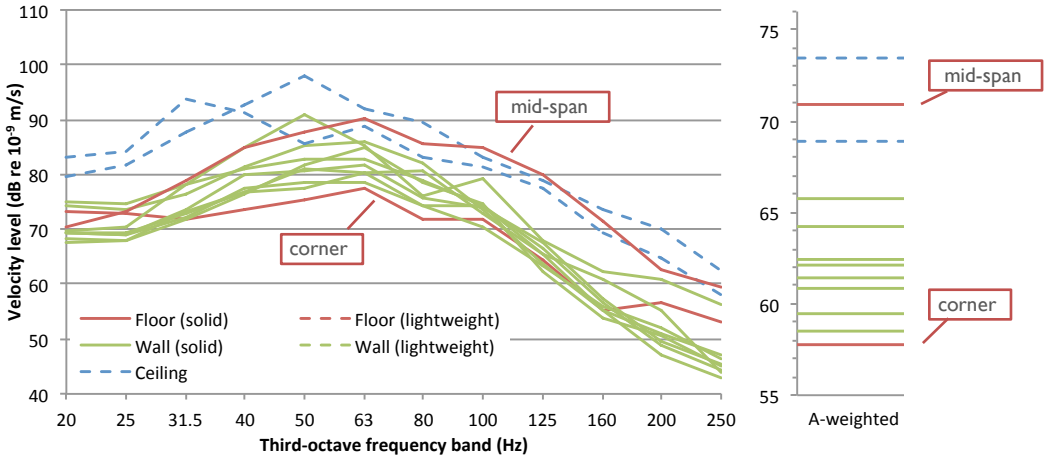

Figure G-33. Hotel 2, Room 3: average maximum sound pressure level of pass-bys at various microphone measurement positions

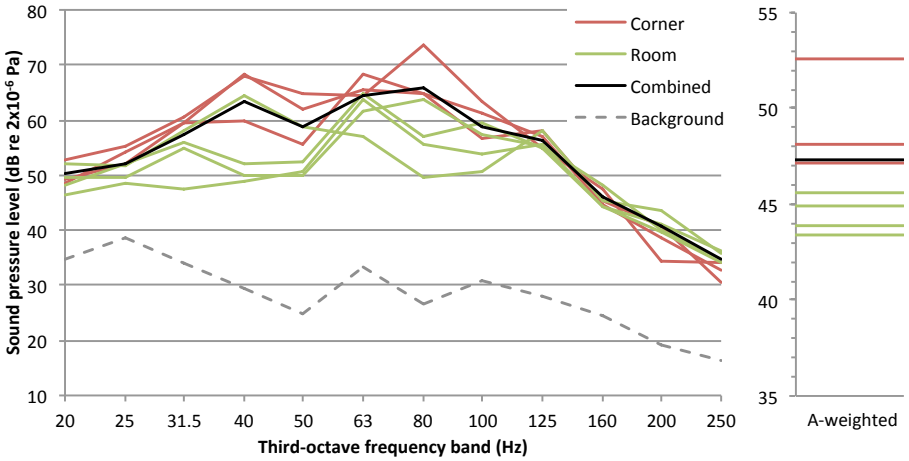

Figure G-32 shows that the vibration levels could vary by up to 10-15 dB when measured at different points on seemingly similar surfaces, although the various solid wall positions gave reasonably similar vibration levels. The ceiling gave the greatest vibration levels for the majority of the frequency range, although above 50 Hz the ceiling vibration levels were similar to the mid-span floor position. The mid-span floor position exhibited vibration levels that were about 10-15 dB greater than at the corner floor position over most of the frequency range.

Figure G-33 shows that sound pressure levels within this room varied by up to about 20 dB, due to acoustic modes. The highest sound pressure levels are at the corner positions, with the lowest at more central room positions.

The reverberation time results for the room are shown in Table G-6. The results are all greater than the minimum values listed in Table 6-1; results below the 31.5 Hz band are likely to be dominated by structural resonances and limitations of the instrumentation.

Table G-6. Hotel 2, Room 3: reverberation time (T_{30}, s)											
1/3 octave frequency band (Hz)											
20	25	31.5	40	50	63	80	100	125	160	200	250
1.58	0.97	1.21	0.83	0.76	1.25	1.43	0.94	0.92	1.03	0.75	0.83

The combined sound pressure level normalised to reverberation time is presented in Figure G-34, with the A-weighted spectrum shown on a secondary scale (to the right of the graph). This shows that the overall A-weighted sound pressure level is dominated by contributions between about 63 and 160 Hz.

Figure G-34. Hotel 2, Room 3: average maximum sound pressure level of pass-bys (combined value) normalised to reverberation time

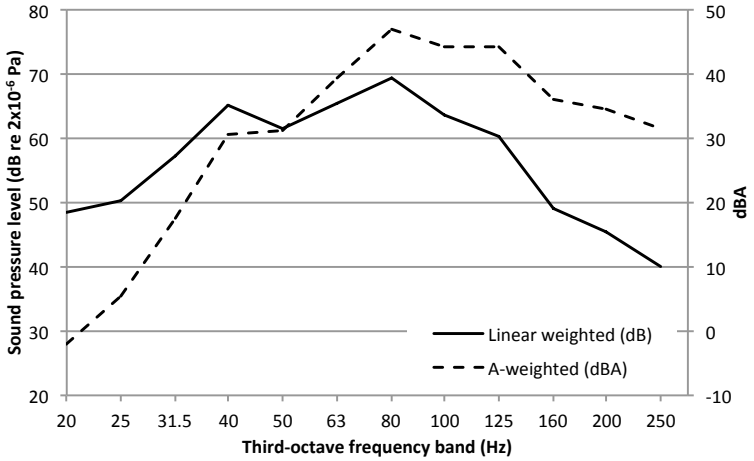

The *LV2P* values for the various vibration measurements and the combined room sound pressure level are shown in Figure G-35. For sound pressure levels normalised to the reverberation time, the $LV2P_n$ values are shown in Figure G-36. For this particular room geometry, ONR 199005 would suggest a $LV2P_n$ of -24 dB.

The results show that the most consistent *LV2P* value is achieved with the mid-span floor vibration measurements, with a value of around -24 dB. When considering a central room position, the sound pressure levels would be slightly lower, and would be predicted within a couple of decibels by the Kurzweil and ONR 199005 approaches.

Grütz's approach for a concrete structure would suggest that to obtain the A-weighted sound pressure level of 47 dBA, the A-weighted vibration velocity level of the surface of interest would be about 87 dBA; this is somewhat greater than any of the measurement positions.

Figure G-35. Hotel 2, Room 3: sound pressure level of pass-bys minus velocity level (dB re $2x10^{4}$ $Pa.m^{-1}.s$)

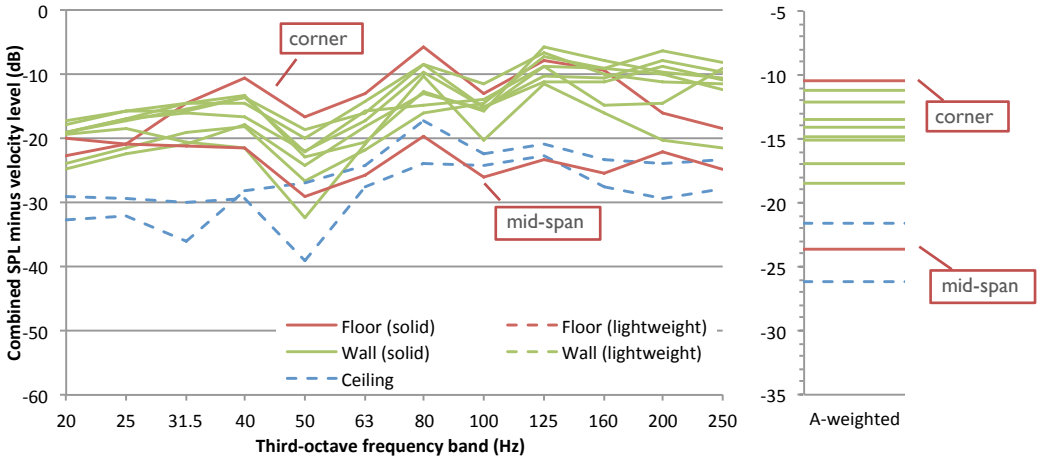

Figure G-36. Hotel 2, Room 3: sound pressure level of pass-bys minus velocity level (normalised to reverberation time) (dB re $2x10^{4}$ $Pa.m^{-1}.s$)

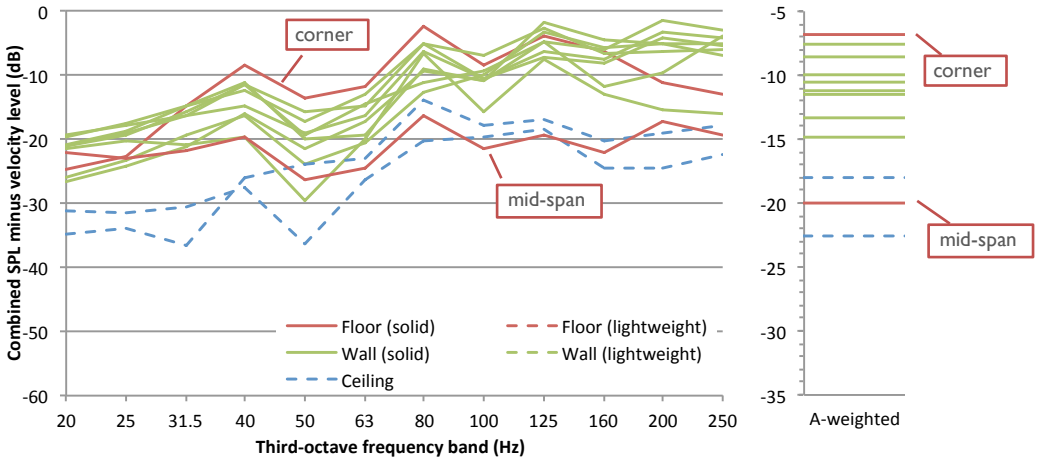

G.7: Hotel 2, Room 4

At the reference vibration position on the floor, a total of 153 train pass-bys were recorded, with the L_{Smax} vertical velocity results shown in Figure G-37. These comprise mainly two different frequency signatures which are seen to differ across the frequency range by up to about 20 dB. Spectra designated as train type A also exhibit two slightly different shapes below 125 Hz. The dominant frequency signatures are likely to be due to trains running on two nearby lines; the District/Circle Line, and the Bakerloo line. Furthermore, each of these lines would be expected to exhibit different frequency signatures for the trains running in two different directions.

Figure G-37. Hotel 2, Room 4: maximum velocity level of pass-bys at reference position (153 pass-bys)

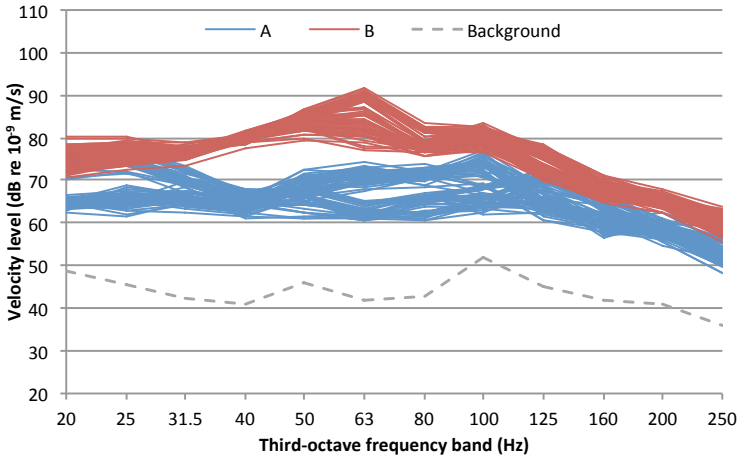

Average L_{Smax} velocity values in each one-third octave band for each measurement position are shown in Figure G-38. It should be noted that for the two floor measurement points, the greater vibration levels were at a mid-span position whereas the lesser vibration levels were at a corner position. The sound pressure results at each microphone position are given in Figure G-39. The combined A-weighted average maximum sound pressure level is 39 dBA.

Figure G-38. Hotel 2, Room 4: average maximum velocity level of pass-bys at various accelerometer measurement positions

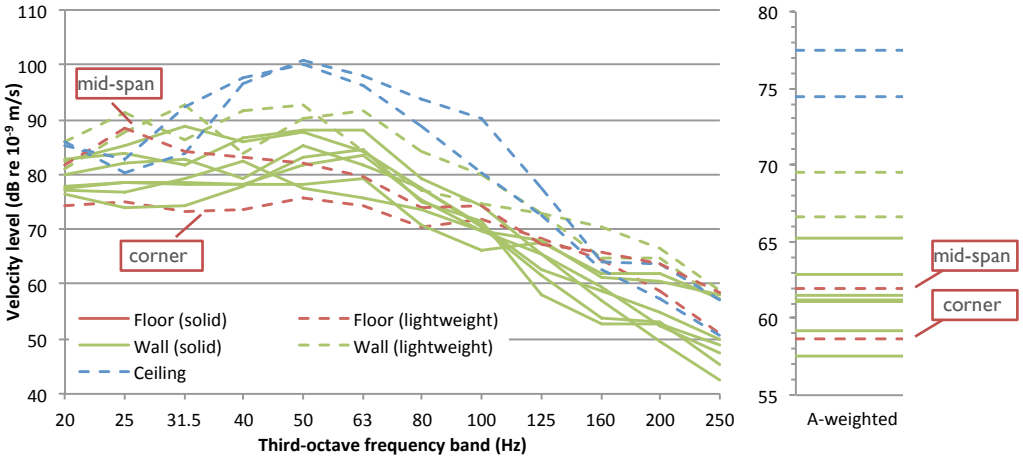

Figure G-39. Hotel 2, Room 4: average maximum sound pressure level of pass-bys at various microphone measurement positions

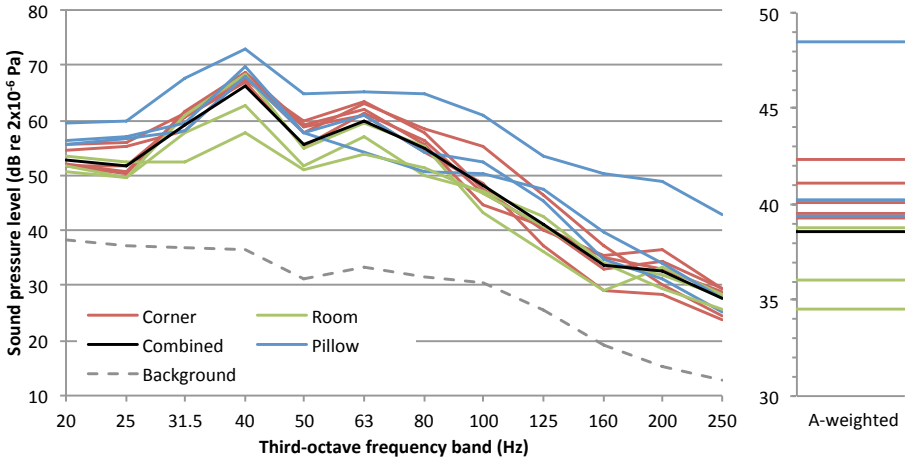

Figure G-38 shows that the vibration levels could vary by up to 10-15 dB when measured at different points on seemingly similar surfaces. The ceiling exhibited the greatest vibration levels over the majority of the frequency range. The mid-span floor vibration was about 10 dB greater than at the corner floor position below 63 Hz.

Figure G-39 shows that sound pressure levels within this room varied by up to about 15-20 dB due to acoustic modes, with one of the pillow positions (near a corner) exhibiting particularly high sound pressure levels.

The reverberation time results for the room are shown in Table G-7. The results are all greater than the minimum values listed in Table 6-1, although only marginally so at some frequencies; results below the 40 Hz band are likely to be dominated by structural resonances and limitations of the instrumentation.

Table G-7. Hotel 2, Room 4: reverberation time (T_{30}, s)

1/3 octave frequency band (Hz)											
20	25	31.5	40	50	63	80	100	125	160	200	250
1.30	1.35	1.00	0.73	0.60	0.54	0.67	0.29	0.33	0.35	0.47	0.33

The combined sound pressure level normalised by reverberation time is presented in Figure G-40, with the A-weighted spectrum shown on a secondary scale (to the right of the graph). This shows that the overall A-weighted sound pressure level is dominated by contributions between 40 and 125 Hz.

Figure G-40. Hotel 2, Room 4: average maximum sound pressure level of pass-bys (combined value) normalised to reverberation time

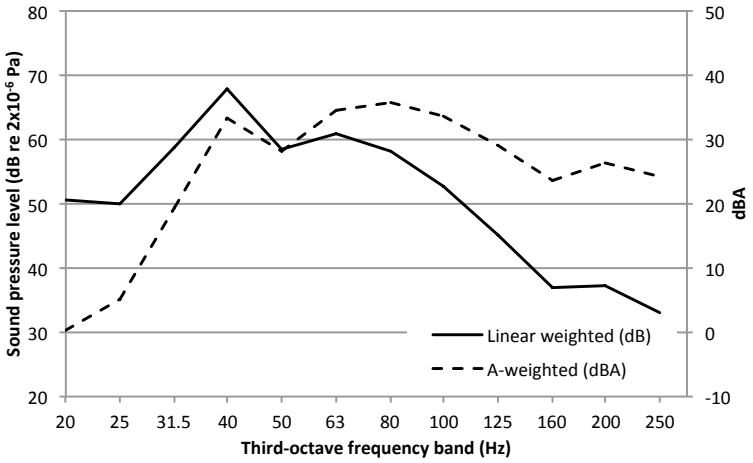

The *LV2P* values for the various vibration measurements and the combined room sound pressure level are shown in Figure G-41. For sound pressure levels normalised to the reverberation time, the $LV2P_n$ values are shown in Figure G-42. For this particular room geometry, ONR 199005 would suggest a $LV2P_n$ of -24 dB.

The results show that none of the surface vibration measurements provide a consistent difference with sound pressure level, although when considering the A-weighted values, the *LV2P* value for the mid-span floor location was about -23 dB. When accounting for the difference between the combined and a central room sound pressure level, the Kurzweil and ONR 199005 predictions would have given overall values similar to those measured.

Grütz's approach for a concrete structure would suggest that to obtain the A-weighted sound pressure level of 39 dBA, the A-weighted vibration velocity level of the surface of interest would be about 74 dBA; this is a similar level to that measured at the ceiling positions.

Figure G-41. Hotel 2, Room 4: sound pressure level of pass-bys minus velocity level (dB re 2x10⁴ Pa.m⁻¹.s)

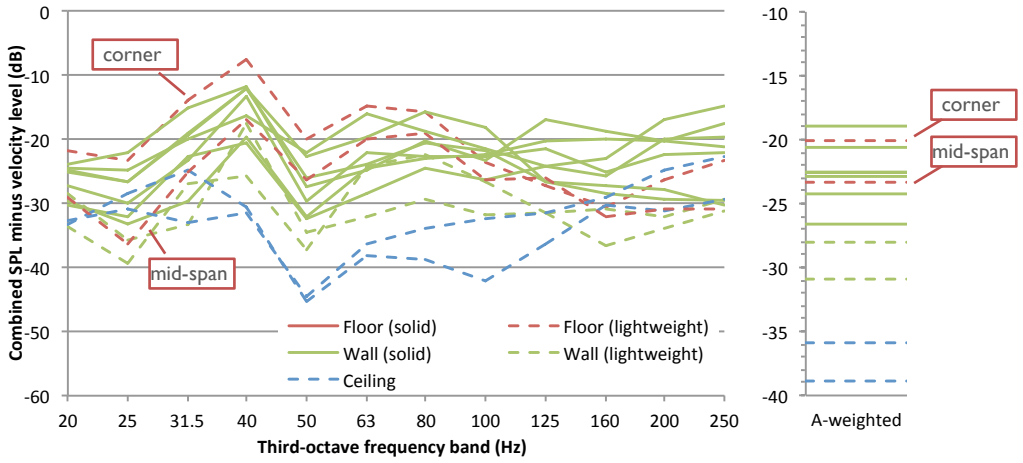

Figure G-42. Hotel 2, Room 4: sound pressure level of pass-bys minus velocity level (normalised to reverberation time) (dB re $2x10^{4}$ $Pa.m^{-1}.s$)

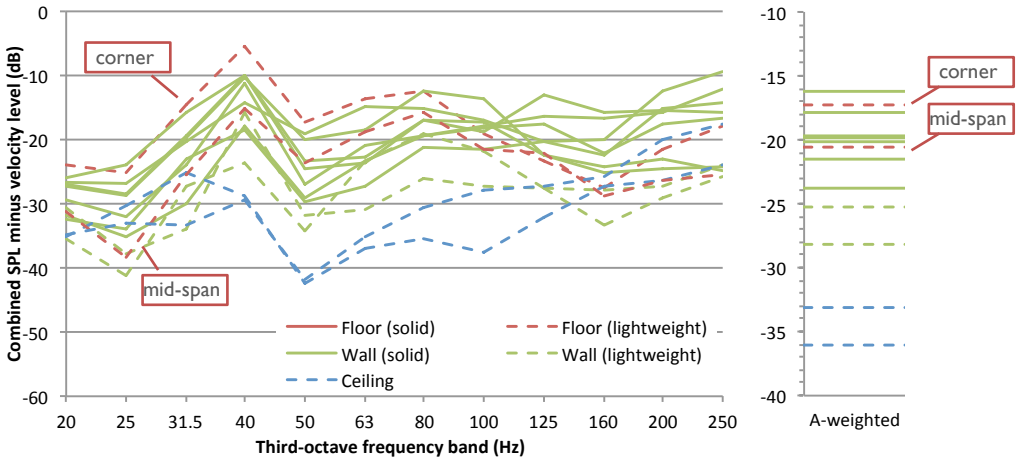

G.8: Hotel 3, Room 1

At the reference vibration position on the windowsill, a total of 121 train pass-bys were recorded, with the L_{Smax} vertical velocity results shown in Figure G-43. These comprise mainly two different frequency signatures which are seen to differ across the frequency range by up to about 20 dB. Spectra designated as train type A also exhibit two slightly different shapes below 125 Hz. The dominant frequency signatures are likely to be due to trains running on two nearby lines; the District/Circle Line, and the Bakerloo line. Furthermore, each of these lines would be expected to exhibit different frequency signatures for the trains running in two different directions.

Figure G-43. Hotel 3, Room 1: maximum velocity level of pass-bys at reference position (121 pass-bys)

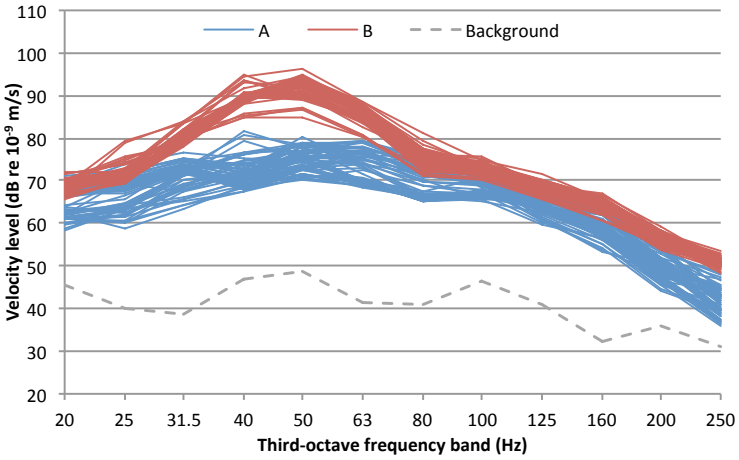

Average L_{Smax} velocity values in each one-third octave band for each measurement position are shown in Figure G-44 (note that the windowsill position has been grouped as a solid floor measurement). The spectrum with the large peak at the 50 Hz band is at the mid-span floor location. The sound pressure results at each microphone position are given in Figure G-45. The combined A-weighted average maximum sound pressure level used for the analysis is 40 dBA.

Figure G-44. Hotel 3, Room 1: average maximum velocity level of pass-bys at various accelerometer measurement positions

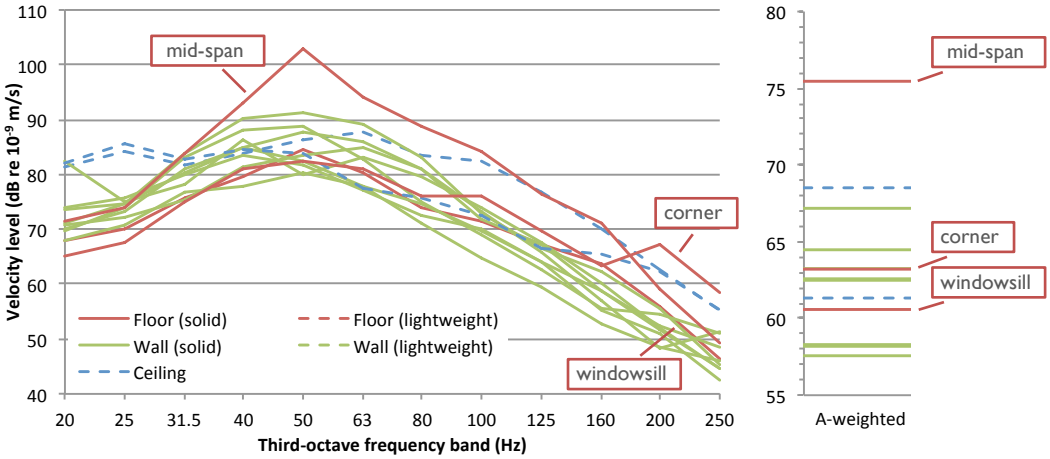

Figure G-45. Hotel 3, Room 1: average maximum sound pressure level of pass-bys at various microphone measurement positions

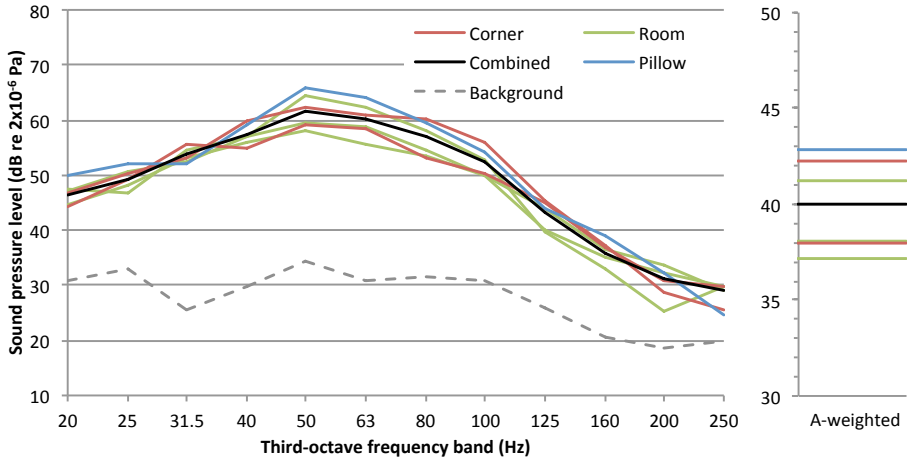

Figure G-44 shows that the vibration levels could vary by up to 10 dB when measured at different points on seemingly similar surfaces, but for the floor the mid-span vibration exceeded the vibration at the corner by up to 20 dB. Whilst for many cases this might be expected to be the case due to structural modes of the floor, in this case it is anticipated to be due to resonant behaviour of the laminate flooring surface.

Figure G-45 shows that sound pressure levels within this room varied by up to about 10 dB due to acoustic modes, with the pillow position (near a corner) exhibiting the greatest sound pressure levels.

The reverberation time results for the room are shown in Table G-8. The results are all greater than the minimum values listed in Table 6-1; results below the 63 Hz band are likely to be dominated by structural resonances and limitations of the instrumentation.

Table G-8. Hotel 3, Room 1: reverberation time (T_{30}, s)											
1/3 octave frequency band (Hz)											
20	25	31.5	40	50	63	80	100	125	160	200	250
1.80	1.07	2.28	0.98	0.76	0.68	0.58	0.46	0.49	0.27	0.31	0.36

The combined sound pressure level normalised to reverberation time is presented in Figure G-46, with the A-weighted spectrum shown on a secondary scale (to the right of the graph). This shows that the overall A-weighted sound pressure level is dominated by contributions between 50 and 125 Hz.

Figure G-46. Hotel 3, Room 1: average maximum sound pressure level of pass-bys (combined value) normalised to reverberation time

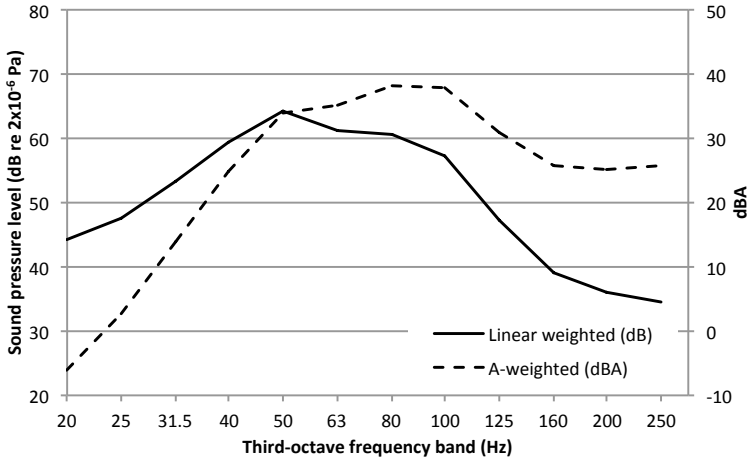

The *LV2P* values for the various vibration measurements and the combined room sound pressure level are shown in Figure G-47. For sound pressure levels normalised to the reverberation time, the $LV2P_n$ values are shown in Figure G-48. For this particular room geometry, ONR 199005 would suggest a $LV2P_n$ of -25 dB.

The results show that none of the surface vibration measurements provide a consistent difference with sound pressure level. Use of the mid-span floor vibration results would lead to overestimates of sound pressure at a central room position by around 11 dB for Kurzweil; the 6 dB for TCRP; and 11 dB for the ONR 199005 approach.

Grütz's approach for a concrete structure would suggest that to obtain the A-weighted sound pressure level of 40 dBA, the A-weighted vibration velocity level of the surface of interest would be about 74 dBA; this is within a few decibels of the mid-span floor vibration measurement.

Figure G-47. Hotel 3, Room 1: sound pressure level of pass-bys minus velocity level (dB re 2x10⁴ Pa.m⁻¹.s)

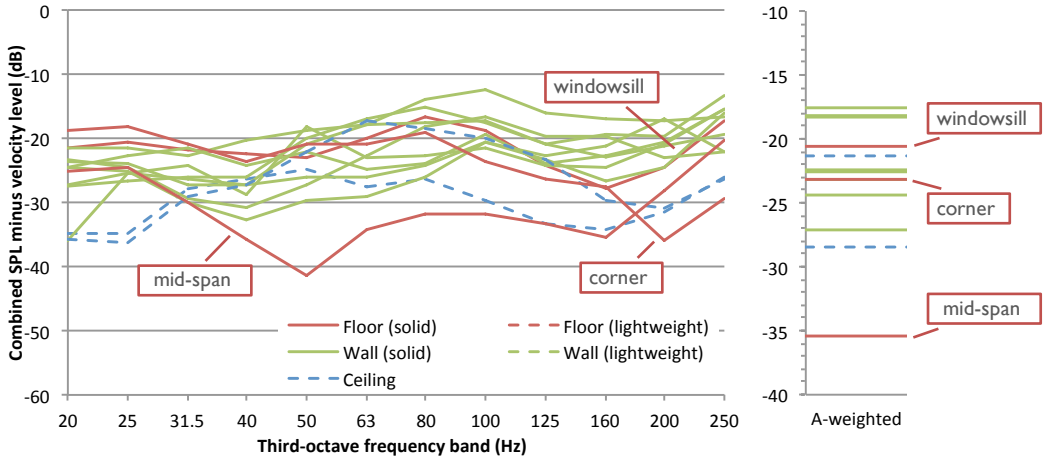

Figure G-48. Hotel 3, Room 1: sound pressure level of pass-bys minus velocity level (normalised to reverberation time) (dB re 2x10⁴ Pa.m⁻¹.s)

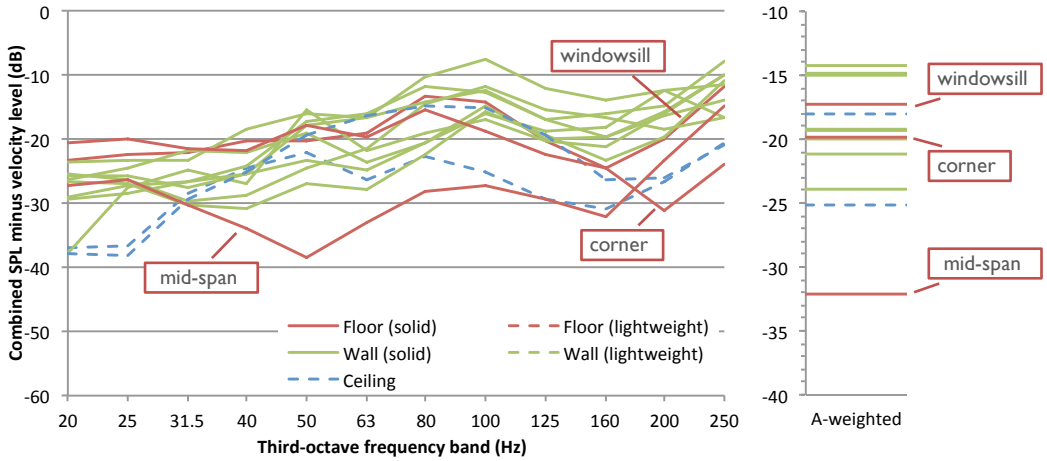

G.9: Hotel 3, Room 2

At the reference vibration position on the windowsill, a total of 109 train pass-bys were recorded, with the L_{Smax} vertical velocity results shown in Figure G-49. These comprise mainly two different frequency signatures which are seen to differ across the frequency range by up to about 10 dB. Within each of these designated main train types, it is seen that there are other groupings of spectra present. The dominant frequency signatures are likely to be due to trains running on two nearby lines; the District/Circle Line, and the Bakerloo line. Furthermore, each of these lines would be expected to exhibit different frequency signatures for the trains running in two different directions.

Figure G-49. Hotel 3, Room 2: maximum velocity level of pass-bys at reference position (109 pass-bys)

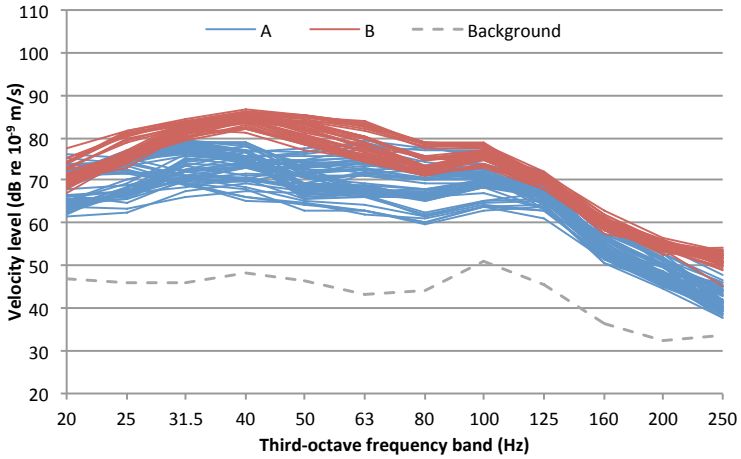

Average L_{Smax} velocity values in each one-third octave band for each measurement position are shown in Figure G-50 (note that the windowsill position has been grouped as a solid floor measurement). The sound pressure results at each microphone position are given in Figure G-51. The combined A-weighted average maximum sound pressure level is 37 dBA.

Figure G-50. Hotel 3, Room 2: average maximum velocity level of pass-bys at various accelerometer measurement positions

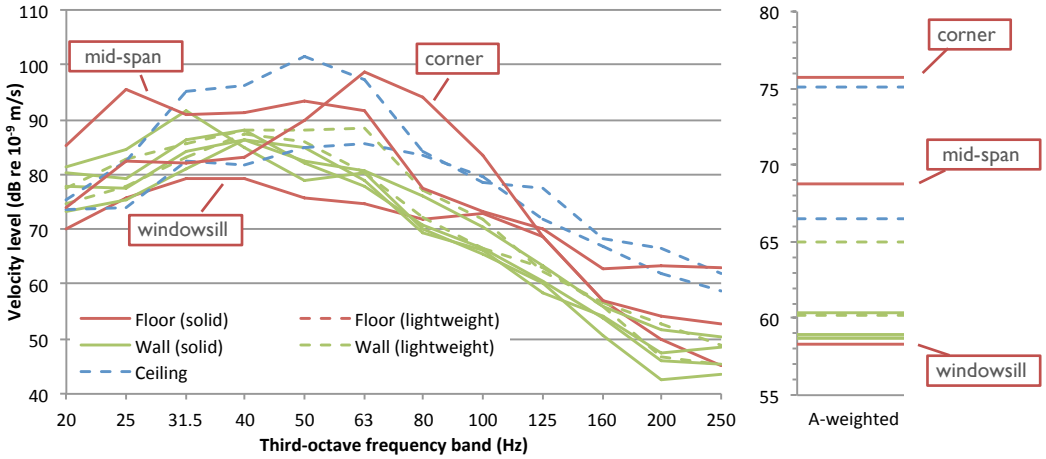

Figure G-51. Hotel 3, Room 2: average maximum sound pressure level of pass-bys at various microphone measurement positions

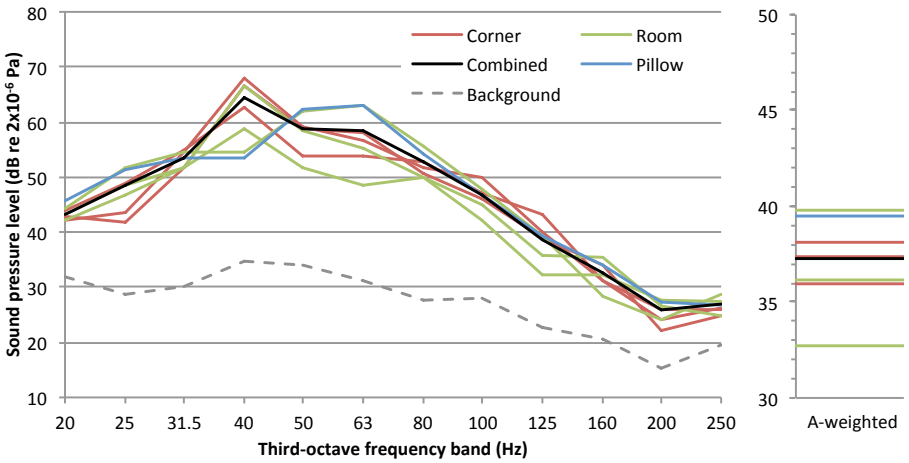

Figure G-50 shows that the vibration levels could vary by up to 10-15 dB when measured at different points on seemingly similar surfaces, and up to 20 dB for different points on the floor. Whilst for many cases this might be expected to be the case due to structural modes of the floor, in this case it is anticipated to be due to non-uniform behaviour of the laminate flooring surface.

Figure G-51 shows that sound pressure levels within this room varied by up to about 15 dB due to acoustic modes.

The reverberation time results for the room are shown in Table G-9. The results are all greater than the minimum values listed in Table 6-1; results below the 63 Hz band are likely to be dominated by structural resonances and limitations of the instrumentation.

Table G-9. Hotel 3, Room 2: reverberation time (T_{30}, s)

1/3 octave frequency band (Hz)											
20	25	31.5	40	50	63	80	100	125	160	200	250
1.22	1.13	1.01	1.03	0.99	0.73	0.54	0.44	0.34	0.31	0.35	0.41

The combined sound pressure level normalised by reverberation time is presented in Figure G-52, with the A-weighted spectrum shown on a secondary scale (to the right of the graph). This shows that the overall A-weighted sound pressure level is dominated by contributions between 40 and 125 Hz.

Figure G-52. Hotel 3, Room 2: average maximum sound pressure level of pass-bys (combined value) normalised to reverberation time

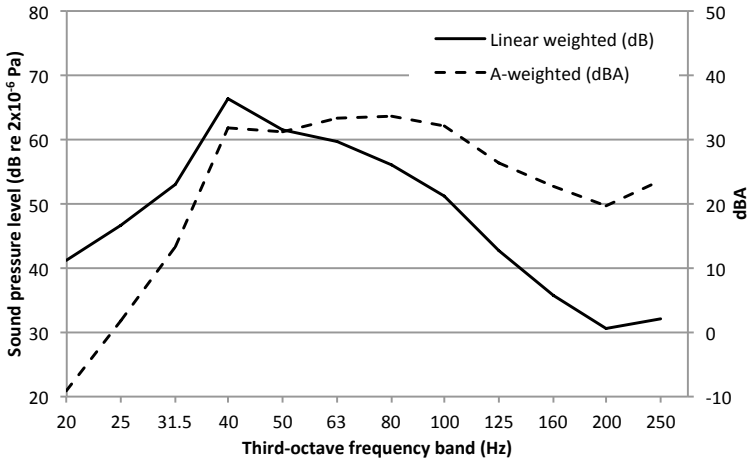

The *LV2P* values for the various vibration measurements and the combined room sound pressure level are shown in Figure G-53. For sound pressure levels normalised to the reverberation time, the $LV2P_n$ values are shown in Figure G-54. For this particular room geometry, ONR 199005 would suggest a $LV2P_n$ of -24 dB.

The results show that the most consistent *LV2P* values were provided by the solid wall locations with values of around -23 dB. Use of the TCRP approach to predict sound pressure levels near the centre of the room from the mid-span floor vibration results would lead to an overestimate of groundborne sound pressure by around 2 dB.

Grütz's approach for a concrete structure would suggest that to obtain the A-weighted sound pressure level of 37 dBA, the A-weighted vibration velocity level of the surface of interest would be about 71 dBA; this is within a few decibels of the mid-span floor vibration measurement.

Figure G-53. Hotel 3, Room 2: sound pressure level of pass-bys minus velocity level (dB re $2x10^{4}$ $Pa.m^{-1}.s$)

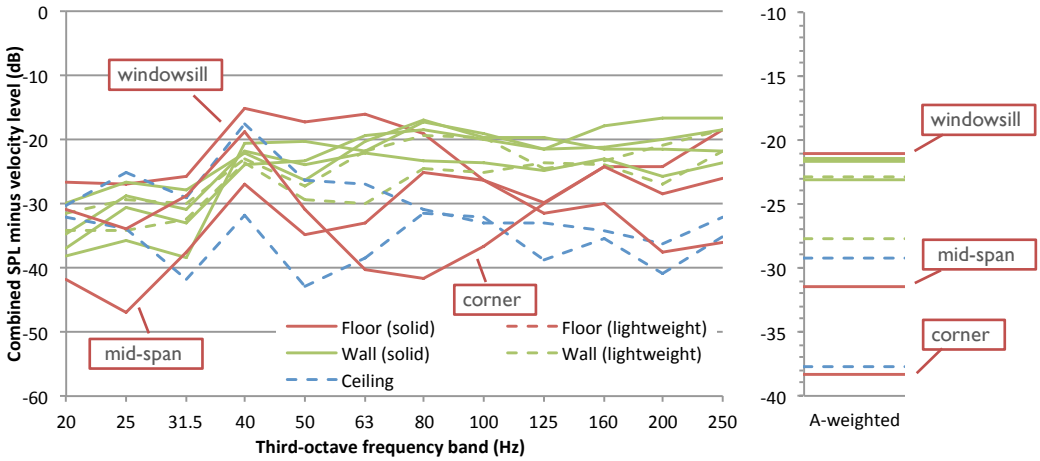

Figure G-54. Hotel 3, Room 2: sound pressure level of pass-bys minus velocity level (normalised to reverberation time) (dB re $2x10^{4}$ $Pa.m^{-1}.s$)

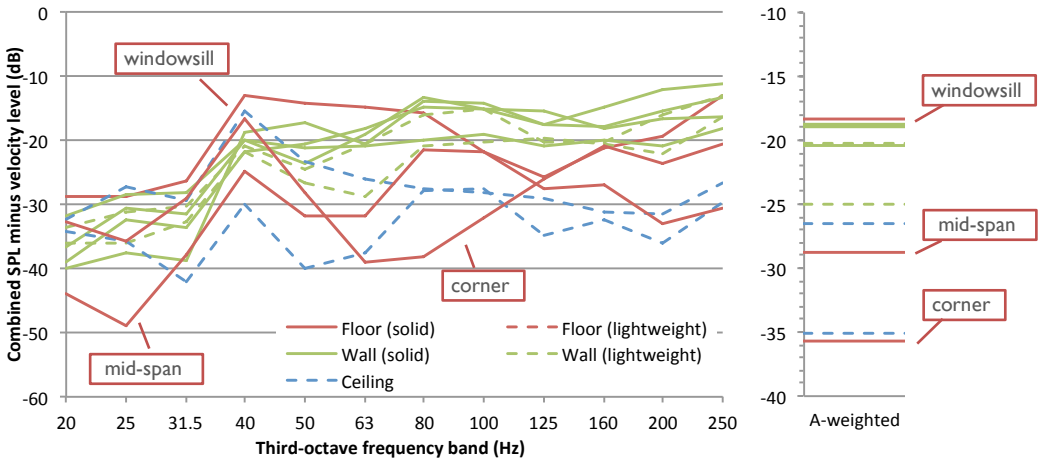

G.10: Hotel 4, Room 1

At the reference positions (both floor positions), a total of 80 train pass-bys were recorded, with the L_{Smax} vertical velocity results for the corner position shown in Figure G-55. These comprise two different frequency signatures that are assumed to correspond to trains running in two different directions in the two nearby tunnels, and which are seen to differ across the frequency range by up to about 10 dB.

Figure G-55. Hotel 4, Room 1: maximum velocity level of pass-bys at reference position (80 pass-bys)

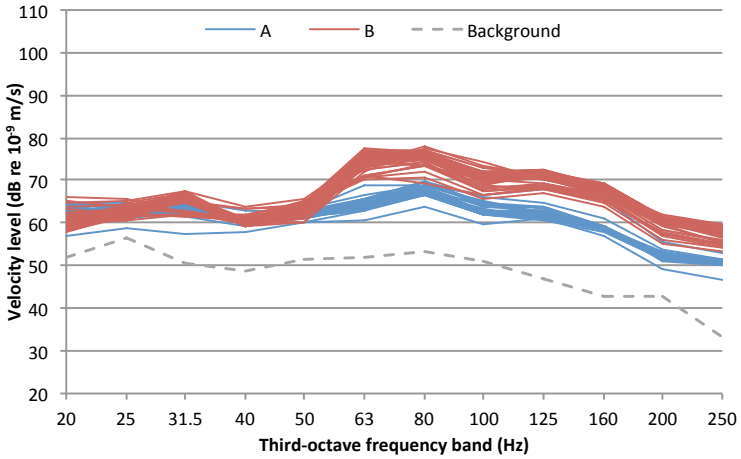

Average L_{Smax} velocity values in each one-third octave band for each measurement position are shown in Figure G-56. The sound pressure results at each microphone position are given in Figure G-57. Note that no corner measurement positions were obtained, and therefore the combined parameter is an estimate based on an assumption that the pillow measurement is likely to have been similar in level to a corner The combined A-weighted average maximum sound pressure level is 35 dBA.

Figure G-56. Hotel 4, Room 1: average maximum velocity level of pass-bys at various accelerometer measurement positions

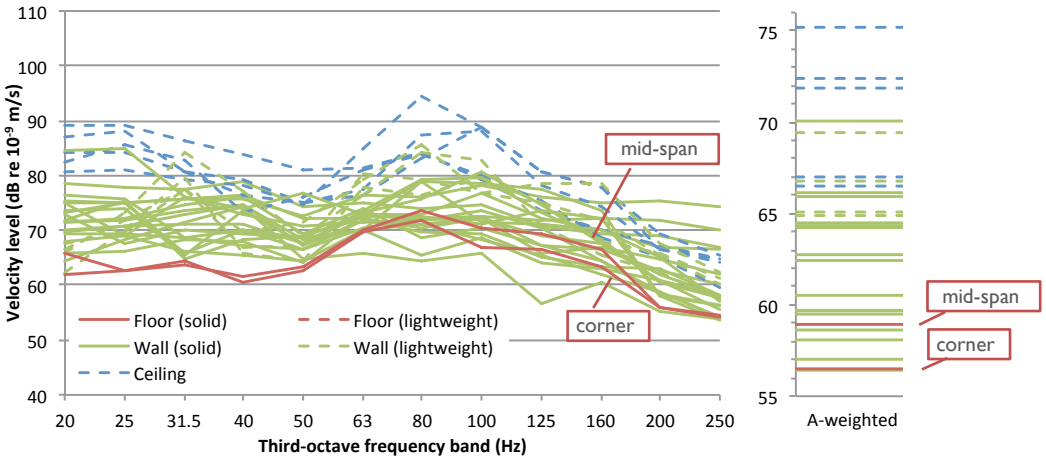

Figure G-57. Hotel 4, Room 1: average maximum sound pressure level of pass-bys at various microphone measurement positions

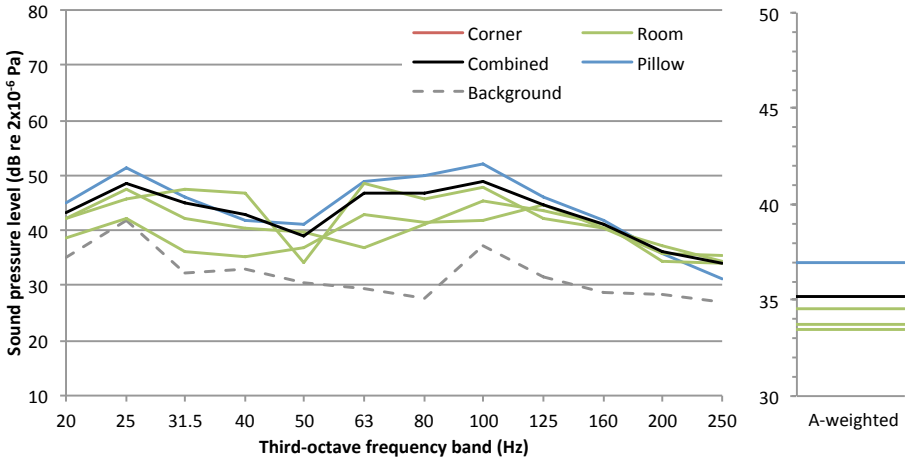

Figure G-56 shows that the vibration levels could vary by up to 10-15 dB when measured at different points on seemingly similar surfaces. The ceiling provided the greatest vibration levels, which were about 20 dB greater than the floor measurements.

Figure G-57 shows that sound pressure levels within this room varied by up to about 10 dB due to acoustic modes.

The reverberation time results for the room are shown in Table G-10. The results are all greater than the minimum values listed in Table 6-1; results below the 31.5 Hz band are likely to be dominated by structural resonances and limitations of the instrumentation.

Table G-10. Hotel 4, Room 1: reverberation time (T_{30}, s)

1/3 octave frequency band (Hz)											
20	25	31.5	40	50	63	80	100	125	160	200	250
1.52	1.30	1.22	0.88	0.59	0.48	0.42	0.38	0.38	0.41	0.42	0.35

The combined sound pressure level normalised by reverberation time is presented in Figure G-58, with the A-weighted spectrum shown on a secondary scale (to the right of the graph). This shows that the overall A-weighted sound pressure level is dominated by contributions between 80 and 250 Hz.

Figure G-58. Hotel 4, Room 1: average maximum sound pressure level of pass-bys (combined value) normalised to reverberation time

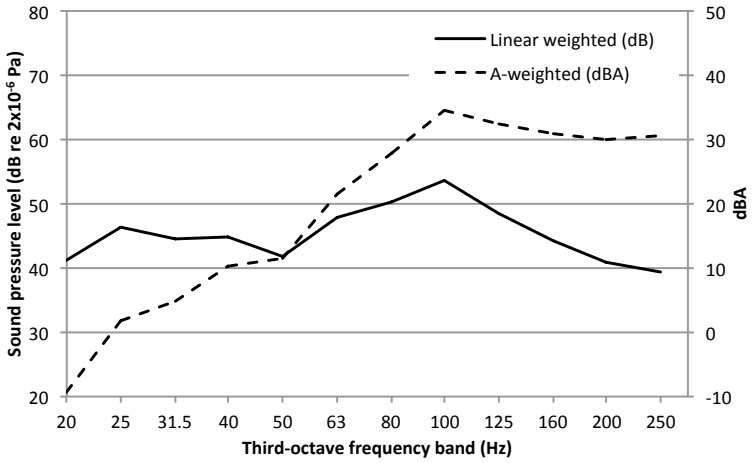

The *LV2P* values for the various vibration measurements and the combined room sound pressure level are shown in Figure G-59. For sound pressure levels normalised to the reverberation time, the $LV2P_n$ values are shown in Figure G-60. For this particular room geometry, ONR 199005 would suggest a $LV2P_n$ of -24 dB.

The results show that the most consistent *LV2P* values were provided by the floor locations, with values of around -23 dB. Use of Kurzweil's approach with the mid-span floor vibration results would lead to a reasonably close estimate of groundborne sound pressure at a room centre location, with the ONR 199005 approach also predicting the sound pressure within a couple of decibels.

Grütz's approach for a concrete structure would suggest that to obtain the A-weighted sound pressure level of 35 dBA, the A-weighted vibration velocity level of the surface of interest would be about 66 dBA; this is around the value of the ceiling measurement with the least vibration or the wall measurements with the higher levels of vibration.

Figure G-59. Hotel 4, Room 1: sound pressure level of pass-bys minus velocity level (dB re $2x10^4$ $Pa.m^{-1}.s$)

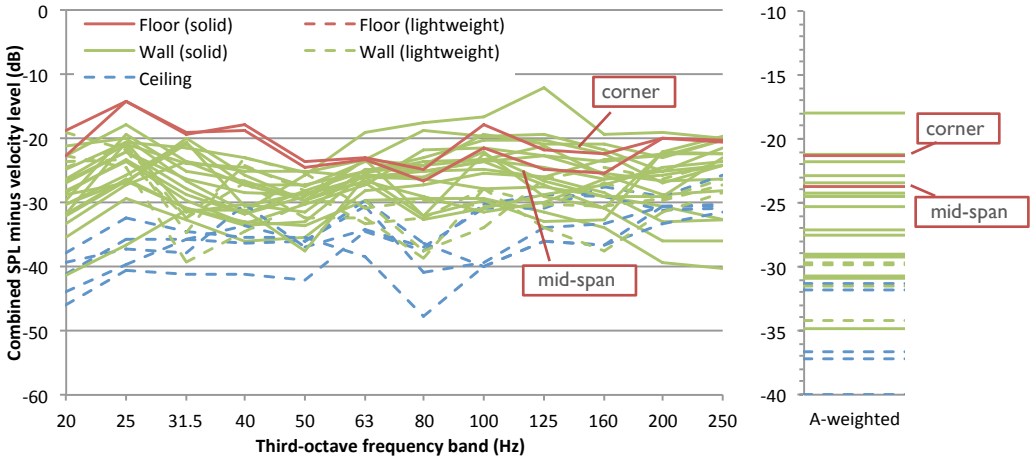

Figure G-60. Hotel 4, Room 1: sound pressure level of pass-bys minus velocity level (normalised to reverberation time) (dB re $2x10^4$ $Pa.m^{-1}.s$)

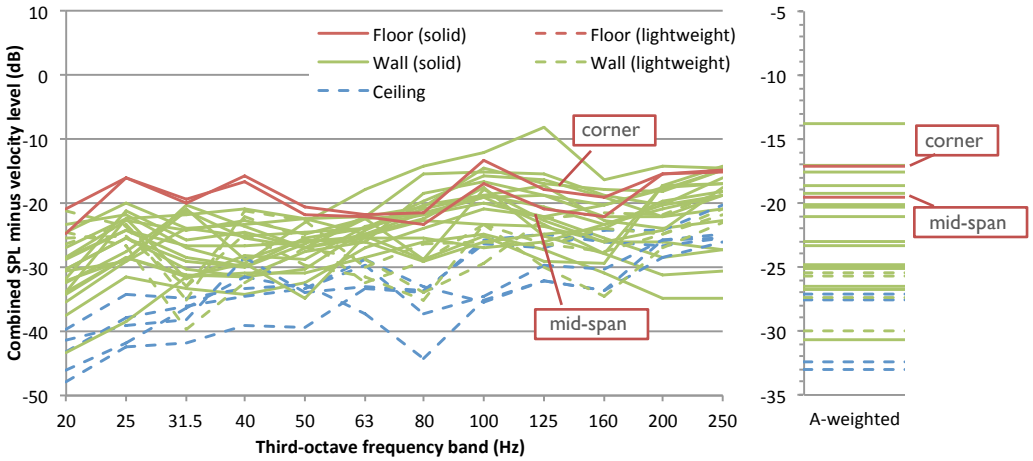

[BLANK PAGE]

APPENDIX H: RE-RADIATED NOISE STUDY RESULTS

The parametric study results for the FE re-radiated noise models are provided in this Appendix. Discussion is provided in Chapter 8.2 of this thesis.

H.1 Default model

H.1.1 Sound and vibration levels

Figure H-1. Rms normal velocity level by surface, default model

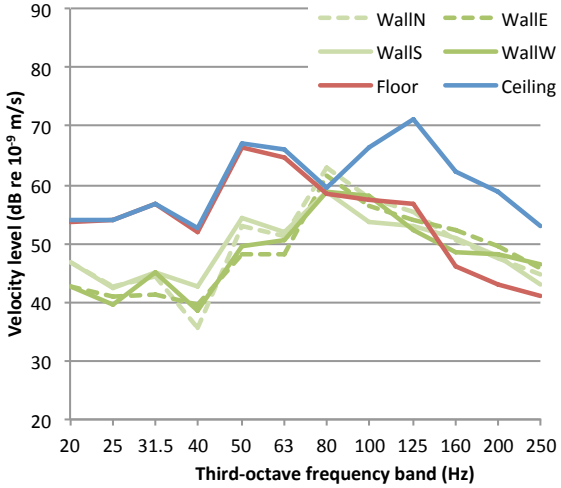

Figure H-2. Sound pressure level contributions by surface, default model

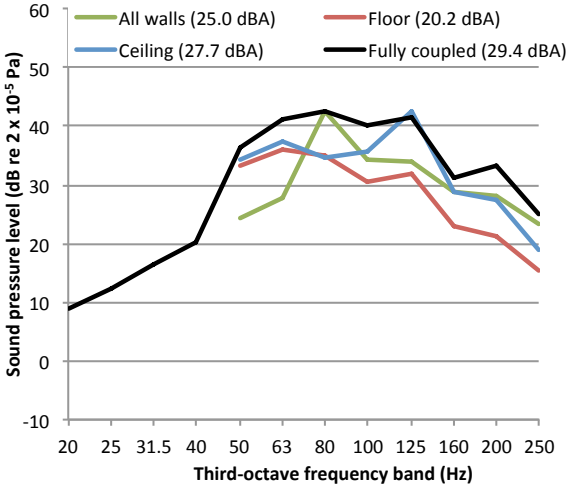

H.1.2 $LV2P_n$ values

Figure H-3. $LV2P_n$ values by surface, relative to total sound pressure level, default model
(dB re $2x10^4$ $Pa.m^{-1}.s$)

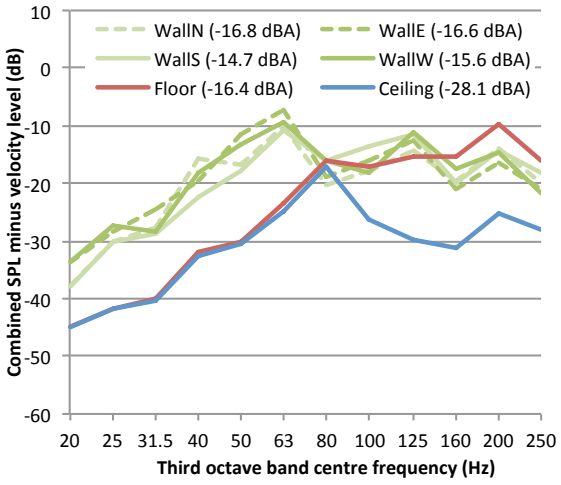

Figure H-4. $LV2P_n$ values by surface, relative to sound pressure level surface contributions, default model
(dB re $2x10^4$ $Pa.m^{-1}.s$)

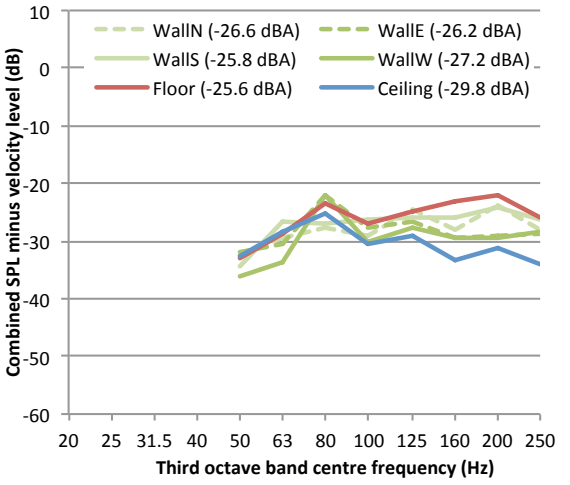

H.2 Room size

H.2.1 Sound and vibration levels

Figure H-5. Rms normal velocity level by surface, room size 2.7 x 2.3 x 2.6 m

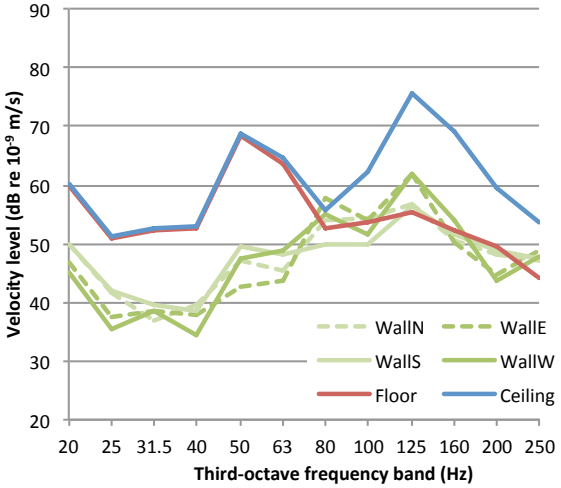

Figure H-6. Sound pressure level contributions by surface, room size 2.7 x 2.3 x 2.6 m

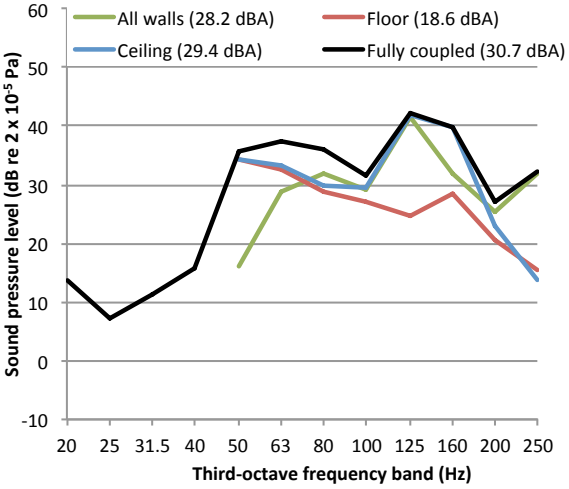

Figure H-7. Rms normal velocity level by surface, room size 6.0 x 5.0 x 2.6 m

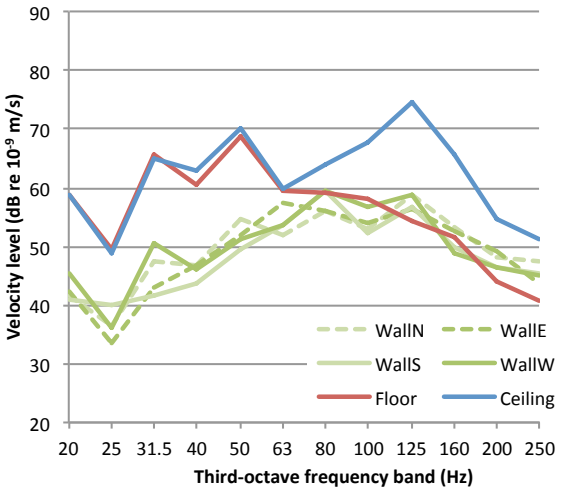

Figure H-8. Sound pressure level contributions by surface, room size 6.0 x 5.0 x 2.6 m

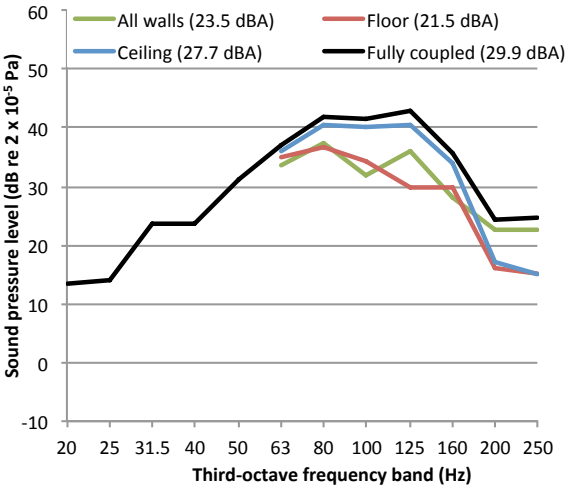

H.2.2 *LV2P$_n$* values

Figure H-9. *LV2P$_n$* values by surface, relative to total sound pressure level, room size 2.7 x 2.3 x 2.6 m
(dB re 2x10^4 Pa.m^{-1}.s)

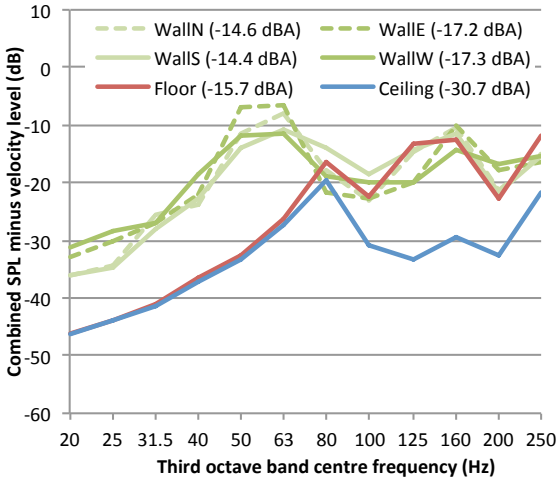

Figure H-10. *LV2P$_n$* values by surface, relative to sound pressure level surface contributions, room size 2.7 x 2.3 x 2.6 m
(dB re 2x10^4 Pa.m^{-1}.s)

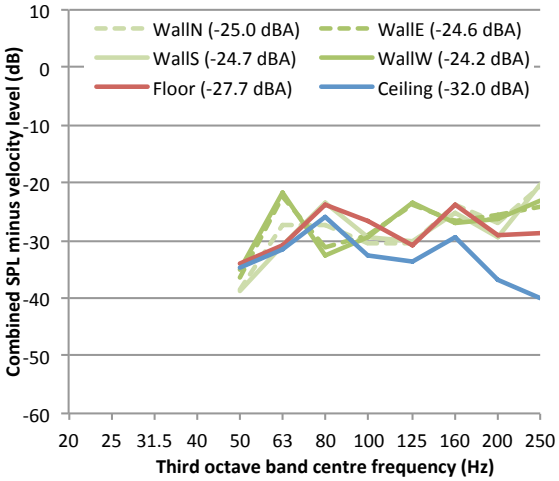

Figure H-11. *LV2P$_n$* values by surface, relative to total sound pressure level, room size 6.0 x 5.0 x 2.6 m
(dB re 2x10^4 Pa.m^{-1}.s)

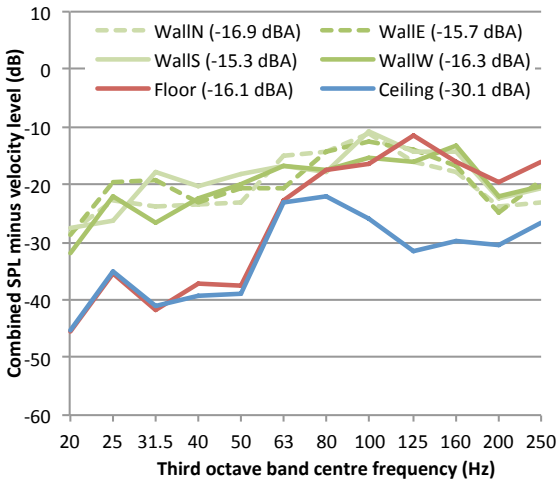

Figure H-12. *LV2P$_n$* values by surface, relative to sound pressure level surface contributions, room size 6.0 x 5.0 x 2.6 m
(dB re 2x10^4 Pa.m^{-1}.s)

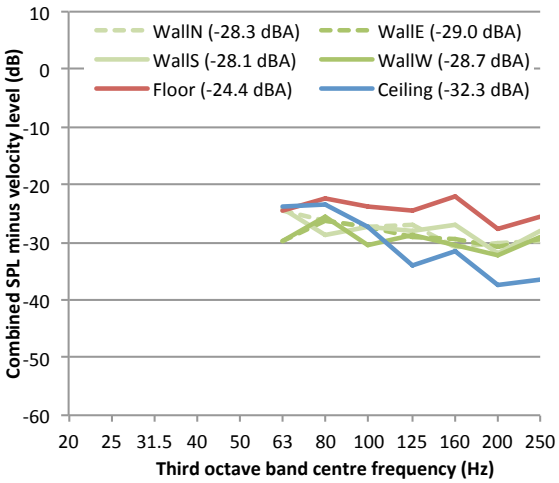

H.3 Ceilings

H.3.1 Sound and vibration levels

Figure H-13. Rms normal velocity level by surface, air in ceiling

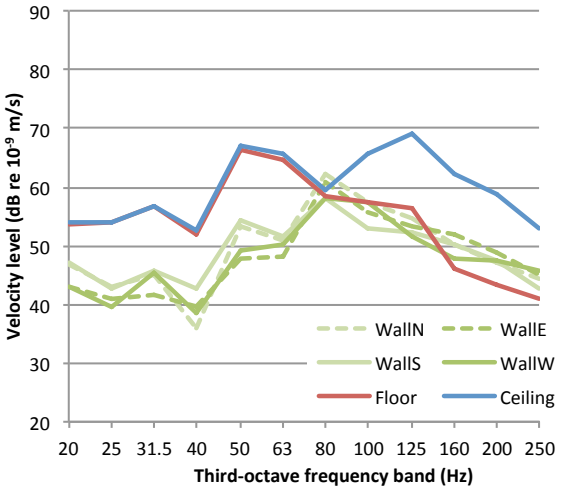

Figure H-14. Sound pressure level contributions by surface, air in ceiling

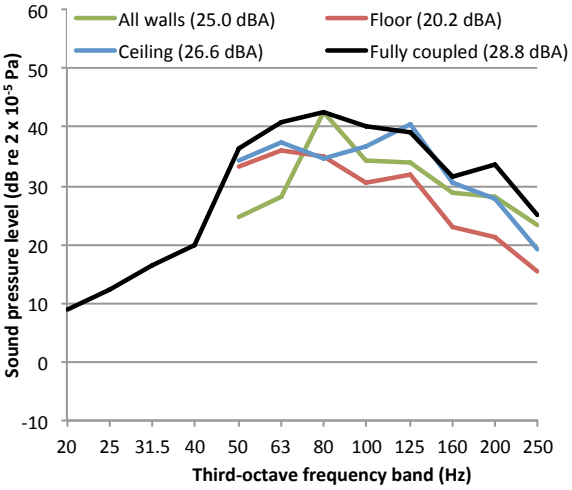

Figure H-15. Rms normal velocity level by surface, no ceiling

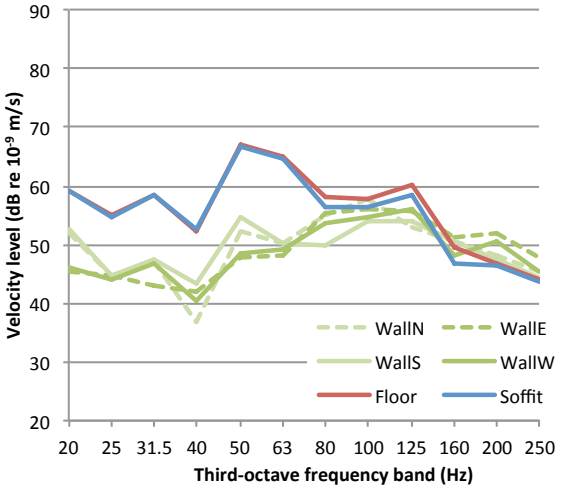

Figure H-16. Sound pressure level contributions by surface, no ceiling

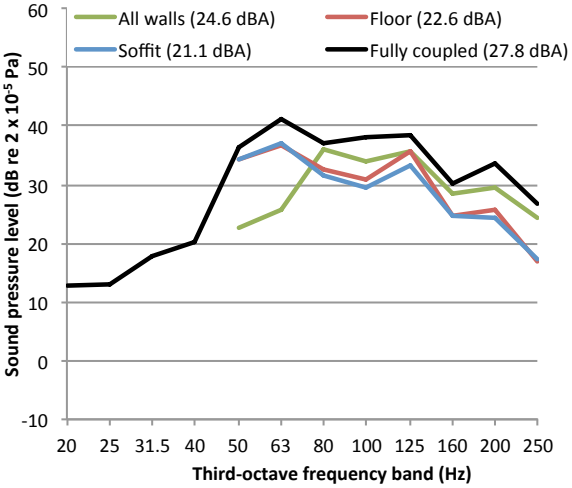

H.3.2 $LV2P_n$ values

Figure H-17. $LV2P_n$ values by surface, relative to total sound pressure level, air in ceiling
(dB re $2x10^4$ Pa.m^{-1}.s)

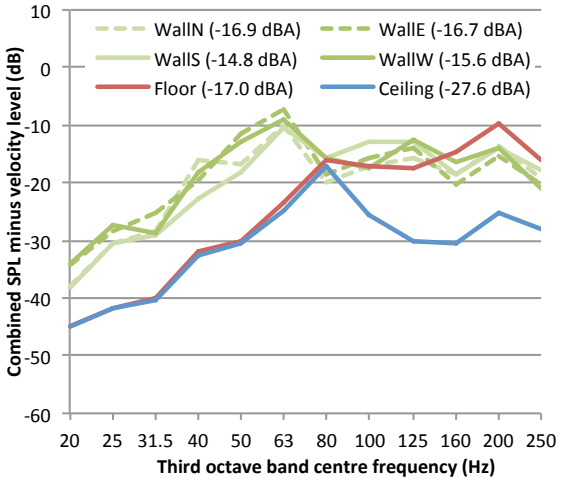

Figure H-18. $LV2P_n$ values by surface, relative to sound pressure level surface contributions, air in ceiling
(dB re $2x10^4$ Pa.m^{-1}.s)

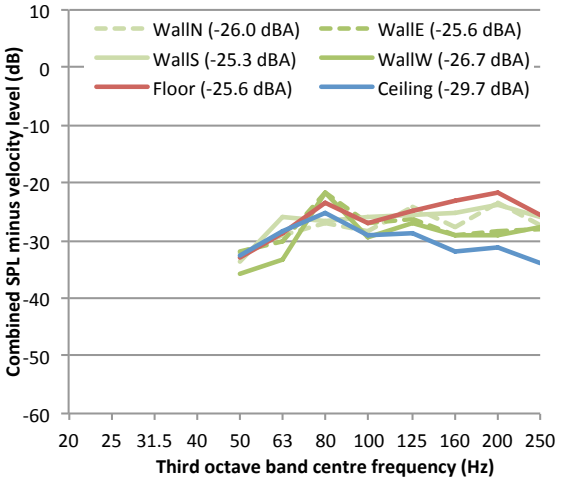

Figure H-19. $LV2P_n$ values by surface, relative to total sound pressure level, no ceiling
(dB re $2x10^4$ Pa.m^{-1}.s)

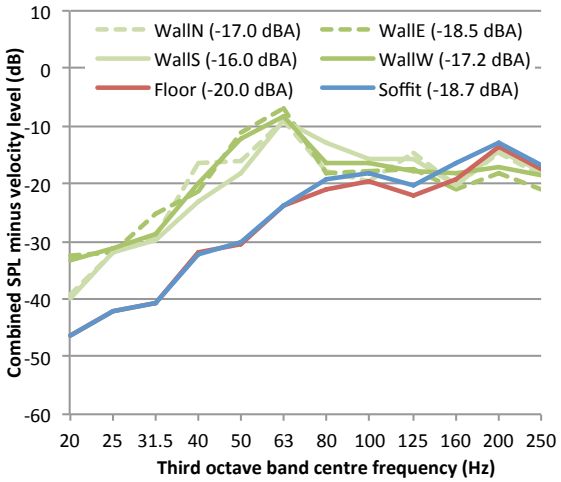

Figure H-20. $LV2P_n$ values by surface, relative to sound pressure level surface contributions, no ceiling
(dB re $2x10^4$ Pa.m^{-1}.s)

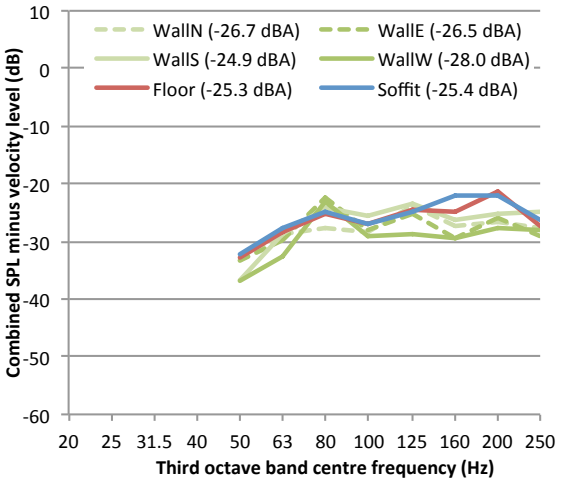

H.4 Walls

H.4.1 Sound and vibration levels

Figure H-21. Rms normal velocity level by surface, non-load-bearing concrete walls

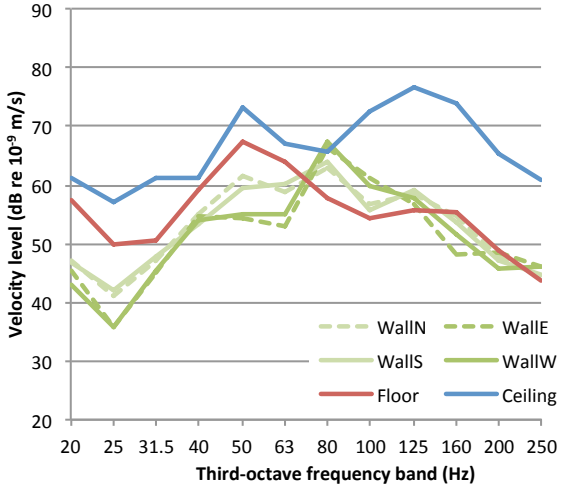

Figure H-22. Sound pressure level contributions by surface, non-load-bearing concrete walls

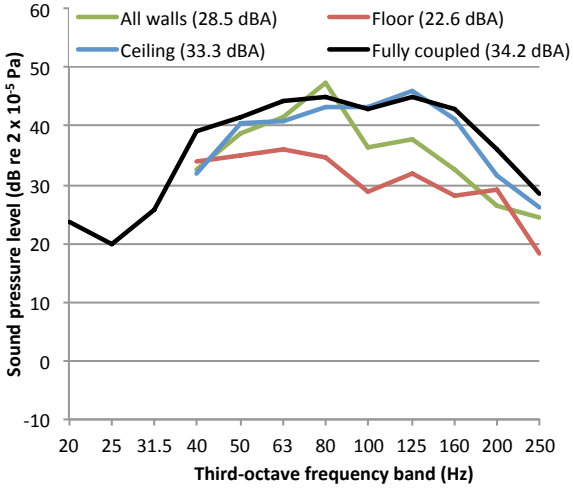

Figure H-23. Rms normal velocity level by surface, non-load-bearing lightweight walls

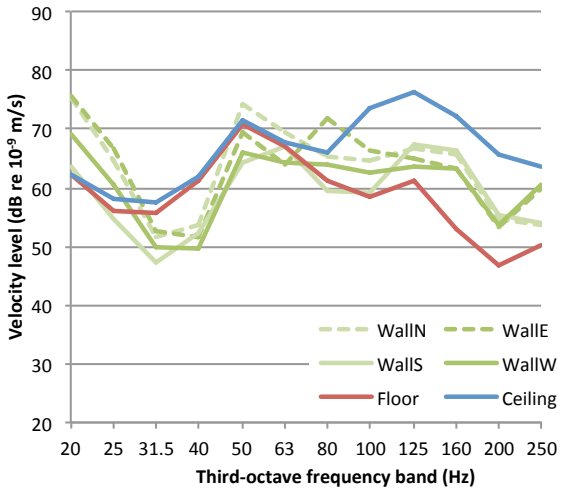

Figure H-24. Sound pressure level contributions by surface, non-load-bearing lightweight walls

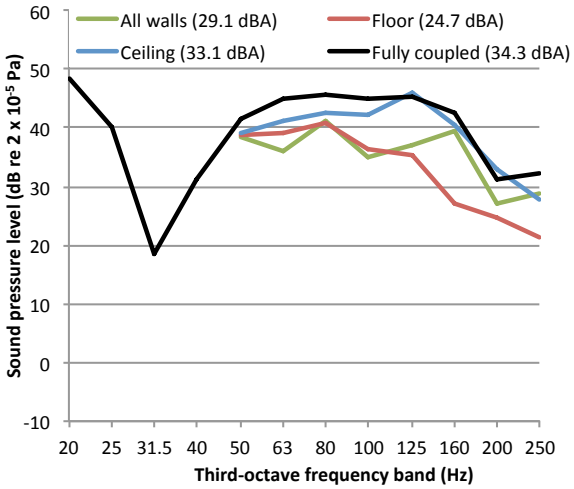

H.4.2 *LV2P$_n$* values

Figure H-25. *LV2P$_n$* values by surface, relative to total sound pressure level, non-load-bearing concrete walls
(dB re 2x10^4 Pa.m^{-1}.s)

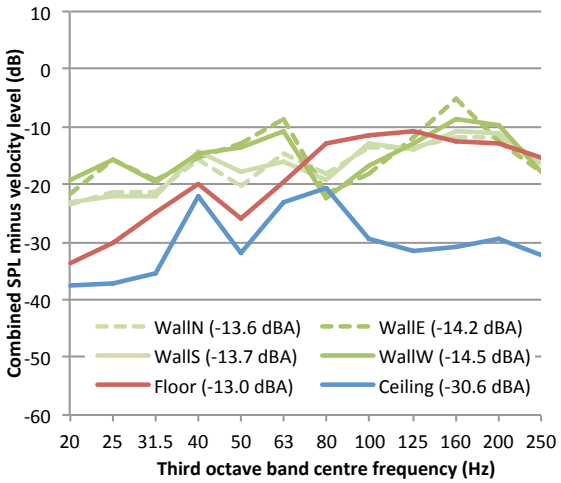

Figure H-26. *LV2P$_n$* values by surface, relative to sound pressure level surface contributions, non-load-bearing concrete walls
(dB re 2x10^4 Pa.m^{-1}.s)

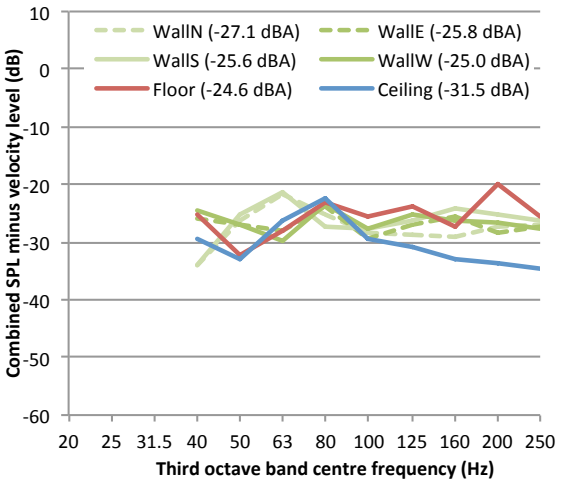

Figure H-27. *LV2P$_n$* values by surface, relative to total sound pressure level, non-load-bearing lightweight walls
(dB re 2x10^4 Pa.m^{-1}.s)

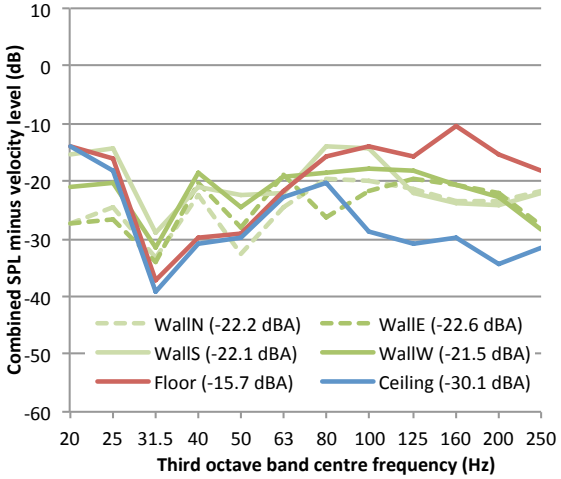

Figure H-28. *LV2P$_n$* values by surface, relative to sound pressure level surface contributions, non-load-bearing lightweight walls
(dB re 2x10^4 Pa.m^{-1}.s)

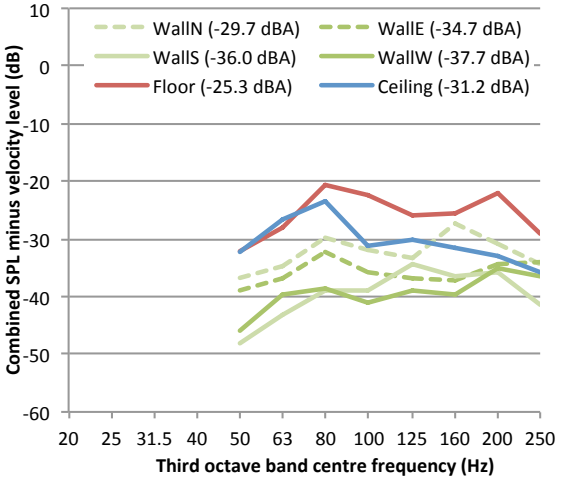

H.5 Force input direction

H.5.1 Sound and vibration levels

Figure H-29. Rms normal velocity level by surface, mainly horizontal force input

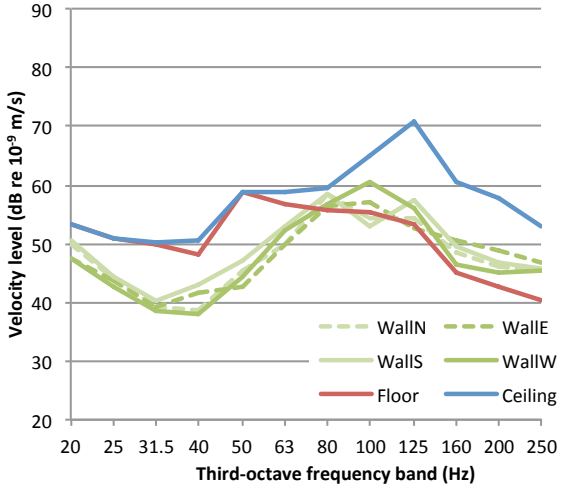

Figure H-30. Sound pressure level contributions by surface, mainly horizontal force input

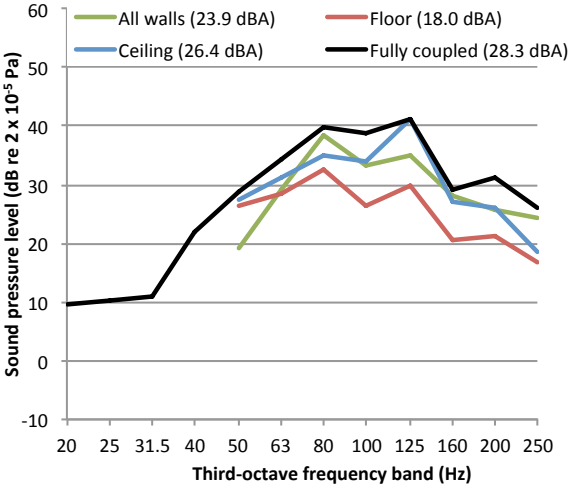

Figure H-31. Rms normal velocity level by surface, vertical-only force input

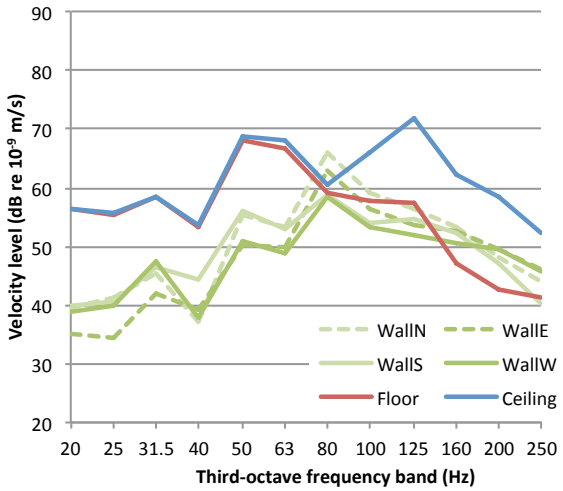

Figure H-32. Sound pressure level contributions by surface, vertical-only force input

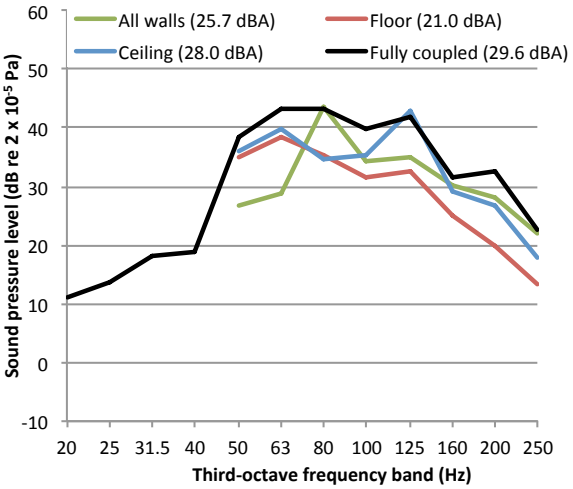

H.5.2 *LV2P$_n$* values

Figure H-33. *LV2P$_n$* values by surface, relative to total sound pressure level, mainly horizontal force input
(dB re 2x10^4 Pa.m^{-1}.s)

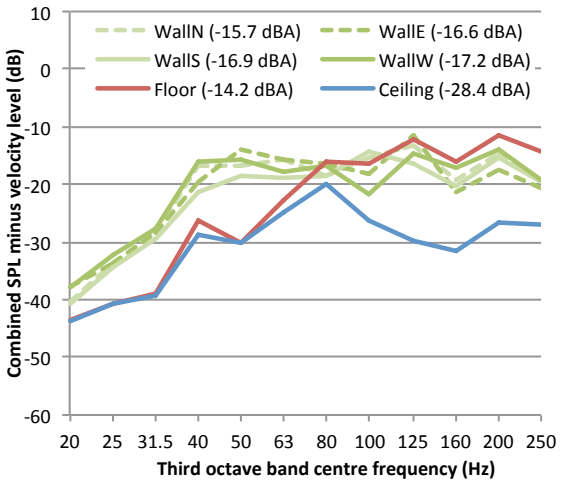

Figure H-34. *LV2P$_n$* values by surface, relative to sound pressure level surface contributions, mainly horizontal force input
(dB re 2x10^4 Pa.m^{-1}.s)

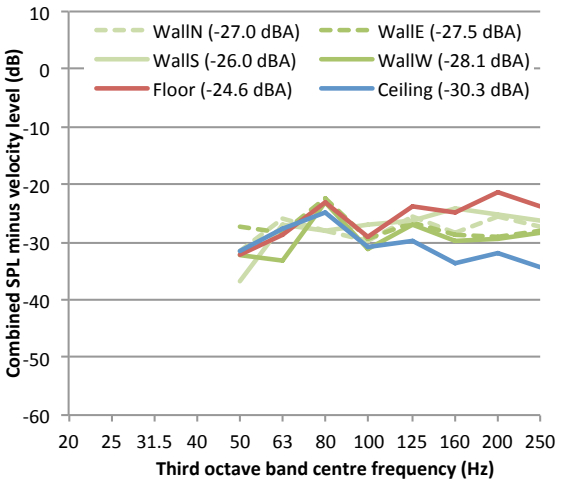

Figure H-35. *LV2P$_n$* values by surface, relative to total sound pressure level, vertical-only force input
(dB re 2x10^4 Pa.m^{-1}.s)

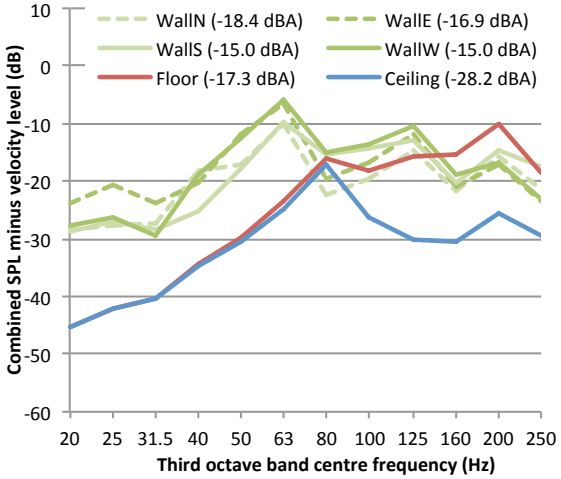

Figure H-36. *LV2P$_n$* values by surface, relative to sound pressure level surface contributions, vertical-only force input
(dB re 2x10^4 Pa.m^{-1}.s)

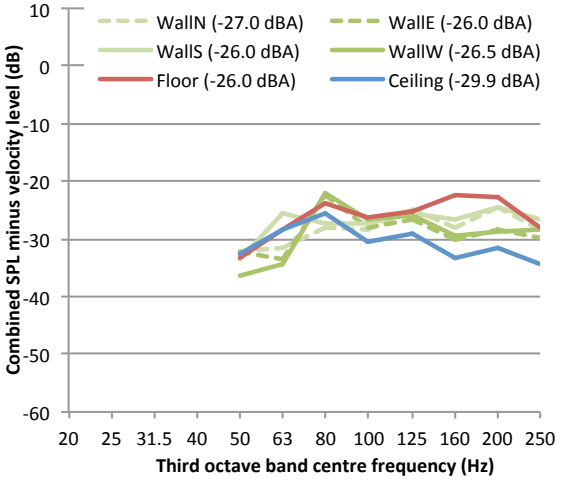

[BLANK PAGE]

REFERENCES

[1] British Standards Institution, Guide to Measurement and evaluation of human exposure to whole-body mechanical vibration and repeated shock, BS 6841:1987, 1987.

[2] International Electrotechnical Commission, Electroacoustics – Sound level meters - Part 1: Specifications, IEC 61672-1:2002, 2002.

[3] United Nations, As world passes 7 billion milestone, UN urges action to meet key challenges, UN News Cent. (2011).

[4] UNFPA, State of World Population 2007: Unleashing the Potential of Urban Growth, 2007.

[5] Department for Transport, Transport Statistics, Great Britain: 2011, 2011.

[6] D.J. Thompson, Railway Noise and Vibration: Mechanisms, Modelling and Means of Control, Elsevier Ltd, 2009.

[7] M. Starnberg, NAT Case study – Results, in: ACOUTRAIN Virtual Certif. Acoust. Perform. Freight Passeng. Trains., Brussels, 2014.

[8] Department of Transport, Calculation of Railway Noise, 1995.

[9] G. Lombaert, G. Degrande, S. François, D.J. Thompson, Ground-borne vibration due to railway traffic, in: 11th Int. Work. Railw. Noise, Uddevalla, Sweden, 2013.

[10] M. Villot, C. Guigou, P. Jean, N. Picard, Deliverable D1.6: Definition of appropriate procedures to predict exposure in buildings and estimate annoyance, 2012.

[11] World Health Organisation, Guidelines for Community Noise, 1999.

[12] British Standards Institution, Guide to evaluation of human exposure to vibration in buildings - Part 1 : Vibration sources other than blasting, BS 6472-1:2008, 2008.

[13] Association of Noise Consultants, Measurement & Assessment of Groundborne Noise & Vibration, 2nd ed., Association of Noise Consultants, 2012.

[14] British Standards Institution, Evaluation and measurement for vibration in buildings - Part 2: Guide to damage levels from groundborne vibration, BS 7385-2:1990, 1993.

[15] British Standards Institution, Guidance on sound insulation and noise reduction for buildings, BS 8233, 2014.

[16] American Public Transport Association, Guidelines for Design of Rapid Transit Facilities, Section 2.7, Noise and Vibration, 1981.

[17] C.E. Hanson, D.A. Towers, L.D. Meister, Transit Noise and Vibration Impact Assessment, Office of Planning and Environment, Federal Transit Administration, 2006.

[18] J.W. Edwards, Survey of Environmental Noise and Vibration from London Underground Trains, in: Internoise '96, 1996: pp. 2029–2032.

[19] Ashdown Environmental Limited, Channel Tunnel Rail Link: Criteria for the Assessment of Vibration from Railways, 1995.

[20] Crossrail, Crossrail Information Paper D10 – Groundborne Noise and Vibration, 2008.

[21] D. Waddington, A. Moorhouse, A. Steele, J. Woodcock, J. Condie, E. Peris, et al., Human Response to Vibration in Residential Environments (NANR209), Final Project Report, London, 2011.

[22] C. Madshus, A.M. Kaynia, High-Speed Railway Lines on Soft Ground: Dynamic Behaviour At Critical Train Speed, J. Sound Vib. 231 (2000) 689–701.

[23] P. Remington, L. Kurzweil, D.A. Towers, Low-Frequency Noise and Vibration from Trains, in: P.M. Nelson (Ed.), Transp. Noise Ref. B., Butterworth & Co., London, 1987.

[24] Ashdown Environmental Limited, Vibration and Groundborne Noise Calculation Procedures for the Channel Tunnel Rail Link: Volume 2 of 2, 1995.

[25] S. Gupta, Y. Stanus, G. Lombaert, G. Degrande, Influence of tunnel and soil parameters on

vibrations from underground railways, J. Sound Vib. 327 (2009) 70–91.

[26] F.E. Richart, J.R. Hall, R.D. Woods, Vibrations of Soil and Foundations, Prentice-Hall, Inc, 1970.

[27] J.P. Wolf, Dynamic Soil-Structure Interaction, Prentice-Hall, Inc, 1985.

[28] S. Timoshenko, J.N. Goodier, Theory of Elasticity, 2nd ed., McGraw-Hill Book Company, 1951.

[29] M.J. Kaldjian, Discussion of "Design Procedures for Dynamically Loaded Foundations," Proc. Am. Soc. Civ. Eng. Soil Mech. Found. Div. 95 (1969) 364–366.

[30] A.M. Kaynia, E. Kausel, Dynamics of piles and pile groups in layered soil media, Soil Dyn. Earthq. Eng. 10 (1991) 386–401.

[31] M. Novak, Dynamic Stiffness and Damping of Piles, Can. Geotech. J. 11 (1974) 574–598.

[32] M. Novak, Vertical Vibration of Floating Piles, J. Eng. Mech. Div. 103 (1977) 153–168.

[33] M. Sheta, M. Novak, Vertical Vibration of Pile Groups, J. Geotech. Eng. Div. 108 (1982) 570–590.

[34] G. Gazetas, N. Makris, Dynamic Pile-Soil-Pile Interaction. Part I: Analysis of Axial Vibration, Earthq. Eng. Struct. Dyn. 20 (1991) 115–132.

[35] N. Makris, G. Gazetas, Dynamic Pile-Soil-Pile Interaction. Part II: Lateral and Seismic Response, Earthq. Eng. Struct. Dyn. 21 (1992) 145–162.

[36] K. Kuo, H.E.M. Hunt, The Role of Structural Foundations in Transmission of Vibration from Underground Railways, in: Int. Congr. Sound Vib., Krakow, 2009.

[37] A.P. Jeary, Damping in tall buildings - A mechanism and a predictor, Earthq. Eng. Struct. Dyn. 14 (1986) 733–750.

[38] B.R. Ellis, An assessment the of accuracy of predicting the fundamental natural frequencies of buildings and the implications concerning the dynamic analysis of structures, Proc. Inst. Civ. Eng. Part 2 (1980) 763–776.

[39] N. Satake, K. Suda, T. Arakawa, A. Sasaki, Y. Tamura, Damping Evaluation Using Full-Scale Data of Buildings in Japan, J. Struct. Eng. 129 (2003) 470–477.

[40] O. Hassan, A Tentative Noise Control Method for Buildings Above Railway Tunnels, Build. Acoust. 9 (2002) 191–218.

[41] A.E.H. Love, The Small Free Vibrations and Deformation of a Thin Elastic Shell, Philos. Trans. R. Soc. London. 179 (1888) 491–546.

[42] A.W. Leissa, Vibration of Plates, National Aeronautics and Space Administration, Columbus, Ohio, 1969.

[43] R.E. Reed, Comparison of Methods in Calculating Frequencies of Corner-Supported Rectangular Plates, National Aeronautics and Space Administration, 1965.

[44] M. Petyt, W.H. Mirza, Vibration of column-supported floor slabs, J. Sound Vib. 21 (1972) 355–364.

[45] R.D. Mindlin, Influence of Rotatory Inertia and Shear on Flexural Motions of Isotropic, Elastic Plates, J. Appl. Mech. Asme. 18 (1951) 31–38.

[46] C.M. Wang, Natural Frequencies Formula for Simply Supported Mindlin Plates, J. Vib. Acoust. 116 (1994) 536–540.

[47] British Standards Institution, Structural use of concrete: Code of practice for special circumstances, BS 8110-2:1985, 1985.

[48] S.-H. Han, J.-K. Kim, Effect of temperature and age on the relationship between dynamic and static elastic modulus of concrete, Cem. Concr. Res. 34 (2004) 1219–1227.

[49] A. Malaikah, K. Al-saif, R. Al-zaid, Prediction of the Dynamic Modulus of Elasticity of Concrete under Different Loading Conditions, in: Int. Conf. Concr. Eng. Technol., Malaysia, 2004.

[50] D. Anderson, Structureborne Railway Noise and Vibration in Buildings, Arup Internal Report, 1992.

[51] H. Kuttruff, Room Acoustics, 5th ed., Spon Press, 2009.

[52] C. Hopkins, Sound Insulation, Elsevier Ltd, 2007.

[53] N.B. Roozen, L. Labelle, M. Rychtáriková, C. Glorieux, Determining radiated sound power of building structures by means of laser Doppler vibrometry, J. Sound Vib. 346 (2015) 81–99.

[54] A. Nagy, P. Fiala, F. Marki, F. Augusztinovicz, Prediction of interior noise in buildings generated by underground rail traffic, J. Sound Vib. 293 (2006) 680–690.

[55] N.B. Roozen, H. Muellner, L. Labelle, M. Rychtáriková, C. Glorieux, Influence of panel fastening on the acoustic performance of light-weight building elements : Study by sound transmission and laser scanning vibrometry, J. Sound Vib. 346 (2015) 100–116.

[56] G. Xie, D.J. Thompson, C.J.C. Jones, The radiation efficiency of baffled plates and strips, J. Sound Vib. 280 (2005) 181–209.

[57] F.J. Fahy, P. Gardonio, Sound and Structural Vibration, 2nd ed., Academic Press Inc. (London) Limited, 2007.

[58] M. Robinson, C. Hopkins, Effects of signal processing on the measurement of maximum sound pressure levels, Appl. Acoust. 77 (2014) 11–19.

[59] M.R. Schroeder, Frequency-Correlation Functions of Frequency Responses in Rooms, J. Acoust. Soc. Am. 34 (1962) 1819–1823.

[60] P. Billeter, A. Egger, Development and assessment of a new approach to determine structure-borne sound in rooms, in: Internoise 2013, Innsbruck, Austria, 2013: pp. 1–8.

[61] British Standards Institution, Mechanical vibration — Ground-borne noise and vibration arising from rail systems — Part 1 : General guidance, BS ISO 14837-1:2005, 2005.

[62] British Standards Institution, Acoustics — Field measurement of sound insulation in buildings and of building elements Part 1 : Airborne sound insulation, BS EN ISO 16283-1:2014, 2014.

[63] C. Simmons, Measurement of Sound Pressure Levels at Low Frequencies in Rooms . Comparison of Available Methods and Standards with Respect to Microphone Positions, Acta Acust. United with Acust. 85 (1999) 88–100.

[64] C. Hopkins, P. Turner, Field measurement of airborne sound insulation between rooms with non-diffuse sound fields at low frequencies, Appl. Acoust. 66 (2005) 1339–1382.

[65] J. Pan, D.H. Bies, The effect of fluid–structural coupling on sound waves in an enclosure—Experimental part, J. Acoust. Soc. Am. 87 (1990) 708.

[66] P. Newell, Recording Studio Design, 1st ed., Focal Press, 2003.

[67] S. Maluski, B.M. Gibbs, The effect of construction material, contents and room geometry on the sound field in dwellings at low frequencies, Appl. Acoust. 65 (2004) 31–44.

[68] The White Book, (2016).

[69] P. Jean, C. Guigou, M. Villot, A 2.5D BEM Model for Ground-Structure Interaction, Build. Acoust. 11 (2004) 157–173.

[70] X. Sheng, C.J.C. Jones, D.J. Thompson, Prediction of ground vibration from trains using the wavenumber finite and boundary element methods, J. Sound Vib. 293 (2006) 575–586.

[71] P. Galvín, S. François, M. Schevenels, E. Bongini, G. Degrande, G. Lombaert, A 2.5D coupled FE-BE model for the prediction of railway induced vibrations, Soil Dyn. Earthq. Eng. 30 (2010) 1500–1512.

[72] Q. Jin, D. Thompson, D. Lurcock, M. Toward, E. Ntotsios, Experimental validation of a numerical model for the ground vibration from trains in tunnels, in: 10th Eur. Congr. Expo. Noise Control Eng., Maastricht, 2015.

[73] S. Gupta, M.F.M. Hussein, G. Degrande, H.E.M. Hunt, D. Clouteau, A comparison of two numerical models for the prediction of vibrations from underground railway traffic, Soil Dyn. Earthq. Eng. 27 (2007) 608–624.

[74] S. Jones, H.E.M. Hunt, The Effect of Voids around Underground Railway Tunnels on Ground Vibration, in: Sixt. Int. Congr. Sound Vib., Krakow, Poland, 2009: pp. 1–8.

[75] E. Ungar, E. Bender, Guidelines for the Preliminary Estimation of Vibration and Noise in Buildings Near Subways, Report BBN-2500B, Cambridge, MA, 1973.

[76] J. Lang, Results of measurements on the control of structure-borne noise from subways, in: Seventh Annu. Conf. Acoust., Budapest, 1971.

[77] L. Kurzweil, Ground-borne noise and vibration from underground rail systems, J. Sound Vib. 66 (1979) 363–370.

[78] J.A. Zapfe, H.J. Saurenman, S. Fidell, Transit Cooperative Research Program: Project D-12 - Ground-Borne Noise and Vibration in Buildings Caused by Rail Transit, 2009.

[79] R.J. Greer, AEL Methodology for the Prediction of Re-Radiated Noise in Residential Buildings from Trains Travelling in Tunnels, in: Internoise '93, 1993.

[80] Austrian Standards Institute, Guideline ONR 199005 Calculation of the secondary airborne noise level from vibration measurements, (2008).

[81] M. Österreicher, L. Ibáñez, On the calculation of the re-radiated sound pressure level from vibration measurements according to ONR 199005, in: Internoise 2013, Innsbruck, Austria, 2013: pp. 1–8.

[82] K. Alten, H. Friedl, R. Flesch, Calculating Ground-Borne Noise From Ground-Borne Vibration – A Comparison of Different Approaches, in: Proc. ISMA2010, 2010: pp. 3431–3440.

[83] H. Kuppelwieser, A. Ziegler, A Tool For Predicting Vibration And Structure-Borne Noise Immissions Caused By Railways, J. Sound Vib. 193 (1996) 261–267.

[84] Ziegler Consultants, SBB, VIBRA-1-2-3 : A software package for ground borne vibration and noise prediction, n.d.

[85] H.. Grütz, A. Said, Zur Ermittlung des sekundären Luftschalls aus oberirdischem Schienenverkehr, Fortschritte Der Akust. - DAGA. (1992).

[86] A. Said, H.. Grütz, R. Garburg, Ermittlung des sekundären Luftschalls aus dem Schienenverkehr, Zeitschrift Für Lärmbekämpfung. 53 (2006) 12–18.

[87] A. Ziegler, Vibrations et sons solidiens dans la proximité des rails ferroviaires, École Polytechnique Fédérale de Lausanne, 2009.

[88] B. Tappauf, Erschütterungen bei Eisenbahnstrecken, Tecnnical University Graz, 2008.

[89] D. Anderson, Engineering Prediction of Railway Vibration Transmission in Buildings, in: Proc. Euronoise 1992, London, 1992.

[90] S. Ljunggren, Transmission of structure-borne sound in buildings above railways, Appl. Acoust. 34 (1991) 193–205.

[91] O. Hassan, Transmission of Structure-borne Sound in Buildings above Railway Tunnels, Build. Acoust. 8 (2001) 269–299.

[92] M. Sanayei, C. Brett, J.A. Zapfe, E. Ungar, E. Hines, Predicting Train-Induced Vibrations in Multi-Story Buildings, in: Struct. 2008 Crossing Borders, American Society of Civil Engineers, Vancouver, 2008.

[93] K.H. Chua, K.W. Lo, T. Balendra, Building response due to subway train traffic, J. Geotech. Eng. (1995) 747–754.

[94] R.J.M. Craik, Sound Transmission through Buildings using Statistical Energy Analysis, Gower Publishing Limited, 1996.

[95] C. Hopkins, Vibration transmission between coupled plates using finite element methods and statistical energy analysis. Part 1: Comparison of measured and predicted data for masonry walls with and without apertures, Appl. Acoust. 64 (2003) 955–973.

[96] C. Hopkins, Statistical Energy Analysis of Coupled Plate Systems With Low Modal Density and Low Modal Overlap, J. Sound Vib. 251 (2002) 193–214.

[97] P. Jean, Boundary and finite elements for 2D soil-structure interaction problems, Acta Acust. United with Acust. 87 (2001) 56–66.

[98] J.P.P. Talbot, H.E.M.E.M. Hunt, A computationally efficient piled-foundation model for studying the effects of ground-borne vibration on buildings, Proc. Inst. Mech. Eng. Part C J. Mech. Eng. Sci. 217 (2003) 975–989.

[99] J.P. Talbot, H.E.M. Hunt, Isolation of buildings from rail-tunnel vibration: a review, Build. Acoust. 10 (2003) 177–192.

[100] L. Pyl, G. Degrande, D. Clouteau, Validation of a Source – Receiver Model for Road Traffic- Induced Vibrations in Buildings . II : Receiver Model, J. Eng. Mech. (2004) 1394–1406.

[101] S.-H. Ju, Finite element analysis of structure-borne vibration from high-speed train, Soil Dyn. Earthq. Eng. 27 (2007) 259–273.

[102] M. Villot, P. Ropars, P. Jean, E. Bongini, F. Poisson, Modeling the influence of structural modifications on the response of a building to railway vibration, Noise Control Eng. 59 (2011) 641–651.

[103] M. Sanayei, A. Kayiparambil P., J. a. Moore, C.R. Brett, Measurement and prediction of train-induced vibrations in a full-scale building, Eng. Struct. 77 (2014) 119–128.

[104] S.F. Teow, Scale-Model Building : Study of Vibration Transmission, University of Southampton, 2015.

[105] J.T. Nelson, H.J. Saurenman, A prediction procedure for rail transportation groundborne noise and vibration, Transp. Res. Rec. 1443 (1987) 26–34.

[106] H.J. Saurenman, J.T. Nelson, G.P. Wilson, Handbook of Urban Rail Noise and Vibration Control, 1982.

[107] Ashdown Environmental Limited, Vibration and Groundborne Noise Calculation Procedures for the Channel Tunnel Rail Link: Volume 1 of 2, 1995.

[108] Ashdown Environmental Limited, Addendum to: Vibration and Groundborne Noise Calculation Procedures for the Channel Tunnel Rail Link, 1996.

[109] H. Gjelstrup, A. Larsen, J. Andersen, H.B. Kock, J. Sandreid, Prediction model for human discomfort related to train induced vibrations in buildings, in: 11th Int. Work. Railw. Noise, Uddevalla, Sweden, 2013.

[110] C. Madshus, B. Bessason, L. Harvik, Prediction model for low frequency vibration from high speed railways on soft ground, J. Sound Vib. 193 (1996) 195–203.

[111] M. Bahrekazemi, Train-Induced Ground Vibration and Its Prediction, PhD Thesis, Royal Institute of Technology, Stockholm, 2004.

[112] C. With, M. Bahrekazemi, A. Bodare, Validation of an empirical model for prediction of train-induced ground vibrations, Soil Dyn. Earthq. Eng. 26 (2006) 983–990.

[113] J. Melke, Noise And Vibration From Underground Railway Lines : Proposals For A Prediction Procedure, J. Sound Vib. 120 (1988) 391–406.

[114] A. Trochides, Ground-borne Vibrations in Buildings Near Subways, Appl. Acoust. 32 (1991) 289–296.

[115] P. Fiala, G. Degrande, F. Augusztinovicz, Numerical modelling of ground-borne noise and vibration in buildings due to surface rail traffic, J. Sound Vib. 301 (2007) 718–738.

[116] A. Romero, P. Galv, J. Maestre, Train-induced building vibration due to high-speed train passage, in: Recent Adv. Struct. Dyn., Pisa, Italy, 2013.

[117] G. Coquel, Propagation and radiation of structure-borne sound generated by railways - Application to nearby buildings, PhD Thesis (in French), University of East Paris, 2009.

[118] M. Villot, S. Bailhache, C. Guigou, P. Jean, Prediction of railway induced vibration and ground borne noise exposure in building and associated annoyance, in: 11th Int. Work. Railw. Noise, Uddevalla, Sweden, 2013.

[119] P. Steinhauser, Railway induced vibrations and structure borne noise – requirements for abatement, in: Internoise 2013, Innsbruck, Austria, 2013: pp. 1–10.

[120] W. Steinhauser, Vibration and ground borne noise forecasts for Lainzer Tunnel and Wienerwaldtunnel, in: Internoise 2013, Innsbruck, Austria, 2013: pp. 1–6.

[121] A. Lackner, W. Herrmann, Projection and verification of solid-borne noise based on measurements using the example of the recently built " Katzenbergtunnel ," in: Internoise 2013, Innsbruck, Austria, 2013: pp. 1–6.

[122] M. Ralbovsky, K. Alten, Predicting vibration immission using Train Simulation : A combination of experimental and numerical solutions to assess railway-induced vibrations prior to construction, in: Internoise 2013, Innsbruck, Austria, 2013: pp. 1–10.

[123] S. Jones, K. Kuo, M.F.M. Hussein, H.E.M. Hunt, Prediction uncertainties and inaccuracies resulting from common assumptions in modelling vibration from underground railways, Proc. Inst. Mech. Eng. Part F J. Rail Rapid Transit. 226 (2012) 501–512.

[124] D.J. Thompson, D.E.J. Lurcock, Predicting Groundborne Railway Noise and Vibration in Buildings: A Comparison of Measurements and Methods, in: Proc. Inst. Acoust., Birmingham, UK, 2014: pp. 139–146.

[125] D.E.J. Lurcock, D.J. Thompson, O.G. Bewes, Attenuation of railway noise and vibration in two concrete frame multi-storey buildings, in: 11th Int. Work. Railw. Noise, Uddevalla, Sweden, 2013.

[126] D.E.J. Lurcock, Predicting Groundborne Noise and Vibration in Buildings from Railways : A Background Study, University of Southampton, 2012.

[127] D.E.J. Lurcock, Predicting Groundborne Noise and Vibration in Buildings from Railways : Interim Project Report, University of Southampton, 2013.

[128] C.J.C. Jones, Groundborne Noise, in: D.J. Thompson (Ed.), Railway Noise and Vibration: Mechanisms, Modelling and Means of Control, Elsevier Ltd, 2009.

[129] R.A.J. Ford, Track and ground vibrations from trains running on conventional ballasted track, Proc. Inst. Mech. Eng. Part F J. Rail Rapid Transit. 206 (1992) 117–126.

[130] M. Petyt, Introduction to Finite Element Vibration Analysis, 2nd Editio, Cambridge University Press, 2010.

[131] D.E.J. Lurcock, D.J. Thompson, O.G. Bewes, Attenuation of Railway Noise and Vibration in Two Concrete Frame Multi-storey Buildings, Noise Vib. Mitig. Rail Transp. Syst. 126 (2015) 297–304.

[132] J. Serra Tur, Ground-borne noise from trains : transmission of vibration through building structures, MSc Thesis, University of Southampton, 2012.

[133] S. Marburg, B. Nolte, Discretization Requirements : How many Elements per Wavelength are Necessary?, in: Comput. Acoust. Noise Propag. Fluids - Finite Bound. Elem. Methods, Springer, 2008.

[134] M.J. Crocker, Handbook of Acoustics, John Wiley & Sons, 1998.

[135] Marshall Day Acoustics Ltd, INSUL, (n.d.).

[136] W.A. Utley, C.N. Pope, The measurement of damping in large panels, Appl. Acoust. 6 (1973) 143–149.

[137] British Standards Institution, Electroacoustics - Octave-band and fractional-octave-band filters: Specifications, BS EN 61260-1:2014, 2014.

[END OF THESIS]